Synthesis and Coordination Studies of Novel Heteroaryl Tetrazoles

A thesis submitted to the National University of Ireland in fulfilment of the requirements for the degree of

Doctor of Philosophy

By

Ursula Sheridan, B.Sc.

Department of Chemistry,
Maynooth University,
Maynooth, Co. Kildare,
Éire.

September 2014

Research Supervisor: Dr. John McGinley
Head of Department: Dr. John Stephens

Dedicated to my parents, Cecilia and Patsy. Thank you for everything.

Table of Contents

Declaration

I hereby certify that this thesis has not been submitted before, in whole or in part, to this or any university for any degree and is, except where otherwise stated, the original work of the author.

Signed:____________________________ Date:__________________________

Maynooth University

Acknowledgements

A sincere thanks to my supervisor Dr. John McGinley for his support, advice and friendship throughout my time here. Despite your long commute to Denmark, you always dedicated the time to discuss work and new ideas, and for that I am truly grateful. It's sad to think that soon there will be no McGinley group to keep things a little colourful inside and outside of the lab. You will be truly missed in the department and I wish you all the best in the future.

Thanks to Prof. John Lowry and Dr. John Stephens for allowing me to conduct my research in the department and for their help throughout my studies. I would especially like to thank Dr. Stephens for the great opportunity to deliver lectures in the department. Thanks to all the academic staff who never refused me when I came knocking at their doors, especially Dr. Denise Rooney, Dr. Sean McCaffery and Dr. Trinidad Velasco-Torrijos. Donna and Carol, you always are so helpful anytime I call in, thanks for everything. I owe a debt of gratitude to the technical staff: Ollie, Barbara and Maryanne for all those Mass Spec. and elemental analysis samples, thank you so much for your patience and persistence; Ken for efficiency in ordering my chemicals and bartering; Ria for everything, you're an absolute saint and how you manage to do all your jobs, walk the dogs AND look after us all I'll never know; Noel, you're an invaluable asset to the department, thanks for all your help and expertise in all things IT and GAA. I am grateful to Dr. Kevin Kavanagh for allowing me to carry out *G. mellonella* work in his lab and for helpful advice. Thanks to Prof. Morten Bjerrum for inviting me to work in the University of Copenhagen and Dr. Constantinos Milios for the solid state fluorescence data presented in this thesis. I've worn out the road between here and DCU to Dr. John Gallagher, thanks so much for your hard work with the X-ray crystal structures and for all your advice and fruitful discussions. I am also very grateful to the IRC and the John and Pat Hume Scholarship for funding.

I leave this place with a lot of memories to cherish, and for these I have to thank my fellow postgraduates who provided so much entertainment over the years. To all the gang that was here when I started: John, Valeria, Sinead, Róisín, Declan, Denis, Rob, Lorna, Foxy, Trish, Murph, Lynn, Joey, Louise, Wayne, Carol and Colin, you were all so helpful when I was stuck with something and I'm so appreciative that you all shared your expertise so willingly when you were always so busy yourselves. To top it all off you provided a great atmosphere to work/play in! I've been so lucky to have made great friends from this experience and to this end a special thanks has to go to Lorna (for your hilarious stories, keeping me company on the many late nights and for being a loyal friend), Declan (for that banked salmon story, the lifts and the introduction to Bhuna), Foxy (for chats and beehroo!), Valeria (for all your sweet treats, Cillian is the luckiest boy ever), Rob (Euphoria ya dope) and Róisín (for comic relief and escapes to the mobile in recent times). Ye were always up for a coffee or a pint or two (or three) and the memories we've shared (wheelbarrow race in the lab anyone?) will remain with me always. To my research group, especially Niall, Sam, Niamh and Haixin for making the West side a fun place to be. Niall thanks so much for your company and chats over the years. The building could be crashing down around you, and you'd still be cool, calm and collected, thanks for making everything 'grand'! Thanks to my lab buddy Haixin, the best word to describe you would be Gent and I still don't think that aptly describes your friendship and generosity to me over the years, thank you so so much for all the papers, help and Chinese culture lessons, thanks to you I know I better get a move on as 25 is over the hill! To all the 'newbies': Rossy Wossy, Chiggy, Barry, HANDrew, Justine, Jessica, Jack (for your boundless energy and enthusiasm), Adam (traitor), Dave, Karen, Ula, Michelle, Collette, thanks so much for the lab banter and nights out over the years. I wish you all the best in the future and hope you enjoy your time here as much as I have. Finno, thanks for our post match analysis chats, it was great to chat to someone who knew as much about football as me (tee hee!). To my writing roomie Ruth, thanks for the venting sessions, advice and distractions (namely The Daily Mail). We started out on our adventures together and it's great we've finished up together too. To everyone, you all make the place what it is and thanks for making life on the bench an enjoyable one. I hope you all know how lucky you are to have each other and please promise me that the tea room will never disappear!

I've been blessed with the most understanding and supportive family and friends. Elaine, Hannah, Donna, Charlotte, Louise, Vanessa, Aisling and Lisa, thanks so much for the comic relief and showing me what I was missing outside of the lab. Thanks for being there and encouraging me whenever it all got too much and for understanding when I couldn't join you on your adventures. I promise you will be sick of the sight of me from now on! A special thanks must go to Marian as you poor thing had to put up with me for the length of this PhD and then some! Thanks so much for the chats and for listening. You've been with me through the highs and lows of this project and I couldn't imagine doing it without you. I'm also so proud of your chemistry knowledge after all these years!

To the Walshs, for always making me feel at home and ensuring I didn't come back up to Maynooth on an empty stomach, a heartfelt thank you.

John, as much as Rob and Dec slag me, I DO realise how incredibly lucky I am to have you in my life. By right, you should be in all the previous paragraphs too, but no amount of paragraphs would ever thank you enough. You've always offered unfailing love, friendship and support and believed in me whenever I doubted myself. Words cannot express how grateful I am for that. I promise we can go on as many holidays as you want now!

A huge thank you to my Mam and Dad. Dad, I may have taken your plea to ''stay in education'' a little too seriously, but I hope I've made you and Mam proud. Thank you for your endless support and encouragement in everything I've ever done.

Abstract

This thesis describes the synthesis, characterisation and coordination studies of an array of heteroaryl 5-substituted tetrazole ligands. A family of 5-substituted pyridyl tetrazole ligands with various functionalities tethered to the tetrazole moiety were prepared and fully characterised. These ligands were reacted with various MX_2 salts (M = Cu, Ni, Co, Zn; X = chloride, thiocyanate). A number of the resulting discrete metal complexes were analysed by X-ray crystallography and their potential application as anti-cancer therapeutics are discussed.

Carboxylate functionalised pyridyl tetrazole ligands were also synthesised and characterised. These ligands were examined for their potential to form coordination polymers. These investigations have been successful and have led to a series of coordination polymers and discrete clusters, some of which were examined by X-ray crystallography. Diamagnetic materials were subjected to solid state fluorescence studies and exhibited (in all but one case) increased emission when compared to the free parent ligands. EPR spectroscopic studies were also performed on Cu(II) materials.

We proceeded to develop these ligands into dicarboxylate systems in order to achieve higher dimensional coordination polymers. This work yielded a plethora of novel 1-D coordination polymers and dinuclear clusters with Cu(II), Ni(II), Co(II), Mn(II) and Zn(II) as the metal ions. Interesting manifestations were observed in these investigations, including the selective hydrolysis of an alkyl ester over an aromatic ester; selective coordination of aromatic carboxylates to hard metal cations; and the presence of coordinatively vacant carboxylate sites which open exciting avenues in the field of post-synthetic modifications. X-ray crystallography was performed on ten products. EPR spectroscopy was performed on Cu(II) materials and the solid state emission spectrum of one Zn(II) complex displayed increased emission compared to its free ligand.

Continuing the theme of coordination polymers, we investigated the ability of carboxylate functionalised bis-tetrazole ligands to form coordination polymers with Cu(II). Two categories of bis-tetrazole systems were synthesised and examined: flexible linked and rigidly linked tetrazoles. Investigations of pyrazine linked tetrazoles that were functionalised with carboxylate groups led to two 2-D coordination polymers, one of which contains water clusters and thus presents future opportunities for removal or substitution of these molecules for guest uptake and future applications.

List of Abbreviations

°C	Degrees Celsius
μ_{eff}	Effective magnetic moment
1-D	One dimensional
2-D	Two dimensional
3-D	Three dimensional
5-ST	5-substituted tetrazole
Å	Angstrom
A	Hyperfine coupling constant
A_{max}	Maximum absorbance
B	Applied magnetic field
B.M.	Bohr magneton
BDT	1,4-benzeneditetrazol-5-yl
Bipy	Bipyridine
Boc	*Tert*-Butyloxycarbonyl
$BrCH_2COOEt$	Ethyl bromoacetate
Bu_2SnO	Dibutyltin oxide
Calcd.	Calculated
$CDCl_3$	Deuterated chloroform
$CdSO_4$	Cadmium sulfate
CE	Conventional electric heating
CH_2Cl_2	Dichloromethane
$Co(SCN)_2$	Cobalt(II) thiocyanate
COSY	Correlation spectroscopy
CP	Coordination polymer
$CuCl_2.2H_2O$	Copper(II) chloride dihydrate
d	*d* orbital
d	Doublet
d_6-DMSO	Deuterated dimethylsulfoxide
DCl	Deuterated hydrochloric acid
DCM	Dichloromethane
dd	Doublet of doublets
DEPT-135	Distortionless Enhancement by Polarisation
DIEA	N,N'-Diisopropylethylamine
DMCC	Dimethylcarbamoyl chloride

DMF	N,N'-dimethylformamide
DMSO	Dimethylsulfoxide
E	Energy
EC	Electrochemistry
en	Ethylenediamine
EPR	Electron paramagnetic spectroscopy
Eqn	Equation
ESI	Electrospray ionisation
Et_3N	Triethylamine
EtOAc	Ethyl acetate
EtOH	Ethanol
ε_{max}	Extinction coefficient
f	*f* orbital
FTIR	Fourier Transform Infrared
G. mellonella	*Galleria mellonella*
g_e	Free electron *g* factor
GHz	Gigahertz
h	Hours
h	Planck's constant
H_2	Molecular hydrogen
H_2NTD	2,6-di(1*H*-tetrazol-5-yl)naphthalene
H_2O	Water
H_2O_2	Hydrogen Peroxide
H_3BTC	Benzene-1,3,5-tricarboxylic acid
HCl	Hydrochloric acid
HKUST	Hong Kong University of Science and Technology
HRMS	High Resolution Mass Spectrometry
HSAB	Hard Soft Acid Base Theory
HSQC	Heteronuclear single quantum coherence spectroscopy
Hz	Hertz
I	Nuclear spin
IC	Internal conversion
IC_{50}	Half maximal inhibitory concentration
IR	Infrared
IRMOF	Isoreticular Metal-Organic Framework
ISC	Intersystem crossing

IUPAC	International Union of Pure and Applied Chemistry
J	Coupling constant (Hz)
K	Kelvin
K_2CO_3	Potassium carbonate
KBr	Potassium bromide
L	Ligand
LAG	Liquid assisted grinding
LED	Light-emitting diode
LiCl	Lithium chloride
lit	Literature value
LLCT	Ligand-ligand charge transfer
LMCT	Ligand-metal charge transfer
Ln	Lanthanide metal
M	Molar
m	Multiplet
m.p.	Melting point
MC	Mechanochemistry
MeCN	Acetonitrile
MeOH	Methanol
mg	Milligrams
$MgSO_4$	Magnesium sulphate
MHz	Megahertz
Min	Minutes
mL	Millilitre
MLCT	Metal-ligand charge transfer
MMCT	Metal-metal charge transfer
mmol	Millimole
$MnCl_2.2H_2O$	Manganese chloride dihydrate
MNDO	Modified neglect of differential overlap
MOF	Metal-Organic Framework
MS	Mass Spectrometry
MW	Microwave
Na_2SO_4	Sodium sulfate
NaCl	Sodium chloride
NaN_3	Sodium azide
NaOH	Sodium hydroxide

NH_4Cl	Ammonium chloride
$NiCl_2$	Anhydrous nickel chloride
$NiCl_2.6H_2O$	Nickel chloride hexahydrate
nm	Nanometer
NMR	Nuclear Magnetic Resonance
p	*p* orbital
Pet. Ether	Petroleum ether
pH	Logarithmic scale of concentration of hydronium ions ($-\log[H_3O^+]$)
phen	Phenanthroline
pK_a	Minus log of association constant K_a of a given solution ($-\log K_a$)
PM3	Parameterised model number 3
POMs	Polyoxometalates
ppm	Parts per million
PSD	Post-synthetic deprotection
PSM	Post-synthetic modification
q	Quartet
quin	Quintet
R_f	Retention value
s	*s* orbital
s	Singlet (NMR)
S	Singlet state
S. aureus	*Staphylococcus aureus*
SAR	Structure-activity relationship
SBU	Secondary building unit
SCN	Thiocyanate
t	Triplet (NMR)
T	Triplet state
Tet	Tetrazole
TGA	Thermogravimetric analysis
THF	Tetrahydrofuran
TLC	Thin Layer Chromatography
$TMSN_3$	Trimethylsilyl azide
US	Ultrasound
UV-Vis	Ultraviolet-visible region
$ZnCl_2$	Zinc(II) chloride
$ZnSO_4$	Zinc sulfate

β	Bohr magneton constant
Δ	Reflux temperature
λ_{max}	Wavelength at maximum absorbance
ν	Frequency (wavenumbers)
τ	Addison parameter

Chapter 1: Introduction

1.1 Introduction to Tetrazoles

Tetrazoles are a class of organic heterocyclic compounds containing a five-membered ring composed of four nitrogen atoms and one carbon atom (Figure 1.1). An increasingly popular functionality, tetrazoles have found many uses as fragments in pharmaceutical drugs (anti-bacterial, anti-allergic, anti-inflammatory, anti-fungal),[1] information recording systems and photography, not to mention a recent increase of interest in employing tetrazoles as greener explosive materials and in pyrotechnics.[2,3] The tetrazole ring has had its greatest influence in the field of medicinal chemistry where it has become an important structural motif in the design of new drugs.[1] This is reflected by the fact that the number of publications and patents in this field of medicinal chemistry has increased substantially in recent years.[4]

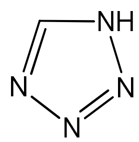

Figure 1.1: Basic structure of tetrazole.

1.1.1 Bioisosteres of Carboxylic Acids - Medicinal Attributes of Tetrazoles

The main reason tetrazoles have received particular interest in medicinal chemistry is that they constitute the most commonly used bioisostere of the carboxylic moiety. Bioisosteres are substituents or groups that impart similar biological properties to a chemical compound. The purpose of exchanging one bioisostere for another is to fine tune the pharmacokinetic or pharmacodynamic properties of a bioactive compound. There are many similarities in the properties of both tetrazole and carboxylic acid moieties. Tetrazoles contain a free N-H which is acidic in nature, having similar acidity to carboxylic acids (pK_a 4.5-4.9 vs. 4.2-4.4 respectively).[5] This is due to the ability of both to stabilise a negative charge by electron delocalisation. Other similarities are that tetrazoles are ionised at physiological pH and exhibit a planar structure like their carboxylic acid counterparts. There are, of course, some differences between the two moieties. Hansch has shown that anionic tetrazoles are almost 10 times more lipophilic than the corresponding carboxylic acid.[5] This increased lipophilicity could account for the higher membrane permeability often seen with tetrazole bioisosteres compared to their carboxylate analogues.[6] A major advantage of tetrazoles over carboxylic acids is that they are resistant to many biological metabolic degradation pathways and long half lives are seen with a number of orally administered tetrazole containing compounds.[7] Tetrazoles also have a larger surface area and a greater ability to delocalise a negative charge, which may aid in receptor-substrate interaction. This could also have a negative impact, whereby it could hinder receptor-substrate interaction due to a local charge density or sterically hindering a change in structural information to allow for binding of a receptor molecule. These observed similarities and differences make tetrazoles interesting bioisosteres which are worth studying further.

The most important group of biologically active compounds based on tetrazoles are the selective antagonists of the receptor angiotensin II. The first representative, Losartan, has been in clinical use since 1994 (Figure 1.2)[8] and is a good example of a drug in which the optimal ratio of anti-hypertensive activity and *per os* bioavailability was achieved. Carboxylic acid analogues of this drug also possessed anti-hypertensive properties but were less active, even when they were administered intravenously. Other bioisosteric replacements of carboxylic acids were examined during the development of this drug, however, these replacements failed to display better properties than the tetrazole derivatives.[9]

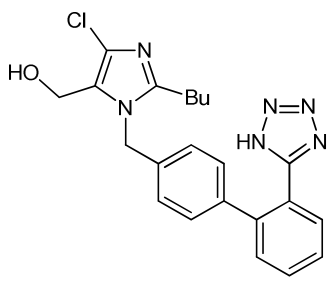

Figure 1.2: Structure of Losartan.[8]

1.1.2 Synthesis of Tetrazoles

With the tetrazole group's increasing importance in medicinal chemistry, the efficient synthesis of tetrazole derivatives has become an important task. This pursuit of improving its synthesis was also evident in the early days of tetrazole development. In 1885, Bladin coined the term tetrazole for a five-membered heteroarene consisting of four nitrogens and proved its existence somewhat mistakenly while he was investigating the reactions of dicyanophenyl hydrazine, the condensation product of cyanogens and phenylhydrazine. Treatment of dicyanophenyl hydrazine with nitrous acid led to the first reported tetrazole containing compound, later known as 5-cyano-2-phenyltetrazole (Figure 1.3).[10]

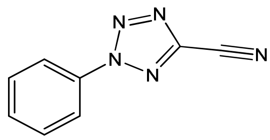

Figure 1.3: The first tetrazole containing compound prepared, 5-cyano-2-phenyltetrazole.

The most interesting compounds containing tetrazole moieties are 5-substituted tetrazoles (5-STs). The first specific and widely used methods for synthesising these derivatives involved the diazotisation of polynitrogen compounds, especially hydrazidines such as **1.11** (Scheme 1.1), which are prepared primarily from imino ethers (imidates) and hydrazine.[11]

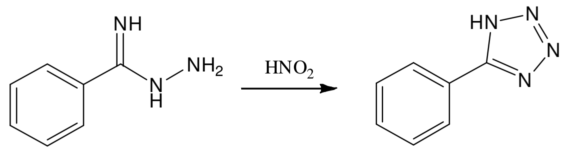

1.11 **1.12**

Scheme 1.1: Synthesis of 5-phenyl-1*H*-tetrazole (**1.12**) from benzimidohydrazide.

The currently favoured approach to obtain 5-STs is to react nitrile moieties with azide groups. A reaction of this type was successfully accomplished for the first time in 1901, when 5-amino-1*H*-tetrazole, known as diazoguanidine at the time, was prepared from cyanamide and hydrazoic acid.[12] In 1910, 1*H*-tetrazole itself was synthesised by a similar reaction, which involved the cycloaddition of hydrazoic acid to hydrogen cyanide.[13] Hydrazoic acid, a toxic and explosive gas, was prepared either in advance or *in situ* and was used as a major reactant for 5-ST formation until the end of the 1950s.[14]

In 1958, Finnegan *et al.* published their fundamental work utilising sodium azide and ammonium chloride in N,N-dimethylformamide (DMF) in the synthesis of 5-STs (Scheme 1.2). Although hydrazoic acid could also be detected in the reaction mixture, this method completely changed the synthetic approaches to 5-STs. Since then, the process has become much safer, reaction times significantly reduced, and the yields of 5-STs have increased. Used to this day for the preparation of 5-STs, it has completely displaced the processes utilising hydrazoic acid.[15] Many new methods and modifications of existing processes have appeared since Finnegans's methodology. The main principle in all of these methodologies is the reaction between a nitrile and an azide moiety. These reactions can be divided into three groups: a) using acidic media, b) using Lewis acids and c) using organometallic and organosilicon azides. There is no clear distinction between these approaches and many of the latest methods combine their advantages.

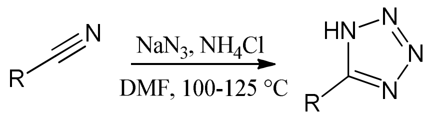

Scheme 1.2: Finnegan's method for the preparation of 5-STs.[15]

The general disadvantage in preparing 5-STs is the long reaction times required. Microwave (MW) irradiation has been widely explored in attempts to overcome this limitation, and has been the subject of intense investigations as a technique, with around 4000 papers been published up to 2012.[16] The benefits of microwave irradiation have been suggested to be the results of thermal effects and so-called ''specific microwave effects''. It is of note, however, that the precise mechanism by which microwave irradiation works in organic reactions remains a contentious issue, with recent high profile publications conflicting with each other.[17]

1.1.2.1 Methods using Acidic Media (Proton Catalysed)

The methods discussed above utilising hydrazoic acid and Finnegan's method also falls into this class. Several modifications have followed, including microwave-assisted preparation of 5-STs which reduced reaction times significantly whilst retaining high yields.[18] Koguro *et al*. carried out significant modifications to Finnegan's method by reacting sodium azide and triethylammonium chloride in toluene (Scheme 1.3).[19] This process was advantageous, as the product could be easily isolated by submerging the reaction mixture into water or alkaline aqueous solution. This methodology was further improved through the use of microwave irradiation.[20]

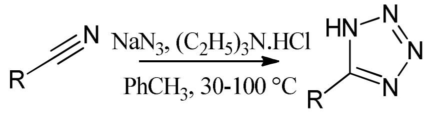

Scheme 1.3: Koguro's method for preparation of 5-STs.[19]

With regard to the preferred mechanism of the reactions in acidic media, the following three hypotheses have been discussed: 1) concerted dipolar [2+3] cycloaddition, 2) anionic two step [2+3] cycloaddition, and 3) activation of the nitrile by protons (*via* an intermediate imidoyl azide). Dimroth and Fester suggested that reactions between nitriles and hydrazoic acid proceeded through the intermediate imidoyl azides.[13] However, this hypothesis was not confirmed for almost one hundred years.[21] Although Finnegan's group formulated the role of acid catalysis in the preparation of 5-STs, they proposed that the principle step of the reaction was the attack of the azide anion on the nitrile carbon, followed by ring closure (hypothesis 2, Scheme 1.4).[15] Several reactions with the use of hydrazoic acid and ammonium azide were performed, with better results seen in the case of the ammonium salt. This hypothesis was confirmed in work by Jursic and Zdravkovski in 1994, in which a two step [2+3] cycloaddition involving nucleophilic attack of the azide ion on the carbon of the nitrile group followed by tetrazole ring closure, was shown to be the preferred mechanism.[22]

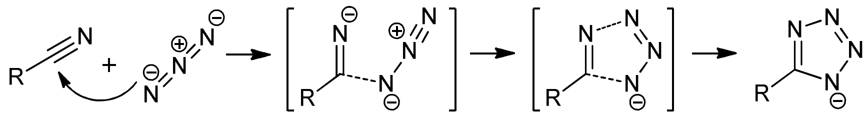

Scheme 1.4: Mechanism of formation of 5-STs through two step [2+3] cycloaddition.

Interestingly, only the two mechanisms corresponding to hypotheses 1 and 2 were considered, with the role of acid catalysis in these reactions not being mentioned. Contradictory data supporting the concerted dipolar [2+3] cycloaddition were presented by Poplavskii *et al.*[23] They discovered that dimethylammonium azide is generally not ionised in DMF and undergoes the reaction as the hydrogen bonded complex $(CH_3)_2NH.HN_3$, and not as azide anion and dimethylammonium cation. The azide part of this complex has a structure and distribution of electron density similar to those of hydrazoic acid and organic azides. Because hydrazoic acid and organic azides are typical 1,3-dipoles in dipolar cycloaddition reactions, the authors suggested that the reaction mechanism is a concerted mechanism (Scheme 1.5).[23]

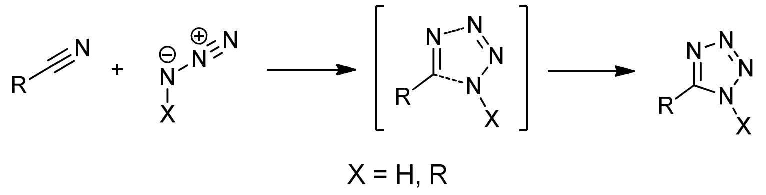

Scheme 1.5: Mechanism of formation of 5-STs through a concerted dipolar [2+3] cycloaddition.

At the same time, they also discovered that tetraalkylammonium azides didn't react with nitriles under certain conditions. These azides only release azide anion, which is not a 1,3-dipole and cannot react by 1,3-dipolar cycloaddition. The fact that tetraalkylammonium azides do not react also rules out the anionic two-step [2+3] cycloaddition mechanism. Also, while virtually all nitriles react with ammonium azide salts at elevated temperature, organic azides only react with the most activated nitriles.[24] The fact that these azide salts and organic azides are electronically very similar, yet have significantly different reactivities, demonstrates that different mechanisms from those proposed in hypotheses 1 and 2 are likely in effect. Himo *et al*. used quantum chemical calculations to probe the energetics of various reaction mechanisms for addition of azides to nitriles. They found that in an acidic medium, the preparation of a 5-ST actually proceeds preferentially through an imidoyl azide intermediate such as **1.13**, which spontaneously cyclises to the 5-ST under the reaction conditions (Scheme 1.6). As in the case of the Pinner synthesis of imidates[25] or the acid hydrolysis of nitriles,[26] protonation of the nitrile increases its reactivity and susceptibility to attack by azide anions. The transition state of this process is significantly lower than those of hypotheses 1 and 2. The ammonium cation acts as a proton transfer mediator, even in the cases where the ammonium salt is not ionised in the reaction medium, which explains why tetraalkylammonium azides would not react. In the case of proton activation by the ammonium part of the salt, the energy barrier, either ionised (NH_4^+) or not ionised (NH_3), was calculated to be ~21 kcal mol^{-1}, whereas all other discussed mechanisms showed higher energetic barriers, with values of 35 kcal mol^{-1} for concerted dipolar [2+3] cycloaddition, 34 kcal mol^{-1} for anionic [2+3] cycloaddition and 31 kcal mol^{-1} for reaction with hydrazoic acid (six-membered transition state).[21] The role of the partial charge on the nitrile carbon is essential. The presence of electron-withdrawing substituents on the nitrile decreases the activation barrier and increases the reactivity of the nitrile towards azide anions. In the cases of the strongest electron acceptors, the energies of the transition states of anionic [2+3] cycloaddition are close to the energies of the ammonium-activated transition states, which is why the anionic mechanism cannot be completely rejected. Moreover, the most electron-poor nitriles react with sodium azide without any additional reactants under very mild conditions.[27]

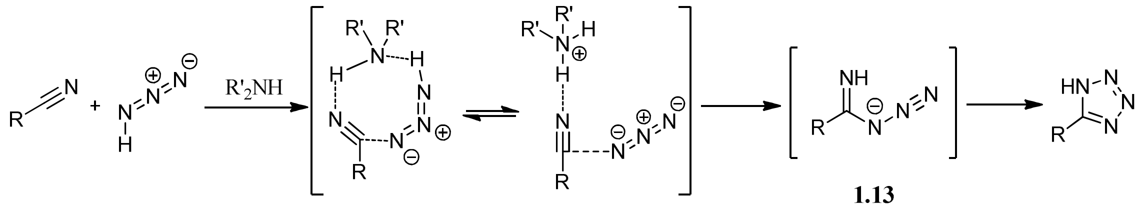

Scheme 1.6: Mechanism of formation of 5-STs *via* imidoyl azide intermediate **1.13**.

Methods using acidic media are widely used both in small laboratories and on an industrial scale.[16] The main drawbacks are the presence of highly toxic and explosive hydrazoic acid in the reaction mixtures. Merck Frosst scientists have recently addressed this issue with successful results. Reaction of a nitrile with sodium azide in the presence of catalytic zinc oxide in aqueous THF proceeded efficiently, and most notably, with only 2 ppm of hydrazoic acid in the reaction vessel headspace as measured by online IR spectroscopy.[28] This modification ensured the safety of the reaction as the pH increased from 5 to 8.

1.1.2.2 Methods Using Lewis Acids

Lewis acids in 5-ST synthesis works by coordinating to nitriles and activating them towards attack by the azide anion, hence in principle, it is a similar method to the acidic media method. After some disappointing but promising results employing aluminium azide and borontrifluoride as Lewis acids in order to synthesise 5-STs, interest in this type of synthesis was regenerated in 1993. Huff *et al.* utilised trimethylaluminium in the synthesis of a series of 5-STs under relatively mild reaction conditions.[29] In these reactions, trimethylsilyl azide ($TMSN_3$) served as the azide donor (Scheme 1.7).

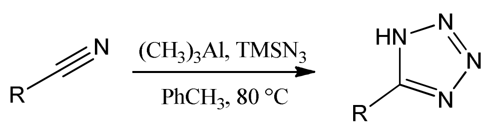

Scheme 1.7: Preparation of 5-STs utilising trimethylaluminium.[29]

The main drawback for these reactions is their water sensitivity, leading to stringent reaction conditions. A major breakthrough in this field came with the publication of work by Sharpless.[30] This method consisted of treatment of a nitrile with sodium azide and zinc bromide in H_2O (Scheme 1.8) and enabled a more environmentally friendly route to 5-STs. Isolation of the product was easily achieved by acidification of the reaction mixture and filtration of the precipitated product. However, this method required the use of high pressure and temperatures of 170 °C for conversion of less reactive nitriles. In 2009, a solvent free method was developed from Sharpless' method which reduced reaction times but larger amounts of azide and zinc salts were required.[31] Microwave assisted methods have also been developed based on Sharpless' work with the result of decreasing reaction times.[32]

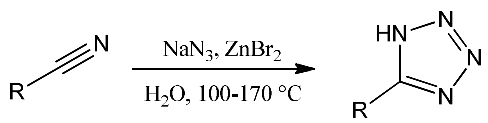

Scheme 1.8: Sharpless' method for preparation of 5-STs.[30]

As in the case of the acid-catalysed synthesis, the mechanism of this type of 5-ST preparation involved a decrease in activation energy when the nitrile was coordinated to a Lewis acid. Activation energies remained unaffected when a Lewis acid was bonded to the azide ion. Activation energies for reactions where the zinc ions were only bonded to azide anions were calculated to be 34 and 36 kcal mol^{-1} for tetrahedral and octahedral coordination of zinc ions, respectively. In comparison, the activation energies of the uncatalysed reactions were 32 kcal mol^{-1} for the reaction with methyl azide and 34 kcal mol^{-1} with azide anions. When the zinc cation was bonded to either a nitrile or both azide and nitrile, the activation energies decreased to 25-30 kcal mol^{-1}, again depending on the numbers and types of ligands. This study confirmed that the Lewis acid coordinates with the nitrile nitrogen. This coordination increases the polarisation of the nitrile moiety and decreases the activation energy of the entire reaction.[33]

1.1.2.3 Methods Using Organometallic and Organosilicon Azides

A notable class of azide donors are that of trialkyltin azides, usually in the form of trimethyltin azide or tri(*n*-butyl)tin azide.[34] Reactions between these tin reactants and nitriles produced 5-STs in high yields, even from sterically hindered and electron rich nitriles. Molloy and co-workers also obtained 5-STs employing organotin azides without the use of solvent.[35] The main drawbacks, however, were the use of toxic reagents in high amounts. In an effort to avoid the use of toxic and volatile trialkyltin chlorides and to decrease the amount of organotin reagents necessary whilst maintaining their advantages, a 5-ST synthesis based on trimethylsilyl azide ($TMSN_3$) in the presence of catalytic amounts of dibutyltin oxide (Bu_2SnO) was developed.[36] The reaction proceeds in a stepwise manner: the nitrile nitrogen binds to the acidic tin atom, which activates the nitrile carbon towards attack of the azide group. The open-chain intermediate then cyclises to the 1-[dimethyl(trimethylsilyloxy)stannyl]-5-ST (**1.17**, Scheme 1.9). The catalytic complex **1.15** is then regenerated through a simple S_N2 reaction between **1.17** and $TMSN_3$ *via* transition state **1.18**. Recently, recovery of the catalyst **1.15** from complex **1.17** has been demonstrated by treatment with azide anions. This meant that only catalytic amounts of $TMSN_3$ and Bu_2SnO together with stoichiometric amounts of inexpensive sodium azide could be used in this new protocol.[37]

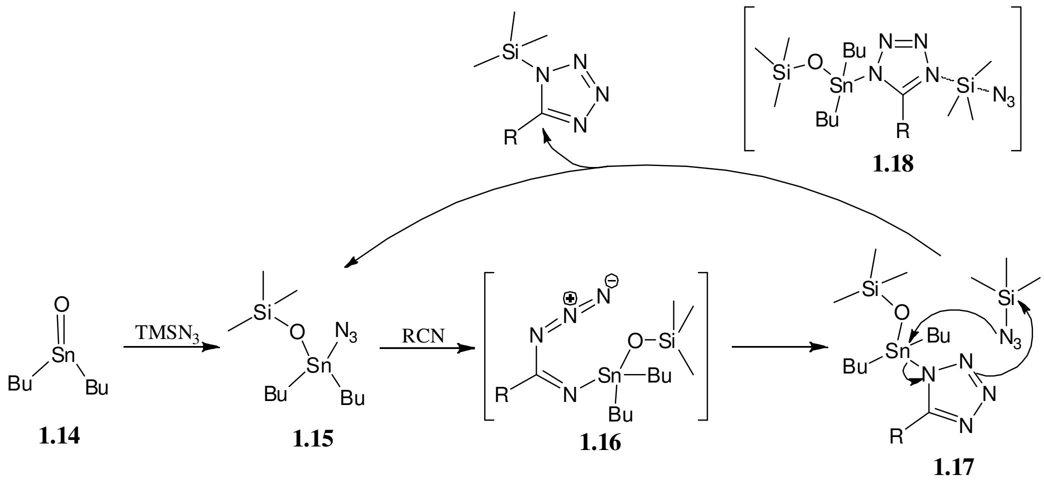

Scheme 1.9: Mechanism for reaction between nitrile and $TMSN_3$ in the presence of dibutyltin oxide.[36]

The most universal method from this group, providing high yields of 5-STs under mild conditions, was published in 2007. Dialkylaluminium azides were the crucial reactants for this procedure and the main source of azide anions, and were prepared *in situ* from the dialkylaluminium chlorides and sodium azide (Scheme 1.10). Their structures combine several advantages: high solubility in organic solvents, a suitable azide donor and typical Lewis acids.[38]

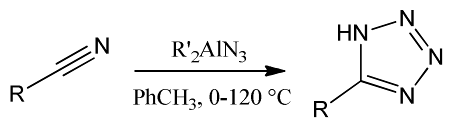

Scheme 1.10: Synthesis of 5-STs by use of dialkylaluminium azides.[38]

Despite the success of these group of reactions, the use of highly toxic organometallic reactants, the residues of which are often present in products meaning necessary careful separation is required, is a major drawback of these procedures.

1.1.3 Functionalisation of 5-Substituted Tetrazoles

5-STs are important intermediates in the synthesis of more complex compounds. Substitution of 5-STs is the most common and effective method for the preparation of 1,5- and 2,5-disubstituted tetrazoles. As well as a wide range of alkyl substituents, aryl, acyl, silyl, vinyl, sulfonyl, phosphoryl and other similar groups can be introduced onto the tetrazole ring.[39] The main problem with 5-ST substitution is its low and hard to control regioselectivity. Tetrazoles exist as tautomeric 1*H*- and 2*H*-tetrazoles (Figure 1.4), and in the presence of base they exist as the corresponding anions, where alkylation can occur at either the N-1 or N-2 positions.

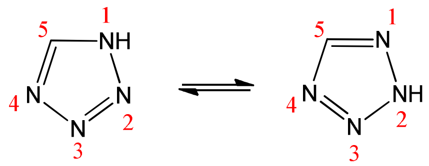

Figure 1.4: Tautomeric forms of tetrazole. The numbering presented will be used in all other cases throughout this thesis unless otherwise stated.

2*H*-tautomers are thought to be more stable than 1*H*-tautomers. In the crystalline state however, the majority of 5-STs exist in the 1*H*-form and are stabilised by hydrogen bonds to neighbouring molecules which results in dimers and larger agglomerates. In media that have high dielectric constants, 1*H*-tautomers are preferred due to their higher polarities. A ^{15}N NMR study of tetrazole in d_6-DMSO revealed that 90-99% of tetrazole exists in the 1*H*-form.[40] However, there are several situations in which the relative proportions of the 2*H*-tautomers strongly increase. This is seen especially in solvents with low polarity, in which the less polar 2*H*-form is better solvated. The presence of an electron-withdrawing substituent at the 5-position increases the polarity of the 2*H*-tautomer and also the relative proportion of the 2*H*-form in polar solvents. In addition, the presence of a bulky substituent in the 5-position or in the *ortho*-position of the phenyl ring in a 5-aryltetrazole can increase the relative proportion of the 2*H*-form.[41]

Alkylation of a tetrazolate anion, either with or without a substituent in the 5-position almost always leads to a mixture of both 1- and 2-alkyltetrazole isomers in various ratios. The ratio of isomers formed during the reaction depends on the reaction temperature and the properties of the substituent at the 5-position. Higher reaction temperatures leads to increased amounts of 1-isomers, whereas electron-accepting properties of substituents at the 5-position increases the amount of 2-isomers produced. Bulky substituents direct substitution to the 2-position of the tetrazole ring.[16] In the next section, several methods of alkylating a tetrazole will be discussed and the regioselectivity of the reactions will be addressed.

1.1.3.1 Alkylation of 5-STs

There are many methods of simple alkylation using a base such as triethylamine (Et_3N), sodium hydroxide (NaOH) and potassium carbonate (K_2CO_3) in an appropriate solvent to yield the desired alkylated products. Tritylation of a 5-ST is one of the most valuable substitutions on the tetrazole ring. The triphenylmethyl group is a fundamental protecting group of 5-STs and is used in the synthesis of more complex structures such as Losartan and its analogues.[42] Alkylation of 5-STs with triphenylmethyl chloride resulted in the formation of only the 2-isomers regardless of the substituents at the 5-position (Scheme 1.11).[43,44] This observation was not surprising, considering the size of the triphenylmethyl moiety. However, even in the case of an unsubstituted tetrazole the same observation was made.[43] Tritylation most probably involves a S_N1 reaction, therefore the rate limiting step is the ionisation of triphenylmethyl chloride to its respective cation. The more stable the carbocation, the higher its selectivity towards one of the two competing nucleophilic centres will be.[45] This is most likely the reason high regioselectivity is seen even in the case of unsubstituted tetrazole.[46]

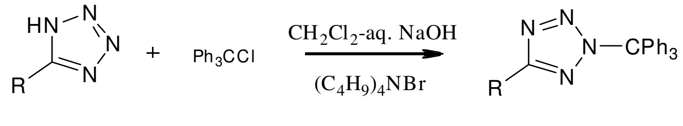

Scheme 1.11: Tritylation of 5-STs under phase-transfer catalysis conditions.[43]

Another highly regioselective reaction occurs in strongly acidic media. Reactions between 5-STs and secondary or tertiary aliphatic alcohols or alkenes in sulfuric acid exclusively produced 2-alkylated products.[47,48] A possible explanation for this is that although 5-STs are weak bases, they are protonated in strong mineral acid solutions. The nitrogen at the 4-position is protonated preferentially, resulting in a 1*H*,4*H*-tetrazolium cation of type **1.19** (Scheme 1.12). The electrophilic attack of a carbocation formed from alcohol or olefin could be directed only to the N-2 or N-3 of the tetrazolium cation, leading exclusively to 2,5-disubstituted tetrazoles (**1.21**). Although an unusual interaction between two cations, MNDO quantum chemical calculations showed a high electron density localised on nitrogen atoms N-2 and N-3. Moreover, decreasing the acidity of the reaction medium led to an increased yield of the 1-isomer, which is in agreement with the proposed mechanism.[48]

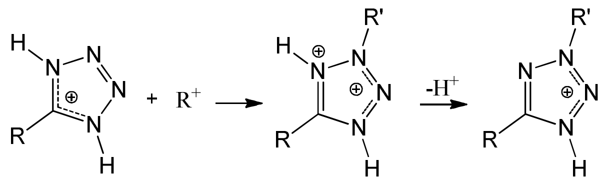

1.19 1.20 1.21

Scheme 1.12: Mechanism of 5-ST alkylation in strongly acidic media.[47]

In 2007, reactions of 5-phenyl-1*H*-tetrazole and 1*H*-tetrazole potassium salts with 2,3,4,6-tetra-*O*-acetyl-α-D-glucopyranosyl bromide (**1.22**) and methyl 2,3,6-tri-*O*-benzyl-4-*O*-triflyl-α-D-glucopyranoside (**1.23**) in boiling acetone were performed (Scheme 1.13).[49] During the reaction of 5-phenyl-1*H*-tetrazole and **1.22**, a mixture of both 1- and 2-isomers were formed. This was in contrast to the reaction with **1.23** which yielded only the 2-isomer. In the first example, 5-phenyl-1*H*-tetrazole could approach a more accessible equatorial site, facilitating the formation of both isomers. In the second case, 5-phenyl-1*H*-tetrazole had to approach a sterically inconvenient axial site, which allowed the formation of only the 2-isomer (Scheme 1.14). It is worthy to note that microwave irradiation on alkylation reactions proceeded with the same regioselectivity, however did increase reaction rates.

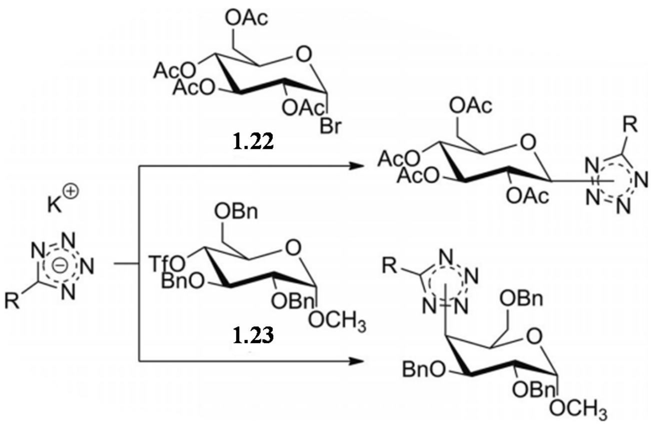

Scheme 1.13: Reactions between potassium salts of 5-STs and glucose derivatives under microwave irradiation.[49]

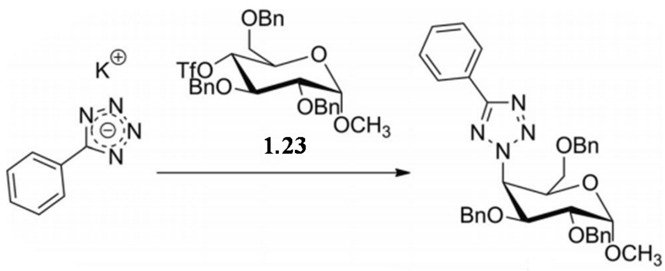

1.24

Scheme 1.14: Sterically controlled formation of a 2,5-disubstituted tetrazole.

1.1.3.2 Arylation of 5-STs

Arylations of 5-STs are described less frequently in the literature than alkylations. An example of this reaction is shown in Scheme 1.15. The reaction of sodium 5-methylsulfanyl-1*H*-tetrazolate and 4-nitrofluorobenzene resulted in the formation of both isomers in a 1:3 ratio. 5-aryltetrazoles did not react under these conditions, however the employment of 2,4-dinitrofluorobenzene resulted in successful reactions with these derivatives under mild conditions.[50]

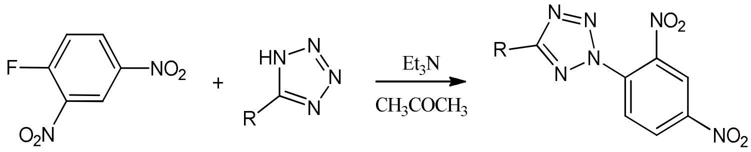

1.25

Scheme 1.15: Arylation of 5-STs with 2,4-dinitrofluorobenzene **1.25**.[50]

Microwave-assisted arylations of 5-STs by treatment of their sodium salts with 4-nitrofluorobenzene in DMSO have recently been described (Scheme 1.16). With 5-aryl-1*H*-tetrazoles the reactions led regioselectively to the formation of 2,5-diaryl-2*H*-tetrazoles. In the cases of more compact substituents such as 5-alkyl-1*H*-tetrazoles however, the reactions yielded mixtures of both regioisomers.[51]

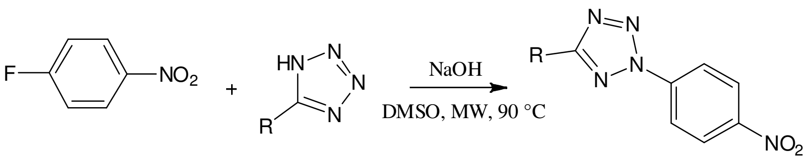

Scheme 1.16: Arylation of 5-STs with 4-nitrofluorobenzene under microwave irradiation conditions.[51]

1.1.3.3 Vinylation of 5-STs

The vinylation of tetrazoles is an interesting concept due to the possibility of subsequent reaction of the vinyl product to form further heterocyclic derivatised tetrazoles. Although several methods for the preparation of 5-substituted 2-vinyl-2*H*-tetrazoles have been published, all have substantial disadvantages. The first direct vinylation methods used mercuric acetate, a toxic mercuric salt, which resulted in low yields. Analogous reactions with palladium(0) catalysts led to low yields with a high tendency to polymerise.[52]

Roh *et al.* recently developed a one-pot regiospecific synthesis of 5-substituted-2-vinyl-2*H*-tetrazoles through a simple procedure without a metal catalyst or organocatalyst. The group found that the reaction of 5-phenyl-1*H*-tetrazole with 1,2-dibromoethane and Et_3N in a 1:1:2 molar ratio in MeCN led to the preferential formation of 5-phenyl-2-vinyl-2*H*-tetrazole. By increasing the ratio of dibromoethane and Et_3N the yield of the vinyl product was seen to rise from 60-80%, while decreasing the amount of dimers formed. The mechanism of the reaction was investigated in order to explain the regiospecificity of the reaction. They proposed that the Et_3N reacted with 1,2-dibromoethane to form (2-bromoethyl)triethylammonium bromide (**1.26**, Scheme 1.17) which reacted with the tetrazole producing **1.27**. Substitution at the 2-position of the tetrazole rings is probably directed by the steric requirements of **1.27**. Under these reaction conditions, **1.27** could undergo spontaneous elimination to produce a vinyl derivative.[53]

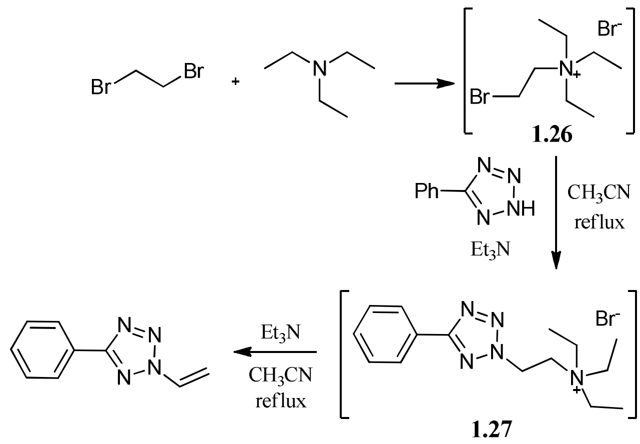

Scheme 1.17: Mechanism of regioselective vinylation.[53]

1.2 Coordination Chemistry – Overview Of Topics Relevant to Thesis

In this section, a brief account of one of the most important bonding theories that rationalise experimental facts such as electronic spectra and magnetic properties of coordination compounds is discussed. The discussion will focus on first row d-block metals, for which this theory of bonding is most successful. The phenomenon of Jahn-Teller distortions will also be discussed.

1.2.1 Crystal Field Theory

Crystal field theory is an electrostatic model which focuses on the interaction of donor electrons from ligands and the metal centre. Each ligand is treated as a point charge and there is an electrostatic interaction between the metal ion and the ligands. However there is also a repulsive interaction between electrons in the d orbitals and the ligand point charges. Of the five d orbitals, three have their lobes directed in between the x, y and z axes, while the other two are directed along these axes (Figure 1.5). As a consequence of this difference, the d orbitals in the presence of ligands are split into groups of different energies. The type of splitting and the magnitude of the energy differences between the orbitals depend on the arrangement and the nature of the ligands. Magnetic properties and electronic spectra, both of which are observable properties, reflect the splitting of the d orbitals and hence these techniques can yield useful information about the electronic structure of coordination compounds.

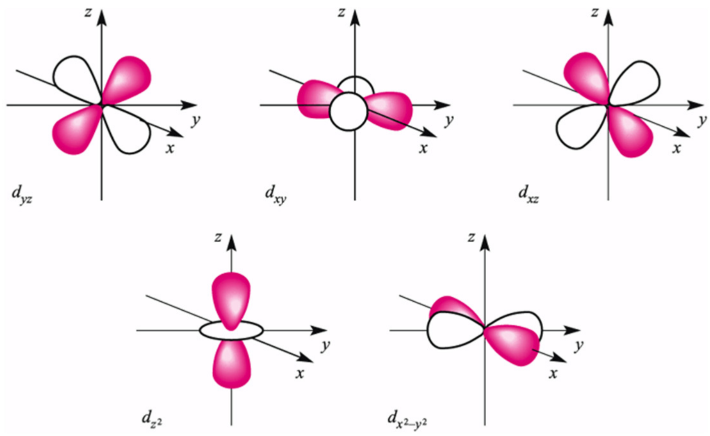

Figure 1.5: Representation of the five d orbitals on a Cartesian axis.

Crystal field theory can be conveniently illustrated by considering a first row metal cation surrounded by six ligands placed on a Cartesion axes at the vertices of an octahedron. If the electrostatic field was spherical, then the energies of the five 3d orbitals would be destabilised by the same amount. However, since the d_{z^2} and $d_{x^2-y^2}$ atomic orbitals point directly at the ligands and the d_{xy}, d_{yz} and d_{xz} atomic orbitals point between them, the d_{z^2} and $d_{x^2-y^2}$ atomic orbitals are destabilized to a greater extent than the d_{xy}, d_{yz} and d_{xz} atomic orbitals (Figure 1.6).

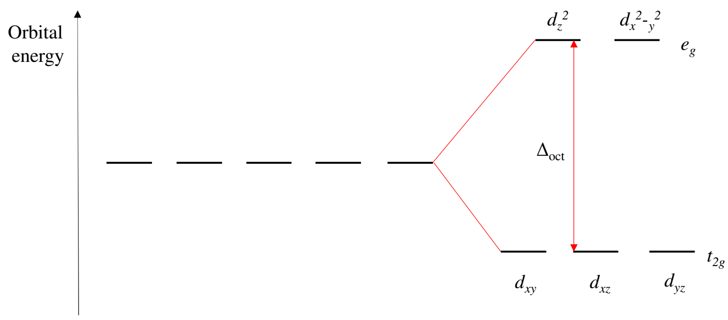

Figure 1.6: Splitting of the d orbitals in an octahedral crystal field.

The energy separation between the energy levels is Δ_{oct}. The magnitude of Δ_{oct} is determined by the strength of the crystal field. Δ_{oct} for a weak crystal field is smaller than for a strong crystal field. Factors governing the magnitude of Δ_{oct} are the identity and oxidation state of the metal ion and the nature of the ligands. For octahedral complexes, Δ_{oct} increases along the spectrochemical series of ligands (seen below), with ambidentate ions appearing in two positions in the series.

$$I^- < Br^- < [NC\underline{S}]^- < Cl^- < F^- < [OH]^- < H_2O < [\underline{N}CS]^- < NH_3 < en < bipy < phen < [CN]^-$$

For d^1, d^2 and d^3 metal ions in an octahedral crystal field, the electrons fill the d orbitals according to Hund's rule and hence will occupy each of the three degenerate orbitals that possess t_{2g} symmetry. For a d^4 ion, two arrangements are possible: the four electrons may occupy the t_{2g} set or may singly occupy four d orbitals (Figure 1.7). Configuration A corresponds to a low-spin arrangement and B to a high-spin arrangement. The preferred configuration is that with the lower energy and depends on whether it is energetically favourable to pair the fourth electron or promote it to the e_g level. The energy required to pair two electrons in the same orbital is termed the pairing energy, P. For high spin metal complexes Δ_{oct} must be less than P, and for low spin metal complexes Δ_{oct} must be greater than P. Therefore, a correlation can be established between types of ligand (strong or weak field ligands) and preferences for high- or low-spin complexes.

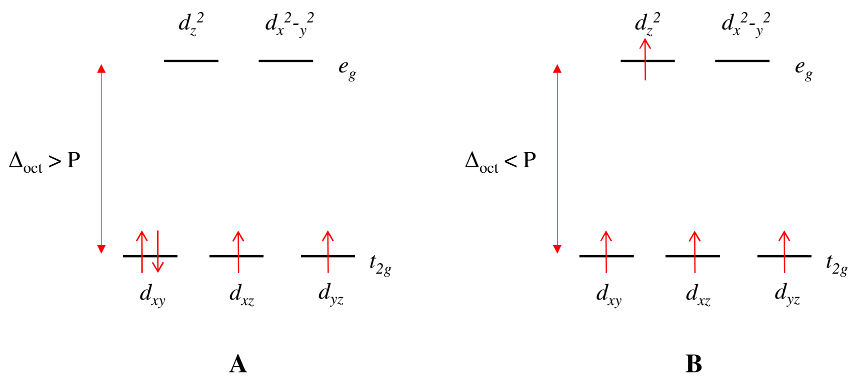

Figure 1.7: A low-spin (A) and high-spin (B) arrangement of electrons for a d^4 ion in an octahedral crystal field.

1.2.2 Jahn-Teller Distortions

In 1937, Hermann Jahn and Edward Teller published their theory which stated that any non-linear system in a degenerate energy state will be unstable and will undergo distortion to form a system of lower symmetry and lower energy, thereby removing degeneracy.[54] These Jahn-Teller distortions are most often associated with transition metal centres. In a ligand field, the splitting of the d orbitals of a metal ion can often lead to degenerate electron configurations that are subject to Jahn-Teller effects. For example, octahedral symmetry d^1, d^2, d^4 (both spin-states), d^5 (low-spin), d^6 (high-spin), d^7 (both spin-states) and d^9 transition ions all have an orbitally degenerate electron configuration that should be Jahn-Teller active. Ions with degenerate occupancy of the e_g subshell nearly always exhibit strong Jahn-Teller distortions, because of the M-L antibonding character of these orbitals.[55] Therefore, the Jahn-Teller effect is pronounced in six-coordinate complexes of high-spin d^4, low-spin d^7 and d^9 ions, with six-coordinate Cu(II) compounds being the most common Jahn-Teller distorted systems. For Cu(II) in an octahedral environment, Jahn-Teller distortions will have the effect of elongating either the two axial metal-ligand bonds or the four equatorial metal-ligand bonds. This is due to one of the e_g atomic orbitals containing an unpaired electron and the other being doubly occupied. If the doubly occupied orbital is in the d_{z^2} orbital, most of the electron density in this orbital will be concentrated between the cation and the two ligands on the *z* axis. Thus there will be greater electrostatic repulsion associated with these ligands than with the other four and the complex is axially elongated. Conversely, occupation of the $d_{x^2-y^2}$ orbital would lead to elongation along the *x* and *y* axes.[56] Both distortions lower the energies of two electrons in the e_g subshell, while raising the energy of only one, yielding a net reduction in electronic energy upon distortion of the complex (Figure 1.8).

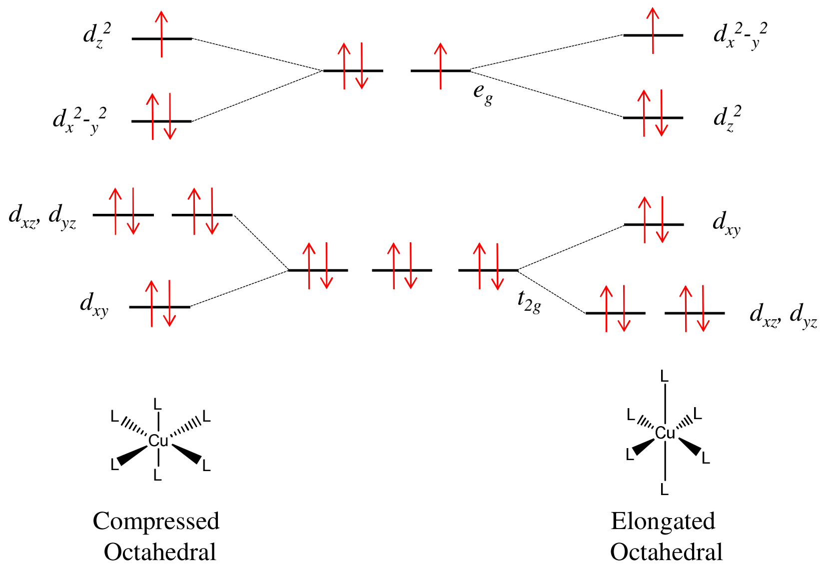

Figure 1.8: The two distortions of an octahedral Cu(II) complex.[55]

1.3 Metals in Anti-Cancer Agents

The origin of research in employing metal compounds against various tumour diseases can be attributed to the serendipitous discovery of the anti-neoplastic properties of cisplatin by Barnett Rosenberg.[57] The clinical use of this drug has been restricted due to dose-dependent side effects and resistance, coupled with a narrow spectrum of activity. This has been somewhat amended by the development of carboplatin and oxaliplatin (Figure 1.9). These metal complexes are used in about 50% of all tumour therapies and display remarkable therapeutic activity in a series of solid tumours.[58]

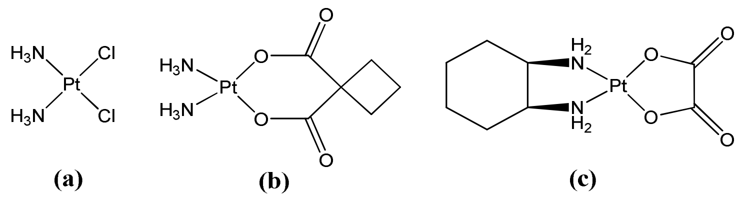

Figure 1.9: Structures of (a) cisplatin; (b) carboplatin and (c) oxaliplatin.

However, these remain to have similar drawbacks to those of cisplatin. The non-desirable effects of cisplatin and its derivatives have had the result of stigmatising the use of metal-based drugs in chemotherapy. In recent years however, this view has lapsed as indicated by the increase in the number of publications in this area. This is because medicinal inorganic chemistry has been realised as a field that offers additional opportunities for the design of therapeutic agents that are not accessible to organic compounds. The wide range of coordination numbers and geometries, available redox states, thermodynamic and kinetic characteristics and intrinsic properties of the metal cation and ligand itself offer a large variety of reactivities to be exploited compared to conventional carbon-based compounds. Therefore an extensive search into alternative strategies, based on different metals with improved pharmacological properties and an extended spectrum of activity, has been undertaken. Metal complexes containing zinc, copper, gold and ruthenium have received considerable attention as potential anti-cancer agents.[59,60] Furthermore, the investigation of ruthenium containing compounds in clinical trials attests to the rich potential of utilising non-platinum metal-based compounds in the treatment of cancer.[61] Copper complexes as anti-cancer agents is a rapidly expanding area of research as illustrated by the increasing number of publications reported since 2000 (Figure 1.10). In Cu(II) complexes, the coordination number varies from four to six allowing different geometries to exist. This variety of arrays allows for an assortment in the choice of ligands and donor atoms. This increase in popularity can also be seen with other d-block metals.

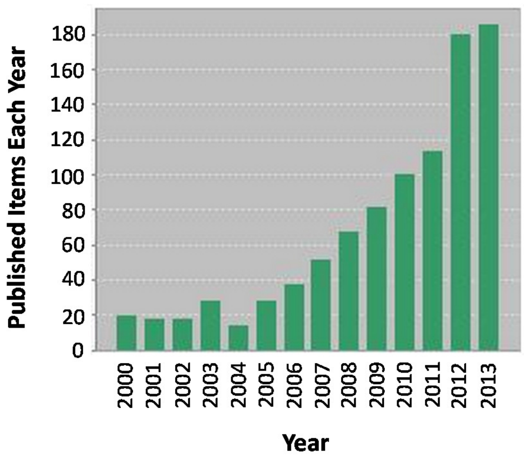

Figure 1.10: Number of articles in Web of Science on the topic ''copper and anti-cancer'' from 2000 to 2013.[62]

The breadth of this area is far too large to satisfactorily cover in this report, however extensive reviews in the literature more than adequately do this area justice and illustrate that the potential of this strategy should not be underestimated.[60,63] As the focus of this thesis is on N-donor systems, a number of relevant examples are shown in Figure 1.11. A brief overview of tetrazole metal complexes and their anti-cancer activites will be undertaken in Chapter 2.

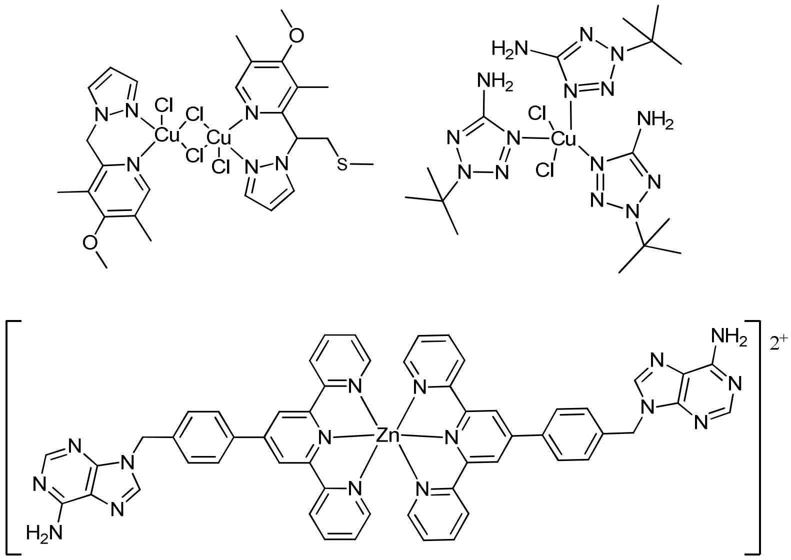

Figure 1.11: A selection of 'non-classical' anti-cancer agents which have shown promising anti-cancer activities.[64]

1.4 Metal-Organic Frameworks

Metal-Organic Frameworks (MOFs) (also known as coordination polymers) are crystalline coordination networks consisting of metal ions/clusters and organic linkers joined in a 1, 2 or 3D fashion.[65,66] A rapidly expanding field in chemical and materials sciences, MOFs display fascinating topologies and exploitable properties for potential applications such as gas adsorption and separation,[67] catalysis,[68] luminescence,[69] sensing,[70] proton conduction,[71] tunable magnetism,[72] explosives,[73] and drug delivery.[74] As well as these appealing aspects of MOFs, their potential scalability to industrial scale have made these materials an attractive target for further study.

1.4.1 Historical Developments and Nomenclature

The relatively young field of MOF synthesis evolved from its foundations in the fields of coordination, materials and zeolite chemistry. In 1989 and 1990, Hoskins' and Robson's seminal work set the basis for the future of MOFs.[75,76] They envisioned the formation of a large range of crystalline, microporous, stable solids, with ion exchange, gas sorption or catalytic properties that further allowed the introduction of functional groups by post-synthetic modification. This vision has subsequently been demonstrated by many scientists and the range of structures continues to expand at an unprecedented rate with more than 20,000 MOF structures reported and studied since the early 1990s.[66] The term MOF was made popular around 1995 by Yaghi *et al.*,[77] a prolific author in the area. In the following years, their potential applications became fully realised with the work by Kitagawa *et al.*,[78] who synthesised a porous 3-D MOF that exhibited gas sorption properties at room temperature; Yaghi *et al.*[79] and Williams *et al.*[80] who reported the syntheses of MOF-5 and HKUST-1 respectively and set the benchmark in MOF chemistry with their high porosities (Figure 1.12); and Férey *et al.*[81] who synthesised non-flexible and flexible porous MOFs. Thereafter, MOFs soon became established as better absorbant materials than conventional porous materials such as zeolites, carbons and silicas. Furthermore, it became clear that with judicious choice of metal ions or secondary building units (SBUs, polyatomic clusters) and linkers, the idea of controlling and designing the frameworks obtained was a real possibility, yielding opportunities to modify pore sizes, shapes and functionalities. In reality, the 'design' of MOFs requires a high degree of predictability to be integrated into the synthesis which is especially hard to realise when extending it to more complicated cases, not to mention consideration of other variables such as temperature, solvent and concentration which also affect product crystallinity and morphology. Nonetheless, the prospect of 'solids by design' has attracted the interests of scientists in both academia and industry.

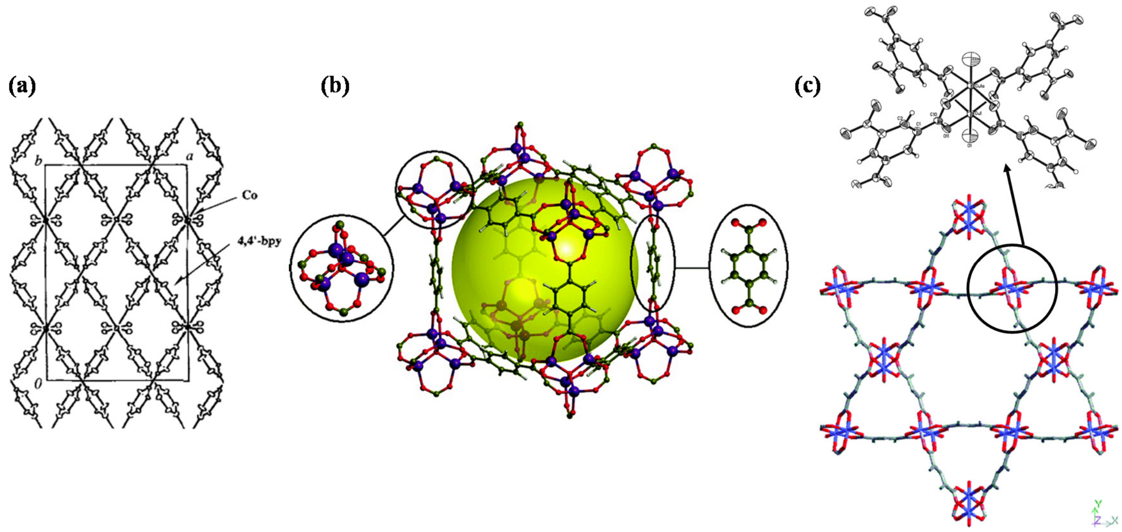

Figure 1.12: Structures of the first porous MOFs (a) a 4,4'-bipyridine linked 3-D porous MOF synthesised by Kitagawa *et al.*;[78] (b) MOF-5[79] and (c) HKUST-1.[80]

With origins in solid state, inorganic and coordination chemistry, the diversity in the focus and the scientific base of those involved in MOF chemistry has led to the use of a variety of terminologies for this class of compounds. Moreover, the nomenclature used is not consistent among research groups and much discussion has taken place regarding the most correct terminology.[82] A IUPAC task group was given the responsibility to produce terminology and nomenclature guidelines for coordination polymers (CPs) and MOFs and their final recommendations were published in 2013.[83] Their conclusions were that the term coordination polymer is the collective term for coordination networks and MOFs since by definition they have ''repeating coordination entities extending in 1-, 2- or 3-dimensions''. They defined a coordination network as a ''coordination compound extending through repeating coordination entities in 1-dimension but with cross-links between two or more individual chains, loops or spiro-links, or a coordination compound extending through repeating coordination entities in 2- or 3- dimensions''. They further define MOFs as ''coordination networks with organic ligands containing potential voids'', with proof of porosity not necessary. Although tasked with the responsibility of setting out guidelines, this report has led to further disputes amongst scientists in this area of chemistry.[84] Despite these disagreements, this thesis will attempt to adhere to these IUPAC recommendations throughout.

1.4.2 Synthesis of Coordination Polymers

Synthesis of CPs involves the use of organic ligands and metal ions or clusters. A plethora of different synthesis methods have been applied over the last 20 years to obtain CPs (Figure 1.13). In addition to room temperature synthesis, conventional electric heating (CE), microwave heating (MW), electrochemistry (EC), mechanochemistry (MC) and ultrasonic (US) methods have been employed. The term conventional synthesis is applied to reactions carried out by conventional electric heating. The reaction temperature is one of the main parameters in the synthesis of CPs and two temperature ranges, solvothermal and nonsolvothermal are normally distinguished which dictate the kind of reaction setups that have to be used. A common definition of solvothermal are those taking place in closed vessels under autogenous pressure above the boiling point of the solvent. Accordingly, nonsolvothermal techniques are those that take place below or at the boiling point of the solvent under ambient pressure. These methods also involve the slow evaporation of the reaction solvent. These methods are well known to grow crystalline solids, as it is possible to tune the reaction conditions, i.e. the rate of nucleation and crystal growth. Methods such as solvent evaporation of a solution of reactants, layering of solutions, or slow diffusion of reactants into each other lead to concentration gradients that allow the formation of CPs. Concentration gradients can also be accomplished using temperature as a variable, i.e. by applying a temperature gradient or slow cooling of the reaction mixture. Alternative synthetic routes have also been developed where the reaction has a different energy source than a conventional hotplate or oven. The development of these other methods is important as different methods can lead to new compounds which cannot be obtained otherwise. Furthermore, different methods can lead to different particle sizes and morphologies that can have an influence on the material's properties. For example, different particle sizes in porous materials can influence the diffusion of guest molecules, which have a direct impact on catalytic reactions or the absorption and separation of molecules. Small crystals may also be employed for the formation of membranes using a seeded growth procedure. Nanocrystalline, non-toxic MOFs with high loading capacities are also envisioned for biomedical applications. For these objectives, MW and US techniques have been applied. High-Throughput Methods (HT) have also been developed to allow efficient investigations into the many parameters involved in CP synthesis.[85]

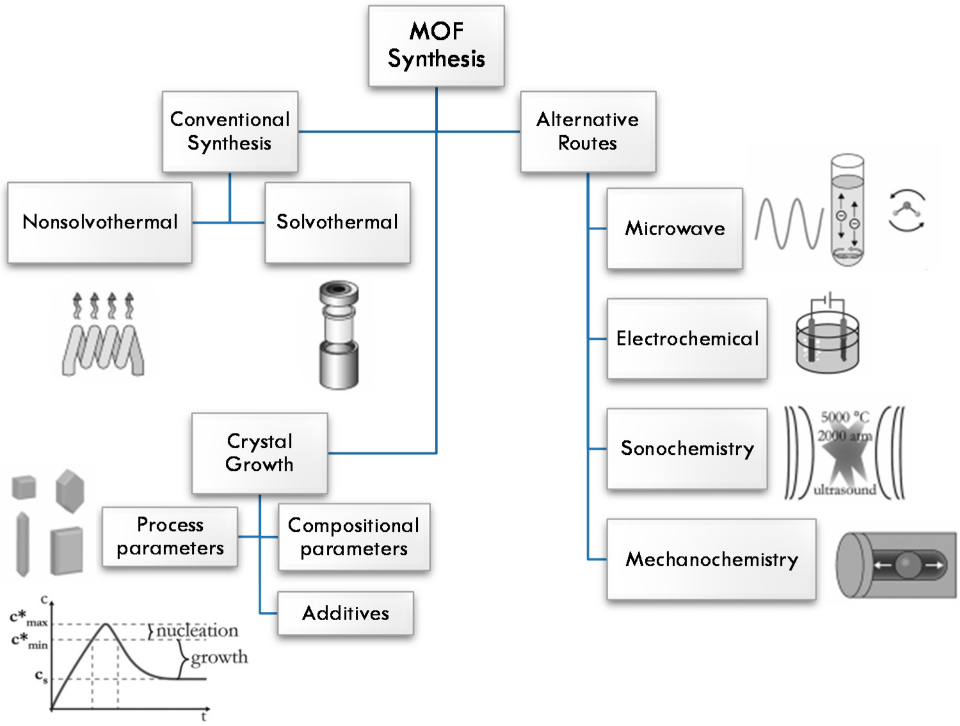

Figure 1.13: MOF synthesis is a multi-faceted task with consideration of synthesis methods and crystal growth necessary.

1.4.2.1 Microwave-Assisted Synthesis

Microwave-assisted heating has mainly been used in organic chemistry,[86] and only recently has been employed in inorganic chemistry and MOF synthesis.[87] This change in focus has been brought about by the desire to reduce reaction times, increase yields and synthesise large amounts of functional materials, which also enhances their industrial applicability. MW has beneficial attributes in that it allows one to monitor temperature and pressure during the reaction, thus allowing more precise control of reaction conditions. With the manipulation of the size and shape of the crystals becoming an emerging area of MOF research,[88] MW has the benefit of generally producing homogenous sometimes nanoscale materials which are key for their applications in magnetic resonance imaging[89] and drug delivery.[90] On the other hand, working with microwaves raises some concern with respect to safety and reproducibility. Although reactions are fast and usually proceed at low temperatures, the morphology and phase purity of the products can be adversely affected if the reaction conditions are not strictly controlled, thus affecting the mechanical strength, conductivity and chemical reactivity of the products. Different instruments are also unable to deliver the same conditions, ultimately hindering reproducibility.

1.4.2.2 Electrochemical Synthesis

Electrochemical synthesis of MOFs was first reported by BASF researchers in 2005.[91] The objective of this work was to negate the use of metal salts which are commonly used in MOF synthesis, as anions like nitrate, perchlorate and chloride are of concern to large-scale production processes. Instead of using metal salts, the metal ions are continuously introduced by aniodic dissolution to the reaction medium which contains the dissolved linker and a conducting salt. The isolation of the product is then achieved *via* a simple filtration. The pioneering work by BASF resulted in the attainment of four Cu- or Zn-containing compounds with high porosity, one of which was the well-studied HKUST-1 (Figure 1.14) which was tested for its use in gas purification (i.e. removal of tetrahydrothiophene from natural gas) and H_2 storage.[92] In a comparative study on the influence of the synthesis procedure on the properties of HKUST-1, the compound was synthesised by solvothermal, ambient pressure and electrochemical routes in pure EtOH and EtOH/H_2O mixtures.[93] In all cases HKUST-1 was formed, however thermogravimetric analysis (TGA), elemental analysis and sorption experiments showed an inferior quality of the electrochemically synthesised product. This was explained by the incorporation of linker molecules and/or the conducting salt in the pores during crystallisation.

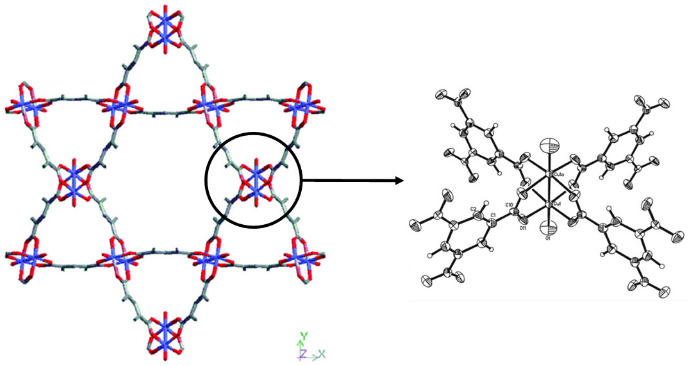

Figure 1.14: Structure of HKUST-1. Oxygen = red, copper = blue, carbon = grey.

1.4.2.3 Mechanochemical Synthesis

The interest in mechanochemical MOF synthesis is due to multiple reasons. One important reason is environmental issues. Reactions can be carried out at room temperature in solvent free conditions which is especially desirable when organic solvents are avoided. Quantitative yields can be obtained in short reaction times (in the range of 10-60 min) and products consisting of small particles are obtained. Another advantage of this technique is the use of metal oxides as starting materials which results in the formation of water as the only side product. The use of mechanochemistry for the synthesis of porous MOFs was first reported in 2006.[94] The mechanochemical synthesis of HKUST-1 was studied in detail.[93,95] Starting from a stoichiometric ratio of Cu^{2+} to benzene-1,3,5-tricarboxylic acid (H_3BTC) (3:2), solvent free grinding as well as liquid-assisted grinding (LAG) resulted in the desired product. Cu salts, grinding conditions (time and frequency), presence/absence of solvent, and nature of the solvent (DMF, MeOH, H_2O/EtOH) were studied. Copper acetate was shown to be the starting material of choice and LAG led to better crystalline products with better sorption properties. The pores of the products contained residual reactants, acetic acid and water molecules which was proven by TGA and TG-MS measurements as well as spectroscopic methods. The guest molecules could be removed by washing followed by thermal treatment, however thermal treatment alone led to small specific surface areas.

1.4.2.4 Sonochemical Synthesis

Sonochemistry involves the application of ultrasonic energy to the reaction mixture. Ultrasound is a cyclic mechanical vibration with a frequency of 20 kHz to 10 kHz. No direct interaction between ultrasound and molecules occurs but areas of high pressure and low pressure are formed when high-energy ultrasound interacts with liquids. In the low pressure regions the pressure drops below the vapour pressure of the liquid and small bubbles or cavities are formed. The bubbles formed grow under the alternating pressure through the diffusion of solute vapour into the volume of the bubble. Thus, ultrasonic energy is accumulated. Once the bubbles reach their maximum size, they become unstable and collapse. This process leads to the rapid release of energy with temperatures of ~5000 K. These 'hot spots' present unusual conditions. The extreme conditions and intense shear forces can lead to the formation of molecules in an excited state, bond breakage and the formation of radicals that will further react.[96] Ultrasonic techniques were first applied to MOF synthesis in 2008 with the goal of finding a fast, energy efficient, environmentally friendly, room temperature method that could easily be carried out. In addition, nanocrystalline particles which are often obtained by sonochemical syntheses were also anticipated to be of advantage for their applications. Three studies were reported on the synthesis of HKUST-1.[93,97,98] The first report investigated the influence of reaction time starting from copper acetate and H_3BTC in a mixed solution of DMF/EtOH/H_2O.[97] Using an ultrasonic bath and varying reaction time, the desired product was obtained after 5 min as a nanocrystalline powder. Increasing the reaction time led to larger crystals and higher yields. Using the same starting materials and the three solvents, the amount of DMF was increased stepwise and the reaction time was varied. In contrast to conventional and MW-assisted heating, DMF was necessary for the formation of HKUST-1. After 1 min, a phase pure and highly crystalline product was obtained. The concentration of DMF was found to have a strong influence on the physical properties of the product.[98] In contrast to these studies, the third report concerns the successful synthesis of HKUST-1 in a mixture of EtOH and H_2O, while a product of poor quality was formed in pure DMF with specific surface areas smaller than optimised products.[93]

1.4.3 Post-Synthetic Modifications

There has been substantial interest in tuning the physical and chemical properties of MOFs by functionalising their pores in order to tailor and modify their host-guest interactions. This relies on the development of MOFs that possess complex chemical functionality that can impart sophisticated chemical and physical properties to these materials. Historically, incorporating functionality into a MOF was achieved by modifying an organic ligand with specific substituents and then using the modified ligand directly in the solvothermal synthesis of the desired MOF. This 'prefunctionalisation' approach has resulted in MOFs with pendant groups such as –Br, –NH_2, –CH_3, and other relatively simple substituents lining the pore channels. However, the preparation of highly functionalised

MOFs has been largely limited by the solvothermal synthetic methods used to prepare most MOFs. Under solvothermal conditions, ligands generally cannot contain functional groups that are thermally labile, result in problematic solubility or can coordinate to metal ions. Unfortunately, many functional groups of interest fall into one or more of these categories. Therefore, the scope of functional groups within the pores of the MOFs has remained relatively limited by this approach.

Another route for obtaining functionalised MOFs is by post-synthetic modification (PSM).[99] PSM, which was originally suggested by Hoskins and Robson[75] in 1990 and formally introduced by Wang and Cohen,[100] is defined as the chemical modification of a framework after it has been synthesised. Rather than synthesising a functionalised MOF directly from a functionalised ligand, a MOF can be synthesised and modified in a heterogeneous manner after the formation of the solid lattice. PSM can be advantageous compared to the prefunctionalisation approach for a number of reasons. Firstly, one has greater control over the types and number of functional groups that can be incorporated into the framework. Secondly, this approach circumvents any incompatibility with the synthetic methods required to obtain the material. Also, the fact that MOFs contain an organic component offers opportunities to employ a vast range of organic transformations. Finally, because MOFs are highly porous, the ability of reagents to access the interior of the solid suggests that functionalisation can be achieved on both the interior and exterior of the material, which is in contrast to many inorganic solids like nanoparticles where only the surface of the materials is available for modification. Apart from removing or absorbing guest molecules, which by themselves are a post-synthetic modification of a MOF material, PSM of MOFs can be broadly divided into three areas (Figure 1.15): covalent PSM, dative PSM and post-synthetic deprotection (PSD). Covalent PSM is defined as the use of a reagent to modify a component (usually the organic linker) of the MOF in a heterogenous manner to form a new covalent bond. This is one of the earliest reported and most examined methods. Dative PSM is defined as the use of a reagent that forms a dative (coordinative) bond with a component of the MOF in a heterogenous and post-synthetic manner. Examples include adding a ligand to the framework that coordinates to the metal in the MOF or adding a metal source which can become bound to the organic linker by dative bonds. PSD is a reaction performed on the MOF in a post-synthetic manner that results in the cleavage of a chemical bond within an intact framework. As post-synthetic modifications are not the focus of this thesis, a brief overview of successful examples of PSM will be presented.

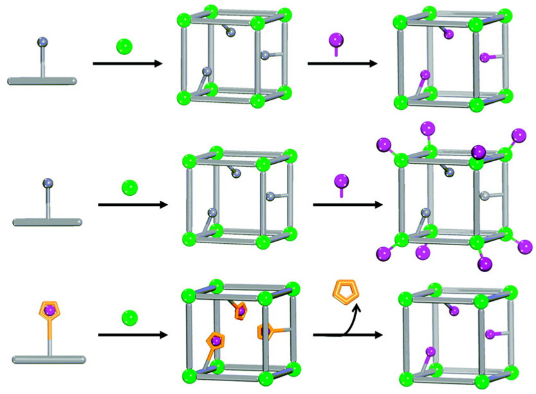

Figure 1.15: Generic schemes for covalent PSM, dative PSM and PSD.

1.4.3.1 Covalent PSM

The earliest example of covalent PSM was encountered in 1999,[101] when 1,3,5-tris(4-ethynylbenzonitrile)benzene derivatives, with a variety of substituents in the 2-position of the central benzene ring, were assembled with silver triflate. Among the substituted ligands employed for the study, one contained a pendant alcohol group on the 2-position (Scheme 1.18). Upon assembly of a MOF from the alcohol-derivitised ligand the MOF was exposed to vapors of trifluoroacetic anhydride, followed by quenching with benzyl alcohol to consume the excess anhydride. Conversion of the alcohol to the ester was confirmed by FTIR and ^{1}H NMR spectroscopy by dissolving the material in d_6-acetone. This first example of covalent PSM highlights the important principles and methods that are now central features in the area of PSM. These features include the use of a ligand possessing a free functional group (a 'tag'), chemical modification in a heterogenous manner, preservation of crystallinity and dissolution of the solid after modification to permit use of solution NMR spectroscopy to characterise the reaction products.

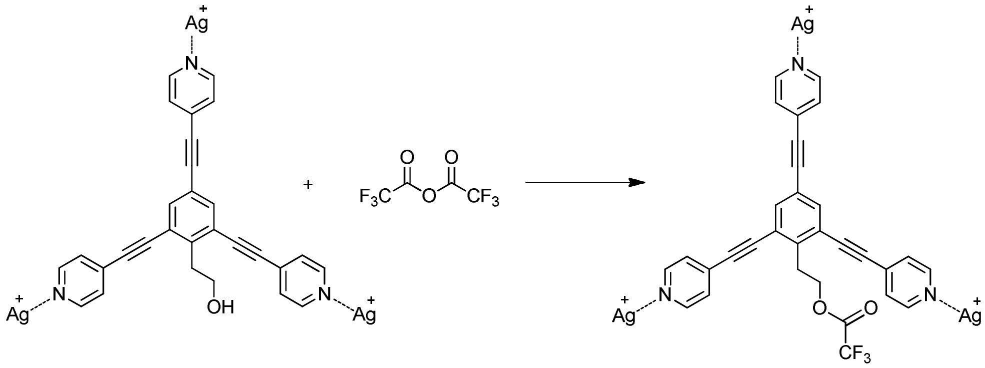

Scheme 1.18: The pendant alcohol group on the symmetrical 1,3,5-tris(4-ethynylbenzonitrile)benzene ligand was not involved in MOF synthesis with silver triflate, allowing it to serve as a chemical handle for covalent PSM with trifluoroacetic anhydride.[101]

Despite these results and the array of possibilities that they promised, the covalent PSM approach only gained worthy attention in earnest in 2007 when Wang and Cohen, who coined the term ''post-synthetic modification'', described the reaction of IRMOF-3 with acetic anhydride.[100] The aromatic amines in IRMOF-3 do not engage in binding to the SBUs and thereby provide the chemical handle for performing PSM. Under mild conditions at room temperature, IRMOF-3 was acetylated in >90% yield with acetic anhydride to produce IRMOF-3-AM1 (Scheme 1.19). The degree of conversion was confirmed by ^{1}H NMR spectroscopy upon digestion of the material in d_6-DMSO and DCl. The material also remained porous, however the surface areas were greatly reduced. Several other reports of covalent PSM of amine-, azide- and aldehyde-tagged MOFs are also now prevalent in the literature.[102]

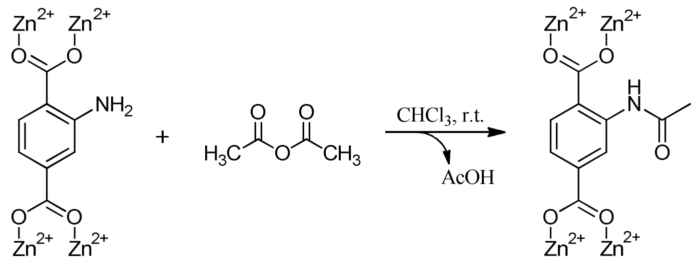

Scheme 1.19: PSM of IRMOF-3 with acetic anhydride.[100]

1.4.3.2 Dative PSM

Dative PSM was reported as far back as 1999,[80] with the original description of HKUST-1. In this early report, the authors noted that the coordinated axial water molecules on the SBUs could be removed by heating HKUST-1 in air to 100 °C. The resulting material could then be immersed in dry pyridine to obtain a material with pyridine molecules bound to the SBU (Scheme 1.20). Importantly, the HKUST-1 derivative could not be directly synthesised by solvothermal methods, demonstrating the importance of dative PSM. Similarly in 2008, Hupp and colleagues demonstrated that axially bound DMF molecules in a Zn(II) paddlewheel SBU could be removed under vacuum with heat (Scheme 1.20).[103] The desolvated MOF could then be treated with pyridine derivatives in DCM that bound to the axial sites left vacant on the SBUs by removal of DMF. Several of the pyridine ligands introduced would decompose under solvothermal conditions demonstrating that dative PSM could be used to introduce thermally labile species into a MOF. Secondly it was shown that H_2 uptake was dependent on the pyridine species coordinated to the SBUs indicating that the MOF properties could be altered by dative PSM.

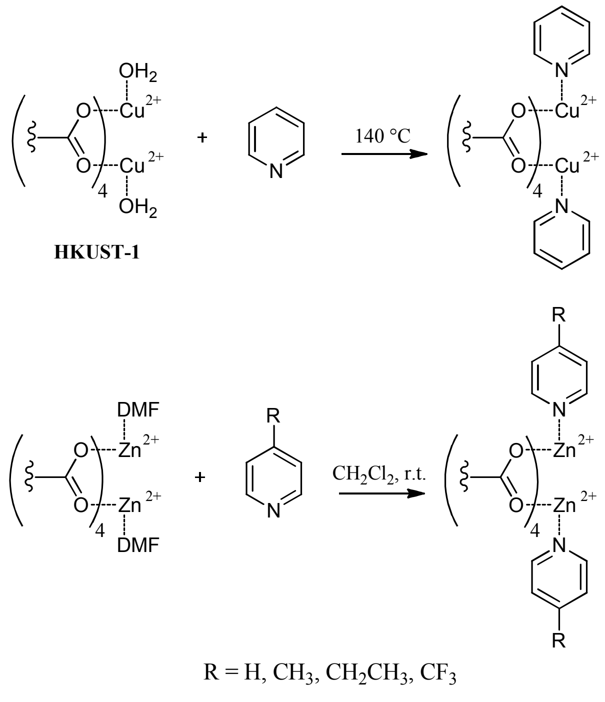

Scheme 1.20: Dative PSM on the SBUs of several MOFs with pyridine derivatives.[80,103]

Another dative PSM approach involves using an organic ligand that contains two or more types of metal binding sites. Under judicious choice of reaction conditions, one of the metal binding groups becomes involved in the framework synthesis and coordinates to the metal centre (forming a SBU). The other metal binding site is not involved structurally and thus is available for post metal insertion.[102,104,105] A recent notable example of this type of dative PSM was reported by Yaghi and Long.[106] The ligand used in this study was 2,2'-bipyridine-5,5'-dicarboxylic acid which possesses the metal-binding 2,2'-bipyridine core that is ubiquitous in MOF chemistry. The challenge with this ligand is that the bipy core binds metal ions so avidly that it is likely to bind metal ions during solvothermal synthesis. Based on the Hard-Soft-Acid-Base (HSAB) theory of coordination chemistry, Yaghi and Long exploited the generally soft nitrogen donors in the ligand due to its π-accepting character and the hard nature of the carboxylate oxygens by selecting a hard oxophilic metal ion to construct the framework. Employing an Al(III) salt resulted in exclusive coordination to the hard carboxylate oxygen donors during solvothermal synthesis, forming the open framework MOF-253 (Scheme 1.21). The free bipy nitrogen sites in MOF-253 were proven accessible by utilising dative PSM on the unit with softer metal ions including Cu(II) and Pd(II). Soaking MOF-253 in CH_3CN solutions of $Cu(BF_4)_2$ or $PdCl_2$ could produce materials where >80% of the bipy ligands were metalated, as determined by elemental analysis.

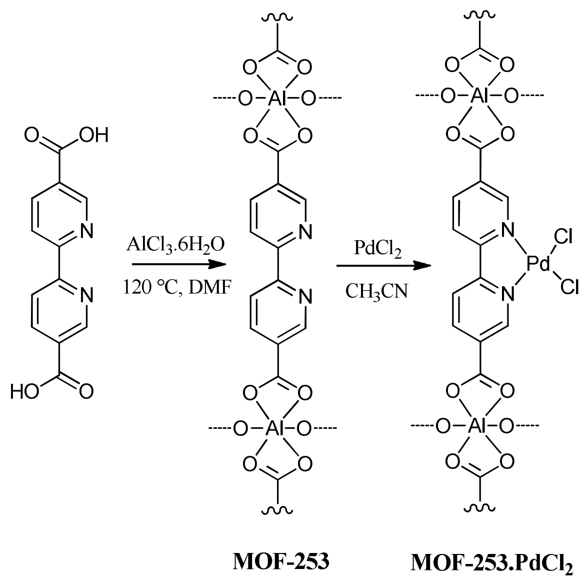

Scheme 1.21: Post-synthetic metalation of MOF-253.[106]

1.4.3.3 Post-Synthetic Deprotection

PSD is a PSM method quickly gaining attention. PSD is based on the concept that a protected or "masked" functional group is introduced onto an organic linker and the linker is then incorporated into a MOF under standard solvothermal conditions. The protecting group is then subsequently removed in a post-synthetic fashion to reveal the desired functionality. Telfer and colleagues clearly demonstrated the utility of PSD in 2010 by validating the ability to prevent framework interpenetration.[107] Framework interpenetration can be problematic for applications like gas absorption, as interpenetrating linkers can occupy the available space. The amine tag on the ligand 2-aminobiphenyl-4,4'-dicarboxylate was protected with a bulky *tert*-butyloxycarbonyl (Boc) protecting group. Combination of this ligand with Zn(II) under solvothermal conditions gave an IRMOF-10 analogue showing a clear absence of framework interpenetration. The bulky *tert*-butyl protecting groups prevented interpenetration, which is generally a difficult feature to control in MOFs produced from extended ligands. Thermolysis of the IRMOF at 150 °C in DMF resulted in removal of the Boc group to generate IRMOF-12-NH_2 with free amine tags within the pores (Scheme 1.22). Attempts to produce this product by directly employing 2-amino-biphenyl-4,4'-dicarboxylate have not been successful.

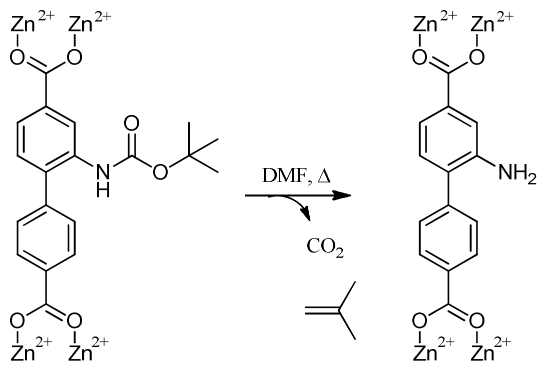

IRMOF-12-NBoc **IRMOF-12-NH_2**

Scheme 1.22: Thermally induced PSD on a protected IRMOF.[107]

The PSM approach to the modification and functionalisation of MOFs has become a vibrant area of research in the last few years. The resulting materials have been shown to engender MOFs with new properties relevant to gas sorption, catalysis and biomedical applications. This will no doubt lead to new exciting contributions to an already rapidly evolving area, which is reflected by the number of reviews published in the last five years.[65,66,96,99,102,108]

1.5 Aims of Thesis

The overall aims of this project are two pronged. Firstly this thesis aims to describe the synthesis and characterisation of pyridyl tetrazole based ligands and their respective metal complexes. This work was carried out with the long term goal of carrying the resulting compounds through to anti-cancer biological testing. The metal ions used included Cu^{2+}, Zn^{2+}, Ni^{2+} and Co^{2+}.

This thesis also aims to describe the development and characterisation of coordination polymers based on heteroaryl carboxylate functionalised tetrazole linkers. The goal in employing these ligands in coordination polymer synthesis was to form open networks or frameworks with potential voids which would endow the materials with interesting properties for potential applications in gas storage, gas separation, chemical sensing or drug delivery. The metal ions employed in this work were Cu^{2+}, Zn^{2+}, Ni^{2+}, Co^{2+} and Mn^{2+}.

We hoped that this work would highlight the versatility and usefulness of heteroaryl tetrazole ligands in the fields of medicinal chemistry and materials chemistry, and that it will add value to both these fields of chemistry.

Chapter 2: Synthesis and Characterisation of Pyridyl Tetrazole Ligands and Their Metal Complexes

2.1 Introduction

2.1.1 Inorganic Complexes in Medicinal Chemistry

The importance of metal-based compounds in medicinal chemistry dates back to the 16th century, with the first reports of their therapeutic effects in the treatment of cancer.[109] Metal-containing drugs are now not just limited to anti-cancer treatments. Silver compounds for example exhibit anti-microbial activity, gold compounds demonstrate anti-arthritic activity, bismuth compounds displays anti-ulcer properties and vanadium exhibits anti-diabetic activity.[110] As discussed in Chapter 1, the synthetic production of tetrazoles has improved over the last decade.[24,30] As a consequence, more attention has been focused on tetrazole compounds and they have become an interesting candidate in the design of new biologically active drugs and also metal-based drugs. This is due to the metal ion binding capabilities of such compounds. Thus, the study of the structures of tetrazole derivatives is relevant to several aspects of medicinal chemistry as is their coordination chemistry given the increasing importance of metal-based drugs which incorporate known therapeutic organic agents.[111]

2.1.2 Metal Complexes of Tetrazoles in Biology

The number of publications and patents describing the synthesis and investigations of the structure and physiochemical properties of metal derivatives with tetrazoles included in their structure has grown intensively. This is due to the wide ranging applications of these compounds which include, but are not limited to, pyrotechniques, organic synthesis and gas generating compositions.[2,112] One of the most important fields where tetrazole-containing coordination compounds are used is in medicinal chemistry. The high physiological activity and low toxicity of tetrazoles means that their metal complexes are substances of versatile biochemical and pharmaceutical relevance.[7] It has been shown that in some cases, the use of metal complexes of biologically active compounds leads to an increase in biological activity. Complexes $Ag_2L_2Cl_2$, ML_2Cl_2 and MLCl (M = Cu(II), Co(II), Ni(II) or Zn(II)) containing the antibiotic Cefazolin as the ligand (Figure 2.1), exhibits higher anti-bacterial activity *in vitro* compared to the free ligand.[113] A similar situation was observed for Zn(II), Cu(II) and Cd(II) complexes with the antibiotic Cefamandole (Figure 2.1).[114] Silver tetrazolate and chelate complexes which were synthesised by the reaction of divalent metal salts with tetrazole-containing Schiff bases also have anti-bacterial activity.[115]

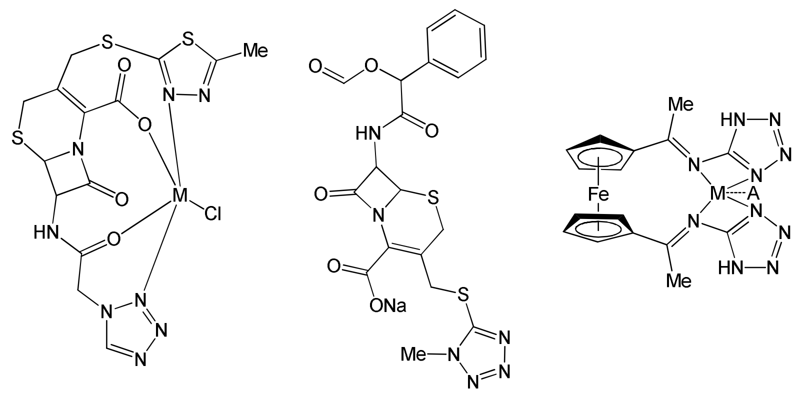

Figure 2.1: Structures of complexes (from left to right) of Cefazolin and Cefamandole, and a chelate complex of a Schiff base. All exhibited better biological activity compared to the free ligands.[113,114,115]

The search for tumour growth inhibitors among tetrazoles has led to the targeted synthesis and investigations of tetrazole containing metal complexes for their biological activity. The ruthenium(II) complex $[Ru(\eta^5\text{-}C_5H_5)(PPh_3)_2(5\text{-Ph-1}H\text{-tetrazole})][PF_6]$ (Figure 2.2) displayed high anti-tumour activity in promyelocytic leukemia cell lines with a lower value of IC_{50} (72 h, 0.69±0.16 μmol L^{-1}; 24 h, 0.95±0.15 μmol L^{-1}) compared to cisplatin.[112] Complexes of Pt(II) with tetrazolo[1,5-*a*]quinolines (Figure 2.2), which are analogs of cisplatin, also exhibit cytotoxic activity against the promyelocytic leukemia cell line HL-60.[112]

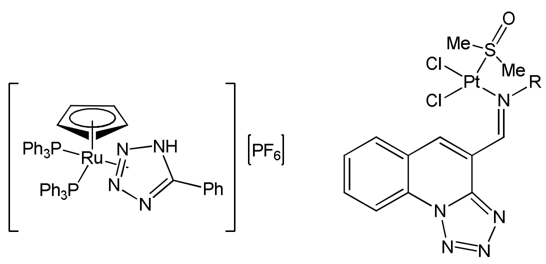

Figure 2.2: Structures of simple tetrazole ligands and metal complexes of tetrazoles which exhibited cytotoxic activities.[112]

Most of the presently used contrast agents are coordination compounds of gadolinium(III) with organic tetrazole ligands.[1] This fact is associated with the high ability of these complexes to decrease proton relaxation time of adjacent water molecules due to dipolar interactions. In recent years, there is an active search for complexes of other paramagnetic metals with the aim of using them instead of higly toxic and expensive gadolinium. It has been shown that an Fe(II) complex with a macrocycle tetrazolyl-containing ligand is a promising contrast agent (Figure 2.3).[116] Tetrazolyl-containing lanthanide complexes (Ln = Eu, Tb, Nb) were also described as potential contrast agents. Polydentate ligands are involved in the formation of such complex compounds (Figure 2.3).[117]

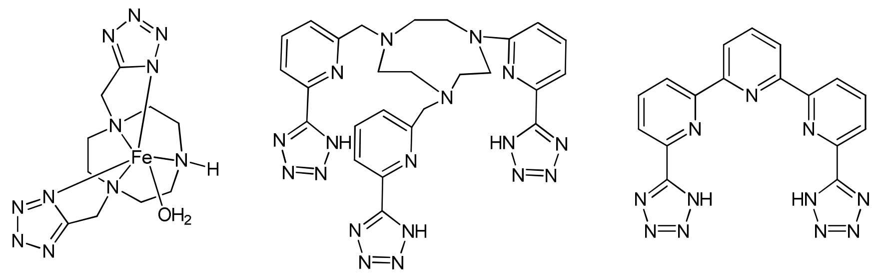

Figure 2.3: A variety of polydentate tetrazole ligands when complexed to metal ions has resulted in the formation of promising contrast agents.[116,117]

Hence, it can be stated that tetrazole derivatives and their metal complexes have an adequate position in the area of medicinal chemistry. These compounds exhibit diverse biological activities and are attractive entities for investigational drug design.

2.1.3 Anti-cancer Activity of Metal Complexed Pyridyl Tetrazoles

McGinley and co-workers have made substantial progress in the area of tetrazole synthesis and metal coordination to tetrazoles.[118] The group's initial studies involving tetrazoles targeted the use of macrocycles which could be used as molecular sensors for metal ions. In nearly all cases, it was found that the cavity size between the tetrazole rings was very small or almost non-existent, with one noteable exception (Figure 2.4).[119] Unfortunately, the metal binding ability of all these macrocycles was not as effective as expected. It was observed that weak binding occurred in solution, but all attempts to isolate and characterise any metal complexes as solids failed as the complexes disintegrated once out of solution.

This work led to the synthesis of macromolecules, instead of macrocycles, which would be capable of binding metal ions.[120] The McGinley group used a substitution reaction to tether two pyridyl tetrazole units to bis-tetrazoles. These tetrazoles were bridged *via* a range of bridging units such as alkyl chains, benzyl and heterocyclic rings. To the pyridyl tetrazole unit, a pendant bromohexyl arm was added for easy attachment to the bis-tetrazole unit (Scheme 2.1). The preparation of the pyridyl tetrazole moiety with the pendant bromohexyl arm was carried out in two steps. Both the N-1 and N-2 isomers (Figure 2.5) were obtained in good yields following chromatographic separation. Transition metal complexes of both compounds were obtained after reactions with several different metal salts. In several cases the complexes were structurally characterised by X-ray crystallography.[121]

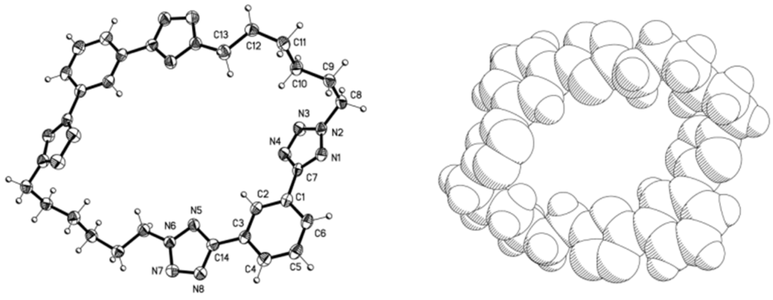

Figure 2.4: X-ray crystal structure and space fill model of a macrocycle with a cavity.[119]

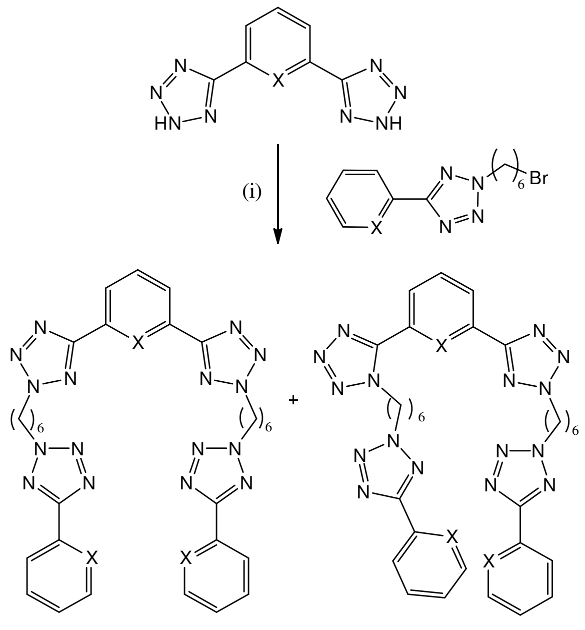

Scheme 2.1: Reagents and conditions: (i) Et_3N, MeCN, Δ, 24 h. X = CH, N.[120]

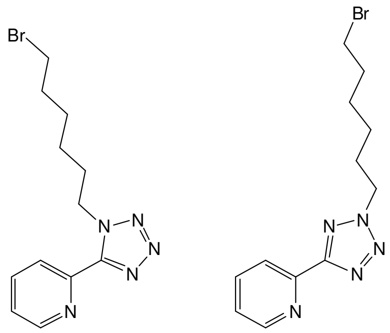

Figure 2.5: Two regioisomers which were synthesised previously in the McGinley group.

The free ligands and their metal complexes were screened against breast, lung, liver and prostate cancer cell lines. Several drug resistant cancer cells lines were also screened. The two copper(II) chloride complexes, one having the pendant arm attached at N-1 of the ligand (**2.3**) and the other having the arm attached at N-2 (**2.4**, Figure 2.6), gave a complete kill across the concentration range of the study (unpublished results), which is rare with toxicity testing. Both of the Cu(II) complexes were very toxic to prostate and breast cancers. Furthermore, the free ligand and free metal salt did not display any significant activity, emphasising the importance of the complex as an entire entity having a key role in its mechanism of action. In addition, the complex showed low IC_{50} values compared to the free metal salt and ligand, with IC_{50} values very close to that of cisplatin under the same conditions. Based on these encouraging results, it was proposed to synthesise a library of metal complexes based on the pyridyl tetrazole template. By varying the pendant arm and metal centre, an improvement in the complex's biological activity could be achieved as well as an insight into the complex's mode of action.

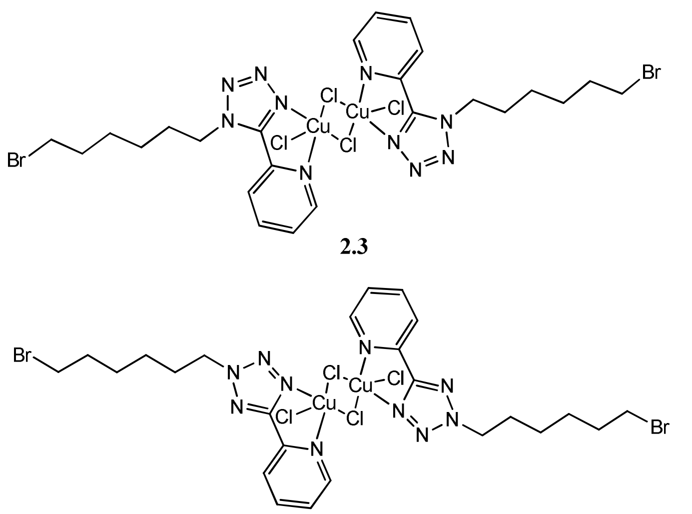

Figure 2.6: Two $CuCl_2$ complexes which showed particularly good anti-cancer activity.

2.2 Aims and Objectives of Chapter

The aim of this body of work was to synthesise a library of ligands with the same metal-binding core as a pyridyl substituted tetrazole and then to alter the pendant arm bonded to the tetrazole ring. Metal complexes would be synthesised from these ligands and different metal salts would also be utilised. The variation in the pendant arm and the metal atom bound would allow an investigation into what functional groups and metals contribute towards the biological activity of the compound. It was intended that a number of variations would be made to these compounds: firstly, the chain length between the tetrazole moiety and the functional group, followed by changing the functional group to methyl groups, alcohols, esters or carboxylic acids and finally to change the metal centre. These derivatives could readily be obtained utilising methods previously established by McGinley and co-workers. Each of these variations would alter the lipophilicity and solubility of the complexes and thus, could affect the biological activity of the complex. The synthesised library could be used in a structure-activity relationship (SAR) study in order to identify the key functionalities which are important for biological activities. Therefore any future variations to the structure of the complexes could be determined.

2.3 Results and Discussion

2.3.1 Synthesis of Ligands

Synthesis of all pyridyl tetrazole ligands in this chapter was carried out utilising methods previously described by McGinley *et al.*[122] The tetrazole moiety is typically obtained *via* a 1,3-dipolar cycloaddition reaction between an azide and a nitrile, where the azide is employed as the 1,3-dipole, whilst the nitrile is employed as the dipolarophile. This [2+3] cycloaddition occurs by a concerted mechanism (Scheme 2.2).[21,123]

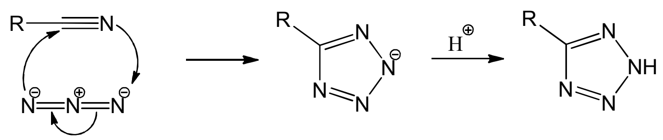

Scheme 2.2: Concerted mechanism of the 1,3-dipolar cycloaddition of a nitrile and azide.[123]

An alternative method of tetrazole synthesis employs ammonium azides as the 1,3-dipole, and a discussion of this method is covered in section 1.1.2.1.[21] Synthesis of 2-(2*H*-tetrazol-5-yl)pyridine (**2.5**) was achieved under these alternative conditions, by reacting sodium azide and 2-cyanopyridine in the presence of ammonium chloride and lithium chloride in anhydrous DMF (Scheme 2.3). Although the use of 10 equivalents of lithium chloride is reported here, it is noteworthy that reactions attempted with significantly lower equivalents also produced compound **2.5** in good yields. Synthesis of **2.5** was confirmed by ^{1}H, ^{13}C NMR and IR spectroscopies. IR spectroscopy suggested the consumption of the nitrile with the disappearance of the associated ν(C≡N) stretch at 2236 cm^{-1}. The disappearance of a ^{13}C peak at 117.2 ppm in the ^{13}C NMR spectrum also supported this. The ^{13}C NMR spectrum also confirmed the formation of a 1,5-tetrazole ring with a signal at 154.9 ppm arising from the C-5 carbon of the tetrazole ring.

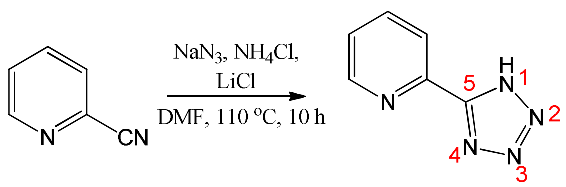

2.5

Scheme 2.3: Synthesis of **2.5** was achieved *via* formation of ammonium azide *in situ*.

Subsequently, **2.5** was reacted with several bromoalkyl compounds in the presence of K_2CO_3 to yield alkylated tetrazoles, with alkylation occurring at either the N-1 or N-2 positions of the ring (Scheme 2.4). The production of two regioisomers arises from the occurrence of tautomerism in tetrazole rings (section 1.1.3). As a result of this phenomenon, when the tetrazole ring is deprotonated, nucleophilic attack can occur from either position, yielding two different products; the N-1 substituted product and the N-2 substituted product.

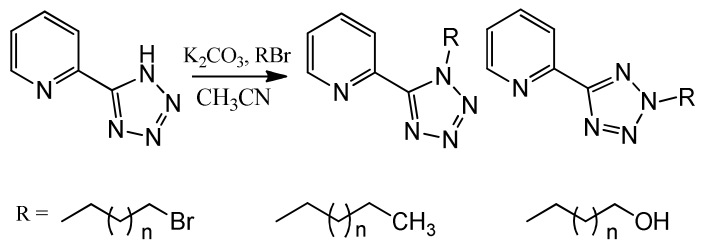

N-1	N-2		N-1	N-2		N-1	N-2	
2.6	**2.7**:	n = 1	**2.12**	**2.13**:	n = 1	**2.18**	**2.19**:	n = 1
2.8	**2.9**:	n = 2	**2.14**	**2.15**:	n = 3	**2.20**	**2.21**:	n = 2
2.1	**2.2**:	n = 4	**2.16**	**2.17**:	n = 5	**2.22**	**2.23**:	n = 4
2.10	**2.11**:	n = 6				**2.24**	**2.25**:	n = 6

Scheme 2.4: Synthesis of alkylated tetrazoles gave rise to two regioisomers.

Thin Layer Chromatography (TLC) was carried out on the crude mixture of isomers, and two well separated spots were observed. Therefore, column chromatography was employed to separate the two regioisomers. In the late 1970's, Butler and McEvoy demonstrated that it is possible to distinguish the N-1 from the N-2 isomer by analysis of their ^{13}C NMR and ^{1}H NMR spectra.[124,125] Employing a variation of organic 5-aryltetrazoles, they reported that the ^{13}C chemical shift values of the tetrazole carbon (C-5) can determine the annular tautomerism. For 5-aryltetrazoles, it was observed that the C-5 chemical shift of the N-1 isomer was positioned significantly more upfield (δC-5 = 152-157 ppm) when compared to that of the N-2 isomer (δC-5 = 162-167 ppm).[125] The two isomers produced by alkylation of **2.5** were readily identifiable by their ^{13}C NMR spectra, with the observation of the tetrazole C-5 resonance signals occurring from 150.1-151.8 ppm for the N-1 isomers, and 164.5-164.9 ppm for the N-2 isomers. These values fit well within the ranges stated by Butler *et al.*[124,125]

In general, the methyl or alkyl protons of substituents on N-1 substituted tetrazoles are more shielded by ~0.15-0.35 ppm in the ^{1}H NMR spectrum relative to the corresponding N-2 isomer.[126] This trend is due to the relative electron density of the –N= moiety over the –C= moiety relative to the alkyl substituents (Figure 2.7).

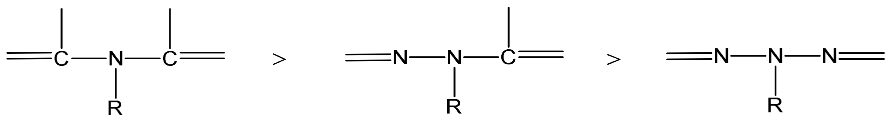

Figure 2.7: Order of chemical shifts of alkyl groups (R) in simple azoles.

However, this relationship may break down depending on the substituents present on the carbon of the tetrazole, for example those that possess anisotropic effects.[127] Throughout the course of this work, the protons of the alkyl group bonded to the tetrazole resonated more downfield in the N-1 isomers when compared to the N-2 isomers. This pattern is in contrast with the trend seen for 5-aryltetrazoles. However, it is consistent with 5-substituted tetrazoles with anisotropic groups in the 5-position. This phenomenon has been reported previously for pyridyl tetrazoles[128] and reinstates the findings by Butler *et al*. that the use of ^{13}C NMR shifts are more reliable than ^{1}H NMR shifts when assigning the position of alkylation on tetrazole rings.[124,125,127]

2.3.1.1 Bromoalkyl Chain Derivatives

The products synthesised from the reaction of **2.5** with 1,3-dibromopropane, 1,4-dibromobutane, 1,6-dibromohexane and 1,8-dibromooctane in the presence of base yielded waxy orange/brown solids with low melting points. Successful synthesis of the alkylbromo substituted tetrazoles was confirmed by employing ^{1}H NMR spectroscopy on the crude residues. The presence of two regioisomers was immediately evident on observation of the ^{1}H NMR spectra, as twice as many of the expected peaks could be distinguished (Figure 2.8). After purification by column chromatography, each regioisomer exhibited the following signals. Four signals attributed to the pyridyl protons were observed at ~7.40-8.79 ppm and a triplet arising from the methylene group bonded to the tetrazole ring was observed at ~4.70-5.15 ppm. A triplet at ~3.39-3.46 ppm was attributed to the methylene group bonded to the terminal bromine atom, with the remaining signals observed from ~1.36-2.08 ppm arising from the remaining protons on the alkyl chain. In all reactions, the N-2 substituted tetrazole was the predominant regioisomer. This could be observed from analysis of the ^{1}H NMR spectra of the crude mixtures as the CH_2-tet protons of the N-1 regioisomers resonated significantly more downfield when compared to the respective signals of the N-2 regioisomer. Therefore a comparison of their relative integrations was possible (Figure 2.8). The slight difference in the observed regioselectivity can be accredited to the features of their structures.

Pokhodylo and co-workers carried out quantum-chemical optimisation of geometries of chloroacetamide alkylated 5-substituted aryl tetrazoles.[129] Experimental data indicated that a co-planar arrangement of the benzene and tetrazole rings was not probable in the 1,5-regioisomers due to the steric hindrance inflicted by the substituent at the N-1 position, causing the benzene ring to deviate from the plane of the molecule (Figure 2.9).

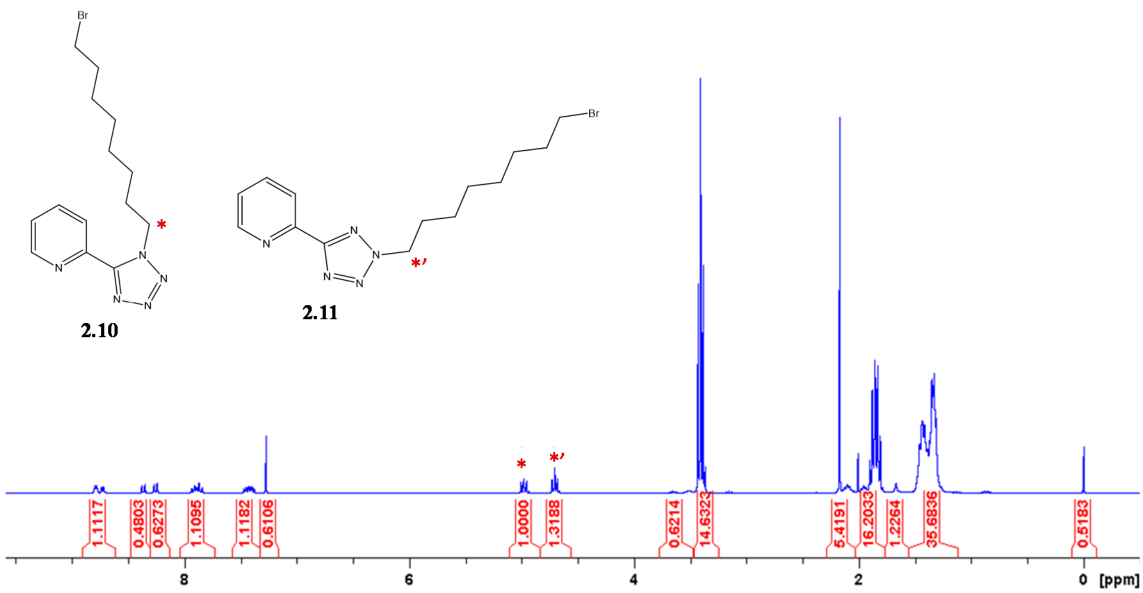

Figure 2.8: Crude ^{1}H NMR spectrum in $CDCl_3$ of **2.10** and **2.11** mixture. Methylene protons beside the tetrazole ring (denoted with *) resonated at significantly different chemical shifts, allowing a comparison of regioselectivity to be carried out.

The 2,5-regioisomers experience no steric hindrance due to the substituent, and therefore the benzene and tetrazole rings can exist in the same plane. This slight steric hindrance is thought to explain the regioselectivity towards N-2 substitution in the alkylation of **2.5**.[129] A ratio of 10:13 was obtained from the bromooctyl (**2.10**, **2.11**), bromohexyl (**2.1**, **2.2**) and bromobutyl (**2.8**, **2.9**) crude mixtures. However, in the case of the bromopropyl derivatives (**2.6**, **2.7**), the regioselectivity for the formation of the N-2 isomer was more prominently evident, with a ratio of 10:33 observed. An increase in steric hindrance is likely to be brought about by the closer proximity of the large bromine atom to the ring systems when compared to the longer chain derivatives.

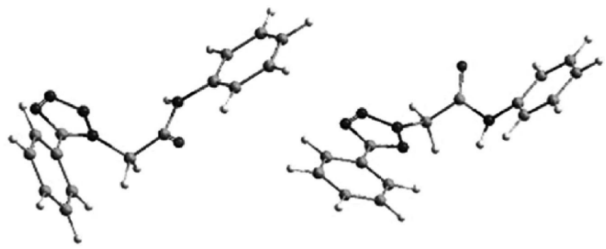

Figure 2.9: The steric structure of the regioisomers obtained through a semi-emperical PM3 method.[129]

In order to see if the cation of the base had any effect on the regioselectivity of the reaction, an experiment employing **2.5**, 1,6-dibromohexane and Cs_2CO_3 as the base was carried out. ^{1}H NMR spectra of the crude mixtures revealed that even though Cs^+ was a bigger cation, the use of Cs_2CO_3 had no effect on the regioselectivity in the alkylation reaction using 1,6-dibromohexane. In fact, a ratio of 10:12 was observed for the N-1 and N-2 isomers; a relative decrease in the yield of the N-2 isomer.

2.3.1.2 Alkyl Chain Derivatives

Synthesis of alkyl chain substituted pyridyl tetrazoles yielded products **2.12-2.17** as oils. All derivatives were characterised by ^{1}H NMR, ^{13}C NMR and IR spectroscopies and HRMS. In the ^{1}H NMR spectra of the products, four signals were observed at ~8.79-7.39 ppm which were attributed to the pyridyl protons. A triplet that integrated for two protons appeared at ~4.70-5.03 ppm which was assigned to the CH_2-tet protons, which were the only alkyl chain protons expected to resonate at this downfield position. The remaining signals at ~0.87-2.00 ppm were assigned to the remaining alkyl chain protons. It was again evident from the ^{1}H NMR spectra that the N-2 substituted products were the marginally major products, with ratios of 10:13 observed in all cases. When the lack of significant regioselectivity observed in the formation of products **2.12-2.17** is compared to the regioselectivity seen in the formation of the bromopropyl derivatives **2.6** and **2.7**, it is evident that the presence of the bromine atom in these derivatives influenced the regioselectivity of the alkylation reaction to some extent.

2.3.1.3 Alcohol Chain Derivatives

Access to compounds **2.18-2.25** was achieved by reacting **2.5** with either 3-bromo-1-propanol, 4-bromo-1-butanol, 6-bromo-1-hexanol or 8-bromo-1-octanol in the presence of base. After work-up and separation of the regioisomers by column chromatography, products were afforded as either low melting white-yellow solids or oils. The typical ^{1}H NMR spectra for these compounds possessed four aromatic pyridyl proton signals resonating at ~7.40-8.78 ppm, a triplet at ~4.72-5.03 ppm representing the CH_2-tet protons, a triplet arising from the methylene protons adjacent to the alcohol group at ~3.62-3.88 ppm and remaining signals were attributed to the alkyl chain. The chemical shift of the alcohol proton varied depending on its proximity to the tetrazole ring, with the shorter chain derivatives resulting in a downfield shift. The hydroxy proton peak also differed in splitting pattern, sometimes appearing as a triplet and other times as a broad singlet. The signal arising from this proton was easily identifiable when not overlapping with other signals, as it was the only signal integrating for one proton. Figure 2.10 presents a ^{1}H NMR spectrum of **2.18** with all relevant signals labelled. Assignment of protons was determined by carrying out COSY spectroscopy. The presence of the alcohol group was also evident in the IR spectrum of the compounds, with a broad OH stretch observed at ~3310-3400 cm^{-1} and a strong absorption at ~1055 cm^{-1} which is a characteristic absorption of a C-O bond in an alcohol. There was no significant variation in the regioselectivity of these alkylation reactions with N-1 and N-2 isomers being produced in a ratio of 10:13.

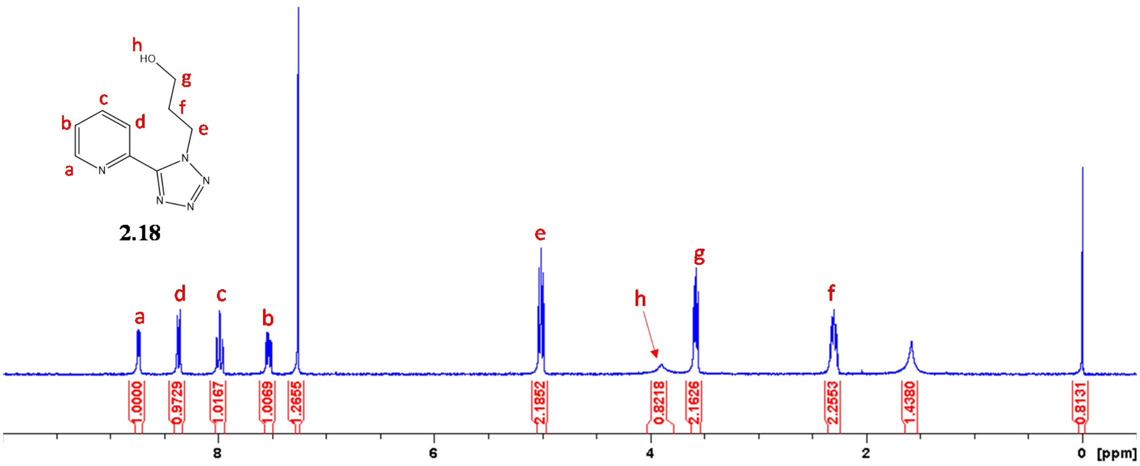

Figure 2.10: ^{1}H NMR spectrum carried out in $CDCl_3$ of **2.18** with relevant proton peaks labelled. Peak at 1.56 ppm arises from residual H_2O in deuterated solvent.

2.3.2 Synthesis of Metal Complexes

Metal complexes were synthesised by reacting a 1:1 stoichiometric ratio of metal salt to ligand in MeOH at reflux temperature for 2 hours. The solutions were then allowed to stand for several days and the solids that formed were isolated and washed with MeOH. Metal salts used included $CuCl_2.2H_2O$, $ZnCl_2$, $NiCl_2.6H_2O$ and $Co(SCN)_2$.

2.3.2.1 Metal Complexes of Bromoalkyl Derivatives

2.3.2.1.1 Copper(II) chloride dihydrate reactions

On addition of $CuCl_2.2H_2O$ to methanolic solutions of bromoalkyl derivatives **2.6-2.11**, vibrant green coloured solutions were observed, with green crystalline solids or powders forming on slow evaporation of the reaction solution. On noting the colour of the solids, further confirmation that copper was complexed to the ligands was achieved by carrying out IR spectroscopy on the green solids. The resulting spectra were compared to those of their respective starting materials and were interpreted in accordance with literature examples of chelating pyridyl-containing azoles,[130] N-alkyltetrazoles and their metal complexes.[131] Characteristic frequencies of the bromoalkyl functionalised pyridyl tetrazoles and their Cu(II) complexes are shown in Table 2.1. Coordination of metal ions leads to significant changes in the frequencies of the ν(C=N) bands of the pyridine and tetrazole rings which are typically located in the region 1640-1450 cm^{-1}. On analysis of the IR spectra of the uncoordinated ligands and their metal complexes, these vibrational bands shifted to different wavenumbers on complexation to Cu(II) which suggested that the ligand molecules were coordinating to the metal centre through chelation of both the pyridine and tetrazole nitrogens.

Table 2.1: Selected frequencies of free ligands* and Cu(II) chloride complexes.

Compound	$C=N_{tet}$ (cm^{-1})	$C=N_{pyr}$ (cm^{-1})	N=N (cm^{-1})
2.6*	1586	1502	1447
2.26	1616	1484	1455
2.7*	1589	1469	1432
2.27	1619	1552	1450
2.8*	1590	1471	1432
2.28	1614	1483	1456
2.9*	1586	1456	1434
2.29	1617	1552	1451
2.10*	1593	1467	1417
2.30	1611	1481	1451
2.11*	1593	1466	1416
2.31	1621	1462	1449

Previous work carried out by the McGinley group on the bromohexyl derivatives, **2.1** and **2.2**, yielded crystal structures of Cu(II) complexes (Figure 2.11).[121] These structures showed that both N-1 and N-2 isomers consisted of dichloro-bridged dimeric units, with the coordination sphere around each atom comprising one pyridine N atom, one tetrazole

N atom and three Cl atoms. The IR spectra of the complexes synthesised in this body of work suggested a resemblance to these structures. Room temperature magnetic moment measurements gave μ_{eff} values in the range of 1.7-2.3 B.M., indicating a 2+ oxidation state of the metal ion. Furthermore, elemental analysis on the metal complexes suggested a 1:1 metal to ligand composition, therefore further indicating that the complexes synthesised were analogous to those in Figure 2.11. A representation of the structures can be seen in Figure 2.12.

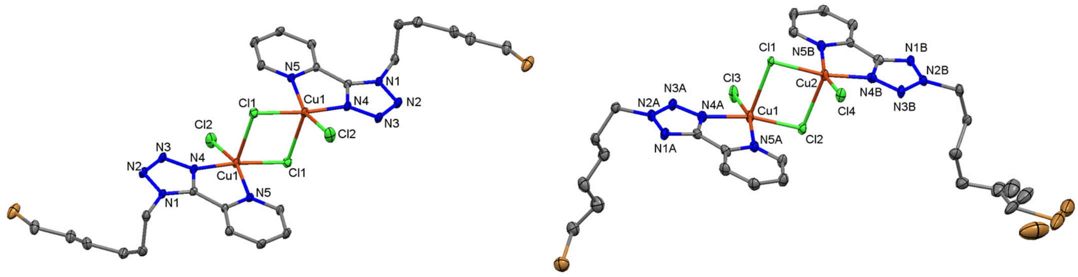

Figure 2.11: Crystal structures of products formed from the reaction of **2.1** and **2.2** with $CuCl_2.2H_2O$, which were previously obtained in the McGinley group. Disorder can be seen in **2.2**.

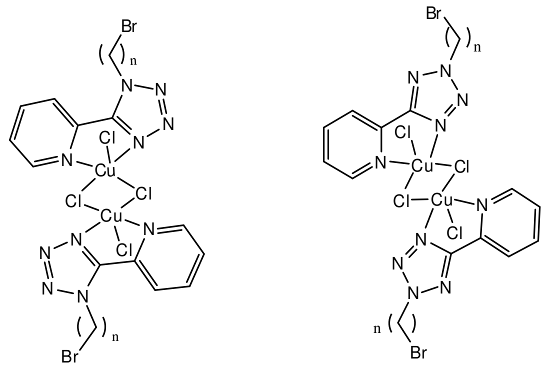

2.26 n = 3
2.28 n = 4
2.30 n = 8

2.27 n = 3
2.29 n = 4
2.31 n = 8

Figure 2.12: Proposed structures of compounds **2.26-2.31**.

2.3.2.1.2 Nickel(II) chloride hexahydrate reactions

Nickel(II) complexes were synthesised in a similar manner to that utilised for the copper(II) complexes, with green coloured reaction solutions producing green solids on slow reduction of the mother liquor. Room temperature magnetic moment measurements indicated that the complex had two unpaired electrons with μ_{eff} values in the range of 2.9-4.2 B.M., which eliminated square planar geometry from our consideration. Hence, the structures of the Ni(II) complexes were believed to be of either tetrahedral (4-coordinate) or square pyramidal/trigonal bipyramidal (5-coordinate) geometry. IR spectroscopy established that the Ni(II) metal centre was coordinating to the pyridine N atom and tetrazole N atoms as ν(C=N) bands arising from the tetrazole rings had shifted from ~1580 cm^{-1} to higher wavenumbers, and ν(C=N) bands arising from the pyridine ring had also shifted (Table 2.2).

Table 2.2: Selected frequencies of free ligands* and Ni(II) chloride complexes.

Compound	$C=N_{tet}$ (cm^{-1})	$C=N_{pyr}$ (cm^{-1})	N=N (cm^{-1})
2.6*	1586	1502	1447
2.32	1614	1481	1455
2.7*	1589	1469	1432
2.33	1614	1549	1452
2.8*	1590	1471	1432
2.34	1613	1481	1457
2.9*	1586	1456	1434
2.35	1613	1545	1451
2.1*	1593	1514	1437
2.36	1608	1478	1457
2.2*	1598	1518	1438
2.37	1615	1451	1261
2.10*	1593	1467	1417
2.38	1606	1478	1459
2.11*	1593	1466	1416
2.39	1614	1463	1452

Elemental analysis of the complexes yielded a ratio of 1:1 metal to ligand composition. In considering the geometrical preferences for Ni(II), it is well known that there are several examples of tetrahedral and square pyramidal/trigonal bipyramidal Ni(II) complexes.[132] However, high spin paramagnetic trigonal bipyramidal Ni(II) complexes are rare,[132] and the manifestation of an intrinsic magnetic moment had to be taken into account. Evidence of bridging or terminal chloride bonds could not be determined due to the presence of other frequencies in the fingerprint region. Despite numerous attempts, no X-ray quality crystals of these complexes were obtained. Therefore, it was tentatively proposed that the Ni(II) complexes formed coordination compounds that were either analogous to the Cu(II) complexes seen in Figure 2.11, with the Ni(II) centre possessing a square pyramidal geometry, or formed a tetrahedral Ni(II) complex. The latter would be deemed most likely as high spin tetrahedral complexes of Ni(II) are more prevalent in the literature.[132] A representation of the proposed complexes can be seen in Figure 2.13.

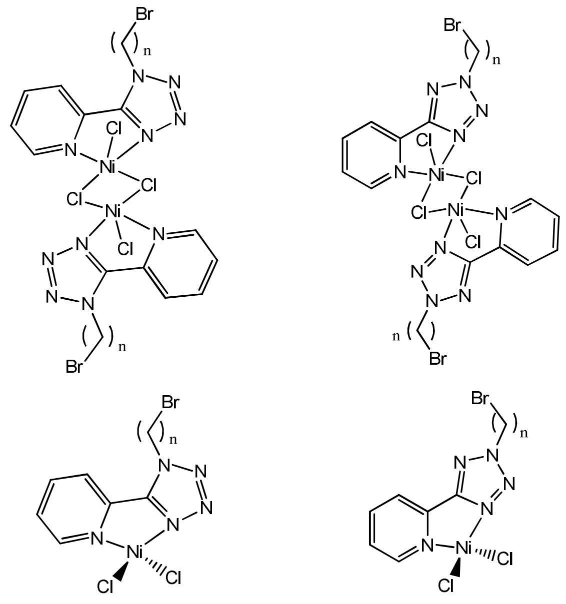

2.32 n = 3
2.34 n = 4
2.36 n = 6
2.38 n = 8

2.33 n = 3
2.35 n = 4
2.37 n = 6
2.39 n = 8

Figure 2.13: Proposed structure of compounds **2.32-2.39**.

2.3.2.1.3 Cobalt(II) thiocyanate reactions

Pink or blue solutions were observed in all reactions involving cobalt(II) thiocyanate, with crystalline rust coloured solids being collected after reduction of the reaction solution. As a 3d^7 system, Co(II) complexes have 3 unpaired electrons and would have a calculated spin-only magnetic moment of 3.8 B.M. for high spin complexes. Octahedral complexes typically have magnetic moments between 4.7 and 5.2 B.M. Tetrahedral complexes are typically below 4.7 B.M. but may be higher for stronger field ligands. Thus, magnetic moments give some indication of geometry but are not completely reliable. Magnetic susceptibility measurements at room temperature recorded μ_{eff} values in the range of 4.6-5.5 B.M., indicating the presence of high spin octahedral Co(II) ions. The IR spectra showed clear indications that complexation to the ligands had occurred (Table 2.3). Coordination to the heterocyclic N atoms was confirmed due to shifting of the ν(C=N)$_{tet}$ band from ~1580 cm^{-1} to ~1610 cm^{-1} and shifting of the ν(C=N)$_{pyr}$ stretch. The presence of thiocyanate groups were revealed in the IR spectra due to an intense absorption at ~2077 cm^{-1} attributed to the asymmetric vibration ν(C-N)$_{SCN}$, which had shifted from 2152 cm^{-1} in the metal salt $Co(SCN)_2$. Elemental analysis of the rust coloured complexes implied that they had a 1:2 metal to ligand composition. It was proposed that the Co(II) complexes were congeners to those synthesised previously by McGinley *et al.*[121] These complexes consisted of an octahedral Co(II) centre that was coordinated to two pyridyl tetrazole ligands, with two thiocyanate anions balancing the 2+ charge on the metal centre (Figure 2.14). These proposed structures are represented in Figure 2.15.

Table 2.3: Selected frequencies of free ligands*, $Co(SCN)_2$ salt and Co(II) complexes.

Compound	$C=N_{tet}$ (cm^{-1})	$C=N_{pyr}$ (cm^{-1})	N=N (cm^{-1})	$(C\text{-}N)_{SCN}$ (cm^{-1})
$Co(SCN)_2$				2152
2.6*	1586	1502	1447	
2.40	1606	1475	1456	2077
2.7*	1589	1469	1432	
2.41	1612	1552	1449	2069
2.8*	1590	1471	1432	
2.42	1607	1478	1435	2070
2.9*	1586	1456	1434	
2.43	1612	1552	1449	2070
2.10*	1593	1467	1417	
2.44	1605	1456	1437	2077
2.11*	1593	1466	1416	
2.45	1610	1471	1447	2069

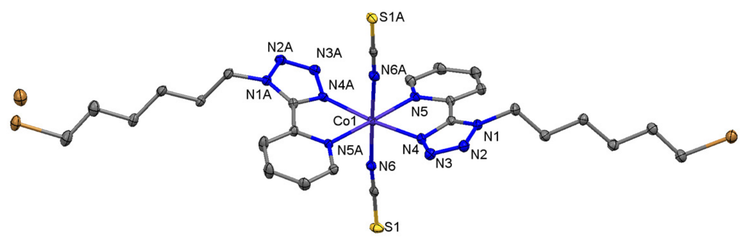

Figure 2.14: Crystal structure of the product obtained from the reaction of **2.1** with $Co(SCN)_2$. Disorder can be seen in the alkyl chain.

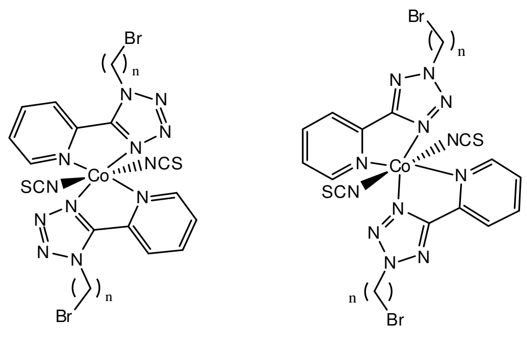

2.40 n = 3
2.42 n = 4
2.44 n = 8

2.41 n = 3
2.43 n = 4
2.45 n = 8

Figure 2.15: Proposed structures for compounds **2.40-2.45**.

2.3.2.1.4 Zinc(II) chloride reactions

Complexation reactions with zinc(II) chloride yielded cream, yellow or orange compounds and generally were the same colour as the starting ligand. Longer reaction times were required in order for $ZnCl_2$ to complex to the ligand, therefore 12 hour reaction times were employed. IR spectroscopy was carried out on the Zn(II) complexes and compared to the spectra of their respective starting materials. In all spectra a shift of the ν(C=N) frequencies of the pyridine and tetrazole ring was observed. In the IR spectra of the ligands, these vibrational bands could be found at ~1471-1500 cm^{-1} and these shifted to ~1500-1600 cm^{-1} on complexation of Zn(II) (Table 2.4). Elemental analysis suggested a 1:1 metal to ligand composition, therefore, it was postulated that a dichloro-bridged species similar to the Cu(II) complexes were present (Figure 2.11) as a coordination number of 5 is most common for Zn(II) complexes.[132] The structures of the proposed complexes can be seen in Figure 2.16.

Table 2.4: Selected frequencies of free ligands* and Zn(II) complexes.

Compound	$C=N_{tet}$ (cm^{-1})	$C=N_{pyr}$ (cm^{-1})	N=N (cm^{-1})
2.6*	1586	1502	1447
2.46	1610	1552	1440
2.7*	1589	1469	1432
2.47	1614	1546	1451
2.8*	1590	1471	1432
2.48	1610	1481	1458
2.9*	1586	1456	1434
2.49	1614	1548	1452
2.1*	1593	1514	1437
2.50	1610	1482	1459
2.2*	1598	1518	1438
2.51	1614	1573	1451
2.10*	1593	1467	1417
2.52	1654	1589	1465
2.11*	1593	1466	1416
2.53	1613	1572	1453

Due to Zn(II) ions being diamagnetic, NMR spectroscopy was also carried out on the complexes. ^1H NMR spectra of the zinc(II) chloride complexes were all obtained in $CDCl_3$. Table 2.5 shows the ^1H NMR spectral data for the four pyridyl tetrazole ligands with the alkyl bromides attached at the N-1 position and the four corresponding zinc(II) chloride complexes, while Table 2.6 contains the ^1H NMR spectral data for the four pyridyl tetrazole ligands with the alkyl bromides attached at the N-2 position and the four corresponding zinc(II) chloride complexes.

Table 2.5: Selected ^{1}H NMR data for the N-1 ligands* and their $ZnCl_2$ complexes.[a]

Compound	pyr-H	pyr-H	pyr-H	pyr-H	CH_2N
2.6*	8.75	8.37	7.93	7.47	5.15
2.46	8.78	8.35	7.95	7.45	5.18
2.8*	8.74	8.37	7.93	7.47	5.04
2.48	8.78	8.36	7.96	7.5	5.02
2.1*	8.77	8.37	7.96	7.52	5.00
2.50	8.92	8.29	8.06	7.61	4.92
2.10*	8.73	8.37	7.90	7.45	4.98
2.52	8.76	8.32	7.97	7.49	4.96

[a] Obtained in $CDCl_3$.

Table 2.6: Selected ^{1}H NMR data for the N-2 ligands* and their $ZnCl_2$ complexes.[a]

Compound	pyr-H	pyr-H	pyr-H	pyr-H	CH_2N
2.7*	8.78	8.26	7.87	7.41	4.91
2.47	8.88	8.31	8.16	7.76	5.01
2.9*	8.78	8.25	7.87	7.40	4.77
2.49	8.96	8.29	8.22	7.84	4.88
2.2*	8.80	8.27	7.90	7.43	4.73
2.51	8.86	8.28	8.19	7.76	4.81
2.11*	8.79	8.25	7.87	7.40	4.70
2.53	8.89	8.31	8.22	7.81	4.81

[a] Obtained in $CDCl_3$.

From the data obtained, it is evident that binding of the zinc chloride has a greater effect on the protons in the series of N-2 ligands, as seen from the larger differences in chemical shift for both the pyridyl proton signals and the signal for the methylene group attached to the tetrazole ring. The ^{1}H NMR spectra of the Zn(II) complexes from the N-1 series of ligands shows only slight variation in signal position compared to the starting ligands. It has previously been observed that the complexation properties of 1- and 2-substituted tetrazole isomers differ greatly due to the electronic properties of the tetrazole ring being influenced by alkyl substituents.[131] Hence, it is proposed that the manifestation of such large differences are due to the differing electronic properties of the N-1 and N-2 isomers.

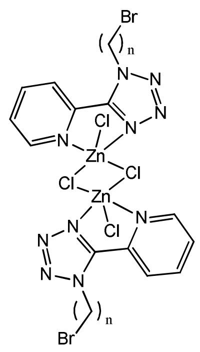

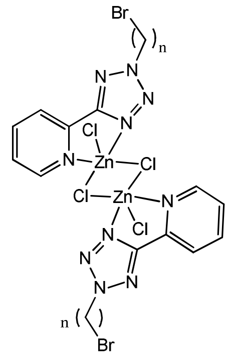

2.46 n = 3
2.48 n = 4
2.50 n = 6
2.52 n = 8

2.47 n = 3
2.49 n = 4
2.51 n = 6
2.53 n = 8

Figure 2.16: Proposed structures of compounds **2.46-2.53**.

2.3.2.2 Metal Complexes of Alkyl Chain Derivatives

2.3.2.2.1 Copper(II) chloride dihydrate reactions

Reactions with $CuCl_2.2H_2O$ resulted in solutions of the ligands turning a vibrant green colour. These solutions produced crystalline green solids on reduction of the mother liquor at room temperature. IR spectra of the green solids indicated that complexation to the pyridine and tetrazole nitrogens had occurred, as ν(C=N) bands from the pyridine and tetrazole rings had shifted (Table 2.7).

Table 2.7: Selected IR frequencies of free ligands* and Cu(II) complexes.

Compound	$C=N_{tet}$ (cm^{-1})	$C=N_{pyr}$ (cm^{-1})	N=N (cm^{-1})
2.12*	1591	1471	1433
2.54	1614	1482	1457
2.13*	1594	1466	1419
2.55	1619	1552	1449
2.14*	1592	1434	1421
2.56	1611	1482	1455
2.15*	1595	1466	1420
2.57	1617	1551	1450
2.16*	1591	1467	1433
2.58	1611	1482	1446
2.17*	1593	1466	1419
2.59	1616	1537	1454

Room temperature magnetic moment measurements yielded expected μ_{eff} values in the range of 1.8-2.1 B.M. indicating the presence of d^9 Cu(II) metal centres. A ratio of 1:1 metal to ligand ratio was suggested in elemental analysis results, therefore it was postulated that these Cu(II) complexes had the same structure as those depicted in Figure 2.11. These proposed structures can be seen in Figure 2.17.

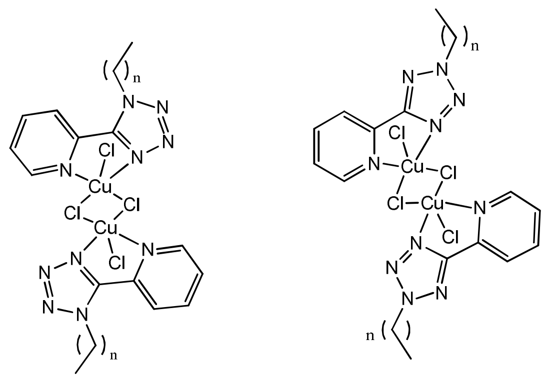

2.54 n = 3
2.56 n = 5
2.58 n = 7

2.55 n = 3
2.57 n = 5
2.59 n = 7

Figure 2.17: Proposed structures of compounds **2.54-2.59**.

2.3.2.2.2 Nickel(II) chloride hexahydrate reactions

Green solutions were observed in reactions with $NiCl_2.6H_2O$ and green or blue solids were recovered from these solutions on slow evaporation of the mother liquor. Room temperature magnetic moment measurements yielded μ_{eff} values in the ranges of 3.1-4.3 B.M., which eliminated square planar geometry from our consideration but did indicate the presence of high spin Ni(II) centres, and conformed with those reported for high spin five-coordinate Ni(II) complexes.[133] IR spectroscopy suggested that the coordination geometry around the Ni(II) centre involved the pyridine and tetrazole nitrogens as shifts could be seen in the characteristic heterocyclic bands (Table 2.8).

Table 2.8: Selected IR frequencies of free ligands* and Ni(II) complexes.

Compound	$C=N_{tet}$ (cm^{-1})	$C=N_{pyr}$ (cm^{-1})	N=N (cm^{-1})
2.12*	1591	1471	1433
2.60	1615	1478	1457
2.13*	1594	1466	1419
2.61	1611	1479	1457
2.14*	1592	1434	1421
2.62	1613	1479	1456
2.15*	1595	1466	1420
2.63	1614	1461	1452
2.16*	1591	1467	1433
2.64	1611	1479	1456
2.17*	1593	1466	1419
2.65	1615	1461	1452

Elemental analysis revealed a 1:1 metal to ligand ratio. Therefore, it was proposed that there were two Ni(II) centres of square pyramidal geometry which were bridged by two chloride atoms, similar to those discussed previously and shown in Figure 2.11. The structures of the proposed complexes can be seen in Figure 2.18. It must also be stated that tetrahedral geometry would also fit the data obtained, however assignments to either geometry was hampered by the fact that metal-chloride (terminal or bridging) IR frequencies could not be distinguished due to their presence in the fingerprint region.

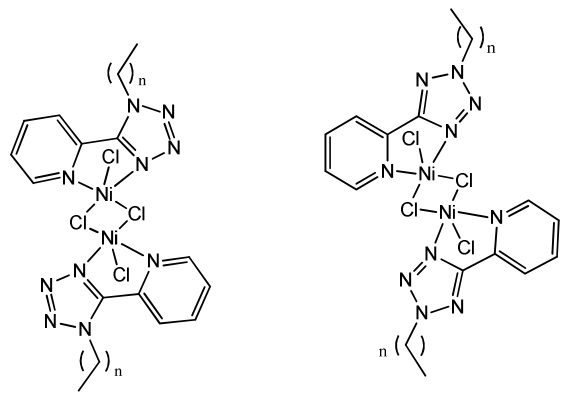

2.60 n = 3
2.62 n = 5
2.64 n = 7

2.61 n = 3
2.63 n = 5
2.65 n = 7

Figure 2.18: Proposed structures of compounds **2.60-2.65**.

2.3.2.2.3 Cobalt thiocyanate reactions

Reactions with cobalt(II) thiocyanate resulted in pink or royal blue solutions. Rust coloured solids were produced on slow evaporation of the reaction solvent. Magnetic measurements at room temperature yielded μ_{eff} values of ~5.0 B.M. which indicated that the geometry of the Co(II) ion was octahedral. IR spectra once again strongly suggested coordination to the pyridyl and tetrazole nitrogens, with the significant shifts observed presented in Table 2.9. Presence of thiocyanate anions were also revealed in the IR spectra.

Table 2.9: Selected IR frequencies of free ligands*, metal salt $Co(SCN)_2$ and Co(II) complexes.

Compound	$C{=}N_{tet}$ (cm^{-1})	$C{=}N_{pyr}$ (cm^{-1})	N=N (cm^{-1})	$(C\text{-}N)_{SCN}$ (cm^{-1})
$Co(SCN)_2$				2152
2.12*	1591	1471	1433	
2.66	1609	1478	1456	2068
2.13*	1594	1466	1419	
2.67	1610	1458	1447	2077
2.14*	1592	1434	1421	
2.68	1609	1476	1456	2067
2.15*	1595	1466	1420	
2.69	1609	1459	1447	2074
2.16*	1591	1467	1433	
2.70	1610	1476	1457	2068
2.17*	1593	1466	1419	
2.71	1609	1541	1447	2074

On slow evaporation of the reaction solvent, crystalline solids of **2.67** and **2.71** were produced which were suitable for X-ray crystallography. The molecular structures are depicted in Figures 2.19 and 2.20. In both structures, the Co(II) atom has an octahedral geometry with the pyridyl tetrazole ligands chelating in the equatorial plane with the two isothiocyanate anions coordinating along the axial direction. Each pyridyl tetrazole ligand binds to the Co(II) atom through one tetrazole nitrogen atom at the N-1 site and through the pyridyl nitrogen atom. The pyridine rings are not co-planar with the tetrazole rings giving both complexes a slightly puckered conformation. The planes between the pyridine and tetrazole rings form interplanar angles of 3.8(5)° and 1.6(5)° in **2.67** and 4.5(4)° in **2.71**. The $Co\text{-}N_{NCS}$ distances are in the range from 2.037(6) to 2.060(6) Å, whereas the remaining Co-N distances are 0.10 Å longer and in the range of 2.140(4) to 2.170(3) Å.

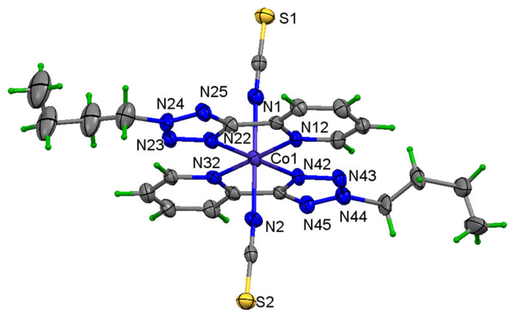

Figure 2.19: A view of **2.67** with atoms depicted with displacement ellipsoids at their 20% probability level.

These bond lengths are typical of Co(II)-N distances involving isothiocyanate and heteroaromatic ring donor groups. The isothiocyanate moieties in both complexes are regular with NCS angles of 178.5(6)°, 176.9(5)° and 178.5(4)°. In **2.67**, the coordination geometry is close to ideal octahedral, with all three *trans* angles within 1° of 180°. **2.71** resides with the cobalt atom on inversion centres and *trans* N-Co-N angles of 180°.

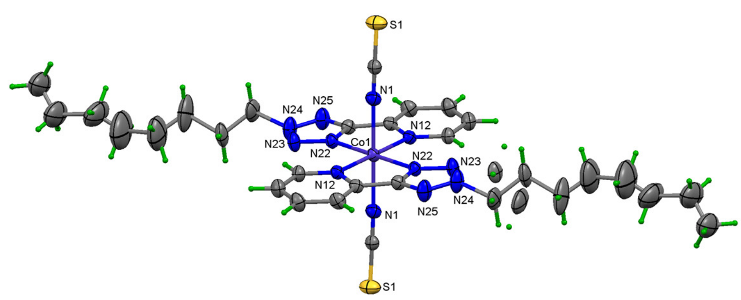

Figure 2.20: A view of **2.71** with atoms depicted with displacement ellipsoids at the 20% probability level; only one component of the disordered *n*-octyl chain is shown.

As a result of X-ray crystallography demonstrating that these octahedral Co(II) complexes were formed and furthermore, due to satisfactory data being obtained for other Co(II) complexes, it was proposed that all Co(II) complexes of alkyl chain functionalised pyridyl tetrazoles were of this type (Figure 2.21).

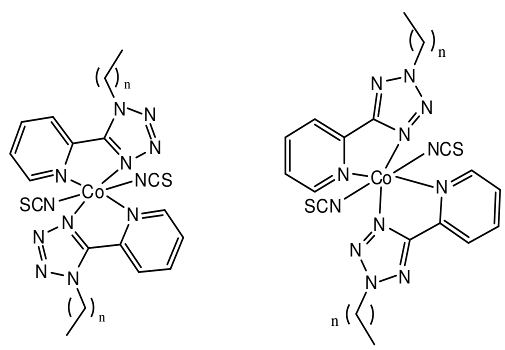

2.66 n = 3
2.68 n = 5
2.70 n = 7

2.67 n = 3
2.69 n = 5
2.71 n = 7

Figure 2.21: Proposed structures of compounds **2.66-2.71**.

2.3.2.2.4 Zinc(II) chloride reactions

Reactions with zinc(II) chloride yielded white or orange solids. IR spectra of the solids indicated that Zn(II) was coordinating to the pyridyl and tetrazole nitrogens as shifts were observed for the characteristic heterocyclic stretches (Table 2.10).

Table 2.10: Selected IR frequencies of free ligands and Zn(II) complexes.

Compound	$C{=}N_{tet}$ (cm^{-1})	$C{=}N_{pyr}$ (cm^{-1})	N=N (cm^{-1})
2.12*	1591	1471	1433
2.72	1609	1482	1459
2.13*	1594	1466	1419
2.73	1614	1547	1453
2.14*	1592	1434	1421
2.74	1610	1480	1460
2.15*	1595	1466	1420
2.75	1613	1547	1454
2.16*	1591	1467	1433
2.76	1610	1481	1460
2.17*	1593	1466	1419
2.77	1610	1543	1452

NMR spectroscopy was also carried out on the solids and all spectra were obtained in $CDCl_3$. On visual inspection, there were clear differences between the spectra of the ligands and the spectra of the Zn(II) complexes. Figure 2.22 displays two ^{1}H NMR spectra; the free ligand (blue) is that of **2.13** and the green spectrum is that of the Zn(II) complex **2.73**. The four pyridyl protons are observed to shift downfield in the metal complex, with the CH_2-tet protons slightly shifting downfield. On comparing NMR data for N-1 and N-2 substituted isomers, it was noted that the CH_2-tet protons shifted upfield for N-1 isomers and downfield for N-2 isomers (Tables 2.11 and 2.12).

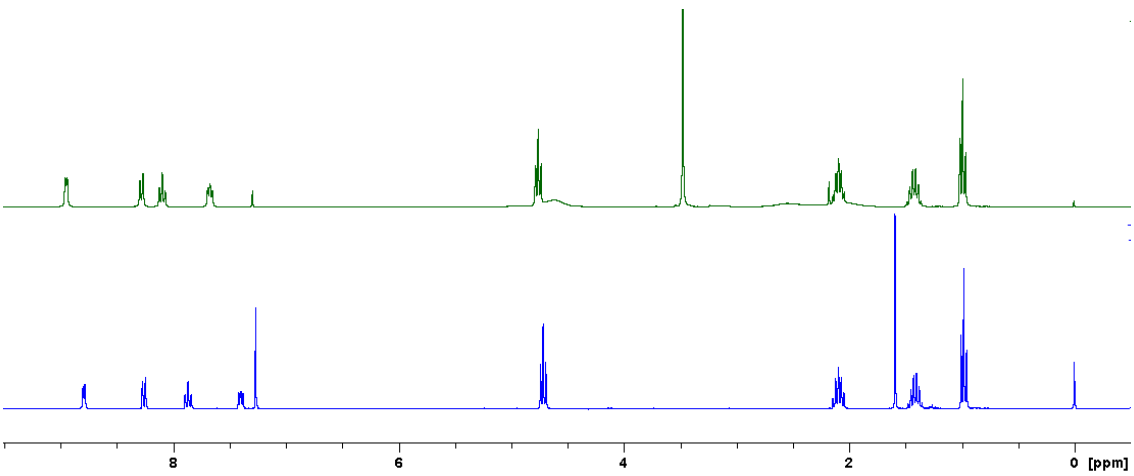

Figure 2.22: Comparison of ^{1}H NMR spectra of free ligand **2.13** (blue) and Zn(II) complex **2.73** (green). Spectra obtained in $CDCl_3$.

Also apparent when comparing the two regioisomers was that the pyridyl protons shifted more significantly for the N-1 isomers than the N-2 isomers, which is contrary to what occurred with the alkylbromo congeners.

Table 2.11: Selected ^{1}H NMR data for the N-1 alkyl chain ligands* and their $ZnCl_2$ complexes.[a]

Compound	pyr-H	pyr-H	pyr-H	pyr-H	CH_2N
2.12*	8.73	8.36	7.91	7.45	4.99
2.72	9.00	8.21	8.12	7.69	4.86
2.14*	8.72	8.36	7.90	7.44	4.97
2.74	9.04	8.26	8.20	7.75	4.81
2.16*	8.73	8.36	7.90	7.45	4.97
2.76	9.11	8.18	8.18	7.76	4.78

[a] Obtained in $CDCl_3$.

Table 2.12: Selected ^{1}H NMR data for the N-2 alkyl chain ligands* and their $ZnCl_2$ complexes.[a]

Compound	pyr-H	pyr-H	pyr-H	pyr-H	CH_2N
2.13*	8.79	8.25	7.86	7.39	4.71
2.73	8.94	8.28	8.09	7.67	4.75
2.15*	8.79	8.26	7.86	7.40	4.70
2.75	9.02	8.34	8.16	7.92	4.82
2.17*	8.78	8.25	7.86	7.39	4.70
2.77	8.87	8.28	8.11	7.69	4.76

[a] Obtained in $CDCl_3$.

Elemental analysis suggested a metal to ligand ratio of 1:1, therefore it was proposed that the Zn(II) complexes were analogous to those synthesised and discussed previously. The proposed structures of these complexes can be seen in Figure 2.23.

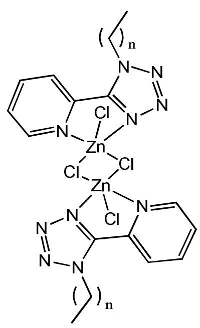

2.72 n = 3
2.74 n = 5
2.76 n = 7

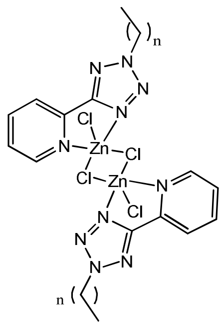

2.73 n = 3
2.75 n = 5
2.77 n = 7

Figure 2.23: Proposed structures of compounds **2.72-2.77**.

2.3.2.3 Metal Complexes of Alcohol Chain Derivatives

2.3.2.3.1 Copper(II) chloride dihydrate reactions

All reactions with $CuCl_2.2H_2O$ resulted in green coloured solutions which produced green solids upon slow evaporation of the mother liquor. The IR spectra of the complexes exhibited the trends seen for the previous metal(II) chlorides, with increased wavenumbers observed for characteristic heterocyclic bands (Table 2.13). This again indicated that coordination was occurring at the pyridine and tetrazole nitrogen atoms. Magnetic moment measurements at room temperature were in the range of 1.7-2.3 B.M. which was typical of a d^9 Cu(II) atom. Elemental analysis of the compounds implied a 1:1 metal to ligand composition, therefore it was proposed that the Cu(II) complexes synthesised were analogous to those synthesised previously (section 2.3.2.1.1). These proposed structures can be seen in Figure 2.24.

Table 2.13: Selected IR frequencies of the free ligands* and Cu(II) complexes.

Compound	$C=N_{tet}$ (cm^{-1})	$C=N_{pyr}$ (cm^{-1})	N=N (cm^{-1})
2.18*	1591	1473	1435
2.78	1613	1484	1455
2.19*	1598	1435	1421
2.79	1618	1459	1447
2.20*	1588	1471	1431
2.80	1614	1551	1481
2.21*	1591	1472	1434
2.81	1614	1548	1457
2.22*	1591	1472	1433
2.82	1615	1484	1456
2.23*	1599	1468	1421
2.83	1617	1463	1453
2.24*	1591	1471	1433
2.84	1615	1486	1458
2.25*	1599	1468	1421
2.85	1617	1463	1453

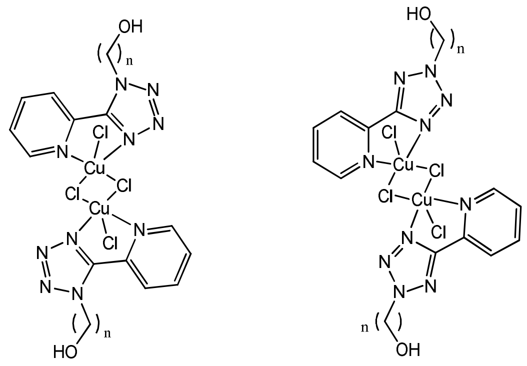

2.78 n = 3
2.80 n = 4
2.82 n = 6
2.84 n = 8

2.79 n = 3
2.81 n = 4
2.83 n = 6
2.85 n = 8

Figure 2.24: Proposed structures of compounds **2.78-2.85**.

2.3.2.3.2 Nickel(II) chloride hexahydrate reactions

All reactions with nickel(II) chloride yielded green solutions and on slow evaporation of the mother liquor produced green or blue solids. Reactions were not carried out with the butanol derivatives **2.20** and **2.21** due to the poor yields observed for these ligands. IR spectra of the complexes displayed the same trends experienced for all previously discussed metal(II) chloride complexes. Characteristic heterocyclic band frequencies and their shifts to higher frequencies can be seen in Table 2.14.

Table 2.14: Selected IR frequencies of free ligands* and Ni(II) complexes.

Compound	$C{=}N_{tet}$ (cm^{-1})	$C{=}N_{pyr}$ (cm^{-1})	N=N (cm^{-1})
2.18*	1591	1473	1435
2.86	1610	1480	1461
2.19*	1598	1435	1421
2.87	1615	1552	1453
2.22*	1591	1472	1433
2.88	1610	1482	1458
2.23*	1599	1468	1421
2.89	1615	1549	1454
2.24*	1591	1471	1433
2.90	1608	1474	1452
2.25*	1599	1468	1421
2.91	1614	1547	1454

Magnetic moments recorded at room temperature yielded μ_{eff} values of 4.0-4.5 B.M. Elemental analysis gave a ratio of 1:1 metal to ligand composition. Hence, it was proposed that the structure of these Ni(II) complexes were either of a tetrahedral or a square pyramidal nature. Unequivocal evidence in order to clarify what geometry existed was not possible to obtain, as bridging metal-chloride and terminal metal-chloride IR frequencies were present in the fingerprint region and were difficult to distinguish. The proposed structures of these complexes can be seen in Figure 2.25.

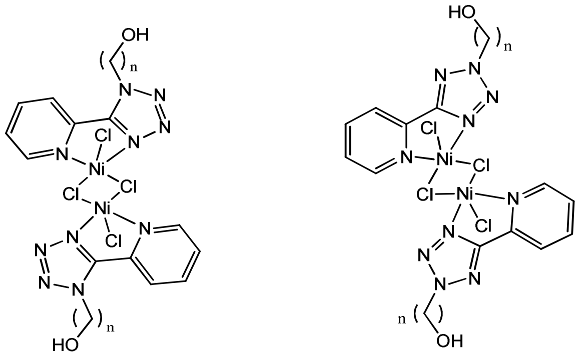

2.86 n = 3
2.88 n = 6
2.90 n = 8

2.87 n = 3
2.89 n = 6
2.91 n = 8

Figure 2.25: Proposed structures of compounds **2.86-2.91**.

2.3.2.3.3 Cobalt(II) thiocyanate reactions

All reactions with $Co(SCN)_2$ were pink in colour and yielded orange or pink crystalline solids. The IR spectra of the complexes exhibited the same indicative band shifts as seen in previously synthesised $Co(SCN)_2$ complexes. The heterocyclic bands shifted to higher frequencies (Table 2.15) and the presence of thiocyanate anions coordinated to the metal centre was revealed through the observation of the $\nu(C\text{-}N)_{SCN}$ stretch moving to lower frequencies.

Table 2.15: Selected IR frequencies of free ligands*, metal salt $Co(SCN)_2$ and Co(II) complexes.

Compound	$C{=}N_{tet}$ (cm^{-1})	$C{=}N_{pyr}$ (cm^{-1})	N=N (cm^{-1})	$(C\text{-}N)_{SCN}$ (cm^{-1})
$Co(SCN)_2$				2152
2.18*	1591	1473	1435	
2.92	1607	1480	1447	2085
2.19*	1598	1435	1421	
2.93	1610	1543	1449	2084
2.22*	1591	1472	1433	
2.94	1608	1479	1461	2095
2.23*	1599	1468	1421	
2.95	1610	1476	1448	2077
2.24*	1591	1471	1433	
2.96	1609	1477	1456	2067
2.25*	1599	1468	1421	
2.97	1610	1476	1448	2081

Elemental analysis of the compounds indicated a 1:2 metal to ligand ratio, therefore it was proposed that all Co(II) complexes in the alkyl alcohol series were of octahedral geometry, with two pyridyl tetrazole ligands and two thiocyanate groups coordinating to the metal centre (Figure 2.26). The attainment of magnetic moment measurements at room temperature yielded values of 4.8-5.5 B.M., which also supported the presence of an octahedral Co(II) centre.

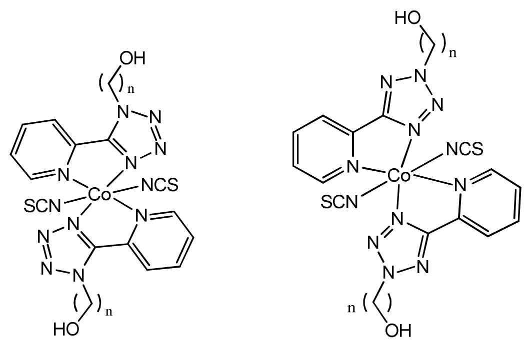

2.92 n = 3	**2.93** n = 3
2.94 n = 6	**2.95** n = 6
2.96 n = 8	**2.97** n = 8

Figure 2.26: Proposed structures of compounds **2.92-2.97**.

2.3.2.3.4 Zinc(II) chloride reactions

Reactions with zinc(II) chloride were carried out under reflux conditions in MeOH for varying times (2 h, 24 h, 3 d). In all cases only free ligand formed in the mother liquor, and this was clearly evident from the ^{1}H NMR spectra of the precipitates formed. The solubility of the alcohol derivatives could have been sufficiently different from other alkylated pyridyl tetrazoles that it nucleated and formed a solid first before binding to the d^{10} metal ion.

2.3.3 *In vivo* Compound Tolerance in *Galleria mellonella*

2.3.3.1 Insects as *in vivo* Models for Testing New Drug Candidates

Insects and mammals have been shown to share many similarities in their innate immune systems.[134,135] For example, the cuticle of insects provides a physical barrier preventing the entry of pathogens, a feature similar to the skin of animals.[134,135] When a pathogen enters the human body, cells known as macrophages and neutrophils can bind to the microbe and engulf them in a process known as phagocytosis.[136] In insects, within the haemolymph (analogous to blood of mammals), haemocytes or blood cells are responsible for the phagocytosis of foreign bodies.[134] These similarities, along with many others, between the innate immune system of insects and mammals have led to the use of insects as *in vivo* models for investigating the virulence of many human pathogens and to evaluate the tolerance of novel therapeutic agents.[137,138,139] An important phase in drug discovery is the assessment of the toxicity of new drug candidates. Before a new drug candidate can reach the clinic it needs to be tested to ensure it is safe and effective.[140] Toxicity testing is usually carried out using animal models such as mice, rabbits, dogs and monkeys.[140] However, the use of mammalian models is expensive, labour intensive, time consuming and requires full ethical consideration. Insects such as *Galleria mellonella* (*G. mellonella*) are lower in cost, do not require a large amount of storage space or experimental work and can give results within 24 to 48 h. These advantages, in combination with the similarity to the mammalian innate immune system render insects a useful preliminary model for the *in vivo* testing of new drug candidates and the evaluation of the therapeutic effect of novel anti-microbial agents. Desbois *et al*. have shown that the treatment of *G. mellonella* infected with *S. aureus* using vancomycin, daptomycin or penicillin improved the survival of the wax moth larvae in a dose dependent manner.[138] The doses administered to the infected *G. mellonella* that were most effective, were similar to those recommended for use in humans. An investigation into the toxicity of Cu(II) and Ag(I) complexes by McCann *et al*. have demonstrated that the level of toxicity exhibited by the test compounds in *G. mellonella* was similar to that observed in Swiss mice.[141] Although the use of mammals as *in vivo* models for testing new drug candidates is necessary, *G. mellonella* can be used as a good preliminary *in vivo* toxicity model. On average, only 500 compounds out of 10,000 compounds synthesised will reach animal testing, with only 10 reaching phase one clinical trials.[140] The use of insects allows for the early optimisation of compounds that exhibit therapeutic potential which in turn reduces the number of mammals used. Insect experiments may also be able to supply information relating to suitable dosages and drug metabolism.[138,142]

2.3.3.2 Examination of the *in vivo* Tolerance of 2.3 and 2.4 in *G. mellonella*

In an effort to further investigate the biological activity of compounds **2.3** and **2.4** (Figure 2.27), complexes which possessed good anti-cancer activity against a range of cell lines (section 2.1.2), *in vivo* toxicity studies were carried out as described in section 2.5.1 using the larvae of the greater wax moth, *G. mellonella*. *G. mellonella* live in beehives in which the larvae feed on honeycomb and undergo metamorphosis to become a grey moth. Working with *G. mellonella* is quite easy. As shown in Figure 2.28, test compounds can be administered into the haemocoel (body cavity) *via* injection into the last left pro-leg. By applying gentle pressure to the sides of the leg, the base of the pro-leg opens and will re-seal once the syringe needle has been removed, without leaving a scar. The toxicity of a given compound is determined by calculating the percentage of *G. mellonella* larvae that survive over a 72 h period. The larvae are monitored every 24 h and death is assessed based on a lack of movement in response to stimulation together with discolouration of the cuticle (melanisation) (Figure 2.29).

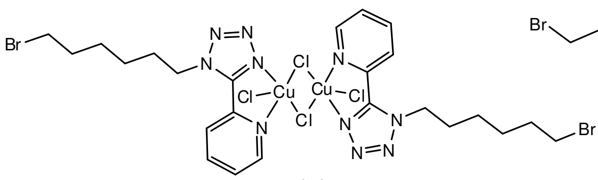

2.3

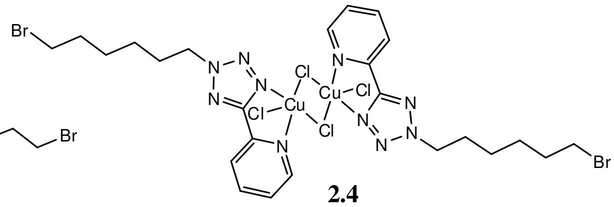

2.4

Figure 2.27: Cu(II) complexes which were synthesised previously in the McGinley group and showed good anti-cancer activity.

Figure 2.28: Compound administration to *G. mellonella* (reprinted with permission).[143]

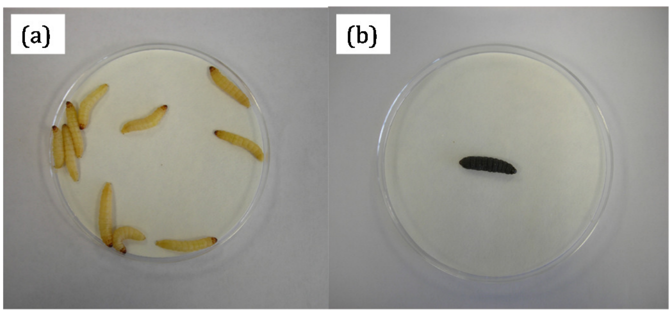

Figure 2.29: Appearance of (a) healthy, living *G. mellonella* larvae and (b) dead *G. mellonella* larvae. Pictures reprinted with permission.

The results of the treatment of *G. mellonella* with **2.3** and **2.4** are presented in Figure 2.30 as the survival of *G. mellonella* larvae (expressed as %) as a function of the compound dosages administered. As can be seen from Figure 2.30, at concentrations of 1-100 µg/mL the minimum survival rate of 73% was observed for compound **2.3**, with a 87% survival rate seen for the highest dose of 100 µg/mL. For compound **2.4**, which was the most active against cancer cell lines, the survival rate was observed to decrease to ~53% on going to a dosage concentration of 100 µg/mL. It was also apparent that larvae death occurred within the first 24 h post injection, with no further decrease in survival rate observed thereafter.

The similarities between the mammalian and insect innate immune systems have allowed insects to be used as models for a variety of *in vivo* studies including microbe virulence, drug efficacy and the toxicity and metabolism of drug candidates.[137,138,142,144] Considering the positive correlation that has been observed between compound toxicity in *G. mellonella* and mice, the results presented here prove encouraging and suggest that they could have applications as low toxicity anti-cancer therapeutic agents.

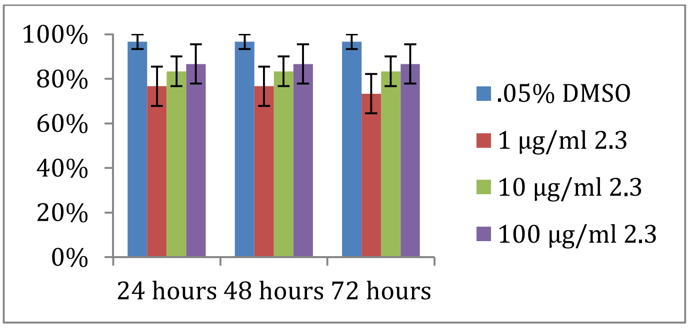

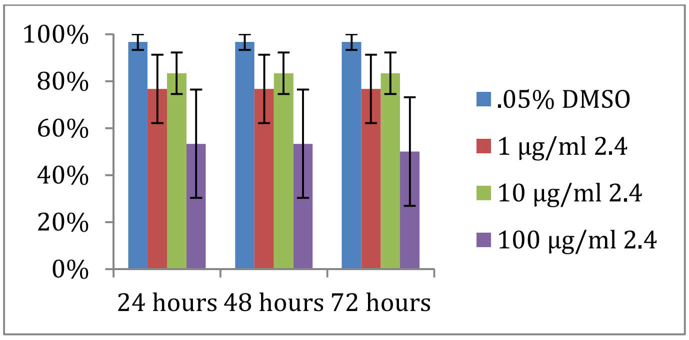

Figure 2.30: Survival of *G. mellonella* larvae (expressed as %) post injection at 24, 48 and 72 h. **2.3** (top graph) displayed low toxicity over incubation time of 72 h. **2.4** (bottom) showed a decrease in survival rates at higher concentrations within 24 h incubation time.

2.4 Conclusions

Herein, the synthesis of a pyridyl tetrazole metal complex library was undertaken with the aim of carrying these compounds forward to anti-cancer testing and SAR screening. The structure of each ligand synthesised was elucidated by means of HRMS, ^{1}H and ^{13}C NMR and IR spectroscopies. Metal complexes synthesised were characterised by IR, UV-Vis spectroscopies, elemental analysis, magnetic moment and in some cases X-ray crystallography.

Synthesis of the ligands involved formation of the tetrazole ring followed by alkylation at the N-1 or N-2 position of the tautomeric tetrazole ring. It was found that the N-2 regioisomer was always the major regioisomer formed, although regioselectivity was never pronounced. The only significant regioselectivity achieved was in the reaction of 1,3-dibromopropane and **2.5**, where the N-2 isomer was formed in a clear majority as a ratio of 10:33 was observed for the N-1 and N-2 isomers respectively.

Synthesis of the metal complexes involved heating a solution of the appropriate metal salt and ligand in MeOH for 2 hours. All reactions with MCl_2 salts were proposed to have resulted in the formation dichloro-bridged dimers, which were analogous to complexes studied previously in the McGinley group. All $Co(SCN)_2$ complexes formed octahedral complexes which were also similar to compounds studied previously. $ZnCl_2$ failed to complex to the alcohol chain derivatives in MeOH, perhaps due to a combination of poor solubility of the ligands and labile coordination bonds to the d^{10} ion. Alternative solvent systems could alleviate this issue.

Future work will involve an investigation into the anti-cancer activities of the complexes synthesised. This work will be carried out in the US National Cancer Institute where compounds are tested against 60 human tumour cell lines for their anti-cancer capabilities. This screening programme is a rich source of information about the mechanisms of growth inhibition and tumour-cell kill and has contributed significantly to the area of cancer chemotherapy.[145]

2.5 Experimental

2.5.1 Instrumentation

^{1}H and ^{13}C NMR (δ ppm; J Hz) spectra were recorded on a Bruker Avance 300 MHz NMR spectrometer using saturated $CDCl_3$ or d_6-DMSO solutions with a $SiMe_4$ reference, with resolutions of 0.18 Hz and 0.01 ppm, respectively. Infrared spectra (cm^{-1}) were recorded as KBr discs or liquid films on NaCl plates using a Perkin Elmer System 2000 FT-IR spectrometer. Solution UV-Vis spectra were recorded using a Unicam UV 540 spectrometer. Melting point analyses were carried out using a Stewart Scientific SMP 1 melting point apparatus and are uncorrected. Electrospray (ESI) mass spectra were collected on an Agilent Technologies 6410 Time of Flight LC/MS. Compounds were dissolved in acetonitrile-water (1:1) solutions containing 0.1% formic acid, unless otherwise stated. The interpretation of mass spectra was made using "Agilent Masshunter Workstation Software". Magnetic susceptibility measurements were carried out at room temperature using a Johnson Matthey Magnetic Susceptibility Balance with $[HgCo(SCN)_4]$ as reference. Microanalyses were carried out at the Microanalytical Laboratory of the National University of Ireland Maynooth using a Thermo Finnigan Elementary Analyzer Flash EA 1112. The results were analysed using the Eager 300 software. All crystal structures resulting from this work were solved by Dr. John Gallagher (Dublin City University) using an Oxford Diffraction Gemini-S Ultra diffractometer. Structures were solved using the SHELXS97 direct methods program. Molecular diagrams were generated using Mercury software. Starting materials were commercially obtained and used without further purification. Solvents used were of HPLC grade. *G. mellonella* in the sixth developmental stage were obtained from The Mealworm Company (Sheffield, England) and stored in wood shavings in the dark at 15 °C. Experiments were personally carried out using ten healthy *G. mellonella* (between 0.20-0.30 g in weight) placed in sterile, 9 cm petri dishes, containing a sheet of Whatmann filter paper and wood shavings. Test compound solutions were made on the day prior to administration. Each compound was dissolved in DMSO and added to sterile, distilled water to give stock solutions of 0.05% (v/v) DMSO. Using a 300 µL Thermo Myjector syringe (29G), sterile test solutions (20 µL) were administered to the larvae by injection. Injections were made into the last, left pro-leg of the *G. mellonella* larvae, directly into the haemocoel. Larvae were then incubated at 37 °C.

Caution! *Nitrogen-rich compounds such as tetrazole derivatives are used as components for explosive mixtures. In our laboratory, the reactions described were run on a few gram scale, and no problems were encountered. However, great caution should be exercised when heating or handling compounds of this type.*

2.5.2 Synthesis of Alkylbromo Pyridyl Tetrazoles

2.5.2.1 Synthesis of 2-(2*H*-tetrazol-5-yl)pyridine (2.5)

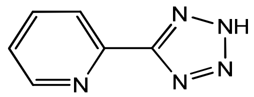

A suspension of 2-cyanopyridine (2.00 g, 19 mmol), NaN_3 (2.81 g, 43 mmol), NH_4Cl (2.32 g, 43 mmol) and LiCl (5.71 g, 134 mmol) in anhydrous DMF (40 mL) was stirred for 10 h at 110 °C. After this time, the solution was cooled and the insoluble salts were removed by filtration. The solvent was then evaporated under reduced pressure and the residue was dissolved in deionised H_2O (200 mL) and acidified with concentrated HCl (3 mL) to initiate precipitation. The product was removed by filtration, washed with H_2O (3 × 40 mL) and dried. The white solid was recrystallised from hot EtOH to yield **2.5** as white needles (2.72 g, 96%). m.p. 221-223 °C (lit. 211 °C).[30] IR (KBr): ν = 2669, 1638, 1621, 1541, 1488, 1459, 1382, 1287, 1229, 1098, 1043, 1016, 976, 800, 755 cm^{-1}. ^1H NMR (d_6-DMSO): δ = 8.79-8.81 (m, 1 H, pyr-H), 8.22-8.24 (m, 1 H, pyr-H), 8.06-8.11 (m, 1 H, pyr-H), 7.61-7.66 (m, 1 H, pyr-H) ppm. ^{13}C NMR (d_6-DMSO): δ = 154.9 (CN_4), 150.0, 143.8 138.1, 125.9, 122.5 ppm. ESI-HRMS: calcd. for $C_6H_6N_5$ $[M+H]^+$ 148.0618, found 148.0624.

NMR data are in agreement with literature values.[30]

2.5.2.2 Synthesis of Alkylbromo Pyridyl Tetrazoles

The general procedure for the synthesis of **2.1, 2.2** and **2.6-2.25** was as follows. To **2.5** (1.00 g, 7 mmol) suspended in MeCN was added K_2CO_3 (9.38 g, 68 mmol). The resulting solution was heated to reflux for 30 min and to the hot solution was added 1,n-dibromoalkane (24 mmol) (n = 3, 4, 6, 8). The reaction mixture was then stirred at reflux temperature for a further 24 h. After cooling the supension was filtered and the filtrate was concentrated under reduced pressure to afford an oil, which was purified by column chromatography on silica gel (Pet. Ether:EtOAc, 2:1). This yielded two isomeric products.

2.5.2.2.1 2-(1-(3-bromopropyl)-1*H*-tetrazol-5-yl)pyridine (2.6)

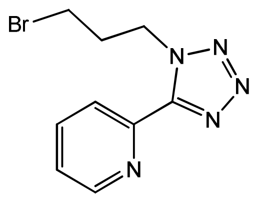

Dark brown solid (0.46 g, 13%). m.p. 190-192 °C. IR (KBr): ν = 2980, 2909, 1624, 1586, 1502, 1447, 1374, 1301, 1166, 1140, 971, 799, 720 cm^{-1}. ^{1}H NMR ($CDCl_3$): δ = 8.73-8.76 (m, 1 H, pyr-H), 8.36-8.39 (m, 1 H, pyr-H), 7.89-7.95 (m, 1 H, pyr-H), 7.44-7.49 (m, 1 H, pyr-H), 5.15 (t, 2 H, J = 6.8 Hz, CH_2N), 3.47 (t, 2 H, J = 6.4 Hz, CH_2Br), 2.53-2.62 (m, 2 H, CH_2) ppm. ^{13}C NMR ($CDCl_3$): δ = 151.8 (CN_4), 149.5, 144.7, 137.5, 125.4, 124.5, 48.2 (CH_2N), 34.8 (CH_2Br), 31.1 ppm. ESI-HRMS: calcd. for $C_9H_{11}N_5Br$ $[M+H]^+$ 268.0192, found 268.0188.

2.5.2.2.2 2-(2-(3-bromopropyl)-2*H*-tetrazol-5-yl)pyridine (2.7)

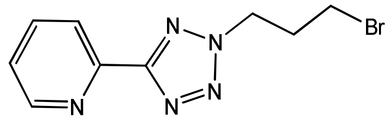

Waxy orange solid (1.38 g, 38%). m.p. 158-160 °C. IR (KBr): ν = 2980, 2931, 1623, 1589, 1533, 1469, 1432, 1357, 1283, 1119, 1042, 993, 799, 740 cm^{-1}. ^{1}H NMR ($CDCl_3$): δ = 8.78-8.79 (m, 1 H, pyr-H), 8.24-8.27 (m, 1 H, pyr-H), 7.82-7.90 (m, 1 H, pyr-H), 7.36-7.43 (m, 1 H, pyr-H), 4.91 (t, 2 H, J = 6.7 Hz, CH_2N), 3.46 (t, 2 H, J = 6.2 Hz, CH_2Br), 2.62-2.71 (m, 2 H, CH_2) ppm. ^{13}C NMR ($CDCl_3$): δ = 164.9 (CN_4), 150.3, 146.6, 137.4, 124.9, 122.4, 51.5 (CH_2N), 31.8 (CH_2Br), 28.7 ppm. ESI-HRMS: calcd. for $C_9H_{11}N_5Br$ $[M+H]^+$ 268.0192, found 268.0205.

2.5.2.2.3 2-(1-(4-bromobutyl)-1*H*-tetrazol-5-yl)pyridine (2.8)

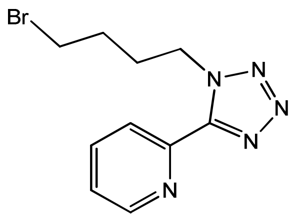

Waxy brown solid (0.86 g, 23%). m.p. 41-45 °C. IR (KBr): ν = 2958, 2865, 1590, 1530, 1471, 1432, 1403, 1330, 1277, 1122, 1092, 993, 796, 742 cm^{-1}. ^{1}H NMR ($CDCl_3$): δ = 8.73-8.75 (m, 1 H, pyr-H), 8.36-8.38 (m, 1 H, pyr-H), 7.90-7.95 (m, 1 H, pyr-H), 7.45-7.49 (m, 1 H, pyr-H), 5.04 (t, 2 H, J = 7.0 Hz, CH_2N), 3.44 (t, 2 H, J = 6.2 Hz, CH_2Br), 2.12-2.22 (m, 2 H, CH_2), 1.89-1.97 (m, 2 H, CH_2) ppm. ^{13}C NMR ($CDCl_3$): δ = 151.7 (CN_4), 149.5, 144.9, 137.5, 125.3, 124.6, 48.6 (CH_2N), 32.5 (CH_2Br), 30.9, 29.2 ppm. ESI-HRMS: calcd. for $C_{10}H_{13}N_5Br$ $[M+H]^+$ 282.0349, found 282.0352.

2.5.2.2.4 2-(2-(4-bromobutyl)-2*H*-tetrazol-5-yl)pyridine (2.9)

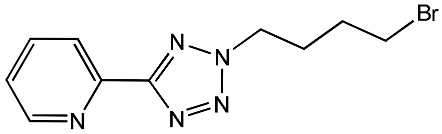

Waxy brown solid (0.62 g, 16%). m.p. 34-36 °C. IR (KBr): ν = 2942, 2866, 1624, 1586, 1456, 1434, 1350, 1292, 1164, 1050, 1010, 792, 750 cm^{-1}. ^{1}H NMR ($CDCl_3$): δ = 8.78-8.80 (m, 1 H, pyr-H), 8.24-8.27 (m, 1 H, pyr-H), 7.84-7.90 (m, 1 H, pyr-H), 7.38-7.43 (m, 1 H, pyr-H), 4.77 (t, 2 H, J = 6.8 Hz, CH_2N), 3.44 (t, 2 H, J = 6.4 Hz, CH_2Br), 2.24-2.34 (m, 2 H, CH_2), 1.89-1.98 (m, 2 H, CH_2) ppm. ^{13}C NMR ($CDCl_3$): δ = 164.9 (CN_4), 150.3, 146.8, 137.1, 124.8, 122.4, 52.4 (CH_2N), 32.1 (CH_2Br), 29.2, 27.8 ppm. ESI-HRMS: calcd. for $C_{10}H_{13}N_5Br$ $[M+H]^+$ 282.0349, found 282.0350.

2.5.2.2.5 2-(1-(8-bromooctyl)-1*H*-tetrazol-5-yl)pyridine (2.10)

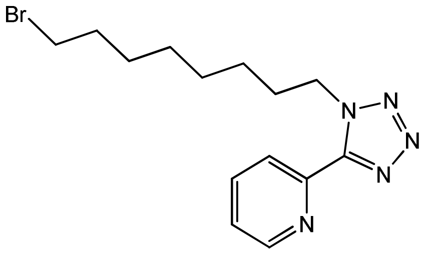

Waxy orange solid (0.77 g, 17%). m.p. 41-44 °C. IR (KBr): ν = 2937, 2860, 1613, 1593, 1467, 1433, 1417, 1354, 1150, 1091, 1043, 991, 803, 747 cm^{-1}. ^{1}H NMR ($CDCl_3$): δ = 8.71-8.74 (m, 1 H, pyr-H), 8.35-8.38 (m, 1 H, pyr-H), 7.87-7.93 (m, 1 H, pyr-H), 7.42-7.47 (m, 1 H, pyr-H), 4.98 (t, 2 H, J = 7.2 Hz, CH_2N), 3.39 (t, 2 H, J = 6.9 Hz, CH_2Br), 1.91-2.00 (m, 2 H, CH_2), 1.78-1.87 (m, 2 H, CH_2), 1.30-1.38 (m, 8 H, CH_2) ppm. ^{13}C NMR ($CDCl_3$): δ = 151.5 (CN_4), 149.4, 145.1 137.4, 125.2, 124.6, 49.5 (CH_2N), 33.9 (CH_2Br), 32.9, 29.8, 28.7, 28.4, 27.9, 26.1 ppm. ESI-HRMS: calcd. for $C_{14}H_{21}N_5Br$ $[M+H]^+$ 338.0975, found 338.0990.

2.5.2.2.6 2-(2-(8-bromooctyl)-2*H*-tetrazol-5-yl)pyridine (2.11)

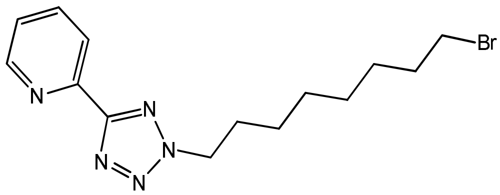

Waxy orange solid (0.86 g, 19%). m.p. 41-50 °C. IR (KBr): ν = 2931, 2852, 1620, 1593, 1466, 1435, 1416, 1351, 1149, 1092, 1042, 989, 803, 746 cm^{-1}. ^{1}H NMR ($CDCl_3$): δ = 8.77-8.80 (m, 1 H, pyr-H), 8.24-8.27 (m, 1 H, pyr-H), 7.83-7.89 (m, 1 H, pyr-H), 7.37-7.42 (m, 1

H, pyr-H), 4.70 (t, 2 H, *J* = 7.1 Hz, CH_2N), 3.39 (t, 2 H, *J* = 6.8 Hz, CH_2Br), 2.05-2.12 (m, 2 H, CH_2), 1.79-1.88 (m, 2 H, CH_2), 1.31-1.43 (m, 8 H, CH_2) ppm. ^{13}C NMR ($CDCl_3$): δ = 164.7 (CN_4), 150.3, 146.9, 137.1, 124.7, 122.3, 53.4 (CH_2N), 33.8 (CH_2Br), 32.6, 29.2, 28.6, 28.4, 27.9, 26.2 ppm. ESI-HRMS: calcd. for $C_{14}H_{21}N_5Br$ $[M+H]^+$ 338.0975, found 338.0983.

2.5.3 Metal Complexation Reactions with Alkylbromo Pyridyl Tetrazoles

2.5.3.1 General Procedure for Metal Complexation Reactions

0.20 g of ligand was dissolved in MeOH (20 mL). To this solution was added 1 equivalent of metal salt ($CuCl_2.2H_2O$, $NiCl_2.6H_2O$, $Co(SCN)_2$ or $ZnCl_2$) in MeOH (20 mL). The resulting solution was heated to reflux under nitrogen for 2 hours. The solution was then cooled to room temperature and allowed to stand for several days. The resulting solids were then isolated by filtration and washed with MeOH.

2.5.3.1.1 [Cu(2.6)Cl$_2$]$_2$ (2.26)

Green solid (0.12 g, 40%). $C_{18}H_{20}Br_2Cl_4Cu_2N_{10}$: calcd. C 26.85, H 2.50, N 17.40%; found C 27.13, H 2.56, N 17.76%. IR (KBr): ν = 2855, 1616, 1484, 1455, 1261, 1167, 1109, 1012, 794, 745, 718 cm^{-1}. λ_{max} (MeOH) 856 nm, ε = 59 $M^{-1}cm^{-1}$. Magnetic moment: 2.12 B.M.

2.5.3.1.2 [Cu(2.7)Cl$_2$]$_2$ (2.27)

Green solid (0.17 g, 57%). $C_{18}H_{20}Br_2Cl_4Cu_2N_{10}$: calcd. C 26.85, H 2.50, N 17.40%; found C 27.66, H 2.47, N 18.44%. IR (KBr): ν = 2860, 1619, 1552, 1450, 1267, 1228, 1064, 1021, 804, 761, 724 cm^{-1}. λ_{max} (MeOH) 800 nm, ε = 36 $M^{-1}cm^{-1}$. Magnetic moment: 2.24 B.M.

2.5.3.1.3 [Cu(2.8)Cl$_2$]$_2$ (2.28)

Green solid (0.19 g, 65%). $C_{20}H_{24}Br_2Cl_4Cu_2N_{10}$: calcd. C 28.83, H 2.90, N 16.81%; found C 28.21, H 2.15, N 16.41%. IR (KBr): ν = 2941, 2851, 1614, 1483, 1456, 1250, 1151, 1012, 791, 746, 718 cm^{-1}. λ_{max} (MeOH) 848 nm, ε = 145 $M^{-1}cm^{-1}$. Magnetic moment: 2.25 B.M.

2.5.3.1.4 [Cu(2.9)Cl$_2$]$_2$ (2.29)

Green solid (0.16 g, 55%). $C_{20}H_{24}Br_2Cl_4Cu_2N_{10}$: calcd. C 28.83, H 2.90, N 16.81%; found C 29.57, H 2.91, N 17.57%. IR (KBr): ν = 2951, 2849, 1617, 1552, 1451, 1259, 1156, 1101, 1062, 1023, 797, 757, 724 cm^{-1}. λ_{max} (MeOH) 832 nm, ε = 145 $M^{-1}cm^{-1}$. Magnetic moment: 2.14 B.M.

2.5.3.1.5 [Cu(2.10)Cl$_2$]$_2$ (2.30)

Green solid (0.21 g, 75%). $C_{28}H_{40}Br_2Cl_4Cu_2N_{10}$: calcd. C 35.57, H 4.26, N 14.82%; found C 36.17, H 4.57, N 15.79%. IR (KBr): ν = 2932, 2855, 1611, 1481, 1451, 1411, 1289, 1229, 1162, 1008, 788 cm^{-1}. λ_{max} (MeOH) 840 nm, ε = 126 M^{-1}cm^{-1}. Magnetic moment: 2.31 B.M.

2.5.3.1.6 [Cu(2.11)Cl$_2$]$_2$ (2.31)

Green solid (0.20 g, 71%). $C_{28}H_{40}Br_2Cl_4Cu_2N_{10}$: calcd. C 35.57, H 4.26, N 14.82%; found C 36.17, H 4.42, N 15.19%. IR (KBr): ν = 2927, 2851, 1621, 1548, 1449, 1283, 1267, 1227, 1010, 796, 757 cm^{-1}. λ_{max} (MeOH) 808 nm, ε = 105 M^{-1}cm^{-1}. Magnetic moment: 2.37 B.M.

2.5.3.1.7 [Ni(2.6)Cl$_2$]$_2$ (2.32)

Dark green solid (0.12 g, 41%). $C_{18}H_{20}Br_2Cl_4Ni_2N_{10}$: calcd. C 27.18, H 2.53, N 17.61%; found C 26.41, H 3.06, N 16.97%. IR (KBr): ν = 2923, 2850, 1614, 1481, 1455, 1297, 1251, 1165, 1112, 1013, 793, 725 cm^{-1}. λ_{max} (MeOH) 348 nm, ε = 86 M^{-1}cm^{-1}. Magnetic moment: 3.19 B.M.

2.5.3.1.8 [Ni(2.7)Cl$_2$]$_2$ (2.33)

Pale green solid (0.14 g, 48%). $C_{18}H_{20}Br_2Cl_4Ni_2N_{10}$: calcd. C 27.18, H 2.53, N 17.61%; found C 27.64, H 3.06, N 17.69%. IR (KBr): ν = 2955, 2853, 1614, 1549, 1452, 1288, 1104, 1026, 806, 762 cm^{-1}. λ_{max} (MeOH) 384 nm, ε = 53 M^{-1}cm^{-1}. Magnetic moment: 3.15 B.M.

2.5.3.1.9 [Ni(2.8)Cl$_2$]$_2$ (2.34)

Pale green solid (0.15 g, 50%). $C_{20}H_{24}Br_2Cl_4Ni_2N_{10}$: calcd. C 29.17, H 2.94, N 17.01%; found C 28.28, H 3.34, N 16.78%. IR (KBr): ν = 2961, 2866, 1613, 1481, 1457, 1252, 1108, 1015, 794, 725 cm^{-1}. λ_{max} (MeOH) 376 nm, ε = 40 M^{-1}cm^{-1}. Magnetic moment: 2.83 B.M.

2.5.3.1.10 [Ni(2.9)Cl$_2$]$_2$ (2.35)

Pale green solid (0.14 g, 47%). $C_{20}H_{24}Br_2Cl_4Ni_2N_{10}$: calcd. C 29.17, H 2.94, N 17.01%; found C 28.49, H 3.51, N 16.24%. IR (KBr): ν = 2951, 2862, 1613, 1545, 1451, 1391, 1259, 1154, 1103, 1025, 805, 763 cm^{-1}. λ_{max} (MeOH) 380 nm, ε = 37 M^{-1}cm^{-1}. Magnetic moment: 3.56 B.M.

2.5.3.1.11 [Ni(2.1)Cl$_2$]$_2$ (2.36)

Pale green solid (0.12 g, 42%). $C_{24}H_{32}Br_2Cl_4Ni_2N_{10}$: calcd. C 32.77, H 3.67, N 15.92%; found C 31.65, H 3.74, N 14.88%. IR (KBr): ν = 2934, 2853, 1608, 1478, 1457, 1252, 1051, 1012, 799, 726 cm^{-1}. λ_{max} (MeOH) 376 nm, ε = 48 M^{-1}cm^{-1}.Magnetic moment: 3.94 B.M.

2.5.3.1.12 [Ni(2.2)Cl$_2$]$_2$ (2.37)

Pale green solid (0.10 g, 35%). $C_{24}H_{32}Br_2Cl_4Ni_2N_{10}$: calcd. C 32.77, H 3.67, N 15.92%; found C 32.45, H 4.16, N 15.80%. IR (KBr): ν = 2935, 2823, 1615, 1451, 1261, 1063, 1027, 801, 756, 731 cm^{-1}. λ_{max} (MeOH) 376 nm, ε = 92 M^{-1}cm^{-1}. Magnetic moment: 4.06 B.M.

2.5.3.1.13 [Ni(2.10)Cl$_2$]$_2$ (2.38)

Pale green solid (0.19 g, 70%). $C_{28}H_{40}Br_2Cl_4Ni_2N_{10}$: calcd. C 35.94, H 4.31, N 14.97%; found C 35.72, H 4.75, N 14.50%. IR (KBr): ν = 2929, 2856, 1606, 1478, 1459, 1436, 1255, 1105, 1014, 802, 725 cm^{-1}. λ_{max} (MeOH) 376 nm, ε = 46 M^{-1}cm^{-1}. Magnetic moment: 3.87 B.M.

2.5.3.1.14 [Ni(2.11)Cl$_2$]$_2$ (2.39)

Pale green solid (0.15 g, 55%). $C_{28}H_{40}Br_2Cl_4Ni_2N_{10}$: calcd. C 35.94, H 4.31, N 14.97%; found C 34.26, H 4.90, N 14.28%. IR (KBr): ν = 2930, 2857, 1614, 1452, 1259, 1156, 1025, 807, 732 cm^{-1}. λ_{max} (MeOH) 384 nm, ε = 194 M^{-1}cm^{-1}. Magnetic moment: 3.49 B.M.

2.5.3.1.15 [Co(2.6)$_2$(NCS)$_2$] (2.40)

Green solid (0.12 g, 45%). $C_{20}H_{20}Br_2CoN_{12}S_2$: calcd. C 33.77, H 2.83, N 23.63%; found C 33.40, H 2.64, N 22.64%. IR (KBr): ν = 2957, 2077, 1606, 1475, 1456, 1435, 1257, 1089, 1010. 788, 723 cm^{-1}. λ_{max}(MeOH) 504 nm, ε = 138 M^{-1}cm^{-1}. Magnetic moment: 5.47 B.M.

2.5.3.1.16 [Co(2.7)$_2$(NCS)$_2$] (2.41)

Green solid (0.15 g, 57%). $C_{20}H_{20}Br_2CoN_{12}S_2$: calcd. C 33.77, H 2.83, N 23.63%; found C 33.52, H 2.95, N 22.85%. IR (KBr): ν = 2958, 2855, 2069, 1612, 1449, 1435, 1260, 1062, 1025, 799, 752, 731 cm^{-1}. λ_{max}(MeOH) 504 nm, ε = 54 M^{-1}cm^{-1}. Magnetic moment: 5.52 B.M.

2.5.3.1.17 [Co(2.8)$_2$(NCS)$_2$] (2.42)

Green solid (0.16 g, 61%). $C_{22}H_{24}Br_2CoN_{12}S_2$: calcd. C 35.74, H 3.27, N 22.73%; found C 36.15, H 3.07, N 23.39%. IR (KBr): ν = 2931, 2855, 2077, 1606, 1456, 1437, 1259, 1103, 1012, 796, 726, 638 cm^{-1}. λ_{max}(MeOH) 516 nm, ε = 44 M^{-1}cm^{-1}. Magnetic moment: 4.82 B.M.

2.5.3.1.18 [Co(2.9)$_2$(NCS)$_2$] (2.43)

Green solid (0.10 g, 38%). $C_{22}H_{24}Br_2CoN_{12}S_2$: calcd. C 35.74, H 3.27, N 22.73%; found C 35.20, H 4.27, N 21.93%. IR (KBr): ν = 2920, 2855, 2069, 1612, 1449, 1387, 1258, 1099, 1025, 799, 753, 731 cm^{-1}. λ_{max}(MeOH) 512 nm, ε = 42 M^{-1}cm^{-1}. Magnetic moment: 4.66 B.M.

2.5.3.1.19 [Co(2.10)$_2$(NCS)$_2$] (2.44)

Rust coloured crystals (0.13 g, 52%). $C_{30}H_{40}Br_2CoN_{12}S_2$: calcd. C 42.31, H 4.73, N 19.74%; found C 41.35, H 4.36, N 19.89%. IR (KBr): ν = 2931, 2855, 2077, 1605, 1456, 1437, 1259, 1103, 1011, 795, 726, 638 cm^{-1}. λ_{max}(MeOH) 516 nm, ε = 32 M^{-1}cm^{-1}. Magnetic moment: 5.27 B.M.

2.5.3.1.20 [Co(2.11)$_2$(NCS)$_2$] (2.45)

Dark green crystals (0.16 g, 64%). $C_{30}H_{40}Br_2CoN_{12}S_2$: calcd. C 42.31, H 4.73, N 19.74%; found C 41.72, H 3.84, N 20.32%. IR (KBr): ν = 2928, 2854, 2069, 1610, 1447, 1281, 1114, 1024, 804, 755, 732 cm^{-1}. λ_{max}(MeOH) 508 nm, ε = 43 M^{-1}cm^{-1}. Magnetic moment: 4.97 B.M.

2.5.3.1.21 [Zn(2.6)Cl$_2$]$_2$ (2.46)

Waxy cream solid (0.17 g, 56%). $C_{18}H_{20}Br_2Cl_4Zn_2N_{10}$: calcd. C 26.73, H 2.49, N 17.32%; found C 26.72, H 2.53, N 16.96%. IR (KBr): ν = 2959, 2850, 2201, 1610, 1565, 1552, 1440, 1418, 1270, 1064, 1021, 896, 740 cm^{-1}. ^{1}H NMR (CDCl$_3$): δ = 8.77-8.79 (m, 1 H, pyr-H), 8.34-8.36 (m, 1 H, pyr-H), 7.92-7.97 (m, 1 H, pyr-H), 7.42-7.47 (m, 1 H, pyr-H), 5.18 (t, 2 H, J = 7.0 Hz, CH$_2$N), 3.49 (t, 2 H, J = 6.2 Hz, CH$_2$Br), 2.12-2.22 (m, 2 H, CH$_2$) ppm. ^{13}C NMR (CDCl$_3$): δ = 157.1 (CN$_4$), 149.5, 148.2, 138.6, 125.7, 124.9, 49.1 (CH$_2$N), 33.2 (CH$_2$Br), 29.4 ppm.

2.5.3.1.22 [Zn(2.7)Cl$_2$]$_2$ (2.47)

Waxy orange solid (0.12 g, 40%). $C_{18}H_{20}Br_2Cl_4Zn_2N_{10}$: calcd. C 26.73, H 2.49, N 17.32%; found C 26.32, H 2.67, N 16.60%. IR (KBr): ν = 2958, 2848, 2233, 1614, 1573, 1546, 1451, 1419, 1288, 1063, 1027, 912, 800, 730 cm^{-1}. ^{1}H NMR ($CDCl_3$): δ = 8.87-8.89 (m, 1 H, pyr-H), 8.28-8.30 (m, 1 H, pyr-H), 8.14-8.19 (m, 1 H, pyr-H), 7.73-7.78 (m, 1 H, pyr-H), 5.01 (t, 2 H, *J* = 6.8 Hz, CH_2N), 3.51 (t, 2 H, *J* = 6.0 Hz, CH_2Br), 2.68-2.74 (m, 2 H, CH_2) ppm. ^{13}C NMR ($CDCl_3$): δ = 161.8 (CN_4), 149.8, 141.8, 141.1, 128.2, 123.0, 52.3 (CH_2N), 40.7(CH_2Br), 31.4 ppm.

2.5.3.1.23 [Zn(2.8)Cl$_2$]$_2$ (2.48)

Waxy orange solid (0.17 g, 59%). $C_{20}H_{24}Br_2Cl_4Zn_2N_{10}$: calcd. C 28.70, H 2.89, N 16.74%; found C 28.34, H 2.25, N 16.68%. IR (KBr): ν = 2949, 2870, 1610, 1481, 1458, 1441, 1252, 1168, 1010, 794, 748, 724 cm^{-1}. ^{1}H NMR ($CDCl_3$): δ = 8.77-8.79 (m, 1 H, pyr-H), 8.34-8.38 (m, 1 H, pyr-H), 7.92-7.98 (m, 1 H, pyr-H), 7.48-7.52 (m, 1 H, pyr-H), 5.02 (t, 2 H, *J* = 7.0 Hz, CH_2N), 3.57 (t, 2 H, *J* = 6.4 Hz, CH_2Br), 2.01-2.05 (m, 2 H, CH_2), 1.93-1.99 (m, 2 H, CH_2) ppm. ^{13}C NMR ($CDCl_3$): δ = 159.1 (CN_4), 149.5, 147.1, 137.6, 125.4, 124.6, 48.8 (CH_2N), 32.5 (CH_2Br), 29.2, 29.1 ppm.

2.5.3.1.24 [Zn(2.9)Cl$_2$]$_2$ (2.49)

Cream solid (0.15 g, 51%). $C_{20}H_{24}Br_2Cl_4Zn_2N_{10}$: calcd. C 28.70, H 2.89, N 16.74%; found C 28.37, H 2.92, N 16.20%. IR (KBr): ν = 2957, 2870, 1614, 1572, 1548, 1452, 1395, 1285, 1064, 1028, 800, 753, 729 cm^{-1}. ^{1}H NMR ($CDCl_3$): δ = 8.95-8.97 (m, 1 H, pyr-H), 8.26-8.32 (m, 1 H, pyr-H), 8.20-8.26 (m, 1 H, pyr-H), 7.81-7.86 (m, 1 H, pyr-H), 4.88 (t, 2 H, *J* = 7.0 Hz, CH_2N), 3.47 (t, 2 H, *J* = 6.2 Hz, CH_2Br), 2.28-2.38 (m, 2 H, CH_2), 1.94-2.04 (m, 2 H, CH_2) ppm. ^{13}C NMR ($CDCl_3$): δ = 161.7 (CN_4), 149.7, 141.7, 141.3, 128.3, 122.9, 54.6 (CH_2N), 43.7 (CH_2Br), 32.1, 29.0 ppm.

2.5.3.1.25 [Zn(2.1)Cl$_2$]$_2$ (2.50)

Waxy cream solid (0.17 g, 60%). $C_{24}H_{32}Br_2Cl_4Zn_2N_{10}$: calcd. C 32.28, H 3.61, N 15.69%; found C 33.01, H 4.00, N 15.12%. IR (KBr): ν = 2931, 2857, 1610, 1543, 1482, 1459, 1249, 1108, 1010, 793, 724 cm^{-1}. ^{1}H NMR ($CDCl_3$): δ = 8.91-8.92 (m, 1 H, pyr-H), 8.28-8.31 (m, 1 H, pyr-H), 8.03-8.08 (m, 1 H, pyr-H), 7.59-7.63 (m, 1 H, pyr-H), 4.92 (t, 2 H, *J* = 7.2 Hz, CH_2N), 3.42 (t, 2 H, *J* = 6.7 Hz, CH_2Br), 1.98-2.07 (m, 2 H, CH_2), 1.83-1.95 (m, 2 H, CH_2), 1.43-1.52 (m, 4 H, CH_2) ppm. ^{13}C NMR ($CDCl_3$): δ = 151.5 (CN_4), 150.0, 143.3, 138.5, 126.3, 124.6, 62.8 (CH_2N), 49.7 (CH_2Br), 33.6, 32.3, 29.3, 27.9 ppm.

2.5.3.1.26 [Zn(2.2)Cl_2]$_2$ (2.51)

Waxy cream solid (0.14 g, 49%). $C_{24}H_{32}Br_2Cl_4Zn_2N_{10}$: calcd. C 32.28, H 3.61, N 15.69%; found C 32.45, H 3.68, N 15.34%. IR (KBr): ν = 2939, 2862, 2231, 1614, 1573, 1451, 1287, 1262, 1063, 1048, 913, 801, 731 cm^{-1}. ^{1}H NMR ($CDCl_3$): δ = 8.84-8.87 (m, 1 H, pyr-H), 8.26-8.30 (m, 1 H, pyr-H), 8.15-8.20 (m, 1 H, pyr-H), 7.74-7.79 (m, 1 H, pyr-H), 4.81 (t, 2 H, J = 7.1 Hz, CH_2N), 3.41 (t, 2 H, J = 6.5 Hz, CH_2Br), 2.12-2.22 (m, 2 H, CH_2), 1.84-1.95 (m, 2 H, CH_2), 1.50-1.56 (m, 4 H, CH_2) ppm. ^{13}C NMR ($CDCl_3$): δ = 162.48 (CN_4), 149.9, 143.2, 140.1, 127.2, 122.7, 54.8 (CH_2N), 44.8, 32.1, 29.2, 25.5, 25.4 ppm.

2.5.3.1.27 [Zn(2.10)Cl_2]$_2$ (2.52)

Sticky orange oil (0.14 g, 50%). $C_{28}H_{40}Br_2Cl_4Zn_2N_{10}.2H_2O$: calcd. C 34.14, H 4.50, N 14.22%; found C 34.11, H 5.08, N 13.53%. IR (neat): ν = 2932, 2856, 1654, 1589, 1465, 1433, 1390, 1253, 1119, 798, 744 cm^{-1}. ^{1}H NMR ($CDCl_3$): δ = 8.75-8.76 (m, 1 H, pyr-H), 8.30-8.33 (m, 1 H, pyr-H), 7.95-7.99 (m, 1 H, pyr-H), 7.47-7.52 (m, 1 H, pyr-H), 4.96 (t, 2 H, J = 7.3 Hz, CH_2N), 3.38 (t, 2 H, J = 6.2 Hz, CH_2Br), 1.92-1.96 (m, 2 H, CH_2), 1.76-1.85 (m, 2 H, CH_2), 1.27-1.35 (m, 8 H, CH_2) ppm. ^{13}C NMR ($CDCl_3$): δ = 151.7 (CN_4), 149.6, 144.1, 137.9, 125.7, 124.6, 49.7 (CH_2N), 37.5 (CH_2Br), 32.7, 29.6, 28.8, 28.5, 27.9, 26.6 ppm.

2.5.3.1.28 [Zn(2.11)Cl_2]$_2$ (2.53)

Cream solid (0.15 g, 53%). $C_{28}H_{40}Br_2Cl_4Zn_2N_{10}$: calcd. C 35.43, H 4.25, N 14.76%; found C 34.91, H 4.22, N 14.21%. IR (KBr): ν = 2926, 2855, 1613, 1572, 1546, 1453, 1395, 1260, 1063, 1027, 804, 756, 731 cm^{-1}. ^{1}H NMR ($CDCl_3$): δ = 8.88-8.89 (m, 1 H, pyr-H), 8.28-8.33 (m, 1 H, pyr-H), 8.19-8.25 (m, 1 H, pyr-H), 7.79-7.83 (m, 1 H, pyr-H), 4.81 (t, 2 H, J = 7.1 Hz, CH_2N), 3.40 (t, 2 H, J = 6.7 Hz, CH_2Br), 2.11-2.16 (m, 2 H, CH_2), 1.80-1.90 (m, 2 H, CH_2), 1.38-1.43 (m, 8 H, CH_2) ppm. ^{13}C NMR ($CDCl_3$): δ = 161.7 (CN_4), 149.8, 142.0, 141.2, 128.1, 122.9, 55.2 (CH_2N), 45.1 (CH_2Br), 34.0, 32.4, 28.9, 27.9, 26.6, 26.1 ppm.

2.5.4 Synthesis of Alkyl Chain Pyridyl Tetrazoles

2.5.4.1 Synthesis of Ligands

Synthesis of alkyl chain functionalised pyridyl tetrazoles **2.12-2.17** was achieved *via* methods outlined in section 2.5.2. Alkylation was carried out using 1-bromobutane, 1-bromohexane and 1-bromooctane.

2.5.4.1.1 2-(1-butyl-1*H*-tetrazol-5-yl)pyridine (2.12)

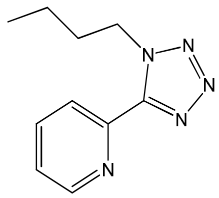

Brown oil (0.85 g, 31%). IR (neat): ν = 2961, 2934, 2874, 1591, 1571, 1532, 1471, 1433, 1409, 1380, 1287, 1121, 1085, 1037, 994, 798, 744 cm^{-1}. ^{1}H NMR ($CDCl_3$): δ = 8.72-7.74 (m, 1 H, pyr-H), 8.35-8.37 (m, 1 H, pyr-H), 7.88-7.93 (m, 1 H, pyr-H), 7.42-7.47 (m, 1 H, pyr-H), 4.99 (t, 2 H, J = 7.3 Hz, CH_2N), 1.89-1.99 (m, 2 H, CH_2), 1.35-1.43 (m, 2 H, CH_2), 0.95 (t, 3 H, J = 7.3 Hz, CH_3) ppm. ^{13}C NMR ($CDCl_3$): δ = 151.7 (CN_4), 149.4, 145.1, 137.4, 125.2, 124.6, 49.4 (CH_2N), 31.9, 19.5, 13.4 ppm. ESI-HRMS: calcd. for $C_{10}H_{13}N_5Na$ $[M+Na]^+$ 226.1069, found 226.1063.

2.5.4.1.2 2-(2-butyl-2*H*-tetrazol-5-yl)pyridine (2.13)

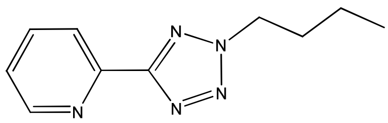

Yellow oil (0.61 g, 22%). IR (neat): ν = 2961, 2935, 2874, 1594, 1571, 1466, 1432, 1419, 1387, 1356, 1156, 1043, 804, 747 cm^{-1}. ^{1}H NMR ($CDCl_3$): δ = 8.78-8.79 (m, 1 H, pyr-H), 8.24-8.26 (m, 1 H, pyr-H), 7.83-7.89 (m, 1 H, pyr-H), 7.37-7.41 (m, 1 H, pyr-H), 4.71 (t, 2 H, J = 7.1 Hz, CH_2N), 2.04-2.11 (m, 2 H, CH_2), 1.37-1.45 (m, 2 H, CH_2), 0.97 (t, 3 H, J = 7.3 Hz, CH_3) ppm. ^{13}C NMR ($CDCl_3$): δ = 164.7 (CN_4), 150.3, 146.9, 137.0, 124.7, 122.3, 53.2 (CH_2N), 31.3, 19.6, 13.3 ppm. ESI-HRMS: calcd. for $C_{10}H_{14}N_5$ $[M+H]^+$ 204.1244, found 204.1248.

2.5.4.1.3 2-(1-hexyl-1*H*-tetrazol-5-yl)pyridine (2.14)

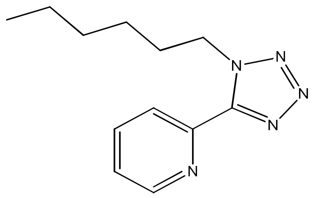

Brown oil (0.43 g, 14%). IR (neat): ν = 2987, 2929, 2858, 2305, 1592, 1434, 1421, 1265, 896, 744, 705 cm^{-1}. ^{1}H NMR ($CDCl_3$): δ = 8.71-8.73 (m, 1 H, pyr-H), 8.35-8.37 (m, 1 H, pyr-H), 7.87-7.93 (m, 1 H, pyr-H), 7.42-7.46 (m, 1 H, pyr-H), 4.97 (t, 2 H, J = 7.3 Hz, CH_2N), 1.90-1.99 (m, 2 H, CH_2), 1.25-1.35 (m, 6 H, CH_2), 0.87 (t, 3 H, J = 7.1 Hz, CH_3) ppm. ^{13}C NMR ($CDCl_3$): δ = 151.6 (CN_4), 149.4, 145.1, 137.4, 125.2, 124.5, 49.6 (CH_2N), 31.1, 29.8, 25.9, 22.3, 13.9 ppm. ESI-HRMS: calcd. for $C_{12}H_{18}N_5$ $[M+H]^+$ 232.1557, found 232.1557.

2.5.4.1.4 2-(2-hexyl-2*H*-tetrazol-5-yl)pyridine (2.15)

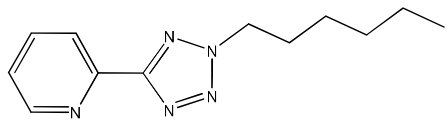

Yellow oil (0.54 g, 17%). IR (neat): ν = 2957, 2929, 2858, 2305, 1595, 1466, 1434, 1420, 1265, 802, 738, 704 cm^{-1}. ^{1}H NMR ($CDCl_3$): δ = 8.77-8.80 (m, 1 H, pyr-H), 8.24-8.27 (m, 1 H, pyr-H), 7.83-7.89 (m, 1 H, pyr-H), 7.37-7.42 (m, 1 H, pyr-H), 4.70 (t, 2 H, J = 7.2 Hz, CH_2N), 2.07-2.14 (m, 2 H, CH_2), 1.25-1.34 (m, 6 H, CH_2), 0.88 (t, 3 H, J = 7.1 Hz, CH_3) ppm. ^{13}C NMR ($CDCl_3$): δ = 164.7 (CN_4), 150.3, 146.9, 137.0, 124.7, 122.3, 53.5 (CH_2N), 31.0, 29.3, 26.0, 22.3, 13.9 ppm. ESI-HRMS: calcd. for $C_{12}H_{18}N_5$ $[M+H]^+$ 232.1557, found 232.1568.

2.5.4.1.5 2-(1-octyl-1*H*-tetrazol-5-yl)pyridine (2.16)

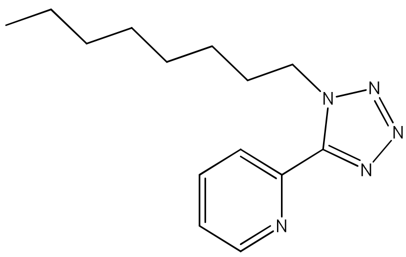

Brown oil (0.82 g, 23%). IR (neat): ν = 2956, 2927, 2856, 1591, 1467, 1433, 1377, 1120, 1036, 797, 743, 730 cm^{-1}. ^{1}H NMR ($CDCl_3$): δ = 8.71-8.74 (m, 1 H, pyr-H), 8.34-8.38 (m, 1 H, pyr-H), 7.87-7.93 (m, 1 H, pyr-H), 7.42-7.47 (m, 1 H, pyr-H), 4.97 (t, 2 H, J = 7.3 Hz, CH_2N), 1.83-1.97 (m, 2 H, CH_2), 1.25-1.30 (m, 10 H, CH_2), 0.86 (t, 3 H, J = 6.9 Hz, CH_3) ppm.

^{13}C NMR ($CDCl_3$): δ = 151.6 (CN_4), 149.4, 145.1, 137.3, 125.2, 124.5, 49.6 (CH_2N), 31.7, 29.8, 29.1, 28.9, 26.2, 22.5, 14.0 ppm. ESI-HRMS: calcd. for $C_{14}H_{22}N_5$ $[M+H]^+$ 260.1870, found 260.1881.

2.5.4.1.6 2-(2-octyl-2*H*-tetrazol-5-yl)pyridine (2.17)

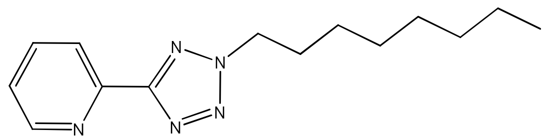

Yellow oil (0.76 g, 22%). IR (neat): ν = 2985, 2927, 2856, 1593, 1571, 1522, 1466, 1432, 1419, 1386, 1356, 1158, 1043, 1015, 803, 746, 726 cm^{-1}. ^1H NMR ($CDCl_3$): δ = 8.77-8.79 (m, 1 H, pyr-H), 8.23-8.27 (m, 1 H, pyr-H), 7.83-7.89 (m, 1 H, pyr-H), 7.37-7.41 (m, 1 H, pyr-H), 4.70 (t, 2 H, J = 7.1 Hz, CH_2N), 2.07-2.12 (m, 2 H, CH_2), 1.23-1.34 (m, 10 H, CH_2), 0.86 (t, 3 H, J = 6.9 Hz, CH_3) ppm. ^{13}C NMR ($CDCl_3$): δ = 164.7 (CN_4), 150.3, 146.9, 137.0, 124.7, 122.3, 53.5 (CH_2N), 31.6, 29.3, 28.9, 28.8 26.2, 22.5, 14.0 ppm. ESI-HRMS: calcd. for $C_{14}H_{21}N_5[M+Na]^+$ 282.1689, found 282.1699.

2.5.5 Metal Complexation Reactions with Alkyl Pyridyl Tetrazoles

2.5.5.1 General Procedure for Metal Complexation Reactions

The attainment of metal complexes was achieved using the same methods utilised in section 2.5.3.

2.5.5.1.1 [Cu(2.12)Cl2]2 (2.54)

Green solid (0.17 g, 51%). $C_{20}H_{26}Cl_4Cu_2N_{10}$: calcd. C 35.57, H 3.88, N 20.74%; found C 35.39, H 3.92, N 20.27%. IR (KBr): ν = 2961, 2868, 1614, 1546, 1482, 1457, 1437, 1378, 1251, 1166, 1049, 1003, 719 cm^{-1}. λ_{max} (MeOH) 836 nm, ε = 110 $M^{-1}cm^{-1}$. Magnetic moment: 2.06 B.M.

2.5.5.1.2 [Cu(2.13)Cl2]2 (2.55)

Green solid (0.12 g, 36%). $C_{20}H_{26}Cl_4Cu_2N_{10}$: calcd. C 35.57, H 3.88, N 20.74%; found C 35.63, H 4.05, N 20.45%. IR (KBr): ν = 2961, 2880, 1619, 1609, 1552, 1461, 1449, 1352, 1269, 1100, 1026, 799, 758, 724 cm^{-1}. λ_{max} (MeOH) 808 nm, ε = 115 $M^{-1}cm^{-1}$. Magnetic moment: 1.98 B.M.

2.5.5.1.3 [Cu(2.14)Cl$_2$]$_2$ (2.56)

Green solid (0.11 g, 35%). $C_{24}H_{34}Cl_4Cu_2N_{10}$: calcd. C 39.41, H 4.68, N 19.15%; found C 39.23, H 4.75, N 18.66%. IR (KBr): ν = 2955, 2927, 2872, 1611, 1541, 1482, 1455, 1382, 1112, 1050, 1008, 792, 751, 719 cm^{-1}. λ_{max} (MeOH) 840 nm, ε = 111 M^{-1}cm^{-1}. Magnetic moment: 2.00 B.M.

2.5.5.1.4 [Cu(2.15)Cl$_2$]$_2$ (2.57)

Green solid (0.12 g, 38%). $C_{24}H_{34}Cl_4Cu_2N_{10}$: calcd. C 39.41, H 4.68, N 19.15%; found C 39.20, H 4.76, N 18.87%. IR (KBr): ν = 2953, 2925, 2858, 1617, 1551, 1450, 1354, 1284, 1103, 1025, 801, 757, 726 cm^{-1}. λ_{max} (MeOH) 812 nm, ε = 129 M^{-1}cm^{-1}. Magnetic moment: 2.04 B.M.

2.5.5.1.5 [Cu(2.16)Cl$_2$]$_2$ (2.58)

Green solid (0.13 g, 43%). $C_{28}H_{42}Cl_4Cu_2N_{10}$: calcd. C 42.70, H 5.37, N 17.78%; found C 41.66, H 5.39, N 17.53%. IR (KBr): ν = 2955, 2924, 2857, 1611, 1540, 1482, 1446, 1384, 1113, 1049, 1007, 792, 748, 719 cm^{-1}. λ_{max} (MeOH) 832 nm, ε = 114 M^{-1}cm^{-1}. Magnetic moment: 1.81 B.M.

2.5.5.1.6 [Cu(2.17)Cl$_2$]$_2$ (2.59)

Green solid (0.10 g, 33%). $C_{28}H_{42}Cl_4Cu_2N_{10}$: calcd. C 42.70, H 5.37, N 17.78%; found C 43.61, H 5.39, N 17.24%. IR (KBr): ν = 2955, 2923, 2850, 1616, 1537, 1466, 1454, 1432, 1360, 1285, 1158, 1014, 801, 765, 726 cm^{-1}. λ_{max} (MeOH) 812 nm, ε = 86 M^{-1}cm^{-1}. Magnetic moment: 2.18 B.M.

2.5.5.1.7 [Ni(2.12)Cl$_2$]$_2$ (2.60)

Green solid (0.29 g, 80%). $C_{20}H_{26}Cl_4N_{10}Ni_2.4H_2O$: calcd. C 32.54, H 4.65, N 18.99%; found C 32.97, H 4.76, N 19.01%. IR (KBr): ν = 2960, 2934, 2873, 1615, 1478, 1457, 1393, 1287, 1224, 1100, 1063, 1027, 802, 758, 732 cm^{-1}. λ_{max} (MeOH) 392 nm, ε = 25 M^{-1}cm^{-1}. Magnetic moment: 3.17 B.M.

2.5.5.1.8 [Ni(2.13)Cl$_2$]$_2$ (2.61)

Pale green solid (0.20 g, 56%). $C_{20}H_{26}Cl_4N_{10}Ni_2.4H_2O$: calcd. C 32.54, H 4.65, N 18.99%; found C 32.71, H 4.69, N 18.87%. IR (KBr): ν = 2961, 2934, 2873, 1611, 1479, 1457, 1294, 1254, 1162, 1050, 1010, 795, 752, 727 cm^{-1}. λ_{max} (MeOH) 392 nm, ε = 19 M^{-1}cm^{-1}. Magnetic moment: 2.91 B.M.

2.5.5.1.9 [Ni(2.14)Cl_2]$_2$ (2.62)

Green solid (0.22 g, 71%)). $C_{24}H_{34}Cl_4Ni_2N_{10}$ .4H_2O: calcd. C 36.31, H 5.33, N 17.64%; found C 36.45, H 5.87, N 17.27%. IR (KBr): ν = 2955, 2926, 2856, 1642, 1613, 1479, 1456, 1415, 1378, 1294, 1253, 1163, 1108, 1012, 796, 752 cm^{-1}. λ_{max} (MeOH) 404 nm, ε = 31 M^{-1}cm^{-1}. Magnetic moment: 3.17 B.M.

2.5.5.1.10 [Ni(2.15)Cl_2]$_2$ (2.63)

Green solid (0.29 g, 93%). $C_{24}H_{34}Cl_4Ni_2N_{10}$.4$H_2O$: calcd. C 36.31, H 5.33, N 17.64%; found C 36.85, H 5.23, N 16.64%. IR (KBr): ν = 2954, 2926, 2856, 1614, 1461, 1452, 1392, 1354, 1286, 1261, 1225, 1157, 1100, 1047, 1063, 1026, 804, 759, 732 cm^{-1}. λ_{max} (MeOH) 400 nm, ε = 17 M^{-1}cm^{-1}. Magnetic moment: 4.27 B.M.

2.5.5.1.11 [Ni(2.16)Cl_2]$_2$ (2.64)

Green solid (0.18 g, 60%). $C_{28}H_{42}Cl_4Ni_2N_{10}$.4$H_2O$: calcd. C 39.55, H 5.93, N 16.48%; found C 39.08, H 5.41, N 12.65%. IR (KBr): ν = 2955, 2925, 2855, 1611, 1479, 1456, 1377, 1254, 1162, 1049, 1012, 797, 752 cm^{-1}. λ_{max} (MeOH) 396 nm, ε = 45 M^{-1}cm^{-1}. Magnetic moment: 4.24 B.M.

2.5.5.1.12 [Ni(2.17)Cl_2]$_2$ (2.65)

Pale green solid (0.21 g, 70%). $C_{28}H_{42}Cl_4Ni_2N_{10}$.2$H_2O$: calcd. C 41.30, H 5.70, N 17.21%; found C 41.05, H 6.11, N 17.25%. IR (KBr): ν = 2955, 2925, 2855, 1615, 1461, 1452, 1392, 1286, 1262, 1226, 1101, 1047, 1063, 1027, 802, 758, 732 cm^{-1}. λ_{max} (MeOH) 396 nm, ε = 21 M^{-1}cm^{-1}. Magnetic moment: 4.37 B.M.

2.5.5.1.13 Co(2.12)$_2$(NCS)$_2$ (2.66)

Green crystalline solid (0.15 g, 53%). $C_{22}H_{26}CoN_{12}S_2$: calcd. C 45.43, H 4.51, N 28.90%; found C 46.15, H 3.74, N 28.43%. IR (KBr): ν = 2960, 2876, 2068, 1609, 1478, 1456, 1291, 1251, 1160, 1045, 1007, 792, 746 cm^{-1}. λ_{max} (MeOH) 520 nm, ε = 40 M^{-1}cm^{-1}. Magnetic moment: 5.43 B.M.

2.5.5.1.14 Co(2.13)$_2$(NCS)$_2$ (2.67)

Rust coloured crystals (0.19 g, 67%). $C_{22}H_{26}CoN_{12}S_2$: calcd. C 45.43, H 4.51, N 28.90%; found C 45.76, H 4.67, N 28.78%. IR (KBr): ν = 2959, 2873, 2077, 1610, 1458, 1447, 1375, 1285, 1256, 1153, 1059, 1046, 802, 754 cm^{-1}. λ_{max} (MeOH) 508 nm, ε = 50 M^{-1}cm^{-1}. Magnetic moment: 5.32 B.M.

2.5.5.1.15 Co(2.14)$_2$(NCS)$_2$ (2.68)

Green crystalline solid (0.18 g, 66%). $C_{26}H_{34}CoN_{12}S_2$: calcd. C 48.97, H 5.37, N 26.36%; found C 49.48, H 6.21, N 25.88%. IR (KBr): ν = 2925, 2854, 2067, 1609, 1476, 1456, 1293, 1106, 1008, 793, 745, 725 cm^{-1}. λ_{max} (MeOH) 520 nm, ε = 56 M^{-1}cm^{-1}. Magnetic moment: 5.05 B.M.

2.5.5.1.16 Co(2.15)$_2$(NCS)$_2$ (2.69)

Rust coloured crystals (0.17 g, 63%). $C_{26}H_{34}CoN_{12}S_2.CH_3OH$: calcd. C 48.42, H 5.72, N 25.11%; found C 48.80, H 6.02, N 24.28%. IR (KBr): ν = 2922, 2852, 2074, 1609, 1459, 1447, 1372, 1154, 1099, 1046, 1025, 802, 756 cm^{-1}. λ_{max} (MeOH) 508 nm, ε = 49 M^{-1}cm^{-1}. Magnetic moment: 3.96 B.M.

2.5.5.1.17 Co(2.16)$_2$(NCS)$_2$ (2.70)

Orange crystalline solid (0.15 g, 58%). $C_{30}H_{42}CoN_{12}S_2.CH_3OH$: calcd. C 51.29, H 6.39, N 23.17%; found C 50.71, H 5.95, N 23.33%. IR (KBr): ν = 2925, 2854, 2068, 1610, 1476, 1457, 1412, 1161, 1010, 789, 725 cm^{-1}. λ_{max} (MeOH) 516 nm, ε = 55 M^{-1}cm^{-1}. Magnetic moment: 6.75 B.M.

2.5.5.1.18 Co(2.17)$_2$(NCS)$_2$ (2.71)

Rust coloured crystals (0.17 g, 65%). $C_{30}H_{42}CoN_{12}S_2$: calcd. C 51.93, H 6.10, N 24.23%; found C 51.47, H 6.11, N 24.09%. IR (KBr): ν = 2923, 2852, 2074, 1609, 1541, 1447, 1389, 1258, 1154, 1099, 1046, 1024, 801, 756 cm^{-1}. λ_{max} (MeOH) 508 nm, ε = 50 M^{-1}cm^{-1}. Magnetic moment: 5.10 B.M.

2.5.5.1.19 [Zn(2.12)Cl$_2$]$_2$ (2.72)

Orange solid (0.21 g, 72%). $C_{20}H_{26}Cl_4Zn_2N_{10}.H_2O$: calcd. C 34.44, H 4.05, N 20.09%; found C 34.13, H 4.30, N 19.49%. IR (KBr): ν = 2961, 2873, 1609, 1535, 1482, 1459, 1445, 1379, 1301, 1252, 1168, 1110, 1049, 1012, 800, 753, 725 cm^{-1}. ^{1}H NMR ($CDCl_3$): δ = 8.99-9.01 (m, 1 H, pyr-H), 8.20-8.22 (m, 1 H, pyr-H), 8.11-8.13 (m, 1 H, pyr-H), 7.69-7.70 (m, 1 H, pyr-H), 4.86 (t, 2 H, J = 7.3 Hz, CH_2N), 1.95-2.02 (m, 2 H, CH_2), 1.41-1.49 (m, 2 H, CH_2), 0.99 (t, 3 H, J = 7.3 Hz, CH_3) ppm. ^{13}C NMR ($CDCl_3$): δ = 150.0 (CN_4), 149.1, 145.1, 138.0, 125.8, 124.4, 49.5 (CH_2N), 31.7, 19.6, 13.4 ppm.

2.5.5.1.20 [Zn(2.13)Cl$_2$]$_2$ (2.73)

White solid (0.19 g, 66%). $C_{20}H_{26}Cl_4Zn_2N_{10}$: calcd. C 35.37, H 3.86, N 20.63%; found C 34.88, H 3.97, N 20.15%. IR (KBr): ν = 2963, 2875, 1614, 1573, 1547, 1453, 1394, 1288, 1259, 1063, 1046, 1028, 804, 757 cm^{-1}. ^{1}H NMR ($CDCl_3$): δ = 8.93-8.95 (m, 1 H, pyr-H), 8.26-8.29 (m, 1 H, pyr-H), 8.06-8.11 (m, 1 H, pyr-H), 7.64-7.69 (m, 1 H, pyr-H), 4.75 (t, 2 H, J = 7.2 Hz, CH_2N), 2.04-2.11 (m, 2 H, CH_2), 1.38-1.45 (m, 2 H, CH_2), 0.98 (t, 3 H, J = 7.3 Hz, CH_3) ppm. ^{13}C NMR ($CDCl_3$): δ = 161.4 (CN_4), 149.8, 141.6, 141.5, 128.3, 122.8, 55.1 (CH_2N), 30.9, 19.5, 13.3 ppm.

2.5.5.1.21 [Zn(2.14)Cl$_2$]$_2$ (2.74)

Orange solid (0.30 g, 83%). $C_{24}H_{34}Cl_4Zn_2N_{10}.3H_2O$: calcd. C 36.50, H 5.11, N 17.75%; found C 36.77, H 5.56, N 17.30%. IR (KBr): ν = 2955, 2927, 2856, 1610, 1480, 1460, 1433, 1377, 1164, 1051, 1013, 796, 747, 724 cm^{-1}. ^{1}H NMR ($CDCl_3$): δ = 9.03-9.04 (m, 1 H, pyr-H), 8.24-8.27 (m, 1 H, pyr-H), 8.18-8.21 (m, 1 H, pyr-H), 7.73-7.77 (m, 1 H, pyr-H), 4.81 (t, 2 H, J = 7.3 Hz, CH_2N), 1.95-2.04 (m, 2 H, CH_2), 1.28-1.36 (m, 6 H, CH_2), 0.86 (t, 3 H, J = 6.9 Hz, CH_3) ppm. ^{13}C NMR ($CDCl_3$): δ = 151.4 (CN_4), 150.7, 140.7, 140.2, 128.0, 125.0, 50.6 (CH_2N), 31.6, 29.0, 26.3, 22.5, 14.0 ppm.

2.5.5.1.22 [Zn(2.15)Cl$_2$]$_2$ (2.75)

White solid (0.26 g, 72%). $C_{24}H_{34}Cl_4Zn_2N_{10}.2CH_3OH$: calcd. C 39.05, H 5.30, N 17.53%; found C 38.18, H 5.30, N 16.81%. IR (KBr): ν = 2925, 2855, 1653, 1613, 1573, 1547, 1454, 1395, 1286, 1260, 1161, 1102, 1063, 1046, 1027, 804, 756, 731 cm^{-1}. ^{1}H NMR ($CDCl_3$): δ = 9.01-9.03 (m, 1 H, pyr-H), 8.33-8.37 (m, 1 H, pyr-H), 8.15-8.17 (m, 1 H, pyr-H), 7.90-7.94 (m, 1 H, pyr-H), 4.82 (t, 2 H, J = 7.1 Hz, CH_2N), 2.10-2.15 (m, 2 H, CH_2), 1.27-1.38 (m, 6 H, CH_2), 0.87 (t, 3 H, J = 7.1 Hz, CH_3) ppm. ^{13}C NMR ($CDCl_3$): δ = 161.1 (CN_4), 149.7, 142.0, 141.3, 128.7, 123.0, 55.5 (CH_2N), 31.6, 28.8, 26.2, 22.5, 14.0 ppm.

2.5.5.1.23 [Zn(2.16)Cl$_2$]$_2$ (2.76)

Orange solid (0.20 g, 86%). $C_{28}H_{42}Cl_4Zn_2N_{10}.4H_2O$: calcd. C 38.93, H 5.84, N 16.23%; found C 37.95, H 5.78, N 15.25%. IR (KBr): ν = 2955, 2927, 2856, 1610, 1481, 1460, 1377, 1297, 1051, 1012, 795, 747, 724 cm^{-1}. ^{1}H NMR (CDCl$_3$): δ = 9.10-9.11 (m, 1 H, pyr-H), 8.17-8.19 (m, 2 H, pyr-H), 7.75-7.79 (m, 1 H, pyr-H), 4.78 (t, 2 H, *J* = 7.3 Hz, CH$_2$N), 2.00-2.05 (m, 2 H, CH$_2$), 1.27-1.38 (m, 10 H, CH$_2$), 0.88 (t, 3 H, *J* = 6.9 Hz, CH$_3$) ppm. ^{13}C NMR (CDCl$_3$): δ = 151.2 (CN$_4$), 151.1, 141.7, 138.8, 128.7, 125.2, 50.8 (CH$_2$N), 31.6, 29.0, 28.9, 28.8, 26.4, 22.6, 14.0 ppm.

2.5.5.1.24 [Zn(2.17)Cl$_2$]$_2$ (2.77)

White solid (0.16 g, 70%). $C_{28}H_{42}Cl_4Zn_2N_{10}$: calcd. C 42.50, H 5.35, N 17.70%; found C 42.86, H 6.23, N 18.35%. IR (KBr): ν = 2926, 2854, 1610, 1571, 1543, 1452, 1393, 1285, 1259, 1158, 1099, 1061, 1045, 1025, 805, 757, 732 cm^{-1}. ^{1}H NMR (CDCl$_3$): δ = 8.86-8.87 (m, 1 H, pyr-H), 8.26-8.29 (m, 1 H, pyr-H), 8.08-8.13 (m, 1 H, pyr-H), 7.66-7.71 (m, 1 H, pyr-H), 4.76 (t, 2 H, *J* = 7.2 Hz, CH$_2$N), 2.07-2.14 (m, 2 H, CH$_2$), 1.28-1.32 (m, 10 H, CH$_2$), 0.88 (t, 3 H, *J* = 6.8 Hz, CH$_3$) ppm. ^{13}C NMR (CDCl$_3$): δ = 162.3 (CN$_4$), 149.9, 143.2, 140.1, 127.2, 122.6, 54.8 (CH$_2$N), 31.6, 29.1, 28.9, 28.7 26.2, 22.5, 14.0 ppm.

2.5.6 Synthesis of Alcohol Pyridyl Tetrazoles

2.5.6.1 Synthesis of Ligands

Access to alkyl alcohol functionalised pyridyl tetrazoles was achieved through similar methods outlined in 2.5.2. Column chromatography was carried out using DCM:EtOAc (1:1) as the mobile phase. The alkylating agents used were 3-bromo-1-propanol, 4-bromo-1-butanol, 6-bromo-1-hexanol or 8-bromo-1-octanol.

2.5.6.1.1 3-(5-(pyridin-2-yl)-1*H*-tetrazol-1-yl)propan-1-ol (2.18)

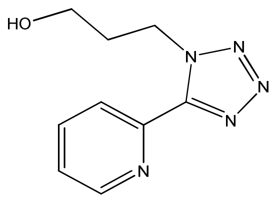

White solid (0.68 g, 24%). m.p. 45-48 °C. IR (KBr): ν = 3316, 2938, 2885, 1591, 1473, 1435, 1131, 1122, 1059, 1038, 993, 806, 749 cm^{-1}. ^{1}H NMR (CDCl$_3$): δ = 8.72-8.76 (m, 1 H, pyr-H), 8.35-8.39 (m, 1 H, pyr-H), 7.95-8.02 (m, 1 H, pyr-H), 7.51-7.55 (m, 1 H, pyr-H), 5.01 (t, 2 H, *J* = 6.2 Hz, CH$_2$N), 3.88 (t, 1 H, *J* = 6.7 Hz, OH), 3.54-3.60 (m, 2 H, CH$_2$O), 2.26-2.34 (m, 2

H, CH_2) ppm. ^{13}C NMR ($CDCl_3$): δ = 150.1 (CN_4), 149.3, 144.6, 138.3, 125.7, 125.5, 57.5 (CH_2OH), 45.6 (CH_2N), 32.6 ppm. ESI-HRMS: calcd for $C_9H_{12}N_5O$ $[M+H]^+$ 206.1036, found 206.1046.

2.5.6.1.2 3-(5-(pyridin-2-yl)-2*H*-tetrazol-2-yl)propan-1-ol (2.19)

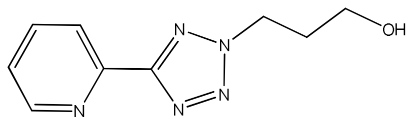

Yellow solid (0.92 g, 33%). m.p. 40-42 °C. IR (KBr): ν = 3368, 2948, 2885, 1651, 1598, 1573, 1435, 1421, 1359, 1060, 804, 749 cm^{-1}. ^1H NMR ($CDCl_3$): δ = 8.76-8.78 (m, 1 H, pyr-H), 8.24-8.27 (m, 1 H, pyr-H), 7.85-7.91 (m, 1 H, pyr-H), 7.40-7.44 (m, 1 H, pyr-H), 4.90 (t, 2 H, J = 6.7 Hz, CH_2N), 3.69-3.74 (m, 2 H, CH_2O), 2.28-2.36 (m, 2 H, CH_2) ppm. ^{13}C NMR ($CDCl_3$): δ = 164.6 (CN_4), 150.2, 146.6, 137.2, 124.9, 122.5, 61.9 (CH_2OH), 50.3 (CH_2N), 31.8 ppm. ESI-HRMS: calcd for $C_9H_{11}N_5NaO$ $[M+Na]^+$ 206.1036, found 206.1046.

2.5.6.1.3 4-(5-(pyridin-2-yl)-1*H*-tetrazol-1-yl)butan-1-ol (2.20)

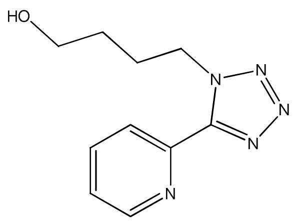

White solid (0.06 g, 0.04%). m.p. 43-36 °C. IR (KBr): ν = 3427, 2976, 2856, 1588, 1571, 1528, 1471, 1431, 1401, 1122, 1103, 1006, 993, 806, 792, 748 cm^{-1}. ^1H NMR ($CDCl_3$): δ = 8.72-8.74 (m, 1 H, pyr-H), 8.36-8.39 (m, 1 H, pyr-H), 7.89-7.94 (m, 1 H, pyr-H), 7.43-7.48 (m, 1 H, pyr-H), 5.03 (t, 2 H, J = 6.6 Hz, CH_2N), 3.71 (t, 2 H, J = 6.7 Hz, CH_2O), 2.04-2.14 (m, 2 H, CH_2), 1.66 (m, 2 H, CH_2) ppm. ^{13}C NMR ($CDCl_3$): δ = 151.7 (CN_4), 149.5, 144.8, 137.5, 125.4, 124.6, 61.7 (CH_2OH), 49.3 (CH_2N), 29.1, 26.8 ppm. ESI-HRMS: calcd for $C_{10}H_{14}N_5O$ $[M+H]^+$ 220.1193, found 220.1199.

2.5.6.1.4 4-(5-(pyridin-2-yl)-2*H*-tetrazol-2-yl)butan-1-ol (2.21)

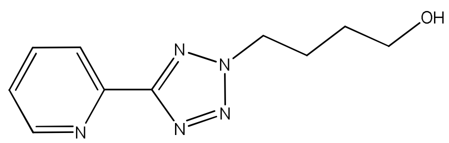

Yellow oil (0.25g, 17%). IR (DCM film): ν = 3395, 2941, 2873, 1591, 1472, 1434, 1410, 1120, 1061, 1035, 994, 799, 745 cm^{-1}. ^1H NMR ($CDCl_3$): δ = 8.75-8.77 (m, 1 H, pyr-H), 8.21-

8.24 (m, 1 H, pyr-H), 7.84-7.89 (m, 1 H, pyr-H), 7.38-7.42 (m, 1 H, pyr-H), 4.77 (t, 2 H, *J* = 7.3 Hz, CH_2N), 3.70 (t, 2 H, *J* = 6.2, CH_2O), 2.17-2.26 (m, 2 H, CH_2), 1.60-1.69 (m, 2 H, CH_2) ppm. ^{13}C NMR ($CDCl_3$): δ = 164.5 (CN_4), 150.1, 146.6, 137.1, 124.8, 122.4, 61.4 (CH_2OH), 53.2 (CH_2N), 29.1, 25.9 ppm. ESI-HRMS: calcd for $C_{10}H_{13}N_5NaO$ $[M+Na]^+$ 242.1012, found 242.1021.

2.5.6.1.5 6-(5-(pyridin-2-yl)-1*H*-tetrazol-1-yl)hexan-1-ol (2.22)

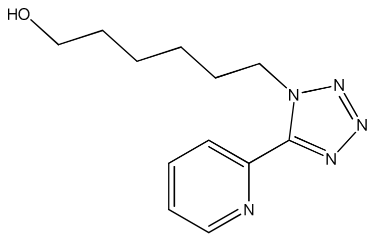

Clear oil (1.48 g, 44%). IR (DCM film): ν = 3402, 2936, 2861, 1591, 1472, 1433, 1409, 1121, 1055, 1038, 994, 798, 747 cm^{-1}. ^1H NMR ($CDCl_3$): δ = 8.72-8.74 (m, 1 H, pyr-H), 8.35-8.38 (m, 1 H, pyr-H), 7.88-7.94 (m, 1 H, pyr-H), 7.43-7.47 (m, 1 H, pyr-H), 4.99 (t, 2 H, *J* = 7.3 Hz, CH_2N), 3.61-3.65 (m, 2 H, CH_2O), 1.95-2.02 (m, 2 H, CH_2), 1.51-1.58 (m, 2 H, CH_2), 1.40-1.42 (m, 5 H, CH_2, OH) ppm. ^{13}C NMR ($CDCl_3$): δ = 151.6 (CN_4), 149.4, 145.0, 137.4, 125.2, 124.6, 62.7 (CH_2OH), 49.5 (CH_2N), 32.4, 29.8, 26.0, 25.1 ppm. ESI-HRMS: calcd for $C_{12}H_{18}N_5O$ $[M+H]^+$ 248.1506, found 248.1514.

2.5.6.1.6 6-(5-(pyridin-2-yl)-2*H*-tetrazol-2-yl)hexan-1-ol (2.23)

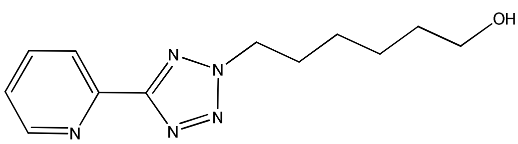

White solid (1.46 g, 43%). m.p. 29-32 °C. IR (KBr): ν = 3321, 2933, 2854, 1599, 1572, 1526, 1468, 1421, 1385, 1356, 1249, 1195, 1160, 1061, 1045, 987, 803, 775, 745 cm^{-1}. ^1H NMR ($CDCl_3$): δ = 8.77-8.79 (m, 1 H, pyr-H), 8.24-8.27 (m, 1 H, pyr-H), 7.84-7.90 (m, 1 H, pyr-H), 7.38-7.42 (m, 1 H, pyr-H), 4.72 (t, 2 H, *J* = 7.1 Hz, CH_2N), 3.61-3.66 (m, 2 H, CH_2O), 2.07-2.17 (m, 2 H, CH_2), 1.52-1.61 (m, 2 H, CH_2), 1.37-1.46 (m, 5 H, CH_2, OH) ppm. ^{13}C NMR ($CDCl_3$): δ = 164.7 (CN_4), 150.3, 146.8, 137.1, 124.8, 122.3, 62.5 (CH_2OH), 53.3 (CH_2N), 32.3, 29.2, 26.0, 25.0 ppm. ESI-HRMS: calcd for $C_{12}H_{17}N_5NaO$ $[M+Na]^+$ 270.1325, found 270.1337.

2.5.6.1.7 8-(5-(pyridin-2-yl)-1*H*-tetrazol-1-yl)octan-1-ol (2.24)

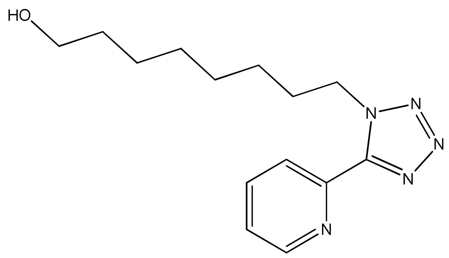

Yellow oil (1.00 g, 27%). IR (DCM film): ν = 3407, 2930, 2858, 1591, 1533, 1471, 1433, 1409, 1376, 1288, 1121, 1055, 994, 798 cm^{-1}. ^{1}H NMR ($CDCl_3$): δ = 8.72-8.73 (m, 1 H, pyr-H), 8.35-8.38 (m, 1 H, pyr-H), 7.88-7.93 (m, 1 H, pyr-H), 7.43-7.47 (m, 1 H, pyr-H), 4.98 (t, 2 H, J = 7.3 Hz, CH_2N), 3.61-3.65 (m, 2 H, CH_2O), 1.93-1.97 (m, 2 H, CH_2), 1.50-1.54 (m, 2 H, CH_2), 1.32-1.34 (m, 9 H, CH_2, OH) ppm. ^{13}C NMR ($CDCl_3$): δ = 151.6 (CN_4), 149.4, 145.0, 137.4, 125.2, 124.5, 62.9 (CH_2OH), 49.6 (CH_2N), 32.6, 29.8, 29.1, 28.9, 26.2, 25.6 ppm. ESI-HRMS: calcd for $C_{14}H_{22}N_5O$ $[M+H]^+$ 276.1819, found 276.1826.

2.5.6.1.8 8-(5-(pyridin-2-yl)-2*H*-tetrazol-2-yl)octan-1-ol (2.25)

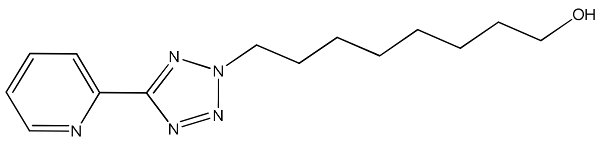

White solid (1.20 g, 32%). m.p. 50-54 °C. IR (KBr): ν = 3321, 2931, 2849, 1599, 1572, 1524, 1468, 1421, 1384, 1063, 1044, 1030, 801, 774, 744, 735 cm^{-1}. ^{1}H NMR ($CDCl_3$): δ = 8.77-8.79 (m, 1 H, pyr-H), 8.24-8.26 (m, 1 H, pyr-H), 7.83-7.89 (m, 1 H, pyr-H), 7.37-7.42 (m, 1 H, pyr-H), 4.70 (t, 2 H, J = 7.1 Hz, CH_2N), 3.60-3.64 (m, 2 H, CH_2O), 2.07-2.12 (m, 2 H, CH_2), 1.50-1.57 (m, 2 H, CH_2), 1.33-1.37 (m, 9 H, CH_2, OH) ppm. ^{13}C NMR ($CDCl_3$): δ = 164.7 (CN_4), 150.3, 146.9, 137.1, 124.7, 122.3, 62.8 (CH_2OH), 53.4 (CH_2N), 32.6, 29.3, 29.0, 28.7, 26.2, 25.5 ppm. ESI-HRMS: calcd for $C_{14}H_{22}N_5O$ $[M+H]^+$ 278.1872, found 278.1877.

2.5.7 Metal Complexation Reactions with Alcohol Pyridyl Tetrazoles

2.5.7.1 General Procedure for Metal Complexation Reactions

Metal complexes of alcohol functionalised pyridyl tetrazoles were synthesised using the methods outlined in section 2.5.3, unless otherwise stated.

2.5.7.1.1 $[Cu(2.18)Cl_2]_2$ (2.78)

Green solid (0.10 g, 61%). $C_{18}H_{22}Cl_4Cu_2N_{10}O_2$: calcd. C 31.81, H 3.26, N 20.62%; found C 32.11, H 3.06, N 20.55%. IR (KBr): ν = 3466, 2933, 1613, 1551, 1484, 1455, 1384, 1283, 1250, 1163, 1113, 1046, 1004, 799, 719 cm^{-1}. λ_{max} (MeOH) 832 nm, ε = 115 $M^{-1}cm^{-1}$. Magnetic moment: 2.56 B.M.

2.5.7.1.2 [Cu(2.19)Cl_2]$_2$ (2.79)

Green solid (0.09 g, 55%). $C_{18}H_{22}Cl_4Cu_2N_{10}O_2$: calcd. C 31.81, H 3.26, N 20.62%; found C 32.18, H 3.13, N 20.36%. IR (KBr): ν = 3506, 2930, 2883, 1618, 1550, 1459, 1447, 1395, 1353, 1333, 1265, 1233, 1154, 1133, 1102, 1041, 1023, 999, 801, 761 cm^{-1}. λ_{max} (MeOH) 844 nm, ε = 147 $M^{-1}cm^{-1}$. Magnetic moment: 1.82 B.M.

2.5.7.1.3 [Cu(2.20)Cl_2]$_2$ (2.80)

Carried out on a 0.03 g scale. Green solid (0.01 g, 20%). $C_{20}H_{26}Cl_4Cu_2N_{10}O_2$: calcd. C 33.96, H 3.70, N 19.80%; found C 33.15, H 3.52, N 19.27%. IR (KBr): ν = 3431, 3100, 3070, 3048, 1614, 1551, 1481, 1457, 1382, 1289, 1112, 1017, 798, 760 cm^{-1}. λ_{max} (MeOH) 829 nm, ε = 112 $M^{-1}cm^{-1}$. Magnetic moment: 1.81 B.M.

2.5.7.1.4 [Cu(2.21)Cl_2]$_2$ (2.81)

Carried out on a 0.09 g scale. Green solid (0.11 g, 75%). $C_{20}H_{26}Cl_4Cu_2N_{10}O_2$: calcd. C 33.96, H 3.70, N 19.80%; found C 34.36, H 3.68, N 19.50%. IR (KBr): ν = 3512, 3103, 2960, 2939, 1614, 1548, 1484, 1457, 1434, 1387, 1293, 1164, 1111, 1051, 1034, 1010, 799 cm^{-1}. λ_{max} (MeOH) 832 nm, ε = 111 $M^{-1}cm^{-1}$. Magnetic moment: 1.75 B.M.

2.5.7.1.5 [Cu(2.22)Cl_2]$_2$ (2.82)

Green solid (0.11 g, 73%). $C_{24}H_{34}Cl_4Cu_2N_{10}O_2$: calcd. C 37.75, H 4.49, N 18.35%; found C 38.10, H 4.42, N 17.89%. IR (KBr): ν = 3443, 2928, 2861, 1615, 1550, 1484, 1456, 1173, 1111, 1051, 1012, 796 cm^{-1}. λ_{max} (MeOH) 840 nm, ε = 105 $M^{-1}cm^{-1}$. Magnetic moment: 1.79 B.M.

2.5.7.1.6 [Cu(2.23)Cl_2]$_2$ (2.83)

Green solid (0.10 g, 66%). $C_{24}H_{34}Cl_4Cu_2N_{10}O_2$: calcd. C 37.75, H 4.49, N 18.35%; found C 36.92, H 4.23, N 17.35%. IR (KBr): ν = 3449, 2935, 2860, 1617, 1554, 1463, 1454, 1430, 1286, 1160, 1072, 1045, 1020, 906, 802, 763, 725 cm^{-1}. λ_{max} (MeOH) 816 nm, ε = 136 $M^{-1}cm^{-1}$. Magnetic moment: 2.14 B.M.

2.5.7.1.7 [Cu(2.24)Cl_2]$_2$ (2.84)

Green solid (0.12 g, 80%). $C_{28}H_{42}Cl_4Cu_2N_{10}O_2$: calcd. C 41.03, H 5.17, N 17.09%; found C 41.89, H 5.38, N 16.93%. IR (KBr): ν = 3429, 2933, 2913, 2852, 1615, 1486, 1458, 1432, 1052, 1010, 798, 754 cm^{-1}. λ_{max} (MeOH) 836 nm, ε = 87 $M^{-1}cm^{-1}$. Magnetic moment: 2.36 B.M.

2.5.7.1.8 [Cu(2.25)Cl_2]$_2$ (2.85)

Green solid (0.14 g, 93%). $C_{28}H_{42}Cl_4Cu_2N_{10}O_2$: calcd. C 41.03, H 5.17, N 17.09%; found C 40.59, H 4.95, N 16.75%. IR (KBr): ν = 3451, 2925, 2854, 1617, 1553, 1464, 1453, 1286, 1160, 1072, 1010, 802, 763, 725 cm^{-1}. λ_{max} (MeOH) 808 nm, ε = 121 $M^{-1}cm^{-1}$. Magnetic moment: 1.81 B.M.

2.5.7.1.9 [Ni(2.18)Cl_2]$_2$ (2.86)

Green solid (0.16 g, 48%). $C_{18}H_{22}Cl_4Ni_2N_{10}O_2$: calcd. C 32.27, H 3.31, N 20.92%; found C 32.82, H 3.93, N 21.44%. IR (KBr): ν = 3379, 1610, 1540, 1480, 1461, 1412, 1299, 1254, 1160, 1108, 1049, 1025, 931, 796, 756, 726, 641, 421 cm^{-1}. λ_{max} (MeOH) 400 nm, ε = 25 $M^{-1}cm^{-1}$; 676 nm, ε = 9 $M^{-1}cm^{-1}$. Magnetic moment: 4.36 B.M.

2.5.7.1.10 [Ni(2.19)Cl_2]$_2$ (2.87)

Green solid (0.10 g, 31%). $C_{18}H_{22}Cl_4Ni_2N_{10}O_2$: calcd. C 32.27, H 3.31, N 20.92%; found C 32.23, H 3.85, N 19.97%. IR (KBr): ν = 3358, 1615, 1552, 1453, 1396, 1357, 1320, 1289, 1262, 1223, 1152, 1099, 1062, 1028, 922, 805, 757, 732 cm^{-1}. λ_{max} (MeOH) 400 nm, ε = 23 $M^{-1}cm^{-1}$; 672 nm, ε = 9 $M^{-1}cm^{-1}$. Magnetic moment: 4.52 B.M.

2.5.7.1.11 [Ni(2.22)Cl_2]$_2$ (2.88)

Green solid (0.11 g, 39%). $C_{24}H_{34}Cl_4Ni_2N_{10}O_2$: calcd. C 38.22, H 4.55, N 18.58%; found C 37.90, H 5.36, N 18.01%. IR (KBr): ν = 3368, 2929, 2859, 1610, 1482, 1458, 1298, 1253, 1169, 1111, 1053, 1012, 795, 756, 726, 427 cm^{-1}. λ_{max} (MeOH) 400 nm, ε = 21 $M^{-1}cm^{-1}$; 680 nm, ε = 8 $M^{-1}cm^{-1}$. Magnetic moment: 4.42 B.M.

2.5.7.1.12 [Ni(2.23)Cl_2]$_2$ (2.89)

Green solid (0.09 g, 32%). $C_{24}H_{34}Cl_4Ni_2N_{10}O_2.2CH_3OH$: calcd. C 38.16, H 5.18, N 17.13%; found C 37.33, H 5.20, N 16.25%. IR (KBr): ν = 3400, 2930, 2858, 1615, 1572, 1549, 1454, 1393, 1354, 1289, 1262, 1227, 1063, 1050, 1028, 805, 762, 732 cm^{-1}. λ_{max} (MeOH) 400 nm, ε = 22 $M^{-1}cm^{-1}$; 676 nm, ε = 8 $M^{-1}cm^{-1}$. Magnetic moment: 4.36 B.M.

2.5.7.1.13 [Ni(2.24)Cl_2]$_2$ (2.90)

Green solid (0.16 g, 55%). $C_{28}H_{42}Cl_4Ni_2N_{10}O_2.2H_2O$: calcd. C 39.74, H 5.48, N 16.56%; found C 38.74, H 5.32, N 15.70%. IR (KBr): ν = 3387, 2919, 2853, 1608, 1538, 1474, 1452, 1409, 1252, 1052, 1008, 797, 727 cm^{-1}. λ_{max} (MeOH) 400 nm, ε = 20 $M^{-1}cm^{-1}$; 680 nm, ε = 7 $M^{-1}cm^{-1}$. Magnetic moment: 4.03 B.M.

2.5.7.1.14 [Ni(2.25)Cl_2]$_2$ (2.91)

Green solid (0.18 g, 62%). $C_{28}H_{42}Cl_4Ni_2N_{10}O_2$: calcd. C 41.50, H 5.23, N 17.30%; found C 42.49, H 6.05, N 17.69%. IR (KBr): ν = 3401, 3095, 2926, 2853, 1614, 1572, 1547, 1454, 1394, 1351, 1289, 1262, 1223, 1163, 1100, 1062, 1049, 1026, 807, 780, 763, 733 cm^{-1}. λ_{max} (MeOH) 400 nm, ε = 20 $M^{-1}cm^{-1}$; 676 nm, ε = 8 $M^{-1}cm^{-1}$. Magnetic moment: 4.20 B.M.

2.5.7.1.15 Co(2.18)$_2$(NCS)$_2$ (2.92)

Carried out on a 0.10 g scale. Purple solid (0.08 g, 59%). $C_{20}H_{22}CoN_{12}O_2S_2$: calcd. C 41.02, H 3.79, N 28.71%; found C 39.76, H 3.71, N 27.92%. IR (KBr): ν = 3434, 2928, 2888, 2085, 1607, 1480, 1447, 1290, 1251, 1161, 1056, 1007, 792, 746, 725 cm^{-1}. λ_{max} (MeOH) 516 nm, ε = 31 $M^{-1}cm^{-1}$. Magnetic moment: 5.53 B.M.

2.5.7.1.16 Co(2.19)$_2$(NCS)$_2$ (2.93)

Carried out on a 0.10 g scale. Rust coloured crystals (0.06 g, 41%). $C_{20}H_{22}CoN_{12}O_2S_2$: calcd. C 41.02, H 3.79, N 28.71%; found C 41.27, H 3.74, N 28.25%. IR (KBr): ν = 3449, 2960, 2872, 2084, 1745, 1610, 1543, 1449, 1351, 1285, 1221, 1157, 1064, 1025, 919, 802, 753, 733, 639 cm^{-1}. λ_{max} (MeOH) 520 nm, ε = 50 $M^{-1}cm^{-1}$. Magnetic moment: 5.32 B.M.

2.5.7.1.17 Co(2.22)$_2$(NCS)$_2$ (2.94)

Carried out on a 0.10 g scale. Rust coloured crystals (0.02 g, 15%). $C_{26}H_{34}CoN_{12}O_2S_2$: calcd. C 46.63, H 5.12, N 25.10%; found C 47.39, H 5.09, N 25.64%. IR (KBr): ν = 3456, 2924, 2875, 2095, 1608, 1461, 1442, 1380, 1066, 1047, 1013, 915, 795, 746, 727 cm^{-1}. λ_{max} (MeOH) 510 nm, ε = 31 $M^{-1}cm^{-1}$. Magnetic moment: 5.22 B.M.

2.5.7.1.18 Co(2.23)$_2$(NCS)$_2$ (2.95)

Carried out on a 0.10 g scale. Rust coloured crystals (0.03 g, 23%). $C_{26}H_{34}CoN_{12}O_2S_2$: calcd. C 46.63, H 5.12, N 25.10%; found C 46.19 , H 4.82, N 24.59%. IR (KBr): ν = 3445, 2930, 2860, 2077, 1610, 1476, 1448, 1391, 1284, 1062, 1047, 1026, 1007, 801, 754, 733 cm^{-1}. λ_{max} (MeOH) 521 nm, ε = 53 M^{-1}cm^{-1}. Magnetic moment: 4.97 B.M.

2.5.7.1.19 Co(2.24)$_2$(NCS)$_2$ (2.96)

Carried out on a 0.10 g scale. Dark green solid (0.10 g, 38%). $C_{30}H_{42}CoN_{12}O_2S_2$: calcd. C 49.64, H 5.83, N 23.16%; found C 50.24, H 5.14, N 22.89%. IR (KBr): ν = 3401, 2928, 2854, 2067, 1609, 1477, 1456, 1049, 1009, 792, 746, 725 cm^{-1}. λ_{max} (MeOH) 523 nm, ε = 48 M^{-1}cm^{-1}. Magnetic moment: 4.87 B.M.

2.5.7.1.20 Co(2.25)$_2$(NCS)$_2$ (2.97)

Carried out on a 0.10 g scale. Rust coloured crystals (0.05 g, 38%). $C_{30}H_{42}CoN_{12}O_2S_2$: calcd. C 49.64, H 5.83, N 23.16%; found C 48.91, H 5.58, N 22.69%. IR (KBr): ν = 3496, 2928, 2855, 2081, 1610, 1476, 1448, 1062, 1047, 1025, 802, 755, 733 cm^{-1}. λ_{max} (MeOH) 520 nm, ε = 50 M^{-1}cm^{-1}. Magnetic moment: 5.10 B.M.

Chapter 3: Ester and Carboxylate Functionalised Pyridyl Tetrazoles

3.1 Introduction

3.1.1 Pyridyl Tetrazole Esters as Organic Linkers in Coordination Polymers

Thus far, a range of functionalised pyridyl tetrazole ligands were synthesised and their metal complexes isolated and characterised. Two ligands which were synthesised during the course of this work were of particular interest and hence are the focus of this chapter. The ligands in question (**3.1** and **3.2**) are shown in Figure 3.1. These ligands not only presented the typical binding pocket of the pyridine and tetrazole nitrogen atoms, but provided another binding site by virtue of the ester functionality.

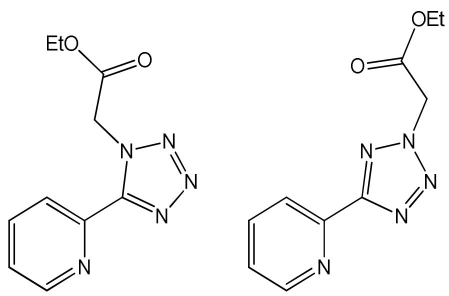

3.1 **3.2**

Figure 3.1: Structures of the two ligands synthesised which provided an additional option for metal binding.

By incorporating both the pyridyl tetrazole nitrogen atoms and the ester oxygen atoms in complexation to the metal atom, there was potential for intermolecular interactions to form. This interaction could result in the formation of coordination polymers (CPs). As discussed in Chapter 1, CPs have attracted immense attention during the last two decades due to their potential applications. Since the structure of CPs have significant implications for their applications, the main goal in CP synthesis is to establish the synthesis conditions that lead to defined inorganic building blocks, without decomposition to the organic linker.[96] Therefore, the knowledge of possible topologies, the functionality of organic linker molecules, as well as the understanding of typical metal coordination environments or the formation conditions of typical inorganic building blocks can help direct synthesis efforts. As of yet, however, it is still difficult to predict and control the structures of such complicated supramolecular assemblies. If CPs could indeed be formed from the employment of **3.1** and **3.2**, an investigation into the synthesis conditions could be undertaken to gain an insight into how the regioisomerism and other variables affect the final structures, thus contributing to the rapidly growing database of knowledge in this field.

3.1.2 Rationale for Employing 3.1 and 3.2 as Organic Linkers in CPs

Some of the most important characteristics of an organic compound used as a linker in CPs are their diverse coordination modes, molecular rigidity and flexibility.[146] As regards diverse metal coordination modes, **3.1** and **3.2** offer a variety of possibilities. Tetrazoles and its derivatives have been employed extensively as multidentate chelating or bridging linkers because of their diverse connecting modes.[146,147] Furthermore, tetrazole ligands can connect discrete or low-dimensional coordination motifs into higher-dimensional architectures *via* hydrogen bonds and π-π interactions.[148] It is also well known that pyridine ring N atoms have a good coordination capacity, hence the combination of both these heterocycles provides numerous opportunities for metal binding. Metal complexes with carboxylic esters have a long tradition in coordination chemistry, with coordination occurring with the carbonyl oxygen in the majority of cases.[149] However, ester oxygens are generally rather weak bases except toward strong Lewis acids such as BF_3.[132] If this group did not interact with the metal centres, this lack of reactivity could be overcome by converting the ester group into an anionic carboxylate group (Figure 3.2). Carboxylate groups are hard bases and are generally more reactive towards metal coordination than ester oxygens.

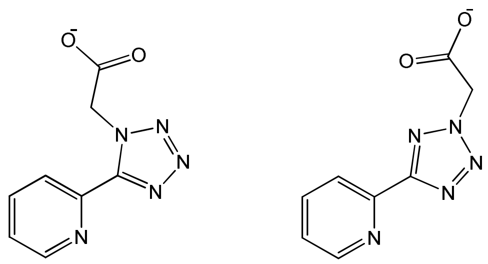

3.1(pytza) 3.2(pytza)

Figure 3.2: The ethyl ester derivatives **3.1** and **3.2** could be converted to a carboxylate group, yielding **3.1(pytza)** and **3.2(pytza)**.

Carboxylate groups may coordinate to a metal ion in one of three modes: monodentate, chelating/bidentate or bridging (Figure 3.3).[150] Furthermore, bridging carboxylates can coordinate to metals in a *syn-syn*, *anti-anti* and *anti-syn* configuration (Figure 3.4).[132]

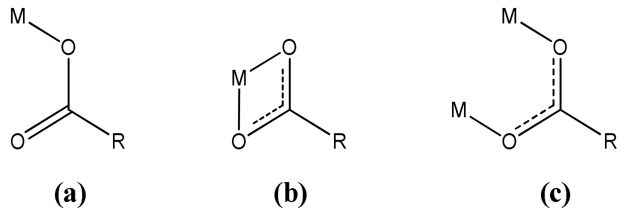

Figure 3.3: The three different coordination modes that carboxylate ions can bind to metals: (a) monodentate; (b) chelating/bidentate; (c) bridging.

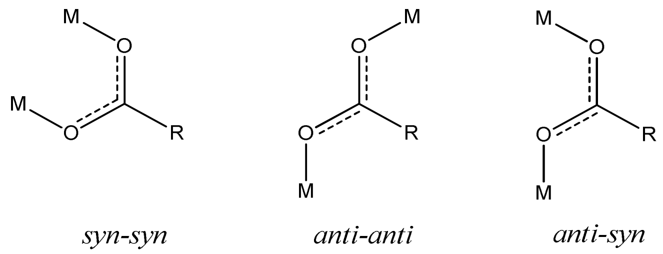

Figure 3.4: The most common forms of bridging carboxylates.

In addition, the anionic nature of the carboxylate linker negates the need for counteranions in the CP framework, and this increases the potential for porosity in the framework products.[151] Therefore these ligands, which have mixed functionalities, could be excellent versatile building blocks, and the combination of these functionalities should allow the incorporation of interesting properties into the resulting networks.

Flexibility is also important in organic linkers in CPs. In these ligands, the oxygen containing functionality is connected to the tetrazole ring *via* a sp^3 CH_2 moiety, which offers flexible orientations and conformational freedom which may provide more possibilities for the construction of CPs. Thus, due to the structural advantages of these type of ligands (Figure 3.5), their potential to be an organic linker is very promising. Despite this fact and that tetrazoles and its pyridyl and alkylated derivatives are easily accessed, there are limited examples of their use in CPs in the literature. More specifically, examples of the use of N-substituted tetrazoles in the synthesis of coordination networks are rare.[152] The synthesis and use of tetrazolate-5-carboxylate ligands is becoming more common, however again reports in the literature are still sparse.[153,154]

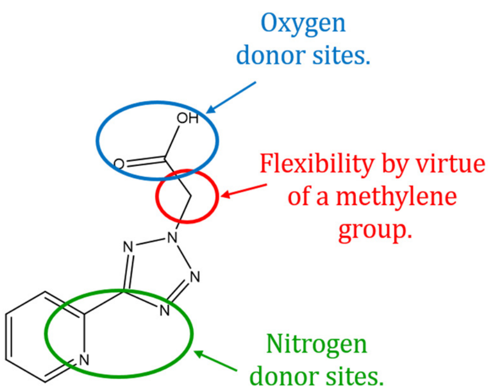

Figure 3.5: The pyridyl tetrazole ligands synthesised in this work possess characteristics that are typical of organic linkers.

3.1.3 Bi- and Multifunctional Tetrazole Based Ligands in CPs

CPs built up by carboxylate or tetrazolate ligands have been increasingly explored for their physical-chemical properties, such as molecular adsorption and recognition,[155,156,157] magnetism,[158] nonlinear optics,[159] luminescence[160] and energetic materials.[161] Although there are limited reports of such ligands, the frequency of relevant examples being published has increased recently. These recent investigations into bifunctional tetrazolate-carboxylate ligands, especially the carboxylate 5-substituted tetrazolates, is a consequence of their four N and two O donor atoms being potential binding centres. These features make them an excellent polydentate ligand. In 2010, Guo and co-workers employed the structurally related 1*H*-tetrazolate-5-formic acid (**3.3**) and 1*H*-tetrazolate-5-acetic acid (**3.4**) (Figure 3.6) in the assembly of Zn(II) and Cd(II) CPs in order to investigate the influence of ligand flexibility, secondary ligand and reaction conditions on the resulting structures.[162,163] When comparing solvothermal reactions which only involved ligands **3.3** and **3.4** in the absence of a secondary ligand, they found that when using the more rigid ligand, **3.3**, an isolated dinuclear structure formed. The lack of any significant intermolecular interactions was ascribed to the nature of the rigid ligand as well as the formation of the six-membered ring (Figure 3.6). On the other hand, when the more flexible **3.4** was employed in the reaction, a 3-D network resulted, with each ligand acting as a tetradentate linker to connect three Zn(II) atoms. These results showed that the bifunctional nature of the ligands played an important role in the attainment of CPs. Furthermore, these results show that flexibility is important in the formation of higher dimensional frameworks and that subtle structural changes to the ligand can govern the final structural topology.

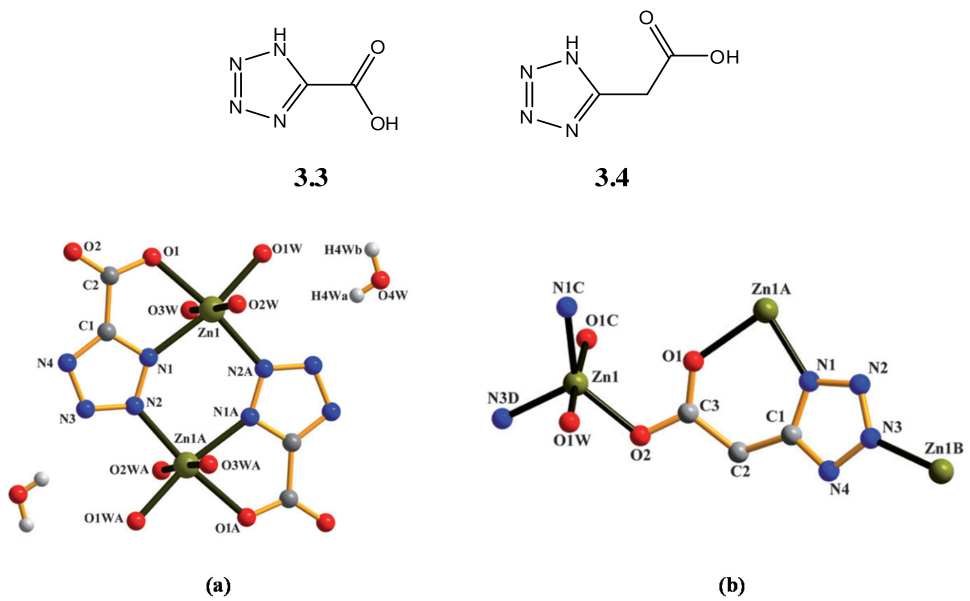

Figure 3.6: Ligands with different flexibilities were used in the synthesis of coordination polymers. (a) Crystal structure of an isolated Zn(II) complex with **3.3** as the coordinating ligand; (b) crystal structure of a subunit of a Zn(II) framework with **3.4** as the coordinating ligand.[163]

An earlier report by Yuan *et al*. involved the *in situ* hydrolysis of tetrazole-5-ethyl acetate to the aforementioned 1*H*-tetrazolate-5-acetic acid (**3.4**) in aqueous NaOH solution under conventional reaction conditions.[154] When $CuCl_2.2H_2O$ was added to this solution, blue crystals formed which on analysis by single crystal X-ray diffraction revealed a heterometallic 2-D network (Figure 3.7), demonstrating that these bifunctional ligands are versatile and adaptable for the coordination requirements of metal atoms. Heterometallic CPs are of great interest as the incorporation of two or more kinds of metal ions can add different functionalities which can be useful in the area of catalysis.[164] The advantages of using bifunctional tetrazolate-carboxylate ligands in this context are recognisable, as the presence of different types of donor atoms can result in preferential coordination to different metal atoms.

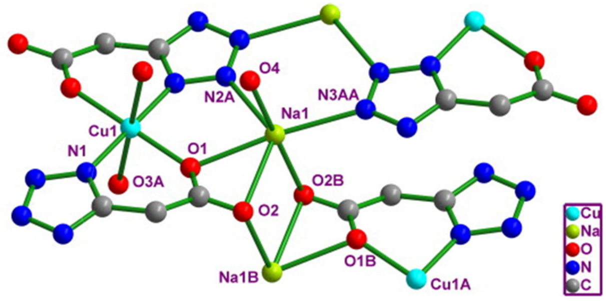

Figure 3.7: Building unit of a Cu-Na coordination polymer.[154]

More recently, Lu *et al*. synthesised two novel 5-(pyrazinyl) tetrazolate CPs, **3.5** and **3.6**, with **3.5** displaying strong luminescent properties suitable for green light luminescent materials.[148] The presence of another aromatic nitrogen heterocycle along with the tetrazolate moiety was clearly advantageous in the attainment of **3.5** as the ligand acted as a tridentate chelating-bridging ligand, which linked neighbouring binuclear subunits to form an infinite chain (Figure 3.8). In **3.6**, the ligand propagates a 1-D chain *via* simultaneous tridentate and bidentate chelating-bridging which further demonstrates the versatility of these type of bifunctional ligands and the advantages of installing another aromatic heterocycle.

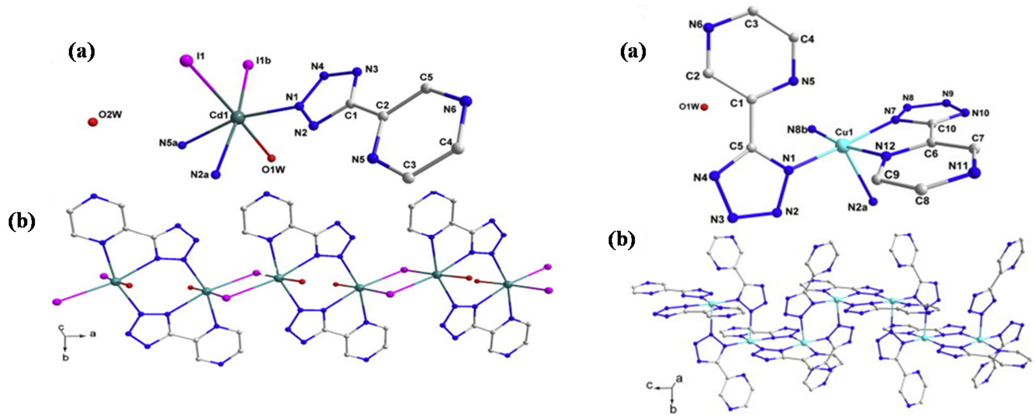

3.5 **3.6**

Figure 3.8: (a) ORTEP drawing of Cd(II) and Cu(II) coordination polymers; (b) 1-D chains formed by bimetallic nodes and bridging halide linkers in the case of **3.5**, and by tetrazolate bridging linkers in the case of **3.6**.[148]

In a rare example of an N-substituted tetrazole being employed in the synthesis of a CP, Li and co-workers reported coordination networks dependent on the ligand 2-(5-(pyrazin-2-yl)-2*H*-tetrazol-2-yl) acetic acid (**3.7**, Figure 3.9).[146] Reactions of Cd(II), Co(II), Zn(II), Mn(II) and Ni(II) salts with **3.7** in pH 6 solutions, either under solvothermal conditions or at room temperature, yielded diverse 1-D and 2-D frameworks. This diversity is owing to the strong combined coordinative abilities of the flexible carboxylate groups, the tetrazole ring and the pyrazine ring which endows the ligand with an abundance of coordination modes. The coordination modes which were present in these frameworks are depicted in Figure 3.10. These results indicate that similar types of multifunctional ligands have great potential in the field of CP synthesis.

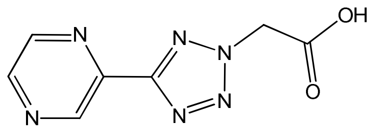

3.7

Figure 3.9: The structure of 2-(5-(pyrazin-2-yl)-2*H*-tetrazol-2-yl) acetic acid.

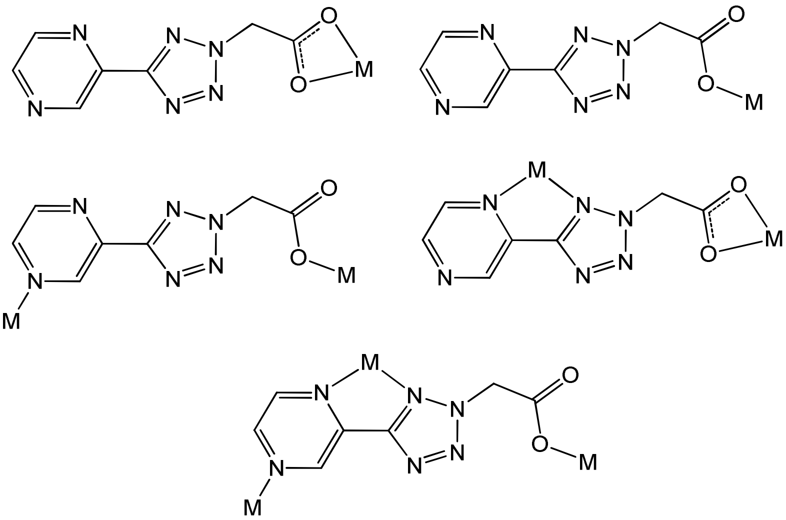

Figure 3.10: The five coordination modes of **3.7** that were observed in the work by Li *et al.*[146]

3.2 Aims and Objectives of Chapter

Although the above examples demonstrate that these type of bi- and multifunctional ligands have excellent potential to form coordination polymers, there are limited examples of similar compounds being exploited for this potential in the literature. For the purpose of our research, and the fact that our previously synthesised ligands bear a resemblance to the above examples, we aimed to investigate multifunctional ligands with a pyridyl tetrazole scaffold for their potential use in the synthesis of high dimensional coordination polymers. We envisaged the use of ethyl acetate N-functionalised pyridyl tetrazoles as organic linkers in the framework syntheses, however the ester functionality could easily be converted to a carboxylic acid if desired. Different metal ions would also be utilised, which would allow an analysis of the influence of metal ion radii on the resulting architectures. The effect of the position of the ester arm on the structures would also be examined. Coordination polymers derived from different ligands are referred to as ''ligand-originated isomers''.[165] Although many different ligands have been investigated for coordination polymer formation, there are few examples of any systematic studies of ligand-originated isomers that arise from differences in regiochemical isomerism in a multifunctional ligand. Hence, these investigations would represent a rare study in this area. Finally, examination of the products by EPR spectroscopy and solid state luminescence was also intended, the concepts of which are also introduced in this chapter.

3.3 Results and Discussion

3.3.1 Synthesis of the Pyridyl Tetrazole Ester Derivatives

Access to the ester functionalised pyridyl tetrazoles was achieved through the alkylation of **2.5** in the presence of K_2CO_3 and ethyl bromoacetate (Scheme 3.1).

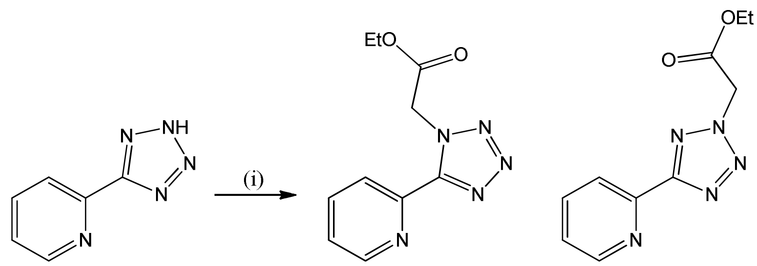

Scheme 3.1: Alkylation of **2.5** yielded two regioisomers **3.1** and **3.2.** Reagents and conditions: (i) K_2CO_3, $BrCH_2COOEt$, CH_3CN, Δ, 24 h.

^{1}H NMR spectroscopy was carried out on the crude residue obtained after filtration and evaporation of the filtrate. It was evident from the ^{1}H NMR spectrum that a mixture of regioisomers were present, as there were double the number of expected peaks observed (Figure 3.11). No significant regioselectivity was observed with the N-1 and N-2 regioisomers being present in a 10:9 ratio. Thin Layer Chromatography using EtOAc and Pet. Ether as the mobile phase showed that the two isomers had very different R_f values. Therefore column chromatography was employed to separate the two isomers. The two isolated isomers were again analysed by NMR spectroscopy and it was deduced from the spectra that the isomer with the highest R_f value (0.58) was the N-1 isomer and the N-2 isomer had the lower R_f value (0.28). The ^{1}H NMR spectra of the regioisomers, which can be seen in Figure 3.11, exhibited four multiplets in the aromatic region (7.42-8.79 ppm) which were attributed to the pyridyl protons; a singlet which integrated for two protons was observed at 5.74 ppm for the N-1 regioisomer and 5.50 ppm for the N-2 regioisomer which arose due to the CH_2-tet protons of the ethyl acetate moiety; the CH_2 protons of the ethoxy group gave rise to a quartet at ~4.20 ppm and the CH_3 protons of the ethoxy group appeared at ~1.20 ppm as a triplet. In the ^{13}C NMR spectra of the isomers, the C-5 of the tetrazole ring gave rise to a signal at 152.1 ppm for the N-1 regioisomer and 164.8 ppm for the N-2 regioisomer. The presence of a carbonyl carbon was implied by resonances observed at 165.9 and 165.2 ppm for the N-1 and N-2 regioisomers respectively. Further confirmation that the ester group was present in the compounds was attained on examination of the IR spectra of the isomers, with a ν(C=O) stretch observed at ~1746 cm^{-1}.

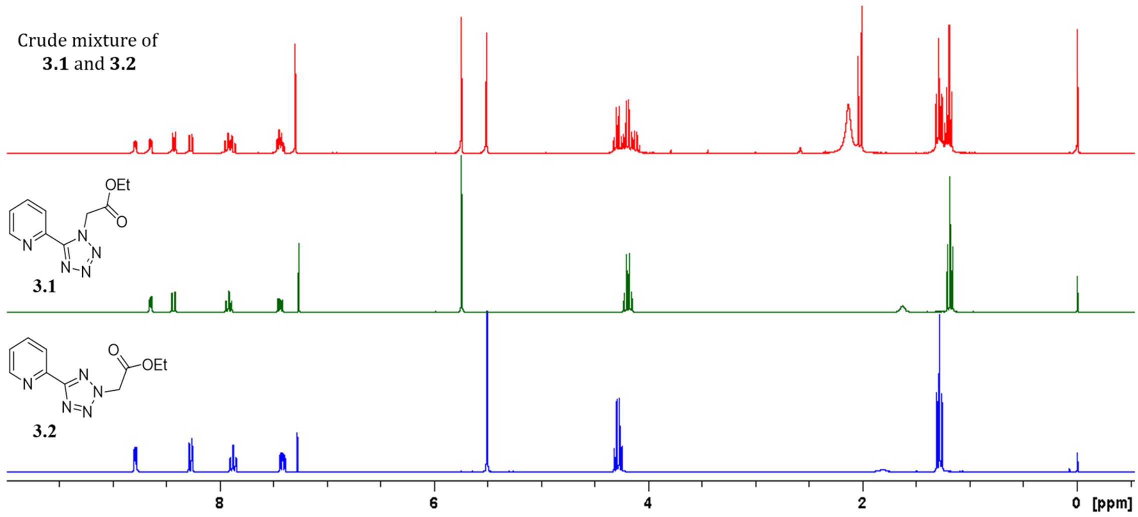

Figure 3.11: ^{1}H NMR spectra of crude mixture of **3.1** and **3.2** (red), purified **3.1** (green) and purified **3.2** (blue), which were all obtained in $CDCl_3$.

Single crystals were obtained for compound **3.1** and were analysed by X-ray crystallography. The results of this analysis are presented in Figure 3.12 and reveal that the pyridine and tetrazole rings are almost co-planar with respect to each other, with the ester pendant arm appearing not to have a pronounced effect on the co-planarity. The methylene group connecting the ester moiety to the tetrazole ring allows the group to orientate itself out of the plane of the heterocyclic systems, being at an angle of 71.1(4)° to the two heterocyclic ring systems.

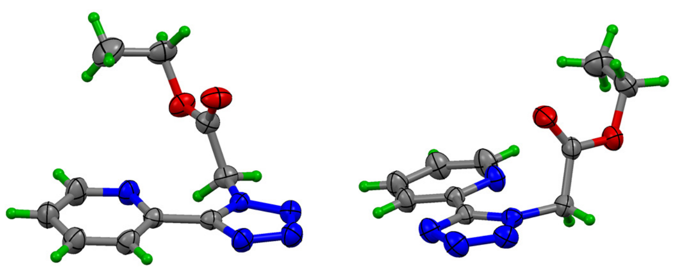

Figure 3.12: Crystal structures of **3.1**. Figure on right demonstrates the non co-planar nature of the ester arm with respect to the pyridyl tetrazole rings. Blue = nitrogen, red = oxygen, grey = carbon, green = hydrogen.

3.3.2 Metal Complexation Reactions

3.3.2.1 Metal Complexation with Pyridyl Tetrazole Ester Derivatives

Metal complexation reactions were carried out in a 1:1 metal to ligand stoichiometric ratio in MeOH. After 2 h at reflux temperature, the reaction solutions were cooled to room temperature and allowed to stand for several days. The resulting solids were then filtered off.

The product from the reaction of **3.1** with $CuCl_2.2H_2O$ was a green crystalline solid. In order to determine if the ester group was coordinating to the Cu(II) atom, IR spectroscopy was undertaken. If the ester group was coordinated to the metal centre, a significant decrease of the ν(C=O) frequency would be expected (with shifts of 50-150 cm^{-1}) and an increase of the ν(C-O) vibration would also be observed.[166] The IR spectrum of the complex showed no such significant shifts for the ν(C=O) and ν(C-O) frequencies, indicating that Cu(II) was not coordinating to the oxygens of the ester moiety. There was however evidence of metal coordination to the pyridine and tetrazole nitrogens, with the heterocyclic bands shifting from 1591, 1474 and 1437 cm^{-1} in the free ligand, to 1615, 1482 and 1456 cm^{-1} in the complex, respectively. Elemental analysis revealed a metal to ligand ratio of 1:1, therefore it was postulated that the complex could be a dimer similar to those synthesised in Chapter 2, as the elemental analysis results were within tolerance of the calculated percentages for a dimer with four chlorine atoms. The magnetic moment of the complex was 1.7 B.M. which was slightly low for a Cu(II) complex, but further suggested that the complex could be a dimer with slight interactions between the Cu(II) atoms. Single green crystals of **3.8** were obtained and analysed by X-ray crystallography, the results of which can be seen in Figure 3.13.

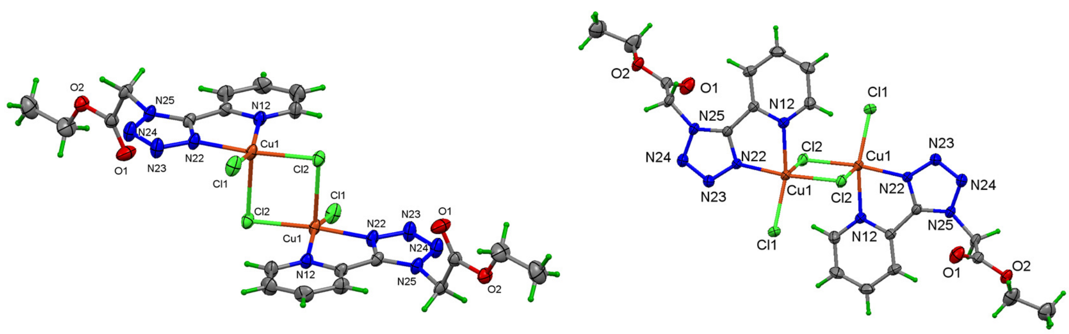

Figure 3.13: Two views of the molecular structure of **3.8** highlighting the square pyramidal Cu geometry and $[Cu(II)(\mu\text{-}Cl)Cl]_2$ unit with displacement ellipsoids at the 30% probability level.

The crystal structure of **3.8** established the 1:1 nature of the molecule. The molecular structure consists of a dichloro-bridged dimeric $[Cu(II)(\mu\text{-}Cl)Cl]_2$ unit, with the coordination sphere about each Cu(II) atom comprising one pyridine N atom, one tetrazole N atom and three chlorine atoms (two of which are μ-Cl bridging chlorines). The dimeric complex lies on a crystallographic inversion centre which lies at the centre of the $[Cu(II)(\mu\text{-}Cl)Cl]_2$ core and this structure is similar to the previously discussed copper dimer complexes in Chapter 2 (Figure 2.11).[121] The coordination geometry of each Cu(II) centre is distorted square pyramidal, with the Addison parameter, $t = 0.22$ (where $t = 0$ for ideal square pyramidal and $t = 1$ for ideal trigonal bipyramidal). Each pyridyl tetrazole ligand binds to the Cu(II) atom through one tetrazole N atom at the N-1 site of the tetrazole ring and through the pyridyl N atom, generating a five-membered chelate ring. The 5-membered tetrazole ring is slightly twisted with respect to the 6-membered pyridyl ring at an angle of 9.9(2)° with the 6 atom co-planar ester group almost orthogonal with the tetrazole-pyridine ligand at 83.79(7)°. In the central core, the four-membered Cu_2Cl_2 ring is planar and is comparable with those of related dichloro-bridged dimers in the literature.[167]

Reaction of **3.2** with $CuCl_2.2H_2O$ yielded a blue crystalline solid, **3.9**. The IR spectrum of the complex again indicated that there was no interaction between the Cu(II) atom and the ester oxygen atoms as no significant shifts were seen for the ν(C=O) and ν(C-O) frequencies. As observed previously, there were shifts seen in the heterocyclic bands of the pyridine and tetrazole rings, indicating that the Cu(II) atom was interacting with the pyridine and tetrazole nitrogens. Magnetic moment measurements at room temperature recorded a μ_{eff} of 2.1 B.M. Elemental analysis yielded a metal to ligand ratio of 1:2, therefore it was proposed that complex **3.9** had only one copper atom coordinating to two ligands through the pyridine and tetrazole nitrogens. In order to counter balance the +2 charge on the Cu(II) it was suggested that two chlorine atoms were also coordinating to the metal centre. The calculated elemental composition of the proposed structure correlated well with the elemental analysis results. The structure was further established when blue crystals of the complex, obtained in MeOH, were analysed by X-ray crystallography. The complex lies on a crystallographic inversion centre (Figure 3.14) with the Cu(II) centre adopting a slightly distorted octahedral coordination geometry. The Cu(II) ion is coordinated by two equatorial pyridyl tetrazole ligands and two axial chloride anions. A *pseudo* Jahn-Teller distortion is observed as elongation along the N22···Cu1···N22 coordination bonds is observed. In **3.9**, there is a slight twist within the ligand so that the planes of the tetrazole and pyridine rings form a dihedral angle of 5.38(13)°; the five atom co-planar ester group is 77.93(5)° to the 11-atom ligand ring atoms (the terminal CH_3 is not included). The coordination at the Cu centre is asymmetric with the Cu-N bond lengths differing by 0.44 Å. Differences can be ascribed to the 5 *vs* 6-coordination and the more symmetrical nature of **3.8** as compared to **3.9** at the Cu centre. There are no classical hydrogen bonds in **3.9**.

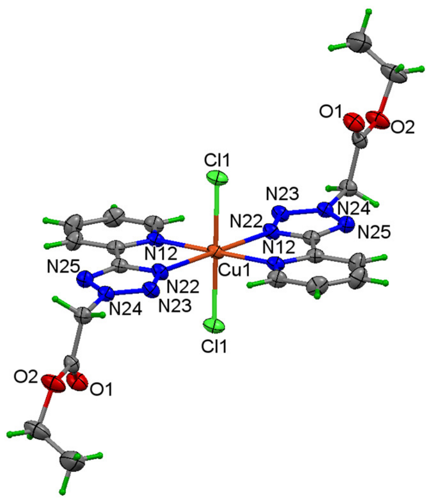

Figure 3.14: The molecular structure of **3.9** with displacement ellipsoids at the 30% probability level.

Taking into consideration that the ester group was not involved in metal coordination, complexes **3.8** and **3.9** were further reacted with either two equivalents of sodium perchlorate or two equivalents of copper salts in an attempt to achieve coordination with the ester. Unfortunately, these reactions yielded crystalline products which on analysis proved to be starting materials **3.8** and **3.9**. At this point, it was decided that conversion of the ester to a carboxylic acid group would have to be undertaken.

3.3.2.2 Metal Complexation of *in situ* Generated Pyridyl Tetrazole Carboxylate Derivatives

Recent work by Yuan and co-workers[154] using the ligand tetrazole-5-ethyl acetate with $CuCl_2.2H_2O$ in NaOH solution resulted in the formation of the polymeric coordination complex seen in Figure 3.7. Two important features of this complex were both the loss of the ester group and the incorporation of the sodium ion into the polymer on complexation. This raised the question as to whether the ligands **3.1** and **3.2** would behave in a similar manner, under similar conditions.

The conversion of an ester to a carboxylic acid is easily achieved using NaOH in MeOH or water.[168] These reaction conditions were suitable for our purposes as they would have a two-fold benefit; firstly, they would give a carboxylate group on the tetrazole unit and this carboxylate could then become involved in inter- and intramolecular interactions, and secondly, as there would be sodium ions in solution, these ions could interact with the carboxylate groups to form heterometallic CPs. In addition, there was also the practical advantage of not having to isolate and purify the carboxylic acid derivatives. The conditions used and the notations used for the *in situ* generated ligands herein are shown in Scheme 3.2.

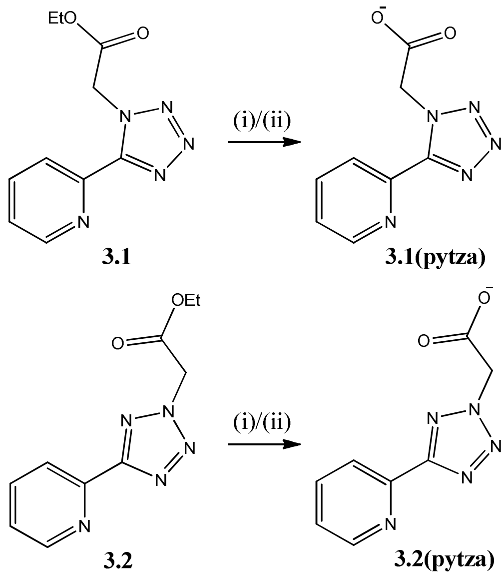

Scheme 3.2: Reagents and conditions: (i) NaOH, MeOH or (ii) NaOH, MeOH:H_2O.

3.3.2.2.1 Reactions with $CuCl_2.2H_2O$

The initial reaction involving **3.1** was carried out in MeOH as the ligand was soluble in this solvent. NaOH was added and the solution was heated to reflux for 1 hour. After this time, it was evident that there was no ester remaining in the solution as there was only a baseline spot present on the TLC plate. $CuCl_2.2H_2O$ in MeOH was added to the pH 8 solution and immediately a blue precipitate formed (**3.10**). IR spectral analysis on the blue solid showed characteristic stretches for the carboxylate group, pyridine and tetrazole rings. In the case of carboxylate derivatives, it is generally accepted that it is possible to distinguish between ionic, monodentate, chelating bidentate or bridging bidentate groups on the basis of calculating the difference in frequency between the anti-symmetric COO^-

($\nu_{asym}(COO^-)$) vibration and the symmetric COO^- ($\nu_{sym}(COO^-)$) vibration.[169,170] The following trend should be seen for $\Delta(\nu_{asym}(COO^-) - \nu_{sym}(COO^-))$:

$$\Delta_{monodentate} > \Delta_{ionic} > \Delta_{bridging\ bidentate} > \Delta_{chelating\ bidentate}$$

Monodentate coordination removes the equivalence of the two oxygen atoms and if the bond orders are significantly affected, a pseudo-ester configuration is obtained. This increases the $\nu_{asym}(COO^-)$, decreases $\nu_{sym}(COO^-)$ and therefore increases the separation (Δ) between the two frequencies.[169] In the IR spectrum of **3.10**, the $\nu_{asym}(COO^-)$ and $\nu_{sym}(COO^-)$ bands were strong bands observed at 1655 cm^{-1} and 1393 cm^{-1}, respectively. The Δ value was therefore 262 cm^{-1}. Carboxylates which have $\Delta > 200$ cm^{-1} typically coordinate in a monodentate fashion.[169] Coordination to the tetrazole and pyridine rings was also evident with the heterocyclic bands shifting to 1614, 1471 and 1456 cm^{-1}, from 1591, 1474, and 1437 cm^{-1} respectively in the uncoordinated ligand. Elemental analysis of the blue solid suggested that no sodium was present in the complex but that a 1:1 metal to ligand ratio was possible. The powder was taken up in water and allowed to stand for several days, after which time, blue block crystals formed. IR spectral analysis of the crystals confirmed that they were the same as the original amorphous solid, therefore X-ray analysis was performed on a single crystal of the sample.

The X-ray crystal structure of **3.10** is shown in Figure 3.15. The crystal structure of **3.10** reveals that the repeating asymmetric unit contains one Cu atom and one ligand, which was the suggested ratio observed in the elemental analysis. Each Cu(II) centre is in a distorted octahedral geometry with elongation observed along the N22···Cu1···N22 axis. The Cu(II) ion is coordinated by four nitrogen atoms of two **3.1(pytza)** ligands in the equatorial plane and two axial oxygen atoms from two other **3.1(pytza)** ligands lying above and below the Cu(II) ion (Figure 3.15). The molecule is neutral overall since the charges on the copper ion are balanced by the two singly charged anionic carboxylate ligands. Thus, each ligand (that exhibits a considerable twist of 15.0(3)° between the pyridine/tetrazole rings) is involved in bonding one copper ion through the pyridine N atom and the tetrazole N-1 atom, in a bidentate manner, while also bonding to a second copper ion through the O2 oxygen atom of the carboxylate group in a monodentate fashion. This method of bridging is common in carboxylate complexes.[171]

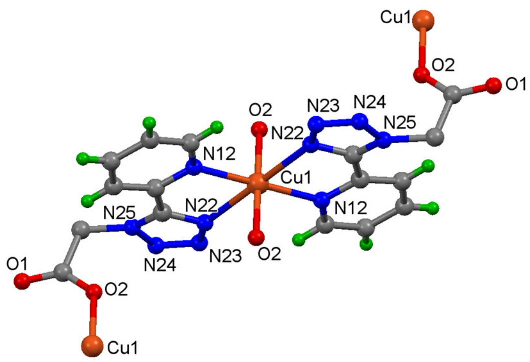

Figure 3.15: The molecular structure of **3.10** with displacement ellipsoids at the 30% probability level and highlighting the Cu-O$_{carboxylate}$ binding.

Only one of the two carboxylate oxygen atoms are involved in bonding within the polymeric chain. The partial packing diagram in Figure 3.16 shows that the complex is oriented in a stepwise manner with interactions between the copper ions and the carboxylate groups only occurring along the stepwise direction. No strong interactions are observed between the 1-D steps.

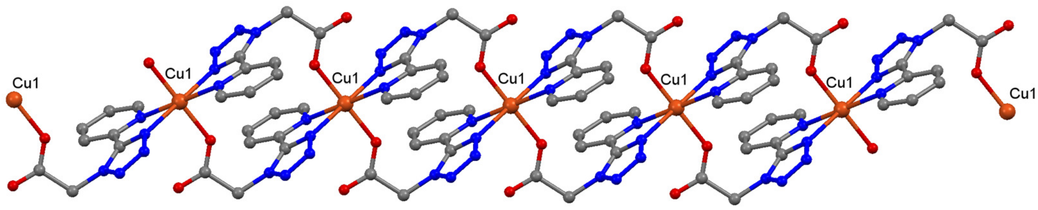

Figure 3.16: The 1-D chain formation in **3.10** (with displacement ellipsoids at the 30% probability level) highlighting the polymeric nature of the Cu-O$_{carboxylate}$ binding. Hydrogen atoms omitted for clarity.

The formation of this 1-D CP was a promising indication that the *in situ* generated carboxylate derivatives could be a useful organic linker in the construction of frameworks. However, improvements on the reaction conditions were sought. This was in order to obtain more crystalline products from the reaction mixture, achieve higher dimensionality in the frameworks and to perhaps incorporate sodium ions into the framework. Hence, the next reaction with **3.1** was carried out in H_2O and MeOH in a 10:1 ratio, as it was thought that the solubility of the complex would have been better and therefore crystalline material could form slowly in the reaction medium. This reaction successfully produced blue-green block crystals on allowing the solution to stand for one day. Interestingly, the

IR spectrum and the elemental analysis of this compound, **3.11**, suggested that it was an entirely different compound to the one synthesised in MeOH. The IR spectrum of compound **3.11** again suggested that monodentate coordination was occurring between a carboxylate oxygen and the Cu(II) ion, with the $\nu_{asym}(COO^{-})$ and $\nu_{sym}(COO^{-})$ bands observed at 1650 cm^{-1} and 1359 cm^{-1}. However, another mode of binding was also evident. Intense bands were present at 1610 cm^{-1} and 1458 cm^{-1}, and these were postulated to be additional $\nu_{asym}(COO^{-})$ and $\nu_{sym}(COO^{-})$ vibrations, respectively. Therefore, a $\Delta(\nu_{asym}(COO^{-}) - \nu_{sym}(COO^{-}))$ value of 152 cm^{-1} would exist. It is generally accepted that Δ values < 200 cm^{-1} belong to chelating and/or bridging carboxylate ligands.[169] Elemental analysis indicated that the composition of the complex was 1:2 metal to ligand, hence it could have been possible for one ligand to be binding in a monodentate manner, and another to be binding in a chelating or bridging manner.

Single crystals of **3.11** were analysed by X-ray crystallography and this revealed that there was indeed two modes of carboxylate coordination present. The molecular structure, shown in Figure 3.17, consists of one ligand behaving in a bridging fashion, *via* one carboxylate oxygen binding in a monodentate manner and two nitrogens binding in a chelating fashion. The second ligand is only involved in chelation through its carboxylate group, with the remaining nitrogen donors at most only engaging in hydrogen bonding. This behaviour is reminiscent of the behaviour of bisphosphines whereby they can bind to metals in typically a bridging or chelating manner or *via* binding through one of the phosphorus atoms.[172] This bonding results in a dimeric molecular complex, with the asymmetric unit comprising one Cu(II) metal centre, one H_2O molecule and two **3.1(pytza)** ligands. The complex is built up about inversion centres midway between the two Cu(II) metal centres.

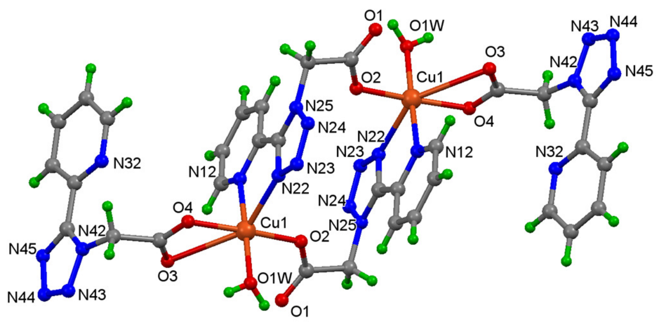

Figure 3.17: The molecular structure of **3.11** with displacement ellipsoids at the 30% probability level.

Each Cu(II) ion is in a distorted octahedral geometry, although the very long Cu1···O3 distance (2.76 Å) implies that a five-coordinate description may be equally valid. The coordination sphere around each Cu(II) centre consists of (i) a pyridine nitrogen atom and a tetrazole N atom from one ligand, (ii) one oxygen atom from the carboxylate group of a second ligand, (iii) two oxygen atoms from the carboxylate group of a third ligand, and (iv) a H_2O molecule that completes the hexa-coordinate geometry. The ligands in **3.11** are not planar, and as has been noted previously, they exhibit a measure of interplanar distortion and exhibit dihedral angles of 7.4(2)° and 6.8(3)° between the planes of the pyridine and tetrazole rings. The 16 membered ring that is formed by the two bridging ligands possesses a square-like cavity with dimensions of 4.13 Å by 5.01 Å.

The coordination of the H_2O molecule to the Cu(II) metal centre is the most obvious difference between the structures of **3.10** and **3.11** and its presence has an effect on the resulting coordination network (Figures 3.18 and 3.19). The water molecule participates in strong hydrogen bonding involving reciprocal water O1W···$O_{carboxylate}$ hydrogen bonds about inversion centres in an inorganic complex that is rich in hydrogen bond acceptors; the intermolecular O···O distances are 2.680(5) and 2.736(5) Å. The strong hydrogen bonding between dimers thus generates a hydrogen bonded chain along the *b*-axis direction. Hydrogen bonded chains are further linked into a 2-D network of hydrogen bonds by a combination of several C-H···O/N interactions (Figures 3.18 and 3.19).

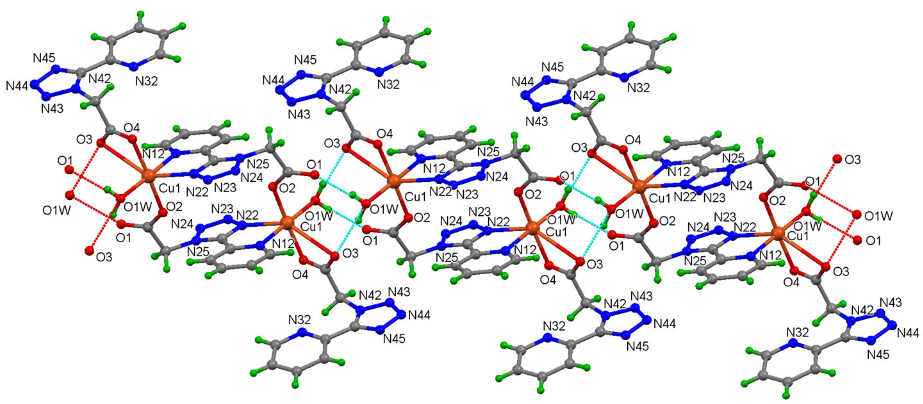

Figure 3.18: The primary hydrogen bonding (shown in blue) involving O1W and linking molecules of **3.11**.

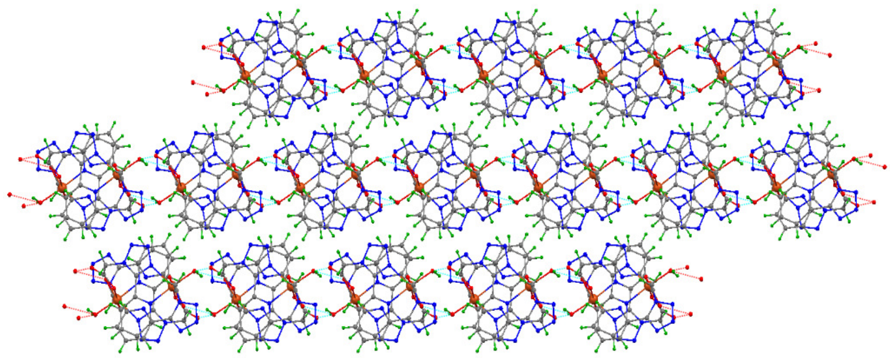

Figure 3.19: A view of hydrogen bonding between molecules of **3.11** in the three hydrogen bonded chains propagating along the *b*-axis direction.

Therefore, it was evident that reaction solvent had a big influence on the resulting structures of the complexes. This prompted similar investigations into the behaviour of the N-2 regioisomer (**3.2**) in different solvents. Thus, *in situ* hydrolysis of **3.2** was carried out in either MeOH or MeOH:H_2O mixtures, and after 1 hour $CuCl_2.2H_2O$ was added to the reactions. In the reaction carried out in MeOH, a pale green precipitate, **3.12**, formed immediately on addition of the metal salt. This precipitate was analysed by IR spectroscopy and again it was evident from the abundance of peaks in the $\nu_{asym}(COO^-)$ and $\nu_{sym}(COO^-)$ region that the ligands were coordinating to the metal centre *via* more than one coordination mode. There was also a broad signal at ~3262 cm^{-1} which suggested that hydroxide anions could be involved in bonding. Elemental analysis suggested a 1:1 metal to ligand ratio. Due to the success of growing crystals of **3.10** from an aqueous solution, attempts at growing crystals of **3.12** were attempted under similar conditions. However, solubility of the complex was very poor in most solvents, and heat was required to dissolve the material into H_2O and DMSO. This often resulted in changes to the molecular structure of **3.12**, and this was evident on performing IR analysis of the materials which formed in the H_2O and DMSO solutions over time. In some cases, conversion to **3.13** was observed (Figure 3.21). Therefore, a proposed structure of **3.12** was tentatively suggested and can be seen in Figure 3.20.

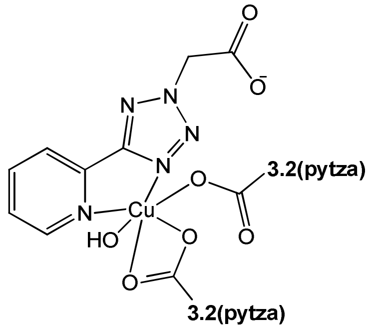

Figure 3.20: Proposed structure of **3.12**.

To investigate the effect of using H_2O as the reaction medium, **3.2** was again hydrolysed *in situ* in a mixture of H_2O and MeOH (10:1). On addition of $CuCl_2.2H_2O$, a blue crystalline solid formed almost immediately. The IR spectrum of the solid displayed a very broad stretch (2973-3433 cm^{-1}) centred at 3166 cm^{-1}, indicating that there could be coordinated H_2O molecules and extensive hydrogen bonding present in the complex. An absence of a peak around 1713 cm^{-1} indicated that the carboxyl group of **3.13** was deprotonated. The $\nu_{asym}(COO^-)$ band was visible at 1628 cm^{-1} and the $\nu_{sym}(COO^-)$ band appeared at 1374 cm^{-1}. This yielded a $\Delta(\nu_{asym}(COO^-) - \nu_{sym}(COO^-))$ value of 254 cm^{-1}, which corresponded to monodentate carboxylate coordination, however it was noted that the $\nu_{asym}(COO^-)$ band was lower in frequency compared to **3.10** and **3.11**. Metal coordination to the pyridyl tetrazole moiety was also alluded to, as shifts in the heterocyclic bands (ν(C=N), ν(N=N)) to 1452, 1465 and 1614 cm^{-1} were visible. Elemental analysis indicated a 1:2 metal to ligand composition.

To achieve single crystals of **3.13** that were suitable for X-ray crystallography, a number of parameters were altered. It was found that by reducing the ratio of MeOH in the reaction medium, the solid became less powdered in appearance and that crystal sizes became bigger. It also became apparent that slow cooling also resulted in larger single crystals. Therefore, the optimum conditions to obtain large single crystals of **3.13** were to employ 100% water as the reaction medium followed by slow cooling after addition of the metal salt. The obtained crystals were solved by X-ray crystallography and the molecular structure and primary hydrogen bonding system of **3.13** is depicted in Figure 3.21.

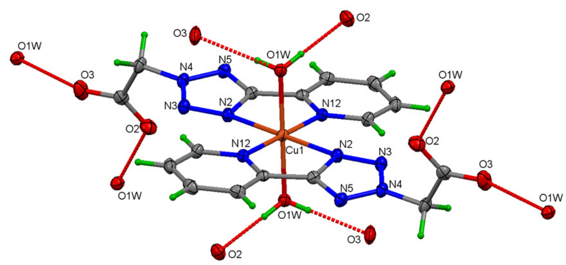

Figure 3.21: The molecular structure of **3.13** with displacement ellipsoids at the 30% probability level including the primary intermolecular O-H⋯O hydrogen bonds.

Each Cu(II) ion is in a distorted octahedral geometry, resulting from the coordination of two **3.2(pytza)** ligands through the pyridine N atom and one tetrazole N atom from each ligand and two H_2O molecules, yielding an isolated complex. Jahn-Teller elongation is observed along the N2⋯Cu1⋯N2 axis (2.34 Å compared to 2.02 Å for all other Cu-L bonds). This observation of an elongated coordination bond between the metal ion and the tetrazole nitrogens correlates well with previously discussed distorted octahedral complexes in this Chapter. Each **3.2(pytza)** ligand is negatively charged through the loss of a carboxylate proton, thereby making the overall molecule neutral. Also, both carboxylate C-O bond lengths are similar in bond length, therefore are intermediate between single and double bonds. This would justify a $\Delta(\nu_{asym}(COO^-) - \nu_{sym}(COO^-))$ value of 254 cm^{-1}, which is typical of ionic carboxylate values and are generally lower than monodentate binding carboxylates. Each H_2O molecule is involved in two hydrogen bond interactions with the carboxylate groups of two different **3.2(pytza)** ligands, as shown in Figures 3.22, forming a 3-D network. This strong O-H⋯O hydrogen bonding creates a large network of interactions throughout the 3-D hydrogen bonded structure with molecular niches, however these niches are too small to contain a solvent molecule.

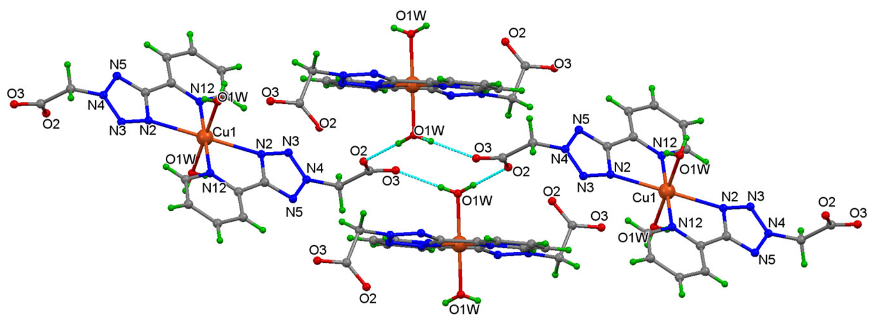

Figure 3.22: Part of the intricate intermolecular O-H⋯O hydrogen bonding in structure of **3.13** with displacement ellipsoids at the 30% probability level.

During the course of this work, Yang and co-workers published their work on CPs utilising 5-(2-pyridyl)tetrazole-2-acetic acid (Figure 3.23).[173] Under solvothermal conditions, and after longer reaction times (48 h), they obtained several hydrogen bonded networks similar to **3.13**. Herein, we present the first Cu(II) coordination network of this type and present a new less stringent synthetic route to obtain such networks.

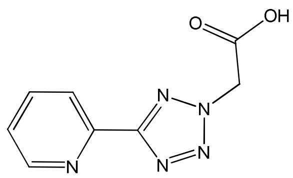

Figure 3.23: 5-(2-pyridyl)tetrazole-2-acetic acid was used in the solvothermal synthesis of coordination architectures.[173]

3.3.2.2.2 Reactions with $ZnCl_2$

Reactions of **3.1** and **3.2** with $ZnCl_2$ were carried out in the same manner as in section 3.3.2.2.1. The reaction of **3.1** with NaOH in MeOH followed by the addition of a methanolic solution of $ZnCl_2$ yielded a clear solution which was allowed to stand for several days. A crystalline creamy white solid formed which was filtered and washed with MeOH. The IR spectrum of the solid, **3.14**, was a simple spectrum. The absence of the characteristic band for the protonated carboxylate group (1724 cm^{-1}) indicated complete deprotonation of **3.1(pytza)**. A $\nu_{asym}(COO^-)$ band could clearly be seen at 1650 cm^{-1}, and the corresponding $\nu_{sym}(COO^-)$ band was observed at 1365 cm^{-1}. This gave a $\Delta(\nu_{asym}(COO^-) - \nu_{sym}(COO^-))$ value of 285 cm^{-1}, suggesting a monodentate coordination of the carboxylate group to the Zn(II) atom. Shifts for the heterocyclic ν(C=N) and ν(N=N) vibrations were also noted to have shifted from 1478, 1438 and 1354 cm^{-1} to 1610, 1474 and 1462 cm^{-1} respectively. This indicated that Zn(II) coordination to the pyridine and tetrazole nitrogens was also occurring. There was no indication of the presence of coordinating solvent molecules or hydrogen bonding in the complex in the IR spectrum, as peaks in the region of 3000 cm^{-1} were only due to aliphatic stretches. Elemental analysis suggested that the composition of the complex was 1:1 metal to ligand ratio. Therefore it was proposed that the Zn(II) atom was in an octahedral geometry, with four coordination sites taken up by chelation to two **3.1(pytza)** ligands *via* four nitrogens and the remaining two coordination sites occupied by two carboxylate oxygens from another two **3.1(pytza)** ligands bonding in a monodentate manner. This would lead to a 1-D polymeric chain like that seen in **3.10**. The proposed structure of the complex is presented in Figure 3.24. The ^1H NMR spectral analysis of **3.14** was carried out in d_6-DMSO and resulted in a simple spectrum. The spectrum showed differences in shifts from those in the free protonated **3.1(pytza)** ^{1}H NMR spectrum, indicating that the complex was not decomposing into free ligand in the d_6-DMSO solution.

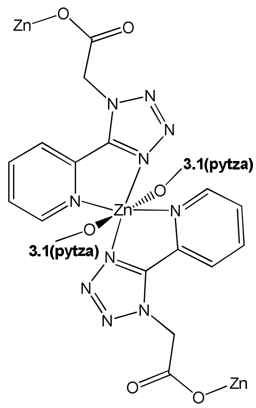

Figure 3.24: Proposed structure of **3.14**.

Five signals in total were observed, which would be expected if the complex had the structure as depicted in Figure 3.22. Four multiplets arising from the pyridyl protons were seen at 7.57, 8.04, 8.25 and 8.68 ppm and a singlet was observed 5.53 ppm which integrated for twice that of the pyridyl protons, hence this signal was assigned to the CH_2-tet protons.

When **3.1** was reacted with NaOH in H_2O:MeOH (10:1) followed by the addition of an aqueous solution of $ZnCl_2$, the resulting clear solution was allowed to stand for several days. The resulting crystalline solids were filtered off and washed with H_2O. On analysis of the IR spectrum of the white solid (**3.15**), it was suggested that the carboxylate was either ionic or adopting a monodentate coordination to the metal centre, as the $\nu_{asym}(COO^-)$ vibration was observed at 1650 cm^{-1} and the $\nu_{asym}(COO^-)$ was observed at 1364 cm^{-1}, yielding a $\Delta(\nu_{asym}(COO^-) - \nu_{sym}(COO^-))$ value of 286 cm^{-1}. There was also a broad stretch centred at ~3126 cm^{-1} indicating the presence of H_2O molecules in the complex. Elemental analysis suggested that the complex possessed a 1:2 metal to ligand ratio. The ^{1}H NMR spectrum of **3.15** displayed five signals: four signals were present in the aromatic region and a singlet was present at 5.48 ppm. Considering the elemental analysis results and the observed NMR signals, it was suggested that the two ligands were in the same environment, thus forming a symmetrical molecule. The proposed structure can be seen in Figure 3.25.

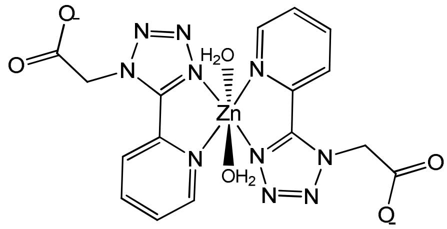

Figure 3.25: Proposed structure of **3.15**.

The reaction of **3.2** with NaOH and $ZnCl_2$ in MeOH resulted in a clear solution which was allowed to stand for several days and the resulting solids were filtered to yield **3.16** as a cream solid which was firstly was analysed by IR spectroscopy. In the IR spectrum, an absence of a peak at 1713 cm^{-1} indicated that the carboxylate was in its deprotonated form. The $\nu_{asym}(COO^-)$ stretch was observed at 1645 cm^{-1} and the $\nu_{sym}(COO^-)$ stretch was observed at 1383 cm^{-1}, yielding a $\Delta(\nu_{asym}(COO^-) - \nu_{sym}(COO^-))$ value of 263 cm^{-1}. This suggested that the carboxylate was binding in a monodentate or ionic manner. Zn(II) coordination to the pyridine and tetrazole nitrogens was also evident with shifts of the ν(C=N) and ν(N=N) bands moving from 1604, 1434 and 1429 in the free ligand to 1611, 1451 and 1417 cm^{-1} in the complex. New bands at higher frequencies (3523, 3423 and 3090 cm^{-1}) appeared in the IR spectrum of the complex. These bands were attributed tentatively to the stretching vibrations of OH groups from coordinated solvent. Elemental analysis of the compound indicated that the composition of the complex was 1:1 metal to ligand. In the ^1H NMR spectrum of the product, there were four multiplets, each with a relative integration of one, corresponding to four aromatic pyridine protons, and a singlet at 5.44 ppm with a relative integration of two, which corresponded to the CH_2-tet protons which would be expected to remain after hydrolysis. On inspection of the ^{13}C NMR spectrum of the product, signals were as expected for the carboxylate, pyridine and tetrazole carbons. Of interest however, were the presence of two signals at 48.5 and 55.3 ppm. One would expect for there to be only one carbon signal for the CH_2-tet carbon in this region. After carrying out a DEPT-135 experiment, it was evident that the signal at 55.3 ppm corresponded to a CH_2 carbon, and that the signal at 48.5 ppm corresponded to either a CH or a CH_3 carbon. Taking into account that the reaction solvent was MeOH, it was postulated that this signal could arise from a coordinated OCH_3 group. The lack of visible signals for these protons in the ^1H NMR spectrum could have been due to overlapping with the substantial d_6-DMSO residual solvent peak. Taking all this information into consideration, a structure was proposed, a representation of which can be seen in Figure

3.26. It was proposed that a dinuclear complex existed, with both Zn(II) atoms in a tetrahedral geometry, as Zn(II) generally prefers this coordination geometry over square planar.[132] One Zn(II) metal centre is coordinated by two **3.2(pytza)** ligands *via* four nitrogens, with the 2^+ charge being counter balanced by two negatively charged **3.2(pytza)** ligands. The second Zn(II) metal centre is proposed to be coordinated by two carboxylate oxygens from two **3.2(pytza)** ligands, both bonding in a monodentate manner, and two methoxy groups, whose negative charge would counter balance the 2^+ charge on this Zn(II) metal centre.

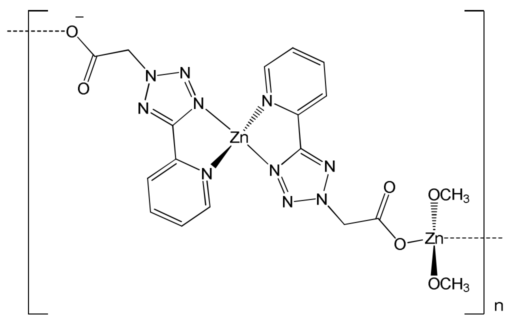

Figure 3.26: The proposed structure of a subunit of the coordination polymer **3.16**.

Reaction of **3.2** with NaOH was then carried out in H_2O, followed by the addition of an aqueous solution of $ZnCl_2$. The resulting crystalline solid, **3.17**, was filtered off and washed with water. The IR spectrum of **3.17** again lacked a peak at 1713 cm^{-1}, indicating that the carboxylate was in the deprotonated form. The spectrum did display a $\nu_{asym}(COO^-)$ stretch at 1638 cm^{-1} and a $\nu_{sym}(COO^-)$ stretch at 1373 cm^{-1}, giving a $\Delta(\nu_{asym}(COO^-) - \nu_{sym}(COO^-))$ value of 265 cm^{-1}. Again, it was noted that the $\nu_{asym}(COO^-)$ and $\nu_{sym}(COO^-)$ stretches were of lower frequencies compared to previous monodentate species, therefore the presence of ionic carboxylates was also taken into consideration. Broad signals (2867-3419 cm^{-1}) centred at 3236 cm^{-1} were also visible in the IR spectrum, which suggested that there were coordinating solvent molecules and hydrogen bonding present in the complex. Elemental analysis of the complex indicated a 1:2 metal to ligand composition. As previously mentioned, work by Yang *et al*. involved the use of 5-(2-pyridyl)tetrazole-2-acetic acid (Figure 3.23) in constructing coordination networks. In the course of this work, they obtained a Zn(II) complex solvothermally after 48 h using a 7:1 ratio of MeOH and H_2O.[174] The data they obtained for this complex correlated with the data obtained for **3.17**. The group also obtained a crystal structure of the complex, and this can be seen in Figure 3.27.

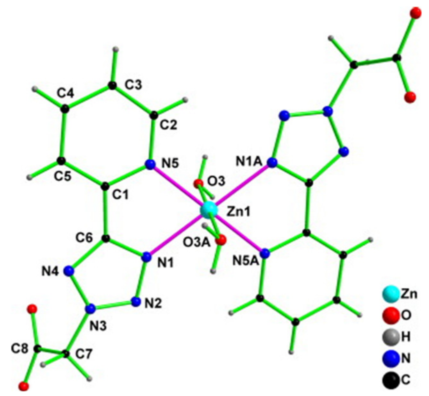

Figure 3.27: Crystal structure of a Zn(II) complex obtained from a solvothermal reaction in H_2O and MeOH after 48 h.[174]

The data obtained for compound **3.17** is in agreement with the crystal structure obtained by Yang and co-workers, and is analogous to the Cu(II) complex **3.13** synthesised previously.

3.3.2.2.3 Reactions with $NiCl_2.6H_2O$

The addition of $NiCl_2.6H_2O$ to a solution of **3.1** and NaOH in MeOH led to a pale blue precipitate forming in solution, which was filtered and dried to yield **3.18**. The blue powder was analysed by IR spectroscopy which revealed that no protonated carboxylate was present as there was an absence of the characteristic peak for such a group. A $\nu_{asym}(COO^-)$ stretch was observed at 1646 cm^{-1} and a $\nu_{sym}(COO^-)$ stretch was observed at 1367 cm^{-1}, giving a $\Delta(\nu_{asym}(COO^-) - \nu_{sym}(COO^-))$ value of 279 cm^{-1}. This suggested that the carboxylate groups were coordinating to the metal in a monodentate manner. Coordination of Ni(II) to the pyridine and tetrazole nitrogens was also evident as significant heterocyclic stretches were observed to shift to 1615, 1479 and 1463 cm^{-1} from 1590, 1473 and 1438 cm^{-1}, which were the heterocyclic frequencies observed in the IR spectrum of the free ligand. There was also a substantial broad stretch visible at 3401 cm^{-1}, indicating that OH groups from solvent or the metal hydrate were possibly present. Elemental analysis indicated that the composition of the complex was 1:1 metal to ligand. Hence, it was proposed that the Ni(II) atom possessed an octahedral geometry, with the coordination sphere being occupied by four **3.1(pytza)** ligands; two ligands coordinating *via* their pyridyl and tetrazole nitrogens and the remaining two coordinating in a monodentate manner *via* their carboxylate oxygens. The presence of solvent which was indicated in the IR spectrum of **3.18** is proposed to be a molecule of water that could be present in the sample. The proposed structure would have the same arrangement as seen for **3.10**, forming a 1-D coordination polymer. When reacting **3.1(pytza)** with $NiCl_2.6H_2O$ in aqueous media (H_2O:MeOH, 10:1) a blue precipitate formed over time. The data obtained for this solid (**3.19**) correlated with that of **3.18**, hence it was proposed that in this case, solvent had no effect on the final structures and **3.19** was the same product as **3.18**.

A pale blue crystalline solid, **3.20**, formed on addition of methanolic $NiCl_2.6H_2O$ to **3.2(pytza)** in NaOH and MeOH. The IR spectrum of **3.20** displayed a $\nu_{asym}(COO^-)$ peak at 1630 cm^{-1} and a $\nu_{sym}(COO^-)$ peak at 1373 cm^{-1}. This gave a $\Delta(\nu_{asym}(COO^-) - \nu_{sym}(COO^-))$ value of 257 cm^{-1} which suggested either a monodentate or an ionic carboxylate was present in the complex. A broad stretch centred at 3234 cm^{-1} was also observed, indicating that some solvent molecules were present and perhaps involved in hydrogen bonding. In the analogous reaction that was carried out in a mixture of H_2O and MeOH, a pale blue solid, **3.21**, precipitated. On IR spectral analysis of this solid, the same stretches were observed, suggesting that in this case the choice of solvent did not affect the final structures. The elemental analysis of both compounds pointed towards a 1:2 metal to ligand composition. Hence, the structure of **3.20** and **3.21** was proposed to comprise of an octahedral Ni(II) centre, with two **3.2(pytza)** ligands binding to the metal centre *via* their pyridine and tetrazole nitrogens and the remaining two coordination sites occupied by two H_2O molecules (Figure 3.28). It was postulated that the degree of hydration of the $NiCl_2$ salt played an important role in the synthesis of this coordination network, as it seemed to provide enough H_2O molecules in both solvents to produce this structure.

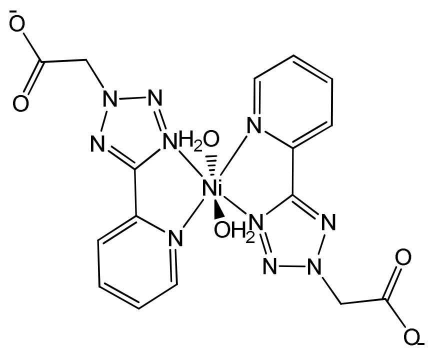

Figure 3.28: Proposed structure of **3.20** and **3.21**.

3.3.2.2.4 Reactions with $Co(SCN)_2$

The reactions of **3.1** and **3.2** with $Co(SCN)_2$ were carried out under the same conditions as in previous sections. In the reaction of **3.1** with NaOH in MeOH followed by the addition of $Co(SCN)_2$, a beige powder, **3.22**, precipitated immediately on addition of the metal salt. The solid was analysed by IR spectroscopy and the IR spectrum revealed that no protonated carboxylate was present as no peak was present at 1724 cm^{-1}. The $\nu_{asym}(COO^-)$ and $\nu_{sym}(COO^-)$ bands were observed at 1649 and 1361 cm^{-1} respectively. This gave a $\Delta(\nu_{asym}(COO^-) - \nu_{sym}(COO^-))$ value of 288 cm^{-1}, indicating that the carboxylate was coordinating to the metal centre in a monodentate manner. It was also evident that metal coordination to the pyridine and tetrazole nitrogens was occurring, as shifts in the ν(C=N) and ν(N=N) bands to higher frequencies compared to the free ligand were visible. The IR spectrum also revealed that no thiocyanate anions were present in the complex, with an absence of a characteristic $\nu(C\text{-}N)_{SCN}$ stretch at ~2070 cm^{-1}. Elemental analysis of **3.22** indicated a 1:1 metal to ligand composition. Hence, it was postulated that the structure of **3.22** was analogous to that of **3.10**; a 1-D polymeric structure with the octahedral Co(II) centre coordinated to two **3.1(pytza)** ligands *via* the pyridine and tetrazole nitrogens, and two **3.1(pytza)** ligands *via* the monodentate coordinating carboxylate oxygens.

A pink solution resulted from the reaction of **3.1** with NaOH in a mixture of H_2O and MeOH followed by the addition of an aqueous solution of $Co(SCN)_2$. On standing for several days an orange solid formed which was isolated. The IR spectrum of the product **3.23** displayed $\nu_{asym}(COO^-)$ and $\nu_{sym}(COO^-)$ stretches at 1650 and 1360 cm^{-1} respectively and complete deprotonation of the carboxylate was indicated by lack of a vibration at 1724 cm^{-1}. The $\Delta(\nu_{asym}(COO^-) - \nu_{sym}(COO^-))$ value was 290 cm^{-1}, therefore monodentate coordination of the carboxylate was possible. However, the $\nu_{asym}(COO^-)$ stretch was broad with a shoulder at 1611 cm^{-1} which alluded to an additional mode of carboxylate coordination being present, especially if the corresponding $\nu_{sym}(COO^-)$ frequency was the peak visible at 1462 cm^{-1}. Comprehensive assignments of these peaks however was hampered due to the heterocyclic stretches of the pyridine and tetrazole rings vibrating in the same region. New bands at ~3429 cm^{-1} indicated solvent molecules were present in the complex and the absence of a $\nu(C\text{-}N)_{SCN}$ stretch at ~2070 cm^{-1} indicated that there were no thiocyanate anions present. Elemental analysis suggested that the composition of the complex was 1:2 metal to ligand, therefore it was proposed that the complex consisted of a dinuclear octahedral Co(II) arrangement. Each Co(II) centre was proposed to coordinate to two nitrogens from one **3.1(pytza)** ligand, one carboxylate oxygen from another **3.1(pytza)** ligand, two oxygens from a third **3.1(pytza)** ligand and a H_2O molecule. This would resemble the arrangement seen in a previously discussed Cu(II) complex, **3.11** (Figure 3.17).

The reaction of **3.2** with NaOH in MeOH followed by the addition of $Co(SCN)_2$ in MeOH yielded a purple solution from which a pink precipitate formed almost immediately. This pink precipitate was filtered and air dried and then subsequently analysed by IR spectroscopy. A number of prominent peaks could be observed in the IR spectrum. An intense band was observed at 1608 cm^{-1} which was assigned to the $\nu_{asym}(COO^{-})$ stretch of the carboxylate group. A strong band was also present at 1397 cm^{-1} which was assigned to the $\nu_{sym}(COO^{-})$ stretch of the carboxylate group. The presence of OH containing groups was also evident as a broad intense band centred at 3393 cm^{-1} was observed. The presence of thiocyanate anions was revealed as two strong $\nu(C\text{-}N)_{SCN}$ stretching frequencies were observed at 2092 and 2116 cm^{-1}. The SCN group may coordinate to a metal through the nitrogen or the sulfur or through both. The $\nu(C\text{-}N)_{SCN}$ stretching frequencies are generally lower in N-bonded complexes (near or below 2050 cm^{-1}) than in S-bonded complexes, which have values near 2100 cm^{-1}. Frequencies well above 2100 cm^{-1} are generally bridging complexes.[150] On observing $\nu(C\text{-}N)_{SCN}$ frequencies appearing near 2100 cm^{-1}, it was proposed that the thiocyanate anions were S-bonded. On observation of the colour of the solid and its μ_{eff} value of 4.5 B.M., it could be presumed that the geometry of the metal centre was octahedral.[132] Therefore the Co(II) centre had to be coordinated by six atoms. If the pink sample was dried under vacuum the colour changed from pink to an intense blue. This implied that solvent molecules present in the octahedral complex were removed, thereby forming a tetrahedral complex. On leaving the solid in air at room temperature for ~1 h, the colour reverted back to pink again, implying that atmospheric water was being absorbed by the complex and hence forming an octahedral complex again. It is well known that Co(II) forms mainly octahedral or tetrahedral species, and there are several cases in which two types with the same ligand are both known. For a d^7 ion like cobalt, ligand field stabilisation energies do not discriminate against either geometry compared to lower or higher d^n ions. Therefore the abundance of complexes with both geometries are due to the small stability difference between them.[132] The change in geometry of the metal centre is concomitant with a change in the crystal field splitting, which is illustrated in Figure 3.29, for octahedral and tetrahedral fields. Δ_{tet} is significantly smaller than Δ_{oct}, implying that smaller amounts of energy are needed for an $t_2 \leftarrow e$ transition in the tetrahedral field than a $e_g \leftarrow t_{2g}$ transition in an octahedral field which often results in octahedral and tetrahedral complexes often having different colours.[56]

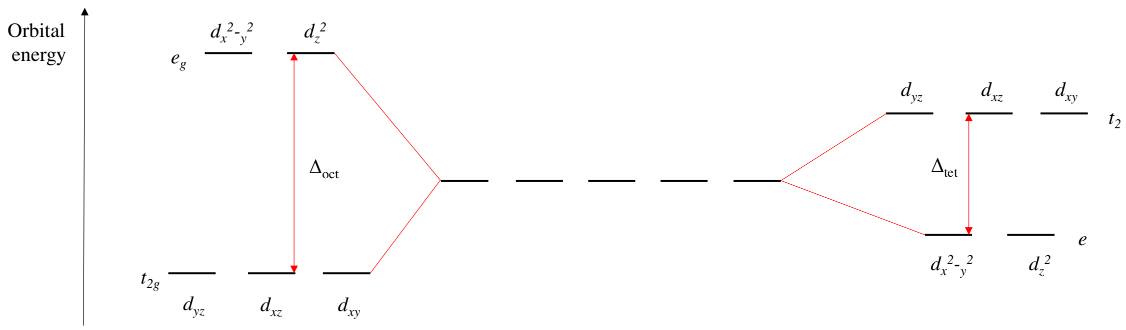

Figure 3.29: Crystal field splitting diagram for octahedral (left hand side) and tetrahedral (right hand side) fields.

Elemental analysis, IR and UV-Vis spectroscopy were carried out on the sample in both its pink and blue states. Elemental analysis indicated that on undergoing a geometry change, solvent molecules were removed as the percentage of carbon and nitrogen increased by ~4%. The IR spectra of both complexes also demonstrated that solvent molecules were removed on going from octahedral to tetrahedral as the broad stretch at 3393 cm^{-1} had decreased in intensity in the blue sample. Hence, two structures were proposed and these can be seen in Figure 3.30.

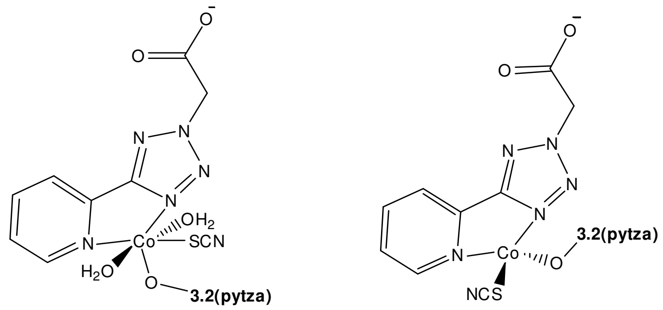

3.24a **3.24b**

Figure 3.30: Proposed structures for **3.24**; **3.24a** represents the proposed octahedral subunit of a coordination polymer and **3.24b** represents the proposed tetrahedral subunit of a coordination polymer which is formed on loss of solvent molecules.

Studies of electronic spectra of metal complexes can provide information about their structure and bonding. The colours of transition metal complexes arise from the splitting of the *d* orbitals caused by the presence of coordinating ligands. When the energy difference between the orbitals matches the energy of incoming light, light is absorbed by the solution and electronic transitions occur between the electronic energy levels. Transitions can occur between *d* orbitals on the metal centre (*d*-*d* transitions) or between metal- and ligand-centred orbitals which transfer charge from metal to ligand or ligand to metal. Electronic transitions obey certain selection rules, one of which is the Laporte selection rule (that there must be a change in parity). Hence, the allowed transitions are $s \rightarrow p$, $p \rightarrow d$, $d \rightarrow f$ and forbidden transitions are $s \rightarrow s$, $p \rightarrow p$, $d \rightarrow d$, $f \rightarrow f$, $s \rightarrow d$, $p \rightarrow f$. The observation of the Laporte forbidden *d*-*d* transitions can be explained by a mechanism called 'vibronic coupling'. Octahedral complexes possess a centre of symmetry, but molecular vibrations result in its temporary loss. When symmetry is briefly lost, mixing of *d* and *p* orbitals occur and a *d*-*d* transition involving an orbital of mixed *pd* character can occur although the absorption is still relatively weak. In tetrahedral complexes, where there is no centre of symmetry, *pd* mixing can occur to a greater extent and so the probability of *d*-*d* transitions occurring is greater than in octahedral complexes.[56] Absorption bands are described by λ_{max} and A_{max} and ε_{max}. ε_{max} indicates how intense an absorption is and is related to A_{max} by the following Beer-Lambert law:

$$A_{max} = \varepsilon l c \qquad \textbf{Eqn. 3.1}$$

where l represents the path length of the cell and c is the molar concentration in the cell. Figure 3.31 displays UV spectra recorded from 5 mM solutions of both the pink (**3.24a**) and blue samples (**3.24b**) (represented by the pink and blue traces respectively). Clear differences between the spectra were observed. The complimentary colour of the absorbed light yields the colour of the sample, therefore you would expect the pink sample to absorb in the green/yellow region of the spectrum. This indeed is manifested in Figure 3.31 as the pink sample possesses a λ_{max} at 512 nm. In the case of blue coloured solutions, you would expect an absorbance in the orange region (600–640 nm) and this is concurrent with the observed λ_{max} of 620 nm. It is also evident from the spectra that the blue solution has a more intense absorbance than the pink solution, with ε_{max} of 13.2 $dm^3mol^{-1}cm^{-1}$ for the pink sample and 137.6 $dm^3mol^{-1}cm^{-1}$ for the blue sample. For centrosymmetric complexes like octahedral complexes, 1-10 $dm^3mol^{-1}cm^{-1}$ would be the typical ε_{max} values for Laporte-forbidden *d*-*d* electronic absorptions. For non-centrosymmetric complexes like tetrahedral complexes a typical ε_{max} value for Laporte-forbidden *d*-*d* electronic absorptions would be 10-1000 $dm^3mol^{-1}cm^{-1}$.[56]

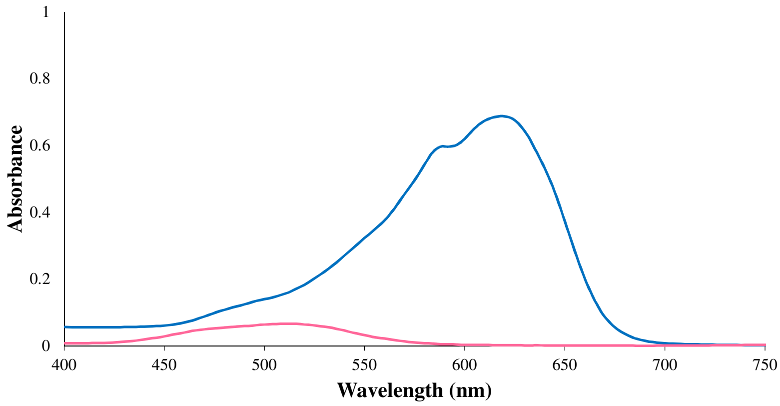

Figure 3.31: UV-Vis spectra of **3.24a** (pink trace) and **3.24b** (blue trace).

Figure 3.32: Colours of **3.24a** (left, in wet DMF) and **3.24b** (right, in dry DMF) in solution.

The extracted ε_{max} values from the spectra further indicated that octahedral and tetrahedral complexes existed. Collating the data obtained for both samples, the two structures proposed for **3.24** correlated well with our findings.

After *in situ* hydrolysis of **3.2** in H_2O and MeOH, the addition of an aqueous solution of $Co(SCN)_2$ resulted in a pink solution, which when allowed to stand for several days formed an orange solid. The IR spectrum of this product, **3.25**, displayed a $\nu_{asym}(COO^-)$ stretch at 1635 cm^{-1} and a corresponding $\nu_{sym}(COO^-)$ stretch at 1372 cm^{-1}. This gave a $\Delta(\nu_{asym}(COO^-) - \nu_{sym}(COO^-))$ value of 263 cm^{-1}, which would generally indicate monodentate coordination. However, the relatively low $\nu_{asym}(COO^-)$ frequency could indicate the presence of non-coordinated carboxylates, since these lower frequencies were a characteristic of our previously synthesised coordination networks with free carboxylates. Broad stretches centred at 3218 cm^{-1} were also visible in the IR spectrum which indicated the presence of coordinating H-bonded water molecules.[175] Elemental analysis suggested that the composition of the complex was 1:2 metal to ligand. Therefore, it was proposed that the complex consisted of an octahedral Co(II) metal centre with two

3.2(pytza) ligands coordinating *via* their pyridine and tetrazole nitrogens and two H_2O molecules filling the coordination sphere. This structure was recently obtained by Yang *et al*. from the reaction of $Co(NO_3)_2$ and 5-(2-pyridyl)tetrazole-2-acetic acid under solvothermal conditions.[173] The crystal structure that they obtained can be seen in Figure 3.33.

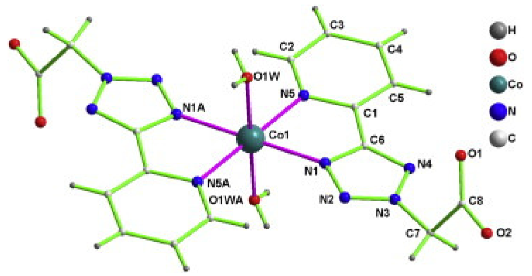

Figure 3.33: Crystal structure obtained by Yang *et al*. for a Co(II) complex of **3.2(pytza)**.[173]

The data obtained for **3.25** correlated well with that reported by Yang *et al*., and was in agreement with the crystal structure.

3.3.3 EPR Spectral Studies

3.3.3.1 EPR Spectroscopy Theory

Electron paramagnetic resonance (EPR) is a branch of spectroscopy in which radiation of microwave frequency is absorbed by molecules, ions or atoms possessing electrons with unpaired spins, hence this non-destructive technique can only be applied to samples having one or more unpaired electrons.[176] The phenomenon of electron spin resonance spectroscopy can be explained by considering a free electron in space without any outside forces. This electron possesses an intrinsic angular momentum and because this electron is charged, the angular motion of this charged particle generates a magnetic field and therefore possesses a magnetic moment. When this unpaired electron interacts with an applied magnetic field, B_0, two energy levels of the magnetic moment result. This phenomenon is called the Zeeman effect. The unpaired electron will have a state of lowest energy when the moment of the electron is aligned with the magnetic field (m_s = -½), and will have a state of highest energy when the moment of the electron is aligned against the magnetic field (m_s = +½) (Figure 3.34).

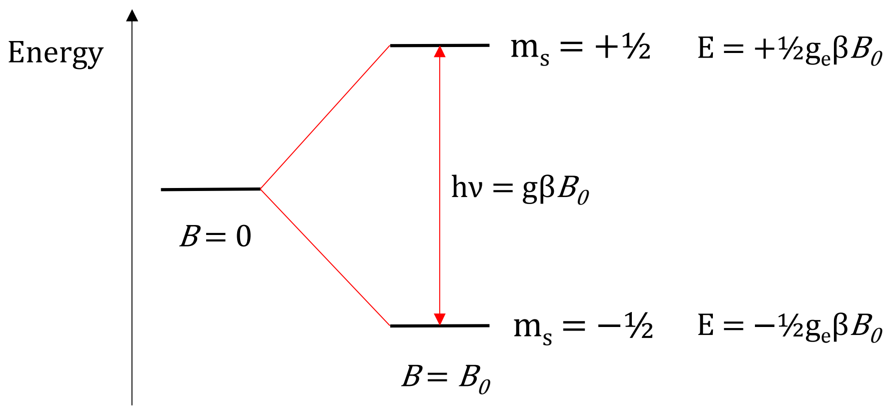

Figure 3.34: Induction of the spin state energies as a function of the magnetic field B_0.

The transition energy between the two states is given by Equation 3.2.

$$\Delta E = g\beta B_0 = h\nu \qquad \textbf{Eqn. 3.2}$$

From the above equation, the g factor can be determined. The magnitude of g contains chemical information on the nature of the bond between the electron and the molecule and the electronic structure of the molecule. The magnitude of g depends on the extent of the spin-orbit coupling, which depends on the size of the nucleus containing the unpaired electron. Therefore, organic free radicals will have a small contribution from spin-orbit coupling, producing g factors very close to the free electron value (g_e = 2.0023) while the g factors of much larger elements, such as metals, may be significantly different from g_e because of huge contribution from spin-orbit coupling. Since β is a constant and the magnitude of B_0 can be measured, to calculate g the value of ΔE must be determined, the energy between the two energy levels. This is done by irradiating the sample with microwaves with a set frequency and sweeping the magnetic field. Absorption of energies will occur when Equation 3.2 is satisfied. The value of g can then be calculated from ν in GHz and B_0 in Gauss using:

$$g = \frac{h\nu}{\beta B_0} \qquad \textbf{Eqn. 3.3}$$

where h = 6.626×10^{-34} J.s and β = 9.274×10^{-28} J/G. Hence, the energies between the two spin states increases linearly as the magnetic field increases. In conventional spectroscopy like NMR, a constant magnetic field is applied to the sample and the frequency of the electromagnetic radiation is scanned. In EPR spectroscopy however, the electromagnetic radiation frequency is kept constant and the magnetic field is scanned. A peak in the absorption will occur when the magnetic field tunes to the two spin states so that their energy difference matches the energy of the radiation. The source of radiation in EPR is called a klystron. An X-band klystron has a spectral band width of about 8.8-9.6 GHz. This makes it impossible to continuously vary the wavelength similarly to optical spectroscopy. Therefore, it is necessary to vary the magnetic field, until the quantum of the radar waves fits between the field-induced energy levels.[176]

In a molecule, orbitals are orientated in a certain direction, hence the magnitude of spin-orbit coupling is direction dependent, or anisotropic. For every paramagnetic molecule, there exists a unique axis system called the principal axis system. The g factors measured along these axes are called the principal g factors and are labelled g_x, g_y and g_z. In the simplest type of EPR spectrum, a metal ion has a totally symmetric environment. Here, the electrons in the different d orbitals have equal interactions in all directions, the orbital moment is equal in all directions and so the total magnetic moment is the same in all directions. When placed in an external field, the magnitude of the total magnetic momentum in the direction of the external field will always be the same. This means it will only have one g factor ($g_x = g_y = g_z$) and only one value of the external field where resonance occurs, thus there will only be one absorption line. This EPR spectrum is said to be isotropic. Figure 3.35 shows an example of a molecule where the paramagnetic metal is coordinated by two equal ligands in the z-direction and four different but equal ligands in both the x- and y-directions. As a result the g factor will be different for the situations where the field B_0 is parallel to the z axis or parallel to either the x or y axes. In a powder sample, the paramagnets are not aligned in a set direction and so are in all possible orientations. Consequently, there are a large number of overlapping absorption lines starting at B_z and ending at $B_{x,y}$. What is detected is the sum of all these lines. The situation where the x- or y-direction is parallel to B occurs much more frequently than one with its z-axis parallel to B. Hence, the total absorption in the x,y-direction is much larger than in the z-direction. This EPR spectrum is said to show axial symmetry (unique axis that differs from the other two, $g_x = g_y \neq g_z$). The last class of EPR spectrum is called rhombic and occurs when all the g factors differ ($g_x \neq g_y \neq g_z$).

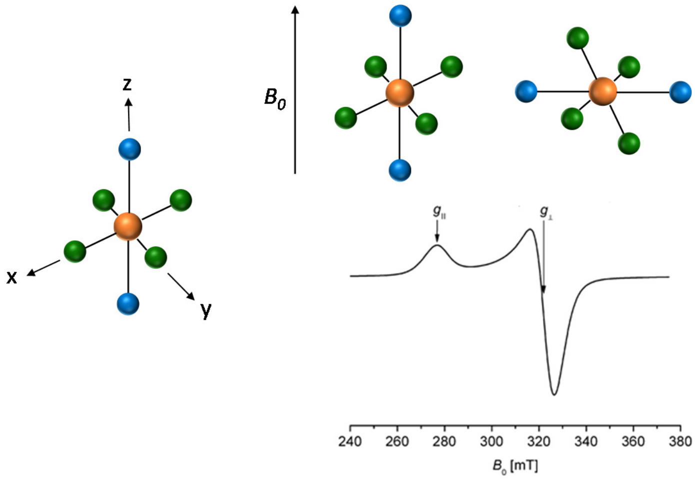

Figure 3.35: Dependency of the g factor on the orientation of the molecules in the magnetic field. The consequential EPR spectrum in this particular case is an axial spectrum.

The interaction of an unpaired electron with the nuclear magnetic moment is termed nuclear hyperfine interaction. The resonance condition becomes

$$hv = g\beta B_0 + hAm_l \qquad \textbf{Eqn. 3.4}$$

where A is called the hyperfine coupling constant and m_l is the magnetic moment quantum number for the nucleus. Since there are $2l + 1$ possible values of m_l ($m_l = \pm l, \pm l-1, \ldots, 0$), the hyperfine interaction terms splits the Zeeman transition into $2l + 1$ lines of equal intensity. The two principal isotopes of copper, ^{63}Cu and ^{65}Cu, both have nuclear spins of $^3/_2$ so that the Zeeman line will be split into four lines ($m_l = {}^3/_2, {}^1/_2, -{}^1/_2, -{}^3/_2$). The hyperfine coupling along g_z for Cu^{2+} is always much greater than that along g_x or g_y, resulting in a large splitting of the g_z line with only minor (often unobservable) splitting of g_x or g_y.

Finally, for practical purposes, the first derivative spectrum instead of the true absorption is recorded. The g factors are very easy to recognise in these types of spectra as it emphasises rapidly changing features of the spectrum, thus enhancing resolution.

3.3.3.2 EPR Spectral Studies on Cu(II) Compounds

The X-band solid state EPR spectra of **3.8 – 3.13** were measured in the solid state at room temperature. Cu(II) has a d^9 configuration and has one unpaired electron, hence it has an effective spin of ½. The configuration of square pyramidal is characterised by the ground state $d_{x^2-y^2}$. Trigonal bipyramidal is also a five coordinated geometry which is characterised by the ground state d_{z^2}. EPR spectra of Cu(II) complexes provides a useful method to distinguish between these two general states.

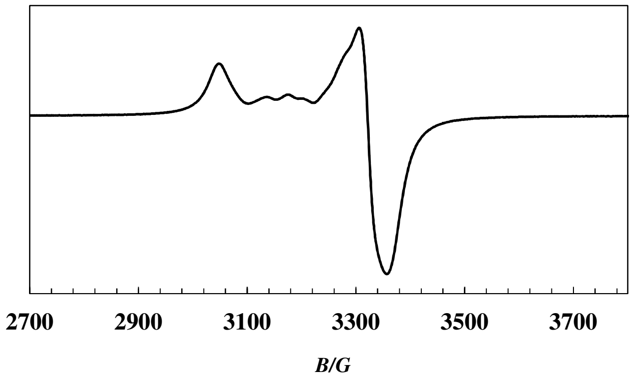

Figure 3.36: Room temperature 9.63 GHz EPR spectrum of a powder sample of **3.8**. (g_x; g_y; g_z) = (2.0477; 2.0739; 2.2586), (A_x;A_y;A_z) = (0; 0; 0:0009 cm^{-1}).

The EPR spectrum for **3.8** is shown in Figure 3.36. It was observed that the g_z factor is greater than the g_x~g_y factors, which in turn is greater than the g_e value. For systems where $g_z > g_y > g_x$, the ratio of (g_y - g_x/g_z - g_y) (called the parameter R) is useful in discriminating between a $d_{x^2-y^2}$ and a d_{z^2} ground state.[177] If R is greater than 1, then the ground state is d_{z^2}. If the ground state is $d_{x^2-y^2}$, then the value of R is less than 1. The EPR spectrum of **3.8** shows the value of R to be less than 1, thus confirming five coordinate square pyramidal geometry, and the spectrum is said to show axial symmetry. The additional lines observed at 3200 G in the spectrum were attributed to crystalline material in the sample, which were greatly reduced on grinding the sample into a powder, however complete removal of these crystalline particle proved difficult, hence their presence in Figure 3.36.

The EPR spectrum of **3.9** was measured in the solid state at room temperature and can be seen in Figure 3.37. The mononuclear complex showed a relatively simple spectrum indicating axial geometry (i.e. there was a unique axis that differed from the other two, g_x = $g_y \neq g_z$). The abstracted g factors show that $g_z > g_x \sim g_y$, indicating that the unpaired electron lies predominantly in the $d_{x^2-y^2}$ orbital.

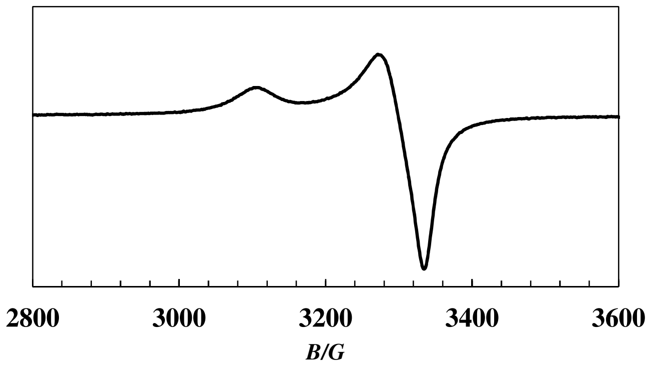

Figure 3.37: Room temperature 9.63 GHz EPR spectrum of a powder sample of **3.9**. (g_x; g_y; g_z) = (2.066; 2.090; 2.223).

The EPR spectrum of **3.10** (Figure 3.38) was measured in the solid state at room temperature. The spectrum indicated axial geometry as $g_z > g_x \sim g_y$ was fulfilled and this would be expected from the regular geometry seen in the crystal structure of **3.10**. Therefore, $d_{x^2-y^2}$ was the ground state.

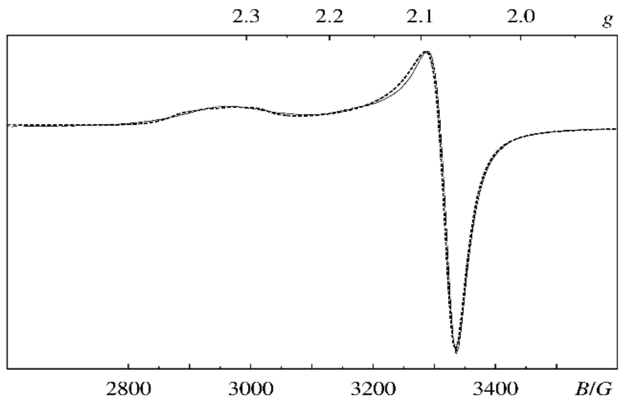

Figure 3.38: Room temperature 9.63 GHz EPR spectrum of a powder sample of **3.10**. The experimental and calculated spectrum is indicated with a solid and dashed line, respectively. The calculated spectrum was obtained from our collaborator using a Hamiltonion equation (Appendix B) with the following spin Hamiltonian parameters: (g_x; g_y; g_z) = (2.070; 2.074; 2.334), (A_x;A_y;A_z) = (0; 0; 0:0044 cm^{-1}).

The X-band spectrum of **3.11** was measured in the solid state at room temperature and can be seen in Figure 3.39. This dimer showed three different g factors ($g_x \neq g_y \neq g_z$), revealing the rhombic symmetry of the coordination sphere. These signals correspond to the three different main axes x, y and z of the magnetic tensor which are all of different length. This can be seen when examining the crystal structure of **3.11**. In this distorted octahedral complex, coordination bond lengths differ greatly (Cu-N_{pyr} 2.040 Å, Cu-N_{tet} 2.282 Å, Cu-H_2O 1.965 Å, Cu-$O_{monodentate}$ 1.939 Å, Cu-$O_{bidentate}$ 2.765 Å, Cu-$O_{bidentate}$ 1.940 Å) therefore the appearance of a rhombic signal is not surprising.

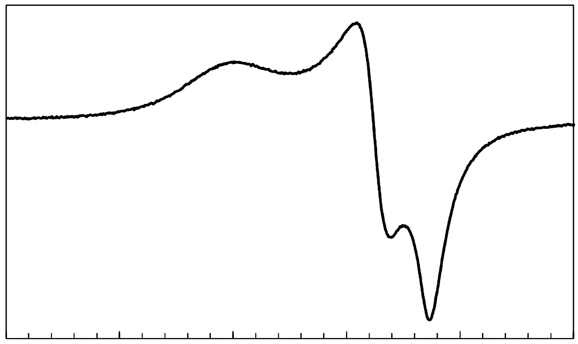

Figure 3.39: Room temperature 9.63 GHz EPR spectrum of a powder sample of **3.11**. (g_x; g_y; g_z) = (2.056; 2.124; 2.312), (A_x;A_y;A_z) = (0; 0; 0:0045 cm^{-1}).

The solid state EPR spectrum for **3.13** (Figure 3.40) measured at room temperature again displayed approximate axial symmetry with g_z > g_x~g_y which was expected for this octahedral complex, which has a $d_{x^2-y^2}$ ground state.

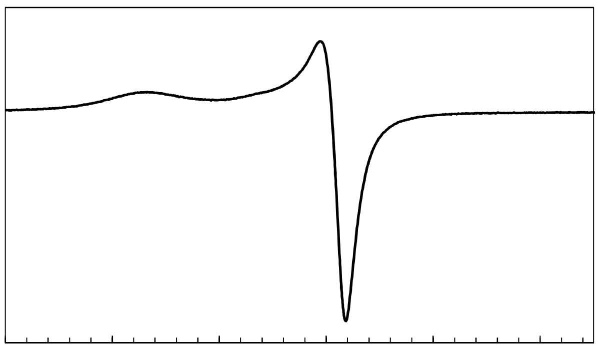

Figure 3.40: Room temperature 9.63 GHz EPR spectrum of a powder sample of **3.13**. (g_{xy}; g_z) = (2.042; 2.555).

3.3.4 Luminescent Properties of CPs

3.3.4.1 Overview of Luminescence

Fluorescence spectroscopy is an area of chemistry which encompasses a broad spectrum of concepts and as such will only be covered here in fundamental detail. Luminescence can be defined as the emission of light upon absorption of energy under the condition that the energy source is not heat based. Luminescence is an occurrence whereby the emission of a photon from an electronic excited state of a molecule occurs at a lower energy (longer wavelength) than the wavelength at which the photon was absorbed.[178] The difference in energy is known as the Stokes shift and can be explained by the Franck-Condon principle. This states that all electronic transitions are vertical, that is, they occur without change in the position of the nuclei.[179] A direct result of the higher energy potential of the excited state is that the vertical transition for the lowest vibrational energy level of the ground state, ν''_0, intersects the excited state at the ν'_n energy level. The excited electron loses energy through non-radiative decay to the lowest vibrational energy level in the excited state: ν'_0. The emitted photon originates from a transition ν'_0 to ν''_n, a point where its vertical transition intersects the ground state potential energy curve. As before, non-radiative decay returns the electron to the lowest vibronic energy level: ν''_0. The above transitions are summarised in Figure 3.41. The energy difference between absorption ($\nu''_0 \rightarrow \nu'_n$) and emission ($\nu'_0 \rightarrow \nu''_n$) is the reason why a Stokes shift occurs.

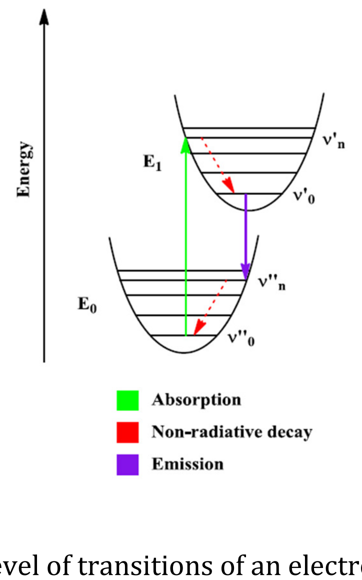

Figure 3.41: Vibrational level of transitions of an electron for both absorption and emission processes. Reprinted with permission.[180]

When a molecule absorbs a photon of energy, a chain of photophysical events occur, including the two main types of luminescence: fluorescence and phosphorescence, depending on the nature of the excited state.[181] In the case of fluorescence, a single electron absorbs this energy and undergoes an electronic transition from the singlet ground state S_0 to a singlet excited state. This excited electron, arbitrarily denoted a, (S_a = $+^1/_2$) is spin paired with the corresponding electron, denoted a*, in the ground state orbital (S_{a^*} = $-^1/_2$). This photo-excited electron decays to the lowest vibrational level of the first excited singlet. The phenomenon of fluorescence results when a spin-allowed singlet-singlet radiative transition (ΔS = 0) from the lowest excited singlet state S_1 to the ground singlet state S_0 occurs. The notation of the singlet state originates from the multiplicity formula M = 2S + 1, where M is the multiplicity of the state and S the number of unpaired electrons. This process has typical lifetimes in the order of 1 ns. Phosphorescence, in comparison, involves a spin-forbidden radiative transition from the triplet state T_1 to the ground state S_0 ($\Delta S \neq 0$). Absorption occurs in the same manner as with the fluorescence absorption transition. In phosphorescence however (a process that can be as a long as several seconds), the electron undergoes a change of spin (S_a = $+^1/_2$ to $-^1/_2$) to the T_1 triplet state. This triplet state is slightly lower in energy than the corresponding S_1 state (due to Hund's rule). Conversion from the S_1 state to the T_1 state (intersystem crossing) becomes possible due to spin-orbit coupling.[182] A summary of the radiative and non-radiative processes are shown in the Jablonski diagram in Figure 3.42.

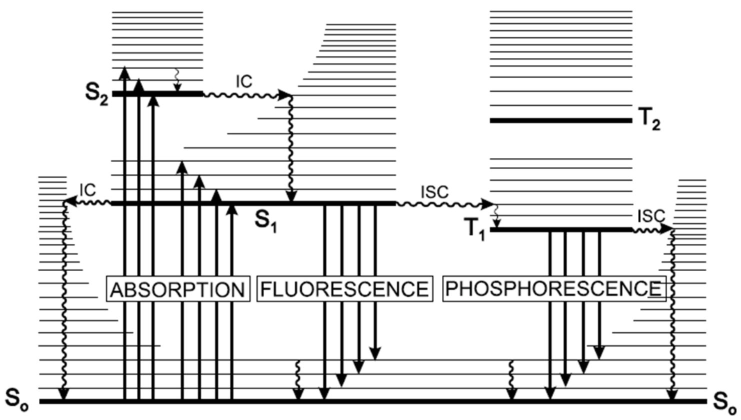

Figure 3.42: Jablonski diagram which shows all the possible transitions between electronic states. S = singlet state, T = triplet state, IC = internal conversion and ISC = intersystem crossing.[179]

3.3.4.2 The Origin of Luminescence in CPs

Fluorescence is commonly observed in aromatic molecules. This is because of the extensive electron delocalisation of the π electrons. This extensive π system lowers the energy required for a $\pi \rightarrow \pi^*$ transition (the lowest energy transition) and as a result yields a larger wavelength emission band than the corresponding absorption band. In CPs and MOFs, a wide range of π-conjugated organic molecules are commonly used as linkers. Usually, the fluorescence emission from organic ligands is similar to their emission behaviour in solution, corresponding to the transition from the lowest excited singlet state to the singlet ground state and the transitions are either $\pi \rightarrow \pi^*$ or $n \rightarrow \pi^*$ in nature. However, the maximum emission wavelength and lifetime of organic linkers in solid MOFs are often different from those of the free molecules. This is because the organic linkers are stabilised within MOFs which reduces the nonradiative decay rate and leads to increased fluorescence intensities, lifetimes and quantum efficiencies.[183] In addition, these structures are often particularly susceptible to π-stacking in the solid state, further enhancing their fluorescence properties. In the solid state, molecular interactions can bring lumophores close together, enabling electronic interactions between the lumophores (e.g. ligand to ligand charge transfer (LLCT)).

Luminescence in MOFs is typically based on the linker rather than on the metal (LLCT), but can also involve charge transfer between the metal and linker (metal to ligand charge transfer (MLCT) or ligand to metal charge transfer (LMCT)), metal-based luminescence, metal to metal charge transfer (MMCT) and sometimes guest molecules may contribute to the emission.[184] Emission from paramagnetic transition-metal complexes is usually not strong because ligand-field transitions (*d*-*d*) may lead to strong reabsorption and/or quenching of fluorescence generated from the organic molecule, which can occur *via* electron or energy transfer through the partially filled *d* orbitals. However, MOFs with transition metal ions without unpaired electrons, especially those having d^{10} configurations, can yield linker-based highly emissive materials. Metal based luminescence is most often seen when lanthanide ions are incorporated in the framework. These mechanisms are not mutually exclusive and more than one emission pathway can co-exist in a competitive manner with another.[184]

The motivation behind studying metal-organic matrices as luminescent materials lies in their advantages over organic molecular solids. The photophysical properties of organic compounds in the solid state has been a rich area of study and recent work on organic solid-state devices has renewed interest in photoabsorption and emission from thin films, monolayers and matrices of these compounds.[185] Controlling these ligand-ligand interactions is important for applications that involve charge transport and to obtain tunable emission colours. In molecular solids, the multitude of weak interactions, such as π-stacking and hydrogen bonding make it difficult to predict the crystal structure *a priori*. CPs have a potential advantage in this context in that they offer a degree of predictability to the structure in a defined, crystalline network that can be useful for extracting structure-property relationships.[184] The presence of both inorganic and organic moieties can provide additional luminescent functionality due to the potential LMCT and MLCT phenomena. This feature has seen CPs investigated for their potential application as inorganic LEDs.[186] The porosity of some CPs further enable the adsorption of guest molecues which can alter the parent framework's photoemission profile, making them excellent candidates for chemosensing.[181]

3.3.4.3 Luminescent Properties of Zn(II) Compounds

The photoluminescence of d^{10} metal complexes has developed into an attractive research field owing to their potential applications in chemical sensors, photochemistry and inorganic LEDs.[181,186] The solid state emission spectra of **3.1(pytzaH)**, **3.2(pytzaH)**, **3.14, 3.15** and **3.16** (Figure 3.43) were measured at room temperature and are depicted in Figure 3.44. It can be seen that they exhibit fluorescence signals with the emission maxima at 452 nm for the free ligand **3.1(pytzaH)**, 436 nm for the free ligand **3.2(pytzaH)**, and 434, 444 and 438 nm for the complexes **3.14**, **3.15** and **3.16** respectively, with λ_{ex} = 350 nm. Compared to the spectrum of the free ligand **3.1(pytzaH)**, complexes **3.14** and **3.15** exhibited slight blue shifts of emission lengths 18 and 8 nm, respectively. The quenching in emission that was observed in **3.14** is tentatively attributed to the tetrazole and pyridine rings been in a rigid non-planar arrangement due to the coordination of Zn(II), which concomitantly would decrease the conjugative effect for the ligand. The free ligand **3.2(pytzaH)** exhibited weak emission bands. Compared to this spectrum, **3.16** was similar in terms of position but an obvious increase in emission was observed. This emission band is mainly due to an intraligand emission state, which is characteristic of fluorescent emissions for Zn(II) complexes with N-donor aromatic ligands.[187,188] The intensity increase of the luminescence for the complexes may be attributed to the chelation of the ligand to the metal centre, which increases the rigidity of the ligands and reduces the non-radiative relaxation process (*via* vibrational motions).[146,188] Cu(II) complexes **3.8**-**3.13** did not exhibit any emissive properties, which was expected as paramagnetic metal ions have low *d-d* transitions which can relax the excitation energy through a non-radiative pathway, thus quenching luminescence.[181] The marked difference in the fluorescence intensities observed for the free ligands is tentatively ascribed to the co-planarity of the N-1 substituted ligand. In the crystal structure of **3.1** (Figure 3.12), this co-planar behaviour was observed and it would be presumed that this would also manifest itself in the structure of the corresponding free acid **3.1(pytzaH)**. The N-2 substituted regioisomer however, may not be capable of adopting this co-planar conformation in the solid state and could disrupt the ligand to ligand transitions if not stacked appropriately. This of course, could be confirmed by undertaking X-ray crystallographic analysis of the crystal structures of both carboxylic acid derivatives **3.1(pytzaH)** and **3.2(pytzaH).**

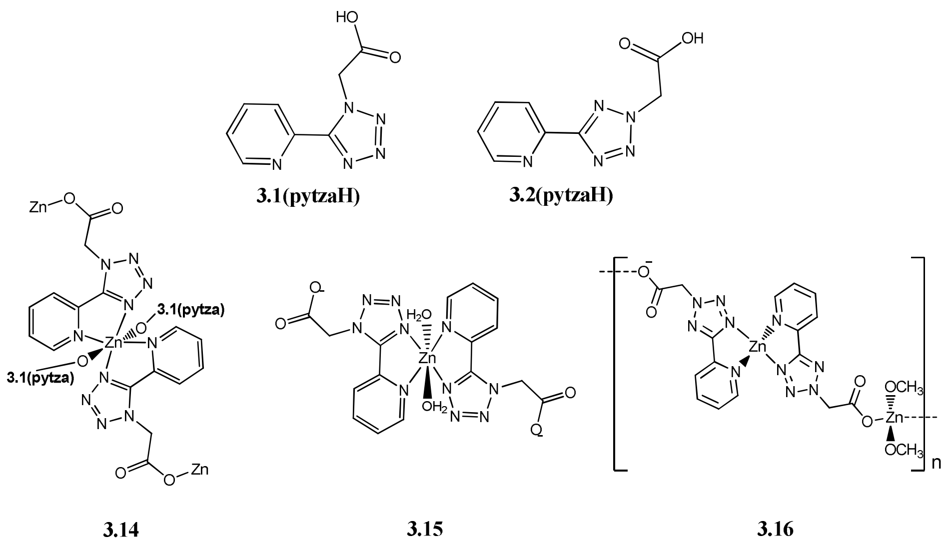

Figure 3.43: Free ligands and Zn(II) complexes that were subject to solid state fluorescence studies.

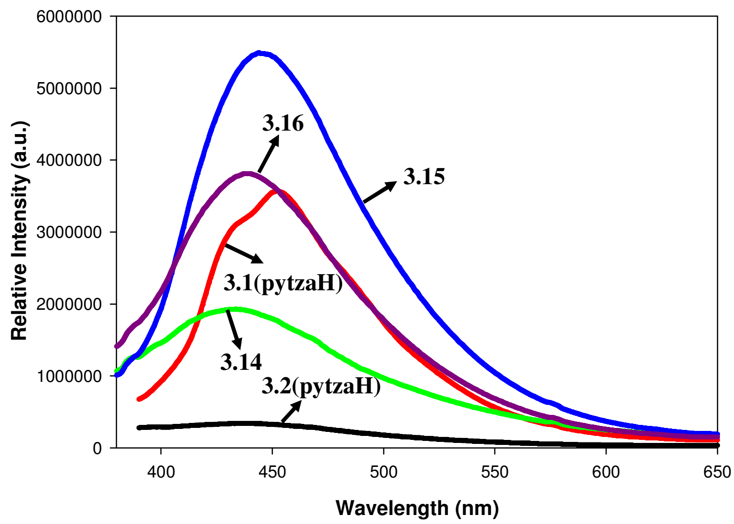

Figure 3.44: Solid state emission spectra for free ligands **3.1(pytzaH)** and **3.2(pytzaH)** and complexes **3.14**, **3.15** and **3.16**. Excitation wavelength was 350 nm.

3.4 Conclusions

For the purpose of investigating the ability of ester and carboxylate functionalised pyridyl tetrazoles to form coordination polymers, **3.1** and **3.2** were synthesised utilising methods previously established. These ligands were then reacted with $CuCl_2.2H_2O$ and displayed interesting coordination chemistry as the position of the alkylation site appeared to have some effect on how the ligand coordinated to the metal centre. These results hinted at the diversity that could be obtained when these regioisomers would be used in coordination polymer synthesis.

Ligands **3.1** and **3.2** were hydrolysed *in situ* to form carboxylates which, in combination with the pyridyl tetrazole binding sites, afforded diverse structures on complexation to metal(II) ions. Regiochemical differences between the linkers played a key role in the formation of these structures and furthermore, solvent also had an affect on what structures were formed. In MeOH, polymeric coordination polymers tended to form whereas when employing water as reaction solvent, hydrogen bonded coordination networks were inclined to form by virtue of coordinating water molecules. It also became apparent that the level of hydration of the metal salt may have provided enough water for these hydrogen bonded networks to form, as seen in the cases where $NiCl_2.6H_2O$ was employed.

X-band EPR spectroscopy was carried out on powdered samples at room temperature on Cu(II) structures and revealed approximate axial symmetry apart from one complex, **3.11**, which showed a rhombic EPR signal. These signals were in agreement with the crystal structures obtained and were typical of Cu(II) complexes with a $d_{x^2-y^2}$ ground state.

Solid state fluorescence spectroscopy was carried out on Zn(II) compounds and their corresponding free acid ligands at room temperature. The emission spectra suggest that the complexes formed could be efficient light emitting materials for potential applications. Investigations will have to be carried out in order to elucidate the reason that the two free acid ligands possessed such different emission profiles. Until such investigations are undertaken, we postulate that the packing of the structures in the solid state could contribute to these differences.

Future work would involve the use of other d^{10} metal ions in the synthesis of these coordination polymers in order to investigate their luminescence properties and to investigate the thermal stabilities of the compounds formed in this chapter. Furthermore, as coordination polymers with low dimensionality were formed in this work, we intended on developing the linkers discussed in this chapter in order to achieve high dimensional, potentially porous materials. The attempts at addressing this issue is the subject of Chapter 4.

3.5 Experimental

3.5.1 Instrumentation

^{1}H and ^{13}C NMR (δ ppm; J Hz) spectra were recorded on a Bruker Avance 300 MHz NMR spectrometer using saturated $CDCl_3$ or d_6-DMSO solutions with a $SiMe_4$ reference, with resolutions of 0.18 Hz and 0.01 ppm, respectively. Infrared spectra (cm^{-1}) were recorded as KBr discs or liquid films between NaCl plates using a Perkin Elmer System 2000 FT-IR spectrometer. Solution UV-Vis spectra were recorded using HPLC grade solvents using a Unicam UV 540 spectrometer. Melting point analyses were carried out using a Stewart Scientific SMP 1 melting point apparatus and are uncorrected. Electrospray (ESI) mass spectra were collected on an Agilent Technologies 6410 Time of Flight LC/MS. Compounds were dissolved in acetonitrile:water (1:1) solutions containing 0.1% formic acid, unless otherwise stated. The interpretation of mass spectra was made with the help of the program "Agilent Masshunter Workstation Software". Magnetic susceptibility measurements were carried out at room temperature using a Johnson Matthey Magnetic Susceptibility Balance with $[HgCo(SCN)_4]$ as reference. EPR spectra were recorded on a Bruker Elexsys E500 spectrometer, operated at the X-band and equipped with an Oxford Instruments cryostat. Solid state UV-Vis measurements were carried out in the Synthetic Bioinorganic Chemistry Laboratory of the University of Crete and were performed on a Perkin Elmer Lambda 950 UV/Vis spectrometer. Solid state fluorescence spectra were also carried out in this laboratory and were recorded on a Jobin-Yvon Horiba, Fluoro Max-P (SPEX) fluorescence spectrometer, with excitation from a cw Xenon arc lamp. Microanalyses were carried out at the Microanalytical Laboratory of the National University of Ireland Maynooth, using a Thermo Finnigan Elementary Analyzer Flash EA 1112. The results were analysed using the Eager 300 software. All crystal structures resulting from this work were solved by Dr. John Gallagher (Dublin City University) using an Oxford Diffraction Gemini-S Ultra diffractometer at 294(1) K. Structures were solved using the SHELXS97 direct methods program. Molecular diagrams were generated using Mercury software. Starting materials were commercially obtained and used without further purification. Solvents used were of HPLC grade.

Caution! *Nitrogen-rich compounds such as tetrazole derivatives are used as components for explosive mixtures. In our laboratory, the reactions described were run on a few gram scale, and no problems were encountered. However, great caution should be exercised when heating or handling compounds of this type.*

3.5.2 Synthesis of 3.1 and 3.2

To **2.5** (2.00 g, 13.60 mmol) dissolved in MeCN (60 mL) was added K_2CO_3 (3.76 g, 27.20 mmol). The resulting solution was heated to reflux for 30 min and to the hot solution was added ethyl bromoacetate (2.27 g, 13.60 mmol). The reaction mixture was then stirred at reflux temperature for a further 24 h. After cooling, the reaction mixture was filtered and the filtrate was concentrated under reduced pressure to afford an oil, which was purified by column chromatography on silica gel (at a ratio of Pet. Ether:EtOAc, 1:2). This gave products **3.1** and **3.2**.

3.5.2.1 Ethyl 2-(5-(pyridin-2-yl)-1*H*-tetrazol-1-yl)acetate (3.1)

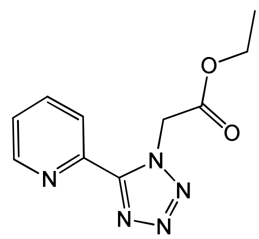

Orange solid (0.70 g, 22%). m.p. 53-55 °C. IR (KBr): ν = 3015, 2989, 2970, 1748, 1591, 1538, 1474, 1437, 1378, 1274, 1251, 1228, 1117, 1019, 809, 751, 728 cm^{-1}. ^{1}H NMR ($CDCl_3$): δ = 8.63-8.66 (m, 1 H, pyr-H), 8.41-8.44 (m, 1 H, pyr-H), 7.88-7.94 (m, 1 H, pyr-H), 7.41-7.46 (m, 1 H, pyr-H), 5.74 (s, 2 H, CH_2N), 4.19 (q, 2 H, J = 7.1 Hz, OCH_2), 1.18 (t, 3 H, J = 7.1 Hz, CH_3) ppm. ^{13}C NMR ($CDCl_3$): δ = 165.9 (C=O), 152.1 (CN_4), 149.2, 144.6, 137.6, 125.4, 124.1, 62.1, 51.1 (CH_2N), 14.0 ppm. ESI-HRMS: calcd. for $C_{10}H_{12}N_5O_2$ $[M+H]^+$ 234.0986, found 234.0983.

3.5.2.2 Ethyl 2-(5-(pyridin-2-yl)-2*H*-tetrazol-2-yl)acetate (3.2)

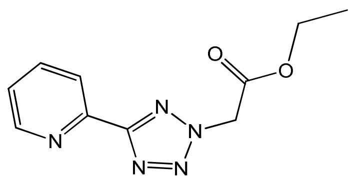

Cream solid (0.74 g, 23%). m.p. 94-96 °C. IR (KBr): ν = 3001, 2958, 1745, 1596, 1520, 1467, 1417, 1368, 1345, 1231, 1051, 1032, 882, 797, 737 cm^{-1}. ^{1}H NMR ($CDCl_3$): δ = 8.78-8.80 (m, 1 H, pyr-H), 8.26-8.29 (m, 1 H, pyr-H), 7.85-7.90 (m, 1 H, pyr-H), 7.39-7.44 (m, 1 H, pyr-H), 5.50 (s, 2 H, CH_2N), 4.28 (q, 2 H, J = 7.1 Hz, OCH_2), 1.28 (t, 3 H, J = 7.1 Hz, CH_3) ppm. ^{13}C NMR ($CDCl_3$): δ = 165.2 (C=O), 164.8 (CN_4), 150.3, 146.5, 137.1, 125.0, 122.5, 62.7, 53.5 (CH_2N), 14.0 ppm. ESI-HRMS: calcd. for $C_{10}H_{12}N_5O_2$ $[M+H]^+$ 234.0986, found 234.0979.

3.5.3 Synthesis of 3.1(pytzaH) and 3.2(pytzaH)

3.1 or **3.2** (0.10 g, 0.43 mmol) were dissolved in EtOH (20 mL). 10 M NaOH (0.1 mL) was added to the solution and the resulting suspension was heated to reflux for 30 min. The solution was allowed to cool and the solid was filtered. The solid was dissolved in deionised H_2O (1 mL) and 6 M HCl was added dropwise until a precipitate formed (pH 3). The solid was filtered and dried.

3.5.3.1 2-(5-(pyridin-2-yl)-1H-tetrazol-1-yl)acetic acid (3.1(pytzaH))

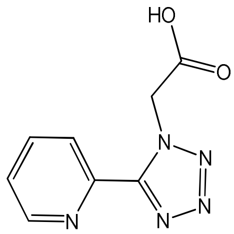

White solid (0.06 g, 68%). m.p. 195-200 °C. IR (KBr): ν = 3460, 3030, 2849, 1724, 1590, 1473, 1438, 1399, 1354, 1293, 1261, 1248, 1129, 1097, 1011, 994, 814, 799, 729, 656, 622, 487 cm^{-1}. ^{1}H NMR ($CDCl_3$): δ = 8.65-8.68 (m, 1 H, pyr-H), 8.41-8.45 (m, 1 H, pyr-H), 7.91-7.97 (m, 1 H, pyr-H), 7.45-7.49 (m, 1 H, pyr-H), 5.78 (s, 2 H, CH_2N) ppm. ^{13}C NMR ($CDCl_3$): δ = 168.8 (C=O), 152.1 (CN_4), 149.2, 144.2, 137.9, 125.7, 124.4, 50.7 (CH_2N) ppm. ESI-HRMS: calcd. for $C_8H_8N_5O_2$ $[M+H]^+$ 206.0673, found 206.0674.

3.5.3.2 2-(5-(pyridin-2-yl)-2H-tetrazol-2-yl)acetic acid (3.2(pytzaH))

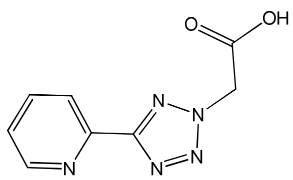

White solid (0.05 g, 62%). m.p. 185-186 °C. IR (KBr): ν = 3441, 2997, 2955, 1713, 1604, 1434, 1348, 1260, 1206, 1166, 1058, 1022, 896, 825, 803, 749, 638, 431 cm^{-1}. ^{1}H NMR (d_6-DMSO): δ = 8.75-8.76 (m, 1 H, pyr-H), 8.15-8.17 (m, 1 H, pyr-H), 8.00-8.05 (m, 1 H, pyr-H), 7.55-7.59 (m, 1 H, pyr-H), 5.78 (s, 2 H, CH_2N) ppm. ^{13}C NMR (d_6-DMSO): δ = 167.3 (C=O), 164.2 (CN_4), 150.2, 145.9, 137.6, 125.3, 122.4, 54.8 (CH_2N) ppm. ESI-HRMS: calcd. for $C_8H_8N_5O_2$ $[M+H]^+$ 206.0673, found 206.0673.

Data obtained agrees with that reported in the literature.[189]

3.5.4 Metal Complexation Reactions

3.5.4.1 Metal Complexes of Ester Derivatives 3.1 and 3.2

3.5.4.1.1 [Cu(3.1)Cl$_2$]$_2$ (3.8)

A solution of $CuCl_2.2H_2O$ (0.15 g, 0.86 mmol) in MeOH (20 mL) was added to a solution of **3.1** (0.20 g, 0.86 mmol) in MeOH (20 mL). The resulting solution was heated to reflux for 2 h. The solution was then allowed to stand at room temperature for several days whereupon green crystals formed. Green crystals (0.12 g, 39%). $C_{20}H_{22}Cl_4Cu_2N_{10}O_4$: calcd. C 32.65, H 3.02, N 19.05%; found C 32.24, H 2.88, N 18.27%. IR (KBr): ν = 3101, 2978, 2947, 1749, 1616, 1556, 1481, 1456, 1373, 1297, 1261, 1230, 1111, 1009, 870, 787, 749 cm^{-1}. λ_{max} (MeOH) 872 nm, ε = 89 M^{-1}cm^{-1}. Magnetic moment: 1.67 B.M.

3.5.4.1.2 [Cu(3.2)Cl$_2$] (3.9)

A solution of $CuCl_2.2H_2O$ (0.15 g, 0.86 mmol) in MeOH (20 mL) was added to a solution of **3.2** (0.20 g, 0.86 mmol) in MeOH (20 mL). The resulting solution was heated to reflux for 2 h. The solution was then allowed to stand at room temperature for several days whereupon blue crystals formed. Blue crystals (0.15 g, 58%). $C_{20}H_{22}Cl_2CuN_{10}O_4$: calcd. C 39.96, H 3.69, N 23.31%; found C 38.99, H 3.63, N 22.76%. IR (KBr): ν = 3005, 2984, 2967, 1749, 1611, 1450, 1388, 1368, 1283, 1214, 1018, 875, 799, 756 cm^{-1}. λ_{max} (MeOH) 800 nm, ε = 61 M^{-1}cm^{-1}. Magnetic moment: 2.17 B.M.

3.5.4.2 Reactions of *in situ* Generated 3.1(pytza) and 3.2(pytza) With Metal Salts

3.5.4.2.1 [Cu(3.1pytza)]$_n$ (3.10)

NaOH (0.01 g, 0.43 mmol) in deionised H_2O (1 mL) was added to a solution of **3.1** (0.10 g, 0.43 mmol) in MeOH (10 mL). The resulting solution was heated to reflux for 1 h. After this time, $CuCl_2.2H_2O$ (0.07 g, 0.43 mmol) was added, then cooled to room temperature and filtered. The blue solid obtained was dissolved in H_2O and by slow evaporation, blue crystals of the product suitable for X-ray crystallography were obtained. $C_{16}H_{12}Cu_2N_{10}O_4$: calcd. C 30.44, H 1.92, N 22.20%; found C 30.68, H 2.24, N 22.41%. IR (KBr): ν = 1651, 1614, 1587, 1471, 1456, 1435, 1392, 1312, 1250, 1123, 926, 814, 793, 745, 730 cm^{-1}. λ_{max} (H_2O) 656 nm, ε = 23 M^{-1}cm^{-1}. Magnetic moment: 2.29 B.M.

3.5.4.2.2 [Cu(3.1pytza)$_2$H$_2$O]$_2$ (3.11)

3.1 (0.20 g, 0.86 mmol) was dissolved in a mixture of deionised H_2O (10 mL) and MeOH (1 mL). NaOH (0.03 g, 0.86 mmol) in deionised H_2O was added to this mixture and the solution was heated to reflux for 1 h. $CuCl_2.2H_2O$ (0.14 g, 0.86 mmol) was added and the resulting solution was allowed to stand for several days whereupon blue block crystals formed. Blue crystals (0.13 g, 65%). $C_{16}H_{14}CuN_{10}O_5$: calcd. C 39.21, H 2.88, N 28.60%; found C 40.09, H 2.55, N 28.95%. IR (KBr): ν = 3133, 3001, 2984, 1650, 1609, 1537, 1471, 1458, 1434, 1359, 1311, 1300, 1243, 1166, 1112, 808, 790, 752 cm^{-1}. λ_{max} (H_2O) 748 nm, ε = 10 $M^{-1}cm^{-1}$. Magnetic moment: 2.02 B.M.

3.5.4.2.3 [Cu(3.2pytza)OH]$_n$ (3.12)

NaOH (0.01 g, 0.43 mmol) in deionised H_2O was added to a solution of **3.2** (0.10 g, 0.43 mmol) in MeOH (10 mL). The resulting solution was refluxed for 1 h, in which time a white precipitate had formed. After this time, $CuCl_2.2H_2O$ (0.07 g, 0.43 mmol) was added and the resulting mixture was cooled to room temperature and filtered. Pale green solid (0.11 g, 92%). $C_8H_7CuN_5O_3$: calcd. C 33.75, H 2.48, N 24.60%; found C 33.56, H 2.49, N 24.17%. IR (KBr): ν = 3414, 3262, 3097, 1661, 1636, 1451, 1416, 1384, 1344, 1287, 1217, 1067, 821, 800, 801, 759, 730, 684, 673 cm^{-1}. λ_{max} (DMSO) 496 nm, ε = 148 $M^{-1}cm^{-1}$. Magnetic moment: 2.50 B.M.

3.5.4.2.4 [Cu(3.2pytza)$_2$(H$_2$O)$_2$] (3.13)

3.2 (0.10 g, 0.43 mmol) was dissolved in a mixture of deionised H_2O (10 mL) and MeOH (1 mL). NaOH (0.01 g, 0.43 mmol) in deionised H_2O was added to this mixture and the solution was heated to reflux for 1 h. $CuCl_2.2H_2O$ (0.07 g, 0.43 mmol) in deionised H_2O was added and the resulting solution was cooled slowly. The resulting pale blue crystals were filtered and air dried. Pale blue crystals (0.09 g, 90%). $C_{16}H_{16}CuN_{10}O_6$: calcd. C 37.82, H 3.18, N 27.58%; found C 37.87, H 3.45, N 26.71%. IR (KBr): ν = 3195, 3022, 1728, 1628, 1614, 1465, 1453, 1420, 1376, 1289, 1221, 1174, 1164, 1066, 1031, 826, 797, 731 cm^{-1}. λ_{max} (H_2O) 760 nm, ε = 33 $M^{-1}cm^{-1}$. Magnetic moment: 1.80 B.M.

3.5.4.2.5 [Zn(3.1pytza)]$_n$ (3.14)

A solution of **3.1** (0.10 g, 0.43 mmol) and NaOH (0.02 g, 0.43 mmol) in MeOH (18 mL) was heated to reflux for 1 h. After this time, a solution of $ZnCl_2$ (0.06 g, 0.43 mmol) in MeOH (5 mL) was added to the reaction. The solution was then allowed to stand at room temperature for several days. The solids formed were filtered off and washed with MeOH. White solid (0.05 g, 50%). $C_{16}H_{12}N_{10}O_4Zn$: calcd. C 40.57, H 2.55, N 29.57%; found C 41.03, H 3.54, N 29.51%. IR (KBr): ν = 3435, 3004, 1650, 1610, 1474, 1462, 1435, 1365, 1314, 1301, 1248, 1165, 1010, 900, 808, 794, 727, 702, 679 cm^{-1}. ^1H NMR (d_6-DMSO): δ = 8.68-8.69 (m, 1 H, pyr-H), 8.23-8.26 (m, 1 H, pyr-H), 8.02-8.07 (m, 1 H, pyr-H), 7.55-7.59 (m, 1 H, pyr-H), 5.53 (s, 2 H CH_2N) ppm. ^{13}C NMR (d_6-DMSO): δ = 170.0 (C=O), 152.4 (CN_4), 150.1, 144.8, 138.5, 126.1, 124.2, 52.2 (CH_2N) ppm.

3.5.4.2.6 [Zn(3.1pytza)$_2$(H_2O)$_2$] (3.15)

A solution of **3.1** (0.10 g, 0.43 mmol) and NaOH (0.02 g, 0.43 mmol) in deionised H_2O (20 mL) was heated under reflux for 1 h. After this time, a solution of $ZnCl_2$ (0.06 g, 0.43 mmol) in H_2O (5 mL) was added to the reaction and heated under reflux for 1 h. The solution was then allowed to stand at room temperature for several days. The solids formed were filtered off and washed with deionised H_2O. White crystals (0.03 g, 28%). $C_{16}H_{16}N_{10}O_6Zn$: calcd. C 37.70, H 3.16, N 27.48% ; found C 36.93, H 4.06, N 28.29%. IR (KBr): ν = 3415, 3126, 3004, 1650, 1610, 1474, 1462, 1364, 1301, 1247, 1165, 1010, 900, 808, 793, 750, 727, 702, 679 cm^{-1}. ^1H NMR (d_6-DMSO): δ = 8.70-8.72 (m, 1 H, pyr-H), 8.22-8.25 (m, 1 H, pyr-H), 8.00-8.08 (m, 1 H, pyr-H), 7.55-7.57 (m, 1 H, pyr-H), 5.48 (s, 2 H CH_2N) ppm. ^{13}C NMR (d_6-DMSO): δ = 166.3 (C=O), 151.9 (CN_4), 149.6, 144.5, 137.9, 125.5, 123.7, 51.0 (CH_2N) ppm.

3.5.4.2.7 [Zn_2(3.2pytza)$_2$(OCH_3)$_2$]$_n$ (3.16)

A solution of **3.2** (0.10 g, 0.43 mmol) and NaOH (0.01 g, 0.43 mmol) in MeOH (10 mL) was heated under reflux for 1 h. After this time, $ZnCl_2$ (0.06 g, 0.43 mmol) was added to the reaction. The resulting clear solution was allowed to stand for several days and the solids formed were filtered. White crystalline solid (0.04 g, 31%). $C_{18}H_{18}N_{10}O_6Zn_2$: calcd. C 35.96, H 3.02, N 23.30%; found C 35.81, H 3.19, N 22.93%. IR (KBr): ν = 3523, 3423, 3090, 3005, 1645, 1611, 1451, 1417, 1383, 1290, 1222, 1145, 1064, 1022, 918, 822, 808, 732, 680, 586 cm^{-1}. ^1H NMR (d_6-DMSO): δ = 8.72-8.75 (m, 1 H, pyr-H), 8.12-8.16 (m, 1 H, pyr-H), 7.97-8.03 (m, 1 H, pyr-H), 7.52-7.57 (m, 1 H, pyr-H), 5.44 (s, 2 H CH_2N) ppm. ^{13}C NMR (d_6-DMSO): δ = 168.9 (C=O), 163.7 (CN_4), 150.1, 146.2, 137.6, 125.1, 122.2, 55.3 (CH_2-tet), 48.5 (OCH_3) ppm.

3.5.4.2.8 [Zn(3.2pytza)$_2$(H$_2$O)$_2$] (3.17)

A solution of **3.2** (0.10 g, 0.43 mmol) and NaOH (0.01 g, 0.43 mmol) in H_2O (10 mL) was heated under reflux for 1 h. After this time, $ZnCl_2$ (0.06 g, 0.43 mmol) was added to the reaction. The solution was allowed to stand at room temperature for several days. Clear block crystals formed which were filtered and washed with deionised H_2O. White crystals (0.05 g, 50%). $C_{16}H_{16}N_{10}O_6Zn$: calcd. C 37.70, H 3.16, N 27.48%; found C 37.76, H 3.07, N 27.04%. IR (KBr): ν = 3419, 3236, 3025. 2867, 1638, 1614, 1547, 1456, 1417, 1373, 1290, 1226, 1145, 1066, 1050, 1031, 929, 901, 827, 801, 757, 731, 700, 685 cm^{-1}. Solid was insoluble in common deuterated solvents.

Data obtained matched that reported in literature.[174]

3.5.4.2.9 [Ni(3.1pytza)]$_n$ (3.18)

3.1 (0.10 g, 0.43 mmol) was dissolved in MeOH. NaOH (0.01 g, 0.43 mmol) in deionised H_2O was added to the solution and this was refluxed for 1 h. After this time $NiCl_2.6H_2O$ (0.10 g, 0.43 mmol) in MeOH was added to the solution and the resulting precipitate was filtered off and washed with MeOH. Blue powder (0.07 g, 62%). $C_8H_6N_5NiO_2$: calcd. C 36.55, H 2.30, N 26.64%; found C 35.80, H 2.71, N 25.75%. IR (KBr): ν = 3401, 3125, 1646, 1479, 1463, 1367, 1304, 1253, 1165, 1113, 1012, 902, 810, 792, 752, 727, 702, 685, 641, 590 cm^{-1}. Magnetic moment: 3.22 B.M.

3.5.4.2.10 [Ni(3.1pytza)]$_n$ (3.19)

A solution of **3.1** (0.10 g, 0.43 mmol) and NaOH (0.01 g, 0.43 mmol) in deionised H_2O (15 mL) was heated to reflux for 1 h. After this time, $NiCl_2.6H_2O$ (0.10 g, 0.43 mmol) in H_2O was added and the resulting green solution was allowed to stand at room temperature for several weeks. The solids formed were filtered off and washed with deionised H_2O. Pale blue powder (0.04 g, 36%). $C_8H_6N_5NiO_2$: calcd. C 36.55, H 2.30, N 26.64%; found C 37.42, H 2.58, N 25.94%. IR (KBr): ν = 3401, 3123, 1643, 1478, 1464, 1365, 1303, 1253, 1165, 1113, 1012, 901, 810, 792, 752, 727, 702, 684, 641, 590 cm^{-1}. Magnetic moment: 3.17 B.M.

3.5.4.2.11 [Ni(3.2pytza)$_2$(H$_2$O)$_2$] (3.20)

A solution of **3.2** (0.20 g, 0.86 mmol) and NaOH (0.03 g, 0.86 mmol) in MeOH (15 mL) was heated to reflux for 1 h. After this time $NiCl_2.6H_2O$ (0.20 g, 0.86 mmol) in MeOH was added and the resulting green solution was allowed to stand at room temperature for 1 week.

The blue solid that formed was filtered and washed with MeOH. Blue crystalline solid (0.09 g, 42%). $C_{16}H_{16}N_{10}NiO_2$: calcd. C 38.20, H 3.21, N 27.84%; found C 37.25, H 3.39, N 27.53%. IR (KBr): ν = 3234, 3026, 1630, 1457, 1418, 1373, 1292, 1230, 1165, 1031, 907, 829, 801, 732, 699, 678, 643 cm^{-1}. Magnetic moment: 2.96 B.M.

3.5.4.2.12 [Ni(3.2pytza)$_2$(H$_2$O)$_2$] (3.21)

A solution of **3.2** (0.20 g, 0.86 mmol) and NaOH (0.03 g, 0.86 mmol) in deionised H_2O (15 mL) was heated to reflux for 1 h. After this time $NiCl_2.6H_2O$ (0.20 g, 0.86 mmol) in deionised H_2O was added and the resulting green solution was allowed to stand at room temperature for 1 week. The blue solid that formed was filtered and washed with deionised H_2O. Blue crystalline solid (0.11 g, 51%). $C_{16}H_{16}N_{10}NiO_2$: calcd. C 38.20, H 3.21, N 27.84%; found C 37.66, H 2.48, N 27.72%. IR (KBr): ν = 3238, 3027, 2978, 1631, 1553, 1458, 1372, 1292, 1231, 1166, 1031, 907, 828, 801, 732, 699, 682, 644, 575, 426 cm^{-1}. Magnetic moment: 3.12 B.M.

3.5.4.2.13 [Co(3.1pytza)]$_n$ (3.22)

3.1 (0.10 g, 0.43 mmol) was dissolved in MeOH (9 mL). NaOH in H_2O (0.01 g, 0.43 mmol) was added to this solution and refluxed for 1 h. $Co(SCN)_2$ (0.08 g, 0.43 mmol) in MeOH was added to the solution and the resulting precipitate was filtered off and washed with MeOH. Beige powder (0.06 g, 53%). $C_8H_6CoN_5O_2$: calcd. C 36.52, H 2.30, N 26.62%; found C 36.96, H 2.64, N 26.27%. IR (KBr): ν = 3124, 2069, 1649, 1612, 1547, 1475, 1462, 1361, 1302, 1249, 1164, 1111, 1009, 913, 901, 809, 793, 751, 727 cm^{-1}. Magnetic moment: 4.92 B.M.

3.5.4.2.14 [Co(3.1pytza)$_2$(H$_2$O)]$_2$ (3.23)

3.1 (0.10 g, 0.43 mmol) was suspended in deionised H_2O (15 mL) and NaOH (0.01 g, 0.43 mmol) in deionised H_2O was added to this solution and the resulting mixture was heated to reflux for 1 h. An aqueous solution of $Co(SCN)_2$ in was added to the solution and the resulting pink solution was allowed to stand at room temperature for several days. The orange solid formed was filtered and washed with H_2O. Orange solid (0.03 g, 29%). $C_{16}H_{14}CoN_{10}O_5$: calcd. C 39.58, H 2.91, N 28.87%; found C 38.97, H 2.49, N 27.93%. IR (KBr): ν = 3124, 1650, 1611, 1547, 1475, 1462, 1433, 1360, 1301, 1247, 1164, 1111, 1008, 913, 800, 793, 751, 727 cm^{-1}. Magnetic moment: 5.17 B.M.

3.5.4.2.15 [Co(3.2pytza)(H_2O)(SCN)]$_n$ (3.24a) and [Co(3.2pytza)(SCN)]$_n$ (3.24b)

3.2 (0.10 g, 0.43 mmol) was dissolved in H_2O. NaOH (0.01 g, 0.43 mmol) in deionised H_2O was added to the solution and this was heated to reflux for 1 h. $Co(SCN)_2$ (0.08 g, 0.43 mmol) in MeOH was added to the mixture. A pink precipitate formed which was filtered off and washed with MeOH to yield **3.24a**. Pink powder (0.13 g, 85%). $C_9H_{10}CoN_6O_4S$: calcd. C 30.26, H 2.82, N 23.53%; found C 30.07, H 2.80, N 23.41%. IR (KBr): ν = 3393, 3024, 2116, 2092, 1608, 1549, 1451, 1423, 1397, 1308, 1225, 1151, 1065, 1047, 1030, 831, 805, 730, 696, 677 cm^{-1}. λ_{max} (DMF:H_2O) 512 nm, ε = 13.2 $M^{-1}cm^{-1}$. Magnetic moment: 4.54 B.M. On drying the sample under vacuum, a blue solid, **3.24b**, was produced. $C_9H_6CoN_6O_2S$: calcd. C 33.66, H 1.88, N 26.17%; found C 34.52, H 2.05, N 26.17%. IR (KBr): ν = 3355, 2092, 2071, 1605, 1450, 1424, 1400, 1310, 1155, 830, 803, 730, 678 cm^{-1}. λ_{max} (DMF) 620 nm, ε = 137.6 $M^{-1}cm^{-1}$. Magnetic moment: 3.23 B.M.

3.5.4.2.16 [Co(3.2pytza)$_2$(H_2O)$_2$] (3.25)

3.2 (0.10 g, 0.43 mmol) was suspended in a mixture of H_2O (10 mL) and MeOH (1 mL). NaOH (0.01 g, 0.43 mmol) in deionised H_2O was added to the mixture and the solution was heated to reflux for 1 h. After this time $Co(SCN)_2$ (0.08 g, 0.43) was added and the resulting solution was left to stand for several days. The resulting solids were filtered off and washed with H_2O. Orange solid (0.08 g, 74%). $C_{16}H_{16}CoN_{10}O_6$: calcd. C 38.18, H 3.20, N 27.83%; found C 37.22, H 3.53, N 26.98%. IR (KBr): ν = 3218, 3026, 2087, 2029, 1635, 1614, 1456, 1417, 1372, 1291, 1227, 1164, 1065, 1050, 1030, 827, 801, 732, 680 cm^{-1}. Magnetic moment: 5.02 B.M.

Data correlates well with literature data.[173]

Chapter 4: Dicarboxylate Functionalised Pyridyl Tetrazoles

4.1 Introduction

As previously discussed in Chapter 1 and Chapter 3, the design and synthesis of coordination polymers (CPs) has received considerable attention over the last number of years. This is due to their potential applications in a number of areas including gas storage, sensors and drug delivery. The general synthetic strategy for designing such materials involves using multidentate ligands containing O- or N-donor groups. Examples of such ligands include polycarboxylic acids and bipyridines. Due to their diverse coordination modes and sensitivity to pH values, symmetrical rigid aromatic O-donor ligands such as phthalic acid and terephthalic acid (Figure 4.1), have been extensively studied. Many multidimensional polymers possessing interesting properties incorporating these type of ligands have been reported[151] and a number have been utilised in combination with N-donor ligands to synthesise mixed linker containing CPs.[190]

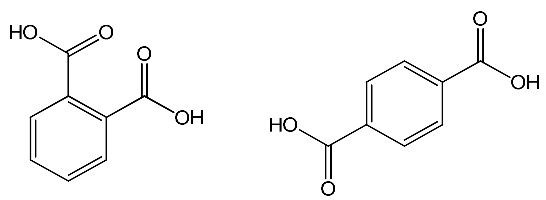

Figure 4.1: Phthalic acid (left) and terephthalic acid (right) are commonly used ligands in coordination polymers due to their high symmetry and diverse coordination modes.

In contrast, asymmetrical and flexible carboxylic acids have rarely been used, and the study on structures constructed from these type of ligands remains undeveloped. The lack of documented examples of multi-carboxylate ligands with rigid and flexible carboxylate groups may be attributed to the unpredictable structure types and also due to their unfavourable crystallisation conditions.[191] Furthermore, examples of asymmetric carboxylates in combination with asymmetric N-donor spacers are extremely limited. The majority of examples report the use of N-donor ligands as ancillary ligands, and these are often symmetrical ligands such as 4,4'-bipyridine.[191,192] N-donors can modify the structures and properties of the resulting materials by the cooperative coordination with carboxylate groups to meet the requirement of coordination geometries of metal ions in the assembly process.[191]

4.1.1 Asymmetric Carboxylates as Linkers in CPs

The most common asymmetrical carboxylate ligand utilised in the construction of CPs is homophthalic acid (Figure 4.2). Compared to symmetrical ligands like phthalic acid and terephthalic acid, homophthalic acid has a relatively flexible ethylic carboxyl group which may not be co-planar with the benzene ring in the molecule. This flexibility endows the ligand with the capacity to adopt various conformations as well as coordination modes.[193]

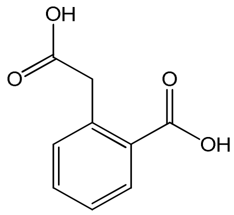

Figure 4.2: Homophthalic acid.

In one example, Wang and co-workers employed homophthalic acid as a ligand along with an N-donor auxiliary ligand, (1,4-bis(imidazol-1-yl-methyl)benzene), to construct MOFs employing solvothermal methods.[192] The resulting networks exhibited diverse structures and coordination modes at the metal ions. It was noted that the nature of the metal ion and its coordination geometry led to variation in the structures obtained, as the synthetic conditions were almost the same. For instance, in complexes **4.1** and **4.2** the Zn(II) is in a tetrahedral geometry with N_2O_2 donor set, while the Cd(II) has an octahedral geometry with O_5N_1 donor set (Figure 4.3). The diversity of the final structures was also attributed to the different conformations adopted by the N-donor ligand and in particular the O-donor ligand whose diverse coordination modes and flexibility allowed adjustments to occur during the assembly process. Several other authors have similarly utilised homophthalic acid in combination with other N-donor auxiliary ligands and have achieved interesting diverse structures.[191,194] Despite the success in employing this ligand as an asymmetric linker, it is apparent that work on this ligand has been documented to the point of exhaustion and there is a distinct paucity of examples utilising other asymmetric linkers. Hence, this is an area that is worth exploiting further and is likely to yield interesting results.

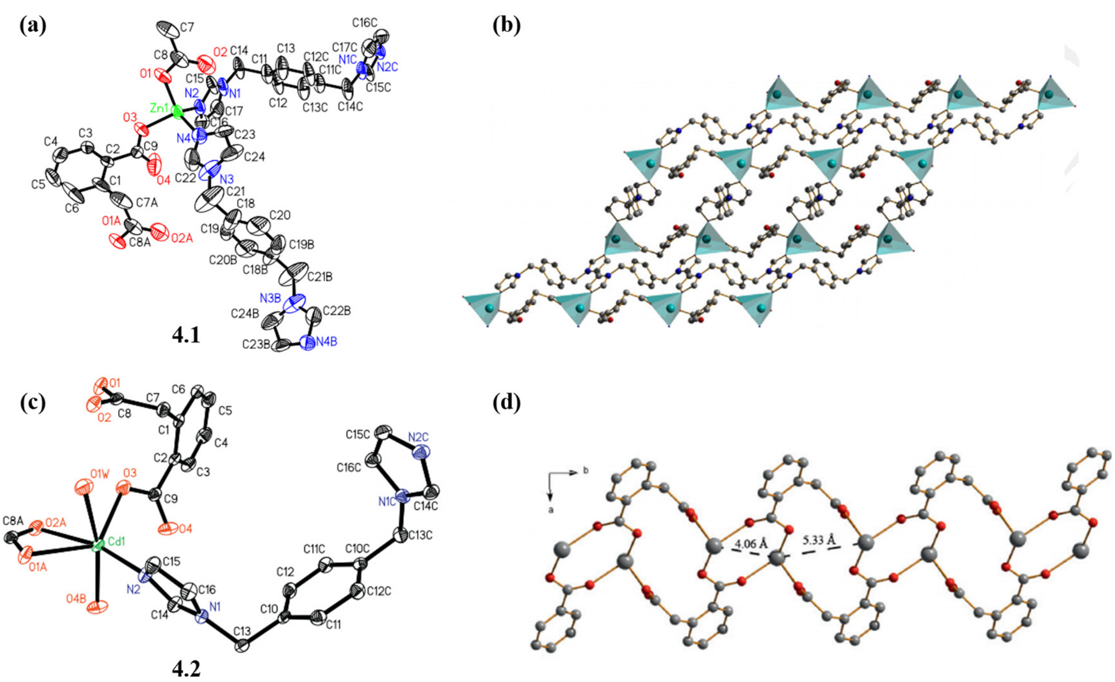

Figure 4.3: (a) and (c) Coordination environments around Zn(II) and Cd(II). Hydrogen atoms are omitted for clarity. (b) Top view of 2-D sheet of **4.1** along the *b*-axis. (d) View of 1-D chain in **4.2**.[192]

4.2 Aims and Objectives of Chapter

Taking the considerations mentioned previously into account, we focused our attention on the construction of CPs based on asymmetric carboxylate ligands. Further developing the linkers used in Chapter 3 (**3.1(pytza)** and **3.2(pytza)**, Figure 4.4), the addition of a carboxylic acid group tethered to the pyridyl unit was proposed (Figure 4.4). **3.1(pytza)** and **3.2(pytza)** possessed the donor capabilities of carboxylate oxygens and pyridyl tetrazole nitrogens. Addition of another carboxylate on the pyridine ring would endow the linker with more coordinative possibilities and could be more conducive to forming higher dimensional infinite arrays. **3.1(pytza)** and **3.2(pytza)** possessed an alkyl carboxylic acid positioned on the tetrazole ring. In the formation of the CPs, it was observed that this group could orientate itself in a number of ways and in most cases, it was not co-planar with the tetrazole ring. In the case of **4.3(pytzda)** and **4.4(pytzda)**, it was anticipated that the combination of an alkyl carboxylate with the co-planar aromatic carboxylate would lead to higher dimensionality and diversity in the frameworks. Considering the breadth of multifunctional linkers, some of which are discussed in Chapter 3, multifunctional linkers with both rigid and flexible carboxylic acid groups are severely under-investigated. Hence, we aimed to further develop the range of asymmetric carboxylate linkers while at the same time incorporating asymmetric N-donors into the linker. To the best of our knowledge, there are no reports in the literature that employ a linker using both asymmetric nitrogen donors and mixed carboxylate groups. Thus, this report is the first to explicitly describe this approach in the synthesis of CPs.

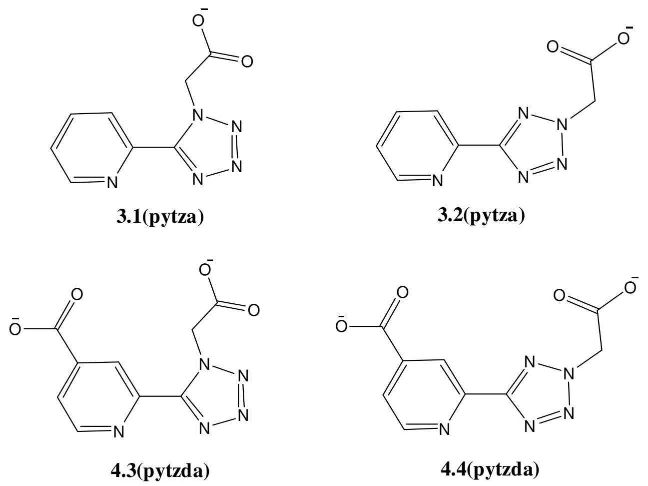

Figure 4.4: Structures of the first generation linkers synthesised in Chapter 3 and the second generation linkers that were intended to be synthesised and employed in the synthesis of CPs.

In previous chapters, synthesis of linkers began with a 1,3-dipolar cycloaddition between 2-cyanopyridine and sodium azide. However, this relied on the nitrile being commercially available. In this case, an appropriate nitrile was not commercially available. Thus, an objective of this work was to develop a strategy to synthesise **4.3** and **4.4**. As before, the ester derivatives would need to be synthesised first in order to aid in the separation of the regioisomers (Figure 4.5). We aimed to carry out the hydrolysis of the esters *in situ* in order to generate **4.3(pytzda)** and **4.4(pytzda)** (Figure 4.4) which would then be available to react with metal salts. As discussed in section 2.3.1, two regioisomers were expected in the formation of **4.3** and **4.4,** thus allowing an investigation into regiochemical effects on the structures of CPs.

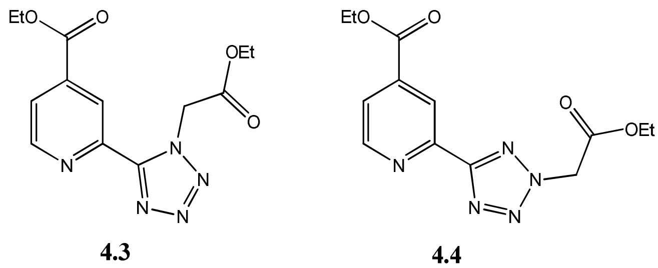

Figure 4.5: Synthesis of ester derivatives **4.3** and **4.4** was intended prior to the synthesis of CPs.

Finally, CPs are of significant interest due to their physical properties,[181] hence we aimed to examine the luminescent properties of the resulting Zn(II) structures and to carry out EPR studies on Cu(II) structures.

Ultimately, our aims were to synthesis **4.3** and **4.4**; to utilise these ligands to construct metal organic complexes with interesting topologies and properties for potential application; to investigate the factors influencing the coordination mode of the ligands and the final structure of the complexes and to investigate the physical properties of the resulting materials.

4.3 Results and Discussion

4.3.1 Synthesis of Diester Pyridyl Tetrazoles 4.3 and 4.4

4.3.1.1 Synthetic Approach

The synthetic strategy developed in order to gain access to the diester derivatives **4.3** and **4.4** involved consideration of pyridine ring reactivities. In order to install a tetrazole moiety in the 2-position of the pyridine, the presence of a nitrile was required in this position. The timing of the instalment of a carboxylic acid moiety in the 4-position also had to be considered. Synthesis could have commenced from either 2-cyanopyridine or isonicotinic acid, however, on examining the potential routes starting from both precursors, a route involving nucleophilic substitution of isonicotinic acid was chosen. This was due to a number of reasons. Firstly, pyridine rings can only undergo electrophilic substitution if they are activated by electron-donating substituents.[123] Nitrile groups and carboxylic acid groups are both electron withdrawing substituents, thus, electrophilic substitution using either of the above starting materials would have proved a difficult task. On the other hand, carrying out nucleophilic substitution on either starting material could have been possible. The most efficient way of carrying out nucleophilic substitution on a pyridine ring is to oxidise the pyridine nitrogen to yield an N-oxide.[123] The N-O moiety of pyridine N-oxides possess a unique functionality which can act effectively as a push electron donor and as a pull electron acceptor group by virtue of the resonance forms shown in Scheme 4.1.[195]

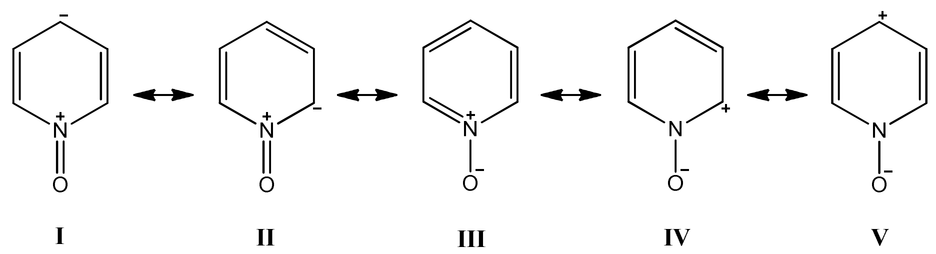

Scheme 4.1: Resonance forms of pyridine-N-oxide.

Secondly, on examination of the literature, nucleophilic substitution on 2-cyanopyridine resulted in low yields and a mixture of products.[196] Thus, nucleophilic substitution starting from isonicotinic acid was considered the best approach, as nitrile attack would only occur at the 2-position due to the carboxylic acid function being present at the 4-position. This group would effectively protect this position.

The nucleophilic substitution of the oxidised pyridine ring was then considered. Classic α-cyanation of pyridine N-oxides is achieved *via* a Reissert-Henze reaction using benzoyl chloride and a cyanide ion.[197] Modifications to this reaction has involved the use of trimethylsilanecarbonitrile (TMSCN) in the presence of different acylating agents.[198,199] In 2008, Huo and colleagues developed a zinc cyanide ($Zn(CN)_2$) mediated direct α-cyanation of isonicotinic acid N-oxide with the objective of avoiding the use of expensive TMSCN.[200] An acylating agent, dimethylcarbamoyl chloride (DMCC), was also used in the reaction and the proposed reaction mechanism is shown in Scheme 4.2. At the initial stage of the reaction, the 1-acyloxypyridinium intermediate ion **4.5** is formed as mentioned in previous reports in the literature.[198,201] The α-cyanation reaction of this intermediate with $Zn(CN)_2$ and elimination of carbon dioxide affords the tetrahedral intermediate **4.6**. Removal of N,N-dimethylcarbamic acid from **4.6** then gives 2-cyanoisonicotinamide (**4.7**).

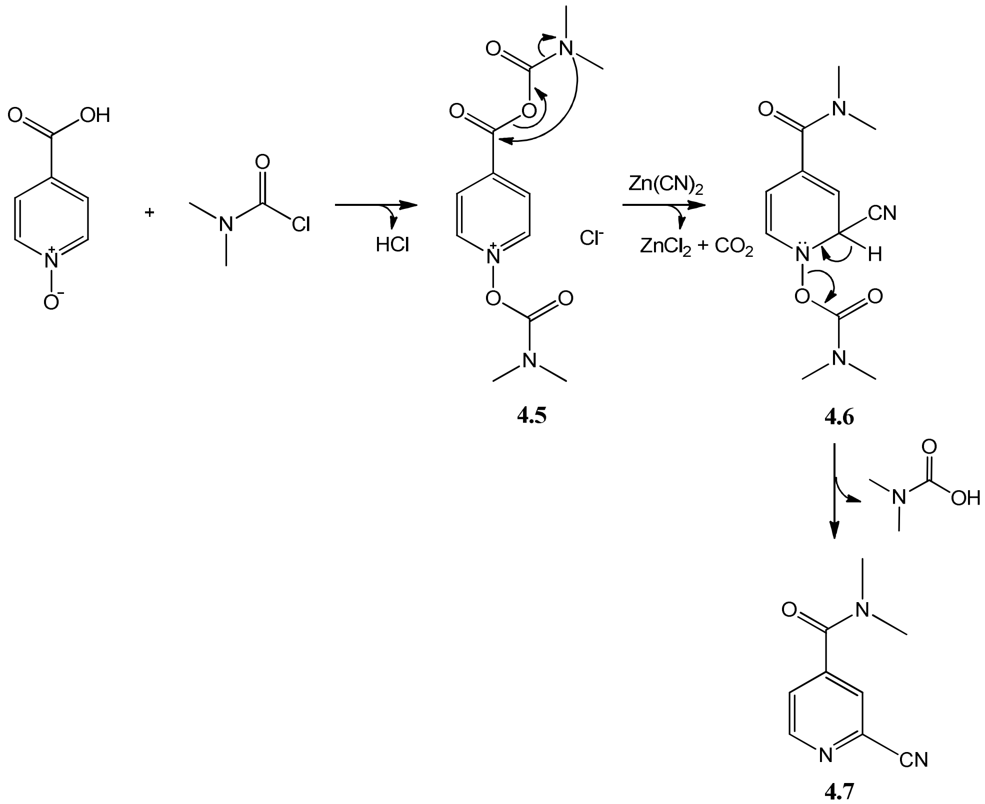

Scheme 4.2: The mechanism proposed by Huo *et al.* for the formation of an α-cyanated pyridine.[200]

We further modified these reaction conditions to suit our purposes and our proposed synthetic route can be seen in Scheme 4.3. Firstly, protection of the carboxylic acid moiety would be carried out to avoid formation of the N-carbamoyl group, followed by oxidation of the pyridine nitrogen to form the N-oxide (**4.9a/4.9b**). Cyanation of the 2-position would be carried out under similar conditions employed by Huo and co-workers to obtain **4.10a/4.10b**. Subsequent 1,3-dipolar cycloaddition and alkylation of the tetrazole ring would yield ligands **4.3** and **4.4** (Scheme 4.3).

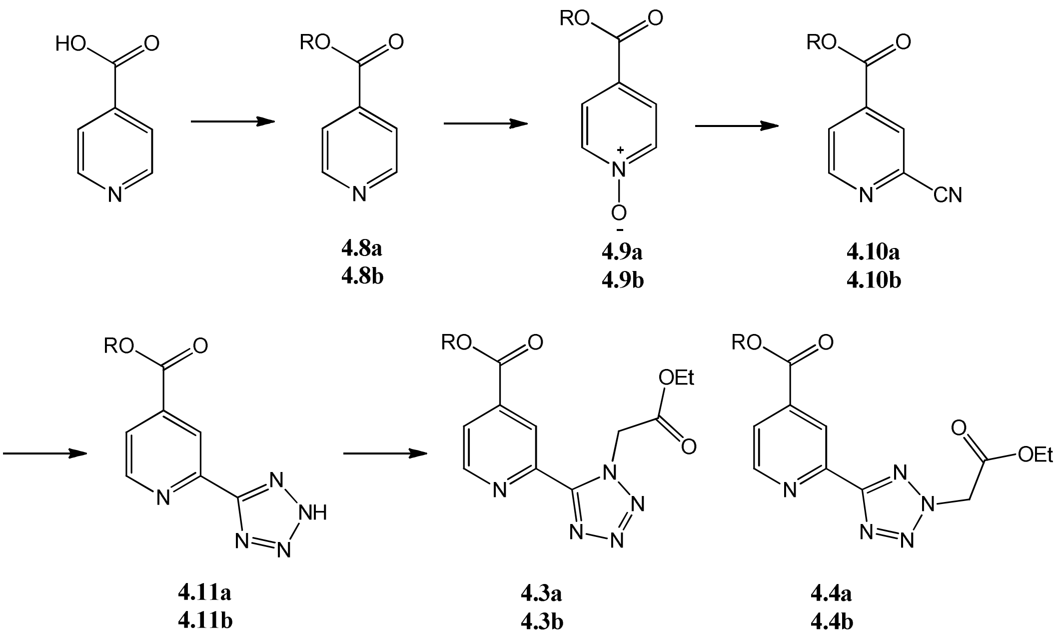

Scheme 4.3: Intended synthetic route to obtain the diester derivatives **4.3a/b** and **4.4a/b**. a: R = Me, b: R = Et.

4.3.1.2 Synthesis of Ligands 4.3 and 4.4

Synthesis commenced with esterification of isonicotinic acid to the methyl ester employing typical esterification conditions.[123,202,203] Characterisation data obtained for the yellow oil (**4.8a**) was in agreement with literature data,[202] with a singlet observed in the ^{1}H NMR spectrum at 3.96 ppm integrating for 3 protons, and a ^{13}C NMR resonance at 52.6 ppm being the main indication of the presence of a methyl ester functionality. In order to activate the 2-position towards nucleophilic attack, oxidation of the pyridine ring was required. Oxidation of heterocycles can be obtained in good yields using peracetic acid. This is a strong oxidant that has uses in disinfection, bleaching of textiles and pulps and in the epoxidation of olefins.[204] Generally, peracetic acid can be prepared in two ways; from hydrogen peroxide or by oxidation of acetaldehyde. For the purpose of this project, the acetic acid-hydrogen peroxide method was used. Sulfuric acid can be used as a strong acid catalyst to accelerate the rate of equilibrium of this reversible reaction, however its use was not required in our case. The process is described by the following scheme:

$$\mathrm{AcOH} + H_2O_2 \xrightleftharpoons{H_2SO_4} \mathrm{AcOOH} + H_2O$$

Scheme 4.4: Formation of peracetic acid from acetic acid and hydrogen peroxide.

The mechanisms of peracetic acid synthesis have been studied previously.[204,205] Using an ^{18}O isotope label, it was found that the reaction did not involve dissociation of the O-O bond in hydrogen peroxide.[204] The hydrolysis of peroxy acids synthesised from $HC^{18}OOH$ or $CH_3C^{18}OOH$ afforded hydrogen peroxide containing no radiolabelled oxygen (^{18}O). This evidence indicated that the bond between the acyl group and oxygen atom was cleaved in both the formation and hydrolysis of peroxy acids.[204] Rubio *et al*. studied the mechanism of formation of peracids taking the reaction between formic acid and hydrogen peroxide as a model for the generation of performic acid.[205] They proposed two routes for the formation of performic acid (Scheme 4.5). Route A consists of the addition of the hydrogen peroxide to the carbonyl carbon to form a tetrahedral transition state with the subsequent loss of a H_2O molecule; Route B is carried out in an acidic medium for the activation of the carbonyl carbon with subsequent addition of the hydrogen peroxide and the loss of a H_2O molecule.[205] Route B is proposed to be the preferred pathway, as the organic acid (in our case acetic acid) can provide a source of H^+ when there is no acid catalyst in the reaction system, thereby accelerating the reaction.

Route A

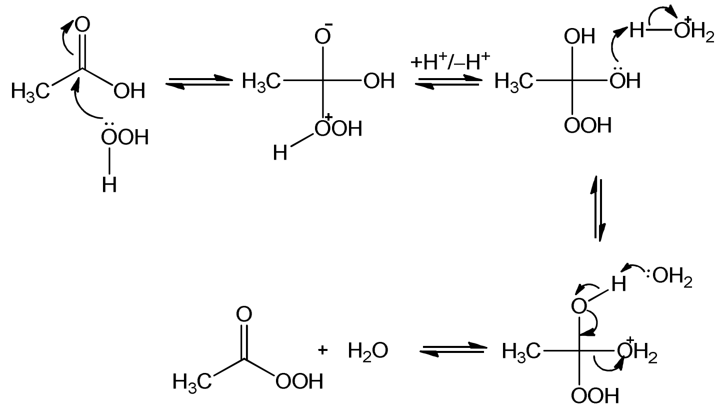

Route B

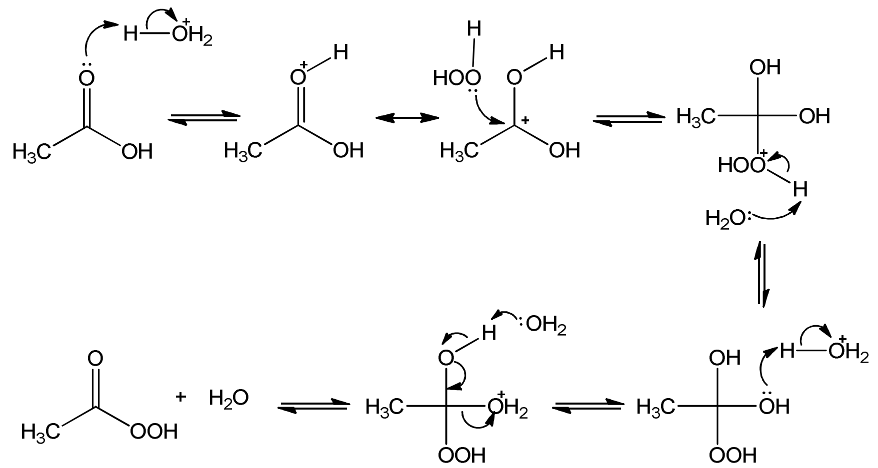

Scheme 4.5: Two proposed routes by which peracetic acid can form, as proposed by Rubio *et al.*[205] Route A involves attack of hydrogen peroxide on the carbonyl carbon of the acid with subsequent loss of H_2O. Route B involves an acid catalysed mechanism with hydrogen peroxide addition and loss of H_2O.

Oxidation of the pyridine ring is achieved by nucleophilic attack from the nitrogen on the peracetic acid oxygen followed by subsequent deprotonation. Oxidation of **4.8a** was achieved in this way and after treatment with base and extraction with ethyl acetate a pale yellow solid was afforded. Confirmation that the pale yellow solid was indeed the N-oxide **4.9a** was attained through characterisation by NMR and IR spectroscopies which was consistent with the data obtained in literature reports.[206,207] The IR spectrum was notably different from the unoxidised pyridine ring **4.8a** with the presence of a ν(N-O) stretching frequency at 1262 cm^{-1}. A cyanation reaction was then carried out utilising a modified method of that carried out by Huo *et al.*[200] The reaction was carried out in toluene, using conventional heating methods employing DMCC as the acylating agent and $Zn(CN)_2$ as the cyanide source. Substitution of the symmetrical N-oxide **4.9a** in the 2-position would result in an additional peak resonating in the ^1H NMR spectrum as symmetry in the molecule would be lost. On analysis of the pale orange product **4.10a**, the successful substitution of a nitrile group at the 2-position was indicated, as three aromatic resonances were observed at 8.07, 8.24 and 8.07 ppm in the ^1H NMR spectrum. The ^{13}C NMR spectrum also displayed three extra signals compared to the spectrum of **4.9a** due to this loss of symmetry, creating eight inequivalent carbon environments. The nitrile ^{13}C signal was observed at 115.5 ppm. The IR spectrum also confirmed the presence of a nitrile group as a ν(C≡N) frequency was positioned at 2237 cm^{-1}. The obtained data for **4.9a** was also consistent with a literature report,[208] indicating that our modified α-cyanation of a pyridine ring was successful. This method afforded comparable yields to those in literature reports (~65%) and offers a safer methodology as cheap $Zn(CN)_2$ is employed which is relatively less toxic than TMSCN, NaCN and KCN. A 1,3-dipolar cycloaddition was then carried out using conditions utilised previously (section 2.3.1). On recovery of the protonated 5-substituted tetrazole **4.11a**, issues were encountered in the acidic work-up. Yields were poor, and often following an extraction, the hydrolysed product was encountered. Although this result was not a considerable diversion from our intended synthetic route, there was concern over the feasibility of purifying regioisomers if a carboxylic acid was present. In addition, the low yields of the methyl ester derivative would have made the synthesis of the coordination polymers an inefficient and time consuming task. Thus, a simple solution was proposed. Taking into consideration the reactivity of a methyl ester towards ester hydrolysis in aqueous acidic conditions, it was anticipated that a less reactive ester would be more stable in these conditions, therefore allowing isolation of the 5-substituted tetrazole with the ester functionality intact. Conversion of the carboxylic acid to a less reactive ethyl ester did indeed alleviate these problems and isolation of **4.11b** was achieved consistently with yields >70% after re-crystallisation in EtOH. Presence of the tetrazole ring was alluded to as another aromatic ^{13}C signal was present in the ^{13}C NMR spectrum accompanied by the concomitant disappearance of the nitrile ^{13}C peak. Consumption of the nitrile was also indicated by the disappearance of a ν(C≡N) frequency in the IR spectrum of **4.11b**. Presence of a broad stretch positioned at 3083 cm^{-1} was attributed to a ν(N-H) frequency, which further pointed towards the presence of a protonated tetrazole ring. This broad stretch was not considered to be a carboxylic acid OH stretch as the presence of ethoxy protons at 1.38 and 4.43 ppm in the ^{1}H NMR spectrum indicated that the ester group remained intact. Finally, analysis by HRMS confirmed the successful synthesis of **4.11b**. Alkylation of **4.11b** using ethyl bromoacetate in the presence of K_2CO_3 yielded two regioisomers, **4.3** and **4.4**. Analysis of the crude mixture of **4.3** and **4.4** by ^{1}H NMR spectroscopy revealed a ratio of ~10:12 of N-1 to N-2 isomers being produced, which represents a distinct lack of regioselectivity. However, in comparison to the ester derivatives **3.1** and **3.2** which were discussed in Chapter 3, which showed similar regioselectivity, this result was to be expected. The two isomers were purified by flash column chromatography and identification and assignment of the position of the alkylated site was possible by analysis of the products by ^{13}C NMR spectroscopy. The C-5 of the tetrazole ring resonated at 151.8 ppm for the N-1 substituted isomer and 164.7 ppm for the N-2 substituted isomer. The protons of the methylene group were again more downfield for the N-1 isomers than for the N-2 isomers due to the anisotropic effects of the pyridine ring (Figure 4.6). The presence of the alkyl ester functionality was also confirmed by the presence of another carbonyl ^{13}C peak at ~165 ppm and another ν(C=O) frequency visible at ~1725 cm^{-1}.

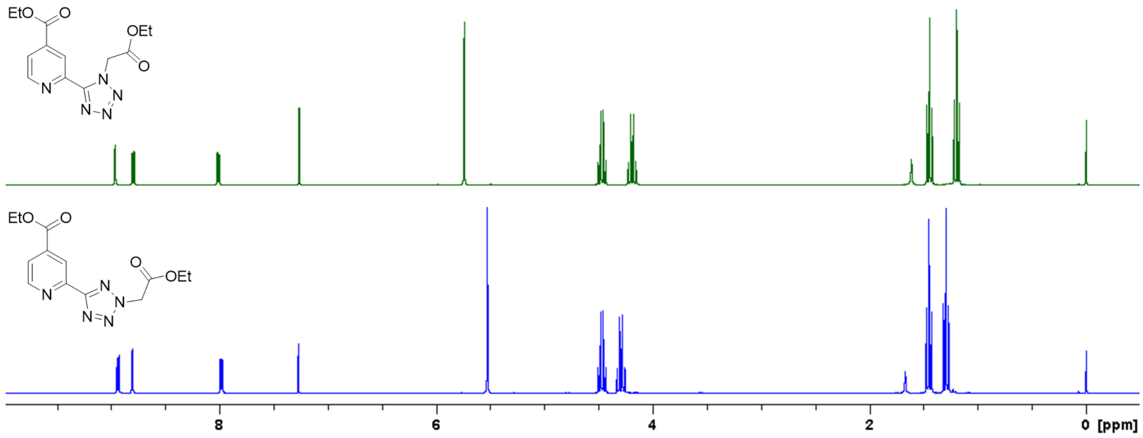

Figure 4.6: ^{1}H NMR spectrum of **4.3** (green) and **4.4** (blue) obtained in $CDCl_3$.

4.3.2 Metal Complexation Reactions

4.3.2.1 Metal Complexation Reactions with Diester Derivatives 4.3 and 4.4

Coordination studies were carried out with **4.3** and **4.4** as it was thought that they could offer interesting coordination chemistry in their own right. One equivalent of metal salt relative to the ligands were employed.

Addition of $CuCl_2.2H_2O$ to a solution of **4.3** in MeOH resulted in a vibrant green solution. After heating the solution to reflux for 2 h, the solution was allowed to sit at room temperature for several days. The resulting green solids (**4.12**) were isolated and characterised. IR analysis on the solid **4.12**, indicated that complexation to the ester moiety was not occurring as there was not a significant shift in the ν(C=O) frequencies. Slight shifts of ~10 cm^{-1} were observed however, suggesting that the ligand had complexed to the Cu(II) ion. Shifts were observed for the heterocyclic frequencies, with ν(C=N)$_{pyr}$, ν(C=N)$_{tet}$ and ν(N=N) frequencies shifting from 1604, 1537 and 1433 cm^{-1} to 1618, 1560 and 1458 cm^{-1} respectively. Elemental analysis suggested that the solid had a 1:1 metal to ligand composition, and the presence of four chloride anions correlated well with these results. Hence, it was proposed that the complex consisted of a dichloro-bridged species, with each Cu(II) centre in a square pyramidal geometry (Figure 4.7).

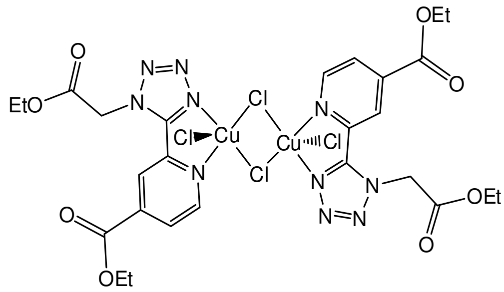

Figure 4.7: Proposed structure of **4.12**.

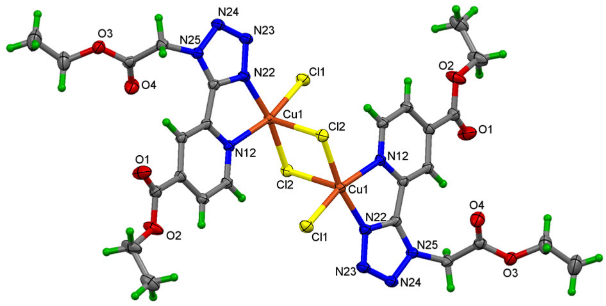

Figure 4.8: Crystal structure of **4.12.**

Crystals suitable for single crystal X-ray diffraction were obtained and the results obtained established that **4.12** was indeed made up of a dichloro-bridged structure (Figure 4.8) and that each Cu(II) ion was coordinated to three chloride anions (two of which were μ-Cl bridging chlorines), a pyridine nitrogen and a tetrazole nitrogen. The dimeric complex lies on a crystallographic inversion centre which lies at the centre of the $[Cu(II)(\mu\text{-}Cl)Cl]_2$ core and this structure is similar to the previously discussed copper dimer complexes in Chapter 2 (Figure 2.11) and Chapter 3 (Figure 3.13). The Cu(II) ion is in a distorted square pyramidal geometry, with a very long Cu1⋯Cl2 bond compared to other coordinative bonds (2.76 Å compared to 2.10-2.25 Å for all other bonds). According to Halcrow, only Cu-L interactions up to 2.4 Å should be considered as genuine Cu-L bonds, with longer bonds representing weaker, secondary interactions.[55] Therefore, on examination of the bond lengths in **4.12**, it could be implied that the complex is more square-planar in geometry. Each pyridyl tetrazole ligand binds to the Cu(II) atom through one tetrazole N atom at the N-1 site of the tetrazole ring and through the pyridyl N atom, generating a five-membered chelate ring. The 5-membered tetrazole ring is slightly twisted with respect to the 6-membered pyridyl ring at an angle of 11.1(3)°.

Addition of $CuCl_2.2H_2O$ to a methanolic solution of **4.4** resulted in an emerald green solution. After heating to reflux for 2 h the solution was allowed to stand at room temperature for several days. The resulting mint green solid, **4.13**, was filtered and dried. IR spectral analysis of the solid revealed that the two ν(C=O) vibrational modes had a smaller difference in frequency than the starting material. Shifts in the heterocyclic frequencies were also observed. Elemental analysis indicated a 1:2 metal to ligand composition. Elemental analysis also suggested that the ethyl groups were no longer present. This could be explained by the process of transesterification. Transesterification is the process of exchanging an ester R group to a different R group of an alcohol.[123] This process was plausible in this case, as MeOH was employed as the reaction solvent and was therefore in excess. This would result in the methyl ester derivative being produced, which would explain the observed elemental analysis results. Therefore, a structure was proposed which is shown in Figure 4.9. This octahedral complex is similar to the complex **3.9** that was discussed in section 3.3.2.1.

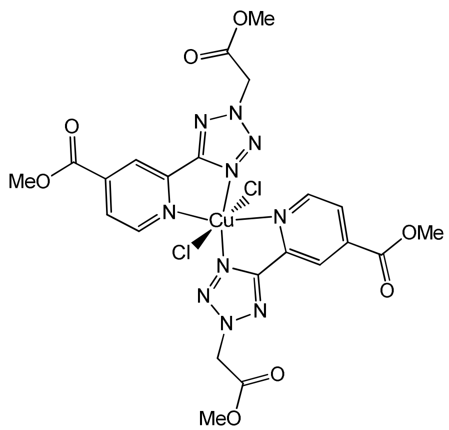

Figure 4.9: Proposed structure of **4.13**.

Reaction of $Co(SCN)_2$ with **4.4** resulted in a pink solution which turned blue on standing at room temperature for several days. An orange/pink crystalline solid, **4.14**, formed which was filtered off, washed with MeOH and dried. The IR spectrum of **4.14** revealed that there was no interaction between the metal ion and the ester moiety, as shifts of ~50 cm^{-1} were not observed for the ν(C=O) frequencies, although smaller shifts were visible. Shifts in the heterocyclic ring frequencies were evident with bands shifting from 1605, 1564, 1427 cm^{-1} to 1622, 1570 and 1432 cm^{-1}. Presence of thiocyanate anions were also revealed, with very strong $\nu(C{=}N)_{SCN}$ frequencies positioned at 2093 and 2081 cm^{-1}. These values are above what classically N-bonded thiocyanato anions would vibrate at, however they are consistent with obtained experimental values reported in the literature.[150] Elemental analysis of **4.14** indicated a 1:2 metal to ligand composition. Elemental analysis also suggested that transesterification had occurred. Taking into consideration the obtained data for **4.14**, a structure was proposed and can be seen in Figure 4.10. The complex consists of an octahedral Co(II) centre, coordinated by two pyridyl tetrazole ligands in the equatorial plane and two isothiocyanate anions in the axial positions.

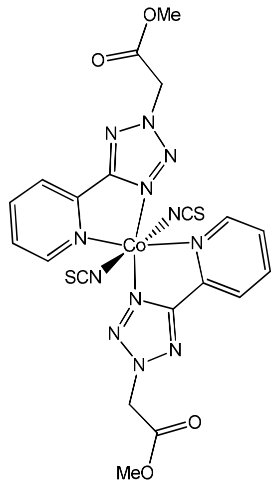

Figure 4.10: Proposed structure of **4.14**.

A crystal was grown of complex **4.14** and was analysed by single crystal X-ray crystallography (Figure 4.11). The results established a distorted octahedral environment around the Co(II) centre and confirmed that transesterification had occurred. The orientations of the ligands, however, are different to what was observed in previous $Co(SCN)_2$ complexes synthesised in this work. Instead of the two pyridyl tetrazole ligands occupying the equatorial planes of the octahedron as had previously been observed, one ligand now occupies the axial position and the other occupies the equatorial position. This is also the case for the thiocyanate anions, which are *cis* to each other. The structure shares similarities with the comprehensively studied $[Ru(bipy\text{-}R)_2(NCS)_2]$ series of complexes.[209]

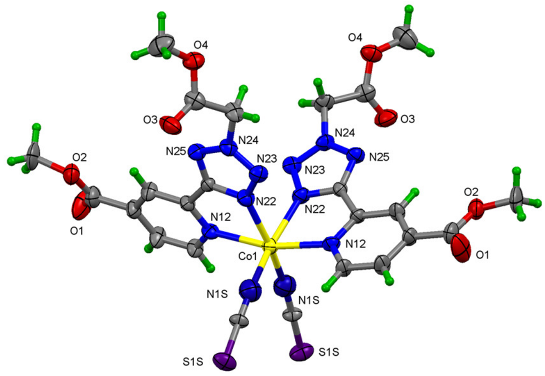

Figure 4.11: Crystal structure of **4.14**.

Comparing these reactions to those carried out with the mono-ester derivatives in Chapter 3, it was again evident that the position of the alkylated site of the tetrazole ring was influencing the geometry that the metal centre was adopting. With the prospect of using the carboxylate derivatives of **4.3** and **4.4** in CP synthesis, these regiochemical effects promised interesting results.

4.3.2.2 *In situ* Hydrolysis and Metal Complexation Reactions with 4.3(pytzda) and 4.4(pytzda)

4.3 and **4.4** were converted to their respective carboxylates *in situ* by nonsolvothermally heating aqueous NaOH solutions of the ligands (Scheme 4.6). After two hours, aqueous solutions of metal salts (one equivalent) were added to the solutions. These solutions were then cooled slowly and allowed to stand at room temperature for several days or in some cases weeks. On slow evaporation of the mother liquor, crystalline solids were obtained and in some instances, crystals formed that were suitable for single crystal X-ray crystallography. Each product was analysed by IR spectroscopy, elemental analysis and magnetic moment measurements. In the case of the Cu(II) products, EPR spectroscopy was also performed. For the Zn(II) products, NMR spectroscopy was also undertaken. One Zn(II) complex, **4.21** was subjected to solid state fluorescence studies.

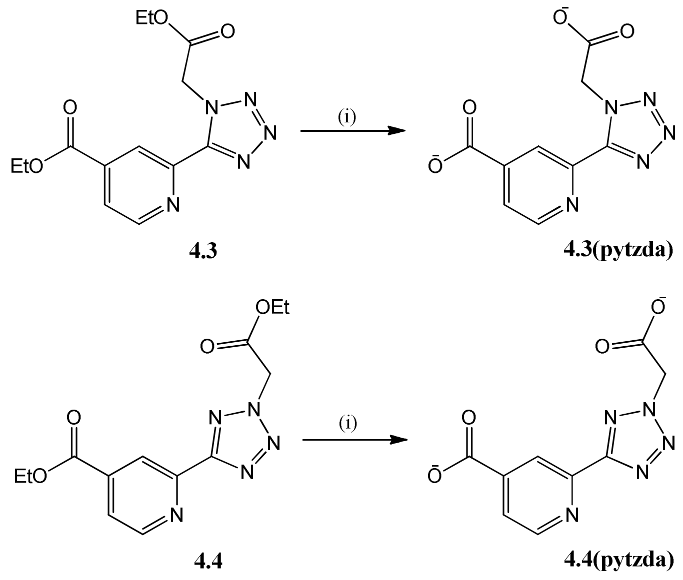

Scheme 4.6: Reagents and conditions: (i) NaOH, H_2O, Δ, 2 h.

4.3.2.2.1 Coordination polymer formation employing 4.3(pytzda)

A blue crystalline solid was obtained in the reaction of **4.3(pytzda)** with $CuCl_2.2H_2O$. IR spectral analysis of the solid **4.15** indicated that no protonated carboxylic acid was present as the peak associated with this vibrational mode was absent (~1726 cm^{-1}). Anti-symmetric carboxylate vibrations ($\nu_{asym}(COO^-)$) were positioned at 1619 cm^{-1} and 1555 cm^{-1}. Corresponding symmetric vibrations ($\nu_{sym}(COO^-)$) were positioned at 1392 and 1365 cm^{-1}. These observations suggested that there were two modes of coordination that the carboxylates were adopting. Also visible in the IR spectrum of **4.15** was a very broad stretch in the range of 2966-3577 cm^{-1} which was centred at 3230 cm^{-1}. This indicated the presence of H_2O molecules coordinating to the metal ion and also that extensive hydrogen bonding was present in the structure. Elemental analysis of **4.15** suggested a 1:1 ratio of metal to ligand. The single blue crystals that were obtained in this reaction were analysed by X-ray crystallography, the results of which can be seen in Figure 4.12. The asymmetric unit of **4.15** consists of a dinuclear structure, with one Cu(II) ion coordinated by two H_2O molecules, a tetrazole nitrogen and a pyridyl nitrogen, and the second Cu(II) centre coordinated by a carboxylate oxygen binding in a monodentate fashion and two H_2O molecules. The Cu1 metal centre displays typical Jahn-Teller axial elongation in its distorted octahedral geometry (Cu1-O1W 2.42 Å, Cu1-N12 2.04 Å, Cu1-N2 1.99 Å). The Cu2 metal centre is also in a distorted octahedral geometry, however the distortions are not quite as pronounced compared to the Cu1 atom. This bonding arrangement generates a 1-D CP (Figure 4.13) that has a wavelike topology. The waves result from a 'kink' created by the coordination geometry around the Cu2 centre. Extensive hydrogen bonding is present throughout the structure by virtue of the H_2O molecules (Figure 4.13). The coordinating H_2O molecules on Cu1 act as both hydrogen bond donors (to carboxylate oxygens) and acceptors (to the H_2O of crystallisation). The coordinating H_2O molecules on Cu2 act solely as hydrogen bond donors to carboxylate oxygens from other polymeric chains.

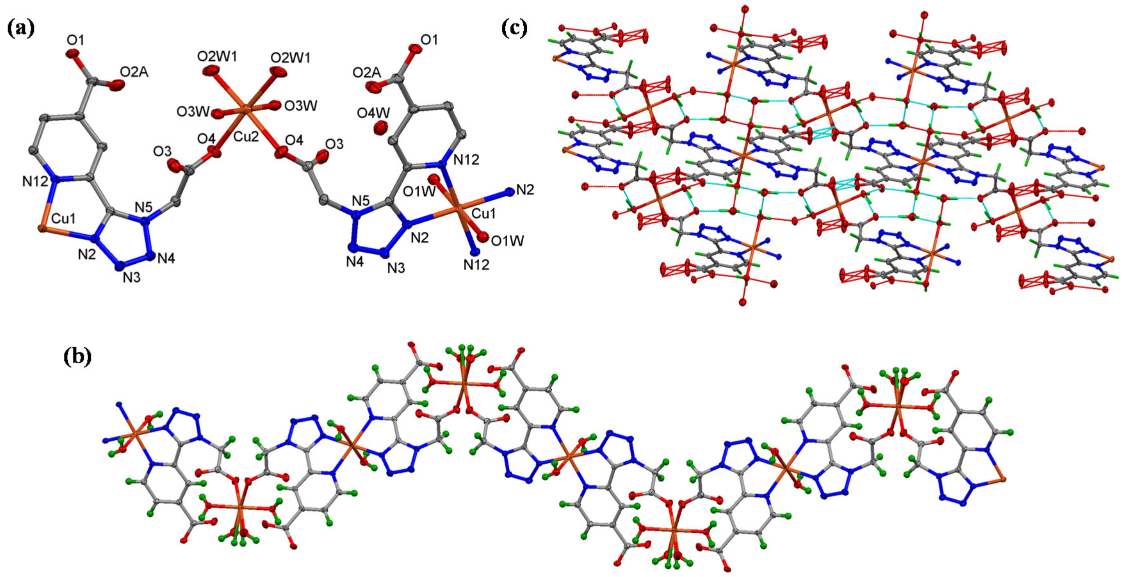

Figure 4.12: (a) Subunit of **4.15**. The Cu2 metal centre gives rise to the 'kink' in the coordination polymer. (b) View along the *c*-axis of **4.15**. (c) Packing diagram viewed along the *b*-axis with hydrogen bonding connecting the polymers visible.

Reaction of **4.3(pytzda)** with $NiCl_2$ yielded blue crystals (**4.16**) on slow evaporation of the mother liquor. On IR analysis of the crystals, it became clear that there were several similarities between the IR spectrum of **4.16** and that of **4.15**. Firstly, $\nu_{asym}(COO^-)$ vibrations were observed at ~1622 and 1553 cm^{-1} with two corresponding $\nu_{sym}(COO^-)$ vibrations at 1389 and 1364 cm^{-1} (Figure 4.13), indicating that there were two different types of carboxylate coordination existing in the structure. These were most likely ionic or monodentate in nature as bidentate or bridging carboxylates would have yielded much smaller $\Delta(\nu_{asym}(COO^-) - \nu_{sym}(COO^-))$ values than those observed in this instance (Δ = 233 and 189 cm^{-1}).[150] A broad peak in the range 3189-2563 cm^{-1} was also observed, which was attributed to hydrogen bonded O-H groups. Elemental analysis indicated a 1:1 metal to ligand composition. The crystal structure obtained for **4.16** was consistent with the data obtained and the X-ray structure can be seen in Figure 4.14. The structure was isomorphic to the Cu(II) coordination polymer **4.15**, apart from the lack of Jahn-Teller distortions observed, which was expected for an octahedral d^8 metal centre. The packing diagram of **4.16** (Figure 4.14) displays these wavelike polymers propagating diagonally.

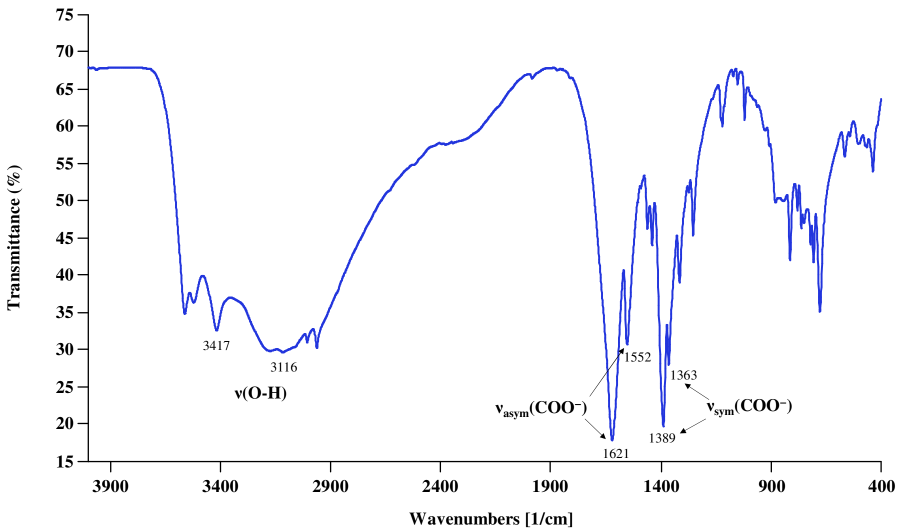

Figure 4.13: IR spectrum of **4.16**.

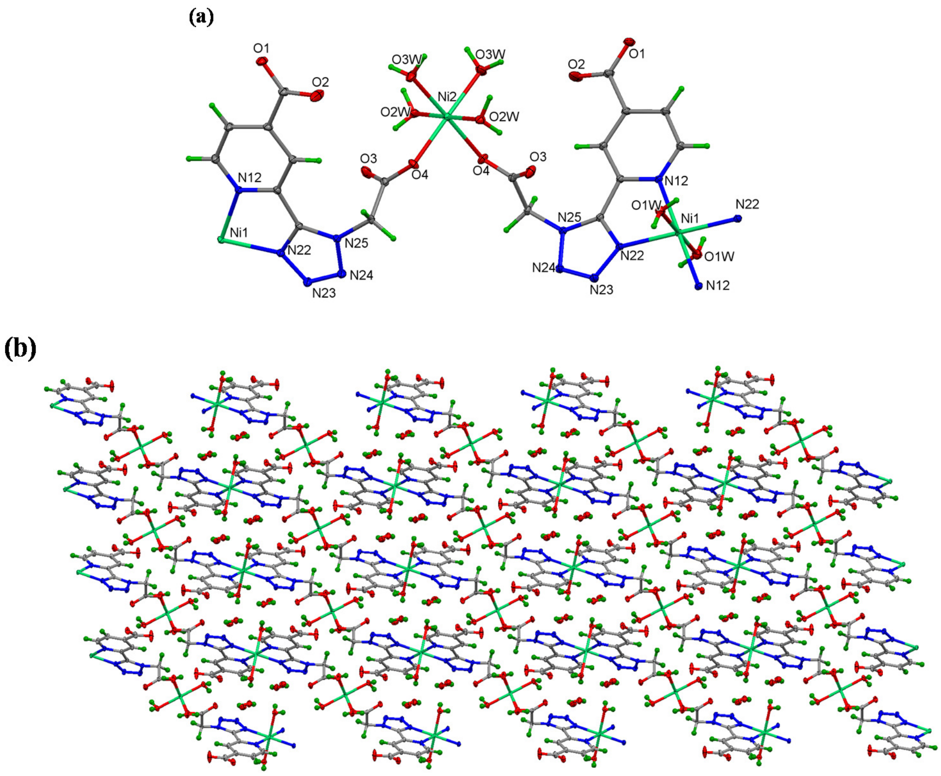

Figure 4.14: (a) Subunit of the coordination polymer **4.16**. (b) View along the *b*-axis of packing diagram of **4.16**.

Reaction of **4.3(pytzda)** with $Co(SCN)_2$ yielded block-like orange crystals (**4.17**) on evaporation of the mother liquor. These crystals were analysed by IR spectroscopy and again the spectrum showed remarkable similarities to those of **4.15** and **4.16**. $\nu_{asym}(COO^-)$ vibrations were positioned at 1621 and 1553 cm^{-1} and $\nu_{sym}(COO^-)$ vibrations were positioned at 1386 and 1362 cm^{-1}. This indicated that there were mixed carboxylate groups present and that they were adopting two modes of coordination. The IR spectrum also indicated the presence of hydrogen bonded O-H bonds as a broad stretch centred at 3130 cm^{-1} was present. An absence of peaks at ~2070 cm^{-1} confirmed that there were no thiocyanate anions present in the structure. Elemental analysis alluded to a 1:1 composition of metal to ligand and analysis of the crystals by X-ray crystallography confirmed this to be the case (Figure 4.15). In **4.17**, both Co(II) centres are in a distorted octahedral geometry, however the distortions are not as pronounced as those observed in **4.15**.

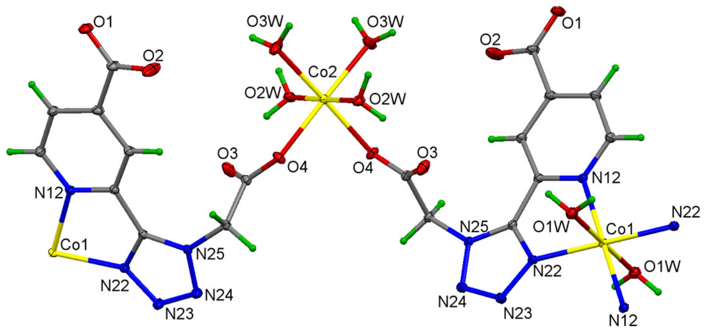

Figure 4.15: Subunit of coordination polymer **4.17**.

Reaction of **4.3(pytzda)** with $ZnCl_2$ yielded opaque white crystals (**4.18**) on slow evaporation of the mother liquor. Elemental analysis suggested a 1:1 metal to ligand composition and IR spectroscopy of the crystals indicated that there were two different modes of carboxylate coordination occurring as splitting of the $\nu_{asym}(COO^-)$ and $\nu_{sym}(COO^-)$ vibrations were evident. It was also noted that the spectrum followed similar patterns observed in the IR spectra of previously discussed products **4.15**-**4.17**. X-ray crystallography established that **4.18** was isomorphic in structure to the previously discussed CPs (Figure 4.16). The distorted octahedral Zn1 metal centre is axially elongated with a Zn1-O1W bond length of 2.23 Å. NMR spectroscopy was performed on the diamagnetic species and this data was in agreement with the crystal structure. As expected, four resonances were observed in the ^1H NMR spectrum, with three peaks in the aromatic region arising from the pyridyl protons and a singlet at 5.56 ppm arising from the methylene group bonded to the tetrazole ring. All of these resonances were observed to have shifted from the free acid, **4.3(pytzdaH)**, ^{1}H NMR resonances.

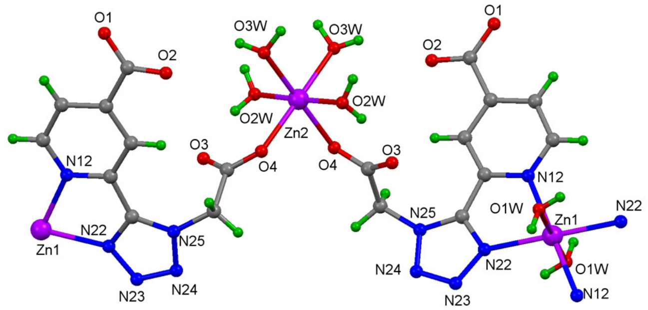

Figure 4.16: Subunit of the coordination polymer **4.18**.

Therefore, a series of isomorphic CPs were synthesised and characterised. The attainment of isostructural complexes is not uncommon with several reports present in the literature.[210,211] These results demonstrate that the coordination environment is determined essentially by the ligand, which is imposing its preferred geometry on the metal ion. This indicates that the ligand is minimising intramolecular ligand interactions through the enforcement of its preferred geometry.[210]

A fascinating structural feature of these CPs is the presence of free aromatic carboxylate chelation sites that are open to metal insertion. Addition of metals to uncoordinated metal sites in CPs is a successful method of post-synthetic modification (PSM).[105] PSM, which was previously described in Chapter 1 (section 1.4.3), has attracted a lot of interest in recent years due to its success in imbuing the parent materials with modified chemical and physical properties. Attainment of CPs with free chelation sites that are available to bind to additional metal ions is difficult, as typically these sites predominantly are involved in the synthesis of the parent framework. For this reason, strategies have been reported in the literature where the CP is post-synthetically appended with a chelating group in order to metallate afterwards. The motivation behind this is to tailor the material towards certain applications like gas separation or absorption. First reported by Rosseinsky and colleagues,[212] this concept has been used by a number of other groups in order to produce MOFs that could potentially be used for gas sorption and catalysis applications.[213] However, this procedure requires a further synthetic step, which can compromise the structural integrity of the parent material. Hence, there are obvious advantages to directly synthesising a framework with free metal binding sites.

4.3.2.2.2 Reactions of 4.4(pytzda)

4.4 was hydrolysed by nonsolvothermally heating it in aqueous NaOH solution. The *in situ* generated carboxylate was then reacted with various metal salts (one equivalent) and the resulting solutions were cooled and evaporated slowly over several days. The resulting crystalline solids were analysed by IR spectroscopy, elemental analysis and magnetic moment measurements and in some cases single crystals were obtained that were suitable for analysis by X-ray crystallography.

Reaction of **4.4(pytzda)** with $CuCl_2.2H_2O$ in H_2O yielded a blue solution which when slowly reduced by slow evaporation yielded a blue crystalline solid (**4.19**). The IR spectrum of **4.19** indicated that no protonated carboxylate was present as there were no vibrational peaks observed at ~1708 and 1744 cm^{-1}. The presence of carboxylates was indicated by the presence of $\nu_{asym}(COO^-)$ vibrations at 1623 and 1602 cm^{-1} and corresponding $\nu_{sym}(COO^-)$ vibrations at 1386 and 1423 cm^{-1}. This gave $\Delta(\nu_{asym}(COO^-) - \nu_{sym}(COO^-))$ values of 237 and 179 cm^{-1}, which indicated both monodentate bound and ionic forms of carboxylate were present in the structure, as bidentate and bridging carboxylates would be expected to have much lower Δ values.[150] A broad stretch was also observed at 3437 cm^{-1} which was attributed to O-H stretches from H_2O molecules which appeared to be involved in hydrogen bonding. Elemental analysis suggested that the blue solid consisted of a 1:1 metal to ligand ratio. The proposed structure of **4.19** can be seen in Figure 4.17. It consists of a dinuclear complex, with each Cu(II) centre in an octahedral geometry. The octahedral geometry is fulfilled through coordination of a pyridine and tetrazole nitrogen, a carboxylate oxygen from a second ligand and three H_2O molecules. This arrangement would give rise to the structure that is depicted in Figure 4.17.

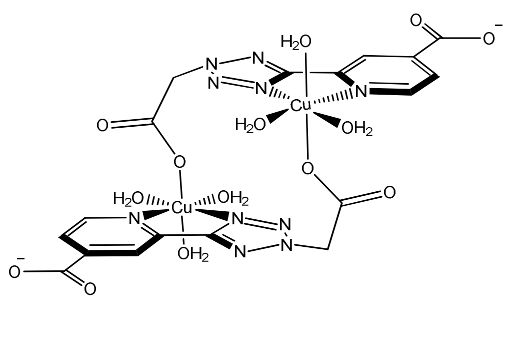

Figure 4.17: Representation of the proposed structure of **4.19**.

Reaction of **4.4(pytzda)** with $Co(SCN)_2$ produced an orange crystalline solid when a dilute solution was allowed to evaporate slowly. An amorphous powder (**4.20**) was produced on addition of the metal salt when more concentrated solutions were employed. The IR spectrum of **4.20** revealed the presence of carboxylates with a broad $\nu_{asym}(COO^-)$ vibration at 1619 cm^{-1} and $\nu_{sym}(COO^-)$ vibrations visible at 1398 and 1382 cm^{-1}. A broad stretch at 3271 cm^{-1} was also observed indicating the presence of H_2O molecules that were possibly involved in hydrogen bonding. Elemental analysis suggested a 1:1 metal to ligand composition and also indicated the presence of solvent molecules. The results of X-ray crystallographic analysis on the single crystals obtained in this reaction can be seen in Figure 4.18. **4.20** crystallises not as a coordination polymer but as an isolated dimeric complex. Each Co(II) centre possesses a distorted octahedral geometry and is coordinated to a pyridine and tetrazole nitrogen, a carboxylate oxygen from a second ligand coordinating in a monodentate manner and three H_2O molecules. As was observed in the case of the N-1 substituted coordination polymers, the aromatic pyridyl carboxylate does not take part in the coordination sphere of the metal ion.

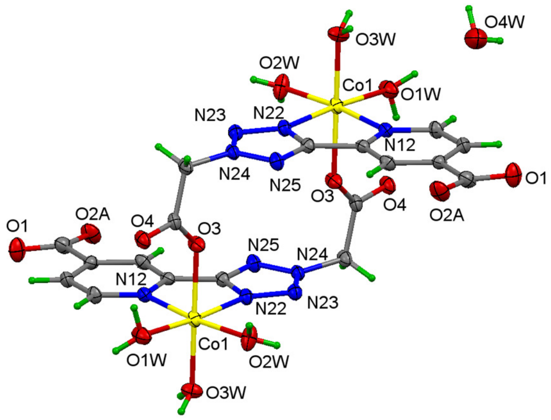

Figure 4.18: X-ray crystal structure of dimer **4.20**.

Reaction of **4.4(pytzda)** with $ZnCl_2$ in H_2O yielded clear block-like crystals (**4.21**) on slow evaporation of the mother liquor. The IR spectrum of the solid, **4.21**, revealed that there was no protonated carboxylate present in the structure. A $\nu_{asym}(COO^-)$ vibration was observed at 1618 cm^{-1}. However, this peak was broad and it was evident that there was a shoulder on this peak, which alluded to the presence of another $\nu_{asym}(COO^-)$ vibration. This opinion was further supported by the observation of two $\nu_{sym}(COO^-)$ vibrations at 1397 and 1381 cm^{-1}. This pointed towards the presence of mixed carboxylates with different coordination modes. Considering the $\Delta(\nu_{asym}(COO^-) - \nu_{sym}(COO^-))$ values were ~237 cm^{-1} it was proposed that the carboxylates were adopting both ionic and monodentate states. A broad stretch centred at 3406 cm^{-1} was also observed. This was proposed to arise from O-

H vibrations from H_2O molecules that were involved in hydrogen bonding. Elemental analysis of **4.21** suggested a 1:1 metal to ligand composition. Single crystals of **4.21** were obtained and were solved by X-ray crystallography. The results of this analysis can be seen in Figure 4.19.

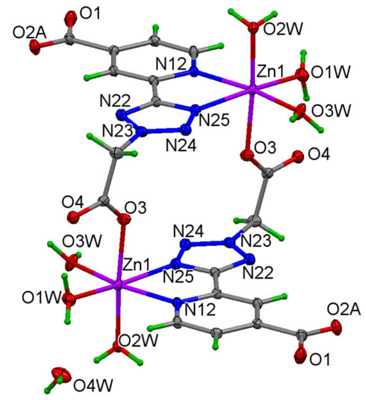

Figure 4.19: Crystal structure of **4.21**.

4.21 crystallises as an isolated dinuclear structure, with two equivalent Zn(II) centres and is isostructural with the Co(II) structure **4.20**. The Zn(II) ion is in a distorted octahedral environment and is coordinated by one pyridyl tetrazole unit from one ligand *via* the pyridyl and tetrazole N-1 nitrogens; a carboxylate oxygen coordinating in a monodentate fashion from a second ligand; and three H_2O molecules. There is a slight variation in the distance between the two metal centres however, with a distance of 7.24(1) Å present in **4.21** compared to 7.09(4) Å in **4.20**. Again, it was noted that the aromatic carboxylate was not partaking in the formation of **4.21**. This led us to believe that the reactivities of the alkyl and aromatic esters were sufficiently different and that this difference could be exploited.

4.3.2.3 Preliminary Attempts at Complexing Aromatic Carboxylate

As discussed previously, the serendipitous attainment of complexes with free metal binding sites offers possibilities of fine-tuning the material for applications like selective adsorption or catalysis. Thus, some preliminary studies were carried out to determine whether coordination to the aromatic carboxylate could be achieved either in tandem with the alkyl carboxylate or post-synthetically.

The previously discussed reactions involved reacting one equivalent of metal salt with the ligands. Therefore, occupation of the alkyl carboxylate site was attempted by reacting **4.3(pytzda)** and **4.4(pytzda)** with two equivalents of metal salt ($CuCl_2.2H_2O$, $NiCl_2.6H_2O$, $Co(SCN)_2$, $ZnCl_2$), however this did not lead to occupation of this site and products **4.15-4.18** and **4.19-4.21** were obtained in each case. Thus, consideration of the Hard-Soft-Acid-Base Theory (HSAB) was taken into account.[214] We proposed that the hardness of the aromatic and alkyl carboxylate oxygens were substantially different so that borderline hard metal cations like Cu^{2+}, Ni^{2+}, Co^{2+} and Zn^{2+} could not coordinate to the harder aromatic carboxylate oxygens. It was also considered that since the ligand itself involved in counterbalancing the charge on the metal atom, that coordination to a second metal centre was restricted by the lack of anionic charges. To examine our first hypothesis both ligands were reacted with one equivalent of a harder metal cation in the form of $Mn(OAc)_2$. In the case of the N-2 isomer a crystalline solid that was of X-ray quality was obtained. The results of X-ray crystallographic analysis on **4.22** can be seen in Figure 4.20.

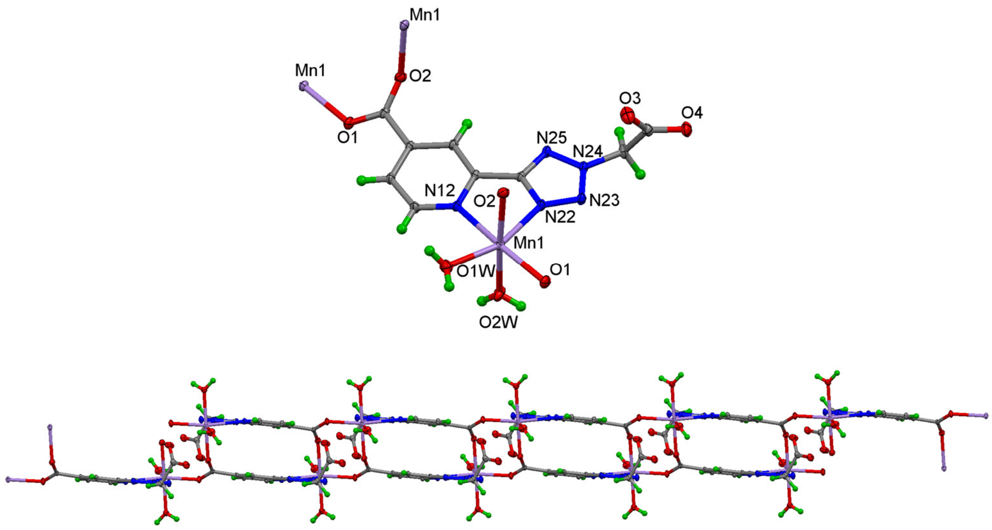

Figure 4.20: Subunit of **4.22** (top) and view of segment of 1-D polymeric chain (bottom).

4.22 crystallises as a 1-D polymer with a ladder like topology. Each subunit of the ladder consists of a distorted octahedral Mn(II) centre coordinated to two N atoms from the chelating pyridyl tetrazole unit, two O atoms of two bridging carboxylates from two additional **4.4(pytzda)** ligands and two O atoms of two H_2O molecules. Therefore, **4.4(pytzda)** chelates one Mn(II) ion using two N atoms and bridges two Mn(II) ions using two O atoms from the same carboxylate, leaving the other uncoordinated carboxylate to form three kinds of O-H···O hydrogen bonds with three coordinated H_2O molecules of three neighbouring units with the O⋯O distances of 2.635(3)-2.932(2) Å. *Cis* elongation of the Mn(II)-N12/N22 bonds are observed, with these bond lengths being 2.3 Å compared to 2.1 Å for all other M-L bonds. This subunit is strikingly similar to a 2,2'-bipyridine 4,4'-dicarboxylic acid Mn(II) helical CP reported by Li *et al*.,[215] with one carboxylate adopting an *anti-syn* conformation and the other remaining coordinatively free. However, the *anti-syn* carboxylate in **4.22** has an opposite orientation compared to the complex reported by Li *et al*., which could explain the topological differences.

These results suggested that our hypothesis was correct: the hardness of the alkyl and aromatic carboxylates were sufficiently different and that the harder Mn(II) cation preferentially coordinated to the harder aromatic carboxylate oxygens. Consequently, it may also confirm our second hypothesis regarding the lack of anions in solution as theoretically Mn(II) should also be able to coordinate to the alkyl carboxylate. The observation of no coordination at this site indicates that it could be required to be free in order to contribute to counterbalancing the charge on the Mn(II) ion.

4.3.2.4 Selective Hydrolysis of Alkyl Ester

Considering the different reactivities observed between the aromatic and alkyl carboxylate, it was anticipated that employing only one equivalent of base would have an effect on the ester hydrolysis. Reacting **4.4** with one equivalent of base for 1 hour followed by the addition of $CuCl_2.2H_2O$ resulted in a blue crystalline solid (**4.23**) forming when the solution was cooled slowly. The single crystals obtained were analysed by X-ray crystallography and a subunit of the structure of **4.23** can be seen in Figure 4.21. The subunit is made up of two Cu(II) centres with distorted octahedral geometry (N-Cu1 posseses a bond length of 2.42 Å compared to ~2.02 Å for all other Cu1-L bonds). Each Cu(II) centre is coordinated by two pyridyl nitrogens, two tetrazole nitrogens and two carboxylate oxygens from two additional ligands coordinating in a monodentate manner. This bonding arrangement leads to a 1-D coordination polymer which is shown in Figure 4.22. Hydrogen bonding is not as pronounced compared to previously discussed structures, however this is to be expected as there were no H_2O molecules present in the structure. As seen in the structures, the alkyl ester was hydrolysed but the aromatic ester was retained. This yielded a coordination polymer with ethyl ester 'tags'. In the packing diagram (Figure 4.23) viewed along the *a*-axis, columns of pyridyl tetrazole ligands alternate between channels of these 'tags'.

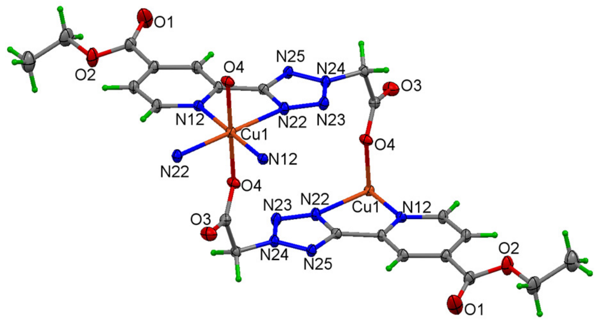

Figure 4.21: Subunit of the coordination polymer **4.23.**

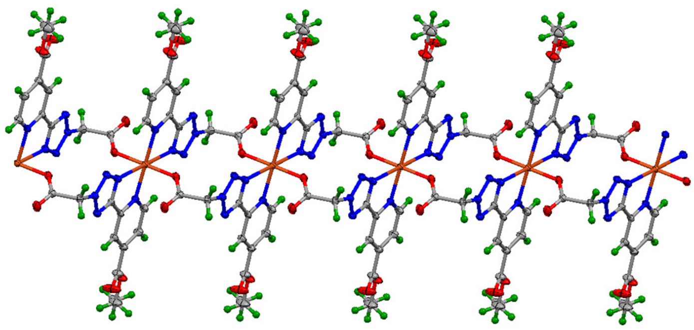

Figure 4.22: Subsection of the bonding arrangement present in **4.23**.

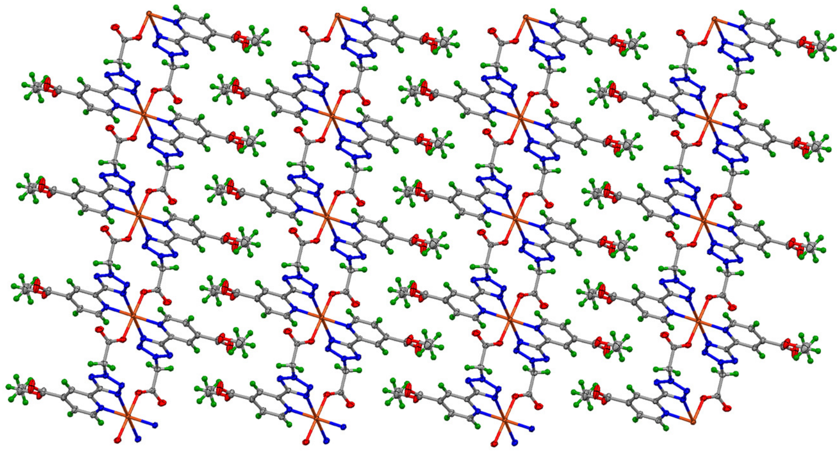

Figure 4.23: Packing diagram of **4.23** viewed along the *a*-axis. Channels of ethyl ester tags alternate between pyridyl tetrazole units.

A 'tag' is defined as a group or functionality that is stable and innocent (i.e. non-structure-defining) during polymer formation, but that can be transformed by a post-synthetic modification.[216] This approach is shown schematically in Scheme 4.7.

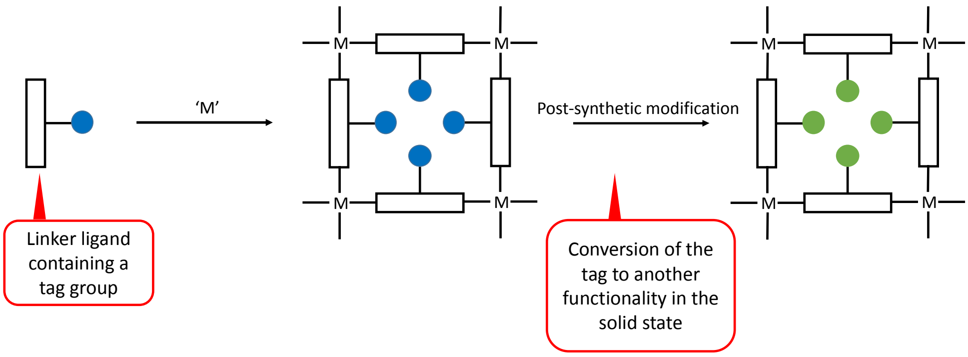

Scheme 4.7: Schematic representation of the post-synthetic modification strategy for CPs. Diagram adapted and edited from Burrows *et al.*[216]

The use of prefunctionalised linkers with tags already bonded is hampered by the fact that they are likely to interfere with CP formation. As well as this, it is not possible to use thermally labile, metal coordinating or solubility lowering functions tagged on the linker.[217] Therefore, the attainment of a network like **4.23** with ethyl ester groups remaining after polymer synthesis is exceptional and offers a large number of possibilities in terms of PSM (section 1.4.3). An increasingly popular approach to forming post-synthetically modified frameworks is to undertake covalent PSM on the preformed CPs by reacting these 'tags' using organic transformations, thereby converting one solid state material into another.[216] This approach, which is currently being investigated on these materials, is beyond the scope of this thesis.

The observed difference in reactivities between the aromatic and alkyl ester could be explained by the studies of Taft.[218] Changes in sterics and nucleophilicity can all be viewed as substituent effects and can influence the reactivity of the groups undergoing change. Therefore, linear free energy relationships (LFER) for these kinds of substituent effects have been developed. Taft developed a scale for LFERs that reflected the steric influence of substituents on various reactions. A parameter that reflected the polar nature of the substituent (σ^*) and a steric parameter (E_s) were both described. The defining reaction was the acid-catalysed hydrolysis of RCO_2Me, and the reference group was a methyl group. To measure the polar and steric substituent constants for the R groups, the hydrolysis was performed in both acidic and basic conditions, with the assumption that polar effects would only influence the base-catalysed hydrolysis. This assumption was made due to the fact that the basic pathway takes a neutral reactant to a negatively charged intermediate in the rate determining step, whereas the acid-catalysed pathway takes a positively charged reactant to a positive intermediate in the rate determining step (Scheme 4.8).

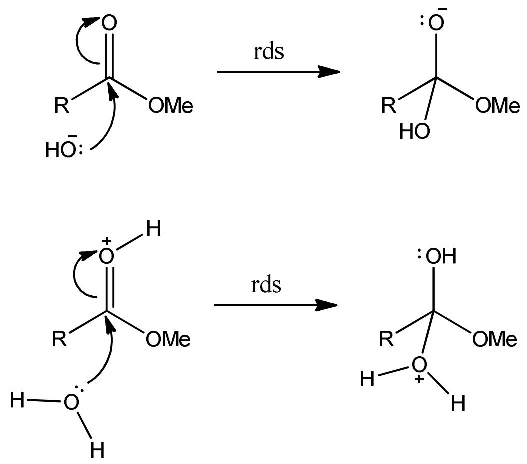

Scheme 4.8: Hydrolysis of RCO_2Me *via* the base-catalysed pathway (top) and acid-catalysed pathway (bottom).

A further assumption was that the steric effects influence the acid and base pathways equally, because they involve similar tetrahedral intermediates. Hence, the steric substituent constant, E_S, was determined solely from the acid-catalysed pathway, as this would not include polar effects (Equation 4.1).

$$log\left(\frac{k_S}{k_{Me}}\right) = E_S \quad \textbf{Eqn. 4.1}$$

The σ* values are determined from Equation 4.2, where subscripts A and B refer to the acid and base pathways and the reference reaction is the hydrolysis of $CH_3CO_2CH_3$. The factor of 2.48 is introduced in order to make the magnitude of these new σ* values similar to Hammett σ values.[219]

$$\sigma * = \frac{1}{2.48}\left[log\left(\frac{k}{k_o}\right)_{\mathrm{B}} - log\left(\frac{k}{k_o}\right)_{\mathrm{A}}\right] \quad \textbf{Eqn. 4.2}$$

The general Taft expression combines the steric and polar substituent scales into one equation (Eqn. 4.3), where ρ* and δ are the sensitivity factors for a new reaction under study to polar and steric effects, respectively.

$$log\left(\frac{k_s}{k_{Me}}\right) = \rho^*\sigma^* + \delta E_s \quad \textbf{Eqn. 4. 3}$$

Table 4.1 gives several E_s and σ* values.

Table 4.1: Selected Taft parameters.

R group	E_s	σ*
-H	1.24	0.49
-Et	-0.07	-0.10
-*i*Pr	-0.47	-0.19
-*t*-Bu	-1.54	-0.30
-CH_2Ph	-0.38	0.22
-Ph	-2.55	0.60

These parameters show that the rate of the hydrolysis reaction is faster when the R group is hydrogen rather than a methyl group, and that it slows as the size of the R group increases (i.e. E_s becomes more negative).[219] Although pyridine was not included in these studies, one can compare it to the phenyl group, which would hydrolyse at a slower rate relative to the R group being a CH_2 or a CH_2Ph group. The rate of hydrolysis of the pyridyl ester must be sufficiently slow in order for yields of >90% to result for complex **4.22**.

4.3.3 EPR Spectral Studies on Cu(II) Compounds

The principles of EPR spectroscopy were previously discussed in section 3.3.3.2. The X-band EPR spectra of **4.15** and **4.23** were measured in the solid state as powders at room temperature. Figure 4.24 displays the EPR spectrum of **4.15**, which resembles an isotropic signal, where g_x = g_y = g_z. It was observed that this signal could have been overlapping with another signal, however it was proposed that the crystallinity of the sample could perturb the signal (samples were ground however crystalline particles always remained). Alternatively, carrying out EPR spectroscopy at a higher resolution might have further resolved this signal into a rhombic signal. The extracted g factor (2.157) was typical of a transition metal unpaired electron as it was much greater than the free electron g value.[176] An isotropic signal implies that the three principle axes are the same and on examination of the bond lengths around the Cu(II) centres (which are all ~2 Å) this was observed to be in agreement with the crystal structure obtained.

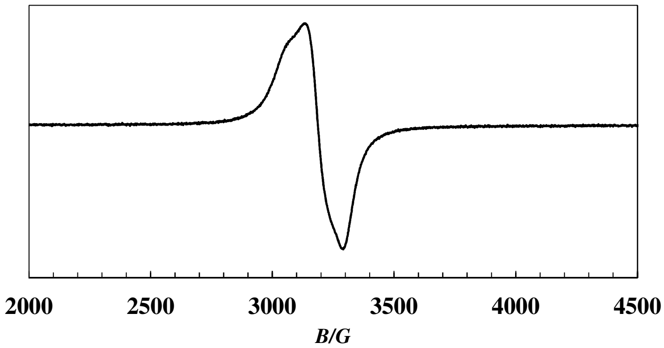

Figure 4.24: Room temperature 9.63 GHz EPR spectrum of a powder sample of **4.15**. $g_x = g_y = g_z = 2.157$.

The EPR spectrum of **4.23** is shown in Figure 4.25. The spectrum displays axial symmetry with the abstracted g factors exhibiting the trend $g_z > g_x \sim g_y$, indicating that the unpaired electron lies predominantly in the $d_{x^2-y^2}$ orbital. This is in agreement with the crystal structure obtained and is consistent with axially elongated octahedral complexes.

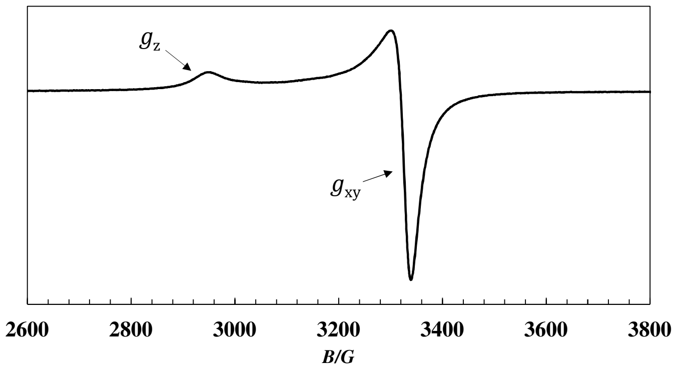

Figure 4.25: Room temperature 9.63 GHz EPR spectrum of a powder sample of **4.23**. $g_{xy}; g_z = 2.042; 2.336$.

4.3.4 Luminescence studies

As discussed in section 3.3.4, d^{10} metal complexes exhibit excellent photoluminescent properties.[220] To investigate the luminescence properties of the asymmetric carboxylate functionalised pyridyl tetrazoles and their Zn(II) complexes, the photoluminescence measurements of **4.4(pytzdaH)** and **4.21** were carried out in the solid state at room temperature by collaborators in the Laboratory of Synthetic Bioinorganic Chemistry, University of Crete. The spectra obtained can be seen in Figure 4.26. It can be seen that they exhibit fluorescence signals with the emission maxima at 425 nm for the free acid and 438 nm for the Zn(II) complex, with λ_{ex} = 350 nm. Compared to the spectra of the free ligand, the spectrum of **4.21** is similar in terms of band shape, hence these emission bands can be attributed to an intraligand emission state.[146] The observed red shift of 13 nm may arise from the coordination effect of the Zn(II) centre to the ligand.[146] The chelation of the ligand to the metal ion effectively increases the conformational rigidity of the ligand reducing energy loss by vibrational relaxation, thus enhancing fluorescence.[146] These results indicate that these compounds may be good candidates for light emitting materials.

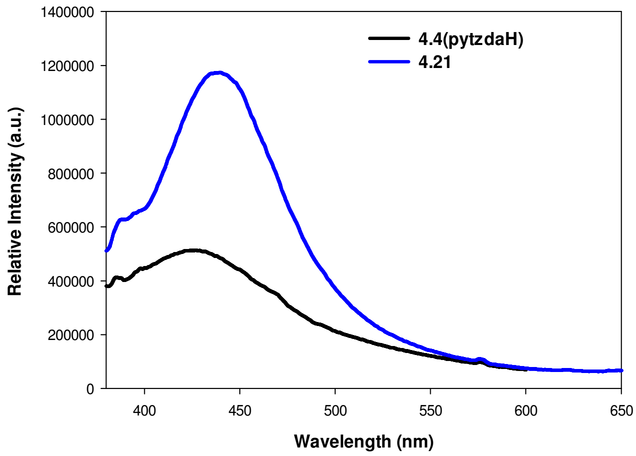

Figure 4.26: Solid state emission spectra for free ligands **4.4(pytzdaH)** and Zn(II) complex **4.21**. Excitation wavelength was 350 nm.

4.4 Conclusions

This chapter dealt with the further development of the organic linkers discussed in Chapter 3 into second generation organic linkers, and their incorporation in the formation of coordination polymers. Another carboxylate group on the pyridine ring was proposed to enhance the ability of the pyridyl tetrazole unit to form novel diverse high dimensional frameworks. Hence, **4.3** and **4.4** were synthesised starting from isonicotinic acid. Taking advantage of the reactivity of pyridine N-oxides, a nitrile group was successfully substituted at the 2-position of the ring, allowing a 1,3-dipolar cycloaddition to be undertaken, which was subsequently followed by alkylation to yield **4.3** and **4.4**.

4.3 and **4.4** were converted to their respective carboxylate derivatives **4.3(pytzda)** and **4.4(pytzda)** *in situ* with aqueous NaOH employing conventional nonsolvothermal heating. Metal salts were added to the solutions and these were allowed to cool slowly. Crystalline solids formed after varying amounts of times (minutes to weeks). These often colourful materials were analysed by IR, EPR and NMR spectroscopies, magnetic moment, elemental analysis, and in some cases X-ray crystallography. On examination of the effect of regioisomerism on final structures, there are clear consequences observed. N-1 substituted **4.3(pytzda)** formed 1-D coordination polymers, whereas **4.4(pytzda)** formed isolated dinuclear structures. This is tentatively attributed to the ease of which the N-2 isomer can suit the coordination geometry requirements of the metal ion by orientating the pendant carboxylate almost perpendicular to itself. The N-1 isomer could possibly be restricted from doing so due to its position, therefore it is much more stable pointing away from itself, allowing a 1-D chain to propagate.

In all cases, employing borderline hard Lewis acids (Cu^{2+}, Ni^{2+}, Co^{2+}, Zn^{2+}) resulted in the aromatic carboxylates remaining free in the complexes. This offers exciting possibilities for post-synthetic metalation. Post-synthetic metalation is a promising new avenue of post-synthetic modification that has developed in recent years, and future work on these compounds would involve taking advantage of these free chelation sites for metal insertion and to investigate their gas absorption and gas separation abilities, as well as catalytic applications. Thus far, attempts to saturate both the alkyl and aromatic carboxylate sites have failed which we believe could be due to two reasons. Firstly, the hardness of the metal ions utilised might not be appropriate for the aromatic carboxylate oxygens, which could be harder donor atoms compared to the alkyl carboxylate oxygens. This was somewhat confirmed by complexing **4.4(pytzda)** with $Mn(OAc)_2$ and achieving coordination with the aromatic carboxylate and not the alkyl carboxylate. Secondly, since the ligands are often themselves counterbalancing the charge on the first row metal complexes, it may be that no further metal insertion could be possible if anions are dissociating. Future work would involve circumventing this issue by the addition of a source of anions if this is indeed the reason why metal insertion is not occurring.

In solid state fluorescence studies, zinc complex **4.21** showed significant enhancement in emission, further indicating that diamagnetic pyridyl tetrazole complexes could be good light emitting materials; an aspect that will be further studied in future work.

In contrast to the prolific bipyridine dicarboxylate ligands used in CP synthesis, studies on asymmetric ligands like **4.3(pytzda)** and **4.4(pytzda)** are less developed. However as demonstrated here, the potential to obtain interesting and diverse structures with intriguing properties with such asymmetric structures is great. Overall, **4.3(pytzda)** and **4.4(pytzda)** proved to be novel versatile ligands in the formation of CPs and dinuclear clusters, and indicate that studies on asymmetric ligands should be investigated further.

4.5 Experimental

4.5.1 Instrumentation

^1H and ^{13}C NMR (δ ppm; J Hz) spectra were recorded on a Bruker Avance 300 MHz NMR spectrometer using saturated $CDCl_3$ or d_6-DMSO solutions with $SiMe_4$ reference, unless indicated otherwise, with resolutions of 0.18 Hz and 0.01 ppm, respectively. Infrared spectra (cm^{-1}) were recorded as KBr discs or liquid films between NaCl plates using a Perkin Elmer System 2000 FT-IR spectrometer. Solution UV-Vis spectra were recorded using HPLC grade solvents using a Unicam UV 540 spectrometer. Melting point analyses were carried out using a Stewart Scientific SMP 1 melting point apparatus and are uncorrected. Electrospray (ESI) mass spectra were collected on an Agilent Technologies 6410 Time of Flight LC/MS. Compounds were dissolved in acetonitrile:water (1:1) solutions containing 0.1% formic acid, unless otherwise stated. The interpretation of mass spectra was made with the help of the program "Agilent Masshunter Workstation Software". Magnetic susceptibility measurements were carried out at room temperature using a Johnson Matthey Magnetic Susceptibility Balance with $[HgCo(SCN)_4]$ as reference. EPR spectra were recorded on a Bruker Elexsys E500 spectrometer, operated at the X-band and equipped with an Oxford Instruments cryostat. Solid state UV-Vis measurements were carried out in the Synthetic Bioinorganic Chemistry Laboratory of the University of Crete and were performed on a Perkin Elmer Lambda 950 UV/Vis spectrometer. Solid state fluorescence spectra were also carried out in this laboratory and were recorded on a Jobin-Yvon Horiba, Fluoro Max-P (SPEX) fluorescence spectrometer, with excitation from a cw Xenon arc lamp. Microanalyses were carried out at the Microanalytical Laboratory of the National University of Ireland Maynooth, using a Thermo Finnigan Elementary Analyzer Flash EA 1112. The results were analysed using the Eager 300 software. All crystal structures resulting from this work were solved by Dr. John Gallagher (Dublin City University) using an Oxford Diffraction Gemini-S Ultra diffractometer at 294(1) K. Structures were solved using the SHELXS97 direct methods program. Molecular diagrams were generated using Mercury software. Starting materials were commercially obtained and used without further purification. Solvents used were of HPLC grade.

Caution! *Nitrogen-rich compounds such as tetrazole derivatives are used as components for explosive mixtures. In our laboratory, the reactions described were run on a few gram scale, and no problems were encountered. However, great caution should be exercised when heating or handling compounds of this type.*

4.5.2 Synthesis of Diester Pyridyl Tetrazoles 4.3 and 4.4

4.5.2.1 4-(Methoxycarbonyl)pyridine (4.8a)

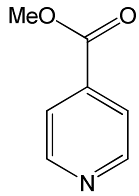

Sulfuric acid (0.24 mL, 4.46 mmol) was added dropwise to a suspension of isonicotinic acid (0.50 g, 4.06 mmol) in MeOH (10 mL) at 0 °C. The solution was then heated to reflux for 18 h. After this time the reaction was cooled to room temperature and the solvent was removed under reduced pressure. The remaining residue was dissolved in deionised H2O, cooled to 0 °C and the pH was adjusted to pH 8 with K_2CO_3. After extraction with chloroform (3 × 10 mL), the combined organic layers were washed with brine, dried over $MgSO_4$ and filtered. The filtrate was concentrated under reduced pressure to yield a yellow oil (0.55 g, 98%). IR (neat): ν = 2955, 1951, 1732, 1599, 1561, 1494, 1437, 1407, 1326, 1287, 1215, 1194, 1121, 1064, 992, 965, 852, 829, 758 cm^{-1}. ^{1}H NMR ($CDCl_3$): δ = 8.78 (d, 2 H, J = 6.0 Hz, pyr-H), 7.84 (d, 2 H, J = 6.0 Hz, pyr-H), 3.96 (s, 3 H, OCH_3) ppm. ^{13}C NMR ($CDCl_3$): δ = 165.4 (C=O), 150.5, 137.2, 122.7, 52.6 (CH_3) ppm.

The acquired data are in agreement with literature reported values.[202]

4.5.2.2 4-(Ethoxycarbonyl)pyridine (4.8b)

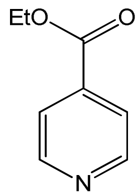

Sulfuric acid (0.48 mL, 8.92 mmol) was added dropwise to a suspension of isonicotinic acid (1.00 g, 8.12 mmol) in EtOH (10 mL) at 0 °C. The solution was then heated to reflux for 18 h. After this time the reaction was cooled to room temperature and the solvent was removed under reduced pressure. The remaining residue was dissolved in deionised H_2O, cooled to 0 °C and the pH was adjusted to pH 8 with K_2CO_3. After extraction with $CHCl_3$ (3 × 10 mL), the combined organic layers were washed with brine, dried over magnesium sulfate and filtered. The filtrate was concentrated under reduced pressure to yield a yellow oil (0.75 g, 62%). IR (DCM film): ν = 2984, 2939, 1728, 1597, 1563, 1466, 1447, 1409, 1368, 1324, 1281, 1214, 1174, 1119, 1064, 1021, 993, 874, 852, 758 cm^{-1}. ^{1}H NMR ($CDCl_3$): δ = 8.72 (d, 2 H, J = 6.0 Hz, pyr-H), 7.79 (d, 2 H, J = 6.0 Hz, pyr-H), 4.36 (q, 2 H, J =

7.1 Hz, OCH_2), 1.35 (t, 3 H, *J* = 7.1 Hz, CH_3) ppm. ^{13}C NMR ($CDCl_3$): δ = 163.8 (C=O), 147.6, 140.3, 124.2, 62.4 (OCH_2), 14.1 (CH_3) ppm. ESI-HRMS: calcd. for $C_8H_9NO_2$ $[M+H]^+$ 152.0706, found 152.0706.

NMR and IR data are in agreement with literature data.[221]

4.5.2.3 4-(Methoxycarbonyl)pyridine-1-oxide (4.9a)

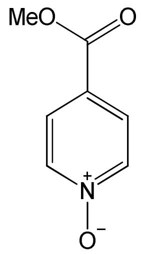

0.49 mL of a H_2O_2 solution (35% w/w) was added to a solution of **4.8a** (0.31 g, 2.18 mmol) in glacial acetic acid (2.25 mL). The mixture was heated at 75 °C for 20 h. The mixture was concentrated under reduced pressure and the resulting residue was taken up in H_2O and made alkaline (pH 8) with K_2CO_3. This basic solution was then extracted with EtOAc (3 × 10 mL) and the combined extracts were washed with brine and dried over anhydrous Na_2SO_4. Evaporation of the solvent yielded a pale yellow solid (0.32 g, 97%). m.p. 123-125 °C (lit. 118-120 °C).[222] IR (KBr): ν = 3120, 3051, 1716, 1610, 1484, 1434, 1299, 1262, 1190, 1169, 1118, 1092, 1024, 957, 858, 771, 683, 634 cm^{-1}. ^1H NMR ($CDCl_3$): δ = 8.21 (d, 2 H, *J* = 7.2 Hz, pyr-H), 7.87 (d, 2 H, *J* = 7.2 Hz, pyr-H), 3.95 (s, 3 H, CH_3) ppm. ^{13}C NMR ($CDCl_3$): δ = 163.8 (C=O), 139.5, 126.6, 126.4, 52.8 (CH_3) ppm. ESI-HRMS: calcd. for $C_7H_7NO_3$ $[M+H]^+$ 154.0499, found 154.0504.

The acquired data are in agreement with literature reported values.[207]

4.5.2.4 4-(Ethoxycarbonyl)pyridine-1-oxide (4.9b)

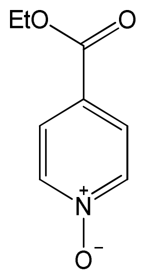

4.48 mL of a H_2O_2 solution (35% w/w) was added to a solution of **4.8b** (3.33 g, 22.04 mmol) in glacial acetic acid (20.52 mL). The mixture was heated at 75 °C for 24 h. The mixture was concentrated under reduced pressure and the resulting residue was taken up in H_2O and made alkaline (pH 8) with K_2CO_3. This basic solution was then extracted with DCM (3 × 10 mL) and the combined extracts were washed with brine and dried over anhydrous $MgSO_4$. Evaporation of the solvent yielded a yellow solid. (3.27 g, 89%). m.p. 59-60 °C (lit. 58 °C).[223] IR (KBr): ν = 3079, 2981, 1720, 1613, 1552, 1474, 1458, 1443, 1369, 1281, 1257, 1167, 1127, 1106, 1092, 1016, 873, 860, 771 cm^{-1}. ^1H NMR ($CDCl_3$): δ = 8.22 (d, 2 H, J = 7.2 Hz, pyr-H), 7.88 (d, 2 H, J = 7.2 Hz, pyr-H), 4.40 (q, 2 H, J = 7.1 Hz, OCH_2), 1.40 (t, 3 H, J= 7.1, CH_3) ppm. ^{13}C NMR ($CDCl_3$): δ = 163.3 (C=O), 139.4, 126.8, 126.3, 61.9 (OCH_2), 14.19 (CH_3) ppm. ESI-HRMS: calcd. for $C_8H_9NO_3$ $[M+H]^+$ 168.0655, found 168.0655.

The NMR and IR data acquired are in agreement with literature values.[223]

4.5.2.5 Methyl-2-cyanoisonicotinate (4.10a)

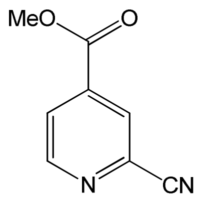

A reaction mixture of **4.9a** (0.20 g, 1.30 mmol), DMCC (0.12 mL, 1.30 mmol) and $Zn(CN)_2$ (0.23 g, 1.96 mmol) in toluene (15 mL) was heated to reflux under an argon atmosphere for 6 h. The reaction mixture was cooled to room temperature and deionised H_2O (10 mL) was added, and stirring was continued for 15 min. The organic layer was separated, washed with brine, dried over $MgSO_4$ and concentrated under reduced pressure to yield an orange solid (0.21 g, 65%) which required no further purification. m.p. 100-103 °C. IR (KBr): ν = 2958, 2852, 2237, 1726, 1441, 1397, 1298, 1209, 1116, 974, 934, 882, 869, 765 cm^{-1}. ^1H NMR ($CDCl_3$): δ = 8.90 (dd, 1 H, J = 4.9, 0.8 Hz, pyr-H), 8.24 (dd, 1 H, J = 1.5, 0.8 Hz, pyr-H), 8.07 (dd, 1 H, J = 4.9, 1.5 Hz, pyr-H), 4.01 (s, 3 H, OCH_3) ppm. ^{13}C NMR ($CDCl_3$): δ = 162.6 (C=O), 151.0, 137.7, 133.8, 126.6, 125.0, 115.5 (CN), 52.3 (OCH_3) ppm. ESI-HRMS: calcd. for $C_8H_6N_2O_2$ $[M+H]^+$ 163.0502, found 163.0509.

NMR data is in agreement with literature data.[208]

4.5.2.6 Ethyl-2-cyanoisonicotinate (4.10b)

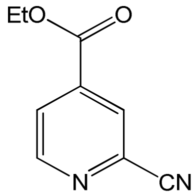

A reaction mixture of **4.9b** (3.64 g, 21.82 mmol), DMCC (3.01 mL, 32.73 mmol) and $Zn(CN)_2$ (3.84 g, 32.73 mmol) in toluene (40 mL) was heated under reflux under an argon atmosphere for 2 h. The reaction mixture was cooled to room temperature and H_2O (30 mL) was added, and stirring was continued for 15 min. The organic layer was separated, washed with brine, dried over $MgSO_4$ and concentrated under reduced pressure to yield a brown solid. This was then passed through a silica plug using EtOAc:Pet. Ether in a 2:1 ratio as the eluent yielding a yellow oil which solidified on ice. Orange solid (3.28 g, 85%). m.p. 39-40 °C (lit. 42-44 °C).[224] IR (KBr): ν = 2988, 2964, 2238, 1728, 1597, 1557, 1470, 1402, 1393, 1370, 1298, 1281, 1202, 1113, 1015, 990, 918, 890, 862, 763, 686 cm^{-1}. ^{1}H NMR ($CDCl_3$): δ = 8.90 (dd, 1 H, J = 4.9, 0.9 Hz, pyr-H), 8.25 (dd, 1 H, J = 1.5, 0.9 Hz, pyr-H), 8.10 (dd, 1 H, J = 4.9, 1.5 Hz, pyr-H), 4.47 (q, 2 H, J = 7.1 Hz, OCH_2), 1.44 (t, 3 H, J = 7.1 Hz, CH_3) ppm. ^{13}C NMR ($CDCl_3$): δ = 163.1 (C=O), 151.9, 139.0, 134.7, 127.6, 126.1, 116.6 (CN), 62.6 (OCH_2), 14.1 (CH_3) ppm. ESI-HRMS: calcd. for $C_9H_8N_2O_2$ $[M+H]^+$ 177.0659, found 177.0659.

NMR data is in agreement with literature data.[224]

4.5.2.7 Methyl-2(1*H*-tetrazol-5-yl)isonicotinate (4.11a)

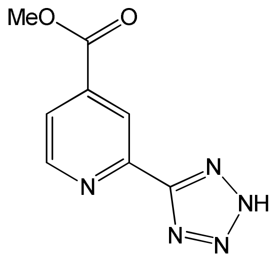

4.10a (0.20 g, 1.25 mmol), NaN_3 (0.09 g, 1.38 mmol), NH_4Cl (0.07 g, 1.38 mmol) and LiCl (0.03 g, 0.62 mmol) were heated at 110 °C in DMF for 12 h. The reaction mixture was filtered and the filtrate concentrated under reduced pressure. The residue was then taken up in deionised H_2O and 1 M HCl was added slowly until precipitation initiated. The mixture was then filtered and the solid dried. Brown solid (0.15 g, 62%). m.p. 163-166 °C. IR (KBr): ν = 3071, 2922, 1724, 1547, 1438, 1416, 1393, 1336, 1295, 1270, 1247, 1198, 1173, 1054, 1031, 967, 755, 746 cm^{-1}. ^{1}H NMR (d_6-DMSO): δ = 9.01 (d, 1 H, J = 4.9 Hz, pyr-

H), 8.56 (s, 1 H, pyr-H), 8.04 (d, 1 H, *J* = 4.9 Hz, pyr-H), 4.03 (s, 3 H, OCH_3) ppm. ^{13}C NMR (d_6-DMSO): δ = 164.3 (C=O), 153.3, 151.4, 144.9, 138.6, 124.5, 121.0, 53.0 (OCH_3) ppm. ESI-HRMS: calcd. for $C_8H_7N_5O_2$ $[M+H]^+$ 206.0673, found 206.0677.

4.5.2.8 Ethyl-2(1*H*-tetrazol-5-yl)isonicotinate (4.11b)

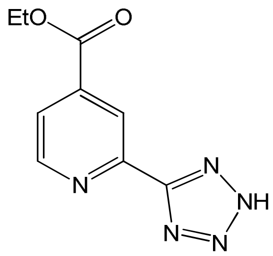

4.10b (2.28 g, 12.93 mmol), NaN_3 (0.93 g, 14.22 mmol), NH_4Cl (0.76 g, 14.22 mmol) and LiCl (0.27 g, 6.47 mmol) were heated at 110 °C in DMF (20 mL) for 12 h. The reaction mixture was cooled to room temperature, filtered and the filtrate was concentrated under reduced pressure. The remaining residue was redissolved in deionised H_2O and 1 M HCl was added dropwise until precipitation was initiated. When the formation of a precipitate ceased, the mixture was filtered. The collected precipitate was recrystallised from hot EtOH, yielding white crystals which were filtered off and washed with cold EtOH. White crystalline solid (2.13 g, 75%). m.p. 186-191 °C. IR (KBr): ν = 3085, 2900, 2751, 1721, 1613, 1566, 1468, 1445, 1421, 1384, 1367, 1317, 1289, 1248, 1216, 1140, 1120, 1025, 1000, 896, 865, 762, 745, 726, 683 cm^{-1}. ^1H NMR (d_6-DMSO): δ = 9.01 (d, 1 H, *J* = 4.9 Hz, pyr-H), 8.56 (s, 1 H, pyr-H), 8.04 (d, 1 H, *J* = 4.9 Hz, pyr-H), 4.43 (q, 2 H, *J* = 7.2 Hz, OCH_2), 1.38 (t, 3 H, *J* = 7.2 Hz, CH_3) ppm. ^{13}C NMR (d_6-DMSO): δ = 163.7 (C=O), 154.5, 151.4, 144.8, 138.8, 124.6, 121.0, 62.0 (OCH_2), 13.9 (CH_3) ppm. ESI-HRMS: calcd. for $C_9H_{10}N_5O_2$ $[M+H]^+$ 220.0829, found 220.0830.

4.5.2.9 Synthesis of 4.3 and 4.4

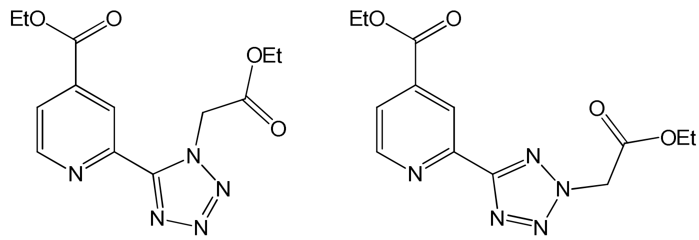

4.11b (1.30 g, 5.93 mmol) was heated to reflux with K_2CO_3 (0.90 g, 6.52 mmol) in MeCN (20 mL) for 30 min. Ethyl bromoacetate (1.09 g, 6.52 mmol) was added to the mixture and the reaction was further heated to reflux for 24 h. The reaction was then cooled to room temperature and filtered and the filtrate was concentrated under reduced pressure. The remaining residue which consisted of two isomers was separated by column chromatography using Pet. Ether:EtOAc (2:1) as the eluent. The two regioisomers were recrystallised from a mixture of DCM and Pet. Ether.

4.5.2.9.1 Ethyl 2-(1-(2-ethoxy-2-oxoethyl)-1*H*-tetrazol-5-yl)isonicotinate (4.3)

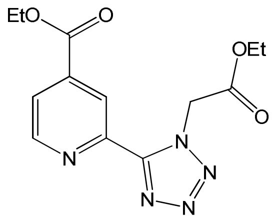

White solid (0.65 g, 37%). m.p. 78-80 °C. IR (KBr): ν = 2980, 2908, 1758, 1733, 1604, 1537, 1433, 1392, 1275, 1301, 1253, 1214, 1143, 1121, 1102, 1020, 993, 875, 772, 751, 722, 707, 681, 590 cm^{-1}. ^{1}H NMR ($CDCl_3$): δ = 8.97 (dd, 1 H, *J* = 1.5, 0.9 Hz, pyr-H), 8.80 (dd, 1 H, *J* = 5.0, 0.9 Hz, pyr-H), 8.01 (dd, 1 H, *J*= 5.0, 1.5 Hz, pyr-H), 5.74 (s, 2 H, CH_2-tet), 4.47 (q, 2 H, *J* = 7.1 Hz, CH_2), 4.19 (q, 2 H, *J* = 7.1 Hz, CH_2), 1.44 (t, 3 H, *J* = 7.1 Hz, CH_3), 1.19 (t, 3 H, *J* = 7.1 Hz, CH_3) ppm. ^{13}C NMR ($CDCl_3$): δ = 165.8 (C=O), 163.9 (C=O), 151.8 (CN_4), 150.0, 145.5, 139.6, 124.7, 123.5, 62.4 (OCH_2), 62.2 (OCH_2), 51.1 (CH_2-tet), 14.2 (CH_3), 14.0 (CH_3) ppm. ESI-HRMS: calcd. for $C_{13}H_{16}N_5O_4$ $[M+H]^+$ 306.1197, found 306.1195.

4.5.2.9.2 Ethyl 2-(2-(2-ethoxy-2-oxoethyl)-2*H*-tetrazol-5-yl)isonicotinate (4.4)

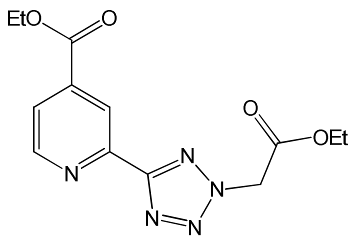

White solid (0.72 g, 40%). m.p. 89-92 °C. IR (KBr): ν = 3075, 2994, 2952, 1756, 1716, 1605, 1564, 1473, 1427, 1376, 1355, 1299, 1259, 1220, 1201, 1174, 1110, 1098, 1050, 1025, 886, 874, 783, 763, 682 cm^{-1}. ^{1}H NMR ($CDCl_3$): δ = 8.94 (dd, 1 H, *J* = 4.9, 0.8 Hz, pyr-H), 8.80 (dd, 1 H, *J* = 1.6, 0.8 Hz, pyr-H), 7.98 (dd, 1 H, *J*= 4.9, 1.6 Hz, pyr-H), 5.54 (s, 2 H, CH_2-tet), 4.47 (q, 2 H, *J* = 7.1 Hz, CH_2), 4.29 (q, 2 H, *J* = 7.1 Hz, CH_2), 1.45 (t, 3 H, *J* = 7.1 Hz, CH_3), 1.29 (t, 3 H, *J* = 7.1 Hz, CH_3) ppm. ^{13}C NMR ($CDCl_3$): δ = 164.7 (C=O), 164.7 (CN_4), 163.9 (C=O), 147.4, 139.1, 124.2, 121.8, 62.8 (OCH_2), 62.1 (OCH_2), 53.6 (CH_2-tet), 14.2 (CH_3), 14.0 (CH_3) ppm. ESI-HRMS: calcd. for $C_{13}H_{16}N_5O_4$ $[M+H]^+$ 306.1197, found 306.1197.

4.5.2.10 2-(1-(Carboxymethyl)-1*H*-tetrazol-5-yl)isonicotinic acid (4.3(pytzdaH))

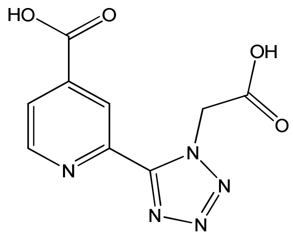

4.3 (0.30 g, 0.98 mmol) was dissolved in EtOH (20 mL). NaOH (0.20 mL, 10 M NaOH) was added to the solution and was heated to reflux overnight. The reaction mixture was concentrated under reduced pressure and the remaining residue was then dissolved in deionised H_2O (3 mL). 1 M HCl was added to the solution whilst stirring until precipitation commenced. The mixture was then allowed to stir at room temperature for 1 h, filtered and the precipitate was washed with H_2O. White solid (0.18 g, 75%). m.p. 165-170 °C. IR (KBr): ν = 3431, 3014, 2573, 1726, 1640, 1548, 1432, 1403, 1271, 1246, 1123, 1092, 912, 819, 783, 747, 730, 673, 546 cm^{-1}. ^{1}H NMR (d_6-DMSO): δ = 8.94 (dd, 1 H, J = 4.9, 0.8 Hz, pyr-H), 8.64 (dd, 1 H, J = 1.5, 0.8 Hz, pyr-H), 8.02 (dd, 1 H, J= 4.9, 1.5 Hz, pyr-H), 5.75 (s, 2 H, CH_2-tet) ppm. ^{13}C NMR (d_6-DMSO): δ = 167.8 (C=O), 165.1 (C=O), 151.7 (CN_4), 150.9, 144.8, 140.1, 124.7, 122.3, 50.9 (CH_2-tet) ppm. ESI-HRMS: calcd. for $C_9H_8N_5O_4$ $[M+H]^+$ 250.0571, found 250.0567.

4.5.2.11 2-(2-(Carboxymethyl)-2H-tetrazol-5-yl)isonicotinic acid (4.4(pytzdaH))

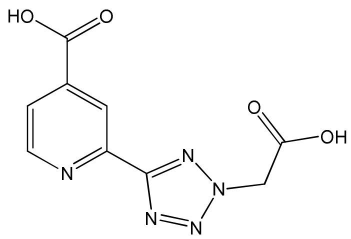

4.4 (0.30 g, 0.98 mmol) was dissolved in EtOH (20 mL). NaOH (0.20 mL, 10 M NaOH) was added to the solution and was heated under reflux for 4 h. The reaction mixture was concentrated under reduced pressure and the remaining residue was then dissolved in deionised H_2O (3 mL). 1 M HCl was added to the solution whilst stirring until precipitation commenced. The mixture was then allowed to stir at room temperature for 1 h, filtered and the precipitate was washed with H_2O. White solid (0.16 g, 66%). m.p. 225-230 °C. IR (KBr): ν = 3421, 3026, 2901, 2595, 2508, 1744, 1708, 1615, 1565, 1474, 1416, 1396, 1372, 1286, 1261, 1232, 1199, 1178, 1118, 1095, 1004, 876, 856, 818, 761, 722, 666, 645 cm^{-1}. ^{1}H NMR (d_6-DMSO): δ = 8.95 (dd, 1 H, J = 4.9, 0.8 Hz, pyr-H), 8.52 (dd, 1 H, J = 1.5, 0.8 Hz, pyr-H), 7.98 (dd, 1 H, *J*= 4.9, 1.5 Hz, pyr-H), 5.80 (s, 2 H, CH_2-tet) ppm. ^{13}C NMR (d_6-DMSO): δ = 167.3 (C=O), 165.4 (C=O), 163.7 (CN_4), 151.4, 146.9, 139.6, 124.1, 121.0, 53.8 (CH_2-tet) ppm. ESI-HRMS: calcd. for $C_9H_8N_5O_4$ $[M+H]^+$ 250.0571, found 250.0559.

4.5.3 Metal Complexation Reactions

4.5.3.1 Complexes of Diester Pyridyl Tetrazoles 4.3 and 4.4

4.5.3.1.1 [Cu(4.3)Cl_2]$_2$ (4.12)

4.3 (0.10 g, 0.33 mmol) was dissolved in MeOH (10 mL). A solution of $CuCl_2.2H_2O$ (0.06 g, 0.33 mmol) in MeOH (5 mL) was added to this solution and the reaction was heated under reflux for 2 h. The solution was allowed to stand until the solvent evaporated off to leave a green oily residue. MeOH was added to this residue and allowed to stand again producing a green crystalline solid which was filtered and dried. Green crystalline solid (0.06 g, 43%). $C_{26}H_{30}Cu_2Cl_4N_{10}O_8$: calcd. C 35.51, H 3.44, N 15.93%; found C 35.01, H 3.27, N 14.96%. IR (KBr): ν = 3437, 3414, 2989, 2918, 1749, 1728, 1624, 1558, 1457, 1390, 1371, 1293, 1262, 1234, 1147, 1124, 1013, 867, 794, 713, 688 cm^{-1}. λ_{max} (MeOH) 880 nm, ε = 90 M^{-1}cm^{-1}. Magnetic moment: 1.78 B.M.

4.5.3.2 [Cu(4.4)Cl_2] (4.13)

4.4 (0.20 g, 0.65 mmol) was dissolved in MeOH (15 mL). A solution of $CuCl_2.2H_2O$ (0.11 g, 0.65 mmol) in MeOH (10 mL) was added to the ligand solution and heated under reflux for 2 h. The solution was allowed to stand for several days at room temperature. The resulting solids were collected by filtration. Crystalline blue solid (0.04 g, 18%). $C_{22}H_{22}Cl_2CuN_{10}O_8$: calcd. C 38.35, H 3.22, N 20.33%; found C 37.36, H 2.47, N 21.14%. IR (KBr): ν = 3436, 1744, 1732, 1628, 1561, 1421, 1369, 1301, 1253, 1233, 1020, 761 cm^{-1}. λ_{max} (MeOH) 890 nm, ε = 110 M^{-1}cm^{-1}. Magnetic moment: 2.12 B.M.

4.5.3.3 Co(4.4)$_2$(NCS)$_2$ (4.14)

4.4 (0.20 g, 0.65 mmol) was dissolved in MeOH (10 mL). Co(SCN)$_2$ (0.11 g, 0.65 mmol) in MeOH (10 mL) was added to the solution and the resulting purple solution was heated to reflux for 2 h. The solution was allowed to cool at room temperature and stood for several days until dryness. MeOH (5 mL) was added to the residue and this solution was allowed to stand for 12 h, after which time a pink crystalline solid formed. This solid was filtered and washed with MeOH and dried. Crystalline pink solid (0.09 g, 38%). $C_{24}H_{22}CoN_{12}O_8S_2$: calcd. C 39.51, H 3.04, N 23.04%; found C 40.29, H 3.03, N 22.37%. IR (KBr): ν = 3444, 2955, 2093, 2081, 1762, 1732, 1622, 1565, 1543, 1432, 1368, 1347, 1304, 1214, 1112, 1060, 1005, 969, 810, 758, 585 cm^{-1}. λ_{max} (MeOH) 516 nm, ε = 45 $M^{-1}cm^{-1}$. Magnetic moment: 4.73 B.M.

4.5.4 Metal Complexation Reactions with Dicarboxylate Pyridyl Tetrazoles

4.5.4.1 Reactions with 4.3(pytzda)

4.5.4.1.1 $[Cu_2(4.3(pytzda)_2(H_2O)_6]_n$ (4.15)

4.3 (0.05 g, 0.16 mmol) was suspended in a solution of NaOH (0.01 g, 0.32 mmol) and deionised H_2O (9 mL). This solution was heated to reflux for 2 h, after which time the solution was homogenous. $CuCl_2.2H_2O$ (0.03 g, 0.16 mmol) in H_2O (2 mL) was added to the hot solution and the reaction was then allowed to stand at room temperature for 1 day, after which time blue block crystals were obtained (0.04 g, 61%). $C_{18}H_{22}Cu_2N_{10}O_{14}.H_2O$: calcd. C 28.92, H 3.24, N 18.74%; found C 28.86, H 3.41, N 18.18%. IR (KBr): ν = 3412, 2966, 1618, 1554, 1464, 1437, 1394, 1368, 1313, 1257, 1111, 1021, 881, 810, 780, 716, 705, 684, 560 cm^{-1}. Magnetic moment: 2.97 B.M.

4.5.4.1.2 $[Ni_2(4.3(pytzda)_2(H_2O)_6]_n$ (4.16)

Procedure was similar to that described for **4.15**, except that $NiCl_2$ (0.02 g, 0.16 mmol) in H_2O was added and the solution was cooled slowly and allowed to stand for several days. Blue block crystals formed as well as crystals of starting ligand. These were filtered and washed with deionised H_2O and MeOH. Blue crystals (0.04 g, 66%). $C_{18}H_{22}N_{10}Ni_2O_{14}.H_2O$: calcd. C 29.30, H 3.28, N 18.98%; found C 28.31, H 3.62, N 18.12%. IR (KBr): ν = 3563, 3419, 3189, 1622, 1553, 1440, 1389, 1364, 1317, 1254, 1121, 813, 707, 678 cm^{-1}. Magnetic moment: 4.37 B.M.

4.5.4.1.3 $[Co_2(4.3(pytzda)_2(H_2O)_6]_n$ (4.17)

Procedure was similar to that described for **4.15**, except that $Co(SCN)_2$ (0.03 g, 0.16 mmol) in deionised H_2O was added and the solution was cooled slowly and allowed to stand for several days. After 1 week, orange crystals formed. These were collected by filtration and washed with deionised H_2O. Orange crystals (0.03 g, 54%). $C_{18}H_{22}Co_2N_{10}O_{14}.H_2O$: calcd. C 29.28, H 3.28, N 18.97%; found C 29.39, H 3.52, N 18.25%. IR (KBr): ν = 3565, 3130, 3005, 2963, 1621, 1553, 1461, 1440, 1386, 1362, 1316, 1255, 1120, 1018, 880, 813, 760, 721, 707, 673, 540, 438 cm^{-1}. Magnetic moment: 6.56 B.M.

4.5.4.1.4 [Zn_2(4.3(pytzda)$_2$(H_2O)$_6$]$_n$ (4.18)

Procedure was similar to that described for **4.15**, except that a solution of $ZnCl_2$ (0.02 g, 0.16 mmol) in H_2O (2 mL) was added to the solution and the reaction was then allowed to stand at room temperature for several weeks, after which time white crystals formed which were filtered off from the mother liquor, washed with deionised H_2O and dried. White crystals (0.03 g, 51%). $C_{18}H_{22}Zn_2N_{10}O_{14}.H_2O$: calcd. C 28.78, H 3.22, N 18.65%; found C 28.85, H 3.47, N 17.88%. IR (KBr): ν = 3372, 1662, 1591, 1553, 1538, 1435, 1401, 1387, 1329, 1315, 1266, 1255, 1131, 1020, 816, 786, 786, 747, 725, 707, 685 cm^{-1}. ^{1}H NMR (d_6-DMSO): δ = 8.77-8.79 (m, 2 H, pyr-H), 8.43 (s, 2 H, pyr-H), 7.78-7.79 (m, 2 H, pyr-H), 5.56 (s, 4 H CH_2N) ppm. ^{13}C NMR (d_6-DMSO): δ = 169.7 (C=O), 168.0 (C=O), 152.3 (CN_4), 150.2, 144.7, 143.5, 124.5, 122.5, 51.8 (CH_2N) ppm.

4.5.4.2 Reactions with 4.4(pytzda)

4.5.4.2.1 [Cu_2(4.4pytza)$_2$(H_2O)$_6$] (4.19)

4.4 (0.05 g, 0.16 mmol) was suspended in a solution of NaOH (0.01 g, 0.32 mmol) in deionised H_2O (9 mL). The mixture was then heated to reflux for 2 h after which time the solution was homogenous. $CuCl_2.2H_2O$ (0.03 g, 0.16 mmol) in deionised H_2O was added to this solution and on slow cooling blue microcrystals formed which were filtered and washed with deionised H_2O. Blue crystalline solid (0.04 g, 66%). $C_{18}H_{22}Cu_2N_{10}O_{14}.H_2O$: calcd. C 28.92, H 3.24, N 18.74%; found C 29.14, H 2.83, N 19.53%. IR (KBr): ν = 3437, 3069, 1623, 1602, 1473, 1423, 1386, 1353, 1281, 1249, 1219, 1061, 1026, 919, 876, 816, 788, 749, 726, 690, 676, 591 cm^{-1}. Magnetic moment: 2.12 B.M.

4.5.4.2.2 [Co_2(4.4pytza)$_2$(H_2O)$_6$] (4.20)

4.4 (0.05 g, 0.16 mmol) was suspended in a solution of NaOH (0.02 g, 0.32 mmol) in deionised H_2O (9 mL). The resulting mixture was heated under reflux for 2 h, after which time the solution was homogenous. $Co(SCN)_2$ (0.03 g, 0.16 mmol) in deionised H_2O was added and the solution was cooled slowly and allowed to stand for several days. Orange crystals formed which were filtered and washed with deionised H_2O. Orange crystals (0.04 g, 66%). $C_{18}H_{22}Co_2N_{10}O_{14}.H_2O$: calcd. C 29.28, H 3.28, N 18.97%; found C 29.39, H 3.51, N 18.58%. IR (KBr): ν = 3271, 1619, 1541, 1423, 1382, 1304, 1253, 1147, 1066, 1013, 826, 798, 749, 709, 681, 595, 392 cm^{-1}. Magnetic moment: 5.88 B.M.

4.5.4.2.3 [Zn_2(4.4pytza)$_2$(H_2O)$_6$] (4.21)

4.4 (0.10 g, 0.32 mmol) was suspended in a solution of NaOH (0.03 g, 0.65 mmol) in deionised H_2O (9 mL). The resulting mixture was heated under reflux for 2 h, after which time the solution was homogenous. $ZnCl_2$ (0.04 g, 0.32 mmol) in H_2O was added and the solution was cooled slowly and allowed to stand for several days. Clear crystals formed which were collected by filtration and washed with deionised H_2O. White crystalline solid (0.10 g, 80%). $C_{18}H_{22}Zn_2N_{10}O_{14}.H_2O$: calcd. C 28.78, H 3.22, N 18.65%; found C 27.83, H 3.32, N 17.94%. IR (KBr): ν = 3406, 1618, 1562, 1540, 1420, 1397, 1381, 1322, 1302, 1254, 1068, 1014, 825, 749, 709, 681, 594 cm^{-1}. ^{1}H NMR (d_6-DMSO): δ = 8.82-8.84 (m, 2 H, pyr-H), 8.49 (s, 2 H, pyr-H), 7.90-7.92 (m, 2 H, pyr-H), 5.50 (s, 4 H, CH_2-tet) ppm. ^{13}C NMR (d_6-DMSO): δ = 169.1 (C=O), 168.6 (C=O), 163.6 (CN_4), 150.7, 146.6, 143.7, 124.4, 121.8, 55.2 ppm.

4.5.4.2.4 [$Cu_2(C_{11}H_{10}N_5O_4)_2$]$_n$ (4.23)

4.4 (0.02 g, 0.06 mmol) was reacted with NaOH (1 mg, 0.03 mmol) under reflux in H_2O for 2 h, after which time the solution was homogenous. $CuCl_2.2H_2O$ (0.01 g, 0.06 mmol) in H_2O (2 mL) was added to the hot solution and the reaction was then cooled slowly. A blue crystalline solid formed which was filtered and washed with H_2O and air dried. Blue crystalline solid (0.02 g, 99%). $C_{22}H_{20}Cu_2N_{10}O_8$: calcd. C 38.88, H 2.97, N 20.61%; found C 38.17, H 3.15, N 20.07%. IR (KBr): ν = 3429, 2968, 1720, 1624, 1537, 1472, 1434, 1426, 1382, 1353, 1309, 1253, 1187, 1061, 911, 881, 818, 767, 753, 690, 593 cm^{-1}. Magnetic moment: 2.77 B.M.

Chapter 5: Bis-Tetrazole Systems

5.1 Introduction

This chapter deals with the synthesis and employment of bis-tetrazole organic linkers in the formation of coordination polymers (CPs). The occurrence of bis-tetrazole CPs in the literature has increased enormously in recent years, with particular prominence in the last five years. This increased interest is due to a number of advantages; bis-tetrazole systems have abundant coordination sites with eight N atoms, which may be conducive to the diversity of networks, and with the development of solvothermal synthesis, the attainment of *in situ* generated tetrazole based CPs has attracted substantial interest, especially in cases where the novel CPs cannot be directly prepared from the ligands or by conventional methods.

Several bis-tetrazoles with various linkers joining the two heterocycles have been investigated. CPs employing 1,4-benzeneditetrazol-5-yl (BDT) (Figure 5.1) have been well documented in recent years. The earliest reported use of this linear ligand in terms of supramolecular architectures was by Molloy and co-workers in 2000.[225] However, it was the group of Dincă and Long in 2006 who identified that the carboxylate groups on a lot of commonly used bridging linkers at the time could be replaced by heterocyclic ligands, specifically tetrazoles or tetrazolates as in the case of BDT, with the result of forming analogous porous MOF structures exhibiting reversible H_2 uptake with enhanced binding capabilities.[155] This work demonstrated the utility of bis-tetrazole based ligands for producing robust MOFs with permanent porosity, and for possessing topologies and gas sorption characteristics mimicking those of carboxylate-based materials. In addition, with the discovery that tetrazoles gave rise to new structure types that had not yet been accessible using carboxylate chemistry and that changes in metal counteranion, solvent and reaction conditions influenced the topology and stability of the resulting frameworks, new opportunities became available to synthesise materials with drastically differing structures and properties. Accordingly, studies on BDT and its derivatives have steadily increased over the years.[226]

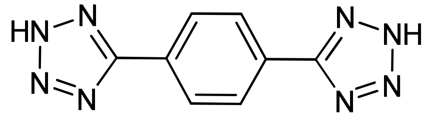

Figure 5.1: 1,4-benzeneditetrazol-5-yl (BDT).

One such derivative was developed by Jeong and colleagues, who synthesised and employed 2,6-di(1*H*-tetrazol-5-yl)naphthalene (H_2NTD) (Figure 5.2), a ligand which contained a naphthyl group as a rigid linker connecting two tetrazole units.[227] They reacted this ligand under solvothermal conditions with $MnCl_2.2H_2O$ in DMF and MeOH at two different temperatures, resulting in two different MOFs due to the formation of trinuclear and pentanuclear SBUs. The free tetrazoles at the terminal ends of the naphthyl group provided a means of counterbalancing the charge on the metal centre, and this state of deprotonation with four possible donor nitrogen atoms offered diverse coordination modes and coordination chemistry.

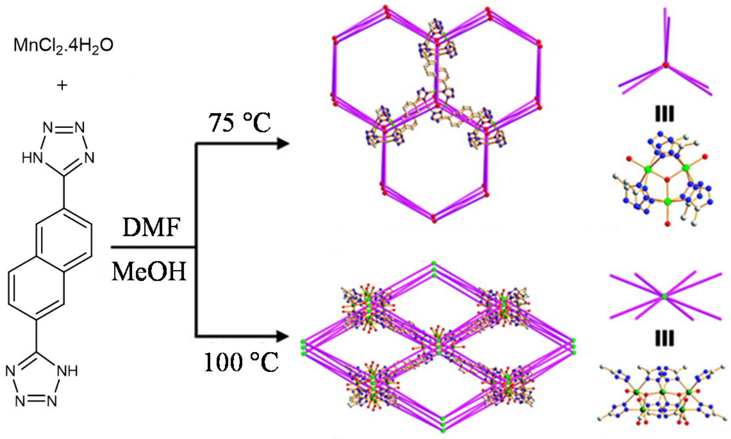

Figure 5.2: Reacting H_2NTD with $MnCl_2.4H_2O$ at different temperatures yielded two different MOFs with different topologies.[227]

Examples of other rigidly linked bis-tetrazoles are prevalent in the literature and ligands belonging to this group are depicted in Figure 5.3.

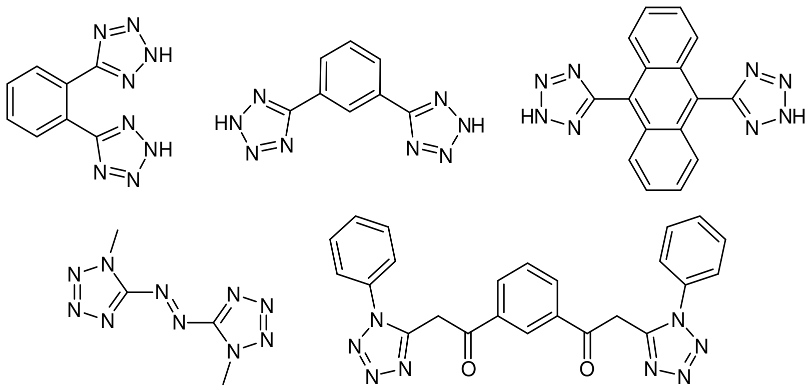

Figure 5.3: A number of rigidly linked tetrazole ligands used to prepare CPs.

Bis-tetrazoles with more flexible linkers have also been examined for their ability to form coordination networks. Sun *et al*. synthesised bis-tetrazole methylene *in situ* from malononitrile with the aim of expanding the repertoire of tetrazole based MOFs.[220] This ligand had abundant coordination sites with eight N atoms and in addition, the tetrazoles were separated by an alkyl ''CH_2'' spacer, which could add flexibility to the structure and endow the ligand with flexible bridging capabilities. Solvothermal reactions with $CdSO_4$ and $ZnSO_4$ and a secondary ligand, 2,2'-bipyridine, produced 2-D networks where the ligands were adopting a bidentate chelating or bridging mode (Figure 5.4). The bidentate chelating mode was made possible by the proximity of the two tetrazole rings to each other. When the secondary ligand was changed to 4,4'-bipyridine, a 3-D network was obtained (Figure 5.4), with the bis(tetrazole) methylene ligand retaining the bidentate chelating and bridging modes, but being further connected through pillars of 4,4'-bipyridine to generate a 3-D architecture.

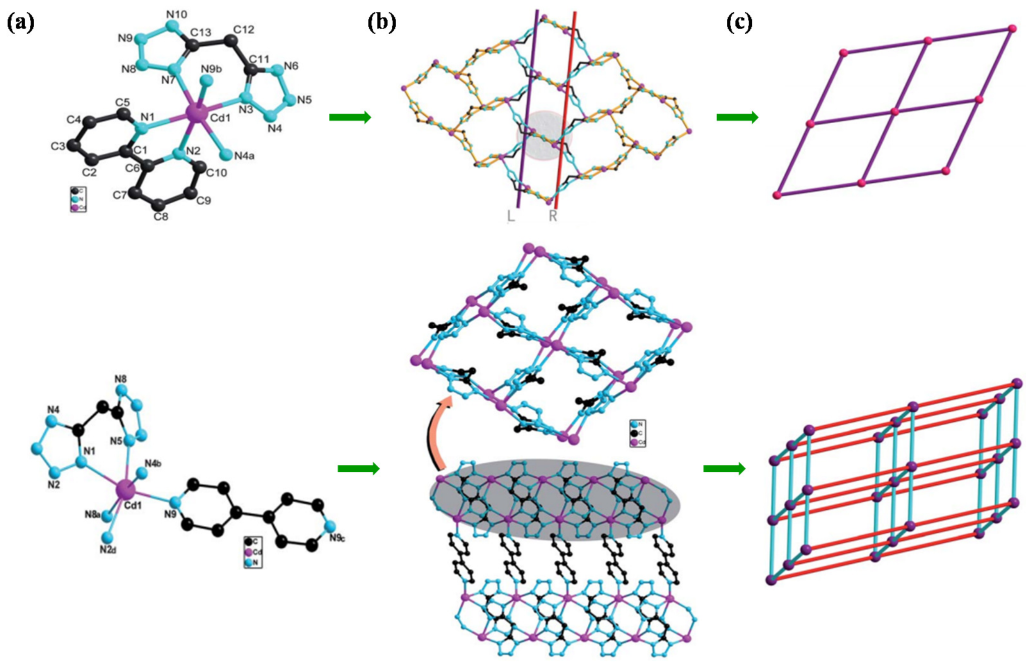

Figure 5.4: (a) Ball and stick plot showing coordination geometry around the Cd centres; (b) Perspective view of the 2-D networks, which in the case of the employment of 4,4'-bipy are joined by terminal bipy nitrogens; (c) Schematic representation of the topologies formed.[220]

Bis-tetrazole systems with increased flexibility between the tetrazole rings are rare. The paucity in examples of flexible tetrazole ligands can be attributed to the success of conformationally rigid organic ligands yielding well defined coordination spheres. The use of geometrically fixed organic building blocks allows targeting of frameworks with certain topologies and such frameworks usually exhibit relatively high thermal and mechanical stability. In contrast to the prolific production of MOFs based on rigid ligands, the design, synthesis and applications of MOFs based on flexible ligands have so far not attracted as much attention. Indeed, increased flexibility makes it more difficult to forecast and control the final structures due to the ligands adopting different conformations, and crystallinity of the products can also be hampered. The structures of MOFs based on flexible ligands are more dependent on the various and subtle reaction parameters including temperature, time and pH. These factors severly hinder the development of knowledge and concepts that allow the rational design and prediction of extended network architectures with flexible organic ligands. Nonetheless, it presents an alluring challenge for supramolecular and materials chemists to harness the benefits of flexible ligands in a way that also produces crystalline predictable structures. These benefits include generating structural diversity that is inaccessible from rigid building blocks, generating homochiral MOFs due to the abundance of flexible chiral ligands (amino acids, peptides) and endowing the molecular architecture with a ''breathing'' ability and adaptive recognition properties. Wang and colleagues recognised the benefits of flexible organic linkers and improved their rigid tetrazole-based ligands[228] by introducing flexible $(CH_2)_4$ backbones, aiming to construct helix/loop subunits in polyoxometalates (POMs).[229] POMs are a subset of metal oxides which usually consist of three or more transition metal oxyanions linked together by shared oxygen atoms to form a large closed 3-D framework. The transition metals are usually group 5 or 6 transition metals in their high oxidation states. POMs have recently been incorporated into the developing field of MOF chemistry, creating a new research field of POM-based MOFs.[230] This is because they are highly regarded as being structurally outstanding SBUs due to their coordination ability, structural diversity and promising properties, such as catalytic activity, magnetism and electrochemical activities.[229] Wang and co-workers suggested that flexible polydentate ligands may form the helix/loop subunits with ease owing to their flexibility and conformational freedom, which can make them conform to the coordination environment of the metal ions and POMs.[229] The ligands synthesised are shown in Figure 5.5. They reported that the position of the N donor atom on the pyridine ring had an effect on the formation of helical subunits. The ligand with side N donors in the pyridyl group were conducive to forming helix/loop subunits, whereas terminal N donors led to dinuclear subunits (Figure 5.5). Furthermore, the influence of the flexible backbone was evident as the group stated that previously studied rigid precursors exclusively yielded isolated multinuclear units.

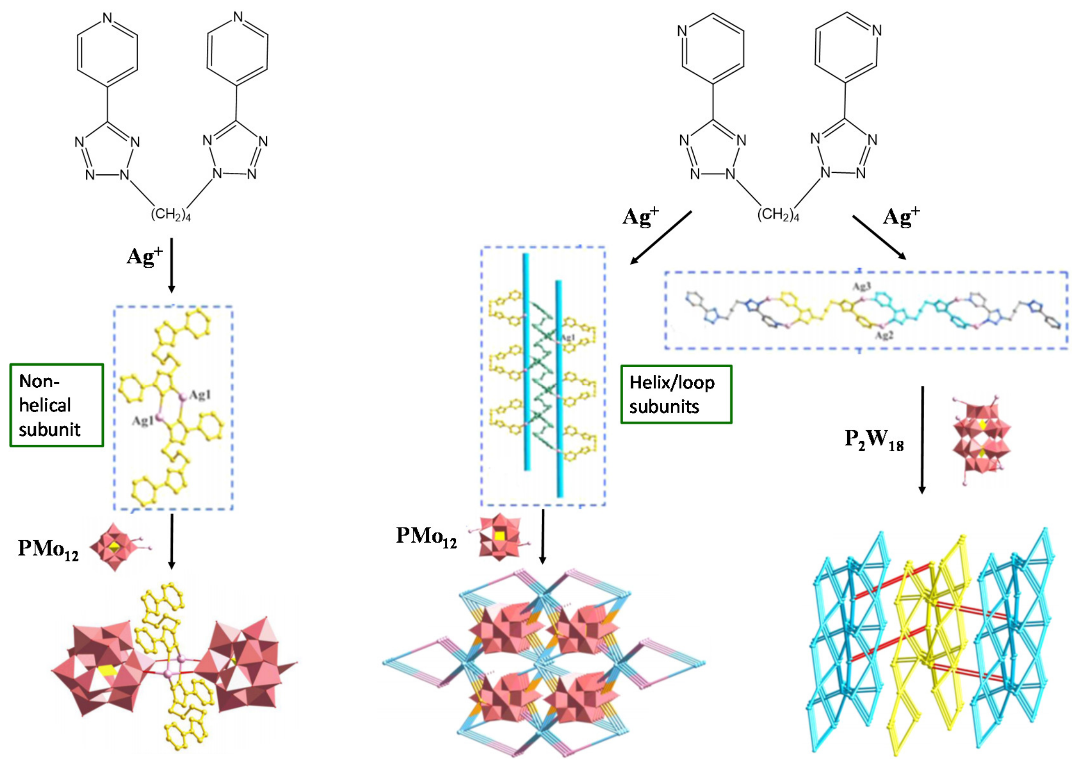

Figure 5.5: Schematic illustration of POM-based MOFs containing different Ag-ligand subunits. Diagram adapted and edited from Wang *et al.*[229]

Similar ligands (some of which are shown in Figure 5.6), albeit much simpler, have been employed in the synthesis of CPs whilst taking advantage of their flexibility.[231,232] The use of bis-tetrazoles in these flexible systems is extremely limited, and the example presented by Wang *et al.* is indeed unique.[229] This led us to question the applicability and usefulness of our tetrazole ligands in bis-systems, with both rigid and flexible backbones.

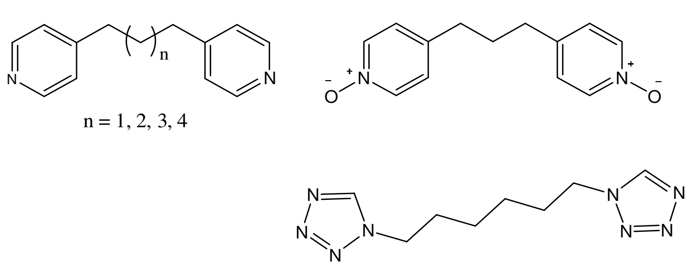

Figure 5.6: Flexible ligands with a $(CH_2)_n$ backbone have been employed in the synthesis of coordination polymers. Their occurrence is limited however, which may be partly due to the many polymorphs possible due to their conformational freedom.

5.2 Aims and Objectives of Chapter

In light of the above mentioned motivations, the goal of this chapter was to synthesise novel bis-tetrazole ligands and to investigate their potential to form multidimensional CPs. In our previous work, we successfully designed a series of pyridyl tetrazole ligands with a flexible tethered carboxylate group and introduced them into CP systems, and obtained novel networks and multinuclear clusters. In this work, we further developed these systems into bis-tetrazole systems, where the linkers introduced to join these moieties were varied. One approach was to introduce more flexibility into the precursors *via* introducing a flexible $(CH_2)_3$ backbone with the aim of forming frameworks with potential voids. Unlike the ligands presented in Figures 5.5 and 5.6, we aimed to synthesise pyridyl tetrazoles linked *via* this flexible backbone through the pyridine ring and not the tetrazole rings (Figure 5.7). These ligands would possess distinctive advantages in that they could provide multiple coordination sites by virtue of possessing pyridine and tetrazole N donors and carboxylate O donors; the carboxylate groups could allow for an expansion in dimensionality; and the relatively long spacer and the two pyridyl groups can rotate along its C−C bonds to form nine main configurations, as observed in previous reports, thereby enabling the ligand to adopt versatile coordination modes and conformations (Figure 5.8).

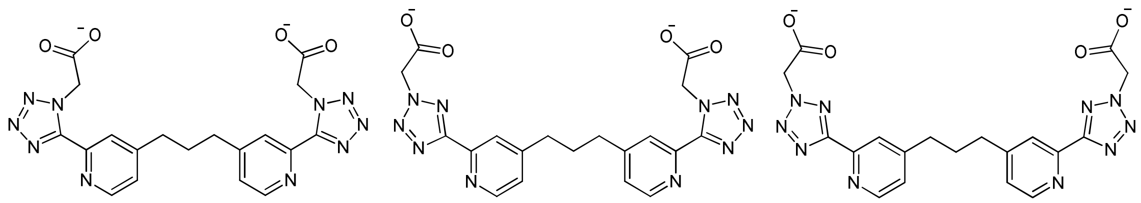

5.1(bptzap) **5.2(bptzap)** **5.3(bptzap)**

Figure 5.7: The flexible bis-tetrazole systems that were intended to be synthesised in this work.

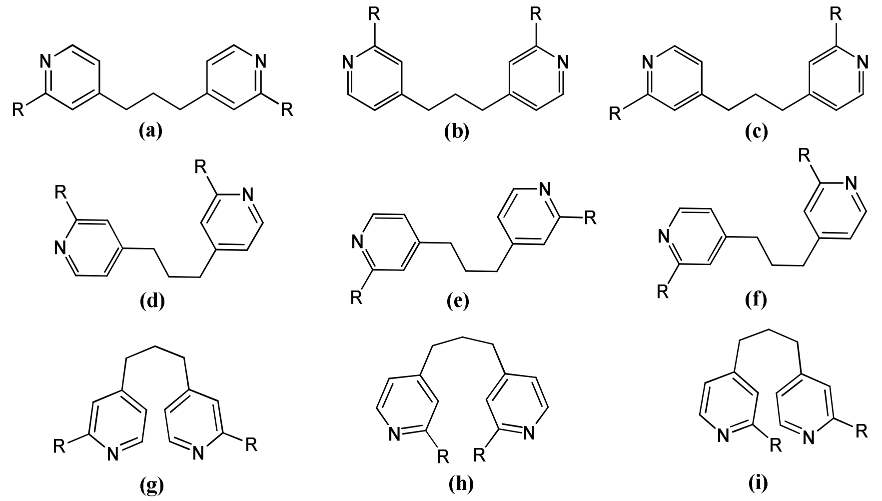

Figure 5.8: The main conformations of trimethylene linked heterocycles.

The second contrary approach was to connect two tetrazole rings by a more rigid linker; hence we aimed to make the ligands presented in Figure 5.9. These ligands would not have as much conformational freedom as the **bptzap** series, and would allow an investigation into the effect of spacer flexibility on CP structures. In addition, pyrazine nitrogens are well known for their donor capacities, therefore we expected coordination to the metal centres from this moiety would lead to higher dimensionality. The ligands would also possess tetrazole nitrogens and flexible carboxylate oxygen donor atoms, further increasing the probability of forming diverse structures with high dimensionality.

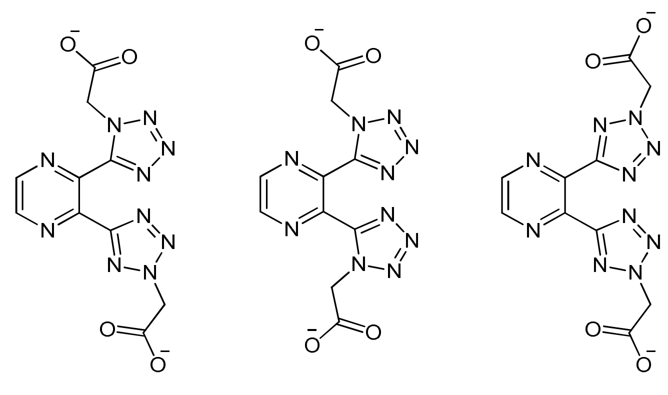

5.4(pzbtza) **5.5(pzbtza)** **5.6(pzbtza)**

Figure 5.9: Bis-tetrazole ligands linked by a rigid pyrazine linker, which were synthesised as part of this work.

Therefore, the overall aims of this chapter were to synthesise novel bis-tetrazole ligands with different spacer groups. The **bptzap** series would possess a flexible $(CH_2)_3$ backbone and the **pzbtza** series would include a rigid pyrazine spacer. These ligands would be produced with the aim of synthesising CPs with exciting topologies and properties for potential applications. The expected formation of regioisomers would also allow an assessment of how tetrazole substitution position would influence the final structures. We also aimed to gain higher dimensional CPs through using these ligands. Ultimately, we aimed to expand the area of rigid and flexible bis-tetrazole ligands in the realm of MOF chemistry and verify whether our improved strategy is rational for the construction of high dimensional materials. This may offer informative examples for the targeted syntheses of CPs. Importantly, to the best of our knowledge, research on these bis-tetrazole ligands in CPs have not been reported to date. Hence, this chapter represents a novel area of exploration.

5.3 Results and Discussion

5.3.1 Synthesis of Ligands

5.3.1.1 Synthesis of Bis-Tetrazole Ligands with Flexible $(CH_2)_3$ Backbone

The synthesis of **5.1**, **5.2** and **5.3** was achieved using a similar approach to that discussed in Chapter 4 (section 4.3.1.1). The synthetic route employed in this chapter is depicted in Scheme 5.1.

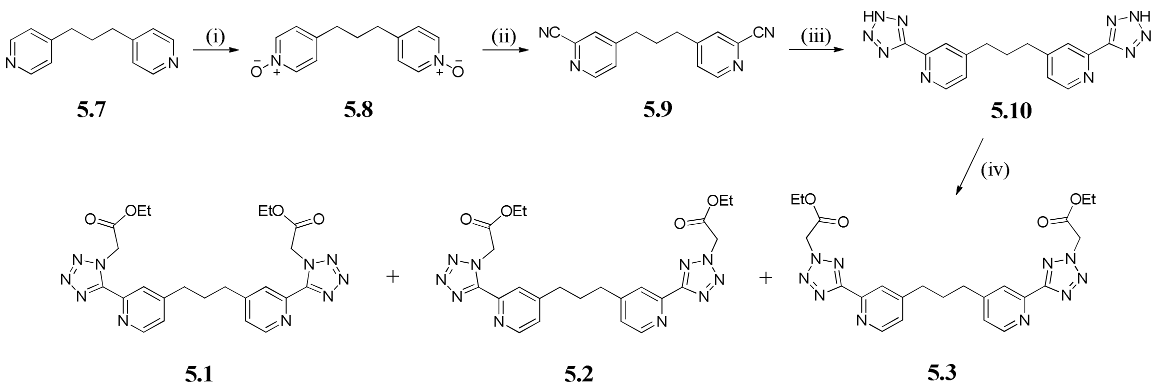

Scheme 5.1: Reagents and Conditions: i) H_2O_2, CH_3COOH, 79 °C, 20 h, 75%; ii) DMCC, $Zn(CN)_2$, DMF, 25 °C, 1 h, 34%; iii) NaN_3, NH_4Cl, DMF, 110 °C, 10 h, 93%; iv) K_2CO_3, $BrCH_2COOEt$, CH_3CN, 82 °C, 24 h, 10% (**5.1**), 16% (**5.2**), 28% (**5.3**).

Access to these ligands was achieved by firstly oxidising commercially available 4,4'-trimethylenebipyridine to the corresponding 1,3-bis(4-pyridyl)propane-N,N'-dioxide (**5.8**). The formation of the N-oxide would activate the 2-position of the pyridine ring towards nucleophilic substitution by virtue of the electron resonance contributors discussed in section 4.3.1.1. Formation of the bis-N,N'-dioxide **5.8** was confirmed by the presence of a ν(N-O) frequency at 1230 cm^{-1} in the IR spectrum. The acquired data for **5.8** was consistent with that reported in the literature.[233] The α-cyanation of **5.8** has been reported once previously by Deng and colleagues, who employed TMSCN and benzoyl chloride to gain access to the bis-cyano derivative **5.9**.[232] Considering the success of our α-cyanation method described in Chapter 4, we undertook α-cyanation of **5.8** using the conditions of $Zn(CN)_2$ and dimethylcarbamoyl chloride (DMCC) in toluene. However, problems were encountered due to the completely insoluble nature of **5.8** in toluene. Even when prolonged reaction times under reflux were employed, analysis by TLC revealed that no traces of product was formed at all, thus indicating that **5.8** was not dissolving even in trace amounts overtime. Hence, further modifications to this method were required.

Solubility testing showed that **5.8** was insoluble in many solvents. It did however dissolve in DMF over time, hence, the α-cyanation of **5.8** was attempted in DMF under heated conditions. On work up of this reaction, a brown sticky residue was obtained. The ^{1}H NMR spectrum revealed that the residue contained a mixture of products, which when separated by flash column chromatography, yielded trace amounts of desired product and monosubstituted product. On probing the reason why this would have happened, the reactivity of the acyl chloride came into question. It was plausible for the very reactive acyl chloride to react with DMF, and on searching the literature, there were a number of examples of this incidence happening.[234] On heating, DMF and DMCC can react to form N,N,N',N'-tetramethylformamidinium chloride (Figure 5.10). Crude amidinium salts are notoriously intractable, being dark sticky oils,[235] which correlated well with our observations. The crude ^{1}H NMR spectrum also alluded to the presence of this species, as methyl signals were observed at ~3 ppm, and a singlet at 8.17 ppm was attributed to an imine proton. Hence, it was believed that the brown residue remaining on the column was this undesired product. No further pursuit of this product or its characterisation was carried out.

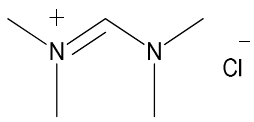

Figure 5.10: N,N,N',N'-tetramethylformamidinium chloride.

Since formation of this product was tentatively proposed, prevention of this undesired reaction from occurring was attempted. The acylating agent, DMCC, was added slowly over one hour to a reaction mixture of $Zn(CN)_2$ and **5.8** in DMF at 0 °C. The reaction was then allowed to slowly warm up to room temperature overnight. After work up and extraction with DCM, the crude mixture was again analysed by ^{1}H NMR spectroscopy. Methyl peaks and a singlet at 8.17 ppm were again visible in the spectrum, however the presence of three aromatic signals was also observed, indicating successful substitution of the pyridine ring. A comparison of the relative integrations for the peaks indicated that formation of the amidinium side product was somewhat alleviated. The mixture was passed through a silica plug using EtOAc and Pet. Ether as the eluent in a 3:1 ratio. This yielded a white crystalline solid with isolated yields of around 30%. As well as the ^{1}H NMR spectrum displaying three aromatic signals, there was further evidence that a nitrile group was present at the 2-position of the pyridine ring. In the IR spectrum of **5.9**, a sharp peak was positioned at 2237 cm^{-1}, which was attributed to the ν(C≡N) vibrational mode. In the ^{13}C NMR spectrum, a peak concomitant with a nitrile carbon was observed at 117.2 ppm. To address the poor yields obtained in this reaction, several attempts at optimisation were carried out. Longer reaction times resulted in no increase in yields. Employing a different acylating agent, benzoyl chloride, also resulted in a side reaction with DMF. Different solvents were also utilised, but in all cases, no product was observed. DMF was the only solvent capable of dissolving both $Zn(CN)_2$ and **5.8** in sufficient quantities to react. Although these yields were not ideal, no further optimisation was carried out at this point. The collated data acquired for **5.9** was consistent with that reported by Deng *et al.*[232] Synthesis of the ligands continued with a 1,3-dipolar cycloaddition using conditions described previously (section 2.3.1). The product, **5.10**, was analysed by NMR and IR spectroscopies and HRMS. The IR spectrum of **5.10** displayed a broad stretch at ~3386 cm^{-1} which was indicative of the ν(N-H) vibrational mode of the protonated tetrazole. Additional stretching frequencies in the region 1562-1633 cm^{-1} indicated the presence of tetrazole rings. Furthermore, the ν(C≡N) frequency was absent which was anticipated if it had been consumed during the reaction. The presence of two tetrazole rings was also indicated by the ^1H NMR spectrum which exhibited five resonances: three aromatic signals and two alkyl chain resonances attributed to the propyl chain protons. This implied a symmetrical system and therefore indicated bis-substitution. The tetrazole quaternary C-5 peak was positioned at 154.9 ppm in the ^{13}C NMR spectrum, which is typical of C-5 resonances of protonated tetrazole rings. Finally, HRMS analysis revealed the presence of a molecular ion peak at m/z 335.1476 which corresponded to (**5.10**+H)$^+$ with an error of −0.03 ppm. Thus, the data acquired for **5.10** supported the presence of two tetrazole rings being present. Alkylation of **5.10** was then carried out in the presence of base, using ethyl bromoacetate. On analysis of the crude residue by ^1H NMR spectroscopy, the spectrum initially appeared complicated. However, it could be deduced that there were three products present in the mixture, most plausibly the N-1, N-1'; N-2, N-2' and N-1, N-2' substituted regioisomers. The crude mixture was separated by flash column chromatography using a gradient system. This was necessary to obtain the products with low R_f values in a clean, well separated manner. On first attempt, traces of a fourth monosubstituted product was also produced, however in very small quantities. This was alleviated by using more equivalents of K_2CO_3 and ethyl bromoacetate. The separated fractions were analysed by NMR spectroscopy and the ^{13}C NMR spectra of the compounds revealed the substitution on the tetrazole rings. The first product to elute was the N-1, N-1' regioisomer **5.1**, as indicated by the single C-5 resonance peak at 152.2 ppm. The second product to elute was the N-1, N-2' regioisomer **5.2** as indicated by the additional ^{13}C

resonances present which supported the presence of asymmetry in the molecule. The ^{1}H NMR spectrum also clearly showed that this was the case (Figure 5.11). The ^{13}C NMR spectrum exhibited a C-5 resonance at 164.1 ppm for the N-2 substituted ring and at 151.4 ppm for the N-1 substituted ring. The ^{1}H NMR spectrum showed the same trends as seen in previous alkylated tetrazoles, with the N-1 methylene group being more deshielded in the N-1 substituted tetrazoles than the N-2 substituted tetrazole rings. The final product that eluted was the N-2, N-2’ regioisomer **5.3** which was confirmed by ^{13}C NMR spectroscopy where the single C-5 resonance for the tetrazole ring resonated at 164.8 ppm.

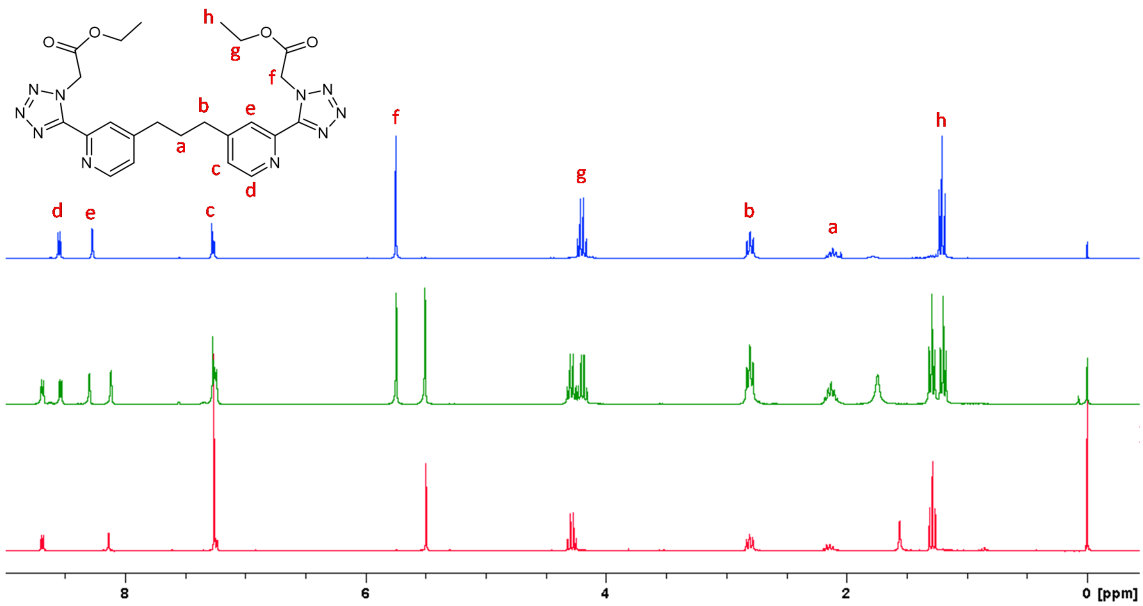

Figure 5.11: ^{1}H NMR spectra, obtained in $CDCl_3$, of **5.1** (blue), **5.2** (green) and **5.3** (red). Relevant signals are labelled for **5.1**.

Single crystals of **5.1** were grown and analysed by X-ray crystallography (Figure 5.12). **5.1** crystallises with the ester groups being almost orthogonal with respect to the plane of the tetrazole rings (66(1)°). This observation is similar to that seen in other N-1 ester functionalised tetrazoles that were synthesised previously in this thesis. There is also a notable bend in the molecule; the propyl chain is in the same plane as one pyridyl tetrazole unit, with the other pyridyl tetrazole being nearly perpendicular to this plane. There are no intermolecular hydrogen bonds present in the packing diagram.

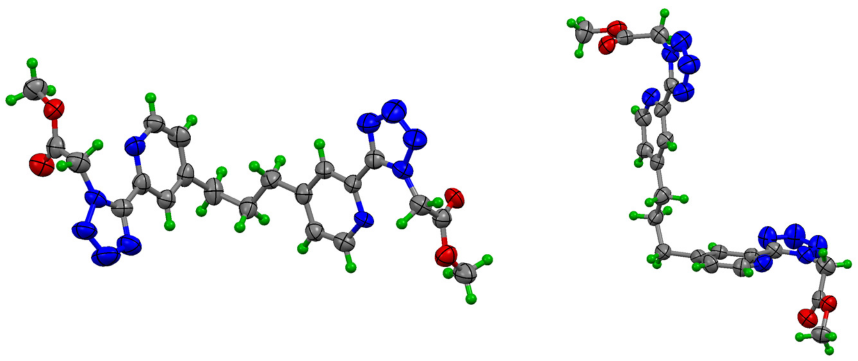

Figure 5.12: View of the molecular structure of **5.1**, and view of conformational bend in the molecule.

5.3.1.2 Synthesis of Bis-Tetrazole Ligands with Rigid Pyrazine Backbone

The synthesis of ligands **5.4**, **5.5** and **5.6** was achieved by the synthetic route shown in Scheme 5.2. 2,3-di(1*H*-tetrazol-5-yl)pyrazine (**5.12**) was synthesised from the 2,3-pyrazinedicarbonitrile precursor in 67% yield as an orange crystalline solid. The acquired data for **5.12** correlated well with literature values.[120,156]

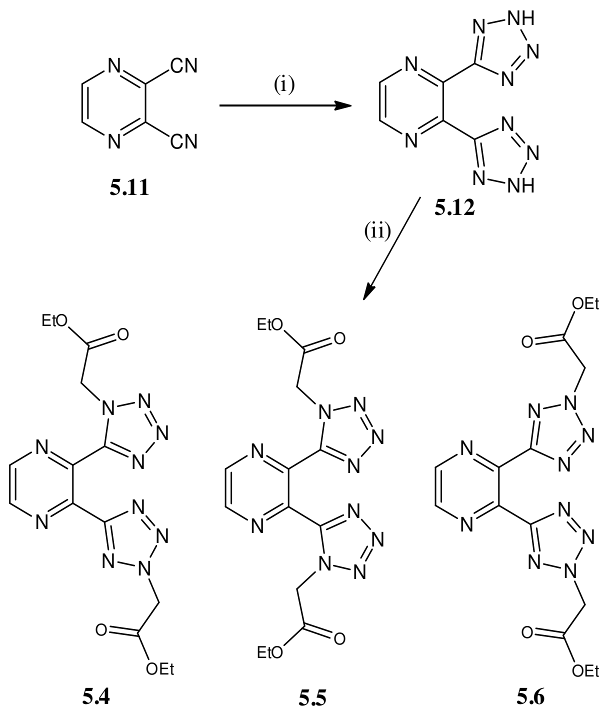

Scheme 5.2: Synthetic scheme for the synthesis of **5.4**, **5.5** and **5.6**. Reagents and conditions: i) NaN_3, NH_4Cl, LiCl, DMF, 110 °C, 12 h, 67%; ii) DIEA, $BrCH_2COOEt$, MeCN, 82 °C, 24 h, 23% (**5.4**), 10% (**5.5**), 9% (**5.6**).

The McGinley group has previously achieved alkylation of **5.12** employing Et_3N.[120] Utilising these conditions for our purposes did lead to alkylation, however it also unsurprisingly hydrolysed the ester groups and there was concern over the feasibility of separating carboxylic acid derivatives by column chromatography if it was required. N,N-Diisopropylethylamine (DIEA) was therefore employed instead, as it is an organic base which is non-nucleophilic. This is due to the steric bulk of the isopropyl and ethyl groups which allow only a proton to be abstracted from a substrate.[236] Thus, **5.12** was reacted with DIEA and ethyl bromoacetate in MeCN at reflux temperature for 24 h. The resulting orange clear solution was reduced *in vacuo* and washed with H_2O in order to remove excess DIEA. TLC analysis of the crude mixture revealed three spots which were overlapping, and the crude ^1H NMR spectrum also indicated the presence of three products. Several combinations of TLC solvent systems were investigated, however clear separation of the spots remained unattainable. On attempting to purify the residue by column chromatography using the best solvent system observed by TLC, the spots eluted at the same time, therefore separation of the regioisomers had to be achieved by other means. In hypothesising that the regioisomers' solubilities might be sufficiently different from each other, slow precipitation of the products was attempted in many solvents. It was found that a mixture of MeOH, Pet. Ether and $CHCl_3$ produced a crystalline solid, which was filtered and dried. ^1H NMR spectroscopy alluded to the asymmetric nature of this solid (**5.4**) as all signals were split due to this asymmetry (Figure 5.13). The ^{13}C NMR spectrum also had many resonances present, with the tetrazole C-5 carbons resonating at 162.1 ppm for the N-2 substituted tetrazole and 150.8 ppm for the N-1 substituted tetrazole. Asymmetry was also confirmed by IR spectroscopy as two ν(C=O) vibrational modes were positioned at 1745 and 1757 cm^{-1}. On sitting the filtrate for a further day, another crop of white solid formed (**5.5**) which when analysed by ^1H NMR spectroscopy proved to be a symmetrically substituted compound, which was evident by the ^1H NMR spectrum obtained (Figure 5.13). The position of the alkyl ester on the tetrazole ring was elucidated by analysing the ^{13}C NMR spectrum for **5.5**, which had a peak at 150.5 ppm that indicated that **5.5** was the N-1, N-1' substituted isomer. The IR spectrum also had a single ν(C=O) stretch at 1750 cm^{-1}. Isolation of the remaining N-2, N-2' isomer proved difficult. This isomer always remained in the filtrate and therefore was in the presence of other impurities as well as traces of **5.4** and **5.5**. Therefore as it crystallised out of solution, it was often along with these impurities. After several recrystallisations of this regioisomer however, clean product (**5.6**) was eventually obtained. Prolonged periods of time in the presence of MeOH did occasionally result in transesterification to the methyl ester derivatives. The ^{1}H NMR spectrum of **5.6** is represented by the blue spectrum in Figure 5.13. The symmetrical nature of the molecule was immediately obvious, as a singlet integrating for two protons which was associated with the pyrazine protons was observed. A single singlet attributed to the methylene group bonded to the tetrazole ring was also present, as was a quartet integrating for four protons and a triplet integrating for six protons which were attributed to the ethoxy protons. The N-2 substituted nature of the tetrazole rings was confirmed by ^{13}C NMR spectroscopy where the anticipated C-5 of the tetrazole ring was positioned at 162.6 ppm. The IR spectrum of **5.6** was similar to **5.5** with a single ν(C=O) vibrational mode positioned at 1745 cm^{-1}.

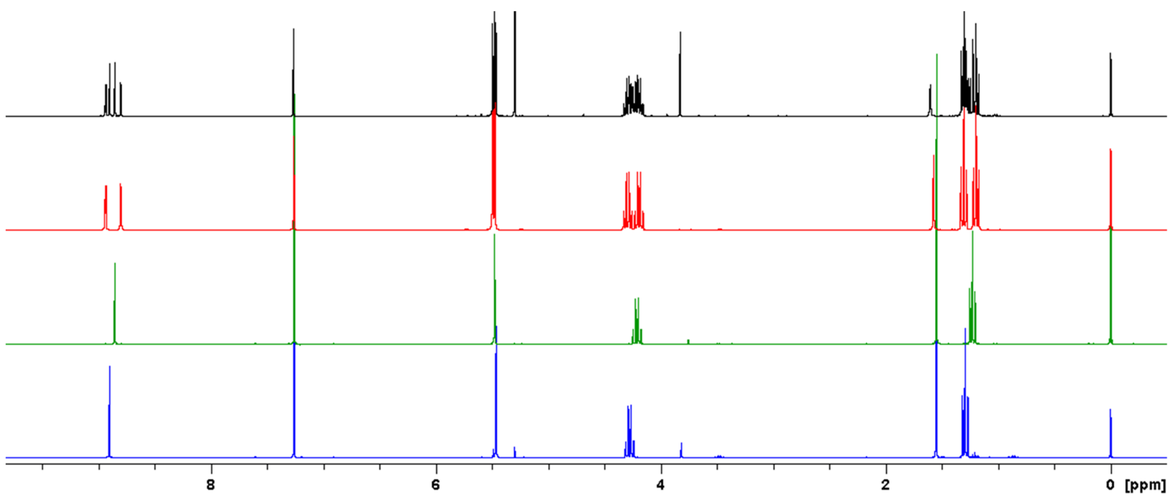

Figure 5.13: ^{1}H NMR spectra of crude mixture (black), **5.4** (red), **5.5** (green) and **5.6** (blue) which were carried out in $CDCl_3$ (with some H_2O present at 1.56 ppm).

Single crystals of **5.4** and **5.5** were analysed by X-ray crystallography and the results of this analysis can be seen in Figures 5.14 and 5.15. In **5.4**, neither of the tetrazole rings are co-planar with the pyrazine ring, with the N-1 substituted tetrazole ring being especially twisted with respect to the pyrazine ring (forms a dihedral angle of 69.5(3)° compared to 7.3(3)° for N-2 the tetrazole ring). We can conclude from this observation that the position of the substituent in the N-1 substituted tetrazole is greatly hindering the existence of co-planar systems.

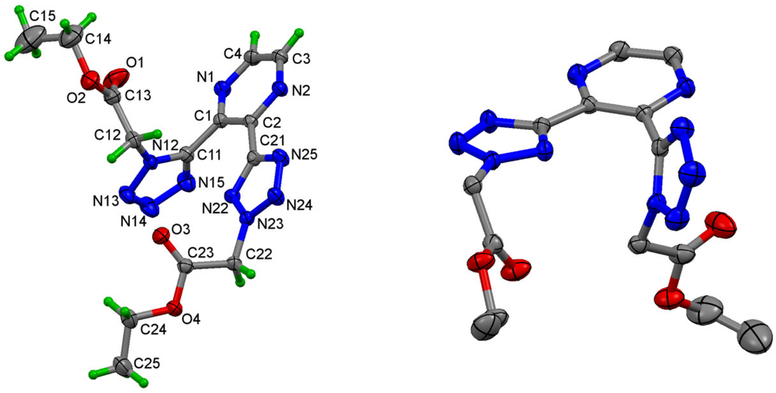

Figure 5.14: Crystal structure of **5.4** viewed from two perspectives**.** Figure on right has hydrogen atoms omitted for clarity.

The crystal structure of **5.5** can be seen in Figure 5.15. In comparison to the crystal structure for **5.4**, **5.5** shows considerable puckering between both tetrazole rings and the pyrazine ring, with the plane of the pyrazine ring and the tetrazole rings forming a dihedral angle of 35.4(6)° for the N12 substituted ring and 30.1(6)° for the N22 substituted ring. Again, it can be deduced that the substitution at the N-1 position of the tetrazole ring causes a significant amount of steric hindrance in these type of systems, so much so that even puckering of the pyrazine ring is observed in the crystal structure.

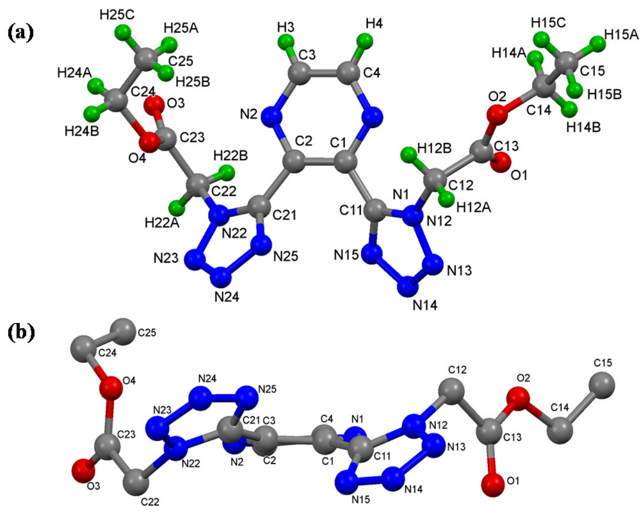

Figure 5.15: (a) Crystal structure of **5.5** viewed along the *a*-axis**,** (b) structure viewed with pyrazine pointing back into the page, highlighting the distortion of the tetrazole rings from the plane of the pyrazine ring. Hydrogen atoms are omitted for clarity.

5.3.2 Metal Complexation Reactions

5.3.2.1 Metal Complexation Reactions with Flexible Bis-Tetrazole Ligands

Reactions of **5.1** with $CuCl_2.2H_2O$, $Cu(NO_3)_2$, $Cu(OAc)_2$ in MeOH resulted in the attainment of unreacted ligand. Reaction of **5.1** with $CuCl_2.2H_2O$ in EtOH however did yield a green precipitate. This solid (**5.13**) was filtered, dried and analysed by IR spectroscopy, elemental analysis and magnetic moment measurements. Room temperature magnetic moment measurements yielded a μ_{eff} value of 1.9 B.M which was a typical value of a d^9 metal ion. The IR spectrum of **5.13** displayed frequency shifts when compared to the starting ligand **5.1**. Complexation to the ester moiety was not alluded to as there were no significant shifts observed for the ν(C=O) vibration. Complexation to the pyridine and tetrazole moieties was suggested as shifts in the heterocyclic frequencies were observed. Elemental analysis alluded to a 1:1 metal to ligand composition. The material was very insoluble which led us to believe that the material was polymeric. A structure was proposed which can be seen in Figure 5.16. It was proposed that the Cu(II) ion was in an octahedral environment, coordinated by two pyridine and tetrazole N-1 nitrogens and two chloride anions. The Cu(II) ion was proposed to connect two different ligands, propagating a 1-D coordination polymer.

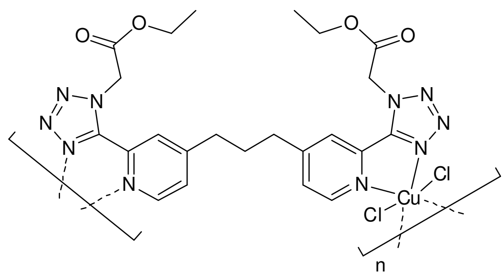

Figure 5.16: Proposed structure of a subunit of coordination polymer **5.13**.

Reacting **5.2** with $CuCl_2.2H_2O$ in EtOH resulted in a dark green precipitate forming in solution. The solid was analysed by IR spectroscopy and compared to that of the starting material. The ν(C=O) vibrational mode had shifted to a lower wavenumber and was now positioned at 1743 cm^{-1}, which indicated that no complexation was occurring to the ester moiety but that complexation to the ligand had occurred. Shifts in the heterocyclic stretches were observed which indicated that there were interactions with the heterocyclic nitrogens and the metal atom. Elemental analysis suggested that the solid had a 2:1 metal to ligand ratio. The solid was insoluble in most solvents, so it was proposed that the material was polymeric. With this in mind, a structure was tentatively assigned to the solid and this structure can be seen in Figure 5.17. The structure consists of dichloro-bridged subunits with each Cu(II) centre possessing a square pyramidal geometry. The polymeric chain propagates through coordination of another subunit to the coordinatively unsaturated Cu(II) centre shown in Figure 5.17. Elemental analysis correlated well with the calculated values for this structure, and chloride bridging has been observed before in pyridyl tetrazole complexes synthesised in this thesis (Chapter 2 and 3).

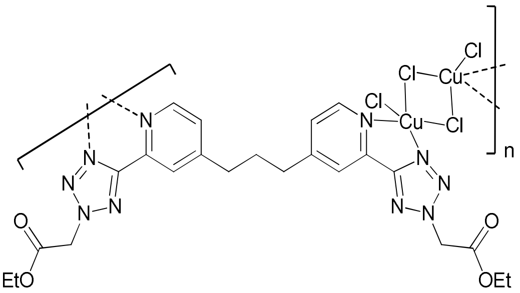

Figure 5.17: Proposed structure of **5.14**, which could be a subunit of a polymeric chain.

On reacting *in situ* generated dicarboxylates **5.1(bptzap)**, **5.2(bptzap)** and **5.3(bptzap)** with metal salts, insoluble powders formed from the solution. IR spectroscopy, elemental analysis and magnetic moment analysis was carried out on these products, however, definitive structures could not be suggested. This was due to the many conformations that the ligands could adopt. It was reasonable to assume coordination to the carboxylate oxygens and the pyridyl tetrazole nitrogens as IR analysis suggested that this was the case. The attainment of single crystals was attempted by changing reaction parameters however, the formation of an amorphous powder was not avoided. The use of solvothermal techniques has proved to be a useful technique in order to obtain crystalline products. This method will be pursued in future work as a means to obtain single crystals and characterise the structures formed by the flexible **bptzap** series.

5.3.2.2 Metal Complexation Reactions with Rigid Pyrazine Ligands

5.4 was nonsolvothermally converted to **5.4(pzbtza)** *in situ* using aqueous NaOH. After heating this solution for two hours, $CuCl_2.2H_2O$ was added to the solution and the resulting blue solution was cooled slowly and allowed to stand for several days. Block shaped royal blue crystals formed after this time which were filtered and dried. The IR spectrum of the blue solid **5.15** revealed that no protonated carboxylic acid was present in the structure. Monodentate coordination to Cu(II) was suggested as a $\nu_{asym}(COO^-)$ vibration was observed at 1660 cm^{-1} and the corresponding $\nu_{sym}(COO^-)$ was positioned at 1377 cm^{-1}, yielding a $\Delta(\nu_{asym}(COO^-) - \nu_{sym}(COO^-))$ value of 283 cm^{-1}. A broad strong stretch was positioned at 3419 cm^{-1} which indicated coordinating H_2O molecules and possible hydrogen bonding. The presence of H_2O was also alluded to in elemental analysis studies. The single crystals obtained were analysed by X-ray crystallography and the results proved to be quite interesting (Figure 5.18). **5.15** crystallises as a 2-D coordination polymer which extends along the *a*- and *b*-axis. These sheets are further connected into a 3-D hydrogen bonded network. There are two crystallographically unique Cu(II) cations in the asymmetric unit. Each Cu(II) centre possesses a distorted square pyramidal geometry. It is coordinated to one H_2O molecule, two tetrazole nitrogens from the same ligand but different rings and two carboxylate oxygens from two different ligands coordinating in a monodentate fashion. Two nitrogen atoms (N22A, N12A for Cu1; N22B, N12B for Cu2) and two oxygens (O1A, O3A for Cu1; O1B, O3B for Cu2) form the base of the pyramid and one H_2O molecule (O1W for Cu1 and O2W for Cu2) occupies the apical position. Each ligand therefore is coordinated to three Cu(II) atoms *via* their N-1 nitrogens of the tetrazole rings and its two carboxylate oxygens. This correlated well with the observations seen in the IR spectrum of **5.15**. There was no coordination observed to the pyrazine and tetrazole nitrogens to form a chelate ring, which was somewhat surprising. However, this could be plausibly explained by the sterics of the system. When compared to the crystal structure of the ligand **5.4**, the coordination of Cu(II) has the effect of puckering both tetrazole rings. Therefore the N-1 substituted tetrazole is now less twisted with respect to the pyrazine ring and the N-2 substituted tetrazole is now more twisted with respect to the pyrazine ring when compared to free ligand **5.4**. However, the N-1 substituted ring is still more twisted relative to the N-2 substituted ring (torsion angles of 43.7(6)° and −40.7(6)° for N-2; −47.7(6)° and 50.2(6)° for N-1). The seven membered chelate ring formed is puckered due to this twisting. A fascinating structural feature of **5.15** are the clusters of acyclic hexanuclear H_2O molecules that are present in the asymmetric unit (Figure 5.19).

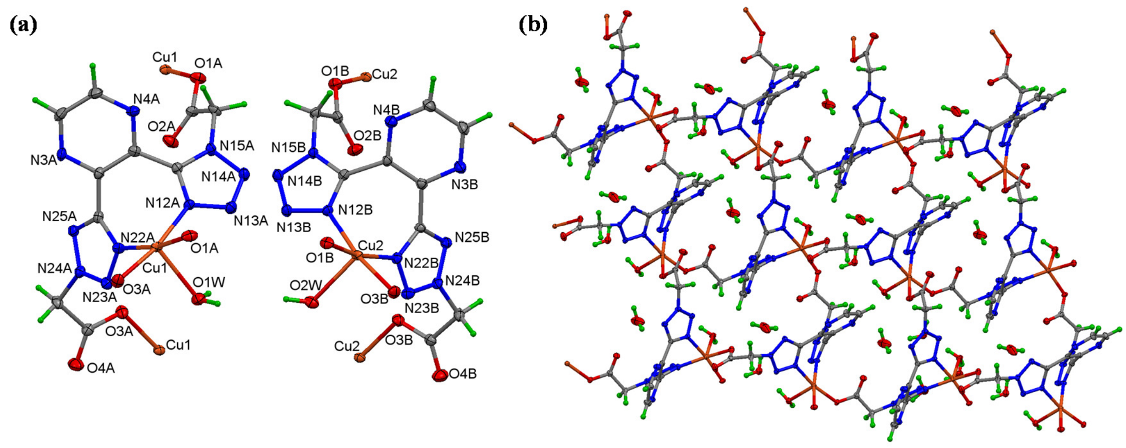

Figure 5.18: (a) Subunit of **5.15**, uncoordinated H_2O molecules omitted for clarity; (b) 2-D MOF with potential voids occupied by uncoordinated H_2O molecules.

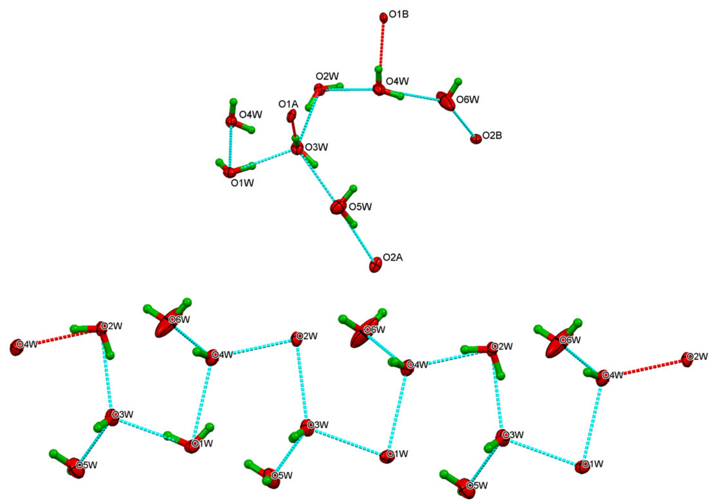

Figure 5.19: Hexameric H_2O cluster that is present in the asymmetric unit of **5.15** (top) and 1-D H_2O chain viewed along the *b*-axis (bottom).

O1W acts as both a hydrogen bond acceptor and donor, O2W acts as a double hydrogen bond donor (both O1W and O2W are also coordinated to Cu1 and Cu2 respectively), O3W and O4W acts as a double hydrogen bond donor and double hydrogen bond acceptor and O5W and O6W acts as a double hydrogen bond donor and acceptor. The O···O distances in the hexanuclear cluster fall in the range of 2.709(6)-2.833(6) Å with an average value of 2.763 Å, compared with 2.76 Å (−90 °C) in hexagonal ice or 2.74 Å in cubic ice.[237,238,239] This cluster is also stabilised in the network through O_{water}-H···$O_{carboxyl}$ hydrogen bonds. Throughout the 2-D coordination sheet, four crystallographically independent H_2O molecules (O1W, O2W, O3W, O4W) are hydrogen bonded to each other forming an infinite

H_2O chain with a curl conformation (Figure 5.19). The arrangement mode of the H_2O molecules within the chain can be described as ⋯O2W⋯O3W⋯O1W⋯O4W⋯. The overall $[(H_2O)_4]_n$ chain can be represented by C4, according to the H_2O cluster nomenclature described by Infantes and co-workers.[240,241] The literature relating to the structure of pure H_2O in both the solid and liquid state as well as in mixed-component systems, is extensive.[238] An improved understanding of the three-dimensional structural aspects of H_2O has important implications in the area of structural biology. Several examples have demonstrated the importance of H_2O structuring, including the structures of *Scapharca* dimeric haemoglobin,[242] actinidin[243] and carbonic anhydrase C.[244] There is much evidence that alludes to the presence of ordered H_2O clusters in the active clefts of these proteins, but unambiguous positional information is still rare. It is thought that H_2O molecules contribute to the complex stability by mediating hydrogen bonds between functional groups of the protein and the ligands, and by filling potential voids or holes inside the binding site.[245] Given the influence of H_2O on the structure and function of biological systems and its fundamental role in almost all branches of natural sciences it is not surprising that hydrogen bonded H_2O aggregates have received much attention. Accurate structural data of low dimensional H_2O structures is key in the elucidation of the complex interplay of biological, chemical and structural properties of H_2O, which is surprisingly still not fully understood. Coordination compounds, MOF structures, and suitable organic compounds can provide ideal void spaces to trap fractions of ice or other hydrogen bonded H_2O aggregates and these have been utilised to simulate H_2O crystallisation in restricted environments.[246] Over the years, such structures have been characterised and categorised;[240] examples include defined oligomeric H_2O aggregates $(H_2O)_n$ (n = 2-100),[239,247] 1-D chains or tapes[248] and 2-D layered structures.[249] The precise structural data and the cooperative association of the water cluster and crystal host in **5.15** may be helpful in improving our understanding of the contribution of water clusters to the stability and function of biological assemblies, as well as the anomalous properties of water.

Reaction of **5.5(pzbtza)** and $CuCl_2.2H_2O$ in aqueous NaOH resulted in the formation of pale blue block-like crystals on standing for 1 day. The crystals were analysed by IR spectroscopy, elemental analysis and X-ray crystallography. The IR spectrum of **5.16** indicated that there was no protonated carboxylate present. The presence of a $\nu_{asym}(COO^-)$ vibration at 1640 cm^{-1} with a corresponding $\nu_{sym}(COO^-)$ vibration positioned at 1380 cm^{-1} suggested that the deprotonated carboxylates were adopting a monodentate coordination to the metal centre. A broad stretch at 3050 cm^{-1} alluded to the presence of H_2O in the structure. Elemental analysis suggested a 1:1 metal to ligand ratio. The crystal structure of **5.16** reveals mononuclear subunits, with the Cu(II) ion in an axially distorted octahedral environment. Bond lengths between the Cu(II) ion and the axial water molecules are 2.32 and 2.56 Å for O1W and O2W, respectively. These lengths are in contrast to the equatorially coordinated ligands, with bond lengths of ~2.00 Å being observed. The equatorial plane of the octahedron is occupied by two tetrazole N-1 nitrogens from the same ligand, two carboxylate oxygens from two different ligands adopting a monodentate binding mode and two H_2O molecules which occupy the axial positions. The bonding arrangement leads to a 2-D coordination polymer, with each ligand bonded to three Cu(II) atoms (Figure 5.20).

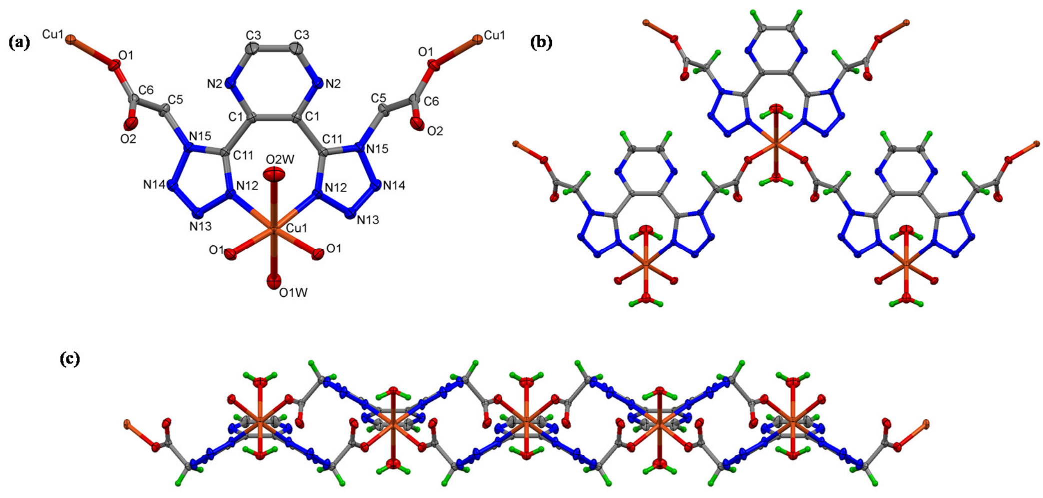

Figure 5.20: (a) Repeating unit of coordination polymer **5.16** viewed along the *b*-axis, hydrogen atoms omitted for clarity; (b) subsection of **5.16** viewed along *b*-axis; (c) view of propagation in **5.16** viewed along *c*-axis.

Each asymmetric unit extends in two directions forming a 2-D coordination layer, propagating along the crystallographic *a*- and *c*-axes. Despite the presence of coordinated H_2O molecules, there are no hydrogen bonds observed between the sheets, and no other significant interactions are present. Hydrogen bonding does exist between O2 and O1W and between O1 and O2W on the same 2-D sheet however. To describe the topology of **5.16**, the underlying net can be termed as having a 4-connected topology with the Cu(II) centre acting as a 4-coordinated node. This mode of bonding is schematically represented in Figure 5.21. The space surrounded by these nodes are filled by the pyrazine ring, however we believe that extending the length of the linker between the tetrazole ring and carboxyl group could expand these pores.

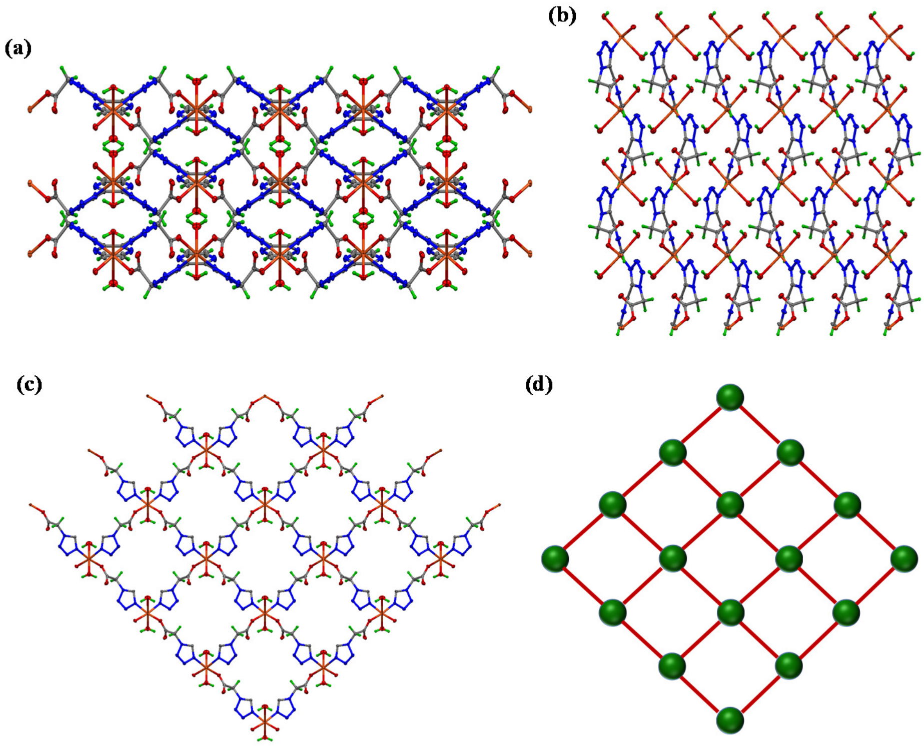

Figure 5.21: (a) Packing diagram viewed along *c*-axis showing 2-D sheets stacked on top of one another; (b) packing diagram viewed along *a*-axis, no interactions occur between the sheets; (c) perspective view of the 2-D network of **5.16** and (d) simplified schematic of 2-D topology of **5.16**. Pyrazine ring was omitted for clarity in (c) and (d).

5.3.3 EPR Studies

The X-band EPR spectra of **5.15** was measured in the solid state as a powder at room temperature. Figure 5.22 displays the EPR spectrum of **5.15**, which resembles an isotropic signal, where $g_x = g_y = g_z$. It was thought that this signal could have been overlapping with another signal, however it was proposed that the crystallinity of the sample could perturb the signal (samples were ground however crystalline particles always remained). The extracted g factor (2.191) was typical of a transition metal unpaired electron as it was much greater than the free electron g_e value.[176] An isotropic signal implies that the three principle axes are the same and on examination of the bond distances around the Cu(II) centres (which are all ~2 Å) this was observed to be in agreement with the crystal structure obtained.

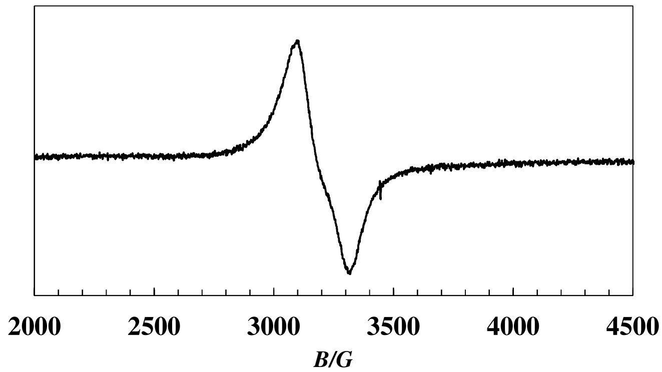

Figure 5.22: Room temperature 9.63 GHz EPR spectrum of a powder sample of **5.15**. $g_x = g_y = g_z = 2.19$.

5.4 Conclusions

In previous chapters, carboxylate functionalised pyridyl tetrazoles were employed in the synthesis of CPs with the result of forming 1-D CPs or isolated bimetallic units. The work outlined in this chapter aimed to increase the dimensionality of these polymers by utilising carboxylate functionalised bis-tetrazole systems. Furthermore, the bis-tetrazole ligands were linked *via* a rigid pyrazine ring or a flexible propyl chain backbone, allowing an examination of how flexibility of the backbone affects the final structures. Higher dimensionality was successfully achieved with 2-D coordination polymers being formed when the pyrazine bis-tetrazole systems were employed. The 2-D coordination polymer based on the asymmetric substituted pyrazine bis-tetrazole was further connected into a 3-D coordination network through hydrogen bonding between H_2O molecules. These H_2O molecules were connected as a 1-D chain thoughout the structure. H_2O aggregates in crystal hosts are gaining a lot of interest in recent years as they provide diverse environments in which to obtain precise structural information about the bonding properties of H_2O.

Elucidation of the CPs formed in experiments utilising trimethylene linked pyridyl tetrazoles proved difficult. Crystalline samples were difficult to obtain which hampered elucidation of the structures by X-ray crystallography. Despite microwave synthesis yielding similar results, we maintain that the use of alternative synthesis methods could alleviate these issues and yield crystalline products. Hence, future efforts will include the use of solvothermal synthesis. Although dramatic advancement has been made, research into CPs based on flexible ligands is still at an early stage of development. As previously stated, flexible ligands themselves can adopt different conformations with distinct symmetries as a consequence of rotations around single bonds during the self-assembly process, which greatly deters the ability to design and predict the form of extended network architectures. As the synthesis conditions such as reaction temperature, solvents, counteranions, organic templates, pH *etc.* can influence the conformations of flexible ligands and therefore the final structures, a high degree of predictability must be integrated prior to synthesis. Further research efforts are indispensable to fully understand the structural features and the structure-property relationship in framework materials, in order to establish reliable strategies for the design and synthesis of targeted flexible based CPs.

Further future work involves incorporating higher dimensionality into the frameworks thereby forming 3-D frameworks which would possess potential voids. One possible way this could be achieved is through the use of a mixed linker approach which has been proven to be successful in obtaining porous frameworks. Hence, we intend on adding 4,4'-bipyridine as it is an excellent bridging ligand and could be capable of connecting the 2-D coordination sheets synthesised in this chapter *via* coordination to two Cu(II) atoms on two separate sheets. In addition, elongation of the linkages between the carboxylate and tetrazole ring will be carried out with the aim of extending the pore sizes in the frameworks.

5.5 Experimental

5.5.1 Instrumentation

^{1}H and ^{13}C NMR (δ ppm; J Hz) spectra were recorded on a Bruker Avance 300 MHz NMR spectrometer using saturated $CDCl_3$ or d_6-DMSO solutions with a $SiMe_4$ reference, with resolutions of 0.18 Hz and 0.01 ppm, respectively. Infrared spectra (cm^{-1}) were recorded as KBr discs or liquid films between NaCl plates using a Perkin Elmer System 2000 FT-IR spectrometer. Solution UV-Vis spectra were recorded using HPLC grade solvents using a Unicam UV 540 spectrometer. Melting point analyses were carried out using a Stewart Scientific SMP 1 melting point apparatus and are uncorrected. Electrospray (ESI) mass spectra were collected on an Agilent Technologies 6410 Time of Flight LC/MS. Compounds were dissolved in acetonitrile:water (1:1) solutions containing 0.1% formic acid, unless otherwise stated. The interpretation of mass spectra was made with the help of the program "Agilent Masshunter Workstation Software". Magnetic susceptibility measurements were carried out at room temperature using a Johnson Matthey Magnetic Susceptibility Balance with $[HgCo(SCN)_4]$ as reference. EPR spectra were recorded on a Bruker Elexsys E500 spectrometer, operated at the X-band and equipped with an Oxford Instruments cryostat. Microanalyses were carried out at the Microanalytical Laboratory of the National University of Ireland Maynooth, using a Thermo Finnigan Elementary Analyzer Flash EA 1112. The results were analysed using Eager 300 software. All crystal structures resulting from this work were solved by Dr. John Gallagher (Dublin City University) using an Oxford Diffraction Gemini-S Ultra diffractometer at 294(1) K. Structures were solved using the SHELXS97 direct methods program. Molecular diagrams were generated using Mercury software. Starting materials were commercially obtained and used without further purification. Solvents used were of HPLC grade.

Caution! *Nitrogen-rich compounds such as tetrazole derivatives are used as components for explosive mixtures. In our laboratory, the reactions described were run on a few gram scale, and no problems were encountered. However, great caution should be exercised when heating or handling compounds of this type.*

5.5.2 Synthesis of Flexible Bis-Tetrazole Ligands 5.1, 5.2 and 5.3

5.5.2.1 1,3-bis(4-pyridyl)propane-N,N'-dioxide (5.8)

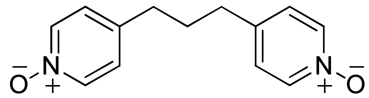

A mixture of 4,4'-trimethylenedipyridine (6.00 g, 30.30 mmol), acetic acid (24 mL), and 35% H_2O_2 (12 mL) was heated at 70–80 °C for 3 h. An additional portion of H_2O_2 (9 mL) was added and heating was continued for a further 9 h. The excess acetic acid and H_2O were removed under reduced pressure. H_2O (12 mL) was introduced, and the mixture was concentrated to dryness under vacuum. Acetone (90 mL) was added to the remaining oil to yield a white precipitate, which was filtered off and washed twice with hot acetone to remove unreacted 4,4'-trimethylenedipyridine. The crude product was recrystallised in EtOH to give 5.22 g of ligand (75% yield). m.p. 220-223 °C. IR (KBr): ν = 3089, 3005, 1501, 1486, 1459, 1412, 1254, 1230, 1200, 1170, 1112, 1043, 890, 864, 812, 761, 576 cm^{-1}. ^{1}H NMR (d_6-DMSO): δ = 8.11 (d, 4 H, J = 6.7 Hz, pyr-H), 7.27 (d, 4 H, J = 6.7 Hz, pyr-H), 2.58 (t, 4 H, J = 7.6 Hz, pyr-CH_2), 1.86 (quin, 2 H, J = 7.6 Hz, CH_2) ppm. ^{13}C NMR (d_6-DMSO): δ = 139.8 (pyr-C), 138.2 (pyr-CH), 126.3 (pyr-CH), 32.6 (pyr-CH_2), 30.0 (CH_2) ppm. ESI-HRMS: calcd. for $C_{13}H_{15}N_2O_2$ $[M+H]^+$ 231.1128, found 231.1133.

The NMR and IR data are in agreement with the reported values.[233]

5.5.2.2 1,3-bis(4-pyridyl-3-cyano)propane (5.9)

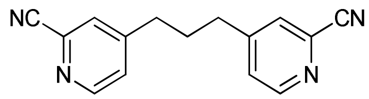

To a suspension of **5.8** (0.20 g, 0.87 mmol) in anhydrous DMF (20 mL) was added $Zn(CN)_2$ (0.31 g, 2.61 mmol). The mixture was stirred at room temperature under argon for 30 min before DMCC (0.32 mL, 3.47 mmol) was added dropwise at 0 °C over 1 h. The reaction was then brought up to room temperature and stirred for 24 h. 10% aqueous K_2CO_3 (10 mL) was added to the solution and stirred for 15 min. The solution was then extracted with DCM (3 × 10 mL) and the combined organic extracts were washed with brine and dried over $MgSO_4$. After removing the insoluble solids by filtration the volatiles were removed under reduced pressure to yield a brown oil. This crude product was passed through a silica plug using EtOAc and Pet. Ether (3:1) as the eluent and recrystallised from a mixture of DCM and Pet. Ether to yield a white crystalline solid (0.07 g, 34%). m.p. 120-122 °C. IR (KBr): ν = 3030, 2921, 2237, 1597, 1552, 1462, 1405, 1384, 1261, 1147, 1086, 1069, 1022, 991, 902, 840, 758 cm^{-1}. ^{1}H NMR ($CDCl_3$): δ = 8.63 (d, 2 H, J = 5.0 Hz, pyr-H), 7.54 (s, 2 H, pyr-H), 7.34 (d, 2 H, J = 5.0 Hz, pyr-H), 2.75 (t, 4 H, J = 7.8 Hz, pyr-CH_2), 2.03 (quin, 2 H, J = 7.8 Hz, CH_2) ppm. ^{13}C NMR ($CDCl_3$): δ = 151.6, 151.2, 134.2, 128.5, 126.8, 117.2 (CN), 34.2 (pyr-CH_2), 30.1 (CH_2) ppm. ESI-HRMS: calcd. for $C_{15}H_{13}N_4$ $[M+H]^+$ 249.1135, found 249.1140.

The NMR and IR data are in agreement with the reported literature values.[232]

5.5.2.3 1,3-bis(2-(2*H*-tetrazol-5-yl)pyridin-4-yl)propane (5.10)

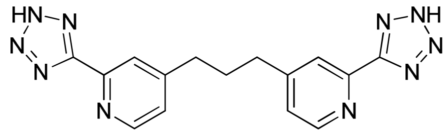

5.9 (0.83 g, 3.34 mmol), NaN_3 (0.48 g, 7.35 mmol), NH_4Cl (0.39 g, 7.35 mmol) and LiCl (0.07 g, 1.67 mmol) were heated to reflux in DMF (20 mL) for 10 h. The inorganic solids were removed by filtration and the filtrate was concentrated under reduced pressure. The residue was then redissolved in deionised H_2O (20 mL) and acidified with 1 M HCl until precipitation ceased. The precipitate was filtered off and washed with deionised H_2O and air dried. Yellow solid (1.04 g, 93%). m.p. 220-223 °C. IR (KBr): ν = 3386, 3042, 2874, 2777, 1597, 1633, 1613, 1562, 1493, 1484, 1406, 1384, 1261, 1149, 1086, 1069, 1024, 1000, 846, 760 cm^{-1}. ^{1}H NMR (d_6-DMSO): δ = 8.66 (d, 2 H, J = 5.1 Hz, pyr-H), 8.09 (s, 2 H, pyr-H), 7.50 (d, 2 H, J = 5.1 Hz, pyr-H), 2.81 (t, 4 H, J = 7.8 Hz, pyr-CH_2), 2.03 (quin, 2 H, J = 7.8 Hz, CH_2) ppm. ^{13}C NMR (d_6-DMSO): δ = 154.9 (CN_4), 152.9, 149.8, 143.7, 126.0, 122.5, 33.7 (pyr-CH_2), 29.9 (CH_2) ppm. ESI-HRMS: calcd. for $C_{15}H_{15}N_{10}$ $[M+H]^+$ 335.1476, found 335.1476.

5.5.2.4 Synthesis of 5.1, 5.2 and 5.3

5.10 (0.90 g, 2.69 mmol) and K_2CO_3 (0.78 g, 5.66 mmol) were heated to reflux for 30 min after which time ethyl bromoacetate (0.62 mL, 6.66 mmol) was added. The reaction was then further heated under reflux for 24 h. The solution was then cooled and filtered and the filtrate was concentrated under reduced pressure. The remaining brown oil consisted of three regioisomers which were separated by column chromatography, starting with 2:1 EtOAc:Pet. Ether and finishing with 100% EtOAc.

5.5.2.4.1 Diethyl 2,2'-(5,5'-(4,4'-(propane-1,3-diyl)bis(pyridine-4,2-diyl))bis(1*H*-tetrazole-5,1-diyl))diacetate (5.1)

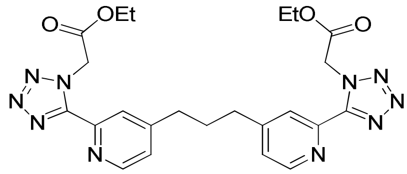

Yellow solid (0.14 g, 10%). m.p. 116-119 °C. IR (KBr): ν = 2989, 2960, 1748, 1603, 1537, 1479, 1462, 1431, 1403, 1379, 1298, 1230, 1118, 1030, 993, 852 cm^{-1}. ^{1}H NMR ($CDCl_3$): δ = 8.54 (d, 2 H, *J* = 5.0 Hz, pyr-H), 8.27 (s, 2 H, pyr-H), 7.26 (d, 2 H, *J* = 5.0 Hz, pyr-H), 5.74 (s, 4 H, CH_2-tet), 4.20 (q, 4 H, *J* = 7.1 Hz, OCH_2), 2.80 (t, 4 H, *J* = 7.7 Hz, pyr-CH_2), 2.11 (quin, 2 H, *J* = 7.7 Hz, CH_2), 1.20 (t, 6 H, *J* = 7.1 Hz, CH_3) ppm. ^{13}C NMR ($CDCl_3$): δ = 166.0 (C=O), 152.2 (pyr-C), 152.2 (CN_4), 149.3 (pyr-CH), 144.5 (C-CN_4), 125.6 (pyr-CH), 124.0 (pyr-CH), 62.1 (OCH_2), 51.1 (tet-CH_2), 34.5 (pyr-CH_2), 30.3 (CH_2), 14.0 (CH_3) ppm. ESI-HRMS: calcd. for $C_{23}H_{27}N_{10}O_4$ $[M+H]^+$ 507.2211, found 507.2232.

5.5.2.4.2 Ethyl 2-(5-(4-(3-(2-(1-(2-ethoxy-2-oxoethyl)-1*H*-tetrazol-5-yl)pyridin-4-yl)propyl)pyridin-2-yl)-2*H*-tetrazol-2-yl)acetate (5.2)

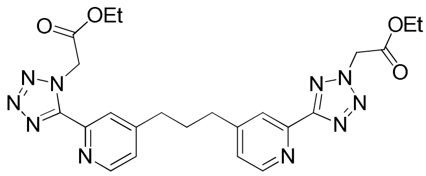

Yellow solid (0.21 g, 16%). m.p. 58-60 °C. IR (KBr): ν = 2930, 1750, 1733, 1606, 1560, 1430, 1387, 1223, 1118, 1025, 854, 793 cm^{-1}. ^{1}H NMR ($CDCl_3$): δ = 8.68 (d, 1 H, *J* = 4.8 Hz, pyr-H), 8.54 (d, 1 H, *J* = 5.1 Hz, pyr-H), 8.29 (s, 1 H, pyr-H), 8.11 (s, 1 H, pyr-H), 7.24-7.27 (m, 2 H, pyr-H), 5.74 (s, 2 H, tet-CH_2), 5.50 (s, 2 H, tet-CH_2), 4.28 (q, 2 H, 7.2 Hz, OCH_2), 4.19 (q, 2 H, 7.2 Hz, OCH_2), 2.77-2.82 (m, 4 H, pyr-CH_2), 2.07-2.17 (m, 2 H, CH_2), 1.29 (t, 3 H, *J* = 7.2 Hz, CH_3), 1.19 (t, 3 H, *J* = 7.2 Hz, CH_3) ppm. ^{13}C NMR ($CDCl_3$): δ = 165.0, 164.1, 163.8, 151.4, 151.2, 150.6, 149.4 (pyr-CH), 148.2 (pyr-CH), 145.5, 143.4, 124.6 (pyr-CH), 124.1 (pyr-CH), 123.0 (pyr-CH), 121.5 (pyr-CH), 61.7 (OCH_2), 61.0 (OCH_2), 52.5 (tet-CH_2), 50.1 (tet-CH_2), 33.5 (pyr-CH_2), 29.3 (CH_2), 13.1 (CH_3) ppm. ESI-HRMS: calcd for $C_{23}H_{27}N_{10}O_4$ $[M+H]^+$ 507.2211, found 507.2229.

5.5.2.4.3 Diethyl 2,2'-(5,5'-(4,4'-(propane-1,3-diyl)bis(pyridine-4,2-diyl))bis(2*H*-tetrazole-5,2-diyl))diacetate (5.3)

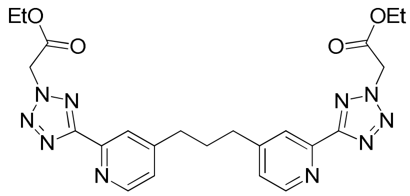

Orange solid (0.38 g, 28%). m.p. 138-141 °C. IR (KBr): ν = 2999, 2956, 1743, 1632, 1607, 1559, 1523, 1479, 1419, 1387, 1370, 1348, 1222, 1053, 1021, 994, 840 cm^{-1}. ^{1}H NMR ($CDCl_3$): δ = 8.68 (d, 2 H, J = 5.1 Hz, pyr-H), 8.13 (s, 2 H, pyr-H), 7.24 (d, 2 H, J = 5.1 Hz, pyr-H), 5.50 (s, 4 H, CH_2-tet), 4.28 (q, 4 H, J = 7.1 Hz, OCH_2), 2.80 (t, 4 H, J = 7.7 Hz, pyr-CH_2), 2.13 (quin, 2 H, J = 7.7 Hz, CH_2), 1.28 (t, 6 H, J = 7.1 Hz, CH_3) ppm. ^{13}C NMR ($CDCl_3$): δ = 165.0 (C=O), 164.8 (CN_4), 151.8 (pyr-C), 150.4 (pyr-CH), 146.5 (C-CN_4), 125.1 (pyr-CH), 122.6 (pyr-CH), 62.8 (OCH_2), 53.5 (tet-CH_2), 34.6 (pyr-CH_2), 30.5 (CH_2), 14.0 (CH_3) ppm. ESI-HRMS: calcd. for $C_{23}H_{27}N_{10}O_4$ $[M+H]^+$ 507.2211, found 507.2198.

5.5.3 Synthesis of Rigid Bis-Tetrazole Ligands 5.4, 5.5 and 5.6

5.5.3.1 2,3-bis(1*H*-tetrazol-5-yl)pyrazine (5.12)

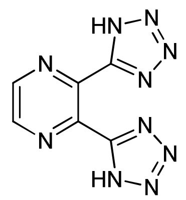

NaN_3 (0.52 g, 8.07 mmol), NH_4Cl (0.43 g, 8.07 mmol) and LiCl (0.08 g, 1.88 mmol) were added to a solution of 2,3-dicyanopyrazine (0.50 g, 3.84 mmol) in anhydrous DMF (20 mL). The suspension was then heated at 110 °C for 12 h, cooled to room temperature and filtered. The filtrate was then concentrated under reduced pressure. The residue was then dissolved in deionised H_2O (20 mL) and acidified with conc. HCl until precipitation initiated. The solids were then filtered off, washed with H_2O and dried. The solid was recrystallised from hot EtOH to yield an orange crystalline solid (0.56 g, 67%). IR (KBr): ν = 3418, 2828, 2855, 1651, 1601, 1452, 1278 cm^{-1}. ^{1}H NMR (d_6-DMSO): δ = 9.11 (s, 2 H, pyz-H), 3.56 (s, 2 H, NH) ppm. ^{13}C NMR (d_6-DMSO): δ = 153.3 (CN_4), 146.1, 139.8 ppm. ESI-HRMS: calcd. for $C_6H_5N_{10}$ $[M+H]^+$ 217.0693, found 217.0698.

5.5.3.2 Synthesis of 5.4, 5.5 and 5.6

DIEA (8.46 mL, 48.60 mmol) was added to a suspension of **5.12** (3.50 g, 16.20 mmol) in MeCN (20 mL) and the solution was heated to reflux for 1 h. After this time, ethyl bromoacetate (3.95 mL, 35.64 mmol) was added and the reaction was further heated to reflux for 24 h. The orange solution was then cooled to room temperature and concentrated under reduced pressure. The residue was then redissolved in DCM (30 mL), washed with water (3 × 15 mL) and the organic extracts were dried over $MgSO_4$. The volatiles were removed under reduced pressure. The three regioisomers were separated by recrystallisation of the residue in $CHCl_3$, Pet. Ether and MeOH. Sequential filtration of the filtrate over time yielded the three purified products.

5.5.3.2.1 Ethyl 2-(5-(3-(1-(2-ethoxy-2-oxoethyl)-1*H*-tetrazol-5-yl)pyrazin-2-yl)-2*H*-tetrazol-2-yl)acetate (5.4)

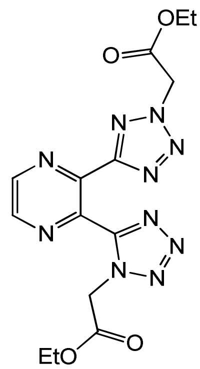

White block crystals (1.46 g, 23%). IR (KBr): ν = 2997, 2953, 1757, 1745, 1470, 1443, 1417, 1406, 1373, 1350, 1300, 1276, 1249, 1220, 1154, 1101, 1023, 1014, 993, 892, 881, 808 cm^{-1}. ^1H NMR ($CDCl_3$): δ = 8.94 (d, 1 H, J = 2.3 Hz, pyz-H), 8.80 (d, 1 H, J = 2.3 Hz, pyz-H), 5.49 (s, 2 H, CH_2-tet), 5.47 (s, 2 H, CH_2-tet), 4.29 (q, 2 H, J = 7.2 Hz, OCH_2), 4.19 (q, 2 H, J = 7.2 Hz, OCH_2), 1.30 (t, 3 H, J = 7.2 Hz, CH_3), 1.20 (t, 3 H, J = 7.2 Hz, CH_3) ppm. ^{13}C NMR ($CDCl_3$): δ = 165.1 (C=O), 164.5 (C=O), 162.1, 150.8, 145.5, 144.1, 143.3, 139.9, 62.9, 62.6, 53.7, 49.9, 13.9 ppm. ESI-HRMS: calcd. for $C_{14}H_{17}N_{10}O_4$ $[M+H]^+$ 389.1429, found 389.1416.

5.5.3.2.2 Diethyl 2,2'-(5,5'-(pyrazine-2,3-diyl)bis(1*H*-tetrazole-5,1-diyl))diacetate (5.5)

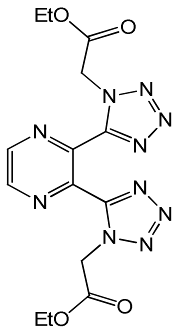

White needle like crystals (0.64 g, 10%). IR (KBr): ν = 2943, 1750, 1634, 1466, 1440, 1418, 1396, 1376, 1264, 1231, 1147, 1094, 1031, 884, 799, 772 cm^{-1}. ^{1}H NMR ($CDCl_3$): δ = 8.85 (s, 2 H, pyz-H), 5.47 (s, 4 H, CH_2-tet), 4.21 (q, 4 H, J = 7.2 Hz, OCH_2), 1.23 (t, 6 H, J = 7.2 Hz, CH_3) ppm. ^{13}C NMR ($CDCl_3$): δ = 165.1 (C=O), 150.5 (CN_4), 144.7, 140.9, 148.9, 62.7 (CH_2-tet), 49.9 (OCH_2), 14.0 (CH_3) ppm. ESI-HRMS: calcd. for $C_{14}H_{17}N_{10}O_4$ $[M+H]^+$ 389.1429, found 389.1434.

5.5.3.2.3 Diethyl 2,2'-(5,5'-(pyrazine-2,3-diyl)bis(2*H*-tetrazole-5,2-diyl))diacetate (5.6)

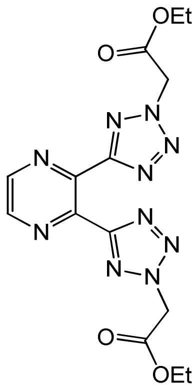

White needle like crystals (0.55 g, 9%). IR (KBr): ν = 2980, 1745, 1416. 1371, 1341, 1233, 1075, 1017, 876 cm^{-1}. ^{1}H NMR ($CDCl_3$): δ = 8.90 (s, 2 H, pyz-H), 5.46 (s, 4 H, CH_2-tet), 4.27 (q, 4 H, J = 7.1 Hz, OCH_2), 1.29 (t, 6 H, J = 7.1 Hz, CH_3) ppm. ^{13}C NMR ($CDCl_3$): δ = 164.6 (C=O), 162.6 (CN_4), 145.0, 142.4, 62.8 (CH_2-tet), 53.5 (OCH_2), 14.0 (CH_3) ppm. ESI-HRMS: calcd. for $C_{14}H_{17}N_{10}O_4$ $[M+H]^+$ 389.1429, found 389.1438.

5.5.4 Metal Complexation Reactions with 5.1 and 5.2

5.5.4.1 [Cu(5.1)Cl_2]$_n$ (5.13)

5.1 (0.04 g, 0.08 mmol) was dissolved in EtOH (15 mL). $CuCl_2.2H_2O$ (0.01 g, 0.08 mmol) in EtOH (5 mL) was added to the solution. The resulting mixture was heated to reflux for 2 h, cooled to room temperature and filtered. Green solid (0.03 g, 59%). $C_{23}H_{26}Cl_2CuN_{10}O_4$: calcd. C 43.10, H 4.09, N 21.85%; found C 43.85, H 4.11, N 21.99%. IR (KBr): ν = 3414, 2961, 1747, 1637, 1622, 1554, 1481, 1490, 1459, 1430, 1401, 1376, 1342, 1296, 1249, 1219, 1116, 1013, 867, 852, 623 cm^{-1}. Magnetic moment: 1.92 B.M.

5.5.4.2 [Cu_2(5.2)Cl_4]$_n$ (5.14)

5.2 (0.10 g, 0.20 mmol) was dissolved in EtOH (20 mL). $CuCl_2.2H_2O$ (0.03 g, 0.20 mmol) in EtOH (5 mL) was added to the solution. The resulting mixture was heated to reflux for 2 h, cooled to room temperature and filtered. Green solid (0.07 g, 92%). $C_{23}H_{26}Cl_4Cu_2N_{10}O_4$: calcd. C 35.63 , H 3.38, N 18.06%; found C 35.98, H 3.69, N 18.09%. IR (KBr): ν = 3440, 2982, 2938, 1750, 1622, 1565, 1475, 1440, 1397, 1372, 1347, 1262, 1220, 1063, 1019, 874, 853, 771, 580 cm^{-1}. Magnetic moment: 1.78 B.M.

5.5.5 Metal Complexation Reactions of 5.4 and 5.5

5.5.5.1 [Cu(5.4)(H_2O)$_2$]$_n$ (5.15)

5.4 (0.10 g, 0.26 mmol) was suspended in deionised H_2O (15 mL). NaOH (0.02 g, 0.52 mmol) was added and the mixture was heated under reflux for 2 h. $CuCl_2.2H_2O$ (0.04 g, 0.26 mmol) was added in deionised H_2O and the solution was cooled slowly and allowed to stand for several days. The resulting solids were filtered off and washed with deionised H_2O. Blue crystalline solid (0.07 g, 60%). $C_{10}H_8CuN_{10}O_5.2H_2O$: calcd. C 26.82, H 2.70, N 31.28%; found C 26.59, H 2.66, N 31.48%. IR (KBr): ν = 3419, 3001, 1660, 1636, 1480, 1433, 1377, 1353, 1328, 1305, 1216, 1176, 1108, 1087, 1032, 879, 821, 751, 718, 691, 547 cm^{-1}. Magnetic moment: 1.96 B.M.

5.5.5.2 [Cu(5.5)(H_2O)$_2$]$_n$ (5.16)

5.5 (0.03 g, 0.08 mmol) was suspended in deionised H_2O (6 mL). NaOH (6 mg, 0.16 mmol) was added to the mixture and the reaction was heated under reflux for 2 h. $CuCl_2.2H_2O$ (0.03 g, 0.16 mmol) in deionised H_2O was added to the solution which was then cooled slowly. A blue crystalline solid formed (0.02 g, 49%) which was filtered off and washed with deionised H_2O. $C_{10}H_6CuN_{10}O_4.2H_2O$: calcd. C 27.95, H 2.35, N 32.59%; found C 28.24, H

3.03, N 32.08%. IR (KBr): ν = 3524, 3050, 1640, 1452, 1422, 1380, 1304, 1149, 1125, 1101, 1032, 955, 889, 955, 889, 819, 718, 682, 590, 553, 454, 384 cm^{-1}. Magnetic Moment: 2.11 B.M.

Chapter 6: Conclusions and Future Work

6.1 Conclusions

This thesis comprises a collection of molecular assemblies based on heteroaryl tetrazole ligands. To address the first goal of the work carried out in this thesis, the synthesis and characterisation of an array of novel ligands were described. The synthesis of these ligands was facile; an aspect which is useful as easy access to a huge library of derivatives is key in the efficient determination of structure-activity relationships. All ligands were subjected to complexation reactions resulting in the formation and characterisation of novel coordination complexes. Copper(II), nickel(II), zinc(II) and cobalt(II) metal salts were employed in these complexation reactions. These complexes were prepared in moderate to good yields and remained stable for an extended period. *In vivo* toxicity studies in *G. mellonella* larvae on two complexes which showed promising anti-cancer activity revealed a high tolerance to the complexes, which is a promising result considering the positive correlations between *G. mellonella* larvae studies and mammalian studies in mice. These complexes and free ligands are intended to be investigated further for their anti-cancer activities through the US National Cancer Institute which will yield useful information on their mechanisms of action and will contribute to the direction of future efforts in the area of cancer chemotherapy.

In Chapter 3, the pyridyl tetrazole chelating unit was exploited further, in the production of coordination networks and coordination polymers. This was achieved by substituting the tetrazole ring with an ethyl ester group, which was capable of forming a carboxylate *in situ*, which prevented the ligand from behaving as a terminal coordinating ligand and allowed it to act as a bridging ligand. These derivatives were reacted with copper(II), zinc(II), nickel(II) and cobalt(II) metal salts in different ratios of water methanol solutions. This work produced X-ray crystal structures of products obtained in copper (II) chloride reactions. This analysis revealed that solvent composition was an important parameter as 1-D extended structures were obtained in solutions with a higher percentage of methanol, and coordination networks and dinuclear clusters were obtained in the cases where water was employed as reaction solvent with Cu(II) pyridyl tetrazole subunits hydrogen bonding to neighbouring subunits. The position of the ester group on the tetrazole ring also had an effect on the final structures. The ligands acted as either bridging linkers with coordination occurring through both nitrogens and carboxylate oxygens (**3.10**, **3.11**) or terminal ligands coordinating through either nitrogens only (**3.13**) or carboxylate oxygens only (**3.11**). This work also resulted in the formation of Zn(II) coordination polymers and discrete complexes which were subjected to solid state fluorescence studies. This demonstrated the potential for the use of these products and their derivatives as light emitting materials. Overall, we showed that carboxylate functionalised pyridyl tetrazole derivatives were useful as bridging ligands in coordination polymers. However, improvements to these linkers were required as in some cases the ligand was acting as a terminal ligand and thus prevented the extension of the frameworks and the opportunity to obtain higher dimensional structures.

Chapter 4 attempted to address these issues by synthesising ligands with an *in situ* generated carboxylate moiety on both the tetrazole and pyridine rings. This was proposed to enhance the ligands' ability to extend in three directions, thereby forming 3-D extended structures. Although we were unsuccessful in producing coordination polymers of high dimensionality, our investigations have led to the production of four novel 1-D coordination polymers and three dinuclear cluster formations. These products are structurally very interesting. The structural formations were affected by the position of the carboxylate group on the tetrazole ring, with extended structures being formed when using the N-1 substituted ligand and dinuclear clusters forming as a result of employing the N-2 substituted ligand. The choice of metal ion did not seem to have any effect on the final structures as isomorphic structures were obtained when using either of the ligands. The presence of an uncomplexed ionic carboxylate was detrimental in terms of forming higher dimensional structures, however this structural aspect does open avenues of carrying out post-synthetic modifications on the products. The ligands also displayed a high capacity for manipulation, as employing a harder metal ion (Mn(II)) coordinated to this free carboxylate group but left the alternate tetrazole carboxylate coordinatively free. This study also presented a different mode of carboxylate binding (bridging) that was not encountered up to this point in these investigations. The scope for manipulation was also demonstrated in the selective hydrolysis of the alkyl ester over the aromatic ester. The 1-D coordination polymer synthesised in this investigation again provides scope for covalent post-synthetic modifications. Therefore, the manipulation of these interesting structural aspects could provide an interesting topic of study in future explorations. The behaviour of these ligands also displayed a striking resemblance to bipy dicarboxylic derivatives. Thus, the novel building units reported in this work could provide analogs to the ubiquitous bipy molecules and comparative studies on the properties of the resulting frameworks could yield interesting results.

The theme of attempting to form high dimensional coordination polymers was continued in Chapter 5, with bis-tetrazole systems being considered as potential linkers in the formation of frameworks with potential voids. Carboxylate functionalised pyridyl tetrazole units (like those discussed in Chapter 3) were linked by a trimethylene chain through the pyridine moieties. These were then reacted with metal salts in both the ester and carboxylate forms. These studies led to the formation of polymeric materials that were in the form of amorphous powders. The difficulty in attaining X-ray quality crystals hampered the accurate structural assignment of these products, which theoretically could produce a variety of products due to the conformational freedom of the starting ligands. Future work would involve the employment of different synthetic methods in order to obtain crystalline products. This is an area worthy of further investigation as the power of flexible based coordination polymers have only begun to be harnessed and promise a wealth of applications. The utilisation of rigidly linked tetrazole rings in coordination polymer synthesis yielded interesting results. Synthesis of the pyrazine linked carboxylate functionalised tetrazoles was easily achieved, however clean separation of the regioisomers was a laborious task. In contrast to the flexible ligands discussed above, the reaction of two of these regioisomers with copper(II) chloride in aqueous sodium hydroxide solution yielded blue crystalline products which were suitable for X-ray crystallography. The use of these ligands achieved our aim of obtaining higher dimensional extended frameworks, with 2-D coordination polymers forming. We reported the formation of a coordination polymer that exhibited an interesting pocket where water clusters resided (**5.15**). The topic of stabilised water clusters continuously generates considerable interest among both theoretical and experimental chemists. Crystal lattice host environments such as those provided by MOFs are increasingly being exploited for quantitative characterisation of the hydrogen bonded networks that exist in aqueous solution. These hydrophilic environments also raise the possibility of encapsulation of biomolecules. A proof of concept could be achieved by encapsulating a simple sugar molecule or polar amino acid into the hydrophilic pockets. The motivation behind the increased interest in encapsulating biomolecules is the desire to control the functions, properties and the stability of the trapped molecules.

In addition to the previously mentioned opportunities for future development, the addition of secondary ligands in the synthesis of these frameworks, such as 4,4'-bipyridine, could lead to connection of the layers, thereby forming 3-D architectures. The use of the free tetrazole derivatives synthesised in this work as organic linkers also offers an attractive and under investigated avenue of research.

In summary, a small contribution to the fields of medicinal chemistry and coordination polymers has been achieved. We have proven that heteroaryl tetrazole ligands are extremely useful and versatile in the construction of discrete and extended molecular aggregates.

References

1. V. A. Ostrovskii, R. E. Trifonov and E. A. Popova, *Russ. Chem. Bull.*, 2012, **61**, 768-780.
2. J. J. Sabatini and J. D. Moretti, *Chem. Eur. J.*, 2013, **19**, 12839-12845.
3. J. J. Sabatini, A. V. Nagori, G. Chen, P. Chu, R. Damavarapu and T. M. Klapötke, *Chem. Eur. J.*, 2012, **18**, 628-631.
4. K. Chauhan, P. Singh, V. Kumar, P. K. Shukla, M. I. Siddiqi and P. M. S. Chauhan, *Eur. J. Med. Chem.*, 2014, **78**, 442-454; D. Habibi, P. Rahmani, F. Ahmadi, H. Bokharaei and Z. Kaboudvand, *Lett. Org. Chem.*, 2014, **11**, 145-151; A. T. Nguyen-Trung, D. Tritsch, C. Grosdemange-Billiard and M. Rohmer, *Biorg. Med. Chem. Lett.*, 2013, **23**, 1643-1647; R. K. Pal, H. Yasmin, L. Nahar, B. K. Datta, A. K. A. Chowdhury, J. K. Kundu, S. C. Bachar and S. D. Sarker, *Med. Chem.*, 2012, **8**, 874-882; J. Demnitz and S. Jorgensen, WO2014001363A1, 2014.
5. C. Hansch and A. Leo, *Exploring QSAR*, American Chemical Society, Washington, D.C., 1995.
6. C. Liljebris, S. D. Larsen, D. Ogg, B. J. Palazuk and J. E. Bleasdale, *J. Med. Chem.*, 2002, **45**, 1785-1798.
7. M. Malik, M. Wani, S. Al-Thabaiti and R. Shiekh, *J. Incl. Phenom. Macrocycl. Chem.*, 2014, **78**, 15-37.
8. D. J. Carini, J. V. Duncia, P. E. Aldrich, A. T. Chiu, A. L. Johnson, M. E. Pierce, W. A. Price, J. B. Santella and G. J. Wells, *J. Med. Chem.*, 1991, **34**, 2525-2547.
9. R. J. Herr, *Biorg. Med. Chem.*, 2002, **10**, 3379-3393.
10. J. A. Bladin, *Ber. Dtsch. Chem. Ges.*, 1885, **18**, 1544-1551.
11. F. R. Benson, *Chem. Rev.*, 1947, **41**, 1-61.
12. A. Hantzsch and A. Vagt, *Liebigs Ann. Chem.*, 1901, **314**, 339-369.
13. O. Dimroth and G. Fester, *Ber. Dtsch. Chem. Ges.*, 1910, **43**, 2219-2223.
14. J. S. Mihina and R. M. Herbst, *J. Org. Chem.*, 1950, **15**, 1082-1092; R. M. Herbst and K. R. Wilson, *J. Org. Chem.*, 1957, **22**, 1142-1145.
15. W. G. Finnegan, R. A. Henry and R. Lofquist, *J. Am. Chem. Soc.*, 1958, **80**, 3908-3911.
16. J. Roh, K. Vávrová and A. Hrabálek, *Eur. J. Org. Chem.*, 2012, **2012**, 6101-6118.
17. M. R. Rosana, Y. Tao, A. E. Stiegman and G. B. Dudley, *Chem. Sci.*, 2012, **3**, 1240-1244; C. O. Kappe, B. Pieber and D. Dallinger, *Angew. Chem. Int. Ed.*, 2013, **52**, 1088-1094; G. B. Dudley, A. E. Stiegman and M. R. Rosana, *Angew. Chem. Int. Ed.*, 2013, **52**, 7918-7923; C. O. Kappe, *Angew. Chem. Int. Ed.*, 2013, **52**, 7924-7928.
18. M. Alterman and A. Hallberg, *J. Org. Chem.*, 2000, **65**, 7984-7989.
19. K. Koguro, T. Oga, S. Mitsui and R. Orita, *Synthesis*, 1998, **1998**, 910-914.
20. J. Roh, T. V. Artamonova, K. Vávrová, G. I. Koldobskii and A. Hrabálek, *Synthesis*, 2009, **2009**, 2175-2178.
21. F. Himo, Z. P. Demko, L. Noodleman and K. B. Sharpless, *J. Am. Chem. Soc.*, 2002, **124**, 12210-12216.
22. B. S. Jursic and Z. Zdravkovski, *J. Mol. Struct.*, 1994, **118**, 11-22.
23. I. E. Titova, V. S. Poplavskii, G. I. Koldobskii, V. A. Ostrovskii, V. D. Nikolaev and G. B. Erusalimskii, *Khim. Geterotsikl. Soedin.*, 1986, 1086-1089.
24. Z. P. Demko and K. B. Sharpless, *Org. Lett.*, 2001, **3**, 4091-4094.
25. S. Caron, L. Wei, J. Douville and A. Ghosh, *J. Org. Chem.*, 2010, **75**, 945-947.
26. M. J. Sullivan and M. L. Kilpatrick, *J. Am. Chem. Soc.*, 1945, **67**, 1815-1823.

27. M.-J. Crawford, T. M. Klapötke and H. Radies, *J. Fluorine Chem.*, 2008, **129**, 1199-1205.
28. M. l. Girardin, S. J. Dolman, S. Lauzon, S. p. G. Ouellet, G. Hughes, P. Fernandez, G. Zhou and P. D. O'Shea, *Org. Process Res. Dev.*, 2011, **15**, 1073-1080.
29. B. E. Huff and M. A. Staszak, *Tetrahedron Lett.*, 1993, **34**, 8011-8014.
30. Z. P. Demko and K. B. Sharpless, *J. Org. Chem.*, 2001, **66**, 7945-7950.
31. S. Rostamizadeh, H. Ghaieni, R. Aryan and A. Amani, *Chin. Chem. Lett.*, 2009, **20**, 1311-1314.
32. Z. Zhao, W. H. Leister, R. G. Robinson, S. F. Barnett, D. Defeo-Jones, R. E. Jones, G. D. Hartman, J. R. Huff, H. E. Huber, M. E. Duggan and C. W. Lindsley, *Biorg. Med. Chem. Lett.*, 2005, **15**, 905-909; J.-J. Shie and J.-M. Fang, *J. Org. Chem.*, 2007, **72**, 3141-3144.
33. F. Himo, Z. P. Demko, L. Noodleman and K. B. Sharpless, *J. Am. Chem. Soc.*, 2003, **125**, 9983-9987.
34. J. V. Duncia, M. E. Pierce and J. B. Santella, *J. Org. Chem.*, 1991, **56**, 2395-2400; K. Sisido, K. Nabika, T. Isida and S. Kozima, *J. Organomet. Chem.*, 1971, **33**, 337-346.
35. A. Goodger, M. Hill, M. F. Mahon, J. McGinley and K. C. Molloy, *Dalton Trans.*, 1996, 847-852.
36. S. J. Wittenberger and B. G. Donner, *J. Org. Chem.*, 1993, **58**, 4139-4141.
37. D. Cantillo, B. Gutmann and C. O. Kappe, *J. Am. Chem. Soc.*, 2011, **133**, 4465-4475.
38. V. Aureggi and G. Sedelmeier, *Angew. Chem. Int. Ed.*, 2007, **46**, 8440-8444.
39. V. A. Ostrovskii and A. O. Koren, *Heterocycles*, 2000, **53**, 1421-1448.
40. D. S. Wofford, D. M. Forkey and J. G. Russell, *J. Org. Chem.*, 1982, **47**, 5132-5137.
41. R. E. Trifonov and V. A. Ostrovskii, *Russ. J. Org. Chem.*, 2006, **42**, 1585-1605.
42. S.-e. Yoo, S.-H. Lee, S.-K. Kim and S.-H. Lee, *Biorg. Med. Chem.*, 1997, **5**, 445-459.
43. L. V. Myznikov, T. V. Artamonova, V. K. Bel'skii, A. I. Stash, N. K. Skvortsov and G. I. Koldobskii, *Russ. J. Org. Chem.*, 2002, **38**, 1360-1369.
44. B. E. Huff, M. E. LeTourneau, M. A. Staszak and J. A. Ward, *Tetrahedron Lett.*, 1996, **37**, 3655-3658.
45. D. Bethell and V. Gold, *Carbonium ions, an introduction*, Academic Press, London, New York, 1967.
46. G. I. Koldobskii and R. B. Kharbash, *Russ. J. Org. Chem.*, 2003, **39**, 453-470.
47. A. O. Koren and P. N. Gaponik, *Khim. Geterotsikl. Soedin.*, 1990, 1643-1647; P. N. Gaponik, S. V. Voitekhovich and B. G. Klyaus, *Russ. J. Org. Chem.*, 2004, **40**, 598-600.
48. A. O. Koren and P. N. Gaponik, *Khim. Geterotsikl. Soedin.*, 1991, 1280-1281.
49. M. R. Couri, I. Luduvico, L. Santos, R. Alves, M. A. Prado and R. F. Gil, *Carbohydr. Res.*, 2007, **342**, 1096-1100.
50. L. V. Alam, R. V. Kharbash and G. I. Koldobskii, *Russ. J. Org. Chem.*, 2000, **36**, 916-918.
51. Y. A. Efimova, T. V. Artamonova and G. I. Koldobskii, *Russ. J. Org. Chem.*, 2010, **46**, 612-614.
52. C. J. Moody, C. W. Rees and R. G. Young, *J. Chem. Soc., Perkin Trans. 1*, 1991, 329-333.

53. J. Roh, K. Vavrova and A. Hrabalek, *Tetrahedron Lett.*, 2010, **51**, 1411-1414.
54. H. A. Jahn and E. Teller, *Proc. R. Soc. London, Ser. A*, 1937, **161**, 220-235.
55. M. A. Halcrow, *Chem. Soc. Rev.*, 2013, **42**, 1784-1795.
56. C. E. Housecroft and A. G. Sharpe, *Inorganic Chemistry*, 2nd edn., Pearson, England, 2005.
57. B. Rosenberg, *Interdiscip. Soc. Rev.*, 1978, **3**, 134-147.
58. M. A. Jakupec, M. Galanski, V. B. Arion, C. G. Hartinger and B. K. Keppler, *Dalton Trans.*, 2008, 183-194.
59. E. R. T. Tiekink, *Crit. Rev. Oncol. Hematol.*, 2002, **42**, 225-248.
60. C. Santini, M. Pellei, V. Gandin, M. Porchia, F. Tisato and C. Marzano, *Chem. Rev.*, 2013, **114**, 815-862.
61. E. S. Antonarakis and A. Emadi, *Cancer Chemother. Pharmacol.*, 2010, **66**, 1-9.
62. *Web of Science*, http://apps.webofknowledge.com/CitationReport.do?product=UA&search_mode=CitationReport&SID=R11h5NGCHFeVd8jkgDR&page=1&cr_pqid=3&viewType=summary, Accessed 1st September, 2014.
63. M. Frezza, S. Hindo, D. Chen, A. Davenport, S. Schmitt, D. Tomco and Q. P. Dou, *Curr. Pharm. Des.*, 2010, **16**, 1813-1825.
64. Q. Jiang, J. Zhu, Y. Zhang, N. Xiao and Z. Guo, *BioMetals*, 2009, **22**, 297-305; S. Tardito, I. Bassanetti, C. Bignardi, L. Elviri, M. Tegoni, C. Mucchino, O. Bussolati, R. Franchi-Gazzola and L. Marchio, *J. Am. Chem. Soc.*, 2011, **133**, 6235-6242; S. V. Voitekhovich, T. V. Serebryanskaya, A. S. Lyakhov, P. N. Gaponik and O. A. Ivashkevich, *Polyhedron*, 2009, **28**, 3614-3620.
65. H.-C. Zhou, J. R. Long and O. M. Yaghi, *Chem. Rev.*, 2012, **112**, 673-674.
66. W. Lu, Z. Wei, Z.-Y. Gu, T.-F. Liu, J. Park, J. Park, J. Tian, M. Zhang, Q. Zhang, T. Gentle Iii, M. Bosch and H.-C. Zhou, *Chem. Soc. Rev.*, 2014, **43**, 5561-5593.
67. D. M. D'Alessandro, B. Smit and J. R. Long, *Angew. Chem. Int. Ed.*, 2010, **49**, 6058-6082; J.-R. Li, J. Sculley and H.-C. Zhou, *Chem. Rev.*, 2011, **112**, 869-932; J. A. Mason, M. Veenstra and J. R. Long, *Chem. Sci.*, 2014, **5**, 32-51; J.-R. Li, J. Yu, W. Lu, L.-B. Sun, J. Sculley, P. B. Balbuena and H.-C. Zhou, *Nat. Commun.*, 2013, **4**, 1538.
68. H. R. Moon, D.-W. Lim and M. P. Suh, *Chem. Soc. Rev.*, 2013, **42**, 1807-1824; A. Dhakshinamoorthy and H. Garcia, *Chem. Soc. Rev.*, 2012, **41**, 5262-5284; M. Yoon, R. Srirambalaji and K. Kim, *Chem. Rev.*, 2011, **112**, 1196-1231.
69. C.-Y. Sun, X.-L. Wang, X. Zhang, C. Qin, P. Li, Z.-M. Su, D.-X. Zhu, G.-G. Shan, K.-Z. Shao, H. Wu and J. Li, *Nat. Commun.*, 2013, **4**; H.-L. Jiang, D. Feng, K. Wang, Z.-Y. Gu, Z. Wei, Y.-P. Chen and H.-C. Zhou, *J. Am. Chem. Soc.*, 2013, **135**, 13934-13938; J. Heine and K. Muller-Buschbaum, *Chem. Soc. Rev.*, 2013, **42**, 9232-9242.
70. L. E. Kreno, K. Leong, O. K. Farha, M. Allendorf, R. P. Van Duyne and J. T. Hupp, *Chem. Rev.*, 2011, **112**, 1105-1125.
71. T. Yamada, K. Otsubo, R. Makiura and H. Kitagawa, *Chem. Soc. Rev.*, 2013, **42**, 6655-6669; M. Yoon, K. Suh, S. Natarajan and K. Kim, *Angew. Chem. Int. Ed.*, 2013, **52**, 2688-2700.
72. E. Coronado and G. Minguez Espallargas, *Chem. Soc. Rev.*, 2013, **42**, 1525-1539; M. Kurmoo, *Chem. Soc. Rev.*, 2009, **38**, 1353-1379; N. Berg and L. F. Jones, *CrystEngComm*, 2011, **13**, 5510-5518.
73. Q. Zhang and J. n. M. Shreeve, *Angew. Chem. Int. Ed.*, 2014, **53**, 2540-2542.

74. S. R. Miller, D. Heurtaux, T. Baati, P. Horcajada, J.-M. Greneche and C. Serre, *Chem. Commun.*, 2010, **46**, 4526-4528; W. J. Rieter, K. M. Pott, K. M. L. Taylor and W. Lin, *J. Am. Chem. Soc.*, 2008, **130**, 11584-11585; C.-Y. Sun, C. Qin, X.-L. Wang and Z.-M. Su, *Exp. Opin. Drug Deliv.*, 2013, **10**, 89-101.
75. B. F. Hoskins and R. Robson, *J. Am. Chem. Soc.*, 1990, **112**, 1546-1554.
76. B. F. Hoskins and R. Robson, *J. Am. Chem. Soc.*, 1989, **111**, 5962-5964.
77. O. M. Yaghi, G. Li and H. Li, *Nature*, 1995, **378**, 703-706; O. M. Yaghi and H. Li, *J. Am. Chem. Soc.*, 1995, **117**, 10401-10402.
78. M. Kondo, T. Yoshitomi, H. Matsuzaka, S. Kitagawa and K. Seki, *Angew. Chem. Int. Ed. Engl.*, 1997, **36**, 1725-1727.
79. H. Li, M. Eddaoudi, M. O'Keeffe and O. M. Yaghi, *Nature*, 1999, **402**, 276-279.
80. S. S.-Y. Chui, S. M.-F. Lo, J. P. H. Charmant, A. G. Orpen and I. D. Williams, *Science*, 1999, **283**, 1148-1150.
81. C. Serre, F. Millange, C. Thouvenot, M. Noguès, G. Marsolier, D. Louër and G. Férey, *J. Am. Chem. Soc.*, 2002, **124**, 13519-13526; K. Barthelet, J. Marrot, D. Riou and G. Férey, *Angew. Chem. Int. Ed.*, 2002, **41**, 281-284; C. Serre, C. Mellot-Draznieks, S. Surblé, N. Audebrand, Y. Filinchuk and G. Férey, *Science*, 2007, **315**, 1828-1831.
82. R. Robson, *Dalton Trans.*, 2008, 5113-5131.
83. R. Batten Stuart, R. Champness Neil, X.-M. Chen, J. Garcia-Martinez, S. Kitagawa, L. Öhrström, M. O'Keeffe, M. Paik Suh and J. Reedijk, *Pure Appl. Chem.*, 2013, **85**, 1715.
84. R. A. Fischer, *Angew. Chem. Int. Ed.*, 2014, **53**, 5716-5717.
85. R. Banerjee, A. Phan, B. Wang, C. Knobler, H. Furukawa, M. O'Keeffe and O. M. Yaghi, *Science*, 2008, **319**, 939-943.
86. D. M. P. Mingos and D. R. Baghurst, *Chem. Soc. Rev.*, 1991, **20**, 1-47; C. Oliver Kappe, *Chem. Soc. Rev.*, 2008, **37**, 1127-1139.
87. J. Klinowski, F. A. Almeida Paz, P. Silva and J. Rocha, *Dalton Trans.*, 2011, **40**, 321-330.
88. F. Di Renzo, *Catal. Today*, 1998, **41**, 37-40.
89. J. Della Rocca and W. Lin, *Eur. J. Inorg. Chem.*, 2010, **2010**, 3725-3734.
90. K. M. L. Taylor-Pashow, J. Della Rocca, R. C. Huxford and W. Lin, *Chem. Commun.*, 2010, **46**, 5832-5849.
91. U. Mueller, H. Puetter, M. Hesse and H. Wessel, WO2005049892A1, 2005.
92. U. Mueller, M. Schubert, F. Teich, H. Puetter, K. Schierle-Arndt and J. Pastre, *J. Mater. Chem.*, 2006, **16**, 626-636.
93. M. Schlesinger, S. Schulze, M. Hietschold and M. Mehring, *Microporous Mesoporous Mater.*, 2010, **132**, 121-127.
94. A. Pichon, A. Lazuen-Garay and S. L. James, *CrystEngComm*, 2006, **8**, 211-214.
95. A. Pichon and S. L. James, *CrystEngComm*, 2008, **10**, 1839-1847; W. Yuan, A. L. Garay, A. Pichon, R. Clowes, C. D. Wood, A. I. Cooper and S. L. James, *CrystEngComm*, 2010, **12**, 4063-4065; M. Klimakow, P. Klobes, A. F. Thünemann, K. Rademann and F. Emmerling, *Chem. Mater.*, 2010, **22**, 5216-5221; H. Yang, S. Orefuwa and A. Goudy, *Microporous Mesoporous Mater.*, 2011, **143**, 37-45.
96. N. Stock and S. Biswas, *Chem. Rev.*, 2011, **112**, 933-969.
97. Z.-Q. Li, L.-G. Qiu, T. Xu, Y. Wu, W. Wang, Z.-Y. Wu and X. Jiang, *Mater. Lett.*, 2009, **63**, 78-80.

98. N. A. Khan and S. H. Jhung, *Bull. Korean Chem. Soc.*, 2009, **30**, 2921-2926.
99. Z. Wang and S. M. Cohen, *Chem. Soc. Rev.*, 2009, **38**, 1315-1329.
100. Z. Wang and S. M. Cohen, *J. Am. Chem. Soc.*, 2007, **129**, 12368-12369.
101. Y. H. Kiang, G. B. Gardner, S. Lee, Z. Xu and E. B. Lobkovsky, *J. Am. Chem. Soc.*, 1999, **121**, 8204-8215.
102. S. M. Cohen, *Chem. Rev.*, 2011, **112**, 970-1000.
103. O. K. Farha, K. L. Mulfort and J. T. Hupp, *Inorg. Chem.*, 2008, **47**, 10223-10225.
104. K. K. Tanabe and S. M. Cohen, *Chem. Soc. Rev.*, 2011, **40**, 498-519.
105. J. D. Evans, C. J. Sumby and C. J. Doonan, *Chem. Soc. Rev.*, 2014, **43**, 5933-5951.
106. E. D. Bloch, D. Britt, C. Lee, C. J. Doonan, F. J. Uribe-Romo, H. Furukawa, J. R. Long and O. M. Yaghi, *J. Am. Chem. Soc.*, 2010, **132**, 14382-14384.
107. R. K. Deshpande, J. L. Minnaar and S. G. Telfer, *Angew. Chem. Int. Ed.*, 2010, **49**, 4598-4602.
108. J. R. Long and O. M. Yaghi, *Chem. Soc. Rev.*, 2009, **38**, 1213-1214.
109. B. Desoize, *Crit. Rev. Oncol. Hematol.*, 2002, **42**, 213-215.
110. R. Huang, A. Wallqvist and D. G. Covell, *Biochem. Pharmacol.*, 2005, **69**, 1009-1039.
111. S. J. Wittenberger, *Org. Prep. Proced. Int.*, 1994, **26**, 499-531.
112. N. G. Pavel, V. V. Sergei and A. I. Oleg, *Russ. Chem. Rev.*, 2006, **75**, 507.
113. Z. H. Chohan, C. T. Supuran and A. Scozzafava, *J. Enzyme Inhib. Med. Chem.*, 2004, **19**, 79-84; J. Anacona and P. Alvarez, *Transition Met. Chem.*, 2002, **27**, 856-860.
114. A. A. M. Aly, A. H. Osman, N. A. El-Maali and G. A. A. Al-Hazmi, *J. Therm. Anal. Calorim.*, 2004, **75**, 159-168; A. H. Osman, A. A. M. Aly, N. A. El-Maali and G. A. A. Al-Hazmi, *Synth. React. Inorg. Met.-Org. Chem.*, 2002, **32**, 1289-1300; A. H. Osman, N. A. El-Maali, A. A. M. Aly and G. A. Al-Hazmi, *Synth. React. Inorg. Met.-Org. Chem.*, 2002, **32**, 763-781.
115. Z. H. Chohan, A. Scozzafava and C. T. Supuran, *J. Enzyme Inhib. Med. Chem.*, 2002, **17**, 261-266; Z. H. Chohan, A. Scozzafava and C. T. Supuran, *Synth. React. Inorg. Met.-Org. Chem.*, 2003, **33**, 241-257; Z. H. Chohan, *Synth. React. Inorg. Met.-Org. Chem.*, 2004, **34**, 833-846.
116. F. Touti, A. K. Singh, P. Maurin, L. Canaple, O. Beuf, J. Samarut and J. Hasserodt, *J. Med. Chem.*, 2011, **54**, 4274-4278.
117. M. Giraud, E. S. Andreiadis, A. S. Fisyuk, R. Demadrille, J. Pécaut, D. Imbert and M. Mazzanti, *Inorg. Chem.*, 2008, **47**, 3952-3954.
118. A. Fleming, F. Kelleher, M. F. Mahon, J. McGinley and V. Prajapati, *Tetrahedron*, 2005, **61**, 7002-7011; A. D. Bond, A. Fleming, F. Kelleher, J. McGinley and V. Prajapati, *Tetrahedron*, 2006, **62**, 9577-9581; A. F. M. Fleming, F. Kelleher, M. F. Mahon, J. McGinley, K. C. Molloy and V. Prajapati, *Acta Crystallogr. Sect. E*, 2004, **60**, o2388-o2389; S. Bhandari, M. F. Mahon, J. G. McGinley, K. C. Molloy and C. E. E. Roper, *Dalton Trans.*, 1998, 3425-3430.
119. A. D. Bond, A. Fleming, F. Kelleher, J. McGinley, V. Prajapati and S. Skovsgaard, *Tetrahedron*, 2007, **63**, 6835-6842.
120. J. Gaire, J. McGinley, A. Fleming and F. Kelleher, *Tetrahedron*, 2012, **68**, 5935-5941.
121. A. D. Bond, A. Fleming, J. Gaire, F. Kelleher, J. McGinley, V. McKee and U. Sheridan, *Polyhedron*, 2012, **33**, 289-296.

122. A. Fleming, J. Gaire, F. Kelleher, J. McGinley and V. McKee, *Tetrahedron*, 2011, **67**, 3260-3266.
123. J. Clayden, N. Greeves and P. Wothers, *Organic Chemistry*, 1st edn., Oxford University Press, New York, 2008.
124. R. N. Butler and T. M. McEvoy, *P. Roy. Irish Acad. B.*, 1977, **77**, 359-364.
125. R. N. Butler and T. M. McEvoy, *J. Chem. Soc., Perkin Trans. 2*, 1978, 1087-1090.
126. R. N. Butler, *Can. J. Chem.*, 1973, **51**, 2315-2322.
127. R. N. Butler, T. M. McEvoy, F. L. Scott and J. C. Tobin, *Can. J. Chem.*, 1977, **55**, 1564-1566.
128. P. Steel, *J. Chem. Crystallogr.*, 1996, **26**, 399-402.
129. N. T. Pokhodylo, R. D. Savka, V. S. Matiichuk and N. D. Obushak, *Russ. J. Gen. Chem.*, 2010, **80**, 836-841.
130. T. J. Lane, I. Nakagawa, J. L. Walter and A. J. Kandathil, *Inorg. Chem.*, 1962, **1**, 267-276.
131. D. M. M., P. N. Gaponik, V. N. Naumenko, A. I. Lesnikovich and M. V. Nikanovich, *Spectrochim. Acta*, 1987, **43**, 349-353.
132. F. A. Cotton and G. Wilkinson, *Advanced Inorganic Chemistry*, 5th edn., Wiley, New York, 1988.
133. L. Sacconi and I. Bertini, *J. Am. Chem. Soc.*, 1966, **88**, 5180-5185.
134. K. Kavanagh and E. P. Reeves, *FEMS Microbiol. Rev.*, 2004, **28**, 101-112.
135. J. A. Hoffmann, *Curr. Opin. Immunol.*, 1995, **7**, 4-10; D. A. Kimbrell and B. Beutler, *Nat. Rev. Genet.*, 2001, **2**, 256-267.
136. C. A. Janeway, P. Travers, M. Walport and M. J. Shlomchik, *Immunobiology: the immune system in health and disease*, 6th edn., Garland Science Publishing, New York, 2005.
137. G. Jander, L. G. Rahme and F. M. Ausubel, *J. Bacteriol.*, 2000, **182**, 3843-3845.
138. A. P. Desbois and P. J. Coote, *J. Antimicrob. Chemother.*, 2011, **66**, 1785-1790.
139. A. Kellett, M. O'Connor, M. McCann, O. Howe, A. Casey, P. McCarron, K. Kavanagh, M. McNamara, S. Kennedy, D. D. May, P. S. Skell, D. O'Shea and M. Devereux, *MedChemComm*, 2011, **2**, 579-584.
140. G. L. Patrick, *An Introduction to Medicinal Chemistry*, 3rd edn., Oxford University Press Inc., New York, 2005.
141. M. McCann, A. L. S. Santos, B. A. da Silva, M. T. V. Romanos, A. S. Pyrrho, M. Devereux, K. Kavanagh, I. Fichtner and A. Kellett, *Toxicology Research*, 2012, **1**, 47-54.
142. H. Hamamoto, A. Tonoike, K. Narushima, R. Horie and K. Sekimizu, *Comp. Biochem. Physiol., C: Toxicol. Pharmacol.*, 2009, **149**, 334-339.
143. K. Kavanagh and J. P. Fallon, *Fungal Biology Reviews*, 2010, **24**, 79-83.
144. M. Brennan, D. Y. Thomas, M. Whiteway and K. Kavanagh, *FEMS Immunol. Med. Microbiol.*, 2002, **34**, 153-157.
145. R. H. Shoemaker, *Nat. Rev. Cancer*, 2006, **6**, 813-823.
146. J. Yang, L. Shen, G.-W. Yang, Q.-Y. Li, W. Shen, J.-N. Jin, J.-J. Zhao and J. Dai, *J. Solid State Chem.*, 2012, **186**, 124-133.
147. G. Aromí, L. A. Barrios, O. Roubeau and P. Gamez, *Coord. Chem. Rev.*, 2011, **255**, 485-546.
148. H.-F. Chen, W.-B. Yang, L. Lin, X.-G. Guo, X.-j. Dui, X.-Y. Wu, C.-Z. Lu and C.-J. Zhang, *J. Solid State Chem.*, 2013, **201**, 215-221.
149. B. Schreiner and W. Beck, *Z. Anorg. Allg. Chem.*, 2010, **636**, 499-505.

150. K. Nakamoto, *Infrared and Raman Spectra of Inorganic and Coordination Compounds Part B*, 6th edn., Wiley, New Jersey, 2009.
151. C. A. Williams, A. J. Blake, C. Wilson, P. Hubberstey and M. Schröder, *Cryst. Growth Des.*, 2008, **8**, 911-922.
152. F.-M. Jian, S.-D. Zhu, S. Jin, Z.-G. Zhou and Y.-B. Lu, *Inorg. Chem. Commun.*, 2013, **36**, 155-158; Y.-B. Lu, S. Jin, F.-M. Jian, Y.-R. Xie and G.-T. Luo, *J. Mol. Struct.*, 2014, **1061**, 14-18.
153. G.-W. Yang, D.-Y. Chen, C. Zhai, X.-Y. Tang, Q.-Y. Li, F. Zhou, Z.-F. Miao, J.-N. Jin and H.-D. Ding, *Inorg. Chem. Commun.*, 2011, **14**, 913-915; Q.-Y. Li, D.-Y. Chen, M.-H. He, G.-W. Yang, L. Shen, C. Zhai, W. Shen, K. Gu and J.-J. Zhao, *J. Solid State Chem.*, 2012, **190**, 196-201.
154. G.-W. Yang, Q.-Y. Li, Y. Zhou, P. Sha, Y.-S. Ma and R.-X. Yuan, *Inorg. Chem. Commun.*, 2008, **11**, 723-726.
155. M. Dincă, A. F. Yu and J. R. Long, *J. Am. Chem. Soc.*, 2006, **128**, 8904-8913.
156. J.-R. Li, Y. Tao, Q. Yu, X.-H. Bu, H. Sakamoto and S. Kitagawa, *Chem. Eur. J.*, 2008, **14**, 2771-2776.
157. S. Horike, S. Hasegawa, D. Tanaka, M. Higuchi and S. Kitagawa, *Chem. Commun.*, 2008, 4436-4438.
158. E.-Q. Gao, N. Liu, A.-L. Cheng and S. Gao, *Chem. Commun.*, 2007, 2470-2472; J.-P. Zhao, B.-W. Hu, E. C. Sañudo, Q. Yang, Y.-F. Zeng and X.-H. Bu, *Inorg. Chem.*, 2009, **48**, 2482-2489; E.-Q. Gao, P.-P. Liu, Y.-Q. Wang, Q. Yue and Q.-L. Wang, *Chem. Eur. J.*, 2009, **15**, 1217-1226.
159. L. K. Li, Y. L. Song, H. W. Hou, Y. T. Fan and Y. Zhu, *Eur. J. Inorg. Chem.*, 2005, **2005**, 3238-3249.
160. L. J. Charbonnière, N. Weibel, P. Retailleau and R. Ziessel, *Chem. Eur. J.*, 2007, **13**, 346-358; M. Li, Z. Li and D. Li, *Chem. Commun.*, 2008, 3390-3392.
161. R. Wang, Y. Guo, Z. Zeng, B. Twamley and J. n. M. Shreeve, *Chem. Eur. J.*, 2009, **15**, 2625-2634.
162. Q.-Y. Chen, Y. Li, F.-K. Zheng, W.-Q. Zou, M.-F. Wu, G.-C. Guo, A. Q. Wu and J.-S. Huang, *Inorg. Chem. Commun.*, 2008, **11**, 969-971; M.-F. Wu, F.-K. Zheng, G. Xu, A. Q. Wu, Y. Li, H.-F. Chen, S.-P. Guo, F. Chen, Z.-F. Liu, G.-C. Guo and J.-S. Huang, *Inorg. Chem. Commun.*, 2010, **13**, 250-253.
163. M.-F. Wu, F.-K. Zheng, A. Q. Wu, Y. Li, M.-S. Wang, W.-W. Zhou, F. Chen, G.-C. Guo and J.-S. Huang, *CrystEngComm*, 2010, **12**, 260-269.
164. S. Nayak, K. Harms and S. Dehnen, *Inorg. Chem.*, 2011, **50**, 2714-2716.
165. M. Kim, J. A. Boissonnault, P. V. Dau and S. M. Cohen, *Angew. Chem.*, 2011, **123**, 12401-12404.
166. M. F. Lappert, *J. Chem. Soc.*, 1961, 817-822.
167. M. F. Mahon, J. McGinley, D. A. Rooney and J. M. D. Walsh, *Inorg. Chim. Acta*, 2009, **362**, 2353-2360; S. Mandal, F. Lloret and R. Mukherjee, *Inorg. Chim. Acta*, 2009, **362**, 27-37; F. Allen, *Acta Crystallogr. Sect. B*, 2002, **58**, 380-388.
168. J. March and M. B. Smith, *March's Advanced Organic Chemistry: Reactons, Mechanisms and Structure*, 6th edn., Wiley-Blackwell, New York, 2007.
169. G. B. Deacon and R. J. Phillips, *Coord. Chem. Rev.*, 1980, **33**, 227-250.
170. D. Martini, M. Pellei, C. Pettinari, B. W. Skelton and A. H. White, *Inorg. Chim. Acta*, 2002, **333**, 72-82.
171. W.-Q. Kan, J. Yang, Y.-Y. Liu and J.-F. Ma, *Polyhedron*, 2011, **30**, 2106-2113; S.-Y. Liao, W. Gu, L.-Y. Yang, T.-H. Li, M. Zhang, L. Wang and X. Liu, *Polyhedron*, 2012, **36**, 38-44.

172. B. Shankar, P. Elumalai, R. Shanmugam, V. Singh, D. T. Masram and M. Sathiyendiran, *Inorg. Chem.*, 2013, **52**, 10217-10219.
173. B. J. Wang, J. H. Zou, W. X. Li, Z. Wang, B. Xu, S. Li, Y. S. Zhai, D. L. Zhu, Q. Y. Li and G. W. Yang, *J. Organomet. Chem.*, 2014, **749**, 428-432.
174. Q.-Y. Li, G.-W. Yang, X.-Y. Tang, Y.-S. Ma, F. Zhou, W. Liu, J. Chen and H. Zhou, *Inorg. Chem. Commun.*, 2010, **13**, 254-257.
175. G. E. Kostakis, C. E. Anson and A. K. Powell, *Bioinorg. Chem. Appl.*, 2010, **2010**.
176. R. S. Drago, *Physical Methods in Chemistry*, 1st edn., W. B. Saunders Company, Philadelphia, 1977.
177. S. Chandra and R. Kumar, *Spectrochim. Acta, Pt. A: Mol. Biomol. Spectrosc.*, 2005, **61**, 437-446.
178. S. A and S. G. Schulman, *Introduction to Fluorescence Spectroscopy*, 1st edn., John Wiley & Sons, New York, 1999.
179. B. Valeur, *Molecular Fluorescence Principles and Applications*, 1st edn., John Wiley & Sons, Weinheim, 2002.
180. J. M. D. Walsh, PhD, NUI Maynooth, 2010.
181. Z. Hu, B. J. Deibert and J. Li, *Chem. Soc. Rev.*, 2014, **43**, 5815-5840.
182. J. R. Lakowicz, *Principles of Fluorescence Spectroscopy*, 3rd edn., John Wiley & Sons, New York, 2006.
183. Y. Cui, Y. Yue, G. Qian and B. Chen, *Chem. Rev.*, 2011, **112**, 1126-1162.
184. M. D. Allendorf, C. A. Bauer, R. K. Bhakta and R. J. T. Houk, *Chem. Soc. Rev.*, 2009, **38**, 1330-1352.
185. F. C. Spano, *Annu. Rev. Phys. Chem.*, 2006, **57**, 217-243.
186. D. F. Sava Gallis, L. E. S. Rohwer, M. A. Rodriguez and T. M. Nenoff, *Chem. Mater.*, 2014, **26**, 2943-2951.
187. S.-L. Zheng, J.-H. Yang, X.-L. Yu, X.-M. Chen and W.-T. Wong, *Inorg. Chem.*, 2003, **43**, 830-838.
188. X. Li, B.-L. Wu, C.-Y. Niu, Y.-Y. Niu and H.-Y. Zhang, *Cryst. Growth Des.*, 2009, **9**, 3423-3431.
189. P. Zhu and H.-M. Li, *J. Mol. Struct.*, 2011, **992**, 106-110.
190. Y.-H. Wan, L.-P. Jin and K.-Z. Wang, *J. Mol. Struct.*, 2003, **649**, 85-93.
191. G.-Z. Liu, L.-Y. Xin and L.-Y. Wang, *CrystEngComm*, 2011, **13**, 3013-3020.
192. Y. Wang, S.-Q. Shen, J.-H. Zhou, T. Wang, S.-N. Wang and G.-X. Liu, *Inorg. Chem. Commun.*, 2013, **30**, 5-12.
193. J. He, Y. Wang, W. Bi, X. Zhu and R. Cao, *J. Mol. Struct.*, 2006, **787**, 63-68.
194. A. D. Burrows, R. W. Harrington, M. F. Mahon and S. J. Teat, *Eur. J. Inorg. Chem.*, 2003, **2003**, 766-776; A. D. Burrows, R. W. Harrington, M. F. Mahon and C. E. Price, *Dalton Trans.*, 2000, 3845-3854; E. Shyu, M. A. Braverman, R. M. Supkowski and R. L. LaDuca, *Inorg. Chim. Acta*, 2009, **362**, 2283-2292; M. A. Braverman, R. J. Staples, R. M. Supkowski and R. L. LaDuca, *Polyhedron*, 2008, **27**, 2291-2300.
195. S. Youssif, *ARKIVOC*, 2001, **2**, 242-268.
196. G. Heinisch and G. Loetsch, *Heterocycles*, 1987, **26**, 731-744.
197. W. K. Fife and E. F. V. Scriven, *Heterocycles*, 1984, **22**, 2375-2394.
198. W. K. Fife, *J. Org. Chem.*, 1983, **48**, 1375-1377.
199. Y. Yuan, O. Elbegdorj, J. Chen, S. K. Akubathini, F. Zhang, D. L. Stevens, I. O. Beletskaya, K. L. Scoggins, Z. Zhang, P. M. Gerk, D. E. Selley, H. I. Akbarali, W. L. Dewey and Y. Zhang, *J. Med. Chem.*, 2012, **55**, 10118-10129.

200. Z. Huo, T. Kosugi and Y. Yamamoto, *Tetrahedron Lett.*, 2008, **49**, 4369-4371.
201. A. R. Katritzky and A. R. Lagowski, *Chemistry of the Heterocyclic N-Oxides*, Academic Press, London, 1971.
202. K.-G. Liu, X.-Q. Cai, X.-C. Li, D.-A. Qin and M.-L. Hu, *Inorg. Chim. Acta*, 2012, **388**, 78-83.
203. L.-R. Zhang, Z.-J. Liu, H. Zhang, J. Sun, Y. Luo, T.-T. Zhao, H.-B. Gong and H.-L. Zhu, *Biorg. Med. Chem.*, 2012, **20**, 3615-3621; L. Feng, K.-W. Yang, L.-S. Zhou, J.-M. Xiao, X. Yang, L. Zhai, Y.-L. Zhang and M. W. Crowder, *Biorg. Med. Chem. Lett.*, 2012, **22**, 5185-5189.
204. X. Zhao, T. Zhang, Y. Zhou and D. Liu, *J. Mol. Catal. A: Chem.*, 2007, **271**, 246-252.
205. M. Rubio, G. Ramírez-Galicia and L. J. López-Nava, *J. Mol. Struct.*, 2005, **726**, 261-269.
206. S. D. Taylor, F. Mirzaei, A. Sharifi and S. L. Bearne, *J. Org. Chem.*, 2006, **71**, 9420-9430.
207. J. Yin, B. Xiang, M. A. Huffman, C. E. Raab and I. W. Davies, *J. Org. Chem.*, 2007, **72**, 4554-4557.
208. N. Sato, M. Ando, S. Ishikawa, M. Jitsuoka, K. Nagai, H. Takahashi, A. Sakuraba, H. Tsuge, H. Kitazawa, H. Iwaasa, S. Mashiko, A. Gomori, R. Moriya, N. Fujino, T. Ohe, A. Ishihara, A. Kanatani and T. Fukami, *J. Med. Chem.*, 2009, **52**, 3385-3396.
209. S. Kämper, A. Paretzki, J. Fiedler, S. Záliš and W. Kaim, *Inorg. Chem.*, 2012, **51**, 2097-2104.
210. E. Cole, R. C. B. Copley, J. A. K. Howard, D. Parker, G. Ferguson, J. F. Gallagher, B. Kaitner, A. Harrison and L. Royle, *Dalton Trans.*, 1994, 1619-1629.
211. A. Palma, J. F. Gallagher, H. Muller-Bunz, J. Wolowska, E. J. L. McInnes and D. F. O'Shea, *Dalton Trans.*, 2009, 273-279.
212. M. J. Ingleson, J. Perez Barrio, J.-B. Guilbaud, Y. Z. Khimyak and M. J. Rosseinsky, *Chem. Commun.*, 2008, 2680-2682.
213. C. J. Doonan, W. Morris, H. Furukawa and O. M. Yaghi, *J. Am. Chem. Soc.*, 2009, **131**, 9492-9493.
214. R. G. Pearson, *J. Am. Chem. Soc.*, 1963, **85**, 3533-3539.
215. P.-Z. Li, N. Muramatsu, G. Maruta, S. Takeda and Q. Xu, *Inorg. Chem. Commun.*, 2011, **14**, 411-414.
216. A. D. Burrows, C. G. Frost, M. F. Mahon and C. Richardson, *Angew. Chem. Int. Ed.*, 2008, **47**, 8482-8486.
217. H. Hintz and S. Wuttke, *Chem. Commun.*, 2014.
218. R. W. Taft, *J. Am. Chem. Soc.*, 1952, **74**, 2729-2732.
219. E. V. Anslyn and D. A. Dougherty, *Modern Physical Organic Chemistry*, University Science Books, California, 2006.
220. L. Sun, L. Ma, J.-B. Cai, L. Liang and H. Deng, *CrystEngComm*, 2012, **14**, 890-898.
221. I. Chiarotto, M. Feroci, G. Sotgiu and A. Inesi, *Tetrahedron*, 2013, **69**, 8088-8095.
222. J. L. Abernethy, D. Srulevitch and M. J. Ordway, *J. Org. Chem.*, 1975, **40**, 3445-3447.
223. S. Duric and C. C. Tzschucke, *Org. Lett.*, 2011, **13**, 2310-2313.
224. T. Sakamoto, S. Kaneda, S. Nishimura and H. Yamanaka, *Chem. Pharm. Bull.*, 1985, **33**, 565-571.

225. S. Bhandari, M. F. Mahon, K. C. Molloy, J. S. Palmer and S. F. Sayers, *Dalton Trans.*, 2000, 1053-1060.
226. W. Ouellette, A. V. Prosvirin, K. Whitenack, K. R. Dunbar and J. Zubieta, *Angew. Chem. Int. Ed.*, 2009, **48**, 2140-2143; E. Yang, Q.-R. Ding, Y. Kang and F. Wang, *CrystEngComm*, 2013, **15**, 10563-10568; J. Tao, Z.-J. Ma, R.-B. Huang and L.-S. Zheng, *Inorg. Chem.*, 2004, **43**, 6133-6135.
227. S. Jeong, X. Song, S. Jeong, M. Oh, X. Liu, D. Kim, D. Moon and M. S. Lah, *Inorg. Chem.*, 2011, **50**, 12133-12140.
228. X. Wang, Y. Wang, G. Liu, A. Tian, J. Zhang and H. Lin, *Dalton Trans.*, 2011, **40**, 9299-9305; A. Tian, X. Lin, J. Ying, J. Zhang, H. Lin, G. Liu, D. Zhao, N. Li and X. Wang, *Dalton Trans.*, 2013, **42**, 9809-9812; X. Wang, N. Li, A. Tian, J. Ying, G. Liu, H. Lin, J. Zhang and Y. Yang, *Dalton Trans.*, 2013, **42**, 14856-14865.
229. X.-L. Wang, N. Li, A.-X. Tian, J. Ying, T.-J. Li, X.-L. Lin, J. Luan and Y. Yang, *Inorg. Chem.*, 2014.
230. D.-Y. Du, J.-S. Qin, S.-L. Li, Z.-M. Su and Y.-Q. Lan, *Chem. Soc. Rev.*, 2014, **43**, 4615-4632.
231. M. J. Plater, M. R. S. J. Foreman, T. Gelbrich, S. J. Coles and M. B. Hursthouse, *Dalton Trans.*, 2000, 3065-3073; X.-J. Feng, W. Yao, M.-F. Luo, R.-Y. Ma, H.-W. Xie, Y. Yu, Y.-G. Li and E.-B. Wang, *Inorg. Chim. Acta*, 2011, **368**, 29-36; L.-L. Liu, C.-X. Yu, Y. Zhou, J. Sun, P.-P. Meng, D. Liu and R.-J. Sa, *Inorg. Chem. Commun.*, 2014, **40**, 194-199.
232. D. Deng, L. Liu, B.-M. Ji, G. Yin and C. Du, *Cryst. Growth Des.*, 2012, **12**, 5338-5348.
233. L.-P. Zhang, W.-J. Lu and T. C. W. Mak, *Chem. Commun.*, 2003, 2830-2831.
234. H. H. Wasserman and J. L. Ives, *J. Org. Chem.*, 1985, **50**, 3573-3580; L. De Vries, *J. Am. Chem. Soc.*, 1978, **100**, 926-933.
235. R. W. Alder, M. E. Blake, S. Bufali, C. P. Butts, A. G. Orpen, J. Schutz and S. J. Williams, *J. Chem. Soc., Perkin Trans. 1*, 2001, 1586-1593.
236. K. L. Sorgi, in *Encyclopedia of Reagents for Organic Synthesis*, John Wiley & Sons, Ltd, 2001.
237. L.-L. Han, X.-Y. Zhang, J.-S. Chen, Z.-H. Li, D.-F. Sun, X.-P. Wang and D. Sun, *Cryst. Growth Des.*, 2014, **14**, 2230-2239.
238. D. Eisenberg and W. Kauzmann, *The Structure and Properties of Water*, Oxford University Press, Oxford, U.K., 1969.
239. L. J. Barbour, G. W. Orr and J. L. Atwood, *Nature*, 1998, **393**, 671-673.
240. L. Infantes, J. Chisholm and S. Motherwell, *CrystEngComm*, 2003, **5**, 480-486.
241. L. Infantes and S. Motherwell, *CrystEngComm*, 2002, **4**, 454-461.
242. W. E. Royer, A. Pardanani, Q. H. Gibson, E. S. Peterson and J. M. Friedman, *Proc. Natl. Acad. Sci. USA*, 1996, **93**, 14526-14531.
243. E. N. Baker, *J. Mol. Biol.*, 1980, **141**, 441-484.
244. A. Liljas, K. K. Kannan, P. C. Bergsten, I. Waara, K. Fridborg, B. Strandberg, U. Carlbom, L. Jarup, S. Lovgren and M. Petef, *Nature (London), New Biol.*, 1972, **235**, 131-137.
245. F. A. Quiocho, D. K. Wilson and N. K. Vyas, *Nature*, 1989, **340**, 404-407.
246. F. N. Keutsch, J. D. Cruzan and R. J. Saykally, *Chem. Rev.*, 2003, **103**, 2533-2578; S. Pal, N. B. Sankaran and A. Samanta, *Angew. Chem. Int. Ed.*, 2003, **42**, 1741-1743.
247. P. S. Lakshminarayanan, E. Suresh and P. Ghosh, *Angew. Chem. Int. Ed.*, 2006, **45**, 3807-3811.

248. Y. Jin, Y. Che, S. R. Batten, P. Chen and J. Zheng, *Eur. J. Inorg. Chem.*, 2007, **2007**, 1925-1929.
249. N. S. Oxtoby, A. J. Blake, N. R. Champness and C. Wilson, *Chem. Eur. J.*, 2005, **11**, 4643-4654.

Appendix

Appendix A: Crystal Structure Data

Table A1: Crystal data and structure refinement for crystal structures.

	2.67	**2.71**	**3.1**
Chemical formula	$C_{22}H_{26}CoN_{12}S_2$	$C_{30}H_{42}CoN_{12}S_2$	$C_{10}H_{11}N_5O_2$
M_r	581.60	693.81	233.24
Crystal system, space group	Orthorhombic, $Pca2_1$	Monoclinic, $P2_1/c$	Triclinic, $P\bar{1}$
Temperature (K)	294(1)	294(1)	294(2)
a, b, c (Å)	15.9466 (4), 8.4530 (2), 20.6129 (5)	13.5506 (10), 8.4428 (5), 15.9122 (10)	9.3222 (18), 9.591 (2), 14.147 (3)
V (Å^3)	2778.55 (12)	99.063 (7)	1167.3 (4)
Z	4	1797.7 (2)	4
μ (mm^{-1})	0.80	2	0.10
Crystal size (mm)	0.39 × 0.22 × 0.10	0.36 × 0.36 × 0.07	0.26 × 0.26 × 0.08
T_{min}, T_{max}	0.745, 0.924	0.804, 0.957	-
No. of measured, independent and observed reflections	14564, 5529, 4007	17401, 4759, 3108	8885, 5053, 2449
R_{int}	0.026	0.046	0.054
(sin θ/λ)$_{max}$ (Å^{-1})	0.658	0.694	0.658
$R[F^2 > 2\sigma(F^2)]$, $wR(F^2)$, S	0.052, 0.132, 1.04	0.080, 0.199, 1.12	0.065, 0.178, 1.03
No. of reflections	5529	4759	5053
No. of parameters	337	224	310
No. of restraints	37	5	0
H-atom treatment	H-atom parameters constrained	H-atom parameters constrained	H atoms treated by a mixture of independent and constrained refinement
Δρ$_{max}$, Δρ$_{min}$ (e Å^{-3})	0.41, -0.22	0.34, -0.22	0.17, -0.19

	3.8	**3.9**	**3.10**
Chemical formula	$C_{20}H_{22}Cl_4Cu_2N_{10}O_4$	$C_{20}H_{22}Cl_2CuN_{10}O_4$	$C_{16}H_{12}CuN_{10}O_4$
M_r	735.38	600.93	471.91
Crystal system, space group	Triclinic, $P\bar{1}$	Monoclinic, $P2_1/c$	Triclinic, $P\bar{1}$
Temperature (K)	294(1)	294(1)	294(1)
a, b, c (Å)	7.3592 (4), 9.3625 (16), 11.3789 (6)	12.1566 (2), 13.9335 (2), 7.9649 (2)	6.7133 (10), 8.5824 (10), 8.6551 (15)
V (Å^3)	716.54 (13)	1303.08 (4)	454.85 (12)
Z	1	2	1
μ (mm^{-1})	1.90	1.09	1.25
Crystal size (mm)	0.30 × 0.19 × 0.04	0.44 × 0.33 × 0.07	0.35 × 0.20 × 0.13
T_{min}, T_{max}	0.599, 0.928	0.645, 0.928	0.668, 0.854
No. of measured, independent and observed reflections	5106, 3092, 2625	11779, 3440, 2909	2823, 1595, 1387
R_{int}	0.019	0.021	0.049
(sin θ/λ)$_{max}$ (Å^{-1})	0.655	0.696	0.596
$R[F^2 > 2\,\sigma\,(F^2)]$, $wR(F^2)$, S	0.032, 0.080, 1.04	0.033, 0.087, 1.04	0.098, 0.290, 1.17
No. of reflections	3092	3440	1595
No. of parameters	182	170	142
H-atom treatment	H-atom parameters constrained	H-atom parameters constrained	H-atom parameters constrained
Δρ$_{max}$, Δρ$_{min}$ (e Å^{-3})	0.36, -0.23	0.31, -0.28	1.38, -0.96

	3.11	**3.13**	**4.12**
Chemical formula	$C_{32}H_{28}Cu_2N_{20}O_{10}$	$C_{16}H_{16}CuN_{10}O_6$	$C_{13}H_{15}Cl_2CuN_5O_4$
M_r	979.84	507.93	439.74
Crystal system, space group	Triclinic, $P\bar{1}$	Monoclinic, $P2_1/c$	Monoclinic, $P2_1/n$
Temperature (K)	294(1)	294(1)	294(1)
a, *b*, *c* (Å)	8.1940 (15), 10.9986 (6), 11.5081 (18)	7.6237 (4), 8.2017 (4), 15.3936 (9)	11.9377 (4), 11.9258 (3), 12.5922 (4)
V (Å^3)	1002.3 (2)	957.51 (9)	1736.57 (9)
Z	1	2	4
μ (mm^{-1})	1.14	1.20	1.60
Crystal size (mm)	0.36 × 0.22 × 0.10	0.29 × 0.13 × 0.07	0.26 × 0.26 × 0.08
T_{min}, T_{max}	0.684, 0.894	0.722, 0.920	-
No. of measured, independent and observed reflections	7342, 4311, 3241	6468, 2206, 1801	16620, 4605, 3669
R_{int}	0.039	0.039	0.042
(sin θ/λ)$_{max}$ (Å^{-1})	0.659	0.670	0.694
$R[F^2 > 2\sigma(F^2)]$, $wR(F^2)$, S	0.065, 0.178, 1.05	0.040, 0.088, 1.06	0.036, 0.100, 1.07
No. of reflections	4311	2206	4605
No. of parameters	297	159	229
H-atom treatment	H atoms treated by a mixture of independent and constrained refinement	H atoms treated by a mixture of independent and constrained refinement	H atoms treated by a mixture of independent and constrained refinement
Δρ$_{max}$, Δρ$_{min}$ (e Å^{-3})	1.38, -0.96	0.31, -0.40	0.50, -0.46

	4.14	**4.15**	**4.16**
Chemical formula	$C_{26}H_{40}CoN_{10}O_8S_2$	$C_{24}H_0CuN_{10}NiO_{10}$	$C_{18}H_{26}N_{10}Ni_2O_{16}$
M_r	743.73	710.59	755.91
Crystal system, space group	Monoclinic, $C2/c$	Monoclinic, $C2/c$	Monoclinic, $C2/c$
Temperature (K)	294(1)	294(1)	294(1)
a, *b*, *c* (Å)	7.0879 (9), 17.764 (2), 25.587 (4)	25.7006 (5), 8.1798 (1), 13.2019 (3)	25.7294 (18), 8.2627 (5), 13.0543 (11)
V (Å^3)	3220.4 (7)	2749.17 (9)	2745.1 (3)
Z	4	4	4
μ (mm^{-1})	0.73	1.54	1.47
Crystal size (mm)	0.26 × 0.26 × 0.08	0.29 × 0.25 × 0.11	0.28 × 0.26 × 0.05
No. of measured, independent and observed reflections	11970, 3596, 2632	10043, 3052, 2628	12342, 3649, 2965
R_{int}	0.087	0.032	0.025
(sin θ/λ)$_{max}$ (Å^{-1})	0.659	0.657	0.695
$R[F^2 > 2\sigma(F^2)]$, $wR(F^2)$, S	0.197, 0.489, 2.80	0.043, 0.124, 1.08	0.030, 0.080, 1.03
No. of reflections	3596	3052	3649
No. of parameters	216	246	253
No. of restraints	0	2	6
H-atom treatment	H atoms treated by a mixture of independent and constrained refinement	H atoms treated by a mixture of independent and constrained refinement	H atoms treated by a mixture of independent and constrained refinement
Δρ$_{max}$, Δρ$_{min}$ (e Å^{-3})	1.93, -0.96	0.90, -1.10	0.36, -0.55

	4.17	**4.18**	**4.20**
Chemical formula	$C_{18}H_{26}Co_2N_{10}O_{16}$	$C_{18}H_{26}Zn_2N_{10}O_{16}$	$C_{18}H_{26}Co_2N_{10}O_{16}$
M_r	756.35	766.01	756.35
Crystal system, space group	Monoclinic, *C*2/*c*	Monoclinic, *C*2/*c*	Triclinic, $P\bar{1}$
Temperature (K)	294(1)	294(1)	294(1)
a, *b*, *c* (Å)	25.9119 (15), 8.3153 (6), 13.1125 (12)	25.957 (2), 8.3140 (5), 13.069 (1)	6.4953 (14), 9.523 (2), 12.686 (3)
V (Å^3)	2795.7 (4)	2788.26	719.4 (3)
Z	4	-	1
μ (mm^{-1})	1.28	-	1.25
Crystal size (mm)	0.33 × 0.23 × 0.16	-	0.41 × 0.06 × 0.02
No. of measured, independent and observed reflections	14425, 3712, 3285	-	5149, 3152, 2352
R_{int}	0.018	-	0.045
(sin θ/λ)$_{max}$ (Å^{-1})	0.692	-	0.668
$R[F^2 > 2\sigma(F^2)]$, $wR(F^2)$, S	0.024, 0.063, 1.03	-	0.050, 0.112, 1.02
No. of reflections	3712	-	3152
No. of parameters	243	-	241
No. of restraints	0	-	6
H-atom treatment	H atoms treated by a mixture of independent and constrained refinement	H atoms treated by a mixture of independent and constrained refinement	H atoms treated by a mixture of independent and constrained refinement
Δρ$_{max}$, Δρ$_{min}$ (e Å^{-3})	0.33, -0.28	-	0.41, -0.43

	4.21	**4.22**	**4.23**
Chemical formula	$C_{18}H_{26}N_{10}O_{16}Zn_2$	$C_{18}H_{18}Mn_2N_{10}O_{12}$	$C_{22}H_{20}CuN_{10}O_8$
M_r	769.23	676.30	616.02
Crystal system, space group	Triclinic, $P\bar{1}$	Triclinic, $P\bar{1}$	Triclinic, $P\bar{1}$
Temperature (K)	294(1)	294(1)	294(1)
a, *b*, *c* (Å)	6.5046 (11), 9.5405 (14), 12.6769 (16)	6.8548 (9), 9.4400 (13), 9.823 (2)	7.0463 (13), 7.2925 (15), 13.188 (3)
V (Å^3)	721.46 (19)	590.65 (16)	624.9 (2)
Z	1	1	1
μ (mm^{-1})	1.76	1.16	0.94
Crystal size (mm)	0.60 × 0.35 × 0.28	0.66 × 0.37 × 0.18	0.38 × 0.21 × 0.16
No. of measured, independent and observed reflections	6307, 3687, 3278	5275, 3088, 2822	4549, 2714, 2190
R_{int}	0.015	0.025	0.036
(sin θ/λ)$_{max}$ (Å^{-1})	0.691	0.701	0.657
$R[F^2 > 2\sigma(F^2)]$, $wR(F^2)$, S	0.028, 0.068, 1.04	0.032, 0.084, 1.07	0.073, 0.188, 1.17
No. of reflections	3687	3088	2714
No. of parameters	250	207	188
No. of restraints	6	0	0
H-atom treatment	H atoms treated by a mixture of independent and constrained refinement	H atoms treated by a mixture of independent and constrained refinement	H atoms treated by a mixture of independent and constrained refinement
Δρ$_{max}$, Δρ$_{min}$ (e Å^{-3})	0.34, -0.31	0.47, -0.55	0.91, -0.39

	5.1	**5.4**	**5.5**
Chemical formula	$C_{21}H_{22}N_{10}O_4$	$C_{14}H_{16}N_{10}O_4$	$C_{14}H_{16}N_{10}O_4$
M_r	478.49	388.37	388.37
Crystal system, space group	Orthorhombic, $Pna2_1$	Triclinic, P^-1	Monoclinic, $P2_1/n$
Temperature (K)	294(1)	294(1)	294 (1)
a, b, c (Å)	28.642 (3), 5.0441 (5), 31.148 (3)	9.1675 (9), 10.0494 (16), 10.9931 (18)	8.6939 (10), 7.8854 (9), 26.452 (3)
V (Å^3)	4499.9 (8)	907.4 (2)	1808.35
Z	8	2	4
μ (mm^{-1})	0.10	0.11	-
Crystal size (mm)	1.20 × 0.16 × 0.15	0.55 × 0.45 × 0.20	-
No. of measured, independent and observed reflections	31339, 5181, 2654	8086, 4698, 3391	-
R_{int}	0.095	0.022	-
$(\sin \theta/\lambda)_{max}$ (Å^{-1})	0.658	0.692	-
$R[F^2 > 2\sigma(F^2)]$, $wR(F^2)$, S	0.095, 0.279, 1.09	0.055, 0.158, 1.03	-
No. of reflections	5181	4698	-
No. of parameters	635	256	-
No. of restraints	1	0	-
H-atom treatment	H atoms treated by a mixture of independent and constrained refinement	H atoms treated by a mixture of independent and constrained refinement	H atoms treated by a mixture of independent and constrained refinement
$\Delta\rho_{max}$, $\Delta\rho_{min}$ (e Å^{-3})	0.61, -0.36	0.44, -0.30	-

	5.15	**5.16**
Chemical formula	$C_{10}H_{12}CuN_{10}O_7$	$C_{10}H_{10}CuN_{10}O_6$
M_r	447.84	429.82
Crystal system, space group	Orthorhombic, $Pna2_1$	Orthorhombic, $Pna2_1$
Temperature (K)	294(1)	294 (1)
a, b, c (Å)	12.3497 (5), 9.0242 (4), 29.5410 (18)	12.9001 (5), 9.9112 (5), 11.9877 (5)
V (Å^3)	3292.2 (3)	1532.69 (12)
Z	8	4
μ (mm^{-1})	1.39	868
Crystal size (mm)	0.55 × 0.35 × 0.15	0.77 × 0.45 × 0.03
No. of measured, independent and observed reflections	27488, 8420, 7389	5315, 1789, 1665
R_{int}	0.043	0.025
$(\sin \theta/\lambda)_{max}$ (Å^{-1})	0.688	0.667
$R[F^2 > 2\sigma(F^2)]$, $wR(F^2)$, S	0.041, 0.102, 1.06	0.037, 0.096, 1.09
No. of reflections	8420	1789
No. of parameters	543	134
No. of restraints	19	3
H-atom treatment	H atoms treated by a mixture of independent and constrained refinement	H atoms treated by a mixture of independent and constrained refinement
$\Delta\rho_{max}$, $\Delta\rho_{min}$ (e Å^{-3})	0.90, -0.59	0.38, -0.44

Table A2: Atomic coordinates for **2.67**.

	x	*y*	*z*		*x*	*y*	*z*
Co1	0.37686(4)	0.75512(7)	0.30593(8)	**H25A**	0.6807	0.3504	0.0224
S1	0.19364(13)	0.9709(2)	0.14246(10)	**H25B**	0.7618	0.43	-0.0056
C1	0.2586(4)	0.8964(6)	0.1942(3)	**H25C**	0.676	0.5205	-0.0077
N1	0.3038(3)	0.8447(5)	0.2321(3)	**C31**	0.4176(3)	1.0803(5)	0.3564(3)
S2	0.55750(13)	0.5410(2)	0.47153(9)	**N32**	0.4452(3)	0.9753(4)	0.3125(3)
C2	0.4940(4)	0.6165(6)	0.4189(3)	**C33**	0.5151(4)	1.0130(6)	0.2792(4)
N2	0.4492(3)	0.6663(6)	0.3788(3)	**H33**	0.5343	0.9438	0.2475
C11	0.3348(3)	0.4325(5)	0.2543(3)	**C34**	0.5590(3)	1.1508(7)	0.2906(3)
N12	0.3070(2)	0.5362(4)	0.2989(3)	**H34**	0.6088	1.1719	0.2687
C13	0.2395(5)	0.4981(6)	0.3318(4)	**C35**	0.5277(4)	1.2555(6)	0.3348(3)
H13	0.2198	0.5697	0.3625	**H35**	0.5551	1.3513	0.3415
C14	0.1961(3)	0.3588(6)	0.3238(3)	**C36**	0.4567(4)	1.2216(6)	0.3695(3)
H14	0.1494	0.3352	0.3489	**H36**	0.4358	1.2911	0.4006
C15	0.2247(4)	0.2560(6)	0.2770(4)	**C41**	0.3413(3)	1.0286(6)	0.3904(3)
H15	0.1958	0.1624	0.2689	**N42**	0.3065(3)	0.8891(5)	0.3752(2)
C16	0.2951(3)	0.2908(6)	0.2425(3)	**N43**	0.2384(3)	0.8779(5)	0.4105(3)
H16	0.3159	0.2205	0.2118	**N44**	0.2362(4)	1.0098(5)	0.4453(3)
C21	0.4115(4)	0.4821(6)	0.2229(3)	**N45**	0.2983(3)	1.1068(5)	0.4339(2)
N22	0.4476(3)	0.6189(5)	0.2365(3)	**C42**	0.1697(4)	1.0433(10)	0.4936(4)
N23	0.5166(3)	0.6283(6)	0.2010(3)	**H42A**	0.189	1.008	0.5359
N24	0.5180(4)	0.4943(6)	0.1678(3)	**H42B**	0.1617	1.1569	0.496
N25	0.4536(3)	0.3990(6)	0.1783(3)	**C43**	0.0932(4)	0.9729(13)	0.4808(4)
C22	0.5881(6)	0.4455(9)	0.1225(5)	**H43A**	0.1021	0.8599	0.4767
H22A	0.6196	0.3605	0.1427	**H43B**	0.0736	1.011	0.4391
H22B	0.5635	0.4038	0.083	**C44**	0.0220(6)	1.0001(13)	0.5314(5)
C23	0.6409(7)	0.5599(13)	0.1068(6)	**H44A**	0.0082	1.1119	0.5326
H23A	0.6554	0.617	0.146	**H44B**	-0.0277	0.9431	0.5176
H23B	0.6118	0.6334	0.0785	**C45**	0.0425(6)	0.954(2)	0.5901(6)
C24	0.7254(8)	0.5083(14)	0.0720(6)	**H45A**	0.0005	0.8827	0.6064
H24A	0.7616	0.5997	0.0669	**H45B**	0.0465	1.0441	0.6182
H24B	0.7545	0.4313	0.0987	**H45C**	0.0957	0.9004	0.5888
C25	0.7100(10)	0.4487(19)	0.0170(8)				

Table A3: Bond lengths (Å) for **2.67**.

Atom1	Atom2	Length	Atom1	Atom2	Length	Atom1	Atom2	Length	Atom1	Atom2	Length
Co1	**N1**	2.061(6)	**C14**	**C15**	1.376(9)	**C24**	**H24B**	0.97	**C41**	**N45**	1.308(7)
Co1	**N2**	2.037(6)	**C15**	**H15**	0.931	**C24**	**C25**	1.26(2)	**N42**	**N43**	1.311(7)
Co1	**N12**	2.165(3)	**C15**	**C16**	1.361(9)	**C25**	**H25A**	0.96	**N43**	**N44**	1.326(7)
Co1	**N22**	2.156(5)	**C16**	**H16**	0.929	**C25**	**H25B**	0.96	**N44**	**N45**	1.307(7)
Co1	**N32**	2.161(4)	**C21**	**N22**	1.322(7)	**C25**	**H25C**	0.96	**N44**	**C42**	1.48(1)
Co1	**N42**	2.140(5)	**C21**	**N25**	1.338(8)	**C31**	**N32**	1.342(7)	**C42**	**H42A**	0.972
S1	**C1**	1.615(6)	**N22**	**N23**	1.324(7)	**C31**	**C36**	1.374(7)	**C42**	**H42B**	0.97
C1	**N1**	1.149(8)	**N23**	**N24**	1.324(8)	**C31**	**C41**	1.471(7)	**C42**	**C43**	1.38(1)
S2	**C2**	1.615(6)	**N24**	**N25**	1.323(8)	**N32**	**C33**	1.347(9)	**C43**	**H43A**	0.97
C2	**N2**	1.171(8)	**N24**	**C22**	1.51(1)	**C33**	**H33**	0.929	**C43**	**H43B**	0.97
C11	**N12**	1.345(7)	**C22**	**H22A**	0.971	**C33**	**C34**	1.379(8)	**C43**	**C44**	1.56(1)
C11	**C16**	1.376(7)	**C22**	**H22B**	0.97	**C34**	**H34**	0.931	**C44**	**H44A**	0.97
C11	**C21**	1.446(8)	**C22**	**C23**	1.32(1)	**C34**	**C35**	1.365(8)	**C44**	**H44B**	0.97
N12	**C13**	1.312(9)	**C23**	**H23A**	0.97	**C35**	**H35**	0.93	**C44**	**C45**	1.31(2)
C13	**H13**	0.93	**C23**	**H23B**	0.97	**C35**	**C36**	1.370(9)	**C45**	**H45A**	0.96
C13	**C14**	1.376(8)	**C23**	**C24**	1.59(2)	**C36**	**H36**	0.931	**C45**	**H45B**	0.96
C14	**H14**	0.928	**C24**	**H24A**	0.97	**C41**	**N42**	1.340(7)	**C45**	**H45C**	0.96

Table A4: Bond angles (°) for **2.67.**

Atom1	Atom2	Atom3	Angle	Atom1	Atom2	Atom3	Angle	Atom1	Atom2	Atom3	Angle
N1	Co1	N2	179.9(2)	C21	N22	N23	107.3(5)	H34	C34	C35	120.8
N1	Co1	N12	88.5(2)	N22	N23	N24	104.4(5)	C34	C35	H35	119.5
N1	Co1	N22	90.1(2)	N22	N23	N24	104.4(5)	C34	C35	C36	121.0(5)
N1	Co1	N32	90.9(2)	N23	N24	N25	115.0(5)	H35	C35	C36	119.5

N1	Co1	N42	90.1(2)	N23	N24	C22	124.4(6)	C31	C36	C35	117.0(5)
N2	Co1	N12	91.5(2)	N25	N24	C22	120.5(6)	C31	C36	H36	121.4
N2	Co1	N22	89.8(2)	C21	N25	N24	100.5(5)	C35	C36	H36	121.6
N2	Co1	N32	89.2(2)	N24	C22	H22A	108.6	C31	C41	N42	119.5(5)
N2	Co1	N42	90.0(2)	N24	C22	H22B	108.5	C31	C41	N45	127.6(5)
N12	Co1	N22	76.6(2)	N24	C22	C23	115.0(8)	N42	C41	N45	112.8(5)
N12	Co1	N32	179.3(2)	H22A	C22	H22B	107.5	Co1	N42	C41	113.9(3)
N12	Co1	N42	103.1(2)	H22A	C22	C23	108.5	Co1	N42	N43	140.0(4)
N22	Co1	N32	103.8(2)	H22B	C22	C23	108.5	C41	N42	N43	106.1(4)
N22	Co1	N42	179.7(2)	C22	C23	H23A	108	N42	N43	N44	105.2(5)
N32	Co1	N42	76.5(2)	C22	C23	H23B	108	N43	N44	N45	114.2(5)
S1	C1	N1	178.5(6)	C22	C23	C24	117(1)	N43	N44	C42	122.9(5)
Co1	N1	C1	175.1(5)	H23A	C23	H23B	107	N45	N44	C42	122.9(5)
S2	C2	N2	177.0(6)	H23A	C23	C24	108	C41	N45	N44	101.7(5)
Co1	N2	C2	176.9(5)	H23B	C23	C24	108	N44	C42	H42A	108.5
N12	C11	C16	122.4(5)	C23	C24	H24A	110	N44	C42	H42B	108.5
N12	C11	C21	113.3(5)	C23	C24	H24B	110	N44	C42	C43	114.9(7)
C16	C11	C21	124.2(5)	C23	C24	C25	110(1)	H42A	C42	H42B	107.5
Co1	N12	C11	115.7(3)	H24A	C24	H24B	108	H42A	C42	C43	108.6
Co1	N12	C13	126.7(4)	H24A	C24	C25	110	H42B	C42	C43	108.6
C11	N12	C13	117.6(5)	H24B	C24	C25	110	C42	C43	H43A	108.2
N12	C13	H13	118	C24	C25	H25A	110	C42	C43	H43B	108.1
N12	C13	C14	124.1(6)	C24	C25	H25B	109	C42	C43	C44	116.8(8)
H13	C13	C14	117.9	C24	C25	H25C	109	H43A	C43	H43B	107.3
C13	C14	H14	121.4	H25A	C25	H25B	109	H43A	C43	C44	108.1
C13	C14	C15	117.2(6)	H25A	C25	H25C	110	H43B	C43	C44	108
H14	C14	C15	121.4	H25B	C25	H25C	109	C43	C44	H44A	109
C14	C15	H15	119.9	N32	C31	C36	124.0(5)	C43	C44	H44B	109
C14	C15	C16	120.2(6)	N32	C31	C41	113.3(5)	C43	C44	C45	113.1(9)
H15	C15	C16	119.9	C36	C31	C41	122.7(5)	H44A	C44	H44B	108
C11	C16	C15	118.4(5)	Co1	N32	C31	116.5(4)	H44A	C44	C45	109
C11	C16	H16	120.8	Co1	N32	C33	126.1(4)	H44B	C44	C45	109
C15	C16	H16	120.8	C31	N32	C33	117.3(5)	C44	C45	H45A	110
C11	C21	N22	121.8(5)	N32	C33	H33	118.8	C44	C45	H45B	110
C11	C21	N25	125.4(5)	N32	C33	C34	122.2(6)	C44	C45	H45C	109
N22	C21	N25	112.7(5)	H33	C33	C34	119	H45A	C45	H45B	109
Co1	N22	C21	112.3(4)	C33	C34	H34	120.8	H45A	C45	H45C	109
Co1	N22	N23	140.3(4)	C33	C34	C35	118.4(5)	H45B	C45	H45C	109

Table A5: Atomic coordinates for **2.71**.

	x	*y*	*z*		*x*	*y*	*z*
Co1	0.5	0	0.5	**C11**	0.4187(3)	-0.3240(4)	0.4497(2)
S1	0.24260(11)	0.20554(18)	0.28451(9)	**N12**	0.4889(2)	-0.2224(3)	0.43083(17)
C1	0.3271(3)	0.1341(4)	0.3584(2)	**C13**	0.5378(3)	-0.2611(5)	0.3681(2)
N1	0.3880(3)	0.0864(4)	0.4106(2)	**H13**	0.5861	-0.1919	0.3541
C11	0.5813(3)	0.3240(4)	0.5503(2)	**C14**	0.5200(4)	-0.3999(6)	0.3229(3)
N12	0.5111(2)	0.2224(3)	0.56917(17)	**H14**	0.5562	-0.4241	0.2796
C13	0.4622(3)	0.2611(5)	0.6319(2)	**C15**	0.4490(4)	-0.5010(5)	0.3421(3)
H13	0.4139	0.1919	0.6459	**H15**	0.4355	-0.5944	0.3114
C14	0.4800(4)	0.3999(6)	0.6771(3)	**C16**	0.3970(4)	-0.4647(5)	0.4074(3)
H14	0.4438	0.4241	0.7204	**H16**	0.3489	-0.5332	0.4223
C15	0.5510(4)	0.5010(5)	0.6579(3)	**C21**	0.3704(3)	-0.2715(4)	0.5202(2)
H15	0.5645	0.5944	0.6886	N22	0.3929(2)	-0.1318(4)	0.55766(18)
C16	0.6030(4)	0.4647(5)	0.5926(3)	**N23**	0.3407(3)	-0.1187(4)	0.6206(2)
H16	0.6511	0.5332	0.5777	**N24**	0.2898(3)	-0.2521(5)	0.6177(3)
C21	0.6296(3)	0.2715(4)	0.4798(2)	**N25**	0.3049(3)	-0.3504(5)	0.5570(3)
N22	0.6071(2)	0.1318(4)	0.44234(18)	**C31A**	0.1930(16)	-0.280(3)	0.6553(12)
N23	0.6593(3)	0.1187(4)	0.3794(2)	**H31A**	0.1787	-0.3924	0.6566
N24	0.7102(3)	0.2521(5)	0.3823(3)	**H31B**	0.1372	-0.2279	0.6204
N25	0.6951(3)	0.3504(5)	0.4430(3)	**C32A**	0.2066(18)	-0.219(3)	0.7368(10)
C31A	0.8070(16)	0.280(3)	0.3447(12)	**H32A**	0.2616	-0.2704	0.7727
H31A	0.8213	0.3924	0.3434	**H32B**	0.2193	-0.1055	0.7364
H31B	0.8628	0.2279	0.3796	**C33**	0.1025(9)	-0.2559(15)	0.7680(8)
C32A	0.7934(18)	0.219(3)	0.2632(10)	**H33A**	0.0906	-0.3692	0.7687
H32A	0.7384	0.2704	0.2273	**H33B**	0.0476	-0.2061	0.7308
H32B	0.7807	0.1055	0.2636	**C34**	0.1105(10)	-0.2007(18)	0.8404(8)
C33	0.8975(9)	0.2559(15)	0.2320(8)	**H34A**	0.1787	-0.2187	0.8678
H33A	0.9094	0.3692	0.2313	**H34B**	0.1016	-0.0869	0.8349

H33B	0.9524	0.2061	0.2692	**C35**	0.0436(14)	-0.258(3)	0.8993(12)
C34	0.8895(10)	0.2007(18)	0.1596(8)	**H35A**	0.0865	-0.2539	0.9542
H34A	0.8213	0.2187	0.1322	**H35B**	0.0366	-0.3693	0.8855
H34B	0.8984	0.0869	0.1651	**C36**	-0.0250(8)	-0.229(2)	0.9144(9)
C35	0.9564(14)	0.258(3)	0.1007(12)	**H36A**	-0.0238	-0.1144	0.9143
H35A	0.9135	0.2539	0.0458	**H36B**	-0.0699	-0.258	0.863
H35B	0.9634	0.3693	0.1145	**C37**	-0.0885(9)	-0.2665(19)	0.9852(7)
C36	1.0250(8)	0.229(2)	0.0856(9)	**H37A**	-0.0721	-0.1879	1.0297
H36A	1.0238	0.1144	0.0857	**H37B**	-0.0666	-0.3682	1.0097
H36B	1.0699	0.258	0.137	**C38**	-0.1780(8)	-0.2709(17)	0.9673(7)
C37	1.0885(9)	0.2665(19)	0.0148(7)	**H38A**	-0.1994	-0.3791	0.9597
H37A	1.0721	0.1879	-0.0297	**H38B**	-0.2075	-0.224	1.0124
H37B	1.0666	0.3682	-0.0097	**H38C**	-0.1985	-0.2132	0.9156
C38	1.1780(8)	0.2709(17)	0.0327(7)	**C31B**	0.7524(12)	0.2950(17)	0.3029(11)
H38A	1.1994	0.3791	0.0403	**H31C**	0.7067	0.2662	0.2519
H38B	1.2075	0.224	-0.0124	**H31D**	0.7671	0.4073	0.3012
H38C	1.1985	0.2132	0.0844	**C32B**	0.8410(18)	0.203(4)	0.3116(18)
S1	0.75740(11)	-0.20554(18)	0.71549(9)	**H32C**	0.8252	0.0907	0.3085
C1	0.6729(3)	-0.1341(4)	0.6416(2)	**H32D**	0.883	0.2243	0.3657
N1	0.6120(3)	-0.0864(4)	0.5894(2)				

Table A6: Bond lengths (Å) for **2.71**.

Atom1	Atom2	Length	Atom1	Atom2	Length	Atom1	Atom2	Length	Atom1	Atom2	Length
Co1	**N1**	2.044	**C31A**	**H31D**	1.34	**C36**	**H36A**	0.97	**C31A**	**H31A**	0.97
Co1	**N12**	2.17	**C31A**	**C32B**	0.99(4)	**C36**	**H36B**	0.97	**C31A**	**H31B**	0.97
Co1	**N22**	2.146	**C31A**	**H32D**	1.13	**C36**	**C37**	1.55(2)	**C31A**	**C32A**	1.38(3)
Co1	**N1**	2.044	**H31A**	**C31B**	1.33	**C37**	**H37A**	0.97	**C32A**	**H32A**	0.97
Co1	**N12**	2.17	**H31B**	**C32B**	1.1	**C37**	**H37B**	0.97	**C32A**	**H32B**	0.97
Co1	**N22**	2.146	**C32A**	**H32A**	0.97	**C37**	**C38**	1.20(2)	**C32A**	**C33**	1.60(3)
S1	**C1**	1.623(4)	**C14**	**C15**	1.357(7)	**C38**	**H38A**	0.96	**C33**	**H33A**	0.97
C1	**N1**	1.148(5)	**C32B**	**H32D**	0.97	**C38**	**H38B**	0.96	**C33**	**H33B**	0.97
C11	**N12**	1.349(5)	**C32A**	**H32B**	0.97	**C38**	**H38C**	0.96	**C33**	**C34**	1.23(2)
C11	**C16**	1.374(5)	**C32A**	**C33**	1.60(3)	**S1**	**C1**	1.623(4)	**C34**	**H34A**	0.97
C11	**C21**	1.454(5)	**C32A**	**C31B**	1.11(3)	**C1**	**N1**	1.148(5)	**C34**	**H34B**	0.97
N12	**C13**	1.323(5)	**C32A**	**H31C**	1.23	**C11**	**N12**	1.349(5)	**C34**	**C35**	1.48(3)
C13	**H13**	0.93	**C32A**	**C32B**	0.93(3)	**C11**	**C16**	1.374(5)	**C35**	**H35A**	0.97
C13	**C14**	1.376(6)	**C32A**	**H32C**	1.33	**C11**	**C21**	1.454(5)	**C35**	**H35B**	0.97
C14	**H14**	0.929	**H32A**	**C31B**	1.21	**N12**	**C13**	1.323(5)	**C35**	**C36**	1.03(2)
C14	**C15**	1.357(7)	**H32B**	**C32B**	1.32	**C13**	**H13**	0.93	**C36**	**H36A**	0.97
C15	**H15**	0.93	**C33**	**H33A**	0.97	**C13**	**C14**	1.376(6)	**C36**	**H36B**	0.97
C15	**C16**	1.379(8)	**C33**	**H33B**	0.97	**C14**	**H14**	0.929	**C36**	**C37**	1.55(2)
C16	**H16**	0.93	**C33**	**C34**	1.23(2)	**C15**	**H15**	0.93	**C37**	**H37A**	0.97
C21	**N22**	1.335(5)	**C33**	**C32B**	1.64(3)	**C15**	**C16**	1.379(8)	**C37**	**H37B**	0.97
C21	**N25**	1.318(6)	**C34**	**H34A**	0.97	**C16**	**H16**	0.93	**C37**	**C38**	1.20(2)
N22	**N23**	1.319(5)	**C34**	**H34B**	0.97	**C21**	**N22**	1.335(5)	**C38**	**H38A**	0.96
N23	**N24**	1.318(6)	**C34**	**C35**	1.48(3)	**C21**	**N25**	1.318(6)	**C38**	**H38B**	0.96
N24	**N25**	1.314(7)	**C35**	**H35A**	0.97	**N22**	**N23**	1.319(5)	**C38**	**H38C**	0.96
N24	**C31A**	1.54(2)	**C35**	**H35B**	0.97	**N23**	**N24**	1.318(6)	**C31B**	**H31C**	0.97
N24	**C31B**	1.51(2)	**C35**	**C36**	1.03(2)	**N24**	**N25**	1.314(7)	**C31B**	**H31D**	0.97
C31A	**H31A**	0.97	**C31A**	**C31B**	0.92(2)	**N24**	**C31A**	1.54(2)	**C32B**	**H32C**	0.97
C31A	**H31B**	0.97									

Table A7: Bond angles (°) for **2.71**.

Atom1	Atom2	Atom3	Angle	Atom1	Atom2	Atom3	Angle	Atom1	Atom2	Atom3	Angle
N1	Co1	N12	91.6	C33	C32A	H32C	96	H31B	C31A	C32A	110
N1	Co1	N22	89.7	C31B	C32A	H31C	49	C31A	C32A	H32A	111
N1	Co1	N1	180	C31B	C32A	C32B	88(3)	C31A	C32A	H32B	111
N1	Co1	N12	88.4	C31B	C32A	H32C	108	C31A	C32A	C33	103(2)
N1	Co1	N22	90.3	H31C	C32A	C32B	134	H32A	C32A	H32B	109
N12	Co1	N22	76.7	H31C	C32A	H32C	124	H32A	C32A	C33	111
N12	Co1	N1	88.4	C32B	C32A	H32C	47	H32B	C32A	C33	111
N12	Co1	N12	180	C32A	H32A	C31B	60	C32A	C33	H33A	111
N12	Co1	N22	103.3	C32A	H32B	C32B	45	C32A	C33	H33B	111
N22	Co1	N1	90.3	C32A	C33	H33A	111	C32A	C33	C34	105(1)
N22	Co1	N12	103.3	C32A	C33	H33B	111	H33A	C33	H33B	109
N22	Co1	N22	180	C32A	C33	C34	105(1)	H33A	C33	C34	111

N1	Co1	N12	91.6	C32A	C33	C32B	33(1)	H33B	C33	C34	111
N1	Co1	N22	89.7	H33A	C33	H33B	109	C33	C34	H34A	107
N12	Co1	N22	76.7	H33A	C33	C34	111	C33	C34	H34B	107
S1	C1	N1	178.6(4)	H33A	C33	C32B	112	C33	C34	C35	120(1)
Co1	N1	C1	177.7	H33B	C33	C34	111	H34A	C34	H34B	107
N12	C11	C16	123.0(3)	H33B	C33	C32B	79	H34A	C34	C35	107
N12	C11	C21	113.4(3)	C34	C33	C32B	129(2)	H34B	C34	C35	107
C16	C11	C21	123.6(4)	C33	C34	H34A	107	C34	C35	H35A	103
Co1	N12	C11	115.6	C33	C34	H34B	107	C34	C35	H35B	103
Co1	N12	C13	126.4	C33	C34	C35	120(1)	C34	C35	C36	137(2)
C11	N12	C13	117.7(3)	H34A	C34	H34B	107	H35A	C35	H35B	105
N12	C13	H13	118.7	H34A	C34	C35	107	H35A	C35	C36	103
N12	C13	C14	122.5(4)	H34B	C34	C35	107	H35B	C35	C36	103
H13	C13	C14	118.8	C34	C35	H35A	103	C35	C36	H36A	103
C13	C14	H14	120.3	C34	C35	H35B	103	C35	C36	H36B	102
C13	C14	C15	119.4(4)	C34	C35	C36	137(2)	C35	C36	C37	138(2)
H14	C14	C15	120.3	H35A	C35	H35B	105	H36A	C36	H36B	105
C14	C15	H15	120.2	H35A	C35	C36	103	H36A	C36	C37	102
C14	C15	C16	119.6(5)	H35B	C35	C36	103	H36B	C36	C37	102
H15	C15	C16	120.2	C35	C36	H36A	103	C36	C37	H37A	107
C11	C16	C15	117.8(4)	C35	C36	H36B	102	C36	C37	H37B	108
C11	C16	H16	121.2	C35	C36	C37	138(2)	C36	C37	C38	119(1)
C15	C16	H16	121.1	H36A	C36	H36B	105	H37A	C37	H37B	107
C11	C21	N22	121.0(3)	H36A	C36	C37	102	H37A	C37	C38	107
C11	C21	N25	127.2(4)	H36B	C36	C37	102	H37B	C37	C38	108
N22	C21	N25	111.7(3)	C36	C37	H37A	107	C37	C38	H38A	109
Co1	N22	C21	112.9	C36	C37	H37B	108	C37	C38	H38B	109
Co1	N22	N23	139.6	C36	C37	C38	119(1)	C37	C38	H38C	109
C21	N22	N23	107.5(3)	H37A	C37	H37B	107	H38A	C38	H38B	109
N22	N23	N24	104.0(3)	H37A	C37	C38	107	H38A	C38	H38C	110
N23	N24	N25	115.1(4)	H37B	C37	C38	108	H38B	C38	H38C	109
N23	N24	C31A	126.1(9)	C37	C38	H38A	109	N24	C31B	C31A	74(2)
N23	N24	C31B	116.1(7)	C37	C38	H38B	109	N24	C31B	H31A	94
N25	N24	C31A	115.4(9)	C37	C38	H38C	109	N24	C31B	C32A	129(2)
N25	N24	C31B	125.9(7)	H38A	C38	H38B	109	N24	C31B	H32A	141
C31A	N24	C31B	35(1)	H38A	C38	H38C	110	N24	C31B	H31C	111
C21	N25	N24	101.6(4)	H38B	C38	H38C	109	N24	C31B	H31D	111
N24	C31A	H31A	110	S1	C1	N1	178.6(4)	C31A	C31B	H31A	47
N24	C31A	H31B	110	Co1	N1	C1	177.7	C31A	C31B	C32A	85(2)
N24	C31A	C31B	71(2)	N12	C11	C16	123.0(3)	C31A	C31B	H32A	133
N24	C31A	H31D	91	N12	C11	C21	113.4(3)	C31A	C31B	H31C	154
N24	C31A	C32B	127(3)	C16	C11	C21	123.6(4)	C31A	C31B	H31D	91
N24	C31A	H32D	128	Co1	N12	C11	115.6	H31A	C31B	C32A	105
H31A	C31A	H31B	108	Co1	N12	C13	126.4	H31A	C31B	H32A	125
H31A	C31A	C31B	89	C11	N12	C13	117.7(3)	H31A	C31B	H31C	150
H31A	C31A	H31D	43.3	N12	C13	H13	118.7	H31A	C31B	H31D	43.8
H31A	C31A	C32B	121	N12	C13	C14	122.5(4)	C32A	C31B	H32A	49
H31A	C31A	H32D	104	H13	C13	C14	118.8	C32A	C31B	H31C	72
H31B	C31A	C31B	160	C13	C14	H14	120.3	C32A	C31B	H31D	115
H31B	C31A	H31D	151	C13	C14	C15	119.4(4)	H32A	C31B	H31C	31.1
H31B	C31A	C32B	68	H14	C14	C15	120.3	H32A	C31B	H31D	98
H31B	C31A	H32D	18.8	C14	C15	H15	120.2	H31C	C31B	H31D	109
C31B	C31A	H31D	46	C14	C15	C16	119.6(5)	C32A	H31C	C31B	59
C31B	C31A	C32B	95(3)	H15	C15	C16	120.2	C31A	H31D	C31B	43
C31B	C31A	H32D	149	C11	C16	C15	117.8(4)	C31A	C32B	H31B	55
H31D	C31A	C32B	116	C11	C16	H16	121.2	C31A	C32B	C32A	91(3)
H31D	C31A	H32D	139	C15	C16	H16	121.1	C31A	C32B	H32B	115
C32B	C31A	H32D	54	C11	C21	N22	121.0(3)	C31A	C32B	C33	123(3)
C31A	H31A	C31B	44	C11	C21	N25	127.2(4)	C31A	C32B	H32C	123
C31A	H31B	C32B	57	N22	C21	N25	111.7(3)	C31A	C32B	H32D	70
H32A	C32A	H32B	109	Co1	N22	C21	112.9	H31B	C32B	C32A	146
H32A	C32A	C33	111	Co1	N22	N23	139.6	H31B	C32B	H32B	138
H32A	C32A	C31B	71	C21	N22	N23	107.5(3)	H31B	C32B	C33	129
H32A	C32A	H31C	30.3	N22	N23	N24	104.0(3)	H31B	C32B	H32C	105
H32A	C32A	C32B	157	N23	N24	N25	115.1(4)	H31B	C32B	H32D	20
H32A	C32A	H32C	147	N23	N24	C31A	126.1(9)	C32A	C32B	H32B	48
H32B	C32A	C33	111	N25	N24	C31A	115.4(9)	C32A	C32B	C33	71(2)
H32B	C32A	C31B	117	C21	N25	N24	101.6(4)	C32A	C32B	H32C	89
H32B	C32A	H31C	99	N24	C31A	H31A	110	C32A	C32B	H32D	160
H32B	C32A	C32B	87	N24	C31A	H31B	110	H32B	C32B	C33	93

H32B	C32A	H32C	40.5	N24	C31A	C32A	108(2)	H32B	C32B	H32C	41
C33	C32A	C31B	128(2)	H31A	C31A	H31B	108	H32B	C32B	H32D	149
C33	C32A	H31C	140	H31A	C31A	C32A	110	C33	C32B	H32C	111
C33	C32A	C32B	76(2)	C32A	H32C	C32B	44	C33	C32B	H32D	111
C31A	H32D	C32B	56	H32C	C32B	H32D	109				

Table A8: Atomic coordinates for **3.1**.

	x	*y*	*z*		*x*	*y*	*z*
O1A	0.4670(2)	-0.1773(3)	0.90610(16)	**N25A**	0.1066(2)	0.0015(3)	0.76322(19)
O2A	0.6848(2)	-0.1098(3)	0.80803(16)	**O1B**	0.6675(2)	0.5772(2)	0.76928(15)
C1A	0.4905(3)	-0.0932(4)	0.7248(2)	**O2B**	0.8671(2)	0.4991(3)	0.83915(15)
H1AA	0.535	-0.003	0.6779	**C1B**	0.9019(3)	0.6551(3)	0.6716(2)
H1AB	0.5211	-0.1719	0.6955	**H1BA**	0.9427	0.7347	0.6845
C2A	0.5424(3)	-0.1312(4)	0.8242(2)	**H1BB**	0.9819	0.5882	0.6567
C3A	0.7536(3)	-0.1427(5)	0.8970(3)	**C2B**	0.7973(3)	0.5736(3)	0.7640(2)
H3AA	0.8546	-0.1762	0.8812	**C3B**	0.7755(4)	0.4129(5)	0.9350(3)
H3AB	0.703	-0.2217	0.9525	**H3BA**	0.707	0.4788	0.9625
C4A	0.7493(5)	-0.0105(5)	0.9287(3)	**N25B**	0.6958(3)	0.7528(4)	0.4700(2)
H4AA	0.7871	0.0716	0.8711	**C4B**	0.8679(6)	0.3359(7)	1.0055(3)
H4AB	0.808	-0.0297	0.9805	**H4BA**	0.9283	0.2636	0.9809
H4AC	0.65	0.0128	0.9551	**H4BB**	0.8091	0.2872	1.0702
C11A	0.2840(3)	0.1679(3)	0.7741(2)	**H4BC**	0.9289	0.4047	1.0133
N12A	0.4253(2)	0.1766(3)	0.7744(2)	**C11B**	0.7756(3)	0.4929(3)	0.5445(2)
C13A	0.4650(3)	0.2990(4)	0.7854(3)	**N12B**	0.8576(3)	0.4048(3)	0.6102(2)
H13	0.5635	0.3071	0.7857	**C13B**	0.8684(4)	0.2609(4)	0.6183(3)
C14A	0.3699(4)	0.4139(4)	0.7965(3)	**H13A**	0.9253	0.1979	0.6634
H3BB	0.7198	0.3432	0.922	**C14B**	0.8012(5)	0.2022(5)	0.5647(4)
H14	0.4031	0.4972	0.8039	**H14A**	0.8123	0.1015	0.573
C15A	0.2262(4)	0.4024(4)	0.7963(3)	**C15B**	0.7181(5)	0.2916(6)	0.4990(4)
H15	0.1585	0.478	0.8036	**H15A**	0.6703	0.2531	0.462
C16A	0.1822(3)	0.2770(4)	0.7852(2)	**C16B**	0.7045(4)	0.4419(5)	0.4873(3)
H16	0.0841	0.2666	0.7852	**H16A**	0.6489	0.506	0.4418
C21A	0.2417(3)	0.0345(3)	0.7596(2)	**C21B**	0.7671(3)	0.6505(3)	0.5336(2)
N22A	0.3327(2)	-0.0728(3)	0.73792(16)	**N22B**	0.8281(3)	0.7150(3)	0.58551(17)
N23A	0.2523(3)	-0.1742(3)	0.72797(19)	**N23B**	0.7945(3)	0.8611(3)	0.5532(2)
N24A	0.1166(3)	-0.1288(3)	0.7434(2)	**N24B**	0.7161(4)	0.8820(3)	0.4836(2)

Table A9: Bond lengths (Å) for **3.1**.

Atom1	Atom2	Length	Atom1	Atom2	Length	Atom1	Atom2	Length	Atom1	Atom2	Length
O1A	**C2A**	1.195(3)	**C11A**	**C21A**	1.465(5)	**O2B**	**C2B**	1.319(3)	**C11B**	**C21B**	1.463(4)
O2A	**C2A**	1.327(3)	**N12A**	**C13A**	1.332(5)	**O2B**	**C3B**	1.478(4)	**N12B**	**C13B**	1.341(5)
O2A	**C3A**	1.453(5)	**C13A**	**H13**	0.93	**C1B**	**H1BA**	0.97	**C13B**	**H13A**	0.93
C1A	**H1AA**	0.97	**C13A**	**C14A**	1.373(5)	**C1B**	**H1BB**	0.97	**C13B**	**C14B**	1.354(8)
C1A	**H1AB**	0.97	**C14A**	**H14**	0.93	**C1B**	**C2B**	1.495(3)	**C14B**	**H14A**	0.931
C1A	**C2A**	1.496(4)	**C14A**	**C15A**	1.356(6)	**C1B**	**N22B**	1.440(4)	**C14B**	**C15B**	1.349(7)
C1A	**N22A**	1.447(3)	**C15A**	**H15**	0.93	**C3B**	**H3BA**	0.97	**C15B**	**H15A**	0.93
C3A	**H3AA**	0.97	**C15A**	**C16A**	1.376(6)	**C3B**	**H3BB**	0.971	**C15B**	**C16B**	1.390(8)
C3A	**H3AB**	0.97	**C16A**	**H16**	0.93	**C3B**	**C4B**	1.415(6)	**C16B**	**H16A**	0.93
C3A	**C4A**	1.474(7)	**C21A**	**N22A**	1.342(4)	**C4B**	**H4BA**	0.96	**C21B**	**N22B**	1.337(5)
C4A	**H4AA**	0.96	**C21A**	**N25A**	1.317(4)	**C4B**	**H4BB**	0.961	**C21B**	**N25B**	1.315(4)
C4A	**H4AB**	0.959	**N22A**	**N23A**	1.346(4)	**C4B**	**H4BC**	0.96	**N22B**	**N23B**	1.345(4)
C4A	**H4AC**	0.96	**N23A**	**N24A**	1.295(4)	**C11B**	**N12B**	1.338(4)	**N23B**	**N24B**	1.292(5)
C11A	**N12A**	1.329(4)	**N24A**	**N25A**	1.360(4)	**C11B**	**C16B**	1.371(6)	**N24B**	**N25B**	1.353(5)
C11A	**C16A**	1.366(4)	**O1B**	**C2B**	1.195(3)						

Table A10: Bond angles (°) for **3.1**.

Atom1	Atom2	Atom3	Angle	Atom1	Atom2	Atom3	Angle	Atom1	Atom2	Atom3	Angle
C2A	O2A	C3A	117.3(3)	C14A	C15A	H15	120.5	C3B	C4B	H4BB	109.5
H1AA	C1A	H1AB	108	C14A	C15A	C16A	118.9(4)	C3B	C4B	H4BC	109.5
H1AA	C1A	C2A	109.3	H15	C15A	C16A	120.5	H4BA	C4B	H4BB	109.5
H1AA	C1A	N22A	109.4	C11A	C16A	C15A	119.4(3)	H4BA	C4B	H4BC	109.5
H1AB	C1A	C2A	109.4	C11A	C16A	H16	120.3	H4BB	C4B	H4BC	109.4
H1AB	C1A	N22A	109.4	C15A	C16A	H16	120.3	N12B	C11B	C16B	122.9(3)
C2A	C1A	N22A	111.2(3)	C11A	C21A	N22A	126.4(3)	N12B	C11B	C21B	116.8(3)

O1A	C2A	O2A	125.1(3)	C11A	C21A	N25A	125.4(3)	C16B	C11B	C21B	120.3(3)
O1A	C2A	C1A	124.8(3)	N22A	C21A	N25A	108.2(2)	C11B	N12B	C13B	116.8(3)
O2A	C2A	C1A	110.1(3)	C1A	N22A	C21A	131.9(2)	N12B	C13B	H13A	118.1
O2A	C3A	H3AA	109.4	C1A	N22A	N23A	119.6(2)	N12B	C13B	C14B	123.7(4)
O2A	C3A	H3AB	109.5	C21A	N22A	N23A	108.5(2)	H13A	C13B	C14B	118.2
O2A	C3A	C4A	110.7(3)	N22A	N23A	N24A	106.6(3)	C13B	C14B	H14A	120.4
H3AA	C3A	H3AB	108.1	N23A	N24A	N25A	110.4(3)	C13B	C14B	C15B	119.1(5)
H3AA	C3A	C4A	109.5	C21A	N25A	N24A	106.3(2)	H14A	C14B	C15B	120.4
H3AB	C3A	C4A	109.5	C2B	O2B	C3B	116.3(3)	C14B	C15B	H15A	120.4
C3A	C4A	H4AA	109.5	H1BA	C1B	H1BB	108.1	C14B	C15B	C16B	119.3(5)
C3A	C4A	H4AB	109.5	H1BA	C1B	C2B	109.6	H15A	C15B	C16B	120.4
C3A	C4A	H4AC	109.5	H1BA	C1B	N22B	109.7	C11B	C16B	C15B	118.1(4)
H4AA	C4A	H4AB	109.4	H1BB	C1B	C2B	109.6	C11B	C16B	H16A	121
H4AA	C4A	H4AC	109.4	H1BB	C1B	N22B	109.6	C15B	C16B	H16A	120.9
H4AB	C4A	H4AC	109.5	C2B	C1B	N22B	110.3(2)	C11B	C21B	N22B	126.7(3)
N12A	C11A	C16A	122.7(3)	O1B	C2B	O2B	124.6(3)	C11B	C21B	N25B	124.6(3)
N12A	C11A	C21A	116.4(3)	O1B	C2B	C1B	124.4(3)	N22B	C21B	N25B	108.6(3)
C16A	C11A	C21A	120.9(3)	O2B	C2B	C1B	111.0(2)	C1B	N22B	C21B	132.1(3)
C11A	N12A	C13A	116.7(3)	O2B	C3B	H3BA	109.9	C1B	N22B	N23B	119.1(3)
N12A	C13A	H13	117.9	O2B	C3B	H3BB	109.9	C21B	N22B	N23B	108.3(3)
N12A	C13A	C14A	124.2(3)	O2B	C3B	C4B	108.8(4)	N22B	N23B	N24B	106.2(3)
H13	C13A	C14A	117.9	H3BA	C3B	H3BB	108.3	N23B	N24B	N25B	111.1(3)
C13A	C14A	H14	120.9	H3BA	C3B	C4B	110	C21B	N25B	N24B	105.7(3)
C13A	C14A	C15A	118.1(4)	H3BB	C3B	C4B	110	C3B	C4B	H4BA	109.5
H14	C14A	C15A	121								

Table A11: Atomic coordinates for **3.8**.

	x	*y*	*z*		*x*	*y*	*z*
Cu1	0.07253(4)	0.04101(3)	0.15893(3)	**Cu1**	-0.07253(4)	-0.04101(3)	-0.15893(3)
Cl1	0.01740(12)	0.26811(7)	0.24750(6)	**Cl1**	-0.01740(12)	-0.26811(7)	-0.24750(6)
Cl2	0.23095(9)	0.12090(7)	0.02982(6)	**Cl2**	-0.23095(9)	-0.12090(7)	-0.02982(6)
O1	-0.3484(3)	-0.4888(2)	0.24153(18)	**O1**	0.3484(3)	0.4888(2)	-0.24153(18)
O2	-0.2852(3)	-0.56783(19)	0.41069(16)	**O2**	0.2852(3)	0.56783(19)	-0.41069(16)
C1	-0.0859(4)	-0.3442(3)	0.4185(2)	**C1**	0.0859(4)	0.3442(3)	-0.4185(2)
H1A	-0.0897	-0.3084	0.5064	**H1A**	0.0897	0.3084	-0.5064
H1B	0.0301	-0.3794	0.4154	**H1B**	-0.0301	0.3794	-0.4154
C2	-0.2565(4)	-0.4744(3)	0.3445(2)	**C2**	0.2565(4)	0.4744(3)	-0.3445(2)
C3	-0.4395(5)	-0.7058(4)	0.3476(3)	**C3**	0.4395(5)	0.7058(4)	-0.3476(3)
H3A	-0.4056	-0.7739	0.2785	**H3A**	0.4056	0.7739	-0.2785
H3B	-0.5553	-0.6789	0.3132	**H3B**	0.5553	0.6789	-0.3132
C4	-0.4706(5)	-0.7820(4)	0.4413(4)	**C4**	0.4706(5)	0.7820(4)	-0.4413(4)
H4A	-0.3576	-0.8131	0.4714	**H4A**	0.3576	0.8131	-0.4714
H4B	-0.5758	-0.8705	0.4025	**H4B**	0.5758	0.8705	-0.4025
H4C	-0.4987	-0.7123	0.5111	**H4C**	0.4987	0.7123	-0.5111
C11	0.1150(3)	-0.2476(3)	0.2030(2)	**C11**	-0.1150(3)	0.2476(3)	-0.2030(2)
N12	0.1846(3)	-0.1524(2)	0.14395(18)	**N12**	-0.1846(3)	0.1524(2)	-0.14395(18)
C13	0.2970(4)	-0.1997(3)	0.0696(2)	**C13**	-0.2970(4)	0.1997(3)	-0.0696(2)
H13	0.3484	-0.1351	0.0292	**H13**	-0.3484	0.1351	-0.0292
C14	0.3395(4)	-0.3407(3)	0.0509(3)	**C14**	-0.3395(4)	0.3407(3)	-0.0509(3)
H14	0.4196	-0.3695	-0.0006	**H14**	-0.4196	0.3695	0.0006
C15	0.2636(4)	-0.4377(3)	0.1080(3)	**C15**	-0.2636(4)	0.4377(3)	-0.1080(3)
H15	0.2891	-0.534	0.0946	**H15**	-0.2891	0.534	-0.0946
C16	0.1485(4)	-0.3911(3)	0.1861(3)	**C16**	-0.1485(4)	0.3911(3)	-0.1861(3)
H16	0.095	-0.455	0.2263	**H16**	-0.095	0.455	-0.2263
C21	-0.0039(3)	-0.1796(3)	0.2811(2)	**C21**	0.0039(3)	0.1796(3)	-0.2811(2)
N22	-0.0473(3)	-0.0512(2)	0.27228(18)	**N22**	0.0473(3)	0.0512(2)	-0.27228(18)
N23	-0.1591(4)	-0.0128(3)	0.3505(2)	**N23**	0.1591(4)	0.0128(3)	-0.3505(2)
N24	-0.1832(4)	-0.1136(3)	0.4075(2)	**N24**	0.1832(4)	0.1136(3)	-0.4075(2)
N25	-0.0846(3)	-0.2185(2)	0.36602(18)	**N25**	0.0846(3)	0.2185(2)	-0.36602(18)

Table A12: Bond lengths (Å) for **3.8**.

Atom1	Atom2	Length	Atom1	Atom2	Length	Atom1	Atom2	Length	Atom1	Atom2	Length
Cu1	**Cl1**	2.2281(8)	**C4**	**H4A**	0.96	**N22**	**N23**	1.345(4)	**C4**	**H4B**	0.96
Cu1	**Cl2**	2.2496(8)	**C4**	**H4B**	0.96	**N23**	**N24**	1.293(4)	**C4**	**H4C**	0.96
Cu1	**N12**	2.094(2)	**C4**	**H4C**	0.96	**N24**	**N25**	1.355(4)	**C11**	**N12**	1.349(4)
Cu1	**N22**	1.998(2)	**C11**	**N12**	1.349(4)	**Cu1**	**Cl1**	2.2281(8)	**C11**	**C16**	1.375(4)

Cu1	**Cl2**	2.6524(6)	**C11**	**C16**	1.375(4)	**Cu1**	**Cl2**	2.2496(8)	**C11**	**C21**	1.464(3)
Cl2	**Cu1**	2.6524(6)	**C11**	**C21**	1.464(3)	**Cu1**	**N12**	2.094(2)	**N12**	**C13**	1.337(4)
O1	**C2**	1.191(3)	**N12**	**C13**	1.337(4)	**Cu1**	**N22**	1.998(2)	**C13**	**H13**	0.93
O2	**C2**	1.320(4)	**C13**	**H13**	0.93	**O1**	**C2**	1.191(3)	**C13**	**C14**	1.378(4)
O2	**C3**	1.460(3)	**C13**	**C14**	1.378(4)	**O2**	**C2**	1.320(4)	**C14**	**H14**	0.93
C1	**H1A**	0.97	**C14**	**H14**	0.93	**O2**	**C3**	1.460(3)	**C14**	**C15**	1.362(5)
C1	**H1B**	0.97	**C14**	**C15**	1.362(5)	**C1**	**H1A**	0.97	**C15**	**H15**	0.93
C1	**C2**	1.502(3)	**C15**	**H15**	0.93	**C1**	**H1B**	0.97	**C15**	**C16**	1.380(5)
C1	**N25**	1.460(4)	**C15**	**C16**	1.380(5)	**C1**	**C2**	1.502(3)	**C16**	**H16**	0.93
C3	**H3A**	0.969	**C16**	**H16**	0.93	**C1**	**N25**	1.460(4)	**C21**	**N22**	1.321(4)
C3	**H3B**	0.97	**C21**	**N22**	1.321(4)	**C3**	**H3A**	0.969	**C21**	**N25**	1.329(3)
C3	**C4**	1.470(6)	**C21**	**N25**	1.329(3)	**C3**	**H3B**	0.97	**N22**	**N23**	1.345(4)
C3	**C4**	1.470(6)	**C4**	**H4A**	0.96	**N24**	**N25**	1.355(4)	**N23**	**N24**	1.293(4)

Table A13: Bond angles (°) for **3.8**.

Atom1	Atom2	Atom3	Angle	Atom1	Atom2	Atom3	Angle	Atom1	Atom2	Atom3	Angle
Cl1	Cu1	Cl2	94.87(3)	H13	C13	C14	118.9	O2	C2	C1	109.6
Cl1	Cu1	N12	158.86(6)	C13	C14	H14	120.1	O2	C3	H3A	110
Cl1	Cu1	N22	92.06(6)	C13	C14	C15	119.7(3)	O2	C3	H3B	110
Cl1	Cu1	Cl2	107.73(3)	H14	C14	C15	120.2	O2	C3	C4	108.2
Cl2	Cu1	N12	93.82(6)	C14	C15	H15	120.4	H3A	C3	H3B	108.4
Cl2	Cu1	N22	172.23(6)	C14	C15	C16	119.1(3)	H3A	C3	C4	110.1
Cl2	Cu1	Cl2	93.03(2)	H15	C15	C16	120.4	H3B	C3	C4	110
N12	Cu1	N22	78.48(8)	C11	C16	C15	118.3(3)	C3	C4	H4A	109.4
N12	Cu1	Cl2	90.99(6)	C11	C16	H16	120.8	C3	C4	H4B	109.5
N22	Cu1	Cl2	88.20(6)	C15	C16	H16	120.9	C3	C4	H4C	109.5
Cu1	Cl2	Cu1	86.97(2)	C11	C21	N22	118.8(2)	H4A	C4	H4B	109.4
C2	O2	C3	116.0(2)	C11	C21	N25	133.7(2)	H4A	C4	H4C	109.5
H1A	C1	H1B	108.1	N22	C21	N25	107.5(2)	H4B	C4	H4C	109.5
H1A	C1	C2	109.6	Cu1	N22	C21	115.7(2)	N12	C11	C16	123.1
H1A	C1	N25	109.6	Cu1	N22	N23	136.3(2)	N12	C11	C21	110.9
H1B	C1	C2	109.6	C21	N22	N23	107.9(2)	C16	C11	C21	125.9
H1B	C1	N25	109.6	N22	N23	N24	109.0(2)	Cu1	N12	C11	115.5
C2	C1	N25	110.2(2)	N23	N24	N25	107.4(2)	Cu1	N12	C13	126.5
O1	C2	O2	126.5(3)	C1	N25	C21	133.6(2)	C11	N12	C13	117.4
O1	C2	C1	123.9(2)	C1	N25	N24	118.2(2)	N12	C13	H13	118.8
O2	C2	C1	109.6(2)	C21	N25	N24	108.1(2)	N12	C13	C14	122.3
O2	C3	H3A	110	Cl2	Cu1	Cl1	107.73(3)	H13	C13	C14	118.9
O2	C3	H3B	110	Cl2	Cu1	Cl2	93.03(2)	C13	C14	H14	120.1
O2	C3	C4	108.2(3)	Cl2	Cu1	N12	90.99(6)	C13	C14	C15	119.7
H3A	C3	H3B	108.4	Cl2	Cu1	N22	88.20(6)	H14	C14	C15	120.2
H3A	C3	C4	110.1	Cl1	Cu1	Cl2	94.87(3)	C14	C15	H15	120.4
H3B	C3	C4	110	Cl1	Cu1	N12	158.86(6)	C14	C15	C16	119.1
C3	C4	H4A	109.4	Cl1	Cu1	N22	92.06(6)	H15	C15	C16	120.4
C3	C4	H4B	109.5	Cl2	Cu1	N12	93.82(6)	C11	C16	C15	118.3
C3	C4	H4C	109.5	Cl2	Cu1	N22	172.23(6)	C11	C16	H16	120.8
H4A	C4	H4B	109.4	N12	Cu1	N22	78.48(8)	C15	C16	H16	120.9
H4A	C4	H4C	109.5	Cu1	Cl2	Cu1	86.97(2)	C11	C21	N22	118.8
H4B	C4	H4C	109.5	C2	O2	C3	116.0(2)	C11	C21	N25	133.7
N12	C11	C16	123.1(2)	H1A	C1	H1B	108.1	N22	C21	N25	107.5
N12	C11	C21	110.9(2)	H1A	C1	C2	109.6	Cu1	N22	C21	115.7
C16	C11	C21	125.9(2)	H1A	C1	N25	109.6	Cu1	N22	N23	136.3
Cu1	N12	C11	115.5(2)	H1B	C1	C2	109.6	C21	N22	N23	107.9
Cu1	N12	C13	126.5(2)	H1B	C1	N25	109.6	N22	N23	N24	109.0
C11	N12	C13	117.4(2)	C2	C1	N25	110.2(2)	N23	N24	N25	107.4
N12	C13	H13	118.8	O1	C2	O2	126.5(3)	C1	N25	C21	133.6
N12	C13	C14	122.3(3)	O1	C2	C1	123.9(2)	C1	N25	N24	118.2
C21	N25	N24	108.1(2)								

Table A14: Atomic coordinates for **3.9**.

	x	*y*	*z*		*x*	*y*	*z*
Cu1	0	0	0	**C11**	-0.17093(15)	-0.01373(11)	0.2017(2)
Cl1	0.14071(4)	0.02890(4)	0.24980(6)	**N12**	-0.09436(12)	-0.06348(10)	0.14131(19)
C11	0.17093(15)	0.01373(11)	-0.2017(2)	**C13**	-0.08438(18)	-0.15771(13)	0.1745(3)
N12	0.09436(12)	0.06348(10)	-0.14131(19)	**H13**	-0.0307	-0.1924	0.135
C13	0.08438(18)	0.15771(13)	-0.1745(3)	**C14**	-0.1500(2)	-0.20546(14)	0.2644(3)

H13	0.0307	0.1924	-0.135	**H14**	-0.142	-0.2713	0.2829
C14	0.1500(2)	0.20546(14)	-0.2644(3)	**C15**	-0.2277(2)	-0.15416(15)	0.3266(3)
H14	0.142	0.2713	-0.2829	**H15**	-0.2724	-0.1848	0.389
C15	0.2277(2)	0.15416(15)	-0.3266(3)	**C16**	-0.23874(19)	-0.05654(14)	0.2955(3)
H15	0.2724	0.1848	-0.389	**C2**	0.40819(15)	-0.30780(13)	0.0307(3)
C16	0.23874(19)	0.05654(14)	-0.2955(3)	**H16**	-0.2906	-0.0205	0.3367
H16	0.2906	0.0205	-0.3367	**C21**	-0.18028(14)	0.08867(11)	0.1570(2)
C21	0.18028(14)	-0.08867(11)	-0.1570(2)	**N22**	-0.11370(13)	0.13187(10)	0.0688(2)
N22	0.11370(13)	-0.13187(10)	-0.0688(2)	**N23**	-0.14811(12)	0.22143(10)	0.0455(2)
N23	0.14811(12)	-0.22143(10)	-0.0455(2)	**N24**	-0.23295(12)	0.22856(10)	0.12000(18)
N24	0.23295(12)	-0.22856(10)	-0.12000(18)	**N25**	-0.25693(13)	0.14763(10)	0.19140(19)
N25	0.25693(13)	-0.14763(10)	-0.19140(19)	**C1**	-0.29937(16)	0.31588(12)	0.1106(2)
C1	0.29937(16)	-0.31588(12)	-0.1106(2)	**H1A**	-0.3167	0.3269	0.2212
H1A	0.3167	-0.3269	-0.2212	**H1B**	-0.2555	0.37	0.0871
H1B	0.2555	-0.37	-0.0871	**C2**	-0.40819(15)	0.30780(13)	-0.0307(3)
O1	0.44061(12)	-0.23783(10)	0.1146(2)	**O1**	-0.44061(12)	0.23783(10)	-0.1146(2)
O2	0.46239(13)	-0.39084(11)	0.0430(2)	**O2**	-0.46239(13)	0.39084(11)	-0.0430(2)
C3	0.5742(2)	-0.3967(2)	0.1665(4)	**C3**	-0.5742(2)	0.3967(2)	-0.1665(4)
H3A	0.6242	-0.4368	0.1194	**H3A**	-0.6242	0.4368	-0.1194
H3B	0.6076	-0.3331	0.187	**H3B**	-0.6076	0.3331	-0.187
C4	0.5620(3)	-0.4368(4)	0.3276(5)	**C4**	-0.5620(3)	0.4368(4)	-0.3276(5)
H4A	0.5341	-0.5014	0.3081	**H4A**	-0.5341	0.5014	-0.3081
H4B	0.5092	-0.3989	0.3703	**H4B**	-0.5092	0.3989	-0.3703
H4C	0.6347	-0.437	0.4116	**H4C**	-0.6347	0.437	-0.4116
Cl1	-0.14071(4)	-0.02890(4)	-0.24980(6)				

Table A15: Bond lengths (Å) for **3.9**.

Atom1	Atom2	Length	Atom1	Atom2	Length	Atom1	Atom2	Length	Atom1	Atom2	Length
Cu1	**Cl1**	2.2986	**C16**	**H16**	0.93	**C3**	**H3B**	0.971	**C21**	**N25**	1.323(2)
Cu1	**N12**	2.008	**C21**	**N22**	1.344(2)	**C3**	**C4**	1.442(5)	**N22**	**N23**	1.314(2)
Cu1	**N22**	2.445	**C21**	**N25**	1.323(2)	**C4**	**H4A**	0.96	**N23**	**N24**	1.320(2)
Cu1	**Cl1**	2.2986	**N22**	**N23**	1.314(2)	**C4**	**H4B**	0.959	**N24**	**N25**	1.329(2)
Cu1	**N12**	2.008	**N23**	**N24**	1.320(2)	**C4**	**H4C**	0.96	**N24**	**C1**	1.451(2)
Cu1	**N22**	2.445	**N24**	**N25**	1.329(2)	**C11**	**N12**	1.345(2)	**C1**	**H1A**	0.97
C11	**N12**	1.345(2)	**N24**	**C1**	1.451(2)	**C11**	**C16**	1.383(3)	**C1**	**H1B**	0.969
C11	**C16**	1.383(3)	**C1**	**H1A**	0.97	**C11**	**C21**	1.468(2)	**C1**	**C2**	1.503(2)
C11	**C21**	1.468(2)	**C1**	**H1B**	0.969	**N12**	**C13**	1.339(2)	**C2**	**O1**	1.190(2)
N12	**C13**	1.339(2)	**C1**	**C2**	1.503(2)	**C13**	**H13**	0.93	**C2**	**O2**	1.323(2)
C13	**H13**	0.93	**C2**	**O1**	1.190(2)	**C13**	**C14**	1.374(4)	**O2**	**C3**	1.459(3)
C13	**C14**	1.374(4)	**C2**	**O2**	1.323(2)	**C14**	**H14**	0.93	**C3**	**H3A**	0.97
C14	**H14**	0.93	**O2**	**C3**	1.459(3)	**C14**	**C15**	1.375(4)	**C3**	**H3B**	0.971
C14	**C15**	1.375(4)	**C3**	**H3A**	0.97	**C15**	**H15**	0.93	**C3**	**C4**	1.442(5)
C15	**H15**	0.93	**C15**	**C16**	1.383(3)	**C21**	**N22**	1.344(2)	**C4**	**H4A**	0.96
C15	**C16**	1.383(3)	**C16**	**H16**	0.93	**C4**	**H4C**	0.96	**C4**	**H4B**	0.959

Table A16: Bond angles (°) for **3.9**.

Atom1	Atom2	Atom3	Angle	Atom1	Atom2	Atom3	Angle	Atom1	Atom2	Atom3	Angle
Cl1	Cu1	N12	90.17	N22	N23	N24	105.4(1)	C14	C15	H15	120.3
Cl1	Cu1	N22	89.34	N23	N24	N25	114.3(1)	C14	C15	C16	119.4(2)
Cl1	Cu1	Cl1	180	N23	N24	C1	121.9(1)	H15	C15	C16	120.3
Cl1	Cu1	N12	89.83	N25	N24	C1	123.5(1)	C11	C16	C15	118.5(2)
Cl1	Cu1	N22	90.66	C21	N25	N24	101.2(1)	C11	C16	H16	120.7
N12	Cu1	N22	76.54	N24	C1	H1A	109.6	C15	C16	H16	120.7
N12	Cu1	Cl1	89.83	N24	C1	H1B	109.6	C11	C21	N22	122.9(1)
N12	Cu1	N12	180	N24	C1	C2	110.2(1)	C11	C21	N25	124.6(1)
N12	Cu1	N22	103.46	H1A	C1	H1B	108.2	N22	C21	N25	112.5(1)
N22	Cu1	Cl1	90.66	H1A	C1	C2	109.6	Cu1	N22	C21	103.4
N22	Cu1	N12	103.46	H1B	C1	C2	109.6	Cu1	N22	N23	149.3
N22	Cu1	N22	180	C1	C2	O1	125.5(2)	C21	N22	N23	106.6(1)
Cl1	Cu1	N12	90.17	C1	C2	O2	108.4(2)	N22	N23	N24	105.4(1)
Cl1	Cu1	N22	89.34	O1	C2	O2	126.1(2)	N23	N24	N25	114.3(1)
N12	Cu1	N22	76.54	C2	O2	C3	117.3(2)	N23	N24	C1	121.9(1)
N12	C11	C16	122.4(2)	O2	C3	H3A	109.8	N25	N24	C1	123.5(1)
N12	C11	C21	115.6(1)	O2	C3	H3B	109.8	C21	N25	N24	101.2(1)
C16	C11	C21	122.1(2)	O2	C3	C4	109.2(3)	N24	C1	H1A	109.6
Cu1	N12	C11	121.5	H3A	C3	H3B	108.3	N24	C1	H1B	109.6

Cu1	N12	C13	120.5	H3A	C3	C4	109.9	N24	C1	C2	110.2(1)
C11	N12	C13	118.1(2)	H3B	C3	C4	109.8	H1A	C1	H1B	108.2
N12	C13	H13	118.6	C3	C4	H4A	109.4	H1A	C1	C2	109.6
N12	C13	C14	122.9(2)	C3	C4	H4B	109.6	H1B	C1	C2	109.6
H13	C13	C14	118.5	C3	C4	H4C	109.4	C1	C2	O1	125.5(2)
C13	C14	H14	120.6	H4A	C4	H4B	109.4	C1	C2	O2	108.4(2)
C13	C14	C15	118.8(2)	H4A	C4	H4C	109.4	O1	C2	O2	126.1(2)
H14	C14	C15	120.6	H4B	C4	H4C	109.5	C2	O2	C3	117.3(2)
C14	C15	H15	120.3	N12	C11	C16	122.4(2)	O2	C3	H3A	109.8
C14	C15	C16	119.4(2)	N12	C11	C21	115.6(1)	O2	C3	H3B	109.8
H15	C15	C16	120.3	C16	C11	C21	122.1(2)	O2	C3	C4	109.2(3)
C11	C16	C15	118.5(2)	Cu1	N12	C11	121.5	H3A	C3	H3B	108.3
C11	C16	H16	120.7	Cu1	N12	C13	120.5	H3A	C3	C4	109.9
C15	C16	H16	120.7	C11	N12	C13	118.1(2)	H3B	C3	C4	109.8
C11	C21	N22	122.9(1)	N12	C13	H13	118.6	C3	C4	H4A	109.4
C11	C21	N25	124.6(1)	N12	C13	C14	122.9(2)	C3	C4	H4B	109.6
N22	C21	N25	112.5(1)	H13	C13	C14	118.5	C3	C4	H4C	109.4
Cu1	N22	C21	103.4	C13	C14	H14	120.6	H4A	C4	H4B	109.4
Cu1	N22	N23	149.3	C13	C14	C15	118.8(2)	H4A	C4	H4C	109.4
C21	N22	N23	106.6(1)	H14	C14	C15	120.6	H4B	C4	H4C	109.5

Table A17: Atomic coordinates for **3.10**.

	x	*y*	*z*		*x*	*y*	*z*
Cu1	0	0	0	**C14**	-0.1511(15)	-0.2106(10)	0.4049(10)
O1	1.1616(8)	0.4033(6)	0.1406(8)	**C21**	0.4584(10)	0.2067(7)	0.0935(8)
O2	0.8982(8)	0.1708(5)	0.0845(6)	**N22**	0.3531(10)	0.1076(7)	0.1739(8)
C1	0.8392(10)	0.4084(8)	0.1897(9)	**N23**	0.4787(11)	0.1388(9)	0.3336(9)
C2	0.9860(10)	0.3209(8)	0.1338(9)	**N24**	0.6543(11)	0.2485(8)	0.3522(8)
C11	0.3636(10)	0.2116(7)	-0.0817(9)	**N25**	0.6461(9)	0.2926(7)	0.2044(7)
N12	0.1476(9)	0.1417(7)	-0.1437(8)	**O1**	-1.1616(8)	-0.4033(6)	-0.1406(8)
C13	0.0462(12)	0.1451(9)	-0.3010(10)	**H14**	-0.0751	-0.2072	0.5157
H13	-0.1042	0.1006	-0.3431	**C15**	-0.3712(14)	-0.2812(10)	0.3407(10)
C14	0.1511(15)	0.2106(10)	-0.4049(10)	**H15**	-0.4468	-0.3293	0.4073
H14	0.0751	0.2072	-0.5157	**C16**	-0.4793(12)	-0.2807(9)	0.1781(10)
C15	0.3712(14)	0.2812(10)	-0.3407(10)	**H16**	-0.6293	-0.3266	0.1335
H15	0.4468	0.3293	-0.4073	**C21**	-0.4584(10)	-0.2067(7)	-0.0935(8)
C16	0.4793(12)	0.2807(9)	-0.1781(10)	**N22**	-0.3531(10)	-0.1076(7)	-0.1739(8)
H16	0.6293	0.3266	-0.1335	**N23**	-0.4787(11)	-0.1388(9)	-0.3336(9)
O2	-0.8982(8)	-0.1708(5)	-0.0845(6)	**N24**	-0.6543(11)	-0.2485(8)	-0.3522(8)
C1	-0.8392(10)	-0.4084(8)	-0.1897(9)	**N25**	-0.6461(9)	-0.2926(7)	-0.2044(7)
C2	-0.9860(10)	-0.3209(8)	-0.1338(9)	**Cu1**	-1	0	0
C11	-0.3636(10)	-0.2116(7)	0.0817(9)	**Cu1**	1	0	0
N12	-0.1476(9)	-0.1417(7)	0.1437(8)	**O2**	-0.1018(8)	0.1708(5)	0.0845(6)
C13	-0.0462(12)	-0.1451(9)	0.3010(10)	**O2**	0.1018(8)	-0.1708(5)	-0.0845(6)
H13	0.1042	-0.1006	0.3431				

Table A18: Bond lengths (Å) for **3.10**.

Atom1	Atom2	Length	Atom1	Atom2	Length	Atom1	Atom2	Length	Atom1	Atom2	Length
Cu1	**N12**	2.084	**C11**	**C16**	1.37(1)	**N22**	**N23**	1.347(9)	**C13**	**H13**	0.93
Cu1	**N22**	2.3	**C11**	**C21**	1.46(1)	**N23**	**N24**	1.274(9)	**C13**	**C14**	1.37(1)
Cu1	**N12**	2.084	**N12**	**C13**	1.32(1)	**N24**	**N25**	1.341(9)	**C14**	**H14**	0.93
Cu1	**N22**	2.3	**C13**	**H13**	0.93	**O1**	**C2**	1.199(8)	**C14**	**C15**	1.37(1)
Cu1	**O2**	1.959	**C13**	**C14**	1.37(1)	**O2**	**C2**	1.265(7)	**C15**	**H15**	0.93
Cu1	**O2**	1.959	**C14**	**H14**	0.93	**O2**	**Cu1**	1.959	**C15**	**C16**	1.37(1)
O1	**C2**	1.199(8)	**C14**	**C15**	1.37(1)	**C1**	**C2**	1.55(1)	**C16**	**H16**	0.93
O2	**C2**	1.265(7)	**C15**	**H15**	0.93	**C1**	**N25**	1.472(9)	**C21**	**N22**	1.33(1)
O2	**Cu1**	1.959	**C15**	**C16**	1.37(1)	**C11**	**N12**	1.343(8)	**C21**	**N25**	1.329(7)
C1	**C2**	1.55(1)	**C16**	**H16**	0.93	**C11**	**C16**	1.37(1)	**N22**	**N23**	1.347(9)
C1	**N25**	1.472(9)	**C21**	**N22**	1.33(1)	**C11**	**C21**	1.46(1)	**N23**	**N24**	1.274(9)
C11	**N12**	1.343(8)	**C21**	**N25**	1.329(7)	**N12**	**C13**	1.32(1)	**N24**	**N25**	1.341(9)

Table A19: Bond angles (°) for **3.10**.

Atom1	Atom2	Atom3	Angle	Atom1	Atom2	Atom3	Angle	Atom1	Atom2	Atom3	Angle
N12	Cu1	N22	76.9	H13	C13	C14	118.3	C16	C11	C21	124.5(7)

N12	Cu1	N12	180	C13	C14	H14	121	Cu1	N12	C11	118.2
N12	Cu1	N22	103.1	C13	C14	C15	118.0(8)	Cu1	N12	C13	122.8
N12	Cu1	O2	95.6	H14	C14	C15	121	C11	N12	C13	118.1(7)
N12	Cu1	O2	84.4	C14	C15	H15	120.2	N12	C13	H13	118.2
N22	Cu1	N12	103.1	C14	C15	C16	119.6(8)	N12	C13	C14	123.5(8)
N22	Cu1	N22	180	H15	C15	C16	120.2	H13	C13	C14	118.3
N22	Cu1	O2	92.9	C11	C16	C15	119.1(8)	C13	C14	H14	121
N22	Cu1	O2	87.1	C11	C16	H16	120.4	C13	C14	C15	118.0(8)
N12	Cu1	N22	76.9	C15	C16	H16	120.4	H14	C14	C15	121
N12	Cu1	O2	84.4	C11	C21	N22	122.0(6)	C14	C15	H15	120.2
N12	Cu1	O2	95.6	C11	C21	N25	131.4(6)	C14	C15	C16	119.6(8)
N22	Cu1	O2	87.1	N22	C21	N25	106.6(6)	H15	C15	C16	120.2
N22	Cu1	O2	92.9	Cu1	N22	C21	107.2	C11	C16	C15	119.1(8)
O2	Cu1	O2	180	Cu1	N22	N23	142.9	C11	C16	H16	120.4
C2	O2	Cu1	132.5	C21	N22	N23	107.2(6)	C15	C16	H16	120.4
C2	C1	N25	111.8(6)	N22	N23	N24	109.6(7)	C11	C21	N22	122.0(6)
O1	C2	O2	129.7(7)	N23	N24	N25	107.8(7)	C11	C21	N25	131.4(6)
O1	C2	C1	116.5(6)	C1	N25	C21	132.4(6)	N22	C21	N25	106.6(6)
O2	C2	C1	113.7(6)	C1	N25	N24	118.6(6)	Cu1	N22	C21	107.2
N12	C11	C16	121.6(7)	C21	N25	N24	108.8(6)	Cu1	N22	N23	142.9
N12	C11	C21	113.9(6)	C2	O2	Cu1	132.5	C21	N22	N23	107.2(6)
C16	C11	C21	124.5(7)	C2	C1	N25	111.8(6)	N22	N23	N24	109.6(7)
Cu1	N12	C11	118.2	O1	C2	O2	129.7(7)	N23	N24	N25	107.8(7)
Cu1	N12	C13	122.8	O1	C2	C1	116.5(6)	C1	N25	C21	132.4(6)
C11	N12	C13	118.1(7)	O2	C2	C1	113.7(6)	C1	N25	N24	118.6(6)
N12	C13	H13	118.2	N12	C11	C16	121.6(7)	C21	N25	N24	108.8(6)
N12	C13	C14	123.5(8)	N12	C11	C21	113.9(6)				

Table A20: Atomic coordinates for **3.11**.

	x	*y*	*z*		*x*	*y*	*z*
Cu1	0.12159(6)	0.71057(4)	0.48120(5)	**Cu1**	-0.12159(6)	1.28943(4)	0.51880(5)
O1W	0.1367(5)	0.5859(3)	0.6056(3)	**O1W**	-0.1367(5)	1.4141(3)	0.3944(3)
H1W	0.047(6)	0.560(4)	0.622(4)	**H1W**	-0.047(6)	1.440(4)	0.378(4)
H2W	0.169(7)	0.531(6)	0.586(5)	**H2W**	-0.169(7)	1.469(6)	0.414(5)
C11	0.1496(6)	0.9494(3)	0.3680(4)	**C11**	-0.1496(6)	1.0506(3)	0.6320(4)
N12	0.0927(5)	0.8337(3)	0.3452(3)	**N12**	-0.0927(5)	1.1663(3)	0.6548(3)
C13	-0.0032(7)	0.8071(4)	0.2338(5)	**C13**	0.0032(7)	1.1929(4)	0.7662(5)
H13	-0.041	0.7275	0.2166	**H13**	0.041	1.2725	0.7834
C14	-0.0471(8)	0.8927(5)	0.1449(4)	**C14**	0.0471(8)	1.1073(5)	0.8551(4)
H14	-0.1146	0.8712	0.0695	**H14**	0.1146	1.1288	0.9305
C15	0.0095(8)	1.0101(5)	0.1682(5)	**C15**	-0.0095(8)	0.9899(5)	0.8318(5)
H15	-0.0194	1.0694	0.1091	**H15**	0.0194	0.9306	0.8909
C16	0.1111(7)	1.0392(4)	0.2822(4)	**C16**	-0.1111(7)	0.9608(4)	0.7178(4)
H16	0.1522	1.1179	0.2999	**H16**	-0.1522	0.8821	0.7001
C21	0.2513(5)	0.9657(3)	0.4917(4)	**C21**	-0.2513(5)	1.0343(3)	0.5083(4)
N22	0.2678(5)	0.8775(3)	0.5718(3)	**N22**	-0.2678(5)	1.1225(3)	0.4282(3)
N23	0.3713(5)	0.9198(3)	0.6754(3)	**N23**	-0.3713(5)	1.0802(3)	0.3246(3)
N24	0.4161(5)	1.0307(3)	0.6603(4)	**N24**	-0.4161(5)	0.9693(3)	0.3397(4)
N25	0.3438(5)	1.0615(3)	0.5460(3)	**N25**	-0.3438(5)	0.9385(3)	0.4540(3)
O1	0.2582(4)	1.3717(3)	0.5573(4)	**O1**	-0.2582(4)	0.6283(3)	0.4427(4)
O2	0.0798(4)	1.2192(2)	0.4884(3)	**O2**	-0.0798(4)	0.7808(2)	0.5116(3)
C1	0.3683(5)	1.1870(3)	0.5097(4)	**C1**	-0.3683(5)	0.8130(3)	0.4903(4)
H1A	0.3765	1.1872	0.4271	**H1A**	-0.3765	0.8128	0.5729
H1B	0.4734	1.2193	0.56	**H1B**	-0.4734	0.7807	0.44
C2	0.2236(6)	1.2680(4)	0.5206(4)	**C2**	-0.2236(6)	0.7320(4)	0.4794(4)
O3	0.1067(4)	0.5302(3)	0.3111(3)	**O3**	-0.1067(4)	1.4698(3)	0.6889(3)
O4	0.3103(4)	0.6341(2)	0.4380(3)	**O4**	-0.3103(4)	1.3659(2)	0.5620(3)
C3	0.3932(6)	0.4864(4)	0.3166(4)	**C3**	-0.3932(6)	1.5136(4)	0.6834(4)
H3A	0.4779	0.5437	0.3045	**H3A**	-0.4779	1.4563	0.6955
H3B	0.4477	0.4307	0.3797	**H3B**	-0.4477	1.5693	0.6203
C4	0.2568(6)	0.5548(3)	0.3561(4)	**C4**	-0.2568(6)	1.4452(3)	0.6439(4)
C31	0.3043(7)	0.5743(4)	0.0437(5)	**C31**	-0.3043(7)	1.4257(4)	0.9563(5)
N32	0.3675(8)	0.6587(4)	0.1226(4)	**N32**	-0.3675(8)	1.3413(4)	0.8774(4)
C33	0.3955(12)	0.7686(6)	0.0777(7)	**C33**	-0.3955(12)	1.2314(6)	0.9223(7)
H33	0.4377	0.8311	0.1319	**H33**	-0.4377	1.1689	0.8681
C34	0.3660(10)	0.7933(6)	-0.0411(6)	**C34**	-0.3660(10)	1.2067(6)	1.0411(6)
H34	0.3898	0.8697	-0.0675	**H34**	-0.3898	1.1303	1.0675
C35	0.3012(10)	0.7038(6)	-0.1198(6)	**C35**	-0.3012(10)	1.2962(6)	1.1198(6)

H35	0.2802	0.7177	-0.202	**H35**	-0.2802	1.2823	1.202
C36	0.2658(10)	0.5909(5)	-0.0783(5)	**C36**	-0.2658(10)	1.4091(5)	1.0783(5)
H36	0.2178	0.5287	-0.1312	**H36**	-0.2178	1.4713	1.1312
C41	0.2787(8)	0.4529(4)	0.0924(4)	**C41**	-0.2787(8)	1.5471(4)	0.9076(4)
N42	0.3261(5)	0.4193(3)	0.2075(3)	**N42**	-0.3261(5)	1.5807(3)	0.7925(3)
N43	0.2792(6)	0.3019(3)	0.2141(4)	**N43**	-0.2792(6)	1.6981(3)	0.7859(4)
N44	0.2091(8)	0.2673(4)	0.1045(4)	**N44**	-0.2091(8)	1.7327(4)	0.8955(4)
N45	0.2077(8)	0.3598(4)	0.0262(4)	**N45**	-0.2077(8)	1.6402(4)	0.9738(4)

Table A21: Bond lengths (Å) for **3.11**.

Atom1	Atom2	Length	Atom1	Atom2	Length	Atom1	Atom2	Length	Atom1	Atom2	Length
Cu1	**O1W**	1.965(3)	**O1**	**C2**	1.221(6)	**N44**	**N45**	1.358(7)	**N24**	**N25**	1.342(5)
Cu1	**N12**	2.040(3)	**O2**	**C2**	1.256(5)	**Cu1**	**O1W**	1.965(3)	**N25**	**C1**	1.470(5)
Cu1	**N22**	2.282(3)	**O2**	**Cu1**	1.939(3)	**Cu1**	**N12**	2.040(3)	**O1**	**C2**	1.221(6)
Cu1	**O3**	2.765(3)	**C1**	**H1A**	0.97	**Cu1**	**N22**	2.282(3)	**O2**	**C2**	1.256(5)
Cu1	**O4**	1.940(3)	**C1**	**H1B**	0.97	**Cu1**	**O3**	2.765(3)	**C1**	**H1A**	0.97
Cu1	**O2**	1.939(3)	**C1**	**C2**	1.520(6)	**Cu1**	**O4**	1.940(3)	**C1**	**H1B**	0.97
O1W	**H1W**	0.85(5)	**O3**	**C4**	1.233(5)	**O1W**	**H1W**	0.85(5)	**C1**	**C2**	1.520(6)
O1W	**H2W**	0.72(7)	**O4**	**C4**	1.273(5)	**O1W**	**H2W**	0.72(7)	**O3**	**C4**	1.233(5)
C11	**N12**	1.353(5)	**C3**	**H3A**	0.97	**C11**	**N12**	1.353(5)	**O4**	**C4**	1.273(5)
C11	**C16**	1.378(6)	**C3**	**H3B**	0.97	**C11**	**C16**	1.378(6)	**C3**	**H3A**	0.97
C11	**C21**	1.463(6)	**C3**	**C4**	1.515(7)	**C11**	**C21**	1.463(6)	**C3**	**H3B**	0.97
N12	**C13**	1.351(6)	**C3**	**N42**	1.435(5)	**N12**	**C13**	1.351(6)	**C3**	**C4**	1.515(7)
C13	**H13**	0.93	**C31**	**N32**	1.305(6)	**C13**	**H13**	0.93	**C3**	**N42**	1.435(5)
C13	**C14**	1.372(7)	**C31**	**C36**	1.370(8)	**C13**	**C14**	1.372(7)	**C31**	**N32**	1.305(6)
C14	**H14**	0.93	**C31**	**C41**	1.483(7)	**C14**	**H14**	0.93	**C31**	**C36**	1.370(8)
C14	**C15**	1.371(8)	**N32**	**C33**	1.356(9)	**C14**	**C15**	1.371(8)	**C31**	**C41**	1.483(7)
C15	**H15**	0.93	**C33**	**H33**	0.93	**C15**	**H15**	0.93	**N32**	**C33**	1.356(9)
C15	**C16**	1.396(7)	**C33**	**C34**	1.35(1)	**C15**	**C16**	1.396(7)	**C33**	**H33**	0.93
C16	**H16**	0.929	**C34**	**H34**	0.93	**C16**	**H16**	0.929	**C33**	**C34**	1.35(1)
C21	**N22**	1.323(5)	**C34**	**C35**	1.346(9)	**C21**	**N22**	1.323(5)	**C34**	**H34**	0.93
C21	**N25**	1.348(5)	**C35**	**H35**	0.93	**C21**	**N25**	1.348(5)	**C34**	**C35**	1.346(9)
N22	**N23**	1.352(4)	**C35**	**C36**	1.386(9)	**N22**	**N23**	1.352(4)	**C35**	**H35**	0.93
N23	**N24**	1.295(5)	**C36**	**H36**	0.93	**N23**	**N24**	1.295(5)	**C35**	**C36**	1.386(9)
N24	**N25**	1.342(5)	**C41**	**N42**	1.335(6)	**N42**	**N43**	1.352(5)	**C36**	**H36**	0.93
N25	**C1**	1.470(5)	**C41**	**N45**	1.314(6)	**N43**	**N44**	1.299(6)	**C41**	**N42**	1.335(6)
N43	**N44**	1.299(6)	**N42**	**N43**	1.352(5)	**N44**	**N45**	1.358(7)	**C41**	**N45**	1.314(6)

Table A22: Bond angles (°) for **3.11**.

Atom1	Atom2	Atom3	Angle	Atom1	Atom2	Atom3	Angle	Atom1	Atom2	Atom3	Angle
O1W	Cu1	N12	176.2(1)	H3B	C3	C4	109.2	C14	C15	C16	118.9(5)
O1W	Cu1	N22	107.4(1)	H3B	C3	N42	109.2	H15	C15	C16	120.6
O1W	Cu1	O3	89.9(1)	C4	C3	N42	111.9(4)	C11	C16	C15	119.0(5)
O1W	Cu1	O4	88.5(1)	O3	C4	O4	124.8(4)	C11	C16	H16	120.5
O1W	Cu1	O2	92.8(1)	O3	C4	C3	120.1(4)	C15	C16	H16	120.5
N12	Cu1	N22	76.2(1)	O4	C4	C3	115.1(4)	C11	C21	N22	121.6(4)
N12	Cu1	O3	87.6(1)	N32	C31	C36	124.2(5)	C11	C21	N25	130.8(4)
N12	Cu1	O4	92.3(1)	N32	C31	C41	116.3(5)	N22	C21	N25	107.6(4)
N12	Cu1	O2	86.1(1)	C36	C31	C41	119.5(5)	Cu1	N22	C21	108.8(3)
N22	Cu1	O3	144.9(1)	C31	N32	C33	116.1(6)	Cu1	N22	N23	144.0(3)
N22	Cu1	O4	96.3(1)	N32	C33	H33	118	C21	N22	N23	107.2(3)
N22	Cu1	O2	88.0(1)	N32	C33	C34	124.2(7)	N22	N23	N24	109.5(3)
O3	Cu1	O4	52.9(1)	H33	C33	C34	117.8	N23	N24	N25	107.7(4)
O3	Cu1	O2	122.2(1)	C33	C34	H34	121	C21	N25	N24	108.0(3)
O4	Cu1	O2	175.0(1)	C33	C34	C35	117.9(7)	C21	N25	C1	134.3(4)
Cu1	O1W	H1W	120(3)	H34	C34	C35	121	N24	N25	C1	117.5(3)
Cu1	O1W	H2W	109(5)	C34	C35	H35	120	Cu1	O2	C2	123.7(3)
H1W	O1W	H2W	102(6)	C34	C35	C36	120.0(7)	N25	C1	H1A	109.3
N12	C11	C16	122.1(4)	H35	C35	C36	120	N25	C1	H1B	109.3
N12	C11	C21	112.3(4)	C31	C36	C35	117.5(6)	N25	C1	C2	111.5(3)
C16	C11	C21	125.6(4)	C31	C36	H36	121.2	H1A	C1	H1B	108
Cu1	N12	C11	120.6(3)	C35	C36	H36	121.3	H1A	C1	C2	109.3
Cu1	N12	C13	120.9(3)	C31	C41	N42	126.5(5)	H1B	C1	C2	109.3
C11	N12	C13	117.9(4)	C31	C41	N45	124.2(5)	O1	C2	O2	127.5(4)
N12	C13	H13	118.7	N42	C41	N45	109.3(5)	O1	C2	C1	117.7(4)
N12	C13	C14	122.7(5)	C3	N42	C41	132.3(4)	O2	C2	C1	114.8(4)

H13	C13	C14	118.6	C3	N42	N43	119.2(4)	Cu1	O3	C4	72.2(2)
C13	C14	H14	120.3	C41	N42	N43	108.0(4)	Cu1	O4	C4	110.1(3)
C13	C14	C15	119.4(5)	N42	N43	N44	106.3(4)	H3A	C3	H3B	108
H14	C14	C15	120.3	N43	N44	N45	110.8(5)	H3A	C3	C4	109.3
C14	C15	H15	120.6	C41	N45	N44	105.6(5)	H3A	C3	N42	109.3
C14	C15	C16	118.9(5)	O2	Cu1	O1W	92.8(1)	H3B	C3	C4	109.2
H15	C15	C16	120.6	O2	Cu1	N12	86.1(1)	H3B	C3	N42	109.2
C11	C16	C15	119.0(5)	O2	Cu1	N22	88.0(1)	C4	C3	N42	111.9(4)
C11	C16	H16	120.5	O2	Cu1	O3	122.2(1)	O3	C4	O4	124.8(4)
C15	C16	H16	120.5	O2	Cu1	O4	175.0(1)	O3	C4	C3	120.1(4)
C11	C21	N22	121.6(4)	O1W	Cu1	N12	176.2(1)	O4	C4	C3	115.1(4)
C11	C21	N25	130.8(4)	O1W	Cu1	N22	107.4(1)	N32	C31	C36	124.2(5)
N22	C21	N25	107.6(4)	O1W	Cu1	O3	89.9(1)	N32	C31	C41	116.3(5)
Cu1	N22	C21	108.8(3)	O1W	Cu1	O4	88.5(1)	C36	C31	C41	119.5(5)
Cu1	N22	N23	144.0(3)	N12	Cu1	N22	76.2(1)	C31	N32	C33	116.1(6)
C21	N22	N23	107.2(3)	N12	Cu1	O3	87.6(1)	N32	C33	H33	118
N22	N23	N24	109.5(3)	N12	Cu1	O4	92.3(1)	N32	C33	C34	124.2(7)
N23	N24	N25	107.7(4)	N22	Cu1	O3	144.9(1)	H33	C33	C34	117.8
C21	N25	N24	108.0(3)	N22	Cu1	O4	96.3(1)	C33	C34	H34	121
C21	N25	C1	134.3(4)	O3	Cu1	O4	52.9(1)	C33	C34	C35	117.9(7)
N24	N25	C1	117.5(3)	Cu1	O1W	H1W	120(3)	H34	C34	C35	121
C2	O2	Cu1	123.7(3)	Cu1	O1W	H2W	109(5)	C34	C35	H35	120
N25	C1	H1A	109.3	H1W	O1W	H2W	102(6)	C34	C35	C36	120.0(7)
N25	C1	H1B	109.3	N12	C11	C16	122.1(4)	H35	C35	C36	120
N25	C1	C2	111.5(3)	N12	C11	C21	112.3(4)	C31	C36	C35	117.5(6)
H1A	C1	H1B	108	C16	C11	C21	125.6(4)	C31	C36	H36	121.2
H1A	C1	C2	109.3	Cu1	N12	C11	120.6(3)	C35	C36	H36	121.3
H1B	C1	C2	109.3	Cu1	N12	C13	120.9(3)	C31	C41	N42	126.5(5)
O1	C2	O2	127.5(4)	C11	N12	C13	117.9(4)	C31	C41	N45	124.2(5)
O1	C2	C1	117.7(4)	N12	C13	H13	118.7	N42	C41	N45	109.3(5)
O2	C2	C1	114.8(4)	N12	C13	C14	122.7(5)	C3	N42	C41	132.3(4)
Cu1	O3	C4	72.2(2)	H13	C13	C14	118.6	C3	N42	N43	119.2(4)
Cu1	O4	C4	110.1(3)	C13	C14	H14	120.3	C41	N42	N43	108.0(4)
H3A	C3	H3B	108	C13	C14	C15	119.4(5)	N42	N43	N44	106.3(4)
H3A	C3	C4	109.3	H14	C14	C15	120.3	N43	N44	N45	110.8(5)
H3A	C3	N42	109.3	C14	C15	H15	120.6	C41	N45	N44	105.6(5)

Table A23: Atomic coordinates for **3.13**.

	x	*y*	*z*		*x*	*y*	*z*
Cu1	0	0	0	**O1W**	-0.2155(3)	-0.0888(2)	0.04715(15)
O1W	0.2155(3)	0.0888(2)	-0.04715(15)	**O2**	0.3292(3)	-0.4082(2)	0.32991(12)
O2	-0.3292(3)	0.4082(2)	-0.32991(12)	**O3**	0.5464(3)	-0.3023(3)	0.42081(12)
O3	-0.5464(3)	0.3023(3)	-0.42081(12)	**C1**	0.2505(3)	-0.2493(3)	0.08296(16)
C1	-0.2505(3)	0.2493(3)	-0.08296(16)	**N2**	0.1831(3)	-0.1141(2)	0.11559(13)
N2	-0.1831(3)	0.1141(2)	-0.11559(13)	**N3**	0.2769(3)	-0.0843(3)	0.19039(13)
N3	-0.2769(3)	0.0843(3)	-0.19039(13)	**N4**	0.3955(3)	-0.2013(2)	0.19970(13)
N4	-0.3955(3)	0.2013(2)	-0.19970(13)	**N5**	0.3854(3)	-0.3083(3)	0.13486(13)
N5	-0.3854(3)	0.3083(3)	-0.13486(13)	**C2**	0.5211(4)	-0.2122(3)	0.27687(17)
C2	-0.5211(4)	0.2122(3)	-0.27687(17)	**H2A**	0.6307	-0.2567	0.2603
H2A	-0.6307	0.2567	-0.2603	**H2B**	0.5453	-0.1032	0.2994
H2B	-0.5453	0.1032	-0.2994	**H1A**	-0.283(5)	-0.113(4)	0.012(2)
H1A	0.283(5)	0.113(4)	-0.012(2)	**H1B**	-0.252(5)	-0.034(4)	0.085(2)
H1B	0.252(5)	0.034(4)	-0.085(2)	**C3**	0.4579(4)	-0.3183(3)	0.34985(17)
C3	-0.4579(4)	0.3183(3)	-0.34985(17)	**C11**	0.1768(3)	-0.3182(3)	-0.00085(16)
C11	-0.1768(3)	0.3182(3)	0.00085(16)	**N12**	0.0546(3)	-0.2238(2)	-0.04625(13)
N12	-0.0546(3)	0.2238(2)	0.04625(13)	**C13**	-0.0231(3)	-0.2805(3)	-0.12183(16)
C13	0.0231(3)	0.2805(3)	0.12183(16)	**H13**	-0.1072	-0.2159	-0.1533
H13	0.1072	0.2159	0.1533	**C14**	0.0156(4)	-0.4302(3)	-0.15527(17)
C14	-0.0156(4)	0.4302(3)	0.15527(17)	**H14**	-0.0419	-0.4667	-0.2078
H14	0.0419	0.4667	0.2078	**C15**	0.1420(4)	-0.5247(3)	-0.10877(18)
C15	-0.1420(4)	0.5247(3)	0.10877(18)	**H15**	0.1716	-0.626	-0.1302
H15	-0.1716	0.626	0.1302	**C16**	0.2244(4)	-0.4689(3)	-0.03056(18)
C16	-0.2244(4)	0.4689(3)	0.03056(18)	**H16**	0.3099	-0.5313	0.0014
H16	-0.3099	0.5313	-0.0014				

Table A24: Bond lengths (Å) for **3.13.**

Atom1	Atom2	Length	Atom1	Atom2	Length	Atom1	Atom2	Length	Atom1	Atom2	Length
Cu1	**O1W**	2.001	**N3**	**N4**	1.317(3)	**C15**	**C16**	1.379(4)	**C2**	**H2B**	0.97
Cu1	**N2**	2.343	**N4**	**N5**	1.326(3)	**C16**	**H16**	0.93	**C2**	**C3**	1.537(4)
Cu1	**N12**	2.028	**N4**	**C2**	1.452(3)	**O1W**	**H1A**	0.74(3)	**C11**	**N12**	1.351(3)
Cu1	**O1W**	2.001	**C2**	**H2A**	0.97	**O1W**	**H1B**	0.81(3)	**C11**	**C16**	1.380(4)
Cu1	**N2**	2.343	**C2**	**H2B**	0.97	**O2**	**C3**	1.241(3)	**N12**	**C13**	1.335(3)
Cu1	**N12**	2.028	**C2**	**C3**	1.537(4)	**O3**	**C3**	1.232(3)	**C13**	**H13**	0.93
O1W	**H1A**	0.74(3)	**C11**	**N12**	1.351(3)	**C1**	**N2**	1.341(3)	**C13**	**C14**	1.375(4)
O1W	**H1B**	0.81(3)	**C11**	**C16**	1.380(4)	**C1**	**N5**	1.329(3)	**C14**	**H14**	0.93
O2	**C3**	1.241(3)	**N12**	**C13**	1.335(3)	**C1**	**C11**	1.468(3)	**C14**	**C15**	1.380(4)
O3	**C3**	1.232(3)	**C13**	**H13**	0.93	**N2**	**N3**	1.316(3)	**C15**	**H15**	0.93
C1	**N2**	1.341(3)	**C13**	**C14**	1.375(4)	**N3**	**N4**	1.317(3)	**C15**	**C16**	1.379(4)
C1	**N5**	1.329(3)	**C14**	**H14**	0.93	**N4**	**N5**	1.326(3)	**C16**	**H16**	0.93
C1	**C11**	1.468(3)	**C14**	**C15**	1.380(4)	**N4**	**C2**	1.452(3)			
N2	**N3**	1.316(3)	**C15**	**H15**	0.93	**C2**	**H2A**	0.97			

Table A25: Bond angles (°) for **3.13**.

Atom1	Atom2	Atom3	Angle	Atom1	Atom2	Atom3	Angle	Atom1	Atom2	Atom3	Angle
O1W	Cu1	N2	91.56	H2A	C2	C3	108.8	N3	N4	N5	114.4(2)
O1W	Cu1	N12	90.2	H2B	C2	C3	108.8	N3	N4	C2	121.5(2)
O1W	Cu1	O1W	180	O2	C3	O3	129.1(3)	N5	N4	C2	124.0(2)
O1W	Cu1	N2	88.44	O2	C3	C2	117.0(2)	C1	N5	N4	101.2(2)
O1W	Cu1	N12	89.8	O3	C3	C2	113.8(2)	N4	C2	H2A	108.8
N2	Cu1	N12	77.13	C1	C11	N12	114.6(2)	N4	C2	H2B	108.8
N2	Cu1	O1W	88.44	C1	C11	C16	123.1(2)	N4	C2	C3	113.8(2)
N2	Cu1	N2	180	N12	C11	C16	122.2(2)	H2A	C2	H2B	107.7
N2	Cu1	N12	102.87	Cu1	N12	C11	119.5	H2A	C2	C3	108.8
N12	Cu1	O1W	89.8	Cu1	N12	C13	122.2	H2B	C2	C3	108.8
N12	Cu1	N2	102.87	C11	N12	C13	118.3(2)	O2	C3	O3	129.1(3)
N12	Cu1	N12	180	N12	C13	H13	118.5	O2	C3	C2	117.0(2)
O1W	Cu1	N2	91.56	N12	C13	C14	123.0(2)	O3	C3	C2	113.8(2)
O1W	Cu1	N12	90.2	H13	C13	C14	118.5	C1	C11	N12	114.6(2)
N2	Cu1	N12	77.13	C13	C14	H14	120.9	C1	C11	C16	123.1(2)
Cu1	O1W	H1A	112	C13	C14	C15	118.2(2)	N12	C11	C16	122.2(2)
Cu1	O1W	H1B	115	H14	C14	C15	120.9	Cu1	N12	C11	119.5
H1A	O1W	H1B	114(4)	C14	C15	H15	120	Cu1	N12	C13	122.2
N2	C1	N5	112.3(2)	C14	C15	C16	120.0(3)	C11	N12	C13	118.3(2)
N2	C1	C11	121.4(2)	H15	C15	C16	120.1	N12	C13	H13	118.5
N5	C1	C11	126.4(2)	C11	C16	C15	118.4(2)	N12	C13	C14	123.0(2)
Cu1	N2	C1	105.5	C11	C16	H16	120.8	H13	C13	C14	118.5
Cu1	N2	N3	145.1	C15	C16	H16	120.8	C13	C14	H14	120.9
C1	N2	N3	106.6(2)	Cu1	O1W	H1A	112	C13	C14	C15	118.2(2)
N2	N3	N4	105.5(2)	Cu1	O1W	H1B	115	H14	C14	C15	120.9
N3	N4	N5	114.4(2)	H1A	O1W	H1B	114(4)	C14	C15	H15	120
N3	N4	C2	121.5(2)	N2	C1	N5	112.3(2)	C14	C15	C16	120.0(3)
N5	N4	C2	124.0(2)	N2	C1	C11	121.4(2)	H15	C15	C16	120.1
C1	N5	N4	101.2(2)	N5	C1	C11	126.4(2)	C11	C16	C15	118.4(2)
N4	C2	H2A	108.8	Cu1	N2	C1	105.5	C11	C16	H16	120.8
N4	C2	H2B	108.8	Cu1	N2	N3	145.1	C15	C16	H16	120.8
N4	C2	C3	113.8(2)	C1	N2	N3	106.6(2)				
H2A	C2	H2B	107.7	N2	N3	N4	105.5(2)				

Table A26: Atomic coordinates for **4.12.**

	x	*y*	*z*		*x*	*y*	*z*
Cu1	0.50860(2)	0.64900(2)	0.47223(2)	**Cu1**	0.49140(2)	0.35100(2)	0.52777(2)
Cl1	0.32131(5)	0.68848(5)	0.40573(5)	**Cl1**	0.67869(5)	0.31152(5)	0.59427(5)
Cl2	0.50972(5)	0.49876(5)	0.36394(4)	**Cl2**	0.49028(5)	0.50124(5)	0.63606(4)
O1	1.07594(16)	0.72270(18)	0.7876(2)	**O1**	-0.07594(16)	0.27730(18)	0.2124(2)
O2	1.10386(15)	0.5743(2)	0.68834(17)	**O2**	-0.10386(15)	0.4257(2)	0.31166(17)
O3	0.87421(15)	1.11677(14)	0.63522(15)	**O3**	0.12579(15)	-0.11677(14)	0.36478(15)
O4	0.81249(19)	0.96975(17)	0.52466(16)	**O4**	0.18751(19)	0.03025(17)	0.47534(16)
C1	1.0428(2)	0.6577(2)	0.7150(2)	**C1**	-0.0428(2)	0.3423(2)	0.2850(2)
C2	1.2238(2)	0.5627(3)	0.7528(3)	**C2**	-0.2238(2)	0.4373(3)	0.2472(3)
H2A	1.2332	0.5987	0.8236	**H2A**	-0.2332	0.4013	0.1764

H2B	1.2757	0.5985	0.7149	H2B	-0.2757	0.4015	0.2851
C3	1.2513(3)	0.4426(3)	0.7677(3)	C3	-0.2513(3)	0.5574(3)	0.2323(3)
H3A	1.2039	0.4091	0.8105	H3A	-0.2039	0.5909	0.1895
H3B	1.3313	0.4338	0.805	H3B	-0.3313	0.5662	0.195
H3C	1.2366	0.4067	0.6974	H3C	-0.2366	0.5933	0.3026
C4	0.7361(2)	1.00615(19)	0.68057(19)	C4	0.2639(2)	-0.00615(19)	0.31943(19)
H4A	0.7843	0.9781	0.7491	H4A	0.2157	0.0219	0.2509
H4B	0.702	1.0763	0.6958	H4B	0.298	-0.0763	0.3042
C5	0.8104(2)	1.02760(19)	0.6018(2)	C5	0.1896(2)	-0.02760(19)	0.3982(2)
C6	0.9560(3)	1.1492(3)	0.5738(3)	C6	0.0440(3)	-0.1492(3)	0.4262(3)
H6A	0.9163	1.1665	0.4986	H6A	0.0837	-0.1665	0.5014
H6B	1.0106	1.089	0.5735	H6B	-0.0106	-0.089	0.4265
C7	1.0165(4)	1.2493(3)	0.6286(4)	C7	-0.0165(4)	-0.2493(3)	0.3714(4)
H7A	1.0582	1.2302	0.7018	H7A	-0.0582	-0.2302	0.2982
H7B	0.961	1.3069	0.6313	H7B	0.039	-0.3069	0.3687
H7C	1.0697	1.2762	0.5883	H7C	-0.0697	-0.2762	0.4117
C11	0.73436(17)	0.73945(17)	0.59534(17)	C11	0.26564(17)	0.26055(17)	0.40466(17)
N12	0.68899(15)	0.65024(15)	0.53290(15)	N12	0.31101(15)	0.34976(15)	0.46710(15)
C13	0.75911(19)	0.56556(19)	0.52473(19)	C13	0.24089(19)	0.43444(19)	0.47527(19)
H13	0.7292	0.5046	0.4807	H13	0.2708	0.4954	0.5193
C14	0.87539(19)	0.56532(19)	0.57973(19)	C14	0.12461(19)	0.43468(19)	0.42027(19)
H14	0.9224	0.5052	0.5722	H14	0.0776	0.4948	0.4278
C15	0.92044(18)	0.65502(18)	0.64559(19)	C15	0.07956(18)	0.34498(18)	0.35441(19)
C16	0.84879(18)	0.74578(18)	0.65282(18)	C16	0.15121(18)	0.25422(18)	0.34718(18)
H16	0.8772	0.8084	0.695	H16	0.1228	0.1916	0.305
C21	0.64425(18)	0.82168(18)	0.59890(18)	C21	0.35575(18)	0.17832(18)	0.40110(18)
N22	0.53495(16)	0.79145(16)	0.55970(17)	N22	0.46505(16)	0.20855(16)	0.44030(17)
N23	0.46794(18)	0.87817(18)	0.5759(2)	N23	0.53206(18)	0.12183(18)	0.4241(2)
N24	0.53279(17)	0.95924(18)	0.62278(19)	N24	0.46721(17)	0.04076(18)	0.37722(19)
N25	0.64472(15)	0.92590(15)	0.63783(15)	N25	0.35528(15)	0.07410(15)	0.36217(15)

Table A27: Bond lengths (Å) for **4.12**.

Atom1	Atom2	Length	Atom1	Atom2	Length	Atom1	Atom2	Length	Atom1	Atom2	Length
Cu1	Cl1	2.2343(6)	C6	H6B	0.97	Cu1	N12	2.099(2)	C4	N25	1.451(3)
Cu1	Cl2	2.2537(6)	C6	C7	1.475(5)	Cu1	N22	2.007(2)	C6	H6A	0.97
Cu1	N12	2.099(2)	C7	H7A	0.96	O1	C1	1.189(3)	C6	H6B	0.97
Cu1	N22	2.007(2)	C7	H7B	0.961	O2	C1	1.325(3)	C6	C7	1.475(5)
Cu1	Cl2	2.7628(6)	C7	H7C	0.961	O2	C2	1.467(3)	C7	H7A	0.96
Cl2	Cu1	2.7628(6)	C11	N12	1.353(3)	O3	C5	1.315(3)	C7	H7B	0.961
O1	C1	1.189(3)	C11	C16	1.380(3)	O3	C6	1.441(5)	C7	H7C	0.961
O2	C1	1.325(3)	C11	C21	1.465(3)	O4	C5	1.197(3)	C11	N12	1.353(3)
O2	C2	1.467(3)	N12	C13	1.332(3)	C1	C15	1.505(3)	C11	C16	1.380(3)
O3	C5	1.315(3)	C13	H13	0.93	C2	H2A	0.971	C11	C21	1.465(3)
O3	C6	1.441(5)	C13	C14	1.389(3)	C2	H2B	0.97	N12	C13	1.332(3)
O4	C5	1.197(3)	C14	H14	0.93	C2	C3	1.471(5)	C13	H13	0.93
C1	C15	1.505(3)	C14	C15	1.378(3)	C3	H3A	0.96	C13	C14	1.389(3)
C2	H2A	0.971	C15	C16	1.396(3)	C3	H3B	0.96	C14	H14	0.93
C2	H2B	0.97	C16	H16	0.93	C3	H3C	0.959	C14	C15	1.378(3)
C2	C3	1.471(5)	C21	N22	1.325(3)	C4	H4A	0.97	C15	C16	1.396(3)
C3	H3A	0.96	C21	N25	1.336(3)	C4	H4B	0.97	C16	H16	0.93
C3	H3B	0.96	N22	N23	1.354(3)	C4	C5	1.508(4)	C21	N22	1.325(3)
C3	H3C	0.959	N23	N24	1.287(3)	C4	N25	1.451(3)	C21	N25	1.336(3)
C4	H4A	0.97	N24	N25	1.361(3)	C6	H6A	0.97	N22	N23	1.354(3)
C4	H4B	0.97	Cu1	Cl1	2.2343(6)	N24	N25	1.361(3)	N23	N24	1.287(3)
C4	C5	1.508(4)	Cu1	Cl2	2.2537(6)						

Table A28: Bond angles (°) for **4.12**.

Atom1	Atom2	Atom3	Angle	Atom1	Atom2	Atom3	Angle	Atom1	Atom2	Atom3	Angle
Cl1	Cu1	Cl2	95.54(2)	Cu1	N12	C11	116.3(1)	H3A	C3	H3C	109.5
Cl1	Cu1	N12	167.38(5)	Cu1	N12	C13	125.1(2)	H3B	C3	H3C	109.5
Cl1	Cu1	N22	91.90(6)	C11	N12	C13	118.2(2)	H4A	C4	H4B	107.9
Cl1	Cu1	Cl2	99.03(2)	N12	C13	H13	118.9	H4A	C4	C5	109.1
Cl2	Cu1	N12	93.79(5)	N12	C13	C14	122.2(2)	H4A	C4	N25	109.1
Cl2	Cu1	N22	168.99(6)	H13	C13	C14	118.9	H4B	C4	C5	109.1
Cl2	Cu1	Cl2	87.60(2)	C13	C14	H14	120.3	H4B	C4	N25	109.2
N12	Cu1	N22	77.72(8)	C13	C14	C15	119.4(2)	C5	C4	N25	112.3(2)

N12	Cu1	Cl2	89.83(5)	H14	C14	C15	120.3	O3	C5	O4	126.8(2)
N22	Cu1	Cl2	99.25(6)	C1	C15	C14	122.9(2)	O3	C5	C4	108.4(2)
Cu1	Cl2	Cu1	92.40(2)	C1	C15	C16	117.9(2)	O4	C5	C4	124.8(2)
C1	O2	C2	117.0(2)	C14	C15	C16	119.1(2)	O3	C6	H6A	110.4
C5	O3	C6	117.5(2)	C11	C16	C15	117.8(2)	O3	C6	H6B	110.4
O1	C1	O2	125.8(2)	C11	C16	H16	121.1	O3	C6	C7	106.5(3)
O1	C1	C15	123.4(2)	C15	C16	H16	121.1	H6A	C6	H6B	108.6
O2	C1	C15	110.7(2)	C11	C21	N22	118.0(2)	H6A	C6	C7	110.4
O2	C2	H2A	109.9	C11	C21	N25	134.3(2)	H6B	C6	C7	110.4
O2	C2	H2B	110	N22	C21	N25	107.7(2)	C6	C7	H7A	109.5
O2	C2	C3	108.6(3)	Cu1	N22	C21	116.1(2)	C6	C7	H7B	109.5
H2A	C2	H2B	108.4	Cu1	N22	N23	135.4(2)	C6	C7	H7C	109.5
H2A	C2	C3	110	C21	N22	N23	107.5(2)	H7A	C7	H7B	109.5
H2B	C2	C3	110	N22	N23	N24	109.4(2)	H7A	C7	H7C	109.5
C2	C3	H3A	109.4	N23	N24	N25	107.6(2)	H7B	C7	H7C	109.4
C2	C3	H3B	109.4	C4	N25	C21	133.2(2)	N12	C11	C16	123.3(2)
C2	C3	H3C	109.4	C4	N25	N24	118.7(2)	N12	C11	C21	110.7(2)
H3A	C3	H3B	109.5	C21	N25	N24	107.8(2)	C16	C11	C21	125.9(2)
H3A	C3	H3C	109.5	Cl2	Cu1	Cl1	99.03(2)	Cu1	N12	C11	116.3(1)
H3B	C3	H3C	109.5	Cl2	Cu1	Cl2	87.60(2)	Cu1	N12	C13	125.1(2)
H4A	C4	H4B	107.9	Cl2	Cu1	N12	89.83(5)	C11	N12	C13	118.2(2)
H4A	C4	C5	109.1	Cl2	Cu1	N22	99.25(6)	N12	C13	H13	118.9
H4A	C4	N25	109.1	Cl1	Cu1	Cl2	95.54(2)	N12	C13	C14	122.2(2)
H4B	C4	C5	109.1	Cl1	Cu1	N12	167.38(5)	H13	C13	C14	118.9
H4B	C4	N25	109.2	Cl1	Cu1	N22	91.90(6)	C13	C14	H14	120.3
C5	C4	N25	112.3(2)	Cl2	Cu1	N12	93.79(5)	C13	C14	C15	119.4(2)
O3	C5	O4	126.8(2)	Cl2	Cu1	N22	168.99(6)	H14	C14	C15	120.3
O3	C5	C4	108.4(2)	N12	Cu1	N22	77.72(8)	C1	C15	C14	122.9(2)
O4	C5	C4	124.8(2)	Cu1	Cl2	Cu1	92.40(2)	C1	C15	C16	117.9(2)
O3	C6	H6A	110.4	C1	O2	C2	117.0(2)	C14	C15	C16	119.1(2)
O3	C6	H6B	110.4	C5	O3	C6	117.5(2)	C11	C16	C15	117.8(2)
O3	C6	C7	106.5(3)	O1	C1	O2	125.8(2)	C11	C16	H16	121.1
H6A	C6	H6B	108.6	O1	C1	C15	123.4(2)	C15	C16	H16	121.1
H6A	C6	C7	110.4	O2	C1	C15	110.7(2)	C11	C21	N22	118.0(2)
H6B	C6	C7	110.4	O2	C2	H2A	109.9	C11	C21	N25	134.3(2)
C6	C7	H7A	109.5	O2	C2	H2B	110	N22	C21	N25	107.7(2)
C6	C7	H7B	109.5	O2	C2	C3	108.6(3)	Cu1	N22	C21	116.1(2)
C6	C7	H7C	109.5	H2A	C2	H2B	108.4	Cu1	N22	N23	135.4(2)
H7A	C7	H7B	109.5	H2A	C2	C3	110	C21	N22	N23	107.5(2)
H7A	C7	H7C	109.5	H2B	C2	C3	110	N22	N23	N24	109.4(2)
H7B	C7	H7C	109.4	C2	C3	H3A	109.4	N23	N24	N25	107.6(2)
N12	C11	C16	123.3(2)	C2	C3	H3B	109.4	C4	N25	C21	133.2(2)
N12	C11	C21	110.7(2)	C2	C3	H3C	109.4	C4	N25	N24	118.7(2)
C16	C11	C21	125.9(2)	H3A	C3	H3B	109.5	C21	N25	N24	107.8(2)

Table A29: Atomic coordinates for **4.14**.

	x	*y*	*z*		*x*	*y*	*z*
Co1	0	0.04287(13)	0.25	**O1**	-0.658(2)	0.0794(10)	0.4561(6)
O1	0.658(2)	0.0794(10)	0.0439(6)	**O2**	-0.4065(16)	0.1432(6)	0.4881(4)
O2	0.4065(16)	0.1432(6)	0.0119(4)	**O3**	0.476(2)	0.2718(6)	0.4175(5)
O3	-0.476(2)	0.2718(6)	0.0825(5)	**O4**	0.4347(15)	0.3902(6)	0.3906(5)
O4	-0.4347(15)	0.3902(6)	0.1094(5)	**C1**	-0.504(3)	0.1003(10)	0.4519(6)
C1	0.504(3)	0.1003(10)	0.0481(6)	**C2**	-0.515(4)	0.1685(13)	0.5324(7)
C2	0.515(4)	0.1685(13)	-0.0324(7)	**H2A**	-0.6303	0.1406	0.5336
H2A	0.6303	0.1406	-0.0336	**H2B**	-0.5423	0.2212	0.5287
H2B	0.5423	0.2212	-0.0287	**H2C**	-0.4421	0.1604	0.5642
H2C	0.4421	0.1604	-0.0642	**C3**	0.364(2)	0.2974(8)	0.3298(6)
C3	-0.364(2)	0.2974(8)	0.1702(6)	**H3A**	0.288	0.3379	0.3151
H3A	-0.288	0.3379	0.1849	**H3B**	0.475	0.292	0.3086
H3B	-0.475	0.292	0.1914	**C4**	0.4264(19)	0.3177(9)	0.3852(6)
C4	-0.4264(19)	0.3177(9)	0.1148(6)	**C5**	0.524(4)	0.4189(12)	0.4386(9)
C5	-0.524(4)	0.4189(12)	0.0614(9)	**H5A**	0.4667	0.3962	0.4682
H5A	-0.4667	0.3962	0.0318	**H5B**	0.5092	0.4725	0.4401
H5B	-0.5092	0.4725	0.0599	**H5C**	0.6564	0.4067	0.4391
H5C	-0.6564	0.4067	0.0609	**C11**	-0.1185(18)	0.1102(7)	0.3531(5)
C11	0.1185(18)	0.1102(7)	0.1469(5)	**N12**	-0.1774(16)	0.0587(6)	0.3177(4)
N12	0.1774(16)	0.0587(6)	0.1823(4)	**C13**	-0.3344(18)	0.0213(8)	0.3265(5)
C13	0.3344(18)	0.0213(8)	0.1735(5)	**H13**	-0.3725	-0.0156	0.3027

H13	0.3725	-0.0156	0.1973	**C14**	-0.444(2)	0.0340(8)	0.3691(6)
C14	0.444(2)	0.0340(8)	0.1309(6)	**H14**	-0.5579	0.0086	0.373
H14	0.5579	0.0086	0.127	**C15**	-0.381(2)	0.0857(8)	0.4060(6)
C15	0.381(2)	0.0857(8)	0.0940(6)	**C16**	-0.2193(19)	0.1248(8)	0.3974(5)
C16	0.2193(19)	0.1248(8)	0.1026(5)	**H16**	-0.177	0.161	0.4212
H16	0.177	0.161	0.0788	**C21**	0.0458(17)	0.1521(6)	0.3382(4)
C21	-0.0458(17)	0.1521(6)	0.1618(4)	**N22**	0.1344(17)	0.1338(6)	0.2937(5)
N22	-0.1344(17)	0.1338(6)	0.2063(5)	**N23**	0.2746(16)	0.1836(7)	0.2879(5)
N23	-0.2746(16)	0.1836(7)	0.2121(5)	**N24**	0.2582(15)	0.2290(6)	0.3277(5)
N24	-0.2582(15)	0.2290(6)	0.1723(5)	**N25**	0.1189(16)	0.2131(6)	0.3597(5)
N25	-0.1189(16)	0.2131(6)	0.1403(5)	**S1S**	0.3574(6)	-0.1604(2)	0.32092(19)
S1S	-0.3574(6)	-0.1604(2)	0.17908(19)	**C1S**	0.2528(16)	-0.0883(7)	0.2994(5)
C1S	-0.2528(16)	-0.0883(7)	0.2006(5)	**N1S**	0.173(2)	-0.0343(7)	0.2825(6)
N1S	-0.173(2)	-0.0343(7)	0.2175(6)				

Table A30: Bond lengths (Å) for **4.14**.

Atom1	Atom2	Length	Atom1	Atom2	Length	Atom1	Atom2	Length	Atom1	Atom2	Length
Co1	**N12**	2.19	**C5**	**H5A**	0.96	**C1S**	**N1S**	1.19(2)	**C5**	**H5C**	0.96
Co1	**N22**	2.17	**C5**	**H5B**	0.96	**O1**	**C1**	1.16(3)	**C11**	**N12**	1.35(2)
Co1	**N1S**	2	**C5**	**H5C**	0.96	**O2**	**C1**	1.37(2)	**C11**	**C16**	1.38(2)
Co1	**N12**	2.19	**C11**	**N12**	1.35(2)	**O2**	**C2**	1.46(2)	**C11**	**C21**	1.44(2)
Co1	**N22**	2.17	**C11**	**C16**	1.38(2)	**O3**	**C4**	1.21(2)	**N12**	**C13**	1.32(2)
Co1	**N1S**	2	**C11**	**C21**	1.44(2)	**O4**	**C4**	1.30(2)	**C13**	**H13**	0.93
O1	**C1**	1.16(3)	**N12**	**C13**	1.32(2)	**O4**	**C5**	1.46(3)	**C13**	**C14**	1.38(2)
O2	**C1**	1.37(2)	**C13**	**H13**	0.93	**C1**	**C15**	1.51(2)	**C14**	**H14**	0.93
O2	**C2**	1.46(2)	**C13**	**C14**	1.38(2)	**C2**	**H2A**	0.96	**C14**	**C15**	1.38(2)
O3	**C4**	1.21(2)	**C14**	**H14**	0.93	**C2**	**H2B**	0.96	**C15**	**C16**	1.36(2)
O4	**C4**	1.30(2)	**C14**	**C15**	1.38(2)	**C2**	**H2C**	0.96	**C16**	**H16**	0.93
O4	**C5**	1.46(3)	**C15**	**C16**	1.36(2)	**C3**	**H3A**	0.97	**C21**	**N22**	1.36(2)
C1	**C15**	1.51(2)	**C16**	**H16**	0.93	**C3**	**H3B**	0.97	**C21**	**N25**	1.31(2)
C2	**H2A**	0.96	**C21**	**N22**	1.36(2)	**C3**	**C4**	1.52(2)	**N22**	**N23**	1.34(2)
C2	**H2B**	0.96	**C21**	**N25**	1.31(2)	**C3**	**N24**	1.43(2)	**N23**	**N24**	1.31(2)
C2	**H2C**	0.96	**N22**	**N23**	1.34(2)	**C5**	**H5A**	0.96	**N24**	**N25**	1.33(2)
C3	**H3A**	0.97	**N23**	**N24**	1.31(2)	**C5**	**H5B**	0.96	**S1S**	**C1S**	1.57(1)
C3	**H3B**	0.97	**N24**	**N25**	1.33(2)	**C3**	**N24**	1.43(2)	**C1S**	**N1S**	1.19(2)
C3	**C4**	1.52(2)	**S1S**	**C1S**	1.57(1)						

Table A31: Bond angles (°) for **4.14.**

Atom1	Atom2	Atom3	Angle	Atom1	Atom2	Atom3	Angle	Atom1	Atom2	Atom3	Angle
N12	Co1	N22	75.5	C16	C11	C21	124(1)	H3B	C3	C4	109
N12	Co1	N1S	96.8	Co1	N12	C11	116.5	H3B	C3	N24	109
N12	Co1	N12	165.2	Co1	N12	C13	125.2	C4	C3	N24	112(1)
N12	Co1	N22	93.4	C11	N12	C13	118(1)	O3	C4	O4	126(1)
N12	Co1	N1S	93.3	N12	C13	H13	118	O3	C4	C3	123(1)
N22	Co1	N1S	92.4	N12	C13	C14	123(1)	O4	C4	C3	110(1)
N22	Co1	N12	93.4	H13	C13	C14	118	O4	C5	H5A	110
N22	Co1	N22	83.7	C13	C14	H14	121	O4	C5	H5B	110
N22	Co1	N1S	167.9	C13	C14	C15	118(1)	O4	C5	H5C	109
N1S	Co1	N12	93.3	H14	C14	C15	121	H5A	C5	H5B	110
N1S	Co1	N22	167.9	C1	C15	C14	118(1)	H5A	C5	H5C	109
N1S	Co1	N1S	93.7	C1	C15	C16	123(1)	H5B	C5	H5C	109
N12	Co1	N22	75.5	C14	C15	C16	119(1)	N12	C11	C16	121(1)
N12	Co1	N1S	96.8	C11	C16	C15	120(1)	N12	C11	C21	114(1)
N22	Co1	N1S	92.4	C11	C16	H16	120	C16	C11	C21	124(1)
C1	O2	C2	115(1)	C15	C16	H16	120	Co1	N12	C11	116.5
C4	O4	C5	117(1)	C11	C21	N22	120(1)	Co1	N12	C13	125.2
O1	C1	O2	125(2)	C11	C21	N25	129(1)	C11	N12	C13	118(1)
O1	C1	C15	126(2)	N22	C21	N25	111(1)	N12	C13	H13	118
O2	C1	C15	109(1)	Co1	N22	C21	113.9	N12	C13	C14	123(1)
O2	C2	H2A	110	Co1	N22	N23	138.6	H13	C13	C14	118
O2	C2	H2B	109	C21	N22	N23	107(1)	C13	C14	H14	121
O2	C2	H2C	109	N22	N23	N24	104(1)	C13	C14	C15	118(1)
H2A	C2	H2B	110	C3	N24	N23	120(1)	H14	C14	C15	121
H2A	C2	H2C	109	C3	N24	N25	124(1)	C1	C15	C14	118(1)
H2B	C2	H2C	109	N23	N24	N25	116(1)	C1	C15	C16	123(1)
H3A	C3	H3B	108	C21	N25	N24	102(1)	C14	C15	C16	119(1)

H3A	C3	C4	109	S1S	C1S	N1S	179(1)	C11	C16	C15	120(1)
H3A	C3	N24	109	Co1	N1S	C1S	169	C11	C16	H16	120
H3B	C3	C4	109	C1	O2	C2	115(1)	C15	C16	H16	120
H3B	C3	N24	109	C4	O4	C5	117(1)	C11	C21	N22	120(1)
C4	C3	N24	112(1)	O1	C1	O2	125(2)	C11	C21	N25	129(1)
O3	C4	O4	126(1)	O1	C1	C15	126(2)	N22	C21	N25	111(1)
O3	C4	C3	123(1)	O2	C1	C15	109(1)	Co1	N22	C21	113.9
O4	C4	C3	110(1)	O2	C2	H2A	110	Co1	N22	N23	138.6
O4	C5	H5A	110	O2	C2	H2B	109	C21	N22	N23	107(1)
O4	C5	H5B	110	O2	C2	H2C	109	N22	N23	N24	104(1)
O4	C5	H5C	109	H2A	C2	H2B	110	C3	N24	N23	120(1)
H5A	C5	H5B	110	H2A	C2	H2C	109	C3	N24	N25	124(1)
H5A	C5	H5C	109	H2B	C2	H2C	109	N23	N24	N25	116(1)
H5B	C5	H5C	109	H3A	C3	H3B	108	C21	N25	N24	102(1)
N12	C11	C16	121(1)	H3A	C3	C4	109	S1S	C1S	N1S	179(1)
N12	C11	C21	114(1)	H3A	C3	N24	109	Co1	N1S	C1S	169

Table A32: Atomic coordinates for **4.15**.

	x	*y*	*z*		*x*	*y*	*z*
Cu1	0.75	0.25	0	**N3**	0.33977(10)	0.4338(3)	0.4058(2)
Cu2	0.5	-0.23387(6)	0.25	**N4**	0.38765(10)	0.3985(3)	0.3961(2)
C1	0.64472(10)	0.1961(3)	0.0263(2)	**N5**	0.39817(9)	0.2499(3)	0.43892(19)
N2	0.68162(9)	0.3089(3)	0.04655(18)	**C2**	0.44856(11)	0.1708(4)	0.4322(2)
N3	0.66023(10)	0.4338(3)	0.0942(2)	**H2A**	0.4634	0.1325	0.4995
N4	0.61235(10)	0.3985(3)	0.1039(2)	**H2B**	0.4726	0.2505	0.4101
N5	0.60183(9)	0.2499(3)	0.06108(19)	**C3**	0.44344(11)	0.0275(4)	0.3583(2)
C2	0.55144(11)	0.1708(4)	0.0678(2)	**O3**	0.39920(9)	-0.0044(3)	0.3100(2)
H2A	0.5366	0.1325	0.0005	**O4**	0.48526(9)	-0.0458(3)	0.35340(18)
H2B	0.5274	0.2505	0.0899	**C11**	0.34298(10)	0.0449(3)	0.5249(2)
C3	0.55656(11)	0.0275(4)	0.1417(2)	**N12**	0.29215(9)	0.0437(3)	0.54177(17)
O3	0.60080(9)	-0.0044(3)	0.1900(2)	**C13**	0.27474(11)	-0.0881(3)	0.5858(2)
O4	0.51474(9)	-0.0458(3)	0.14660(18)	**H13**	0.24	-0.0905	0.5984
C11	0.65702(10)	0.0449(3)	-0.0249(2)	**C14**	0.30663(12)	-0.2217(3)	0.6135(3)
N12	0.70785(9)	0.0437(3)	-0.04177(17)	**H14**	0.2931	-0.3127	0.643
C13	0.72526(11)	-0.0881(3)	-0.0858(2)	**C15**	0.35813(11)	-0.2197(3)	0.5972(2)
H13	0.76	-0.0905	-0.0984	**C16**	0.37692(11)	-0.0824(3)	0.5529(2)
C14	0.69337(12)	-0.2217(3)	-0.1135(3)	**H16**	0.4119	-0.0763	0.5421
H14	0.7069	-0.3127	-0.143	**C17**	0.39428(12)	-0.3651(4)	0.6263(3)
C15	0.64187(11)	-0.2197(3)	-0.0972(2)	**O1**	0.37324(8)	-0.4930(3)	0.6525(2)
C16	0.62308(11)	-0.0824(3)	-0.0529(2)	**O2A**	0.4418(7)	-0.337(2)	0.6420(9)
H16	0.5881	-0.0763	-0.0421	**O2B**	0.4395(7)	-0.355(2)	0.6005(9)
C17	0.60572(12)	-0.3651(4)	-0.1263(3)	**O2W1**	0.4904(3)	-0.4043(9)	0.3668(8)
O1	0.62676(8)	-0.4930(3)	-0.1525(2)	**O2W2**	0.4853(7)	-0.4480(17)	0.323(2)
O2A	0.5582(7)	-0.337(2)	-0.1420(9)	**O3W**	0.57351(9)	-0.2332(3)	0.31303(19)
O2B	0.5605(7)	-0.355(2)	-0.1005(9)	**H3A**	0.5886(16)	-0.321(5)	0.315(3)
O1W	0.77820(9)	0.1357(3)	0.16779(18)	**H3B**	0.5899(16)	-0.167(4)	0.266(3)
H1A	0.8053(16)	0.088(5)	0.162(3)	**O1W**	0.72180(9)	0.3643(3)	-0.16779(18)
H1B	0.7806(16)	0.214(5)	0.204(3)	**H1A**	0.6947(16)	0.412(5)	-0.162(3)
O2W1	0.5096(3)	-0.4043(9)	0.1332(8)	**H1B**	0.7194(16)	0.286(5)	-0.204(3)
O2W2	0.5147(7)	-0.4480(17)	0.177(2)	**Cu1**	0.25	0.25	0.5
O3W	0.42649(9)	-0.2332(3)	0.18697(19)	**N2**	0.81838(9)	0.1911(3)	-0.04655(18)
H3A	0.4114(16)	-0.321(5)	0.185(3)	**N12**	0.79215(9)	0.4563(3)	0.04177(17)
H3B	0.4101(16)	-0.167(4)	0.234(3)	**O4W**	0.70356(12)	-0.1090(4)	0.1962(2)
C1	0.35528(10)	0.1961(3)	0.4737(2)	**H4W1**	0.719(2)	-0.030(7)	0.195(4)
N2	0.31838(9)	0.3089(3)	0.45345(18)	**H4W2**	0.667(2)	-0.088(6)	0.196(4)

Table A33: Bond lengths (Å) for **4.15**.

Atom1	Atom2	Length	Atom1	Atom2	Length	Atom1	Atom2	Length	Atom1	Atom2	Length
Cu1	**N2**	1.999	**N5**	**C2**	1.461(4)	**O1W**	**H1A**	0.81(4)	**N12**	**C13**	1.331(4)
Cu1	**N12**	2.04	**C2**	**H2A**	0.97	**O1W**	**H1B**	0.80(4)	**N12**	**Cu1**	2.04
Cu1	**O1W**	2.422	**C2**	**H2B**	0.97	**O2W1**	**O2W2**	0.68(2)	**C13**	**H13**	0.931
Cu1	**O1W**	2.422	**C2**	**C3**	1.519(4)	**O3W**	**H3A**	0.81(4)	**C13**	**C14**	1.385(4)
Cu1	**N2**	1.999	**C3**	**O3**	1.252(3)	**O3W**	**H3B**	0.96(4)	**C14**	**H14**	0.929
Cu1	**N12**	2.04	**C3**	**O4**	1.240(4)	**C1**	**N2**	1.324(3)	**C14**	**C15**	1.370(4)
Cu2	**O4**	2.125	**C11**	**N12**	1.355(4)	**C1**	**N5**	1.326(4)	**C15**	**C16**	1.383(4)
Cu2	**O2W1**	2.118	**C11**	**C16**	1.376(4)	**C1**	**C11**	1.465(4)	**C15**	**C17**	1.526(4)

Cu2	**O2W2**	2.06	**N12**	**C13**	1.331(4)	**N2**	**N3**	1.355(4)	**C16**	**H16**	0.931
Cu2	**O3W**	1.957	**C13**	**H13**	0.931	**N2**	**Cu1**	1.999	**C17**	**O1**	1.248(4)
Cu2	**O4**	2.125	**C13**	**C14**	1.385(4)	**N3**	**N4**	1.287(4)	**C17**	**O2A**	1.23(2)
Cu2	**O2W1**	2.118	**C14**	**H14**	0.929	**N4**	**N5**	1.352(3)	**C17**	**O2B**	1.26(2)
Cu2	**O2W2**	2.06	**C14**	**C15**	1.370(4)	**N5**	**C2**	1.461(4)	**O2A**	**O2B**	0.56(2)
Cu2	**O3W**	1.957	**C15**	**C16**	1.383(4)	**C2**	**H2A**	0.97	**O2W1**	**O2W2**	0.68(2)
C1	**N2**	1.324(3)	**C15**	**C17**	1.526(4)	**C2**	**H2B**	0.97	**O3W**	**H3A**	0.81(4)
C1	**N5**	1.326(4)	**C16**	**H16**	0.931	**C2**	**C3**	1.519(4)	**O3W**	**H3B**	0.96(4)
C1	**C11**	1.465(4)	**C17**	**O1**	1.248(4)	**C3**	**O3**	1.252(3)	**O1W**	**H1A**	0.81(4)
N2	**N3**	1.355(4)	**C17**	**O2A**	1.23(2)	**C3**	**O4**	1.240(4)	**O1W**	**H1B**	0.80(4)
N3	**N4**	1.287(4)	**C17**	**O2B**	1.26(2)	**C11**	**N12**	1.355(4)	**O4W**	**H4W1**	0.76(6)
N4	**N5**	1.352(3)	**O2A**	**O2B**	0.56(2)	**C11**	**C16**	1.376(4)	**O4W**	**H4W2**	0.95(5)

Table A34: Bond angles (°) for **4.15**.

Atom1	Atom2	Atom3	Angle	Atom1	Atom2	Atom3	Angle	Atom1	Atom2	Atom3	Angle
N2	Cu1	N12	79.97	C1	N5	C2	131.3(2)	N2	N3	N4	109.3(2)
N2	Cu1	O1W	88.7	N4	N5	C2	120.1(2)	N3	N4	N5	107.4(2)
N2	Cu1	O1W	91.3	N5	C2	H2A	109.1	C1	N5	N4	108.4(2)
N2	Cu1	N2	180	N5	C2	H2B	109.1	C1	N5	C2	131.3(2)
N2	Cu1	N12	100.03	N5	C2	C3	112.4(2)	N4	N5	C2	120.1(2)
N12	Cu1	O1W	90.52	H2A	C2	H2B	107.8	N5	C2	H2A	109.1
N12	Cu1	O1W	89.48	H2A	C2	C3	109.1	N5	C2	H2B	109.1
N12	Cu1	N2	100.03	H2B	C2	C3	109.1	N5	C2	C3	112.4(2)
N12	Cu1	N12	180	C2	C3	O3	118.7(3)	H2A	C2	H2B	107.8
O1W	Cu1	O1W	180	C2	C3	O4	114.0(3)	H2A	C2	C3	109.1
O1W	Cu1	N2	91.3	O3	C3	O4	127.3(3)	H2B	C2	C3	109.1
O1W	Cu1	N12	89.48	Cu2	O4	C3	128	C2	C3	O3	118.7(3)
O1W	Cu1	N2	88.7	C1	C11	N12	110.9(2)	C2	C3	O4	114.0(3)
O1W	Cu1	N12	90.52	C1	C11	C16	126.4(2)	O3	C3	O4	127.3(3)
N2	Cu1	N12	79.97	N12	C11	C16	122.7(2)	Cu2	O4	C3	128
O4	Cu2	O2W1	87.7	Cu1	N12	C11	116	C1	C11	N12	110.9(2)
O4	Cu2	O2W2	104.8	Cu1	N12	C13	126.2	C1	C11	C16	126.4(2)
O4	Cu2	O3W	88.4	C11	N12	C13	117.8(2)	N12	C11	C16	122.7(2)
O4	Cu2	O4	87.23	N12	C13	H13	118.9	C11	N12	C13	117.8(2)
O4	Cu2	O2W1	173.2	N12	C13	C14	122.2(3)	C11	N12	Cu1	116
O4	Cu2	O2W2	167.7	H13	C13	C14	118.9	C13	N12	Cu1	126.2
O4	Cu2	O3W	91.4	C13	C14	H14	120.1	N12	C13	H13	118.9
O2W1	Cu2	O2W2	18.6	C13	C14	C15	119.9(3)	N12	C13	C14	122.2(3)
O2W1	Cu2	O3W	83.9	H14	C14	C15	120	H13	C13	C14	118.9
O2W1	Cu2	O4	173.2	C14	C15	C16	118.5(3)	C13	C14	H14	120.1
O2W1	Cu2	O2W1	97.7	C14	C15	C17	121.3(3)	C13	C14	C15	119.9(3)
O2W1	Cu2	O2W2	80.1	C16	C15	C17	120.2(2)	H14	C14	C15	120
O2W1	Cu2	O3W	96.3	C11	C16	C15	118.9(2)	C14	C15	C16	118.5(3)
O2W2	Cu2	O3W	91.8	C11	C16	H16	120.6	C14	C15	C17	121.3(3)
O2W2	Cu2	O4	167.7	C15	C16	H16	120.6	C16	C15	C17	120.2(2)
O2W2	Cu2	O2W1	80.1	C15	C17	O1	116.8(3)	C11	C16	C15	118.9(2)
O2W2	Cu2	O2W2	63.4	C15	C17	O2A	116.9(8)	C11	C16	H16	120.6
O2W2	Cu2	O3W	88.5	C15	C17	O2B	115.7(7)	C15	C16	H16	120.6
O3W	Cu2	O4	91.4	O1	C17	O2A	124.5(8)	C15	C17	O1	116.8(3)
O3W	Cu2	O2W1	96.3	O1	C17	O2B	125.6(8)	C15	C17	O2A	116.9(8)
O3W	Cu2	O2W2	88.5	O2A	C17	O2B	26(1)	C15	C17	O2B	115.7(7)
O3W	Cu2	O3W	179.7	C17	O2A	O2B	80(2)	O1	C17	O2A	124.5(8)
O4	Cu2	O2W1	87.7	C17	O2B	O2A	74(2)	O1	C17	O2B	125.6(8)
O4	Cu2	O2W2	104.8	Cu1	O1W	H1A	105	O2A	C17	O2B	26(1)
O4	Cu2	O3W	88.4	Cu1	O1W	H1B	103	C17	O2A	O2B	80(2)
O2W1	Cu2	O2W2	18.6	H1A	O1W	H1B	117(4)	C17	O2B	O2A	74(2)
O2W1	Cu2	O3W	83.9	Cu2	O2W1	O2W2	76	Cu2	O2W1	O2W2	76
O2W2	Cu2	O3W	91.8	Cu2	O2W2	O2W1	86	Cu2	O2W2	O2W1	86
N2	C1	N5	107.8(2)	Cu2	O3W	H3A	116	Cu2	O3W	H3A	116
N2	C1	C11	119.2(2)	Cu2	O3W	H3B	102	Cu2	O3W	H3B	102
N5	C1	C11	133.0(2)	H3A	O3W	H3B	106(4)	H3A	O3W	H3B	106(4)
Cu1	N2	C1	113.9	N2	C1	N5	107.8(2)	Cu1	O1W	H1A	105
Cu1	N2	N3	139	N2	C1	C11	119.2(2)	Cu1	O1W	H1B	103
C1	N2	N3	107.1(2)	N5	C1	C11	133.0(2)	H1A	O1W	H1B	117(4)
N2	N3	N4	109.3(2)	C1	N2	N3	107.1(2)	N2	Cu1	N12	79.97
N3	N4	N5	107.4(2)	C1	N2	Cu1	113.9	H4W1	O4W	H4W2	111(5)
C1	N5	N4	108.4(2)	N3	N2	Cu1	139				

Table A35: Atomic coordinates for **4.16**.

	x	*y*	*z*		*x*	*y*	*z*
Ni1	0.25	-0.25	0.5	**C1**	-0.10630(8)	0.3698(2)	1.12090(17)
O1	0.12847(5)	0.49456(17)	0.35334(13)	**O3**	-0.10116(6)	0.0088(2)	0.80780(12)
O2	0.05946(7)	0.3555(2)	0.3865(2)	**O4**	-0.01483(5)	0.05098(17)	0.85029(10)
C1	0.10630(8)	0.3698(2)	0.37910(17)	**C2**	-0.05042(7)	-0.1644(2)	0.93098(15)
O3	0.10116(6)	0.0088(2)	0.69220(12)	**H2A**	-0.0259	-0.2419	0.9092
O4	0.01483(5)	0.05098(17)	0.64971(10)	**H2B**	-0.0359	-0.1259	0.9994
C2	0.05042(7)	-0.1644(2)	0.56902(15)	**C3**	-0.05674(7)	-0.0221(2)	0.85555(14)
H2A	0.0259	-0.2419	0.5908	**C11**	-0.15622(7)	-0.0417(2)	1.02176(14)
H2B	0.0359	-0.1259	0.5006	**N12**	-0.20658(6)	-0.04169(18)	1.04154(12)
C3	0.05674(7)	-0.0221(2)	0.64445(14)	**C13**	-0.22361(8)	0.0877(2)	1.08672(17)
C11	0.15622(7)	-0.0417(2)	0.47824(14)	**H13**	-0.258	0.0884	1.101
N12	0.20658(6)	-0.04169(18)	0.45846(12)	**C14**	-0.19219(8)	0.2219(2)	1.11356(18)
C13	0.22361(8)	0.0877(2)	0.41328(17)	**H14**	-0.2055	0.3109	1.1447
H13	0.258	0.0884	0.399	**C15**	-0.14116(7)	0.2226(2)	1.09373(16)
C14	0.19219(8)	0.2219(2)	0.38644(18)	**C16**	-0.12230(7)	0.0871(2)	1.04821(15)
H14	0.2055	0.3109	0.3553	**H16**	-0.0877	0.0828	1.0357
C15	0.14116(7)	0.2226(2)	0.40627(16)	**C21**	-0.14395(7)	-0.1917(2)	0.96998(14)
C16	0.12230(7)	0.0871(2)	0.45179(15)	**N22**	-0.18050(6)	-0.30486(18)	0.94812(12)
H16	0.0877	0.0828	0.4643	**N23**	-0.15881(7)	-0.4270(2)	0.90034(14)
C21	0.14395(7)	-0.1917(2)	0.53002(14)	**N24**	-0.11064(7)	-0.3912(2)	0.89193(13)
N22	0.18050(6)	-0.30486(18)	0.55188(12)	**N25**	-0.10060(6)	-0.24404(17)	0.93577(12)
N23	0.15881(7)	-0.4270(2)	0.59966(14)	**O2W**	-0.07570(6)	0.23283(18)	0.67899(12)
N24	0.11064(7)	-0.3912(2)	0.60807(13)	**H21**	-0.0922(11)	0.323(4)	0.675(2)
N25	0.10060(6)	-0.24404(17)	0.56423(12)	**H22**	-0.0895(11)	0.177(4)	0.718(2)
Ni2	0	0.23152(4)	0.75	**O3W**	-0.01283(8)	0.4068(2)	0.85678(15)
O2W	0.07570(6)	0.23283(18)	0.82101(12)	**H31**	-0.0414(14)	0.443(4)	0.860(2)
H21	0.0922(11)	0.323(4)	0.825(2)	**H32**	0.0107(15)	0.489(5)	0.866(3)
H22	0.0895(11)	0.177(4)	0.782(2)	**O1W**	0.27754(6)	-0.1437(2)	0.64675(13)
O3W	0.01283(8)	0.4068(2)	0.64322(15)	**H11**	0.3024(12)	-0.099(3)	0.648(2)
H31	0.0414(14)	0.443(4)	0.640(2)	**H12**	0.2820(12)	-0.200(4)	0.686(2)
H32	-0.0107(15)	0.489(5)	0.634(3)	**Ni1**	-0.25	-0.25	1
O1W	0.22246(6)	-0.3563(2)	0.35325(13)	**N12**	0.29342(6)	-0.45831(18)	0.54154(12)
H11	0.1976(12)	-0.401(3)	0.352(2)	**N22**	0.31950(6)	-0.19514(18)	0.44812(12)
H12	0.2180(12)	-0.300(4)	0.314(2)	**O4W**	0.20492(10)	0.1145(4)	0.70195(18)
O1	-0.12847(5)	0.49456(17)	1.14666(13)	**H41**	0.1740(12)	0.093(3)	0.6929(19)
O2	-0.05946(7)	0.3555(2)	1.1135(2)	**H42**	0.2179(15)	0.035(5)	0.699(3)
O5W	0.1843(12)	0.219(5)	0.6826(19)				

Table A36: Bond lengths (Å) for **4.16**.

Atom1	Atom2	Length	Atom1	Atom2	Length	Atom1	Atom2	Length	Atom1	Atom2	Length
Ni1	**N12**	2.08	**N12**	**C13**	1.326(2)	**O2W**	**H21**	0.86(3)	**C13**	**H13**	0.931
Ni1	**N22**	2.054	**C13**	**H13**	0.931	**O2W**	**H22**	0.81(3)	**C13**	**C14**	1.387(3)
Ni1	**O1W**	2.132	**C13**	**C14**	1.387(3)	**O3W**	**H31**	0.80(4)	**C14**	**H14**	0.93
Ni1	**O1W**	2.132	**C14**	**H14**	0.93	**O3W**	**H32**	0.91(4)	**C14**	**C15**	1.375(3)
Ni1	**N12**	2.08	**C14**	**C15**	1.375(3)	**O1W**	**H11**	0.74(3)	**C15**	**C16**	1.388(3)
Ni1	**N22**	2.054	**C15**	**C16**	1.388(3)	**O1W**	**H12**	0.69(3)	**C16**	**H16**	0.929
O1	**C1**	1.248(2)	**C16**	**H16**	0.929	**O1**	**C1**	1.248(2)	**C21**	**N22**	1.327(2)
O2	**C1**	1.229(3)	**C21**	**N22**	1.327(2)	**O2**	**C1**	1.229(3)	**C21**	**N25**	1.333(2)
C1	**C15**	1.522(2)	**C21**	**N25**	1.333(2)	**C1**	**C15**	1.522(2)	**N22**	**N23**	1.350(2)
O3	**C3**	1.245(2)	**N22**	**N23**	1.350(2)	**O3**	**C3**	1.245(2)	**N22**	**Ni1**	2.054
O4	**C3**	1.247(2)	**N23**	**N24**	1.294(3)	**O4**	**C3**	1.247(2)	**N23**	**N24**	1.294(3)
O4	**Ni2**	2.057	**N24**	**N25**	1.353(2)	**C2**	**H2A**	0.97	**N24**	**N25**	1.353(2)
C2	**H2A**	0.97	**Ni2**	**O2W**	2.03	**C2**	**H2B**	0.97	**O2W**	**H21**	0.86(3)
C2	**H2B**	0.97	**Ni2**	**O3W**	2.07	**C2**	**C3**	1.527(2)	**O2W**	**H22**	0.81(3)
C2	**C3**	1.527(2)	**Ni2**	**O4**	2.057	**C2**	**N25**	1.459(2)	**O3W**	**H31**	0.80(4)
C2	**N25**	1.459(2)	**Ni2**	**O2W**	2.03	**C11**	**N12**	1.358(2)	**O3W**	**H32**	0.91(4)
C11	**N12**	1.358(2)	**Ni2**	**O3W**	2.07	**C11**	**C16**	1.387(2)	**O1W**	**H11**	0.74(3)
C11	**C16**	1.387(2)	**N12**	**Ni1**	2.08	**C11**	**C21**	1.468(2)	**O1W**	**H12**	0.69(3)
C11	**C21**	1.468(2)	**O4W**	**H42**	0.74(4)	**N12**	**C13**	1.326(2)	**O4W**	**H41**	0.81(3)

Table A37: Bond angles (°) for **4.16**.

Atom1	Atom2	Atom3	Angle	Atom1	Atom2	Atom3	Angle	Atom1	Atom2	Atom3	Angle
N12	Ni1	N22	78.95	C15	C16	H16	120.7	C3	C2	N25	111.3(1)

N12	Ni1	O1W	90.68	C11	C21	N22	120.0(2)	O3	C3	O4	127.7(2)
N12	Ni1	O1W	89.32	C11	C21	N25	132.5(2)	O3	C3	C2	118.9(2)
N12	Ni1	N12	180	N22	C21	N25	107.5(2)	O4	C3	C2	113.4(2)
N12	Ni1	N22	101.05	Ni1	N22	C21	113.4	N12	C11	C16	122.4(2)
N22	Ni1	O1W	90.85	Ni1	N22	N23	139.2	N12	C11	C21	111.3(2)
N22	Ni1	O1W	89.15	C21	N22	N23	107.3(2)	C16	C11	C21	126.3(2)
N22	Ni1	N12	101.05	N22	N23	N24	109.5(2)	C11	N12	C13	118.1(2)
N22	Ni1	N22	180	N23	N24	N25	107.2(2)	C11	N12	Ni1	116.2
O1W	Ni1	O1W	180	C2	N25	C21	131.1(2)	C13	N12	Ni1	125.7
O1W	Ni1	N12	89.32	C2	N25	N24	120.2(1)	N12	C13	H13	118.7
O1W	Ni1	N22	89.15	C21	N25	N24	108.4(1)	N12	C13	C14	122.6(2)
O1W	Ni1	N12	90.68	O4	Ni2	O2W	92.25	H13	C13	C14	118.7
O1W	Ni1	N22	90.85	O4	Ni2	O3W	90.91	C13	C14	H14	120.3
N12	Ni1	N22	78.95	O4	Ni2	O4	87.04	C13	C14	C15	119.5(2)
O1	C1	O2	126.4(2)	O4	Ni2	O2W	88.2	H14	C14	C15	120.2
O1	C1	C15	116.5(2)	O4	Ni2	O3W	177.19	C1	C15	C14	120.4(2)
O2	C1	C15	117.1(2)	O2W	Ni2	O3W	93.81	C1	C15	C16	120.9(2)
C3	O4	Ni2	129	O2W	Ni2	O4	88.2	C14	C15	C16	118.7(2)
H2A	C2	H2B	107.9	O2W	Ni2	O2W	179.39	C11	C16	C15	118.6(2)
H2A	C2	C3	109.4	O2W	Ni2	O3W	85.76	C11	C16	H16	120.7
H2A	C2	N25	109.4	O3W	Ni2	O4	177.19	C15	C16	H16	120.7
H2B	C2	C3	109.4	O3W	Ni2	O2W	85.76	C11	C21	N22	120.0(2)
H2B	C2	N25	109.4	O3W	Ni2	O3W	91.2	C11	C21	N25	132.5(2)
C3	C2	N25	111.3(1)	O4	Ni2	O2W	92.25	N22	C21	N25	107.5(2)
O3	C3	O4	127.7(2)	O4	Ni2	O3W	90.91	C21	N22	N23	107.3(2)
O3	C3	C2	118.9(2)	O2W	Ni2	O3W	93.81	C21	N22	Ni1	113.4
O4	C3	C2	113.4(2)	Ni2	O2W	H21	118	N23	N22	Ni1	139.2
N12	C11	C16	122.4(2)	Ni2	O2W	H22	101	N22	N23	N24	109.5(2)
N12	C11	C21	111.3(2)	H21	O2W	H22	106(3)	N23	N24	N25	107.2(2)
C16	C11	C21	126.3(2)	Ni2	O3W	H31	122	C2	N25	C21	131.1(2)
Ni1	N12	C11	116.2	Ni2	O3W	H32	116	C2	N25	N24	120.2(1)
Ni1	N12	C13	125.7	H31	O3W	H32	108(3)	C21	N25	N24	108.4(1)
C11	N12	C13	118.1(2)	Ni1	O1W	H11	114	Ni2	O2W	H21	118
N12	C13	H13	118.7	Ni1	O1W	H12	113	Ni2	O2W	H22	101
N12	C13	C14	122.6(2)	H11	O1W	H12	106(3)	H21	O2W	H22	106(3)
H13	C13	C14	118.7	O1	C1	O2	126.4(2)	Ni2	O3W	H31	122
C13	C14	H14	120.3	O1	C1	C15	116.5(2)	Ni2	O3W	H32	116
C13	C14	C15	119.5(2)	O2	C1	C15	117.1(2)	H31	O3W	H32	108(3)
H14	C14	C15	120.2	Ni2	O4	C3	129	Ni1	O1W	H11	114
C1	C15	C14	120.4(2)	H2A	C2	H2B	107.9	Ni1	O1W	H12	113
C1	C15	C16	120.9(2)	H2A	C2	C3	109.4	H11	O1W	H12	106(3)
C14	C15	C16	118.7(2)	H2A	C2	N25	109.4	N12	Ni1	N22	78.95
C11	C16	C15	118.6(2)	H2B	C2	C3	109.4	H41	O4W	H42	104(4)
C11	C16	H16	120.7	H2B	C2	N25	109.4				

Table A38: Atomic coordinates for **4.17**.

	x	*y*	*z*		*x*	*y*	*z*
Co1	0.25	-0.25	0.5	**C1**	-0.10713(5)	0.37005(16)	1.12009(12)
O1	0.12951(4)	0.49336(12)	0.35274(9)	**O3**	-0.10125(4)	0.00847(14)	0.81041(9)
O2	0.06065(5)	0.35731(15)	0.38870(14)	**O4**	-0.01538(4)	0.05106(12)	0.85031(7)
C1	0.10713(5)	0.37005(16)	0.37991(12)	**C2**	-0.05006(5)	-0.16258(15)	0.93270(10)
O3	0.10125(4)	0.00847(14)	0.68959(9)	**H2A**	-0.0256	-0.2392	0.9109
O4	0.01538(4)	0.05106(12)	0.64969(7)	**H2B**	-0.0356	-0.1234	1.0005
C2	0.05006(5)	-0.16258(15)	0.56730(10)	**C3**	-0.05686(5)	-0.02178(15)	0.85704(10)
H2A	0.0256	-0.2392	0.5891	**C11**	-0.15499(5)	-0.04146(14)	1.02362(9)
H2B	0.0356	-0.1234	0.4995	**N12**	-0.20504(4)	-0.04223(12)	1.04289(8)
C3	0.05686(5)	-0.02178(15)	0.64296(10)	**C13**	-0.22280(5)	0.08686(16)	1.08659(11)
C11	0.15499(5)	-0.04146(14)	0.47638(9)	**H13**	-0.257	0.0868	1.1002
N12	0.20504(4)	-0.04223(12)	0.45711(8)	**C14**	-0.19221(5)	0.22138(16)	1.11257(13)
C13	0.22280(5)	0.08686(16)	0.41341(11)	**H14**	-0.2059	0.3101	1.1425
H13	0.257	0.0868	0.3998	**C15**	-0.14125(5)	0.22260(15)	1.09373(11)
C14	0.19221(5)	0.22138(16)	0.38743(13)	**C16**	-0.12188(5)	0.08753(15)	1.04957(10)
H14	0.2059	0.3101	0.3575	**H16**	-0.0874	0.0839	1.0377
C15	0.14125(5)	0.22260(15)	0.40627(11)	**C21**	-0.14263(5)	-0.19047(15)	0.97199(9)
C16	0.12188(5)	0.08753(15)	0.45043(10)	**N22**	-0.17895(4)	-0.30253(13)	0.94953(9)
H16	0.0874	0.0839	0.4623	**N23**	-0.15720(5)	-0.42398(14)	0.90188(10)
C21	0.14263(5)	-0.19047(15)	0.52801(9)	**N24**	-0.10934(4)	-0.38856(14)	0.89446(9)
N22	0.17895(4)	-0.30253(13)	0.55047(9)	**N25**	-0.09941(4)	-0.24284(12)	0.93859(9)

N23	0.15720(5)	-0.42398(14)	0.59812(10)	**O2W**	-0.07722(4)	0.23567(13)	0.68245(9)
N24	0.10934(4)	-0.38856(14)	0.60554(9)	**H21**	-0.0928(8)	0.320(3)	0.6782(16)
N25	0.09941(4)	-0.24284(12)	0.56141(9)	**H22**	-0.0915(8)	0.177(3)	0.7191(15)
Co2	0	0.23458(3)	0.75	**O3W**	-0.01138(5)	0.41042(15)	0.85963(11)
O2W	0.07722(4)	0.23567(13)	0.81755(9)	**H31**	-0.0387(10)	0.444(3)	0.8667(19)
H21	0.0928(8)	0.320(3)	0.8218(16)	**H32**	0.0116(9)	0.483(3)	0.8691(17)
H22	0.0915(8)	0.177(3)	0.7809(15)	**O1W**	0.27748(4)	-0.14166(12)	0.64687(8)
O3W	0.01138(5)	0.41042(15)	0.64037(11)	**H11**	0.3054(8)	-0.097(2)	0.6489(15)
H31	0.0387(10)	0.444(3)	0.6333(19)	**H12**	0.2553(8)	-0.078(3)	0.6639(15)
H32	-0.0116(9)	0.483(3)	0.6309(17)	**Co1**	-0.25	-0.25	1
O1W	0.22252(4)	-0.35834(12)	0.35313(8)	**N12**	0.29496(4)	-0.45777(12)	0.54289(8)
H11	0.1946(8)	-0.403(2)	0.3511(15)	**N22**	0.32105(4)	-0.19747(13)	0.44953(9)
H12	0.2447(8)	-0.422(3)	0.3361(15)	**O4W**	0.20722(5)	0.08778(18)	0.69683(11)
O1	-0.12951(4)	0.49336(12)	1.14726(9)	**H41**	0.1760(11)	0.068(3)	0.6911(19)
O2	-0.06065(5)	0.35731(15)	1.11130(14)	**H42**	0.2101(9)	0.163(3)	0.740(2)

Table A39: Bond lengths (Å) for **4.17.**

Atom1	Atom2	Length	Atom1	Atom2	Length	Atom1	Atom2	Length	Atom1	Atom2	Length
Co1	**N12**	2.114	**N12**	**C13**	1.330(2)	**O3W**	**H31**	0.78(3)	**C13**	**C14**	1.385(2)
Co1	**N22**	2.09	**C13**	**H13**	0.929	**O3W**	**H32**	0.84(2)	**C14**	**H14**	0.93
Co1	**O1W**	2.152	**C13**	**C14**	1.385(2)	**O1W**	**H11**	0.81(2)	**C14**	**C15**	1.378(2)
Co1	**O1W**	2.152	**C14**	**H14**	0.93	**O1W**	**H12**	0.84(2)	**C15**	**C16**	1.390(2)
Co1	**N12**	2.114	**C14**	**C15**	1.378(2)	**O1**	**C1**	1.255(2)	**C16**	**H16**	0.929
Co1	**N22**	2.09	**C15**	**C16**	1.390(2)	**O2**	**C1**	1.231(2)	**C21**	**N22**	1.327(2)
O1	**C1**	1.255(2)	**C16**	**H16**	0.929	**C1**	**C15**	1.522(2)	**C21**	**N25**	1.333(2)
O2	**C1**	1.231(2)	**C21**	**N22**	1.327(2)	**O3**	**C3**	1.248(2)	**N22**	**N23**	1.353(2)
C1	**C15**	1.522(2)	**C21**	**N25**	1.333(2)	**O4**	**C3**	1.248(2)	**N22**	**Co1**	2.09
O3	**C3**	1.248(2)	**N22**	**N23**	1.353(2)	**C2**	**H2A**	0.97	**N23**	**N24**	1.292(2)
O4	**C3**	1.248(2)	**N23**	**N24**	1.292(2)	**C2**	**H2B**	0.97	**N24**	**N25**	1.351(2)
O4	**Co2**	2.09	**N24**	**N25**	1.351(2)	**C2**	**C3**	1.528(2)	**O2W**	**H21**	0.81(2)
C2	**H2A**	0.97	**Co2**	**O2W**	2.068	**C2**	**N25**	1.454(2)	**O2W**	**H22**	0.81(2)
C2	**H2B**	0.97	**Co2**	**O3W**	2.101	**C11**	**N12**	1.357(2)	**O3W**	**H31**	0.78(3)
C2	**C3**	1.528(2)	**Co2**	**O4**	2.09	**C11**	**C16**	1.385(2)	**O3W**	**H32**	0.84(2)
C2	**N25**	1.454(2)	**Co2**	**O2W**	2.068	**C11**	**C21**	1.469(2)	**O1W**	**H11**	0.81(2)
C11	**N12**	1.357(2)	**Co2**	**O3W**	2.101	**N12**	**C13**	1.330(2)	**O1W**	**H12**	0.84(2)
C11	**C16**	1.385(2)	**O2W**	**H21**	0.81(2)	**N12**	**Co1**	2.114	**O4W**	**H41**	0.82(3)
C11	**C21**	1.469(2)	**O2W**	**H22**	0.81(2)	**C13**	**H13**	0.929	**O4W**	**H42**	0.84(3)

Table A40: Bond angles (°) for **4.17**.

Atom1	Atom2	Atom3	Angle	Atom1	Atom2	Atom3	Angle	Atom1	Atom2	Atom3	Angle
N12	Co1	N22	77.19	C15	C16	H16	120.6	H2B	C2	N25	109.4
N12	Co1	O1W	90.32	C11	C21	N22	120.0(1)	C3	C2	N25	111.5(1)
N12	Co1	O1W	89.68	C11	C21	N25	132.5(1)	O3	C3	O4	127.6(1)
N12	Co1	N12	180	N22	C21	N25	107.5(1)	O3	C3	C2	119.0(1)
N12	Co1	N22	102.81	Co1	N22	C21	114.32	O4	C3	C2	113.5(1)
N22	Co1	O1W	90.18	Co1	N22	N23	138.33	N12	C11	C16	122.2(1)
N22	Co1	O1W	89.82	C21	N22	N23	107.3(1)	N12	C11	C21	111.1(1)
N22	Co1	N12	102.81	N22	N23	N24	109.5(1)	C16	C11	C21	126.7(1)
N22	Co1	N22	180	N23	N24	N25	107.3(1)	C11	N12	C13	118.4(1)
O1W	Co1	O1W	180	C2	N25	C21	130.9(1)	C11	N12	Co1	117.34
O1W	Co1	N12	89.68	C2	N25	N24	120.2(1)	C13	N12	Co1	124.24
O1W	Co1	N22	89.82	C21	N25	N24	108.5(1)	N12	C13	H13	118.8
O1W	Co1	N12	90.32	O4	Co2	O2W	90.7	N12	C13	C14	122.5(1)
O1W	Co1	N22	90.18	O4	Co2	O3W	91.1	H13	C13	C14	118.8
N12	Co1	N22	77.19	O4	Co2	O4	86.21	C13	C14	H14	120.3
O1	C1	O2	126.5(1)	O4	Co2	O2W	89.67	C13	C14	C15	119.4(1)
O1	C1	C15	116.5(1)	O4	Co2	O3W	175.59	H14	C14	C15	120.2
O2	C1	C15	117.0(1)	O2W	Co2	O3W	93.86	C1	C15	C14	120.4(1)
C3	O4	Co2	130.03	O2W	Co2	O4	89.67	C1	C15	C16	120.8(1)
H2A	C2	H2B	108	O2W	Co2	O2W	179.5	C14	C15	C16	118.8(1)
H2A	C2	C3	109.3	O2W	Co2	O3W	85.79	C11	C16	C15	118.7(1)
H2A	C2	N25	109.3	O3W	Co2	O4	175.59	C11	C16	H16	120.7
H2B	C2	C3	109.3	O3W	Co2	O2W	85.79	C15	C16	H16	120.6
H2B	C2	N25	109.4	O3W	Co2	O3W	91.79	C11	C21	N22	120.0(1)
C3	C2	N25	111.5(1)	O4	Co2	O2W	90.7	C11	C21	N25	132.5(1)
O3	C3	O4	127.6(1)	O4	Co2	O3W	91.1	N22	C21	N25	107.5(1)

O3	C3	C2	119.0(1)	O2W	Co2	O3W	93.86	C21	N22	N23	107.3(1)
O4	C3	C2	113.5(1)	Co2	O2W	H21	118	C21	N22	Co1	114.32
N12	C11	C16	122.2(1)	Co2	O2W	H22	104	N23	N22	Co1	138.33
N12	C11	C21	111.1(1)	H21	O2W	H22	107(2)	N22	N23	N24	109.5(1)
C16	C11	C21	126.7(1)	Co2	O3W	H31	123	N23	N24	N25	107.3(1)
Co1	N12	C11	117.34	Co2	O3W	H32	116	C2	N25	C21	130.9(1)
Co1	N12	C13	124.24	H31	O3W	H32	111(2)	C2	N25	N24	120.2(1)
C11	N12	C13	118.4(1)	Co1	O1W	H11	114	C21	N25	N24	108.5(1)
N12	C13	H13	118.8	Co1	O1W	H12	111	Co2	O2W	H21	118
N12	C13	C14	122.5(1)	H11	O1W	H12	110(2)	Co2	O2W	H22	104
H13	C13	C14	118.8	O1	C1	O2	126.5(1)	H21	O2W	H22	107(2)
C13	C14	H14	120.3	O1	C1	C15	116.5(1)	Co2	O3W	H31	123
C13	C14	C15	119.4(1)	O2	C1	C15	117.0(1)	Co2	O3W	H32	116
H14	C14	C15	120.2	Co2	O4	C3	130.03	H31	O3W	H32	111(2)
C1	C15	C14	120.4(1)	H2A	C2	H2B	108	Co1	O1W	H11	114
C1	C15	C16	120.8(1)	H2A	C2	C3	109.3	Co1	O1W	H12	111
C14	C15	C16	118.8(1)	H2A	C2	N25	109.3	H11	O1W	H12	110(2)
C11	C16	C15	118.7(1)	H2B	C2	C3	109.3	N12	Co1	N22	77.19
C11	C16	H16	120.7	H41	O4W	H42	102(2)				

Table A41: Atomic coordinates for **4.18**.

	x	*y*	*z*		*x*	*y*	*z*
Zn1	0.25	-0.25	0.5	**C1**	-0.10598(7)	0.3666(2)	1.12041(14)
O1W	0.27855(5)	-0.13808(16)	0.65299(11)	**O3**	-0.10172(5)	0.01151(16)	0.81023(10)
H11	0.3047(11)	-0.090(3)	0.652(2)	**O4**	-0.01577(4)	0.05182(14)	0.85129(9)
H12	0.2831(11)	-0.205(4)	0.698(2)	**C2**	-0.05087(6)	-0.16262(19)	0.93203(12)
O1	0.12800(5)	0.49090(15)	0.35314(11)	**H2A**	-0.0266	-0.239	0.9098
O2	0.05996(6)	0.35227(19)	0.38838(17)	**H2B**	-0.0363	-0.1248	1.0005
C1	0.10598(7)	0.3666(2)	0.37959(14)	**C3**	-0.05750(6)	-0.02023(18)	0.85710(11)
O3	0.10172(5)	0.01151(16)	0.68977(10)	**C11**	-0.15570(6)	-0.04276(17)	1.02245(11)
O4	0.01577(4)	0.05182(14)	0.64871(9)	**N12**	-0.20552(5)	-0.04171(15)	1.04157(10)
C2	0.05087(6)	-0.16262(19)	0.56797(12)	**C13**	-0.22271(6)	0.08697(19)	1.08655(14)
H2A	0.0266	-0.239	0.5902	**H13**	-0.2568	0.0875	1.1005
H2B	0.0363	-0.1248	0.4995	**C14**	-0.19157(7)	0.22034(19)	1.11338(15)
C3	0.05750(6)	-0.02023(18)	0.64290(11)	**H14**	-0.2048	0.3091	1.1441
C11	0.15570(6)	-0.04276(17)	0.47755(11)	**C15**	-0.14077(6)	0.22012(18)	1.09407(13)
N12	0.20552(5)	-0.04171(15)	0.45843(10)	**C16**	-0.12203(6)	0.08508(18)	1.04904(12)
C13	0.22271(6)	0.08697(19)	0.41345(14)	**H16**	-0.0876	0.0805	1.037
H13	0.2568	0.0875	0.3995	**C21**	-0.14354(5)	-0.19190(17)	0.97021(11)
C14	0.19157(7)	0.22034(19)	0.38662(15)	**N22**	-0.17929(5)	-0.30531(16)	0.94785(10)
H14	0.2048	0.3091	0.3559	**N23**	-0.15722(6)	-0.42653(17)	0.90055(12)
C15	0.14077(6)	0.22012(18)	0.40593(13)	**N24**	-0.10955(5)	-0.38916(16)	0.89319(11)
C16	0.12203(6)	0.08508(18)	0.45096(12)	**N25**	-0.10017(5)	-0.24292(14)	0.93717(11)
H16	0.0876	0.0805	0.463	**O2W**	-0.07656(5)	0.23723(15)	0.68140(10)
C21	0.14354(5)	-0.19190(17)	0.52979(11)	**H21**	-0.0913(8)	0.325(3)	0.6755(16)
N22	0.17929(5)	-0.30531(16)	0.55215(10)	**H22**	-0.0900(9)	0.178(3)	0.7181(19)
N23	0.15722(6)	-0.42653(17)	0.59945(12)	**O3W**	-0.01080(6)	0.41124(18)	0.86126(14)
N24	0.10955(5)	-0.38916(16)	0.60681(11)	**H31**	-0.0385(12)	0.443(3)	0.872(2)
N25	0.10017(5)	-0.24292(14)	0.56283(11)	**H32**	0.0114(12)	0.493(4)	0.866(2)
Zn2	0	0.23402(3)	0.75	**O1W**	0.22145(5)	-0.36192(16)	0.34701(11)
O2W	0.07656(5)	0.23723(15)	0.81860(10)	**H11**	0.1953(11)	-0.410(3)	0.348(2)
H21	0.0913(8)	0.325(3)	0.8245(16)	**H12**	0.2169(11)	-0.295(4)	0.302(2)
H22	0.0900(9)	0.178(3)	0.7819(19)	**Zn1**	-0.25	-0.25	1
O3W	0.01080(6)	0.41124(18)	0.63874(14)	**N12**	0.29448(5)	-0.45829(15)	0.54157(10)
H31	0.0385(12)	0.443(3)	0.628(2)	**N22**	0.32071(5)	-0.19469(16)	0.44785(10)
H32	-0.0114(12)	0.493(4)	0.634(2)	**O4W**	0.20517(6)	0.1176(2)	0.70022(13)
O1	-0.12800(5)	0.49090(15)	1.14686(11)	**H41**	0.1772(11)	0.077(3)	0.695(2)
O2	-0.05996(6)	0.35227(19)	1.11162(17)	**H42**	0.1853(19)	0.222(5)	0.677(4)

Table A42: Bond lengths (Å) for **4.18**.

Atom1	Atom2	Length	Atom1	Atom2	Length	Atom1	Atom2	Length	Atom1	Atom2	Length
Zn1	O1W	2.229	**C11**	**C16**	1.387(2)	**Zn2**	**O3W**	2.118	**C13**	**H13**	0.93
Zn1	N12	2.107	**C11**	**C21**	1.472(2)	**O2W**	**H21**	0.82(2)	**C13**	**C14**	1.386(2)
Zn1	N22	2.103	**N12**	**C13**	1.330(2)	**O2W**	**H22**	0.80(3)	**C14**	**H14**	0.93
Zn1	O1W	2.229	**C13**	**H13**	0.93	**O3W**	**H31**	0.80(3)	**C14**	**C15**	1.379(3)
Zn1	N12	2.107	**C13**	**C14**	1.386(2)	**O3W**	**H32**	0.89(3)	**C15**	**C16**	1.389(2)

Zn1	N22	2.103	C14	H14	0.93	O1	C1	1.254(2)	C16	H16	0.931
O1W	H11	0.79(3)	O4W	H42	1.03(4)	O2	C1	1.223(2)	C21	N22	1.324(2)
O1W	H12	0.81(3)	C14	C15	1.379(3)	C1	C15	1.524(2)	C21	N25	1.334(2)
O1	C1	1.254(2)	C15	C16	1.389(2)	O3	C3	1.245(2)	N22	N23	1.354(2)
O2	C1	1.223(2)	C16	H16	0.931	O4	C3	1.250(2)	N22	Zn1	2.103
C1	C15	1.524(2)	C21	N22	1.324(2)	C2	H2A	0.969	N23	N24	1.293(2)
O3	C3	1.245(2)	C21	N25	1.334(2)	C2	H2B	0.97	N24	N25	1.351(2)
O4	C3	1.250(2)	N22	N23	1.354(2)	C2	C3	1.529(2)	O2W	H21	0.82(2)
O4	Zn2	2.092	N23	N24	1.293(2)	C2	N25	1.454(2)	O2W	H22	0.80(3)
C2	H2A	0.969	N24	N25	1.351(2)	C11	N12	1.354(2)	O3W	H31	0.80(3)
C2	H2B	0.97	Zn2	O2W	2.054	C11	C16	1.387(2)	O3W	H32	0.89(3)
C2	C3	1.529(2)	Zn2	O3W	2.118	C11	C21	1.472(2)	O1W	H11	0.79(3)
C2	N25	1.454(2)	Zn2	O4	2.092	N12	C13	1.330(2)	O1W	H12	0.81(3)
C11	N12	1.354(2)	Zn2	O2W	2.054	N12	Zn1	2.107	O4W	H41	0.79(3)

Table A43: Bond angles (°) for **4.18**.

Atom1	Atom2	Atom3	Angle	Atom1	Atom2	Atom3	Angle	Atom1	Atom2	Atom3	Angle
O1W	Zn1	N12	89.05	C14	C15	C16	118.9(1)	H2B	C2	N25	109.3
O1W	Zn1	N22	89.38	C11	C16	C15	118.6(1)	C3	C2	N25	111.7(1)
O1W	Zn1	O1W	180	C11	C16	H16	120.7	O3	C3	O4	127.7(1)
O1W	Zn1	N12	90.95	C15	C16	H16	120.7	O3	C3	C2	119.0(1)
O1W	Zn1	N22	90.62	C11	C21	N22	120.7(1)	O4	C3	C2	113.3(1)
N12	Zn1	N22	78	C11	C21	N25	131.9(1)	N12	C11	C16	122.2(1)
N12	Zn1	O1W	90.95	N22	C21	N25	107.4(1)	N12	C11	C21	111.6(1)
N12	Zn1	N12	180	Zn1	N22	C21	112.9	C16	C11	C21	126.2(1)
N12	Zn1	N22	102	Zn1	N22	N23	139.5	C11	N12	C13	118.7(1)
N22	Zn1	O1W	90.62	C21	N22	N23	107.5(1)	C11	N12	Zn1	116.7
N22	Zn1	N12	102	N22	N23	N24	109.3(1)	C13	N12	Zn1	124.6
N22	Zn1	N22	180	N23	N24	N25	107.3(1)	N12	C13	H13	118.9
O1W	Zn1	N12	89.05	C2	N25	C21	131.3(1)	N12	C13	C14	122.3(2)
O1W	Zn1	N22	89.38	C2	N25	N24	119.8(1)	H13	C13	C14	118.9
N12	Zn1	N22	78	C21	N25	N24	108.5(1)	C13	C14	H14	120.3
Zn1	O1W	H11	112	O4	Zn2	O2W	90.97	C13	C14	C15	119.3(2)
Zn1	O1W	H12	111	O4	Zn2	O3W	90.61	H14	C14	C15	120.3
H11	O1W	H12	109(3)	O4	Zn2	O4	87.23	C1	C15	C14	120.5(1)
O1	C1	O2	126.7(2)	O4	Zn2	O2W	90.1	C1	C15	C16	120.5(1)
O1	C1	C15	116.2(2)	O4	Zn2	O3W	175.32	C14	C15	C16	118.9(1)
O2	C1	C15	117.1(2)	O2W	Zn2	O3W	94.09	C11	C16	C15	118.6(1)
C3	O4	Zn2	129.7	O2W	Zn2	O4	90.1	C11	C16	H16	120.7
H2A	C2	H2B	107.9	O2W	Zn2	O2W	178.51	C15	C16	H16	120.7
H2A	C2	C3	109.3	O2W	Zn2	O3W	84.87	C11	C21	N22	120.7(1)
H2A	C2	N25	109.2	O3W	Zn2	O4	175.32	C11	C21	N25	131.9(1)
H2B	C2	C3	109.3	O3W	Zn2	O2W	84.87	N22	C21	N25	107.4(1)
H2B	C2	N25	109.3	O3W	Zn2	O3W	91.85	C21	N22	N23	107.5(1)
C3	C2	N25	111.7(1)	O4	Zn2	O2W	90.97	C21	N22	Zn1	112.9
O3	C3	O4	127.7(1)	O4	Zn2	O3W	90.61	N23	N22	Zn1	139.5
O3	C3	C2	119.0(1)	O2W	Zn2	O3W	94.09	N22	N23	N24	109.3(1)
O4	C3	C2	113.3(1)	Zn2	O2W	H21	117	N23	N24	N25	107.3(1)
N12	C11	C16	122.2(1)	Zn2	O2W	H22	102	C2	N25	C21	131.3(1)
N12	C11	C21	111.6(1)	H21	O2W	H22	111(2)	C2	N25	N24	119.8(1)
C16	C11	C21	126.2(1)	Zn2	O3W	H31	125	C21	N25	N24	108.5(1)
Zn1	N12	C11	116.7	Zn2	O3W	H32	115	Zn2	O2W	H21	117
Zn1	N12	C13	124.6	H31	O3W	H32	109(3)	Zn2	O2W	H22	102
C11	N12	C13	118.7(1)	O1	C1	O2	126.7(2)	H21	O2W	H22	111(2)
N12	C13	H13	118.9	O1	C1	C15	116.2(2)	Zn2	O3W	H31	125
N12	C13	C14	122.3(2)	O2	C1	C15	117.1(2)	Zn2	O3W	H32	115
H13	C13	C14	118.9	Zn2	O4	C3	129.7	H31	O3W	H32	109(3)
C13	C14	H14	120.3	H2A	C2	H2B	107.9	Zn1	O1W	H11	112
C13	C14	C15	119.3(2)	H2A	C2	C3	109.3	Zn1	O1W	H12	111
H14	C14	C15	120.3	H2A	C2	N25	109.2	H11	O1W	H12	109(3)
C1	C15	C14	120.5(1)	H2B	C2	C3	109.3	N12	Zn1	N22	78
C1	C15	C16	120.5(1)	H41	O4W	H42	86(3)				

Table A44: Atomic coordinates for **4.20**.

	x	*y*	*z*		*x*	*y*	*z*
Co1	0.30251(7)	0.80448(5)	0.70179(4)	**H1WA**	-0.668(8)	0.025(5)	0.325(4)

O1W	0.6011(4)	0.9873(3)	0.7244(2)	**H1WB**	-0.693(8)	-0.013(5)	0.218(4)
H1WA	0.668(8)	0.975(5)	0.675(4)	**O2W**	-0.1457(4)	0.0642(3)	0.3848(3)
H1WB	0.693(8)	1.013(5)	0.782(4)	**H2WA**	-0.199(8)	0.014(5)	0.437(4)
O2W	0.1457(4)	0.9358(3)	0.6152(3)	**H2WB**	-0.016(8)	0.080(5)	0.396(4)
H2WA	0.199(8)	0.986(5)	0.563(4)	**O3W**	-0.2374(5)	0.1284(3)	0.1588(2)
H2WB	0.016(8)	0.920(5)	0.604(4)	**H3WA**	-0.298(7)	0.048(5)	0.133(4)
O3W	0.2374(5)	0.8716(3)	0.8412(2)	**H3WB**	-0.229(6)	0.193(5)	0.102(3)
H3WA	0.298(7)	0.952(5)	0.867(4)	**C11**	-0.2713(5)	0.4964(4)	0.2213(3)
H3WB	0.229(6)	0.807(5)	0.898(3)	**N12**	-0.4264(4)	0.3589(3)	0.2164(2)
C11	0.2713(5)	0.5036(4)	0.7787(3)	**C13**	-0.6343(6)	0.3378(4)	0.1608(3)
N12	0.4264(4)	0.6411(3)	0.7836(2)	**H13**	-0.7447	0.2436	0.1562
C13	0.6343(6)	0.6622(4)	0.8392(3)	**C14**	-0.6917(6)	0.4504(4)	0.1100(3)
H13	0.7447	0.7564	0.8438	**H14**	-0.8379	0.4311	0.0716
C14	0.6917(6)	0.5496(4)	0.8900(3)	**C15**	-0.5314(6)	0.5913(4)	0.1163(3)
H14	0.8379	0.5689	0.9284	**C16**	-0.3162(6)	0.6146(4)	0.1739(3)
C15	0.5314(6)	0.4087(4)	0.8837(3)	**H16**	-0.2038	0.7083	0.1805
C16	0.3162(6)	0.3854(4)	0.8261(3)	**C21**	-0.0470(5)	0.5117(4)	0.2832(3)
H16	0.2038	0.2917	0.8195	**N22**	-0.0046(4)	0.3943(3)	0.3266(2)
C21	0.0470(5)	0.4883(4)	0.7168(3)	**N23**	0.2094(5)	0.4444(3)	0.3771(2)
N22	0.0046(4)	0.6057(3)	0.6734(2)	**N24**	0.2841(4)	0.5870(3)	0.3609(2)
N23	-0.2094(5)	0.5556(3)	0.6229(2)	**N25**	0.1309(5)	0.6358(3)	0.3039(2)
N24	-0.2841(4)	0.4130(3)	0.6391(2)	**O1**	-0.7705(4)	0.6937(3)	0.0043(2)
N25	-0.1309(5)	0.3642(3)	0.6961(2)	**O2A**	-0.4129(7)	0.8418(5)	0.0692(3)
O1	0.7705(4)	0.3063(3)	0.9957(2)	**O3**	0.3643(4)	0.7255(3)	0.55952(19)
O2A	0.4129(7)	0.1582(5)	0.9308(3)	**O4**	0.6920(4)	0.8925(3)	0.5423(2)
O3	-0.3643(4)	0.2745(3)	0.44048(19)	**C1**	-0.5816(7)	0.7200(4)	0.0621(3)
O4	-0.6920(4)	0.1075(3)	0.4577(2)	**C2**	0.5109(5)	0.6891(4)	0.4086(3)
C1	0.5816(7)	0.2800(4)	0.9379(3)	**H2A**	0.6102	0.6321	0.4236
C2	-0.5109(5)	0.3109(4)	0.5914(3)	**H2B**	0.5633	0.759	0.3571
H2A	-0.6102	0.3679	0.5764	**C3**	0.5211(5)	0.7761(4)	0.5123(3)
H2B	-0.5633	0.241	0.6429	**O4W**	0.9209(6)	1.0844(5)	0.9111(3)
C3	-0.5211(5)	0.2239(4)	0.4877(3)	**H4WA**	1.005(11)	1.067(7)	0.945(5)
Co1	-0.30251(7)	0.19552(5)	0.29821(4)	**H4WB**	0.887(10)	1.150(7)	0.942(5)
O1W	-0.6011(4)	0.0127(3)	0.2756(2)	**O2B**	0.491(3)	0.157(2)	0.8830(16)

Table A45: Bond lengths (Å) for **4.20**.

Atom1	Atom2	Length	Atom1	Atom2	Length	Atom1	Atom2	Length	Atom1	Atom2	Length
Co1	**O1W**	2.082(2)	**C14**	**C15**	1.379(5)	**Co1**	**O2W**	2.071(3)	**C15**	**C16**	1.382(5)
Co1	**O2W**	2.071(3)	**C15**	**C16**	1.382(5)	**Co1**	**O3W**	2.036(3)	**C15**	**C1**	1.517(6)
Co1	**O3W**	2.036(3)	**C15**	**C1**	1.517(6)	**Co1**	**N12**	2.176(3)	**C16**	**H16**	0.93
Co1	**N12**	2.176(3)	**C16**	**H16**	0.93	**Co1**	**N22**	2.158(2)	**C21**	**N22**	1.344(5)
Co1	**N22**	2.158(2)	**C21**	**N22**	1.344(5)	**O1W**	**H1WA**	0.86(6)	**C21**	**N25**	1.318(4)
Co1	**O3**	2.102(3)	**C21**	**N25**	1.318(4)	**O1W**	**H1WB**	0.82(4)	**N22**	**N23**	1.322(4)
O1W	**H1WA**	0.86(6)	**N22**	**N23**	1.322(4)	**O2W**	**H2WA**	0.88(5)	**N23**	**N24**	1.314(4)
O1W	**H1WB**	0.82(4)	**N23**	**N24**	1.314(4)	**O2W**	**H2WB**	0.79(5)	**N24**	**N25**	1.331(4)
O2W	**H2WA**	0.88(5)	**N24**	**N25**	1.331(4)	**O3W**	**H3WA**	0.76(4)	**N24**	**C2**	1.457(3)
O2W	**H2WB**	0.79(5)	**N24**	**C2**	1.457(3)	**O3W**	**H3WB**	0.96(4)	**O1**	**C1**	1.236(5)
O3W	**H3WA**	0.76(4)	**O1**	**C1**	1.236(5)	**C11**	**N12**	1.344(4)	**O2A**	**C1**	1.283(5)
O3W	**H3WB**	0.96(4)	**O2A**	**C1**	1.283(5)	**O4W**	**H4WB**	0.84(7)	**O3**	**C3**	1.246(4)
C11	**N12**	1.344(4)	**O3**	**C3**	1.246(4)	**C11**	**C16**	1.378(6)	**O4**	**C3**	1.257(4)
C11	**C16**	1.378(6)	**O3**	**Co1**	2.102(3)	**C11**	**C21**	1.467(5)	**C2**	**H2A**	0.97
C11	**C21**	1.467(5)	**O4**	**C3**	1.257(4)	**N12**	**C13**	1.337(4)	**C2**	**H2B**	0.97
N12	**C13**	1.337(4)	**C2**	**H2A**	0.97	**C13**	**H13**	0.93	**C2**	**C3**	1.516(6)
C13	**H13**	0.93	**C2**	**H2B**	0.97	**C13**	**C14**	1.383(6)	**O4W**	**H4WA**	0.69(7)
C13	**C14**	1.383(6)	**C2**	**C3**	1.516(6)	**C14**	**H14**	0.93			
C14	**H14**	0.93	**Co1**	**O1W**	2.082(2)	**C14**	**C15**	1.379(5)			

Table A46: Bond angles (°) for **4.20**.

Atom1	Atom2	Atom3	Angle	Atom1	Atom2	Atom3	Angle	Atom1	Atom2	Atom3	Angle
O1W	Co1	O2W	87.5(1)	N22	C21	N25	112.6(3)	Co1	O3W	H3WB	118(2)
O1W	Co1	O3W	91.5(1)	Co1	N22	C21	111.8(2)	H3WA	O3W	H3WB	108(4)
O1W	Co1	N12	100.0(1)	Co1	N22	N23	141.5(2)	N12	C11	C16	123.7(3)
O1W	Co1	N22	175.9(1)	C21	N22	N23	106.6(3)	N12	C11	C21	114.2(3)
O1W	Co1	O3	90.4(1)	N22	N23	N24	104.9(3)	C16	C11	C21	122.1(3)
O2W	Co1	O3W	91.1(1)	N23	N24	N25	114.8(3)	Co1	N12	C11	115.0(2)
O2W	Co1	N12	172.3(1)	N23	N24	C2	123.5(3)	Co1	N12	C13	128.0(2)

O2W	Co1	N22	94.8(1)	N25	N24	C2	121.4(3)	C11	N12	C13	117.0(3)
O2W	Co1	O3	90.6(1)	C21	N25	N24	101.1(3)	N12	C13	H13	118.7
O3W	Co1	N12	90.6(1)	C3	O3	Co1	131.9(2)	N12	C13	C14	122.6(3)
O3W	Co1	N22	91.8(1)	C15	C1	O1	118.0(3)	H13	C13	C14	118.7
O3W	Co1	O3	177.5(1)	C15	C1	O2A	115.8(4)	C13	C14	H14	120.1
N12	Co1	N22	77.7(1)	O1	C1	O2A	125.5(4)	C13	C14	C15	119.8(4)
N12	Co1	O3	87.5(1)	N24	C2	H2A	109.2	H14	C14	C15	120.1
N22	Co1	O3	86.2(1)	N24	C2	H2B	109.2	C14	C15	C16	118.1(4)
Co1	O1W	H1WA	107(3)	N24	C2	C3	111.9(3)	C14	C15	C1	122.8(3)
Co1	O1W	H1WB	123(4)	H2A	C2	H2B	107.9	C16	C15	C1	119.1(3)
H1WA	O1W	H1WB	109(5)	H2A	C2	C3	109.3	C11	C16	C15	118.7(4)
Co1	O2W	H2WA	122(3)	H2B	C2	C3	109.3	C11	C16	H16	120.7
Co1	O2W	H2WB	124(4)	O3	C3	O4	126.8(3)	C15	C16	H16	120.6
H2WA	O2W	H2WB	108(5)	O3	C3	C2	117.9(3)	C11	C21	N22	121.3(3)
Co1	O3W	H3WA	120(4)	O4	C3	C2	115.3(3)	C11	C21	N25	126.1(3)
Co1	O3W	H3WB	118(2)	O3	Co1	O1W	90.4(1)	N22	C21	N25	112.6(3)
H3WA	O3W	H3WB	108(4)	O3	Co1	O2W	90.6(1)	Co1	N22	C21	111.8(2)
N12	C11	C16	123.7(3)	O3	Co1	O3W	177.5(1)	Co1	N22	N23	141.5(2)
N12	C11	C21	114.2(3)	O3	Co1	N12	87.5(1)	C21	N22	N23	106.6(3)
C16	C11	C21	122.1(3)	O3	Co1	N22	86.2(1)	N22	N23	N24	104.9(3)
Co1	N12	C11	115.0(2)	O1W	Co1	O2W	87.5(1)	N23	N24	N25	114.8(3)
Co1	N12	C13	128.0(2)	O1W	Co1	O3W	91.5(1)	N23	N24	C2	123.5(3)
C11	N12	C13	117.0(3)	O1W	Co1	N12	100.0(1)	N25	N24	C2	121.4(3)
N12	C13	H13	118.7	O1W	Co1	N22	175.9(1)	C21	N25	N24	101.1(3)
N12	C13	C14	122.6(3)	O2W	Co1	O3W	91.1(1)	Co1	O3	C3	131.9(2)
H13	C13	C14	118.7	O2W	Co1	N12	172.3(1)	C15	C1	O1	118.0(3)
C13	C14	H14	120.1	O2W	Co1	N22	94.8(1)	C15	C1	O2A	115.8(4)
C13	C14	C15	119.8(4)	O3W	Co1	N12	90.6(1)	O1	C1	O2A	125.5(4)
H14	C14	C15	120.1	O3W	Co1	N22	91.8(1)	N24	C2	H2A	109.2
C14	C15	C16	118.1(4)	N12	Co1	N22	77.7(1)	N24	C2	H2B	109.2
C14	C15	C1	122.8(3)	Co1	O1W	H1WA	107(3)	N24	C2	C3	111.9(3)
C16	C15	C1	119.1(3)	Co1	O1W	H1WB	123(4)	H2A	C2	H2B	107.9
C11	C16	C15	118.7(4)	H1WA	O1W	H1WB	109(5)	H2A	C2	C3	109.3
C11	C16	H16	120.7	Co1	O2W	H2WA	122(3)	H2B	C2	C3	109.3
C15	C16	H16	120.6	Co1	O2W	H2WB	124(4)	O3	C3	O4	126.8(3)
C11	C21	N22	121.3(3)	H2WA	O2W	H2WB	108(5)	O3	C3	C2	117.9(3)
C11	C21	N25	126.1(3)	Co1	O3W	H3WA	120(4)	O4	C3	C2	115.3(3)
H4WA	O4W	H4WB	111(7)								

Table A47: Atomic coordinates for **4.21**.

	x	*y*	*z*		*x*	*y*	*z*
Zn1	1.00103(3)	-0.31190(2)	0.703999(15)	**H1WA**	1.193(5)	0.513(3)	0.220(2)
O1W	0.8773(3)	-0.48588(17)	0.72469(15)	**H1WB**	1.196(5)	0.478(3)	0.328(2)
H1WA	0.807(5)	-0.513(3)	0.780(2)	**O2W**	0.8609(2)	0.37346(17)	0.15747(11)
H1WB	0.804(5)	-0.478(3)	0.672(2)	**H2WA**	0.926(5)	0.319(3)	0.107(2)
O2W	1.1391(2)	-0.37346(17)	0.84253(11)	**H2WB**	0.848(5)	0.455(3)	0.134(2)
H2WA	1.074(5)	-0.319(3)	0.893(2)	**O3W**	0.7066(3)	0.43851(19)	0.38228(13)
H2WB	1.152(5)	-0.455(3)	0.866(2)	**H3WA**	0.616(5)	0.408(4)	0.402(2)
O3W	1.2934(3)	-0.43851(19)	0.61772(13)	**H3WB**	0.716(6)	0.488(4)	0.434(3)
H3WA	1.384(5)	-0.408(4)	0.598(2)	**C11**	1.2647(3)	0.00585(18)	0.22177(13)
H3WB	1.284(6)	-0.488(4)	0.566(3)	**N12**	1.2845(2)	0.14335(15)	0.21523(11)
C11	0.7353(3)	-0.00585(18)	0.77823(13)	**C13**	1.4726(3)	0.16331(19)	0.15995(14)
N12	0.7155(2)	-0.14335(15)	0.78477(11)	**H13**	1.4897	0.2571	0.1551
C13	0.5274(3)	-0.16331(19)	0.84005(14)	**C14**	1.6434(3)	0.05001(19)	0.10945(14)
H13	0.5103	-0.2571	0.8449	**H14**	1.7714	0.0682	0.0712
C14	0.3566(3)	-0.05001(19)	0.89055(14)	**C15**	1.6203(3)	-0.09059(19)	0.11687(13)
H14	0.2286	-0.0682	0.9288	**C16**	1.4271(3)	-0.11261(18)	0.17465(14)
C15	0.3797(3)	0.09059(19)	0.88313(13)	**H16**	1.4071	-0.2059	0.1816
C16	0.5729(3)	0.11261(18)	0.82535(14)	**C21**	1.0566(3)	-0.00952(18)	0.28330(13)
H16	0.5929	0.2059	0.8184	**N22**	1.0036(3)	-0.13433(17)	0.30359(12)
C21	0.9434(3)	0.00952(18)	0.71670(13)	**N23**	0.8031(2)	-0.08743(16)	0.36122(11)
N22	0.9964(3)	0.13433(17)	0.69641(12)	**N24**	0.7334(2)	0.05507(17)	0.37775(12)
N23	1.1969(2)	0.08743(16)	0.63878(11)	**N25**	0.8953(2)	0.10661(16)	0.32737(11)
N24	1.2666(2)	-0.05507(17)	0.62225(12)	**O1**	1.9638(3)	-0.19470(16)	0.00660(12)
N25	1.1047(2)	-0.10661(16)	0.67263(11)	**O2A**	1.7467(5)	-0.3395(3)	0.0700(2)
O1	0.0362(3)	0.19470(16)	0.99340(12)	**C1**	1.7976(3)	-0.2199(2)	0.06284(15)
O2A	0.2533(5)	0.3395(3)	0.9300(2)	**O3**	0.8669(2)	-0.23007(15)	0.55779(10)
C1	0.2024(3)	0.2199(2)	0.93716(15)	**O4**	0.6988(2)	-0.39284(14)	0.54203(10)

O3	1.1331(2)	0.23007(15)	0.44221(10)	**C2**	0.6795(3)	-0.1903(2)	0.40841(15)
O4	1.3012(2)	0.39284(14)	0.45797(10)	**H2A**	0.5235	-0.1341	0.4244
C2	1.3205(3)	0.1903(2)	0.59159(15)	**H2B**	0.6968	-0.2593	0.3563
H2A	1.4765	0.1341	0.5756	**C3**	0.7577(3)	-0.2788(2)	0.51209(13)
H2B	1.3032	0.2593	0.6437	**O4W**	0.6638(4)	-0.5863(3)	0.91126(17)
C3	1.2423(3)	0.2788(2)	0.48791(13)	**H4WA**	0.759(6)	-0.647(4)	0.938(2)
Zn1	0.99897(3)	0.31190(2)	0.296001(15)	**H4WB**	0.557(7)	-0.599(5)	0.930(3)
O1W	1.1227(3)	0.48588(17)	0.27531(15)	**O2B**	0.1818(19)	0.3410(12)	0.8933(10)

Table A48: Bond lengths (Å) for **4.21**.

Atom1	Atom2	Length	Atom1	Atom2	Length	Atom1	Atom2	Length	Atom1	Atom2	Length
Zn1	**O1W**	2.038(2)	**C14**	**H14**	0.93	**C2**	**C3**	1.527(2)	**C13**	**C14**	1.389(2)
Zn1	**O2W**	2.048(1)	**C14**	**C15**	1.386(3)	**Zn1**	**O1W**	2.038(2)	**C14**	**H14**	0.93
Zn1	**O3W**	2.071(2)	**C15**	**C16**	1.384(3)	**Zn1**	**O2W**	2.048(1)	**C14**	**C15**	1.386(3)
Zn1	**N12**	2.193(1)	**C15**	**C1**	1.518(2)	**Zn1**	**O3W**	2.071(2)	**C15**	**C16**	1.384(3)
Zn1	**N25**	2.233(2)	**C16**	**H16**	0.93	**Zn1**	**N12**	2.193(1)	**C15**	**C1**	1.518(2)
Zn1	**O3**	2.133(1)	**C21**	**N22**	1.322(3)	**Zn1**	**N25**	2.233(2)	**C16**	**H16**	0.93
O1W	**H1WA**	0.81(3)	**C21**	**N25**	1.346(2)	**O1W**	**H1WA**	0.81(3)	**C21**	**N22**	1.322(3)
O1W	**H1WB**	0.88(3)	**N22**	**N23**	1.325(2)	**O1W**	**H1WB**	0.88(3)	**C21**	**N25**	1.346(2)
O2W	**H2WA**	0.84(3)	**N23**	**N24**	1.316(2)	**O2W**	**H2WA**	0.84(3)	**N22**	**N23**	1.325(2)
O2W	**H2WB**	0.77(3)	**N23**	**C2**	1.456(3)	**O2W**	**H2WB**	0.77(3)	**N23**	**N24**	1.316(2)
O3W	**H3WA**	0.73(4)	**N24**	**N25**	1.317(2)	**O3W**	**H3WA**	0.73(4)	**N23**	**C2**	1.456(3)
O3W	**H3WB**	0.89(4)	**O1**	**C1**	1.242(3)	**O3W**	**H3WB**	0.89(4)	**N24**	**N25**	1.317(2)
C11	**N12**	1.349(2)	**O2A**	**C1**	1.277(4)	**C11**	**N12**	1.349(2)	**O1**	**C1**	1.242(3)
C11	**C16**	1.378(2)	**O3**	**C3**	1.238(3)	**O4W**	**H4WB**	0.73(5)	**O2A**	**C1**	1.277(4)
C11	**C21**	1.460(3)	**O3**	**Zn1**	2.133(1)	**C11**	**C16**	1.378(2)	**O3**	**C3**	1.238(3)
N12	**C13**	1.338(2)	**O4**	**C3**	1.252(3)	**C11**	**C21**	1.460(3)	**O4**	**C3**	1.252(3)
C13	**H13**	0.93	**C2**	**H2A**	0.97	**N12**	**C13**	1.338(2)	**C2**	**H2A**	0.97
C13	**C14**	1.389(2)	**C2**	**H2B**	0.969	**C13**	**H13**	0.93	**C2**	**H2B**	0.969
C2	**C3**	1.527(2)	**O4W**	**H4WA**	0.78(3)						

Table A49: Bond angles (°) for **4.21**.

Atom1	Atom2	Atom3	Angle	Atom1	Atom2	Atom3	Angle	Atom1	Atom2	Atom3	Angle
O1W	Zn1	O2W	94.88(7)	N22	C21	N25	112.3(2)	Zn1	O3W	H3WB	118(2)
O1W	Zn1	O3W	90.46(7)	C21	N22	N23	101.2(2)	H3WA	O3W	H3WB	108(4)
O1W	Zn1	N12	99.92(6)	N22	N23	N24	114.9(1)	N12	C11	C16	123.3(2)
O1W	Zn1	N25	173.73(6)	N22	N23	C2	121.5(1)	N12	C11	C21	115.0(2)
O1W	Zn1	O3	90.37(6)	N24	N23	C2	123.5(1)	C16	C11	C21	121.7(2)
O2W	Zn1	O3W	90.01(6)	N23	N24	N25	105.0(1)	Zn1	N12	C11	115.7(1)
O2W	Zn1	N12	91.07(5)	Zn1	N25	C21	110.7(1)	Zn1	N12	C13	127.0(1)
O2W	Zn1	N25	90.43(5)	Zn1	N25	N24	142.5(1)	C11	N12	C13	117.4(1)
O2W	Zn1	O3	174.74(5)	C21	N25	N24	106.7(1)	N12	C13	H13	118.6
O3W	Zn1	N12	169.43(6)	C15	C1	O1	117.7(2)	N12	C13	C14	122.9(2)
O3W	Zn1	N25	92.86(6)	C15	C1	O2A	115.4(2)	H13	C13	C14	118.6
O3W	Zn1	O3	90.28(6)	O1	C1	O2A	126.4(2)	C13	C14	H14	120.5
N12	Zn1	N25	76.62(5)	C3	O3	Zn1	130.5(1)	C13	C14	C15	119.0(2)
N12	Zn1	O3	87.69(5)	N23	C2	H2A	109.2	H14	C14	C15	120.5
N25	Zn1	O3	84.30(5)	N23	C2	H2B	109.2	C14	C15	C16	118.5(2)
Zn1	O1W	H1WA	126(2)	N23	C2	C3	111.9(2)	C14	C15	C1	122.4(2)
Zn1	O1W	H1WB	109(2)	H2A	C2	H2B	108	C16	C15	C1	119.1(2)
H1WA	O1W	H1WB	107(3)	H2A	C2	C3	109.2	C11	C16	C15	118.9(2)
Zn1	O2W	H2WA	115(2)	H2B	C2	C3	109.2	C11	C16	H16	120.5
Zn1	O2W	H2WB	114(2)	O3	C3	O4	127.4(2)	C15	C16	H16	120.6
H2WA	O2W	H2WB	107(3)	O3	C3	C2	117.6(2)	C11	C21	N22	125.7(2)
Zn1	O3W	H3WA	120(3)	O4	C3	C2	114.9(2)	C11	C21	N25	122.0(2)
Zn1	O3W	H3WB	118(2)	O3	Zn1	O1W	90.37(6)	N22	C21	N25	112.3(2)
H3WA	O3W	H3WB	108(4)	O3	Zn1	O2W	174.74(5)	C21	N22	N23	101.2(2)
N12	C11	C16	123.3(2)	O3	Zn1	O3W	90.28(6)	N22	N23	N24	114.9(1)
N12	C11	C21	115.0(2)	O3	Zn1	N12	87.69(5)	N22	N23	C2	121.5(1)
C16	C11	C21	121.7(2)	O3	Zn1	N25	84.30(5)	N24	N23	C2	123.5(1)
Zn1	N12	C11	115.7(1)	O1W	Zn1	O2W	94.88(7)	N23	N24	N25	105.0(1)
Zn1	N12	C13	127.0(1)	O1W	Zn1	O3W	90.46(7)	Zn1	N25	C21	110.7(1)
C11	N12	C13	117.4(1)	O1W	Zn1	N12	99.92(6)	Zn1	N25	N24	142.5(1)
N12	C13	H13	118.6	O1W	Zn1	N25	173.73(6)	C21	N25	N24	106.7(1)
N12	C13	C14	122.9(2)	O2W	Zn1	O3W	90.01(6)	C15	C1	O1	117.7(2)
H13	C13	C14	118.6	O2W	Zn1	N12	91.07(5)	C15	C1	O2A	115.4(2)

C13	C14	H14	120.5	O2W	Zn1	N25	90.43(5)	O1	C1	O2A	126.4(2)
C13	C14	C15	119.0(2)	O3W	Zn1	N12	169.43(6)	Zn1	O3	C3	130.5(1)
H14	C14	C15	120.5	O3W	Zn1	N25	92.86(6)	N23	C2	H2A	109.2
C14	C15	C16	118.5(2)	N12	Zn1	N25	76.62(5)	N23	C2	H2B	109.2
C14	C15	C1	122.4(2)	Zn1	O1W	H1WA	126(2)	N23	C2	C3	111.9(2)
C16	C15	C1	119.1(2)	Zn1	O1W	H1WB	109(2)	H2A	C2	H2B	108
C11	C16	C15	118.9(2)	H1WA	O1W	H1WB	107(3)	H2A	C2	C3	109.2
C11	C16	H16	120.5	Zn1	O2W	H2WA	115(2)	H2B	C2	C3	109.2
C15	C16	H16	120.6	Zn1	O2W	H2WB	114(2)	O3	C3	O4	127.4(2)
C11	C21	N22	125.7(2)	H2WA	O2W	H2WB	107(3)	O3	C3	C2	117.6(2)
C11	C21	N25	122.0(2)	Zn1	O3W	H3WA	120(3)	O4	C3	C2	114.9(2)
H4WA	O4W	H4WB	112(4)								

Table A50: Atomic coordinates for **4.22**.

	x	*y*	*z*		*x*	*y*	*z*
Mn1	0.11467(4)	0.09071(3)	0.33360(3)	**N12**	0.1598(2)	0.34526(15)	0.35196(15)
O1W	-0.1029(2)	0.0493(2)	0.12424(16)	**C13**	0.0787(3)	0.40636(19)	0.24514(18)
H11	-0.206(5)	0.091(3)	0.113(3)	**H13**	0.0233	0.3449	0.151
H12	-0.143(5)	-0.041(4)	0.071(4)	**C14**	0.0732(3)	0.55708(19)	0.26804(18)
O2W	0.3749(2)	0.06798(18)	0.24930(19)	**H14**	0.0157	0.5955	0.1908
H21	0.425(4)	0.114(3)	0.202(3)	**C15**	0.1547(2)	0.64941(17)	0.40794(17)
H22	0.451(5)	0.012(4)	0.276(3)	**C16**	0.2448(2)	0.58879(17)	0.52008(18)
O1	0.1375(2)	0.86896(14)	0.33641(15)	**H16**	0.3035	0.6483	0.6146
O2	0.13193(19)	0.87885(14)	0.56563(14)	**C21**	0.3353(2)	0.36225(17)	0.59694(17)
O3	0.2903(2)	0.2586(2)	0.97601(18)	**N22**	0.3229(2)	0.21374(15)	0.56298(15)
O4	0.5743(2)	0.20756(17)	1.11503(15)	**N23**	0.4217(2)	0.18118(16)	0.68231(16)
C1	0.1409(2)	0.81323(18)	0.44015(19)	**N24**	0.4888(2)	0.30811(16)	0.78137(15)
C2	0.6058(3)	0.3138(2)	0.92887(18)	**N25**	0.4379(2)	0.42532(16)	0.73493(16)
H2A	0.6628	0.4149	0.9812	**Mn1**	0.11467(4)	1.09071(3)	0.33360(3)
H2B	0.7175	0.2555	0.9239	**Mn1**	-0.11467(4)	0.90929(3)	0.66640(3)
C3	0.4743(3)	0.2549(2)	1.0131(2)	**O1**	0.1375(2)	-0.13104(14)	0.33641(15)
C11	0.2445(2)	0.43716(17)	0.48686(17)	**O2**	-0.13193(19)	0.12115(14)	0.43437(14)

Table A51: Bond lengths (Å) for **4.22**.

Atom1	Atom2	Length	Atom1	Atom2	Length	Atom1	Atom2	Length	Atom1	Atom2	Length
Mn1	**O1W**	2.143(1)	**O2W**	**H22**	0.81(4)	**C2**	**H2B**	0.97	**C14**	**H14**	0.93
Mn1	**O2W**	2.147(2)	**O1**	**C1**	1.255(3)	**C2**	**C3**	1.537(3)	**C14**	**C15**	1.385(2)
Mn1	**N12**	2.362(2)	**O1**	**Mn1**	2.114(1)	**C2**	**N24**	1.454(2)	**C15**	**C16**	1.390(2)
Mn1	**N22**	2.312(1)	**O2**	**C1**	1.251(2)	**C11**	**N12**	1.351(2)	**C16**	**H16**	0.93
Mn1	**O1**	2.114(1)	**O2**	**Mn1**	2.162(2)	**C11**	**C16**	1.385(2)	**C21**	**N22**	1.350(2)
Mn1	**O2**	2.162(2)	**O3**	**C3**	1.226(2)	**C11**	**C21**	1.465(2)	**C21**	**N25**	1.325(2)
O1W	**H11**	0.82(3)	**O4**	**C3**	1.258(3)	**N12**	**C13**	1.337(2)	**N22**	**N23**	1.315(2)
O1W	**H12**	0.87(3)	**C1**	**C15**	1.512(2)	**C13**	**H13**	0.93	**N23**	**N24**	1.313(2)
O2W	**H21**	0.83(3)	**C2**	**H2A**	0.97	**C13**	**C14**	1.387(3)	**N24**	**N25**	1.330(2)

Table A52: Bond angles (°) for **4.22**.

Atom1	Atom2	Atom3	Angle	Atom1	Atom2	Atom3	Angle	Atom1	Atom2	Atom3	Angle
O1W	Mn1	O2W	95.38(6)	C1	O2	Mn1	133.3(1)	H13	C13	C14	118.5
O1W	Mn1	N12	90.99(6)	O1	C1	O2	126.7(2)	C13	C14	H14	120.6
O1W	Mn1	N22	160.95(6)	O1	C1	C15	116.0(1)	C13	C14	C15	118.9(2)
O1W	Mn1	O1	97.88(6)	O2	C1	C15	117.3(1)	H14	C14	C15	120.5
O1W	Mn1	O2	88.74(6)	H2A	C2	H2B	107.9	C1	C15	C14	120.8(1)
O2W	Mn1	N12	88.19(6)	H2A	C2	C3	109.3	C1	C15	C16	120.1(1)
O2W	Mn1	N22	90.16(6)	H2A	C2	N24	109.3	C14	C15	C16	119.0(1)
O2W	Mn1	O1	83.83(6)	H2B	C2	C3	109.3	C11	C16	C15	118.1(1)
O2W	Mn1	O2	175.73(6)	H2B	C2	N24	109.3	C11	C16	H16	121
N12	Mn1	N22	70.94(5)	C3	C2	N24	111.7(2)	C15	C16	H16	120.9
N12	Mn1	O1	168.57(5)	O3	C3	O4	127.7(2)	C11	C21	N22	121.0(1)
N12	Mn1	O2	90.65(5)	O3	C3	C2	118.6(2)	C11	C21	N25	126.8(1)
N22	Mn1	O1	100.83(5)	O4	C3	C2	113.7(2)	N22	C21	N25	112.2(1)
N22	Mn1	O2	85.58(5)	N12	C11	C16	123.6(1)	Mn1	N22	C21	115.2(1)
O1	Mn1	O2	96.71(5)	N12	C11	C21	114.0(1)	Mn1	N22	N23	137.9(1)
Mn1	O1W	H11	122(2)	C16	C11	C21	122.4(1)	C21	N22	N23	106.4(1)
Mn1	O1W	H12	119(2)	Mn1	N12	C11	116.9(1)	N22	N23	N24	105.7(1)

H11	O1W	H12	105(3)	Mn1	N12	C13	124.8(1)	C2	N24	N23	120.7(1)
Mn1	O2W	H21	133(2)	C11	N12	C13	117.3(1)	C2	N24	N25	124.8(1)
Mn1	O2W	H22	117(2)	N12	C13	H13	118.4	N23	N24	N25	114.4(1)
H21	O2W	H22	110(3)	N12	C13	C14	123.1(2)	C21	N25	N24	101.2(1)
C1	O1	Mn1	128.2(1)								

Table A53: Atomic coordinates for **4.23**.

	x	*y*	*z*		*x*	*y*	*z*
Cu1	0.5	0.5	0	**O3**	0.9350(7)	0.3624(6)	-0.1762(4)
O1	0.5330(10)	0.2112(11)	0.5214(4)	**O4**	0.7193(6)	0.2634(5)	-0.0490(3)
O2	0.8162(8)	0.2870(8)	0.4734(4)	**C11**	0.5344(8)	-0.2953(7)	-0.2057(4)
O3	0.0650(7)	-0.3624(6)	0.1762(4)	**N12**	0.4444(7)	-0.4160(6)	-0.1455(3)
O4	0.2807(6)	-0.2634(5)	0.0490(3)	**C13**	0.3179(9)	-0.4830(8)	-0.1840(4)
C11	0.4656(8)	0.2953(7)	0.2057(4)	**H13**	0.2535	-0.5644	-0.142
N12	0.5556(7)	0.4160(6)	0.1455(3)	**C14**	0.2813(9)	-0.4348(9)	-0.2834(4)
C13	0.6821(9)	0.4830(8)	0.1840(4)	**H14**	0.1926	-0.4823	-0.3078
H13	0.7465	0.5644	0.142	**C15**	0.3773(9)	-0.3151(8)	-0.3467(4)
C14	0.7187(9)	0.4348(9)	0.2834(4)	**C16**	0.5050(8)	-0.2436(8)	-0.3069(4)
H14	0.8074	0.4823	0.3078	**H16**	0.5704	-0.1617	-0.3477
C15	0.6227(9)	0.3151(8)	0.3467(4)	**C21**	0.6653(8)	-0.2253(7)	-0.1578(4)
C16	0.4950(8)	0.2436(8)	0.3069(4)	**N22**	0.6938(7)	-0.2768(6)	-0.0595(3)
H16	0.4296	0.1617	0.3477	**N23**	0.8228(7)	-0.1938(7)	-0.0427(4)
C21	0.3347(8)	0.2253(7)	0.1578(4)	**N24**	0.8671(7)	-0.0953(6)	-0.1301(3)
N22	0.3062(7)	0.2768(6)	0.0595(3)	**N25**	0.7703(7)	-0.1100(6)	-0.2047(3)
N23	0.1772(7)	0.1938(7)	0.0427(4)	**C1**	0.3491(10)	-0.2640(10)	-0.4572(5)
N24	0.1329(7)	0.0953(6)	0.1301(3)	**C2**	0.1414(13)	-0.2436(13)	-0.5792(5)
N25	0.2297(7)	0.1100(6)	0.2047(3)	**H2A**	0.154	-0.1174	-0.6046
C1	0.6509(10)	0.2640(10)	0.4572(5)	**H2B**	0.2374	-0.341	-0.6256
C2	0.8586(13)	0.2436(13)	0.5792(5)	**C3**	-0.0684(14)	-0.2445(14)	-0.5741(7)
H2A	0.846	0.1174	0.6046	**H3A**	-0.1019	-0.2166	-0.6422
H2B	0.7626	0.341	0.6256	**H3B**	-0.0788	-0.3701	-0.5489
C3	1.0684(14)	0.2445(14)	0.5741(7)	**H3C**	-0.1617	-0.1475	-0.528
H3A	1.1019	0.2166	0.6422	**C4**	0.9976(8)	0.0268(7)	-0.1429(4)
H3B	1.0788	0.3701	0.5489	**H4A**	1.0928	-0.0198	-0.0954
H3C	1.1617	0.1475	0.528	**H4B**	1.0763	0.0183	-0.2131
C4	0.0024(8)	-0.0268(7)	0.1429(4)	**C5**	0.8718(8)	0.2391(8)	-0.1222(4)
H4A	-0.0928	0.0198	0.0954	**Cu1**	0.5	-0.5	0
H4B	-0.0763	-0.0183	0.2131	**O4**	0.2807(6)	0.7366(5)	0.0490(3)
C5	0.1282(8)	-0.2391(8)	0.1222(4)	**N12**	0.4444(7)	0.5840(6)	-0.1455(3)
O1	0.4670(10)	-0.2112(11)	-0.5214(4)	**N22**	0.6938(7)	0.7232(6)	-0.0595(3)
O2	0.1838(8)	-0.2870(8)	-0.4734(4)				

Table A54: Bond lengths (Å) for **4.23**.

Atom1	Atom2	Length	Atom1	Atom2	Length	Atom1	Atom2	Length	Atom1	Atom2	Length
Cu1	**N12**	2.028	**C14**	**H14**	0.931	**C4**	**H4B**	0.97	**C15**	**C1**	1.502(9)
Cu1	**N22**	2.421	**C14**	**C15**	1.381(9)	**C4**	**C5**	1.531(7)	**C16**	**H16**	0.93
Cu1	**O4**	1.962	**C15**	**C16**	1.39(1)	**O1**	**C1**	1.182(9)	**C21**	**N22**	1.348(7)
Cu1	**O4**	1.962	**C15**	**C1**	1.502(9)	**O2**	**C1**	1.29(1)	**C21**	**N25**	1.319(7)
Cu1	**N12**	2.028	**C16**	**H16**	0.93	**O2**	**C2**	1.468(9)	**N22**	**N23**	1.311(8)
Cu1	**N22**	2.421	**C21**	**N22**	1.348(7)	**O3**	**C5**	1.226(7)	**N22**	**Cu1**	2.421
O1	**C1**	1.182(9)	**C21**	**N25**	1.319(7)	**O4**	**C5**	1.261(6)	**N23**	**N24**	1.325(6)
O2	**C1**	1.29(1)	**N22**	**N23**	1.311(8)	**C11**	**N12**	1.345(7)	**N24**	**N25**	1.342(7)
O2	**C2**	1.468(9)	**N23**	**N24**	1.325(6)	**C11**	**C16**	1.386(8)	**N24**	**C4**	1.452(8)
O3	**C5**	1.226(7)	**N24**	**N25**	1.342(7)	**C11**	**C21**	1.462(9)	**C2**	**H2A**	0.97
O4	**C5**	1.261(6)	**N24**	**C4**	1.452(8)	**N12**	**C13**	1.350(9)	**C2**	**H2B**	0.97
O4	**Cu1**	1.962	**C2**	**H2A**	0.97	**C4**	**C5**	1.531(7)	**C2**	**C3**	1.47(1)
C11	**N12**	1.345(7)	**C2**	**H2B**	0.97	**N12**	**Cu1**	2.028	**C3**	**H3A**	0.96
C11	**C16**	1.386(8)	**C2**	**C3**	1.47(1)	**C13**	**H13**	0.93	**C3**	**H3B**	0.96
C11	**C21**	1.462(9)	**C3**	**H3A**	0.96	**C13**	**C14**	1.375(8)	**C3**	**H3C**	0.96
N12	**C13**	1.350(9)	**C3**	**H3B**	0.96	**C14**	**H14**	0.931	**C4**	**H4A**	0.969
C13	**H13**	0.93	**C3**	**H3C**	0.96	**C14**	**C15**	1.381(9)	**C4**	**H4B**	0.97
C13	**C14**	1.375(8)	**C4**	**H4A**	0.969	**C15**	**C16**	1.39(1)			

Table A55: Bond angles (°) for **4.23**.

Atom1	Atom2	Atom3	Angle	Atom1	Atom2	Atom3	Angle	Atom1	Atom2	Atom3	Angle
N12	Cu1	N22	76.5	N23	N24	N25	113.5(4)	C14	C15	C16	118.6(5)
N12	Cu1	O4	87.9	N23	N24	C4	123.8(4)	C14	C15	C1	121.6(5)
N12	Cu1	O4	92.1	N25	N24	C4	122.6(4)	C16	C15	C1	119.7(5)
N12	Cu1	N12	180	C21	N25	N24	101.4(4)	C11	C16	C15	119.5(5)
N12	Cu1	N22	103.5	O1	C1	O2	124.6(7)	C11	C16	H16	120.2
N22	Cu1	O4	83.4	O1	C1	C15	123.2(7)	C15	C16	H16	120.3
N22	Cu1	O4	96.6	O2	C1	C15	112.2(6)	C11	C21	N22	122.5(5)
N22	Cu1	N12	103.5	O2	C2	H2A	110.3	C11	C21	N25	124.9(5)
N22	Cu1	N22	180	O2	C2	H2B	110.3	N22	C21	N25	112.6(5)
O4	Cu1	O4	180	O2	C2	C3	107.0(7)	C21	N22	N23	106.6(4)
O4	Cu1	N12	92.1	H2A	C2	H2B	108.6	C21	N22	Cu1	104.4
O4	Cu1	N22	96.6	H2A	C2	C3	110.3	N23	N22	Cu1	148.7
O4	Cu1	N12	87.9	H2B	C2	C3	110.4	N22	N23	N24	105.8(4)
O4	Cu1	N22	83.4	C2	C3	H3A	109.4	N23	N24	N25	113.5(4)
N12	Cu1	N22	76.5	C2	C3	H3B	109.5	N23	N24	C4	123.8(4)
C1	O2	C2	117.1(6)	C2	C3	H3C	109.5	N25	N24	C4	122.6(4)
C5	O4	Cu1	130.9	H3A	C3	H3B	109	C21	N25	N24	101.4(4)
N12	C11	C16	121.5(5)	H3A	C3	H3C	109	O1	C1	O2	124.6(7)
N12	C11	C21	115.7(5)	H3B	C3	H3C	109	O1	C1	C15	123.2(7)
C16	C11	C21	122.8(5)	N24	C4	H4A	109.4	O2	C1	C15	112.2(6)
Cu1	N12	C11	120.9	N24	C4	H4B	109.3	O2	C2	H2A	110.3
Cu1	N12	C13	120.3	N24	C4	C5	111.3(4)	O2	C2	H2B	110.3
C11	N12	C13	118.9(5)	H4A	C4	H4B	108	O2	C2	C3	107.0(7)
N12	C13	H13	119	H4A	C4	C5	109.4	H2A	C2	H2B	108.6
N12	C13	C14	122.1(5)	H4B	C4	C5	109.4	H2A	C2	C3	110.3
H13	C13	C14	118.9	O3	C5	O4	128.6(5)	H2B	C2	C3	110.4
C13	C14	H14	120.3	O3	C5	C4	116.4(5)	C2	C3	H3A	109.4
C13	C14	C15	119.4(6)	O4	C5	C4	115.0(5)	C2	C3	H3B	109.5
H14	C14	C15	120.3	C1	O2	C2	117.1(6)	C2	C3	H3C	109.5
C14	C15	C16	118.6(5)	Cu1	O4	C5	130.9	H3A	C3	H3B	109
C14	C15	C1	121.6(5)	N12	C11	C16	121.5(5)	H3A	C3	H3C	109
C16	C15	C1	119.7(5)	N12	C11	C21	115.7(5)	H3B	C3	H3C	109
C11	C16	C15	119.5(5)	C16	C11	C21	122.8(5)	N24	C4	H4A	109.4
C11	C16	H16	120.2	C11	N12	C13	118.9(5)	N24	C4	H4B	109.3
C15	C16	H16	120.3	C11	N12	Cu1	120.9	N24	C4	C5	111.3(4)
C11	C21	N22	122.5(5)	C13	N12	Cu1	120.3	H4A	C4	H4B	108
C11	C21	N25	124.9(5)	N12	C13	H13	119	H4A	C4	C5	109.4
N22	C21	N25	112.6(5)	N12	C13	C14	122.1(5)	H4B	C4	C5	109.4
Cu1	N22	C21	104.4	H13	C13	C14	118.9	O3	C5	O4	128.6(5)
Cu1	N22	N23	148.7	C13	C14	H14	120.3	O3	C5	C4	116.4(5)
C21	N22	N23	106.6(4)	C13	C14	C15	119.4(6)	O4	C5	C4	115.0(5)
N22	N23	N24	105.8(4)	H14	C14	C15	120.3	O4	Cu1	N12	87.9
O4	Cu1	N22	83.4	N12	Cu1	N22	76.5				

Table A56: Atomic coordinates for **5.1**.

	x	*y*	*z*		*x*	*y*	*z*
C11A	0.4624(4)	0.2775(15)	0.9600(3)	**C11B**	0.7872(4)	0.7169(18)	0.8494(3)
N12A	0.4969(3)	0.2525(10)	0.9893(3)	**N12B**	0.7519(3)	0.7397(13)	0.8223(3)
C13A	0.4942(3)	0.4045(16)	1.0248(3)	**C13B**	0.7547(3)	0.5881(15)	0.7875(3)
H13A	0.5174	0.3894	1.0455	**H13B**	0.7309	0.6031	0.7674
C14A	0.4576(3)	0.5848(15)	1.0314(3)	**C14B**	0.7901(3)	0.4101(16)	0.7787(3)
H14A	0.4573	0.6865	1.0563	**H14B**	0.7893	0.3068	0.754
C15A	0.4224(3)	0.6145(14)	1.0023(3)	**C15B**	0.8268(3)	0.3890(15)	0.8075(3)
C16A	0.4246(3)	0.4598(16)	0.9655(3)	**C16B**	0.8234(3)	0.5470(17)	0.8446(3)
H16A	0.4016	0.4747	0.9446	**H16B**	0.8461	0.5349	0.8659
C21A	0.4642(3)	0.1146(16)	0.9225(3)	**C21B**	0.7837(3)	0.8902(15)	0.8875(3)
N22A	0.4976(3)	-0.0703(12)	0.9146(2)	**N22B**	0.7501(3)	1.0667(12)	0.8957(2)
N23A	0.4873(4)	-0.1980(18)	0.8777(3)	**N23B**	0.7598(4)	1.186(2)	0.9335(3)
N24A	0.4492(3)	-0.0914(19)	0.8634(3)	**N24B**	0.7990(4)	1.0813(19)	0.9467(3)
N25A	0.4333(3)	0.1033(17)	0.8915(3)	**N25B**	0.8145(3)	0.8997(17)	0.9188(3)
O1A	0.5771(3)	0.2479(11)	0.9135(2)	**O1B**	0.6719(2)	0.7444(12)	0.8987(2)
O2A	0.6034(2)	0.0478(11)	0.97286(19)	**O2B**	0.6446(2)	0.9387(13)	0.8393(2)
C1A	0.5396(3)	-0.1470(17)	0.9390(3)	**C1B**	0.7085(3)	1.1362(17)	0.8735(3)
H1A1	0.5536	-0.3022	0.9259	**H1B1**	0.7164	1.1865	0.8443
H1A2	0.5308	-0.1926	0.9682	**H1B2**	0.6945	1.2888	0.8874

C2A	0.5750(3)	0.0787(16)	0.9399(3)	**C2B**	0.6738(3)	0.9158(16)	0.8724(3)
C3A	0.6377(4)	0.254(2)	0.9780(5)	**C3B**	0.6101(4)	0.733(2)	0.8328(4)
H3A1	0.6584	0.2541	0.9538	**H3B1**	0.625	0.5764	0.8219
H3A2	0.6552	0.2233	1.0038	**H3B2**	0.5871	0.7929	0.8126
H3A3	0.6223	0.4228	0.9799	**H3B3**	0.5952	0.6925	0.8596
O3A	0.1312(2)	0.6188(12)	1.1378(2)	**O3B**	1.1198(3)	0.4161(12)	0.6738(2)
O4A	0.1021(2)	0.4261(11)	1.0787(2)	**O4B**	1.1473(2)	0.5876(11)	0.7357(2)
C4A	0.1607(4)	0.2105(19)	1.1130(3)	**C4B**	1.0896(4)	0.825(2)	0.7011(3)
H4A1	0.1438	0.0613	1.1251	**H4B1**	1.082	0.8704	0.7305
H4A2	0.1692	0.1656	1.0838	**H4B2**	1.1067	0.9725	0.6887
C5A	0.1301(3)	0.4443(14)	1.1126(3)	**C5B**	1.1198(3)	0.5827(16)	0.7006(3)
C6A	0.0703(4)	0.651(2)	1.0740(4)	**C6B**	1.1769(4)	0.3575(19)	0.7422(3)
H6A1	0.0614	0.7144	1.1019	**H6B1**	1.158	0.2068	0.7492
H6A2	0.043	0.5957	1.0585	**H6B2**	1.1983	0.3918	0.7653
H6A3	0.0857	0.7903	1.0584	**H6B3**	1.1941	0.3218	0.7164
C7A	0.3816(4)	0.7933(17)	1.0100(3)	**C7B**	0.8681(4)	0.2179(19)	0.8004(4)
H7A1	0.3534	0.6872	1.0086	**H7B1**	0.8691	0.0866	0.8231
H7A2	0.3802	0.9207	0.9867	**H7B2**	0.8958	0.3267	0.8031
C8A	0.3810(3)	0.9457(16)	1.0522(3)	**C8B**	0.8704(3)	0.0747(16)	0.7579(3)
H8A1	0.4076	1.0647	1.0529	**H8B1**	0.8679	0.2039	0.735
H8A2	0.3844	0.8211	1.0758	**H8B2**	0.8438	-0.0435	0.7557
C9A	0.3361(4)	1.1078(18)	1.0590(4)	**C9B**	0.9149(3)	-0.0859(17)	0.7514(4)
H9A1	0.3386	1.2067	1.0856	**H9B1**	0.913	-0.1814	0.7244
H9A2	0.3328	1.2342	1.0357	**H9B2**	0.9179	-0.215	0.7743
C31A	0.2475(3)	0.6019(16)	1.0955(3)	**C31B**	1.0034(3)	0.4343(16)	0.7174(3)
N32A	0.2153(3)	0.5927(15)	1.0641(2)	**N32B**	1.0356(3)	0.4400(15)	0.7493(3)
C33A	0.2241(4)	0.757(2)	1.0317(4)	**C33B**	1.0280(4)	0.2662(16)	0.7818(3)
H33A	0.203	0.756	1.009	**H33B**	1.0493	0.2617	0.8043
C34A	0.2609(4)	0.9287(19)	1.0283(3)	**C34B**	0.9906(4)	0.0972(16)	0.7835(3)
H34A	0.2638	1.039	1.0046	**H34B**	0.9871	-0.0161	0.8068
C35A	0.2938(3)	0.9361(16)	1.0607(3)	**C35B**	0.9582(3)	0.0936(15)	0.7509(3)
C36A	0.2853(4)	0.7703(16)	1.0950(4)	**C36B**	0.9645(3)	0.2688(15)	0.7166(3)
H36A	0.3056	0.7722	1.1183	**H36B**	0.9433	0.2746	0.6939
C41A	0.2397(3)	0.4198(16)	1.1317(3)	**C41B**	1.0100(3)	0.6278(15)	0.6832(3)
N42A	0.2029(3)	0.2545(12)	1.1378(3)	**N42B**	1.0464(3)	0.7851(13)	0.6770(3)
N43A	0.2113(4)	0.1157(16)	1.1741(3)	**N43B**	1.0386(3)	0.9349(16)	0.6405(3)
N44A	0.2513(4)	0.196(2)	1.1888(3)	**N44B**	0.9978(4)	0.867(2)	0.6285(3)
N45A	0.2703(3)	0.3920(17)	1.1640(3)	**N45B**	0.9785(3)	0.6828(18)	0.6525(3)

Table A57: Bond lengths (Å) for **5.1**.

Atom1	Atom2	Length	Atom1	Atom2	Length	Atom1	Atom2	Length	Atom1	Atom2	Length
C11A	**N12A**	1.35(1)	**C4A**	**H4A2**	0.97	**C11B**	**N12B**	1.32(1)	**C4B**	**H4B2**	0.97
C11A	**C16A**	1.43(1)	**C4A**	**C5A**	1.47(1)	**C11B**	**C16B**	1.35(1)	**C4B**	**C5B**	1.50(1)
C11A	**C21A**	1.43(1)	**C4A**	**N42A**	1.45(1)	**C11B**	**C21B**	1.48(1)	**C4B**	**N42B**	1.46(1)
N12A	**C13A**	1.35(1)	**C6A**	**H6A1**	0.96	**N12B**	**C13B**	1.33(1)	**C6B**	**H6B1**	0.96
C13A	**H13A**	0.929	**C6A**	**H6A2**	0.96	**C13B**	**H13B**	0.929	**C6B**	**H6B2**	0.96
C13A	**C14A**	1.40(1)	**C6A**	**H6A3**	0.96	**C13B**	**C14B**	1.38(1)	**C6B**	**H6B3**	0.96
C14A	**H14A**	0.93	**C7A**	**H7A1**	0.97	**C14B**	**H14B**	0.929	**C7B**	**H7B1**	0.97
C14A	**C15A**	1.36(1)	**C7A**	**H7A2**	0.97	**C14B**	**C15B**	1.39(1)	**C7B**	**H7B2**	0.97
C15A	**C16A**	1.39(1)	**C7A**	**C8A**	1.52(1)	**C15B**	**C16B**	1.41(1)	**C7B**	**C8B**	1.51(1)
C15A	**C7A**	1.50(1)	**C8A**	**H8A1**	0.97	**C15B**	**C7B**	1.48(1)	**C8B**	**H8B1**	0.969
C16A	**H16A**	0.929	**C8A**	**H8A2**	0.972	**C16B**	**H16B**	0.931	**C8B**	**H8B2**	0.97
C21A	**N22A**	1.36(1)	**C8A**	**C9A**	1.54(1)	**C21B**	**N22B**	1.34(1)	**C8B**	**C9B**	1.52(1)
C21A	**N25A**	1.31(1)	**C9A**	**H9A1**	0.97	**C21B**	**N25B**	1.32(1)	**C9B**	**H9B1**	0.97
N22A	**N23A**	1.35(1)	**C9A**	**H9A2**	0.97	**N22B**	**N23B**	1.35(1)	**C9B**	**H9B2**	0.97
N22A	**C1A**	1.47(1)	**C9A**	**C35A**	1.49(1)	**N22B**	**C1B**	1.42(1)	**C9B**	**C35B**	1.54(1)
N23A	**N24A**	1.30(1)	**C31A**	**N32A**	1.35(1)	**N23B**	**N24B**	1.31(2)	**C31B**	**N32B**	1.36(1)
N24A	**N25A**	1.39(1)	**C31A**	**C36A**	1.38(1)	**N24B**	**N25B**	1.34(1)	**C31B**	**C36B**	1.39(1)
O1A	**C2A**	1.19(1)	**C31A**	**C41A**	1.47(1)	**O1B**	**C2B**	1.19(1)	**C31B**	**C41B**	1.46(1)
O2A	**C2A**	1.32(1)	**N32A**	**C33A**	1.33(1)	**O2B**	**C2B**	1.33(1)	**N32B**	**C33B**	1.36(1)
O2A	**C3A**	1.44(1)	**C33A**	**H33A**	0.93	**O2B**	**C3B**	1.45(1)	**C33B**	**H33B**	0.93
C1A	**H1A1**	0.97	**C33A**	**C34A**	1.37(2)	**C1B**	**H1B1**	0.971	**C33B**	**C34B**	1.37(1)
C1A	**H1A2**	0.971	**C34A**	**H34A**	0.928	**C1B**	**H1B2**	0.97	**C34B**	**H34B**	0.929
C1A	**C2A**	1.52(1)	**C34A**	**C35A**	1.38(1)	**C1B**	**C2B**	1.49(1)	**C34B**	**C35B**	1.38(1)
C3A	**H3A1**	0.96	**C35A**	**C36A**	1.38(1)	**C3B**	**H3B1**	0.96	**C35B**	**C36B**	1.40(1)
C3A	**H3A2**	0.96	**C36A**	**H36A**	0.93	**C3B**	**H3B2**	0.96	**C36B**	**H36B**	0.932
C3A	**H3A3**	0.96	**C41A**	**N42A**	1.36(1)	**C3B**	**H3B3**	0.96	**C41B**	**N42B**	1.32(1)
O3A	**C5A**	1.18(1)	**C41A**	**N45A**	1.34(1)	**O3B**	**C5B**	1.18(1)	**C41B**	**N45B**	1.34(1)

O4A	**C5A**	1.33(1)	**N42A**	**N43A**	1.35(1)	**O4B**	**C5B**	1.35(1)	**N42B**	**N43B**	1.38(1)
O4A	**C6A**	1.46(1)	**N43A**	**N44A**	1.30(2)	**O4B**	**C6B**	1.45(1)	**N43B**	**N44B**	1.27(1)
C4A	**H4A1**	0.97	**N44A**	**N45A**	1.37(1)	**C4B**	**H4B1**	0.97	**N44B**	**N45B**	1.31(1)

Table A58: Bond angles (°) for **5.1**.

Atom1	**Atom2**	**Atom3**	**Angle**	**Atom1**	**Atom2**	**Atom3**	**Angle**	**Atom1**	**Atom2**	**Atom3**	**Angle**
N12A	C11A	C16A	122.2(8)	H8A1	C8A	H8A2	107.7	O1B	C2B	O2B	124.5(8)
N12A	C11A	C21A	118.2(8)	H8A1	C8A	C9A	108.9	O1B	C2B	C1B	123.7(8)
C16A	C11A	C21A	119.7(8)	H8A2	C8A	C9A	108.9	O2B	C2B	C1B	111.8(7)
C11A	N12A	C13A	117.3(8)	C8A	C9A	H9A1	109.2	O2B	C3B	H3B1	110
N12A	C13A	H13A	118.8	C8A	C9A	H9A2	109.1	O2B	C3B	H3B2	110
N12A	C13A	C14A	122.1(8)	C8A	C9A	C35A	112.1(8)	O2B	C3B	H3B3	110
H13A	C13A	C14A	119.1	H9A1	C9A	H9A2	108	H3B1	C3B	H3B2	109
C13A	C14A	H14A	119.1	H9A1	C9A	C35A	109.2	H3B1	C3B	H3B3	109
C13A	C14A	C15A	121.7(8)	H9A2	C9A	C35A	109.2	H3B2	C3B	H3B3	109
H14A	C14A	C15A	119.1	N32A	C31A	C36A	123.5(8)	C5B	O4B	C6B	116.1(7)
C14A	C15A	C16A	117.0(8)	N32A	C31A	C41A	115.6(8)	H4B1	C4B	H4B2	108
C14A	C15A	C7A	122.5(8)	C36A	C31A	C41A	120.9(8)	H4B1	C4B	C5B	109.4
C16A	C15A	C7A	120.5(8)	C31A	N32A	C33A	113.6(8)	H4B1	C4B	N42B	109.1
C11A	C16A	C15A	119.6(8)	N32A	C33A	H33A	117	H4B2	C4B	C5B	109.3
C11A	C16A	H16A	120.3	N32A	C33A	C34A	127(1)	H4B2	C4B	N42B	109.2
C15A	C16A	H16A	120.1	H33A	C33A	C34A	116	C5B	C4B	N42B	111.8(8)
C11A	C21A	N22A	124.6(8)	C33A	C34A	H34A	121	O3B	C5B	O4B	125.8(8)
C11A	C21A	N25A	127.1(8)	C33A	C34A	C35A	119.1(9)	O3B	C5B	C4B	125.9(8)
N22A	C21A	N25A	108.2(8)	H34A	C34A	C35A	120	O4B	C5B	C4B	108.3(7)
C21A	N22A	N23A	109.1(7)	C9A	C35A	C34A	123.0(9)	O4B	C6B	H6B1	109.6
C21A	N22A	C1A	131.4(7)	C9A	C35A	C36A	121.6(9)	O4B	C6B	H6B2	109.5
N23A	N22A	C1A	119.5(7)	C34A	C35A	C36A	115.4(9)	O4B	C6B	H6B3	109.5
N22A	N23A	N24A	106.2(9)	C31A	C36A	C35A	121.5(9)	H6B1	C6B	H6B2	109
N23A	N24A	N25A	110.6(9)	C31A	C36A	H36A	119	H6B1	C6B	H6B3	109
C21A	N25A	N24A	105.8(8)	C35A	C36A	H36A	119	H6B2	C6B	H6B3	109
C2A	O2A	C3A	115.0(7)	C31A	C41A	N42A	127.5(8)	C15B	C7B	H7B1	108
N22A	C1A	H1A1	109.4	C31A	C41A	N45A	122.7(8)	C15B	C7B	H7B2	108
N22A	C1A	H1A2	109.5	N42A	C41A	N45A	109.8(8)	C15B	C7B	C8B	116.4(9)
N22A	C1A	C2A	110.9(7)	C4A	N42A	C41A	131.8(8)	H7B1	C7B	H7B2	107
H1A1	C1A	H1A2	108.1	C4A	N42A	N43A	120.9(8)	H7B1	C7B	C8B	108.1
H1A1	C1A	C2A	109.6	C41A	N42A	N43A	107.3(8)	H7B2	C7B	C8B	108.2
H1A2	C1A	C2A	109.4	N42A	N43A	N44A	106.9(9)	C7B	C8B	H8B1	108.7
O1A	C2A	O2A	126.4(8)	N43A	N44A	N45A	112.2(9)	C7B	C8B	H8B2	108.8
O1A	C2A	C1A	123.9(8)	C41A	N45A	N44A	103.8(8)	C7B	C8B	C9B	114.0(8)
O2A	C2A	C1A	109.6(7)	N12B	C11B	C16B	124.8(9)	H8B1	C8B	H8B2	107.7
O2A	C3A	H3A1	110	N12B	C11B	C21B	114.2(8)	H8B1	C8B	C9B	108.8
O2A	C3A	H3A2	109	C16B	C11B	C21B	121.0(9)	H8B2	C8B	C9B	108.7
O2A	C3A	H3A3	110	C11B	N12B	C13B	115.1(8)	C8B	C9B	H9B1	109.4
H3A1	C3A	H3A2	110	N12B	C13B	H13B	117.3	C8B	C9B	H9B2	109.5
H3A1	C3A	H3A3	109	N12B	C13B	C14B	125.4(8)	C8B	C9B	C35B	111.3(8)
H3A2	C3A	H3A3	109	H13B	C13B	C14B	117.2	H9B1	C9B	H9B2	108
C5A	O4A	C6A	113.7(7)	C13B	C14B	H14B	120.7	H9B1	C9B	C35B	109.2
H4A1	C4A	H4A2	108	C13B	C14B	C15B	118.6(8)	H9B2	C9B	C35B	109.4
H4A1	C4A	C5A	109.1	H14B	C14B	C15B	120.8	N32B	C31B	C36B	124.8(8)
H4A1	C4A	N42A	109.1	C14B	C15B	C16B	115.8(8)	N32B	C31B	C41B	115.7(8)
H4A2	C4A	C5A	109.3	C14B	C15B	C7B	123.6(8)	C36B	C31B	C41B	119.5(8)
H4A2	C4A	N42A	109	C16B	C15B	C7B	120.5(8)	C31B	N32B	C33B	115.1(8)
C5A	C4A	N42A	112.2(8)	C11B	C16B	C15B	120.2(8)	N32B	C33B	H33B	118.2
O3A	C5A	O4A	126.6(8)	C11B	C16B	H16B	119.9	N32B	C33B	C34B	123.8(9)
O3A	C5A	C4A	125.3(8)	C15B	C16B	H16B	120	H33B	C33B	C34B	118
O4A	C5A	C4A	108.1(7)	C11B	C21B	N22B	126.6(8)	C33B	C34B	H34B	120
O4A	C6A	H6A1	109	C11B	C21B	N25B	124.8(8)	C33B	C34B	C35B	120.5(9)
O4A	C6A	H6A2	109	N22B	C21B	N25B	108.5(8)	H34B	C34B	C35B	119.7
O4A	C6A	H6A3	109	C21B	N22B	N23B	108.4(7)	C9B	C35B	C34B	123.0(8)
H6A1	C6A	H6A2	110	C21B	N22B	C1B	132.5(7)	C9B	C35B	C36B	119.0(8)
H6A1	C6A	H6A3	110	N23B	N22B	C1B	119.1(8)	C34B	C35B	C36B	117.9(8)
H6A2	C6A	H6A3	109	N22B	N23B	N24B	105.7(9)	C31B	C36B	C35B	117.9(8)
C15A	C7A	H7A1	108.1	N23B	N24B	N25B	110.9(9)	C31B	C36B	H36B	121.1
C15A	C7A	H7A2	108.2	C21B	N25B	N24B	106.5(8)	C35B	C36B	H36B	121
C15A	C7A	C8A	116.9(8)	C2B	O2B	C3B	118.3(7)	C31B	C41B	N42B	127.6(8)
H7A1	C7A	H7A2	107.3	N22B	C1B	H1B1	109	C31B	C41B	N45B	124.9(8)
H7A1	C7A	C8A	107.9	N22B	C1B	H1B2	109	N42B	C41B	N45B	107.5(8)

H7A2	C7A	C8A	108.1	N22B	C1B	C2B	112.7(7)	C4B	N42B	C41B	132.4(8)
C7A	C8A	H8A1	108.8	H1B1	C1B	H1B2	107.9	C4B	N42B	N43B	118.9(8)
C7A	C8A	H8A2	109	H1B1	C1B	C2B	109.2	C41B	N42B	N43B	108.7(8)
C7A	C8A	C9A	113.4(8)	H1B2	C1B	C2B	109	N42B	N43B	N44B	104.0(8)
N43B	N44B	N45B	114.1(9)	C41B	N45B	N44B	105.6(8)				

Table A59: Atomic coordinates for **5.4**.

	x	*y*	*z*		*x*	*y*	*z*
O1	0.2333(2)	0.3357(2)	0.2296(3)	**C12**	0.4844(2)	0.3144(2)	0.28564(19)
O2	0.4245(2)	0.46678(18)	0.18293(18)	**H12A**	0.5215	0.2498	0.2121
O3	0.8634(2)	0.27395(17)	0.38310(16)	**H12B**	0.5684	0.3957	0.3425
O4	1.01035(17)	0.23296(15)	0.53653(15)	**C13**	0.3647(3)	0.3732(2)	0.2316(2)
N1	0.12479(16)	-0.03778(18)	0.14833(16)	**C14**	0.3198(5)	0.5242(4)	0.1156(4)
N2	0.29938(17)	-0.17784(17)	-0.02760(15)	**H14A**	0.3697	0.5627	0.0584
C1	0.27533(18)	-0.00927(18)	0.18508(17)	**H14B**	0.2333	0.4452	0.0599
C2	0.36242(17)	-0.08459(18)	0.09850(16)	**C15**	0.2698(5)	0.6395(6)	0.2130(6)
C3	0.1512(2)	-0.1995(2)	-0.06367(19)	**H15A**	0.1961	0.6719	0.1682
H3	0.1043	-0.2612	-0.1514	**H15B**	0.3546	0.7209	0.2632
C4	0.0646(2)	-0.1337(2)	0.0243(2)	**H15C**	0.2255	0.6026	0.2725
H4	-0.0397	-0.1573	-0.0041	**C22**	0.86378(19)	0.0271(2)	0.36158(19)
C11	0.33769(19)	0.09912(19)	0.32291(17)	**H22A**	0.9486	-0.0112	0.3299
N12	0.42747(16)	0.23385(16)	0.36156(14)	**H22B**	0.8369	-0.0097	0.4279
N13	0.4548(2)	0.2988(2)	0.49580(16)	**C23**	0.9096(2)	0.1925(2)	0.42535(19)
N14	0.3846(2)	0.2051(2)	0.53609(18)	**C24**	1.0784(3)	0.3900(3)	0.6091(3)
N15	0.3089(2)	0.0787(2)	0.43007(17)	**H24A**	1.0008	0.4457	0.6221
C21	0.52396(18)	-0.07175(18)	0.13987(16)	**H24B**	1.1455	0.4245	0.5596
N22	0.60080(16)	-0.00150(17)	0.26418(14)	**C25**	1.1640(3)	0.4090(3)	0.7398(3)
N23	0.73655(15)	-0.02544(16)	0.25044(15)	**H25A**	1.2401	0.3531	0.7254
N24	0.74532(17)	-0.10529(19)	0.12658(17)	**H25B**	1.0963	0.3748	0.7878
N25	0.60980(17)	-0.13615(19)	0.05353(16)	**H25C**	1.2112	0.5115	0.7909

Table A60: Bond lengths (Å) of **5.4**.

Atom1	Atom2	Length	Atom1	Atom2	Length	Atom1	Atom2	Length	Atom1	Atom2	Length
O1	**C13**	1.194(3)	**C2**	**C21**	1.466(2)	**C21**	**N25**	1.353(2)	**C15**	**H15B**	0.96
O2	**C13**	1.318(3)	**C3**	**H3**	0.93	**N22**	**N23**	1.323(2)	**C15**	**H15C**	0.96
O2	**C14**	1.464(5)	**C3**	**C4**	1.374(3)	**N23**	**N24**	1.318(2)	**C22**	**H22A**	0.97
O3	**C23**	1.192(3)	**C25**	**H25C**	0.96	**N23**	**C22**	1.451(2)	**C22**	**H22B**	0.97
O4	**C23**	1.322(2)	**C4**	**H4**	0.93	**N24**	**N25**	1.316(2)	**C22**	**C23**	1.501(3)
O4	**C24**	1.457(3)	**C11**	**N12**	1.341(2)	**C12**	**H12A**	0.97	**C24**	**H24A**	0.97
N1	**C1**	1.340(2)	**C11**	**N15**	1.317(3)	**C12**	**H12B**	0.97	**C24**	**H24B**	0.97
N1	**C4**	1.324(2)	**N12**	**N13**	1.344(2)	**C12**	**C13**	1.496(3)	**C24**	**C25**	1.482(5)
N2	**C2**	1.338(2)	**N12**	**C12**	1.444(3)	**C14**	**H14A**	0.971	**C25**	**H25A**	0.96
N2	**C3**	1.326(2)	**N13**	**N14**	1.291(3)	**C14**	**H14B**	0.97	**C25**	**H25B**	0.96
C1	**C2**	1.402(2)	**N14**	**N15**	1.363(2)	**C14**	**C15**	1.440(7)	**C15**	**H15A**	0.96
C1	**C11**	1.470(2)	**C21**	**N22**	1.321(2)						

Table A61: Bond angles (°) of **5.4**.

Atom1	Atom2	Atom3	Angle	Atom1	Atom2	Atom3	Angle	Atom1	Atom2	Atom3	Angle
C13	O2	C14	117.0(2)	C2	C21	N22	124.6(2)	C14	C15	H15C	109.5
C23	O4	C24	117.3(2)	C2	C21	N25	122.8(2)	H15A	C15	H15B	109.5
C1	N1	C4	116.6(2)	N22	C21	N25	112.5(2)	H15A	C15	H15C	109.5
C2	N2	C3	116.8(2)	C21	N22	N23	101.7(1)	H15B	C15	H15C	109.5
N1	C1	C2	121.2(2)	N22	N23	N24	113.9(2)	N23	C22	H22A	109.3
N1	C1	C11	114.8(2)	N22	N23	C22	123.4(2)	N23	C22	H22B	109.3
C2	C1	C11	123.9(2)	N24	N23	C22	122.6(2)	N23	C22	C23	111.6(2)
N2	C2	C1	120.9(2)	N23	N24	N25	106.3(2)	H22A	C22	H22B	108
N2	C2	C21	115.9(2)	C21	N25	N24	105.6(2)	H22A	C22	C23	109.3
C1	C2	C21	123.1(2)	N12	C12	H12A	109.3	H22B	C22	C23	109.3
N2	C3	H3	119	N12	C12	H12B	109.3	O3	C23	O4	125.6(2)
N2	C3	C4	122.2(2)	N12	C12	C13	111.5(2)	O3	C23	C22	126.0(2)
H3	C3	C4	118.9	H12A	C12	H12B	108	O4	C23	C22	108.5(2)
N1	C4	C3	122.1(2)	H12A	C12	C13	109.3	O4	C24	H24A	110.4
N1	C4	H4	118.9	H12B	C12	C13	109.3	O4	C24	H24B	110.4
C3	C4	H4	119	O1	C13	O2	125.5(2)	O4	C24	C25	106.8(2)

C1	C11	N12	127.1(2)	O1	C13	C12	124.0(2)	H24A	C24	H24B	108.5
C1	C11	N15	124.1(2)	O2	C13	C12	110.4(2)	H24A	C24	C25	110.4
N12	C11	N15	108.7(2)	O2	C14	H14A	109.7	H24B	C24	C25	110.4
C11	N12	N13	108.2(2)	O2	C14	H14B	109.7	C24	C25	H25A	109.5
C11	N12	C12	131.5(2)	O2	C14	C15	110.1(4)	C24	C25	H25B	109.5
N13	N12	C12	120.1(2)	H14A	C14	H14B	108.1	C24	C25	H25C	109.5
N12	N13	N14	106.7(2)	H14A	C14	C15	109.6	H25A	C25	H25B	109.5
N13	N14	N15	110.7(2)	H14B	C14	C15	109.6	H25A	C25	H25C	109.5
C11	N15	N14	105.6(2)	C14	C15	H15A	109.5	H25B	C25	H25C	109.5
C14	C15	H15B	109.4								

Table A62: Atomic coordinates for **5.5**.

	x	*y*	*z*		*x*	*y*	*z*
O1	0.7347(4)	0.7192(4)	0.39463(12)	**C12**	0.5595(5)	0.7767(5)	0.45801(16)
O2	0.5450(3)	0.5354(4)	0.40832(12)	**H12A**	0.4579	0.8173	0.446
O3	1.2331(4)	0.7701(4)	0.72764(13)	**H12B**	0.5482	0.7049	0.4873
O4	0.9863(4)	0.8513(4)	0.73086(12)	**C13**	0.6270(5)	0.6746(6)	0.41677(17)
N1	0.8278(4)	0.6450(4)	0.52309(13)	**C14**	0.5882(6)	0.4284(5)	0.36689(18)
N2	0.9790(4)	0.7139(4)	0.61741(13)	**H14A**	0.6758	0.358	0.378
C1	0.8357(4)	0.8026(5)	0.54211(17)	**H14B**	0.6164	0.4978	0.3387
C2	0.9031(4)	0.8354(5)	0.59022(16)	**C15**	0.4534(6)	0.3213(7)	0.3511(2)
C3	0.9779(5)	0.5595(5)	0.59690(19)	**H15A**	0.478	0.25	0.3235
H3	1.0341	0.4734	0.6137	**H15B**	0.3673	0.3924	0.3406
C4	0.8960(5)	0.5235(5)	0.55156(19)	**H15C**	0.4276	0.2522	0.3791
H4	0.8882	0.4116	0.5406	**C22**	1.1370(5)	0.9941(5)	0.67540(17)
C11	0.7754(5)	0.9377(5)	0.50727(16)	**H22A**	1.1944	1.0879	0.6912
N12	0.6567(4)	0.9187(4)	0.47257(13)	**H22B**	1.1959	0.9511	0.6485
N13	0.6402(5)	1.0658(5)	0.44625(15)	**C23**	1.1247(6)	0.8564(6)	0.71419(18)
N14	0.7480(5)	1.1664(5)	0.46516(15)	**C24**	0.9612(6)	0.7248(8)	0.7697(2)
N15	0.8353(4)	1.0898(4)	0.50318(14)	**H24A**	1.0574	0.7043	0.7898
C21	0.8901(5)	0.9964(5)	0.61744(16)	**H24B**	0.8873	0.7683	0.7922
N22	0.9906(4)	1.0585(4)	0.65299(14)	**C25**	0.9057(8)	0.5700(7)	0.7480(2)
N23	0.9345(5)	1.2038(4)	0.67063(15)	**H25A**	0.98	0.5252	0.7265
N24	0.8021(5)	1.2279(5)	0.64535(16)	**H25B**	0.81	0.5899	0.7284
N25	0.7706(4)	1.0989(4)	0.61186(14)	**H25C**	0.8895	0.4901	0.7745

Table A63: Bond lengths (Å) for **5.5**.

Atom1	Atom2	Length	Atom1	Atom2	Length	Atom1	Atom2	Length	Atom1	Atom2	Length
O1	**C13**	1.194(6)	**C2**	**C21**	1.468(6)	**C21**	**N25**	1.316(5)	**C15**	**H15B**	0.96
O2	**C13**	1.319(5)	**C3**	**H3**	0.93	**N22**	**N23**	1.343(5)	**C15**	**H15C**	0.959
O2	**C14**	1.454(6)	**C3**	**C4**	1.378(7)	**N22**	**C22**	1.455(5)	**C22**	**H22A**	0.969
O3	**C23**	1.195(6)	**C4**	**H4**	0.93	**N23**	**N24**	1.301(6)	**C22**	**H22B**	0.968
O4	**C23**	1.313(6)	**C11**	**N12**	1.337(5)	**N24**	**N25**	1.363(5)	**C22**	**C23**	1.503(6)
O4	**C24**	1.460(7)	**C11**	**N15**	1.315(5)	**C12**	**H12A**	0.97	**C24**	**H24A**	0.971
N1	**C1**	1.341(5)	**N12**	**N13**	1.355(5)	**C12**	**H12B**	0.97	**C24**	**H24B**	0.97
N1	**C4**	1.330(5)	**N12**	**C12**	1.438(5)	**C12**	**C13**	1.509(6)	**C24**	**C25**	1.418(8)
N2	**C2**	1.342(5)	**N13**	**N14**	1.299(6)	**C14**	**H14A**	0.97	**C25**	**H25A**	0.959
N2	**C3**	1.333(5)	**N14**	**N15**	1.356(5)	**C14**	**H14B**	0.971	**C25**	**H25B**	0.96
C1	**C2**	1.385(6)	**C21**	**N22**	1.328(5)	**C14**	**C15**	1.479(7)	**C25**	**H25C**	0.961
C1	**C11**	1.479(6)	**C15**	**H15A**	0.958						

Table A64: Bond angles (°) for **5.5**.

Atom1	Atom2	Atom3	Angle	Atom1	Atom2	Atom3	Angle	Atom1	Atom2	Atom3	Angle
C13	O2	C14	116.3(3)	C2	C21	N22	126.5(4)	C14	C15	H15B	109.4
C23	O4	C24	116.5(4)	C2	C21	N25	124.4(4)	C14	C15	H15C	109.4
C1	N1	C4	116.5(4)	N22	C21	N25	109.0(4)	H15A	C15	H15B	109.6
C2	N2	C3	116.5(4)	C21	N22	N23	108.9(3)	H15A	C15	H15C	109.5
N1	C1	C2	121.6(4)	C21	N22	C22	132.0(4)	H15B	C15	H15C	109.4
N1	C1	C11	115.3(3)	N23	N22	C22	119.1(3)	N22	C22	H22A	108.4
C2	C1	C11	123.0(4)	N22	N23	N24	106.0(4)	N22	C22	H22B	108.5
N2	C2	C1	121.1(4)	N23	N24	N25	110.6(4)	N22	C22	C23	115.2(4)
N2	C2	C21	114.0(3)	C21	N25	N24	105.5(3)	H22A	C22	H22B	107.5
C1	C2	C21	124.7(4)	N12	C12	H12A	109.5	H22A	C22	C23	108.5
N2	C3	H3	119	N12	C12	H12B	109.4	H22B	C22	C23	108.5

N2	C3	C4	122.0(4)	N12	C12	C13	110.9(3)	O3	C23	O4	127.2(5)
H3	C3	C4	119	H12A	C12	H12B	108.1	O3	C23	C22	121.3(4)
N1	C4	C3	121.6(4)	H12A	C12	C13	109.4	O4	C23	C22	111.4(4)
N1	C4	H4	119.2	H12B	C12	C13	109.5	O4	C24	H24A	109.4
C3	C4	H4	119.2	O1	C13	O2	126.6(4)	O4	C24	H24B	109.3
C1	C11	N12	124.5(4)	O1	C13	C12	124.0(4)	O4	C24	C25	111.6(5)
C1	C11	N15	125.7(4)	O2	C13	C12	109.4(4)	H24A	C24	H24B	107.8
N12	C11	N15	109.6(4)	O2	C14	H14A	110.2	H24A	C24	C25	109.4
C11	N12	N13	107.7(3)	O2	C14	H14B	110.2	H24B	C24	C25	109.4
C11	N12	C12	132.8(4)	O2	C14	C15	107.5(4)	C24	C25	H25A	109.5
N13	N12	C12	119.4(3)	H14A	C14	H14B	108.5	C24	C25	H25B	109.4
N12	N13	N14	106.2(4)	H14A	C14	C15	110.3	C24	C25	H25C	109.5
N13	N14	N15	111.2(4)	H14B	C14	C15	110.2	H25A	C25	H25B	109.6
C11	N15	N14	105.3(3)	C14	C15	H15A	109.4	H25A	C25	H25C	109.4
H25B	C25	H25C	109.4								

Table A65: Atomic coordinates for **5.15**.

	x	*y*	*z*		*x*	*y*	*z*
Cu1	0.96278(3)	0.57959(4)	0.405848(13)	**Cu2**	0.71280(3)	0.58152(4)	0.620994(13)
O1W	0.9084(4)	0.7589(3)	0.45156(15)	**O2W**	0.6612(3)	0.7489(3)	0.57198(15)
H11	0.951(3)	0.776(6)	0.4730(12)	**H21**	0.687(4)	0.741(6)	0.5445(9)
H12	0.845(2)	0.735(6)	0.4617(16)	**H22**	0.5926(16)	0.737(5)	0.5702(17)
O1A	0.5933(2)	-0.0449(3)	0.44256(11)	**O1B**	0.3496(2)	-0.0470(3)	0.58924(10)
O2A	0.6178(2)	0.1832(3)	0.41472(12)	**O2B**	0.3722(2)	0.1863(3)	0.61272(11)
O3A	0.5442(2)	0.7924(4)	0.36521(10)	**O3B**	0.2891(2)	0.7868(3)	0.66264(10)
O4A	0.5436(3)	0.9820(3)	0.31658(11)	**O4B**	0.2919(3)	0.9805(3)	0.70971(11)
C1A	0.8555(4)	0.2334(4)	0.37836(18)	**C1B**	0.6133(4)	0.2354(4)	0.65027(17)
C2A	0.8240(3)	0.3130(4)	0.33989(12)	**C2B**	0.5776(3)	0.3134(4)	0.68772(12)
N3A	0.8236(5)	0.2477(4)	0.29893(16)	**N3B**	0.5764(5)	0.2510(4)	0.72899(17)
C3A	0.8579(4)	0.1081(5)	0.29717(15)	**C3B**	0.6118(4)	0.1131(5)	0.73199(14)
H3A	0.8573	0.0595	0.2694	**H3B**	0.6083	0.0649	0.7598
C4A	0.8945(4)	0.0320(4)	0.33480(15)	**C4B**	0.6540(4)	0.0380(5)	0.69488(15)
H4A	0.9215	-0.0635	0.3314	**H4B**	0.6833	-0.0561	0.6989
N4A	0.8917(3)	0.0930(3)	0.37601(13)	**N4B**	0.6532(3)	0.0980(4)	0.65388(12)
C11A	0.8489(3)	0.2911(4)	0.42499(12)	**C11B**	0.6054(3)	0.2895(4)	0.60333(12)
N12A	0.8826(3)	0.4217(3)	0.43905(11)	**N12B**	0.6359(3)	0.4191(3)	0.58689(11)
N13A	0.8623(3)	0.4276(3)	0.48429(12)	**N13B**	0.6108(3)	0.4201(3)	0.54225(11)
N14A	0.8169(3)	0.3057(4)	0.49731(11)	**N14B**	0.5669(3)	0.2954(4)	0.53137(11)
N15A	0.8079(3)	0.2190(4)	0.46054(12)	**N15B**	0.5648(3)	0.2112(4)	0.56911(10)
C21A	0.7875(3)	0.4668(4)	0.33994(12)	**C21B**	0.5379(3)	0.4692(4)	0.68675(12)
N22A	0.8327(3)	0.5806(3)	0.36309(11)	**N22B**	0.5806(3)	0.5814(3)	0.66265(10)
N23A	0.7837(2)	0.7035(4)	0.35073(12)	**N23B**	0.5315(2)	0.7031(4)	0.67517(12)
N24A	0.7111(3)	0.6609(3)	0.32060(10)	**N24B**	0.4607(3)	0.6612(3)	0.70598(10)
N25A	0.7096(3)	0.5155(3)	0.31250(10)	**N25B**	0.4608(3)	0.5169(3)	0.71451(10)
C5A	0.7533(3)	0.0766(4)	0.46319(14)	**C5B**	0.5125(3)	0.0668(4)	0.56978(13)
H5A	0.7404	0.0521	0.4947	**H5C**	0.5583	-0.0033	0.5857
H5B	0.7998	0.0006	0.4505	**H5D**	0.5035	0.0315	0.539
C6A	0.6449(3)	0.0770(4)	0.43771(13)	**C6B**	0.4012(3)	0.0740(4)	0.59304(13)
C7A	0.6428(4)	0.7677(5)	0.29599(18)	**C7B**	0.3929(4)	0.7683(5)	0.72960(17)
H7A	0.5969	0.7148	0.2748	**H7C**	0.439	0.8368	0.7459
H7B	0.6886	0.8345	0.2788	**H7D**	0.3488	0.7163	0.7516
C8A	0.5712(3)	0.8586(4)	0.32890(12)	**C8B**	0.3190(3)	0.8559(4)	0.69828(12)
Cu1	0.46278(3)	-0.07959(4)	0.405848(13)	**Cu2**	0.21280(3)	-0.08152(4)	0.620994(13)
Cu1	0.46278(3)	0.92041(4)	0.405848(13)	**Cu2**	0.21280(3)	0.91848(4)	0.620994(13)
O1A	1.0933(2)	0.5449(3)	0.44256(11)	**O1B**	0.8496(2)	0.5470(3)	0.58924(10)
O3A	1.0442(2)	0.7076(4)	0.36521(10)	**O3B**	0.7891(2)	0.7132(3)	0.66264(10)
O3W	0.7009(3)	0.7151(4)	0.47810(13)	**O5W**	0.6157(3)	0.4985(4)	0.42196(15)
H31	0.666(4)	0.791(4)	0.466(2)	**H51**	0.604(5)	0.398(3)	0.419(3)
H32	0.670(4)	0.633(3)	0.468(2)	**H52**	0.556(4)	0.531(7)	0.436(2)
O4W	0.4480(3)	0.7141(4)	0.54754(13)	**O6W**	0.3336(6)	0.4784(6)	0.5826(3)
H41	0.416(4)	0.797(3)	0.553(2)	**H61**	0.377(7)	0.446(11)	0.605(3)
H42	0.409(4)	0.637(4)	0.553(2)	**H62**	0.277(6)	0.523(12)	0.596(3)

Table A66: Bond lengths (Å) for **5.15**.

Atom1	Atom2	Length	Atom1	Atom2	Length	Atom1	Atom2	Length	Atom1	Atom2	Length
Cu1	**O1W**	2.212(4)	**C11A**	**N12A**	1.317(5)	**Cu2**	**N12B**	2.016(3)	**C11B**	**N15B**	1.331(5)
Cu1	**N12A**	1.993(3)	**C11A**	**N15A**	1.335(5)	**Cu2**	**N22B**	2.044(3)	**N12B**	**N13B**	1.355(5)
Cu1	**N22A**	2.044(4)	**N12A**	**N13A**	1.361(5)	**Cu2**	**O1B**	1.957(3)	**N13B**	**N14B**	1.290(5)
Cu1	**O1A**	1.968(3)	**N13A**	**N14A**	1.293(5)	**Cu2**	**O3B**	1.953(3)	**N14B**	**N15B**	1.349(5)
Cu1	**O3A**	1.946(3)	**N14A**	**N15A**	1.343(5)	**O2W**	**H21**	0.87(3)	**N15B**	**C5B**	1.455(5)
O1W	**H11**	0.84(4)	**N15A**	**C5A**	1.453(5)	**O2W**	**H22**	0.86(2)	**C21B**	**N22B**	1.345(5)
O1W	**H12**	0.87(3)	**C21A**	**N22A**	1.354(5)	**O1B**	**C6B**	1.269(5)	**C21B**	**N25B**	1.328(5)
O1A	**C6A**	1.279(5)	**C21A**	**N25A**	1.333(5)	**O1B**	**Cu2**	1.957(3)	**N22B**	**N23B**	1.308(5)
O1A	**Cu1**	1.968(3)	**N22A**	**N23A**	1.315(5)	**O2B**	**C6B**	1.222(5)	**N23B**	**N24B**	1.318(5)
O2A	**C6A**	1.221(5)	**N23A**	**N24A**	1.321(5)	**O3B**	**C8B**	1.278(5)	**N24B**	**N25B**	1.326(4)
O3A	**C8A**	1.272(5)	**N24A**	**N25A**	1.334(4)	**O3B**	**Cu2**	1.953(3)	**N24B**	**C7B**	1.457(6)
O3A	**Cu1**	1.946(3)	**N24A**	**C7A**	1.473(6)	**O4B**	**C8B**	1.221(5)	**C5B**	**H5C**	0.97
O4A	**C8A**	1.220(5)	**C5A**	**H5A**	0.97	**C1B**	**C2B**	1.383(6)	**C5B**	**H5D**	0.97
C1A	**C2A**	1.400(6)	**C5A**	**H5B**	0.97	**C1B**	**N4B**	1.339(5)	**C5B**	**C6B**	1.538(5)
C1A	**N4A**	1.345(5)	**C5A**	**C6A**	1.536(5)	**C1B**	**C11B**	1.473(6)	**C7B**	**H7C**	0.969
C1A	**C11A**	1.475(6)	**C7A**	**H7A**	0.97	**C2B**	**N3B**	1.343(6)	**C7B**	**H7D**	0.969
C2A	**N3A**	1.346(6)	**C7A**	**H7B**	0.97	**C2B**	**C21B**	1.489(5)	**C7B**	**C8B**	1.521(6)
C2A	**C21A**	1.459(5)	**C7A**	**C8A**	1.549(6)	**N3B**	**C3B**	1.322(6)	**O5W**	**H51**	0.92(3)
N3A	**C3A**	1.330(6)	**O3W**	**H31**	0.88(4)	**C3B**	**H3B**	0.931	**O5W**	**H52**	0.90(5)
C3A	**H3A**	0.93	**O3W**	**H32**	0.89(4)	**C3B**	**C4B**	1.390(6)	**O6W**	**H61**	0.90(9)
C3A	**C4A**	1.383(6)	**O4W**	**H41**	0.86(3)	**C4B**	**H4B**	0.931	**O6W**	**H62**	0.90(9)
C4A	**H4A**	0.93	**O4W**	**H42**	0.86(4)	**C4B**	**N4B**	1.327(6)	**C11B**	**N12B**	1.321(5)
C4A	**N4A**	1.337(6)	**Cu2**	**O2W**	2.187(4)						

Table A67: Bond angles (°) for **5.15**.

Atom1	Atom2	Atom3	Angle	Atom1	Atom2	Atom3	Angle	Atom1	Atom2	Atom3	Angle
O1W	Cu1	N12A	94.1(1)	N23A	N24A	N25A	114.6(3)	H3B	C3B	C4B	119.1
O1W	Cu1	N22A	97.8(1)	N23A	N24A	C7A	122.1(3)	C3B	C4B	H4B	119.3
O1W	Cu1	O1A	91.6(1)	N25A	N24A	C7A	123.2(3)	C3B	C4B	N4B	121.2(4)
O1W	Cu1	O3A	95.7(1)	C21A	N25A	N24A	101.8(3)	H4B	C4B	N4B	119.5
N12A	Cu1	N22A	85.2(1)	N15A	C5A	H5A	109.2	C1B	N4B	C4B	117.0(4)
N12A	Cu1	O1A	91.3(1)	N15A	C5A	H5B	109.3	C1B	C11B	N12B	128.3(3)
N12A	Cu1	O3A	170.0(1)	N15A	C5A	C6A	112.1(3)	C1B	C11B	N15B	124.3(3)
N22A	Cu1	O1A	170.1(1)	H5A	C5A	H5B	107.9	N12B	C11B	N15B	107.3(3)
N22A	Cu1	O3A	91.3(1)	H5A	C5A	C6A	109.1	Cu2	N12B	C11B	126.4(3)
O1A	Cu1	O3A	90.6(1)	H5B	C5A	C6A	109.2	Cu2	N12B	N13B	126.1(2)
Cu1	O1W	H11	114(3)	O1A	C6A	O2A	126.9(4)	C11B	N12B	N13B	107.4(3)
Cu1	O1W	H12	108(3)	O1A	C6A	C5A	112.2(3)	N12B	N13B	N14B	109.4(3)
H11	O1W	H12	111(4)	O2A	C6A	C5A	120.9(3)	N13B	N14B	N15B	107.1(3)
C6A	O1A	Cu1	118.9(2)	N24A	C7A	H7A	109.3	C11B	N15B	N14B	108.7(3)
C8A	O3A	Cu1	112.1(2)	N24A	C7A	H7B	109.3	C11B	N15B	C5B	129.2(3)
C2A	C1A	N4A	122.3(4)	N24A	C7A	C8A	111.3(4)	N14B	N15B	C5B	121.6(3)
C2A	C1A	C11A	124.2(4)	H7A	C7A	H7B	108	C2B	C21B	N22B	126.3(3)
N4A	C1A	C11A	113.5(4)	H7A	C7A	C8A	109.4	C2B	C21B	N25B	122.0(3)
C1A	C2A	N3A	120.4(4)	H7B	C7A	C8A	109.4	N22B	C21B	N25B	111.3(3)
C1A	C2A	C21A	125.0(3)	O3A	C8A	O4A	127.4(4)	Cu2	N22B	C21B	129.2(3)
N3A	C2A	C21A	114.6(4)	O3A	C8A	C7A	115.5(3)	Cu2	N22B	N23B	122.7(2)
C2A	N3A	C3A	116.7(4)	O4A	C8A	C7A	117.1(4)	C21B	N22B	N23B	107.5(3)
N3A	C3A	H3A	118.6	H31	O3W	H32	108(4)	N22B	N23B	N24B	105.2(3)
N3A	C3A	C4A	122.9(4)	H41	O4W	H42	114(4)	N23B	N24B	N25B	114.4(3)
H3A	C3A	C4A	118.5	O2W	Cu2	N12B	91.9(1)	N23B	N24B	C7B	121.5(3)
C3A	C4A	H4A	119.4	O2W	Cu2	N22B	99.6(1)	N25B	N24B	C7B	124.1(3)
C3A	C4A	N4A	121.3(4)	O2W	Cu2	O1B	92.5(1)	C21B	N25B	N24B	101.6(3)
H4A	C4A	N4A	119.3	O2W	Cu2	O3B	97.9(1)	N15B	C5B	H5C	109.4
C1A	N4A	C4A	116.3(4)	N12B	Cu2	N22B	85.7(1)	N15B	C5B	H5D	109.4
C1A	C11A	N12A	126.4(4)	N12B	Cu2	O1B	92.9(1)	N15B	C5B	C6B	111.4(3)
C1A	C11A	N15A	125.7(4)	N12B	Cu2	O3B	169.9(1)	H5C	C5B	H5D	107.9
N12A	C11A	N15A	107.9(3)	N22B	Cu2	O1B	167.9(1)	H5C	C5B	C6B	109.4
Cu1	N12A	C11A	129.9(3)	N22B	Cu2	O3B	90.4(1)	H5D	C5B	C6B	109.3
Cu1	N12A	N13A	123.2(2)	O1B	Cu2	O3B	89.0(1)	O1B	C6B	O2B	127.5(4)
C11A	N12A	N13A	106.6(3)	Cu2	O2W	H21	117(3)	O1B	C6B	C5B	111.9(3)
N12A	N13A	N14A	109.8(3)	Cu2	O2W	H22	104(3)	O2B	C6B	C5B	120.6(3)
N13A	N14A	N15A	106.9(3)	H21	O2W	H22	107(4)	N24B	C7B	H7C	108.9
C11A	N15A	N14A	108.7(3)	C6B	O1B	Cu2	121.9(2)	N24B	C7B	H7D	108.8
C11A	N15A	C5A	130.5(3)	C8B	O3B	Cu2	111.2(2)	N24B	C7B	C8B	113.5(4)

N14A	N15A	C5A	120.7(3)	C2B	C1B	N4B	121.7(4)	H7C	C7B	H7D	107.8
C2A	C21A	N22A	126.5(3)	C2B	C1B	C11B	124.3(4)	H7C	C7B	C8B	108.9
C2A	C21A	N25A	122.4(3)	N4B	C1B	C11B	114.0(4)	H7D	C7B	C8B	108.8
N22A	C21A	N25A	110.8(3)	C1B	C2B	N3B	121.1(4)	O3B	C8B	O4B	126.7(4)
Cu1	N22A	C21A	129.3(3)	C1B	C2B	C21B	124.7(3)	O3B	C8B	C7B	114.9(3)
Cu1	N22A	N23A	122.5(2)	N3B	C2B	C21B	114.2(4)	O4B	C8B	C7B	118.4(4)
C21A	N22A	N23A	108.0(3)	C2B	N3B	C3B	116.9(4)	H51	O5W	H52	104(5)
N22A	N23A	N24A	104.7(3)	N3B	C3B	H3B	118.9	H61	O6W	H62	107(8)
N3B	C3B	C4B	122.0(4)								

Table A68: Atomic coordinates for **5.16**.

	x	*y*	*z*		*x*	*y*	*z*
Cu1	0.5	0.24466(5)	0.63674(6)	**C3**	0.5538(3)	0.2431(4)	1.1138(4)
O1	0.10771(17)	0.3668(2)	1.0691(2)	**H3**	0.5892	0.2197	1.1786
O2	0.1482(2)	0.2499(2)	0.9150(3)	**C11**	0.6204(2)	0.3568(3)	0.8392(2)
C1	0.4456(2)	0.3106(3)	0.9313(2)	**N2**	0.6072(2)	0.2761(3)	1.0228(3)
C3	0.4462(3)	0.2431(4)	1.1138(4)	**N12**	0.6065(2)	0.3412(3)	0.7301(2)
H3	0.4108	0.2197	1.1786	**N13**	0.6875(2)	0.3996(3)	0.6783(2)
C5	0.2300(2)	0.4607(3)	0.9508(3)	**N14**	0.7495(2)	0.4504(4)	0.7514(2)
H5A	0.1914	0.543	0.937	**N15**	0.70910(18)	0.4259(3)	0.8521(2)
H5B	0.276	0.4763	1.0135	**O1**	0.89229(17)	0.3668(2)	1.0691(2)
C6	0.1553(2)	0.3470(3)	0.9786(3)	**O2**	0.8518(2)	0.2499(2)	0.9150(3)
C11	0.3796(2)	0.3568(3)	0.8392(2)	**C5**	0.7700(2)	0.4607(3)	0.9508(3)
N2	0.3928(2)	0.2761(3)	1.0228(3)	**H5A**	0.8086	0.543	0.937
N12	0.3935(2)	0.3412(3)	0.7301(2)	**H5B**	0.724	0.4763	1.0135
N13	0.3125(2)	0.3996(3)	0.6783(2)	**C6**	0.8447(2)	0.3470(3)	0.9786(3)
N14	0.2505(2)	0.4504(4)	0.7514(2)	**H1W**	0.555(2)	0.376(4)	0.473(4)
N15	0.29090(18)	0.4259(3)	0.8521(2)	**H2W**	0.553(3)	0.015(6)	0.750(4)
O1W	0.5	0.4088(3)	0.4984(3)	**Cu1**	0	0.25534(5)	1.13674(6)
H1W	0.445(2)	0.376(4)	0.473(4)	**Cu1**	1	0.25534(5)	1.13674(6)
O2W	0.5	0.0533(5)	0.7813(4)	**O1**	0.39229(17)	0.1332(2)	0.5691(2)
H2W	0.447(3)	0.015(6)	0.750(4)	**O1**	0.60771(17)	0.1332(2)	0.5691(2)
C1	0.5544(2)	0.3106(3)	0.9313(2)				

Table A69: Bond lengths (Å) for **5.16**.

Atom1	Atom2	Length	Atom1	Atom2	Length	Atom1	Atom2	Length	Atom1	Atom2	Length
Cu1	**N12**	2.014	**C1**	**C1**	1.404(4)	**N12**	**N13**	1.346(4)	**C11**	**N12**	1.329(3)
Cu1	**O1W**	2.323	**C3**	**H3**	0.93	**N13**	**N14**	1.289(4)	**C11**	**N15**	1.342(4)
Cu1	**O2W**	2.569	**C3**	**N2**	1.331(6)	**N14**	**N15**	1.337(3)	**N12**	**N13**	1.346(4)
Cu1	**N12**	2.014	**C1**	**C11**	1.467(4)	**O1W**	**H1W**	0.84	**N13**	**N14**	1.289(4)
Cu1	**O1**	1.952	**C3**	**C3**	1.388(5)	**O1W**	**H1W**	0.84	**N14**	**N15**	1.337(3)
Cu1	**O1**	1.952	**C5**	**H5A**	0.97	**O2W**	**H2W**	0.87	**N15**	**C5**	1.462(4)
O1	**C6**	1.262(4)	**C5**	**H5B**	0.97	**O2W**	**H2W**	0.87	**O1**	**C6**	1.262(4)
O1	**Cu1**	1.952	**C5**	**C6**	1.520(4)	**C5**	**C6**	1.520(4)	**O1**	**Cu1**	1.952
O2	**C6**	1.231(4)	**C5**	**N15**	1.462(4)	**C1**	**N2**	1.336(4)	**O2**	**C6**	1.231(4)
C1	**C11**	1.467(4)	**C11**	**N12**	1.329(3)	**C3**	**H3**	0.93	**C5**	**H5A**	0.97
C1	**N2**	1.336(4)	**C11**	**N15**	1.342(4)	**C3**	**N2**	1.331(6)	**C5**	**H5B**	0.97

Table A70: Bond angles (°) for **5.16**.

Atom1	Atom2	Atom3	Angle	Atom1	Atom2	Atom3	Angle	Atom1	Atom2	Atom3	Angle
N12	Cu1	O1W	93.7	H5B	C5	N15	109.6	C3	C3	H3	119.4
N12	Cu1	O2W	88.6	C6	C5	N15	110.1(2)	C3	C3	N2	121.2(4)
N12	Cu1	N12	86	O1	C6	O2	128.2(3)	H3	C3	N2	119.4
N12	Cu1	O1	90.8	O1	C6	C5	112.4(3)	C1	C11	N12	128.7(2)
N12	Cu1	O1	170.3	O2	C6	C5	119.4(3)	C1	C11	N15	124.5(2)
O1W	Cu1	O2W	176.9	C1	C11	N12	128.7(2)	N12	C11	N15	106.7(2)
O1W	Cu1	N12	93.7	C1	C11	N15	124.5(2)	C1	N2	C3	118.2(3)
O1W	Cu1	O1	95.7	N12	C11	N15	106.7(2)	Cu1	N12	C11	134
O1W	Cu1	O1	95.7	C1	N2	C3	118.2(3)	Cu1	N12	N13	118.5
O2W	Cu1	N12	88.6	Cu1	N12	C11	134	C11	N12	N13	107.4(2)
O2W	Cu1	O1	82.1	Cu1	N12	N13	118.5	N12	N13	N14	109.6(3)
O2W	Cu1	O1	82.1	C11	N12	N13	107.4(2)	N13	N14	N15	107.5(3)
N12	Cu1	O1	170.3	N12	N13	N14	109.6(3)	C11	N15	N14	108.7(2)
N12	Cu1	O1	90.8	N13	N14	N15	107.5(3)	C11	N15	C5	132.2(3)

O1	Cu1	O1	90.79	C5	N15	C11	132.2(3)	N14	N15	C5	118.6(3)
C6	O1	Cu1	128	C5	N15	N14	118.6(3)	C6	O1	Cu1	128
C11	C1	N2	113.7(2)	C11	N15	N14	108.7(2)	N15	C5	H5A	109.7
C11	C1	C1	125.5(2)	Cu1	O1W	H1W	89	N15	C5	H5B	109.6
N2	C1	C1	120.7(3)	Cu1	O1W	H1W	89	N15	C5	C6	110.1(2)
H3	C3	N2	119.4	H1W	O1W	H1W	116	H5A	C5	H5B	108.2
H3	C3	C3	119.4	Cu1	O2W	H2W	92	H5A	C5	C6	109.6
N2	C3	C3	121.2(4)	Cu1	O2W	H2W	92	H5B	C5	C6	109.6
H5A	C5	H5B	108.2	H2W	O2W	H2W	104	O1	C6	O2	128.2(3)
H5A	C5	C6	109.6	C1	C1	C11	125.5(2)	O1	C6	C5	112.4(3)
H5A	C5	N15	109.7	C1	C1	N2	120.7(3)	O2	C6	C5	119.4(3)
H5B	C5	C6	109.6	C11	C1	N2	113.7(2)				

Appendix B: EPR Spectroscopy Hamiltonian Equation

Fitting of EPR spectra was performed by Dr. Høgni Weihe in the University of Copenhagen. As the EPR spectra revealed no signature of metal-metal interactions, the spectra were fitted to the spin Hamiltonian

$$\hat{H} = A_x \hat{S}_x \hat{I}_x + A_y \hat{S}_y \hat{I}_y + A_z \hat{S}_z \hat{I}_z + {}_B(g_x \hat{S}_x B_x + g_y \hat{S}_y B_y + g_z \hat{S}_z B_z)$$

being appropriate for mononuclear Cu^{2+} spin systems with quantum numbers (S; *I*) = (1/2, 3/2). The parameters A_x and A_y could not be determined from the broad lines, and A_z could be reliably estimated for compounds **3.8**, **3.10** and **3.11**.